The Impact of Climate Change on Blond Sandstone decay in Glasgow

Laura Jane Duthie
BSc. (Hons) University of Glasgow

Submitted in fulfilment of the requirements for the
Degree of Doctor of Philosophy

School of Geographical and Earth Science
College of Science and Engineering
University of Glasgow

June 2011

Abstract

Glasgow contains many buildings made from local 'blond' sandstones that are showing the legacy of 150 years of urban weathering and this decay may accelerate as climate changes in the future. Most of the blond sandstones are Carboniferous in age and comprise of micaceous quartz arenites with varying amounts of diagenetic minerals including ankerite and kaolinite. Chemical decay can be visually identified in the carbonate minerals, but the combination of quantitative X-ray microanalysis (chemistry of mineral) and Raman spectroscopy (structure of mineral) also allows chemical decay to be observed in both kaolinite and muscovite. The Raman spectroscopy shows a variation in the muscovite minerals between the outermost surface and internal region (20 mm depth), demonstrating that structural decay is occurring within the micas and reduces them to an "ionic slurry state" in a relatively short time frame. The impact of microbial colonisation on the stones was also investigated. Using osmium stained polished blocks, complimented by scanning electron microscope imaging, microorganisms were found to be living cryptoendolithically in a few samples but at very shallow depths (<2 mm). Light penetration results revealed that a thin weathered crust (<1 mm) on the surface of sandstone will restrict the transmission of light into the rock, thereby preventing the colonisation of photosynthetic microbes. As a result, most microbial communities are restricted to the stone surface but only where they will not be subjected to photo-oxidative damage, which frequently occurs during summer months. Consequently, the most extensive microbial colonisation is restricted to the sandstone's surface and during the winter. Using novel internal microclimate monitoring technologies it was found that stone temperature and humidity is decoupled from ambient conditions. During the summer the stone interior is considerably hotter than air temperature, whilst relative humidity is generally comparable to external conditions, whereas in the winter interior temperatures are closely related to ambient conditions and relative humidity is generally much higher. To understand how sandstone buildings will react to a change in climate, current conditions were extrapolated to 2080 using predictive models for the Glasgow region and the impact of these conditions was investigated by accelerated weathering experiments in a climate chamber. Results reveal rapid granular disintegration, the rates of which are independent of grain size. Overall, this study concludes that rates of chemical decay will increase as the climate warms and becomes wetter overall, primarily

through dissolution, decay and loss of diagenetic minerals, and the extent of microbial activity will change, but these effects will be strongly dependent on local microenvironment. Implications of these findings are that more work on conservation and preservation techniques will be very important to protect the stone-built heritage of Scotland.

Table of contents

List of Figures:

List of Tables:

List of Equations:

Acknowledgements

Firstly, I would like to thank NERC and Historic Scotland who funded the project initially and then allowed me the pleasure and responsibility of taking on the research at the School of Geographical and Earth Science.

Although sample collection was a long and arduous process, we got there in the end. I would like to thank the many companies who helped with this; CBC stone, Natural Stone Trading, EBS construction, Robert Gordon University and the BGS.

The excellent supervision then provided by Martin Lee and Vernon Phoenix has been the key to success for this project, where as without there support, assistant, motivation and English. I would never have gotten this far, Thank you for having faith that I would get there in the end. Also thanks to Ewan Hyslop and Craig Kennedy for their assistance in completing the research.

However, there are many people who have provided assistance in this project that I owe thanks to. From Historic Scotland thanks has to be given to Maureen Young, who gave guidance and discussion and Colin Muir, who provided expert laser scanning and Lyn Wilson. Thanks to Dr. John Parnell for undertaking the permeability experiments at Robert Gordon University. To Colin Hunter at the University observatory for letting me take over a small section of their grounds and allowing me to clamber over their roof.

The success of this project comes from having a great network of technical support available, and they all deserve massive thanks. Brian Black and Garry Tait for providing endless support, and always answering my pleas of computer distress. Kenny Roberts for being my personal chauffeur and colleting rock whenever asked. John Gilleece for providing sample preparation training, and conversation during many hours of endless grinding. And finally Peter Chung for SEM training and Robert McDonald for being able to find and fix anything.

The Gregory building contained, and contains some of the most fabulous people (and heels) ever. I have made some excellent friends over the last four years, who have provided me with much tea, cake, wine, laughs and memories. They have supported and

ranted with me when necessary, thank you. A special thanks has to be given to Susan and Clare. Without their wise words and motivation I may never have made it out alive. In addition, throughout the difficult third year I had an amazing flatmate, who provided much tea and dinners. She took on extra cleaning when I was stressed and busy and provided much needed stimulating non-geology conversation. And she is now acting as my local b&b. Thank you Imogen, more than my English can express.

Although I don't think that any of my family really understands what I have actually been doing for the last four years, I hope they understand that they have helped me through those years. They have being there for a yarn and providing ssasarmeat, flaky biscuits and fish. Thank you Mam, Granny, Duthie 2 and Duthie 3.

Finally my biggest thanks of all has to go to Dave. Thank you for listening to me rant and rave and for putting up with many tears. You have supported me and made me believe that I could do it. Thank you for always being there for me, even when we were hundreds of miles apart, you never complained and you made it easy. All I can say is thank you, and oh technically you have now read a whole book.

There are too many people who have given endless support to me in their own ways. So I would like to thank to all the Joys.

Declaration

The material presented in this thesis is the result of independent research carried out at the School of Geographical and Earth Science at the University of Glasgow in conjunction with Historic Scotland, between September 2007 to June 2011. The research was supervised by Dr. Martin Lee, Dr. Vernon Phoenix, Dr. Craig Kennedy and Dr. Ewan Hyslop. This thesis represents my own research and any published or unpublished work by other authors has been given full acknowledgement in the text.

Abbreviations

BGS:	British Geological Survey
BRE:	Building Research Establishment
BSE:	Backscatter electron
CKN:	Clackmannan Group
CL:	Cathodoluminescence
EDS:	Energy Dispersive Spectroscopy
EDX:	Quantitative Energy Dispersive Spectroscopy
EPS:	Extracellular polysaccharide
FEG-SEM:	Quanta 200F Field-emission environmental SEM
FTIR:	Fourier Transform Infrared Spectroscopy
H_P:	Hand held Macam Q203 Quantum Radiometer pyronometer
LASC:	Lausanne Atmospheric Simulation Chamber
LWS:	Leaf Wetness Sensor
LWS-EXT:	Leaf Wetness Sensor External
LWS-INT:	Leaf Wetness Sensor Internal
LR:	London White Resin
OLT:	Optical Light transmission
O_P:	Fixed Kipp and Zonen CMP3 pyronometer at University of Glasgow observatory
PAR:	Photosynthetically active radiation

PE:	Potential evaporation
RH:	Relative Humidity
RSD:	Relative Standard Deviation
SCMG:	Scottish Coal Measures Group
SEG:	Scottish Enterprise Glasgow
SEM:	Scanning electron Microscopy
SP1:	Sample preparation one
SP2:	Sample preparation two
SSD:	Shell to shell deviation
ZS-SEM	Zeiss Sigma Field-emission analytical SEM
SSLG:	Scottish Stone Liaison Group
UKCIP02:	United Kingdom Climate Impact Program 2002
XRD:	X-ray Diffraction

1 Introduction

To successfully undertake this study, all the different factors that may influence the decay of sandstone have to be understood. A comprehensive literature review was conducted regarding all possible factors potentially influencing building sandstone. In addition to this information, it was also important to understand the geological nature of the sandstone and the diagenetic conditions under which they were originally formed, thus providing a background to the sandstones used in the construction of Glasgow. Finally the climatic conditions that the sandstones have encountered since placed into the buildings will have a significant role in past weathering of the buildings. All this information is detailed in the present chapter. However, a definition of weathering is presented first.

1.1 Definition of Weathering

The definition of weathering used is dependent on the circumstance within which it is being referred to. Geomorphologists often use the Reiche, (1962) definition "the response of materials which were in equilibrium within the lithosphere to conditions at or near to its contact with the atmosphere, the hydrosphere and perhaps more importantly, the biosphere".

More recent definitions of weathering have been put forward by Ollier (1991), Selby (1993) and Price (1995). The definition proposed by Ollier (1991) suggests "weathering is the alteration and breakdown of rocks near the earth's surface, mainly by reactions with water and air to form clay, iron oxides and other weathering products". Price (1995) agrees: "weathering is the irreversible response of soil and rock material and masses to their natural or artificial exposure to the near surface geomophological or engineering environment. These authors provide adequate definitions, although fail to outline all the mechanisms of weathering in one definition. Therefore, within this study, Selby's (1993) definition of weathering will be used, "... the process of alteration and breakdown of soil and rock material at and near the Earth's surface by physical, chemical and biotic processes". However, Price (1995) did identify that weathering is caused by individual weathering processes. Therefore these weathering processes will be out detailed next.

1.2 Literature Review of Weathering on Sedimentary Rock

A wealth of research has been published worldwide on the interactions between natural building materials (I.E sandstone, limestone, granite) and the weathering processes that contribute to their deterioration. Various overview studies have also been published on this subject (Whalley and Mcgreevy, 1985; Turkington and Paradise, 2005), although these overviews often focus only on one aspect of weathering such as salt or biological deterioration. The present review will concentrate on decay of sandstone but will examine all factors that can be attributed to the weathering of sandstone buildings and monuments. For this discussion weathering processes have been divided into seven categories: pollution; salt crystallization; freeze-thaw; chemical action; clay expansion; thermal heating and biological activity. These factors have tended to be studied individually to assess their weathering potential on sandstone. Whilst it is important to understand each process individually, efforts must be made to recognise that many of these processes are interrelated. In this review, the literature relevant to each process will be examined in turn to evaluate what is known about their role in stone decay. Key references are listed in Table 1-1.

Table 1-1: Important references for each aspect of stone decay discussed.

Topic	Key References
Overviews	(Whalley and Mcgreevy, 1985; Turkington and Paradise, 2005)
Pollution	(Bluck and Porter, 1991b; Butlin et al., 1992; Sabbioni and Zappia, 1992; Machill et al., 1997; Turkington et al., 2003)
Salt Crystallisation	(Cooke and Smalley, 1968; Winkler and Singer, 1972; Mcgreevy and Smith, 1982; Rodriguez-Navarro and Doehne, 1999; Smith et al., 2002; Mottershead et al., 2003)
Freeze-thaw	(Thomachot and Jeannette, 2002; Hall, 2004)
Chemical	(Lasaga, 1998; Franke, 2009)
Clay Expansion	(Madsen and Muller-Vonmoos, 1989; Chin and Mills, 1991; Maurice et al., 2001; Jimenez-Gonzalez et al., 2008; Sebastián et al., 2008)
Thermal Heating and albedo climate	(Kerr et al., 1984b; Jenkins and Smith, 1990; Warke et al., 1996; Warke and Smith, 1998; Hall et al., 2005; Hall and Andre, 2006; Smith et al., 2008b)
Biological	(Golubic et al., 1981; Friedmann, 1982; Ortega-Calvo et al., 1991; Viles, 1995; Young, 1997; Welton et al., 2003)

1.2.1 *Weathering due to Pollution*

The effects of anthropogenic pollution are particularly important in urban environments, especially those which are, or have been, located in areas of heavy industry (e.g. coal mining and steelworks). Pollution in these areas often manifests itself as a black crust or patina covering the surface of the sandstone. These crusts are often complex in composition but are commonly a combination of fly ash (industrial particulates), soot (vehicle combustion outputs) and salts (mainly gypsum). These substances accumulate on the surface and are thought to be damaging to the sandstone beneath, but they may also protect the stone by reducing the inward flow of water.

Many studies have been have been undertaken on limestone crusts (Moropoulou et al., 1998; Grossi et al., 2003; Török, 2003), but only a few of them have examined crusts on sandstones.

One such study was the National Material Exposure Program (Butlin et al., 1992) which experimentally studied the interactions between pollutants and Portland Limestone, White Mansfield Dolomitic Sandstone and Monks Park Limestone. Some of the experimental blocks were sheltered whereas others were exposed to the local climate at 29 locations throughout Britain, over a period of four years. It was concluded that the main weathering was caused by pollution, although Butlin et al. (1992) did not say which pollutants had accumulated on their sandstone samples. They commented that the problems caused by the pollutants are the removal of cements present and were evident through increased definition of ooids in the limestone samples. Furthermore, chemical analyses showed an increase in the concentrations of soluble ions (Na^+, K^+, NH_4^+, Ca^{2+}, Mg^{2+}, Cl^-, NO_3^-, SO_4^{4-}) near the surface of the sheltered tablets compared to the exposed tablets, with one exception SO_4^{4-}. Butlin et al. (1992) proposed that, due to their exposure, salts may have been washed away by rainfall.

Sabbioni and Zappia (1992) studied the main pollution components within the patina on some northern Italian sandstones and calc-arenite sandstones. They identified anthropogenic aerosols, lead (a vehicle-derived pollutant) and zinc (an oil tracer from refineries) through X-ray diffraction (XRD), differential thermal analysis and thermal gravimetric analysis. The sandstones studied could be divided into two layers: the thin

black patina (1 mm) and an underlying thicker (1 cm) white layer which had a crumbly texture. Gypsum occurred in both layers, although in higher concentrations in the black patina. The sulphur within the gypsum was shown to be derived from atmospheric deposition (gaseous and aerosol SO_2) whilst the calcium was sourced from the minerals within the rock. They suggest a weathering cycle of sulphation-decohesion-detachment was taking place on the sandstone.

Machill et al. (1997) detailed the exact pollutants within the crust by analysing a building constructed from Saxonean Cretaceous sandstone using gas chromatography and mass spectrometry. Numerous substances were identified with three principal sources, atmospheric pollution (denoted by the presence of alphatic hydrocarbons originating from petroleum residues), microorganisms and plants (denoted by alkanols and fatty acids) and thirdly the metabolites of organic materials (shown by carbohydrate derivatives, dicarboxylic and hydroxyl acids). Sabbioni and Zappia (1992) and MacHill et al. (1997) agree that pollutants are damaging but fail to demonstrate the process by which they mediate weathering, only mentioning that the crusts are acidic and promote corrosion.

Laboratory experiments were undertaken by Ausset et al. (1996) using the Lausanne Atmospheric Simulation Chamber (LASC), with the aim of examining sulphation on Jaumont Limestone (calcite = 94%, quartz = 2.5%) and Berne Sandstone (calcite = 23%, quartz = 40%). Samples were either bare or covered in fly ash or soot particles, then placed in the chamber for a year while SO_2 and NO_2 gases were pumped in and the samples were analysed in 3 month intervals. Results show that the two stones behaved very differently, which is to be expected given the mineralogical contrasts. Jaumont Limestone was much more reactive and therefore more SO_2 was deposited on the surface. However, the soot particles seem to shield the sandstones from sulphation for a much longer period of time compared to the bare and fly ash samples.

Lefevre and Ausset (2002) give an in-depth description of how sulphation of sandstone can occur and describe two processes of sulphation, "*below"* and "*above"* the surface. *"Below"* is characterised by gypsum developing due to available calcium in the substrate, then gaseous (SO_2) or liquid (H_2SO_4) penetrates in to the rocks and reacts with the calcite which is then replaced by gypsum. *"Above"* sulphation occurs due to the reaction

between atmospheric SO_2 and calcium ions present in fog, and this reaction then generates precipitates onto the surface of the stone and forms gypsum. In both cases the salts, when created, trap atmospheric particles and produce a blackened colouration. They state that "*below"* sulphation is often more damaging as it leads to fracturing, blistering and slab detachment and is also much more frequently occurring. These observations complimented their previous study (Ausset et al., 1996).

Pollutants do not only have a corrosive effect, they are also visually unsightly after a period of time (Webster et al., 1992). To quantify the time period in which pollution begins to adhere and affect the sandstone, Turkington et al. (2003) mounted blocks of Baumberger Sandstone and a quartz rich Dunhouse Sandstone in various locations throughout Belfast to run exposure trials. These were left for six years and sampled after three months, two years, four years and then at the end. The experiment shows that, within three months, fly ash will adhere preferentially to Dunhouse Buff but by two years it can adhere to both sandstones, due to both lithological and environmental controls. In addition, after six years, the percentage of fly ash pollution on the exposed samples decreases in comparison to the four year tests. Their conclusions suggest that environment is a more significant control on the decay processes rather than the weathering caused by the pollutants, which have adhered to the stone.

1.2.2 ***Summary of Pollution Weathering***

Pollution is still seen as a problem, although its importance as a weathering agent in the future may diminish in the United Kingdom, due to the Clean Air Act 1956 and more recent legalisation by Clean Air For Europe such as the 1996 96/62/EC report on air quality assessment and management, but pollution is still an important topic for many cities worldwide and conservation groups. However, it is unclear the exact role pollution plays in the overall weathering process. These studies previously discussed mention that pollution can cause granular disintegration and the removal of cement, although, these may have been caused instead by climatic conditions and it is difficult to isolate the effect of pollution. In addition, a black crust may actually play a protective role to sandstone, by repelling the attack of microbes (Bluck and Porter, 1991b) and reducing the penetration of water (Young 1995). We therefore have to understand whether climate or pollution is the most damaging process.

1.2.3 *Weathering due to Salts*

Crystallisation of salt within sandstone is one of the main areas of stone weathering research, as its occurrence and consequences vary widely. There are many factors to consider such as the salt solution composition and concentration, pore size, sandstone mineralogy and environmental conditions such as relative humidity and temperature.

One of the earliest studies by Cooke and Smalley (1968) focused on the processes through which the salt caused damage. Three main processes were identified: 1) the initial growth of salt crystals from solution; 2) thermal expansion; 3) salt hydration. Cooke and Smalley (1968) considered initial crystallisation and growth of salt to be the most effective weathering process as this process could cause the most damage. Thermal expansion of salt is only a significant factor within hot desert climates where temperature changes can be in excess of ±54°C daily. Nevertheless, this would result in a volumetric expansion of ~1% for halite (NaCl) salt (Cooke and Smalley, 1968).

Winkler and Wilhelm (1970) investigated "salt burst" by hydration pressures. These salt bursts cause flaking and efflorescence on the surface of sandstone. Hydration pressure is particularly important when sandstone monuments or artefacts move from low to high humidity environments, such as monuments or artefacts which have been open to the natural environment being moved to within a museum. They calculated that the hydration of bassanite ($CaSO_4.0{\cdot}5H_2O$) to gypsum ($CaSO_4{\cdot}2H_2O$) under the condition 65% RH and 30°C has the highest hydration pressure at 842 psi compared to those of $MgSO_4$ hydrates, which are particularly low whilst under the same conditions at 29 psi.

Winkler and Singer (1972) then calculated the pressure exerted by the growth of salt crystals. They combined temperature and saturation level for many salts to reveal crystallisation pressure under a variety of different conditions. Anhydrite ($CaSO_4$), halite (NaCl) and thenardite (Na_2SO_4) repeatedly produced the highest pressures in all circumstances (Table 1-2).

Table 1-2: Table of salt crystallisation pressures.

Salt	Chemical Formula	Cyststallisation Pressure (psi)					
		2		10		50	
		0°C	50°C	0°C	50°C	0°C	50°C
Anhydrite	$CaSO_4$	335	398	1120	1325	1900	2262
Bischofite	$MgCl_2 \cdot 6H_2O$	119	142	397	470	675	803
Dodekahydrate	$MgCl_4 \cdot 12H_2O$	67	80	222	264	378	450
Epsomite	$MgCl_4 \cdot 7H_2O$	105	125	350	415	595	708
Gypsum	$CaSO_4 \cdot 2H_2O$	282	334	938	1110	1595	1900
Halite	NaCl	554	654	1845	2190	3135	3737
Heptahydrite	$NaCO_3 \cdot 7H_2O$	100	119	334	365	568	677
Hexahydrite	$MgSO_4 \cdot 6H_2O$	118	141	395	469	671	300
Kierserite	$MgSO_4 \cdot H_2O$	272	324	910	1079	1543	1840
Mirabilite	$Na_2SO_4 \cdot 10H_2O$	72	83	234	277	397	473
Natron	$Na_2CO_3 \cdot 10H_2O$	78	92	259	308	440	524
Tachhydrite	$2MgCl_2 \cdot CaCl_2 \cdot 12H_2O$	50	59	166	198	282	336
Thenardite	Na_2SO_4	292	345	970	1150	1650	1965
Thermonatrite	$Na_2CO_3 \cdot H_2O$	280	333	935	1109	1590	1891

Calculated for supersaturation ratios of 2, 10 and 50, modified from Winkler and Singer (1972).

Williams and Robinson (1981) conducted laboratory experiments using Ardingly Sandstone from southeast England, to test how salts within sandstone may affect the frost cycle. Blocks were soaked in salt solutions of either sodium chloride, sodium sulphate or a control liquid of water and exposed to cycles of freeze-thaw. Disintegration on the surface was seen in both salt sample sets. However, the blocks soaked in the sodium sulphate showed much more damage whilst the control block suffered the least damage.

McGreevy and Smith (1982) conducted an overview of the methodology used in previous salt weathering experiments in hot deserts, and made many recommendations such as using realistic temperature and relative humidity values and to use salts native to the desert. McGreevy and Smith (1985) incorporated these improvements, where their quartz sandstones were sprayed with $MgSO_4$ and Na_2SO_4 solution and then heated in a climate cabinet, ranging from 22°C to 54°C, over a period of 24 hours and repeated this cycle over 60 times. The damaged surface was then brushed off and analysed. They conclude that the salts caused the detachment of quartz overgrowths because these overgrowths are only lightly “resting” on the quartz grains, therefore allowing salt solutions to exploit these regions. This theme was then revisited in Wright’s (2000) study where she also concluded that the removal of the “resting” quartz overgrowths by salt penetration has lead to weathering.

Smith and McGreevy (1988) then repeated a similar experiment to McGreevy and Smith (1985) but cycled blocks of Darney Sandstone between 22°C and 52°C whilst applying a 10% solution of sodium sulphate and magnesium sulphate to half the blocks daily for sixty days within a climate cabinet. The treated blocks had extensive surface disaggregation and subsurface cracking which were associated with microcrystalline salts, unseen in the control blocks. However, these studies failed to quantify the amount of damage that the salts caused.

To examine the growth and damage potential of sodium chloride (NaCl) and sodium sulphate (Na_2SO_4) salts, Rodriguez-Navarro and Doehne (1999) conducted experiments on their crystallisation at both the microscale and the macroscale. Microscale experiments involved observing the crystallisation of the salt solutions on a glass plate within a range of relative humidity values, and comparing the salts that crystallised within glass test tubes of a range of diameters. The macroscale experiment was to cycle the salt solutions through oolitic limestone. Microscale results show that NaCl salt has three crystallisation stages: 1) euhedral cubic crystals forms; 2) large hopper form crystals appearance at the edge of the droplet; 3) massive skeletal dendritic crystals. Variations in RH conditions did not affect this process. The Na_2SO_4 experiment by comparison has only two stages: 1) prismatic mirabilite crystals form and 2) acicular and dendritic groups of mirabilite form at the centre of the droplet at RH greater than 50%. Below 50%, only thenardite salt crystals grew as prismatic acicular or bulky crystals. The macroscale experiments show that halite precipitation is very slow (minutes) whilst mirabilite is almost instantaneous and that little damage took place to the stone from the growth of halite whilst the mirabilite and thenardite cause considerable damage to the limestone.

The papers discussed thus far are on salt weathering and have been laboratory-based reports and few have included field evidence. However, later studies show a shift on focus toward the incorporation of real world examples.

Mottershead et al. (2003) compared two historic structures in Merseyside: one coastal (Fort Perch Rock at the entrance of the Mersey Estuary) and one inland (Stafford Castle) as both were built from red sandstone of similar composition and age (ten years difference). They compared their recession rates and concluded that the weathering rate

is accelerated by a factor of 1.59 in the coastal building. This is due to marine salts in the area enhancing the weathering at the coastal site.

Přikryl et al. (2007) studied quartz sandstones of the Bohemian National Park in Switzerland. Their results showed that the types of salts present varied as a factor of both aspect and height. Soluble salts such as chlorides and nitrates dominate the south faces whereas the north faces are most likely to have less soluble phases such as gypsum. Their results suggest that aspect and height are of great importance to the production of salts.

Smith et al. (2002) used laboratory based simulation experiments alongside a case study building (St Matthew's Church, Belfast) to examine salt weathering. The church was constructed from Scrabo and Scottish Dumfries sandstones and a combination of ion chromatography, atomic absorption spectroscopy and XRD were used to identify the salts present. These showed that, whilst scaling and flaking was confined to a depth of 15 mm from the outermost surface of the stone, $CaSO_4$ (gypsum) and NaCl (halite) were evident to a maximum depth of 60 mm. For the complimentary laboratory experiments, fresh blocks of Scrabo, Dumfries and Dunhouse sandstones were cycled in a salt corrosion cabinet. Blocks were cycled from 15°C to 50°C twice within 23 hours and were sprayed with 10% $MgSO_4$ solution for three hours whilst cooling down. After 43 cycles, only the Scrabo sandstone showed any significant weight loss. The depth to which salt had penetrated was also studied. In Dunhouse and Dumfries samples, salts were restricted to the outer 20-30 mm compared to the Scrabo sandstone where salt was found in excess of 50 mm depth. From these results, Smith et al. (2002) produced a model of sandstone decay in a wet polluted maritime environment (Figure 1-1).

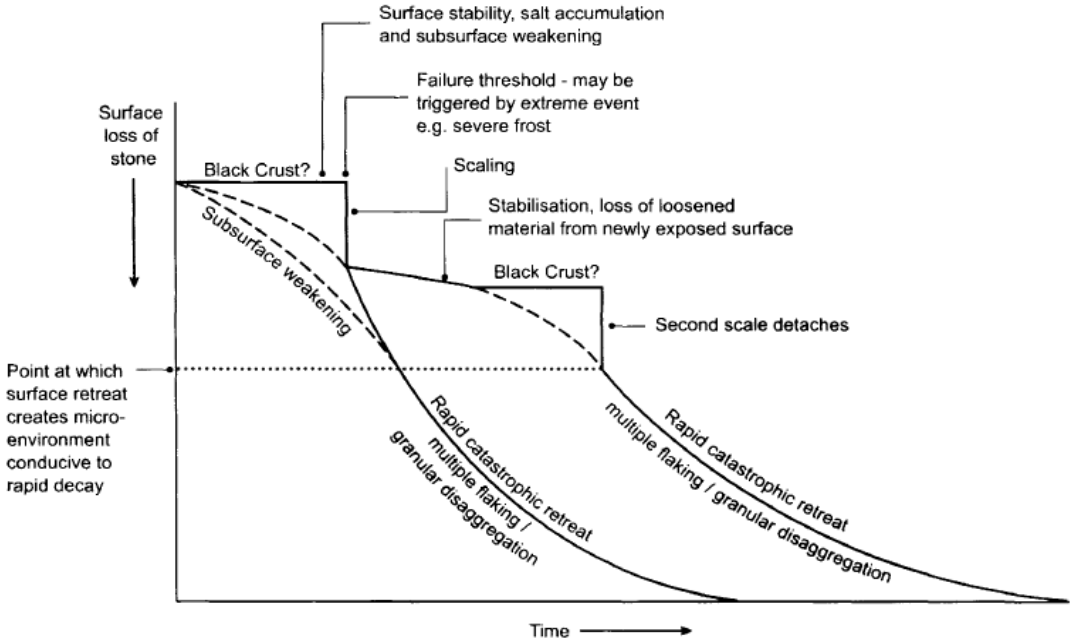

Figure 1-1: Schematic diagram illustrating possible decay pathways of sandstone. Decay pathways associated with the rapid retreat of building sandstone blocks through salt weathering and crust formation (Smith et al., 2002).

The impact of porosity and permeability on salt damage potential was investigated in laboratory experiments by Warke et al. (2006). Fine-grained Stanton Moor sandstone has a large range of permeability values (7.70-205.67 mD) and a porosity of 17% whilst the coarse-grained Stanton Moor has a limited range of permeability values (4.75-113.97 mD) and only 13.5% porosity. These were subjected to the same weathering cycles using a 2.5% solution of sodium sulphate. Their data show that the fine-grained blocks had a greater range of potential for salt and moisture ingress and retention, which would eventually lead to greater damage.

The presence of salts within sandstone may affect the properties of the stone. Franzen and Mirwald (2009) studied the effect of three different salt mixtures on the absorption of moisture. The data indicates that the presence of Mg-sulphates increases moisture uptake compared to Na salts.

1.2.3.1 Summary of Salt Weathering

As outlined, the presence of salt can be very harmful to sandstone. However, it is quite difficult to constrain how damaging it may be, to any one individual building, as the impact depends on many factors: salt composition and concentration, environmental

conditions, temperature, relative humidity and the properties of the particular sandstone in question. Therefore, each case has to be considered individually and all properties and environmental conditions have to be taken into account. Also, it can be seen that there are definite links between pollution and salts. The main pollutants discussed in section 1.2.1 are fly ash and soot, these are normally incorporated into the salt, even though some studies may consider these two constituents as part of the same weathering cycle, we have divided them into two sections, as it can be seen that salt can cause may different forms of weathering.

1.2.4 *Weathering due to Freeze-thaw*

The action of freeze-thaw has been considered a weathering process in sandstone for many years and numerous papers examining sandstone decay in cold climatic conditions argue that the mechanical weathering of freeze-thaw is the dominant breakdown process (Ballantyne and Harris, 1994; Matsuoka, 2001; Kamh, 2005b). Freeze-thaw operates when porous material becomes saturated by water and as temperatures fall, the water cools, and expands by 9% at 0°C (Price, 1995). This cycle might be repeated many hundreds of times and this expansion causes microfracturing, which may eventually lead to failure of the material and could be particularly destructive in cold and wet climates. However, most studies of this topic assume this process occurs without providing any significant evidence. Only a few papers have tried to provide direct evidence for the process of freeze-thaw within sandstone.

Wright (2000) subjected Dunhouse Sandstone to two different temperature regimes: -5°C to +15°C and -12°C to +15°C. The debris produced was then collected and viewed under a Scanning Electron Microscope (SEM) so that particle analyses could be conducted. Within this quartz debris, overgrowth fragments were found and it was suggested that freeze-thaw weathering might have caused their detachment. Thomachot and Jeannette (2004) also simulated freeze-thaw experiments using two sandstones: Vosgien (18% porosity) and Meules (23.5% porosity). Three samples were set up as partial saturation, total saturation and control blocks. These were then subjected to three series of 30 freeze-thaw cycles and then the porous network of the sandstone was studied to identify any changes, using mercury porosimetry and capillary inhibition and dilation. The results showed fracturing within the saturation set of samples, which increased the porosity of

the sandstones, therefore it is assumed that freeze-thaw caused this increase. They state that these results cannot be transposed to natural conditions due to absorption-drying which occurs simultaneously with freeze-thaw.

Hall (2004) investigated freeze-thaw in nature, using cement paving blocks in northern Canada which were embedded with temperature data loggers, recording on a minute interval scale. This fine temporal scale was used so that the exothermic reaction associated with the release of latent heat as the water freezes could be recorded. This small release of heat was observed in their data, which gives unequivocal evidence of freeze-thaw events taking place. However, Hall (2004) also concluded that there is no fixed temperature for the exothermic initiation and that, although the process of freeze-thaw is present within rock, there is no evidence to its effectiveness as a weathering agent.

1.2.4.1 Summary of Freeze-thaw

The research to date shows that freeze-thaw weathering in sandstone may be effective when accelerated and enhanced in laboratory experiments and it definitely occurs in nature. However, it has not been proven in sandstone buildings so its power as a weathering agent in temperate climatic conditions is still unknown, and may only be effective in climates where air temperature dips below freezing on a daily basis. In other circumstances, it may only help accelerate other active decay processes on the sandstone. In addition, many sandstone buildings are warmed from the inside (from central heating systems), again limiting the freeze-thaw that may have otherwise occurred. The water trapped within the pores of sandstone is also salty and these solutions have a much lower freezing point temperature compared to pure water.

1.2.5 *Weathering due to Chemical Decay*

Chemical decay in sandstone is a change to the original bulk chemical composition of the material whether it is an addition or removal of a mineral or some of its constituents. This process is therefore highly individual to each sandstone as sedimentary rocks have a wide ranging primary mineralogy and also highly varied diagenetic histories. Other features important to chemical decay, complimentary to mineralogy, are the porosity and

permeability of the sandstone. Therefore, it is critical to understand the primary characteristics of the sandstone so that it is possible to distinguish between the diagenetic features and weathering characteristics. This has been done for many sandstones such as Stanton Moor (Mckinley et al., 2006) and Saxony sandstones (Götze and Siedel, 2007).

Lasaga (1998) undertook laboratory experiments to deduce the dissolution rate of the main sandstone constituents under varying conditions. The results suggest that carbonate minerals dissolve at a very rapid rate in comparison to the silicates in all conditions (Table 1-3).

Table 1-3: Lifetime of a 1 mm sized grain at 25°C and pH 5.

Mineral	Lifetime	Dissolution rate (log moles $m^{-2}s^{-1}$)
Quartz	34,000,000 yrs	-13.4
Kaolinite	6,000,000 yrs	-13.3
Muscovite	2,600,000 yrs	-13.1
K-Feldspar	921,000 yrs	-12.5
Dolomite	36 days	-5.5

Data from Lasaga (1998).

Whole rock studies into chemical decay were not investigated until later. Since then a few studies have been undertaken to compare weathered sandstone to the unweathered sandstone to identify the specific chemical weathering changes that have occurred.

A common mineral to form within building sandstone weathering is gypsum and this is covered largely in section 1.2.3**.** However, gypsum can also form in the outer layer through the interaction of actinolite (Ca rich mineral) with atmospheric sulphur, as seen in Scrabo Sandstone (Mckinley et al., 2001; Smith et al., 2002). The sulphur reacts with the actinolite and forms gypsum leading to pore spaces being in-filled and blocked.

Friolo et al. (2003) studied Hawkesbury Sandstone composed of 60-68% quartz, 16-25% clays and 7% siderite determined by using a combination of Fourier transform infrared spectroscopy (FTIR), X-Ray diffraction (XRD), SEM, inductively coupled plasma-atomic emission spectroscopy (ICP-AES) and thermal analysis. They showed that when the

siderite ($FeCO_3$) chemically breaks down, a proportion of the released Fe^{3+} is substituted into the kaolinite matrix for Al^{3+}. This replacement of Fe^{3+} for Al^{3+} disrupts the structure of the kaolinite, which then becomes unstable and so weathers at an increased rate.

Sérgio De Melo and César Fonseca Giannini (2007) show that in the unweathered sections of the Furnas Formation in southern Brazil, which is composed predominantly of quartz arenites, the kaolinite present is well crystallised (booklets 50 µm) and cements the sandstone together. Upon the onset of weathering, the kaolinite is dissolved out and reprecitated within cracks or on exposed surfaces as microcrystalline kaolinite (booklets 10 µm). This chemical change in the sandstone leaves it weakened and increases formation of erosional features such as furnes, sinkholes and tunnels.

Franke (2009) simulated chemical weathering on 39 different rock-forming minerals to test their resilience. Mineral chips were immersed in an appropriate exchange resin slurry under conditions of 20˚C and pH 5.5. Weight measurements were taken at intervals dependent on the mineral chip over a period of four years. As expected the calcite weathered at a quicker rate (600 mg $m^{-2}d^{-1}$) compared to the silicate minerals (alkali feldspar 2.10 mg $m^{-2}d^{-1}$).

1.2.5.1 Summary of Chemical Decay

These papers suggest that chemical alteration to the original sandstone is much more likely to be seen in the diagenetic minerals (carbonates, clays and Fe-oxides) compared to the detrital minerals (quartz, Or-rich feldspars and micas). When such chemical reactions do occur, the precipitates are formed closer to the outermost surface. As noted at the beginning of the section, chemical alteration within any sandstone is likely to be highly individualistic due to variable primary composition and so makes chemical decay very difficult to generalise.

1.2.6 *Weathering due to Clays*

Many different types of clay minerals occur within sandstone including illite ($(K,H_3O)(Al,Mg,Fe)_2(Si,Al)_4O_{10}[(OH)_2,(H_2O)]$), kaolinite ($Al_2Si_2O_5(OH)_4$) and montmorillonite ($(Na,Ca)_{0.33}(Al,Mg)_2(Si_4O_{10})(OH)_2{\cdot}nH_2O$), which is a variety of smectite. Illite and kaolinite are

classified as non-expandable, whereas montmorillonite can cause destruction to sandstones by exerting pressure, through shrinking and swelling cyclic behaviour (Piffy 1979). Intracrystalline swelling and also osmotic swelling to a lesser degree, can affect the layered structure of these phyllosilicates. Intracrystalline swelling occurs when the cations binding the clay platelets together become hydrated upon contact with water and rearrange themselves as a layer between the clay layers, thus causing widening (Figure 1-2). This process will double the size of a Na-montmorillonite crystals whereas Ca-montmorillonite expands to a much lesser extent as it cannot absorb as much water (Madsen and Muller-Vonmoos, 1989).

The second swelling process is osmotic swelling, which involves the repulsion between electric double layers. Osmotic swelling is caused by the large differences in concentration between the ions electrically held close to the clay surface and the ions in the pore water of the rock. The irregularities in the crystal lattice are manifested by an excess negative charge, which must be compensated by positive ions close to the surface of the clay. The positive ion concentration decreases with increasing distance from the surface, whereas the concentration of negative ions increases. The negatively charged clay surface and the cloud of ions combine to form the electric double layers causing swelling (Figure 1-2) (Madsen and Muller-Vonmoos, 1989).

Both intracrystalline and osmotic swelling are fully reversible and therefore they can occur repeatedly over a long time period (Madsen and Muller-Vonmoos, 1989).

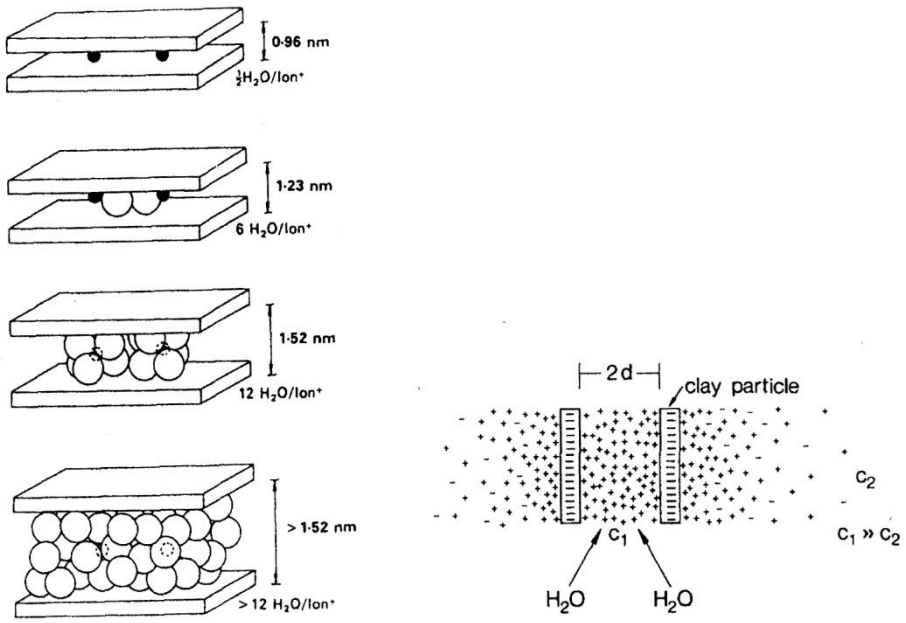

Figure 1-2: Schematic diagrams of intracrystalline and osmotic swelling.

Left) intracrystalline, right) osmotic swelling, taken from Madsen and Muller-Vonmoos (1989).

Two Spanish studies have examined the clays within sandstone from the Tafina region (Cadiz, Spain), which contains ~7 wt% clay. Sebastián et al. (2008) explains how the sandstone experiences weathering through the swelling of smectite and chlorite. Within a low porosity sandstone, this can have a significant impact through both intracrystalline swelling and osmotic reactions. The expansion of the clays within these sandstones leads to the development of several types of weathering phenomena: scaling, flaking and contour scaling. Jimenez-Gonzalez et al. (2008) used the same sandstones from the Tafina region in a second study and various tests were conducted to determine the behaviour of the clay and the mechanics of its swelling. To clarify whether or not the weathering seen is caused by the expansion of clays, one set of samples was soaked in diminoethane dihydrochloride, which adsorbs negative charge and therefore minimises osmotic swelling. Stones were then subjected to repeated wetting and drying cycles before their strength tests were recalculated and compared to their original values. Strength tests showed the treated stone to be stronger than the damaged, non-treated sandstone. The swelling strain test indicated that the clays present expand by 200 µm/m whilst wet, and that swelling inhibitors may prove useful in conservation of sandstone which contain high proportions of swelling clays.

Kaolinite is present in many sandstones as a cement and helps bind detrital grains together. Although it is a non-expandable clay, kaolinite clay lost from the sandstone will

cause structural weaknesses. A few studies have looked at the dissolution of kaolinite in the presence of biological material. Chin and Mills (1991) suspended kaolinite in low molecular weight organic ligands, soil humic acid and organic matter dissolved in stream water. The soil humic acid and stream water did not promote the dissolution of kaolinite although in the presence of the organic ligands, the rate of aluminium dissolution was generally much greater than silicon. Maurice et al. (2001) then showed bacteria could mobilise iron from the kaolinite for metabolism in aerobic environments when iron is a limited nutrient. This increased the weathering rate of the kaolinite and also enhanced the release of Al from the kaolinite.

1.2.6.1 Summary of Clay Weathering

The role of kaolinite has been the focus of this review section due to its abundance in Scottish sandstones and the literature above indicates, that although it is a non-expandable clay, it can still cause damage, sometimes severe. Kaolinite clay weathering occurs both through loss of the clay, which weakens the internal structure, and by the breakdown of the clay as elements are substituted into its structure.

1.2.7 *Weathering due to Thermal Heating*

One of the most significant factors affecting exposed sandstone is the ambient climate, which is directly responsible for weathering, but also drives many associated secondary processes. One of the most studied aspects within this area is the thermal properties of sandstone and research on these thermal properties connected to weathering is described herein. Kerr et al. (1984a) investigate the effects of both albedo and thermal conductivity as controls on weathering regimes. They placed chalk, granite and sandstone samples in Er Rachida, Morocco and measured temperatures at known depths within the stone and the external environment. This showed that the sandstone sample, which had the lowest albedo and thermal conductivity, attains the highest surface temperature whereas the opposite extreme, chalk, which has a high albedo and high thermal conductivity, reaches a much lower surface and sub-surface temperature. They concluded that these sandstone properties should be taken into consideration when assessing weathering controls.

Jenkins and Smith (1990) then used quartz sandstone blocks that were placed in locations throughout Tenerife to investigate how temperature affects weathering mechanisms on the sandstone surface. They embedded sensors at various depths within the stone and on the surface. Results showed that the surface of the sandstone is subject to large fluctuations in temperature and that the temperature change can be very rapid leading to increased thermal stress. They also highlighted the fact that there may be seasonal changes reflected in the weathering patterns.

Warke et al. (1996) then tested the observations by Kerr et al. (1984a) and Jenkins and Smith (1990) within a controlled laboratory experiment. They tested Portland Limestone, Dunhouse Sandstone, Baumberger Sandstone and Pentellic Marble, which all have high albedo values in accordance to the Munsell colour notation. Using a climate chamber, the stones were subjected to periods of heating and cooling to observe how the stone surface temperature corresponds to air temperature. The results indicate that Dunhouse Sandstone and Pentellic Marble conducted the surface heat to deeper layers (and therefore experience uniform heating) compared to the Baumberger sandstone and Portland Limestone. An explanation for this is that the latter two rock types have poor thermal conductivity. Warke et al. (1996) highlight how topography on the surface of the sandstone as seen on the Portland Limestone and Baumberger Sandstone may make them more prone to thermal stress weathering. However, they concluded that these low magnitude events of thermal stress are unlikely to cause catastrophic failure, but still must be considered as a weathering mechanism. Furthermore, they also suggest that the removal of black crust will reduce thermal stress inflicted on the stone as the low albedo surface will be removed leaving a high-albedo surface exposed.

Warke and Smith (1998) continued their work using Portland Limestone, Dunhouse Sandstone and Antrim Basalt. These were tested under direct (natural systems) and indirect (laboratory experiments) light sources, and the subsurface temperature response was quite different. Under natural systems, the varying rock types respond differently due to their thermal properties i.e. albedo and thermal conductivity, whilst indirect light sources cause all lithologies to behave in a similar manner. These results highlighted the need to use realistic temperature regimes gained from both direct and indirect light sources when working with climate chambers.

McGreevy et al. (2000) undertook a similar study investigating the differences of indirect and direct heating of Antrim Chalk, Mounre Granite and Scrabo Sandstone. Temperature measurements were again taken from the subsurface and show that these rock types also respond differently under the conditions. Again, one of the main conclusions is that thermal heating and albedo are important influences on the surface and internal temperatures. McGreevy et al. (2000) also suggest that previously conducted oven/indirect heating based studies may have produced exaggerated results as they had not considered the albedo effect.

The process of thermal cycling has also been linked to the development of tafoni in the Antarctic, where processes such as biological and salt accumulations have been ruled out. The high temperature range experienced on a daily cycle, which has caused thermal stress, has been thought to be a leading factor (Hall and Andre, 2006). Hall et al. (2005) suggests that albedo may not play as much of a significant role as portrayed previously in this section. Hall et al. (2005) painted paving bricks in intervals of 20% reflectivity from black to white and attached temperatures sensors to the surface and base of each block. It was indeed seen that the black blocks became warmest. However, in situations where the surface temperatures exceeded those of the air, the black bricks were at the same temperatures or lower than those of the white bricks. They argue that the effect of albedo is overpowered by the convection of internal heat being expelled to cooler surroundings. However, the white blocks being the warmest only occurs when the sandstone's surface temperature is greater than the air temperature and this circumstance rarely occurs in the natural environment.

1.2.7.1 Summary of Thermal Weathering

The research summarised here shows that two main themes are apparent in the role of weathering: 1) the albedo of the sandstone and 2) the thermal conductivity. However, in these papers, a relatively wide-ranging selection of rock types was analysed. Due to the high albedo and thermal conductivity of many sandstones, its thermal heating does not influence weathering as much in comparison to many of the other rock types tested, such as those with a high percentage of dark coloured minerals. As Scottish sandstones are primarily composed of light coloured minerals (discussed later)

1.2.8 **Weathering due to Biological Activity**

Organic material causes weathering by many processes: e.g. production of chelating agent and acids; physically burrowing into and displacing minerals; leaching and depleting minerals of elements to name a few. These processes are dependent on the type of organism present, whether it is bacteria, cyanobacteria, algae, fungi, lichen or most likely a combination. Their weathering potential has been tested and observed in both the natural environment and in laboratory experiments and both will be discussed in detail within this section. Due to the large amount of information on biodeterioration, a few overview articles have also been written on the subject (Warscheid and Braams, 2000; Burford et al., 2003; De La Torre et al., 2003; Fernandes, 2006).

The relationship between microbes and stone has been discussed since the late 19th century, but the terminology for microbes and their habitation was not clarified until the work of Golubic et al. (1981), who describe those living on the surface as epiliths and those living within pore spaces as cryptoendolithic. After this work, there was an increased interest in their role in weathering. Friedmann (1982) describes how cryptoendolithic organisms weather sandstone in Antarctic conditions. Within rocks which are formed predominantly from translucent minerals, the microbes form a series of layers: surface crust, black zone, white zone and green zone. The black zone is a dense mat of fungal hyphae, but fungal hyphae also form the white zone (but in a looser web network) and the green zone is caused by flourishing algae. The white zone is weak due to leaching of iron compounds, which are transported to the outer crust by the microbes, and as a result, the black zone is enriched in iron. All layers are not always seen but a characteristic weathering pattern emerges, with a step-like weathering cycle occurring as the black and some of the weak white microbial weakened zone peels away, before the pattern repeats itself on the newly exposed surface (Figure 1-3).

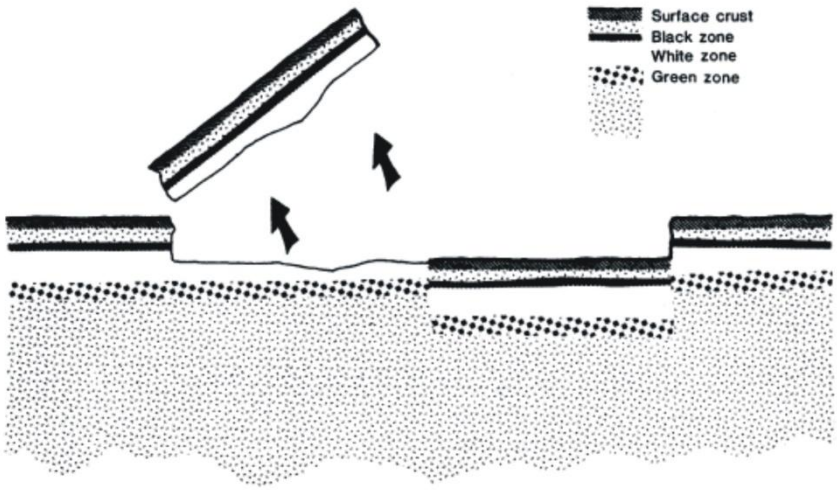

Figure 1-3: Diagram detailing the various layers formed by microbial communities and the step like weathering process.

Diagram taken from Friedmann (1982).

Antarctic microbes were then reinvestigated by Vestal (1988) who showed that the biomass of the cyptoendolithic microbiota was dominated by lichens *Buellia* and *Lechidea*, and had a spatial variation of about 14% over the surface of the samples. Spatial variation was calculated using the amount of lipid phosphate present on the surface of the stone at specific points. Work on cryptoendolithic microbes in extreme cold environments has continued until recently (Wierzchos et al., 2003; Omelon et al., 2006b, and, 2007) in an effort to further the understanding of microbial communities in these extremes. However, it was in the 1990's that the study of the role of microbes in the weathering of sandstone buildings became popularised.

Ortega-Calvo et al. (1991) sampled the most common type of microbe living on a variety of building materials (terracotta, sandstone, limestone, marble and granite) from locations in Spain and Sweden and found cyanobacterium *Microcoleus vaginatus* and the chlorophyte *Klebsormidium flaccidium* to be the most common. Sandstone samples were then inoculated with these two species identified in the case study and, under examination show the cyanobacteria to be firmly bound to the surface by mucilage cementing stone grains. This appears to lead to spontaneous detachment of the microbial films causing disintegration of grains and mechanical deterioration.

Gómez-Alarón et al. (1994) studied the fungi on the church of Carrascosa del Campo in Spain (constructed from sandstone) and isolated seven different genera of fungi, with *Penicillium* being the most numerous. It was found that *Penicillium*, and other fungi such

as *Fusarium,* have the ability to excrete oxalic, fumaric and succinic acids, which are all corrosive to the minerals beneath. Gómez-Alarón et al. (1995) studied the same sandstone but shifted their focus from fungi to cyanobacteria and algae. The cyanobacteria and algae had been observed producing biofilms on the stone surface. The authors state that these biofilms have the potential to retain water and trap soil, dust particles, spores and seeds; this then helping to expose the sandstone surface to more harmful invasion from higher order mosses and plants. Although the presence of a biofilm is not directly harmful, these secondary effects can prove detrimental. Gómez-Alarón et al. (1995) conclude that microbial weathering is complex on natural stone and it cannot be limited to one species, so many should be considered together.

Viles (1995) did not specifically examine biological weathering of buildings but did compile a comprehensive review outlining how the ecology on the rock surface might shape the topography beneath it, publishing a model of how the environment dictates the efficiency of weathering experienced (Figure 1-4). The model suggested that, in wet regions there is more microbial growth on the surface causing more damage, whilst drier environments may cause all growth to occur subsurface. This may suggest that, in a wet climate such as Scotland microbes may be causing more decay on the surface.

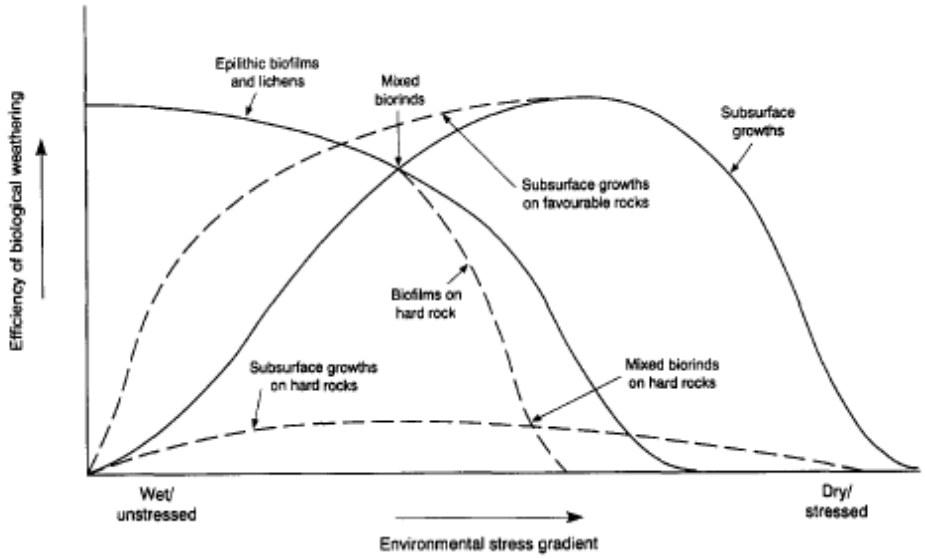

Figure 1-4: Model of the changing effectiveness of biological weathering.

Biological weathering on various rocks types, across differing environmental stress gradients, taken from Viles (1995).

Spanish monuments were once again used by Flores et al. (1997) to classify the algae and bacteria on limestone and granite buildings, and how their presence may influence

weathering. Bacteria belonging to the genera *Bacillus*, *Micrococcus* and *Thiobacillus* were found in addition to *Apatococcus* algae. Flores et al. (1997) suggest that algae may cause mechanical weathering through volumetric change (when wetting and drying cycles occur), but its main role in weathering may be to support the growth of other species. Several species of hetrotrophic bacteria were seen to create biofilms, and it is also thought that *Thiobacillus,* an autotrophic bacterium, can cause damage to the limestone by the transformation of calcium carbonate to calcium sulphate. Although the research was not directly conducted on sandstone, the porous nature may be affected heavily by this process of shrinking and swelling seen within the algae of this study.

Wakefield (1996) considered microbial growth on sandstone in Scotland, studying Hermitage Castle in the Scottish Borders, which is constructed of fine-grained red sandstone as well as a medium-grained quartz rich sandstone but unfortunately the sandstones were both of unknown origin. This study examined algae on the stone, specifically *Trentepohlia*, and showed how this one cyanobacteria can, very efficiently, mechanically decay sandstone through blistering and spalling its surface. This blistering and spalling occurs due to the volume change of the cyanobacteria in sandstone during successive wetting and drying cycles. The Hermitage Castle study also suggests that the volume expansion of a cyanobacteria crust can be as much as 300%, causing massive pressures on the sandstone and therefore potentially exploiting minute fissures.

These studies on sedimentary rocks show that a wide variety of microbes live both within and on the surface of stone and the various authors have made tentative explanations into how they cause weathering. In the early 2000's a few studies concentrated on investigating the impact of microbes on individual minerals rather than whole rock studies before returning to whole rock studies later in the decade.

Welton et al. (2003) conducted laboratory experiments using communities of algae (*Chlorella, Vulgaris, Chlorococcum, Tetrasporum, Scenedesmus obliquus, Oocystis marssonii* and *Stichococcus*) to assess how a blend of algal microbes affect the dominant rock forming minerals: albite, calcite, dolomite, labradorite, orthoclase, quartz and siderite. Mineral chips were immersed in water or an algal mix. The pH was tested weekly and water chemical composition tested fortnightly. After a 90 day period, biologically mediated etching of minerals was seen (Figure 1-5). This showed algae to

have the capability to etch and weather minerals independent of any other microbes, and in particular, the algal populations preferentially affected the carbonate and feldspar mineral chips.

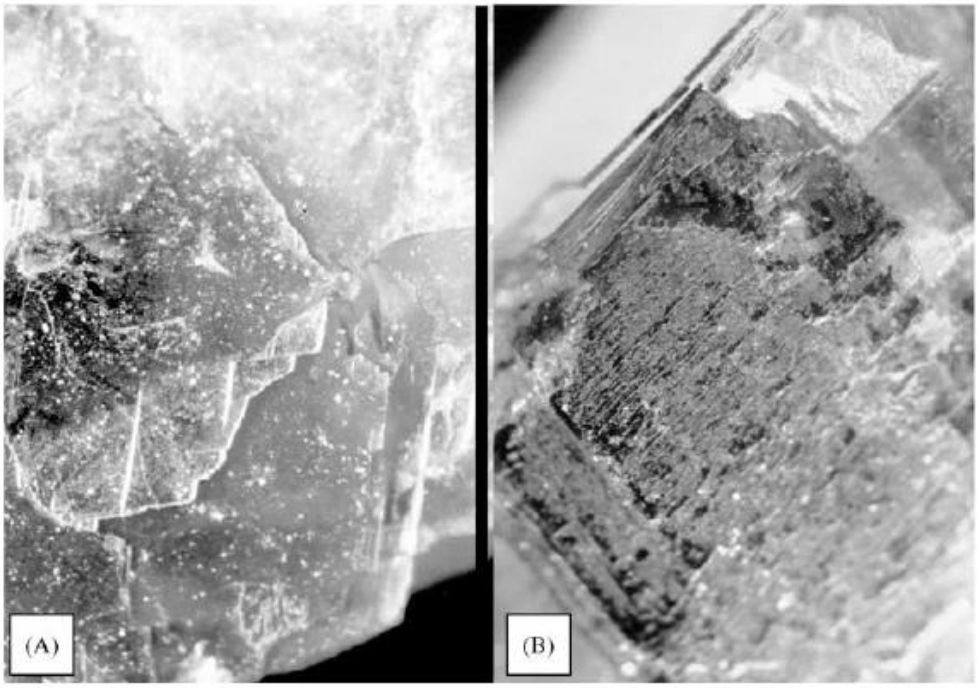

Figure 1-5: Algal weathering on siderite.

A) Siderite surface prior to algal colonisation, B) Siderite surface after 60 days algal colonisation. Both views are 1.5 cm across (Welton et al., 2003).

It was suggested by Bennett et al. (2001) that, in environments where nutrients are scarce, bacteria may weather minerals to gain their nutritional requirements. To test this idea, mineral chips were suspended in polyethylene chambers and buried into aquifers, where the ground water was abundant in carbon and lacking in phosphate. When retrieved, the samples were examined for microbial abundance, their colonization pattern and any changes to the host mineral surface. Results showed that, in these environments, silicate minerals such as Ca-feldspars can become weathered very quickly by the bacteria releasing nutrients from the mineral.

Poikilotrophic fungi were identified settling on a surface of sandstone and forming biofilms by Dornieden et al. (2000) who considered the impact and potential damage of these fungi. They show that, during the initial growth and establishment stage, they cause substantial damage to the substrate by excreting many types of acids. However, once established, the impact is significantly reduced as the fungi lived with a much lower metabolic rate.

Souza-Egipsy et al. (2004) studied the microbial growth on sandstone in the semi-arid Torrollones de Gabarda area of Spain. Using SEM techniques, they compared the weathering effects on the vertical and horizontal surfaces, which yielded significant differences: The vertical surfaces were dominated by grain disintegration, etching and biomineralization by calcium oxalate and entrapment of minerals within extracellular polysaccharides. However, on the horizontal surfaces, holes formed as well as the development of a crust, which favours intense flaking. They also explored the protective aspect of biogeneic soils on these surfaces. Souza-Egipsy et al. (2004) suggest that green algal lichens may have a layer of calcium oxalate, which shields the rock beneath from environmental conditions, and this web of microbes may also protect an unstable surface beneath.

To discover which stone types may be most prone to weathering, Miller et al. (2006) studied the bioreceptivity of Anҫã and Lioz Limestone, Portalegre Granite and Vila Viçosa Marble all from Portugal. After four months of inoculation with microalgae *Stichococcus bacillaris* and cyanobacteria *Gloeocapsa alpine*, results showed that the limestone had the highest biorecepivity whilst granite exhibits the lowest. This could have been expected due to the low porosity of the granite, although this study neglected sandstone, which may have a high bioreceptivity due to its range of porosity.

Suihko et al, (2007) used DNA classification techniques to identify the bacterial and fungal microbiota on six Scottish monuments. These included actinobacteria belonging to the genus *Sterptomyces*, *Arthrobacter* and *Pseudomonas* and fungal species of *Cladosporium*, *Penicillium* and *Philophora*. However, they did not discuss their role in weathering, only documenting the species present.

Now that a good understanding of which microorganisms are likely to be residing on sandstone had been established, Jain et al. (2009) studied the optimal environmental conditions for the growth of fungi. One of the main factors affecting growth is the influence of relative humidity (RH). Whilst keeping temperature constant at 25°C, a mixture of fungi were grown within a range of RH. The study showed that maximum diversity of fungi was found at 96% and 85% RH, while levels lower than 62% RH produced no fungal growth on the sandstone. Jain et al. (2009) state that, in general, one species would gain dominance on the sandstone over time. The fungi are shown to have

a dynamic weathering effect on sandstone as they precipitated minerals such as dolomite whilst also dissolving out cements such as calcium carbonate. Fungi have also been found to excrete higher concentrations of effective chelating agents thus enhancing dissolution of stable aluminosilicates.

1.2.8.1 Review of Biological Activity

A large volume of research has been focused on the relationship between microbial communities and the weathering of sandstone constructions. Most work has been centred on algae, cyanobacteria and fungi as these have been deemed the most detrimental to the sandstone while they are also the most commonly identified living on the buildings. These studies provide information on the products of the organisms and how these damage the stone, but there is often a lack of information on the time scale over which they take place and also to what depth within the stone they cause damage on a building exposed to the environment. In many studies, it seems difficult to specifically state that any weathering observed was exclusively due to microbial decay.

1.3 Research on Sandstone Decay in Scotland

As is evident from the literature review, there is a wealth of information on the weathering of sandstones throughout the world, particularly the Mediterranean countries, as it has been used for construction purposes for centuries. However, these studies are not so relevant to Scotland when understanding the Scottish decay process, for many reasons: 1) the wide range of sandstone mineral compositions, textures and diagenetic histories of the sandstones studied; 2) the local climate in which the weathering has occurred is unlike that of Scotland; 3) differences in weathering time scale. As seen, research on northern British sandstone is limited and focuses mainly on the mechanical breakdown of sandstone as a consequence of salt infiltration and microbes (Wakefield, 1995 and Suihko et al., 2007). Thus far, there is limited detailed understanding of how Scottish sandstones erode and decay. The work that has been undertaken to date is reviewed next.

1.3.1 *Decay of Sandstone within Scotland*

The decay process of Glasgow sandstones was first analysed in detail by Bluck and Porter (1991b), who produced a model of breakdown within the blond and red categories of sandstone (Figure 1-6 andFigure 1-7). They were the first to observe that the blond variety of sandstone is much more susceptible to decay. There model for blond sandstone weathering begins with aqueous fluid entering the rock and then a period of chemical redistribution, when fluids dissolve unstable minerals from the interior of the sandstones and reprecipitate them on or close to the outer surface. This reprecipitation builds up a tough patina, which can become impermeable. Once this chemical stage has been completed a mechanical set of breakdown processes start to take effect. The impermeable layer causes a build up of water within the rock, thus increasing the time that water is in contact with clay minerals, allowing them to expand to a greater degree than achieved by otherwise periodic wetting. The trapped water also increases the risk of freeze-thaw taking place, potentially further increasing mechanical damage (Figure 1-6). Bluck and Porter's (1991b) model is the same for red sandstones but, as their mineralogy is less complex in comparison to blond sandstones, it takes a longer time for a thick patina to develop and therefore there is less decay within the same time scale (Figure 1-7). However, these models were constructed from observations only and were not backed up with experimental data.

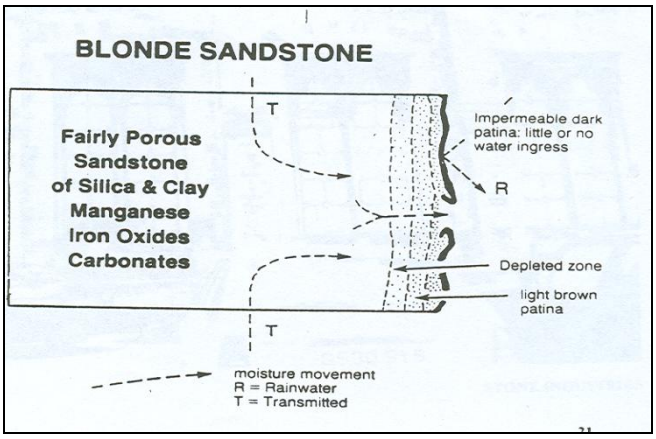

Figure 1-6: Bluck and Porter (1991A) model of fluid flow through a blond sandstone. Showing all the decay steps taken from Bluck and Porter (1991b).

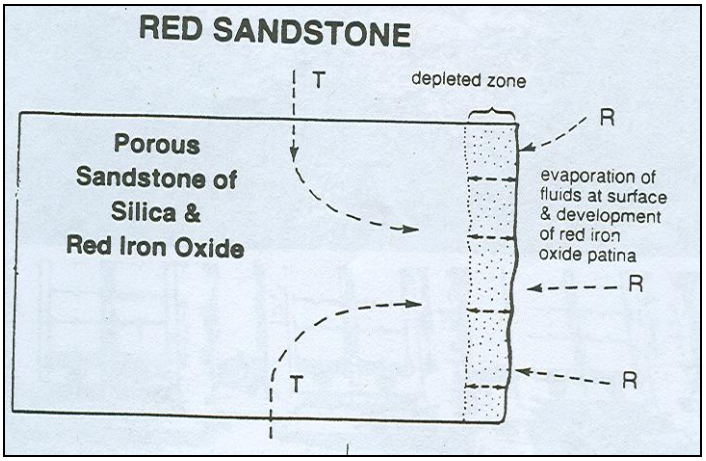

Figure 1-7: Bluck and Porter (1991A) model of fluid flow through a red sandstone. Showing decay steps, taken from Bluck and Porter (1991b).

Bluck and Porter (1991a) also conducted work on how building stones decay after cleaning. This study concluded that a building chemically cleaned in the past will suffer from algal growth in the future, although abrasively cleaned buildings will not. This is thought to be linked to the change in the water flow after the differing cleaning processes.

The work by Bluck and Porter (1991a and b) highlights two important factors to consider in the degradation of sandstone. First is that the original composition of the stone is very important; complex mineralogy equates to complex weathering. Secondly, they show that weathering is not a static process, but will instead vary with time and also with the fluctuation of rainwater and evaporation.

Kamh (2005b) undertook an investigation on sandstone decay using Jedburgh Abbey in the Scottish Borders as a case study. The abbey is approximately 890 years old. He compared weathered samples from the interior and exterior of the building, to fresh samples of similar stone type from a natural exposure. He concluded that one of the most important decay processes was the chemical weathering of feldspar and dolomite and their breakdown. He also hypothesised that “spalling” of quartz overgrowths may be an important factor during the freeze-thaw process.

1.3.1.1 Microbial Decay on Sandstones within Scotland

The effects of microbial communities have long been considered a significant factor in the decay of sandstone. Many microbial decay studies have been carried out in

Mediterranean countries (Ortega-Calvo et al., 1991; Gómez-Alarcón et al., 1995), but few have been undertaken in Scotland. In Scotland, the comparatively cooler and wetter climate will dictate which microbes may be present and their roles in the resulting decay.

As previously outlined in section 1.2.8 Wakefield et al. (1996) conducted an investigation into the effect of filamentous green algae *Trentepohlia* on Scottish sandstone at Hermitage Castle. The weathering observed in this sandstone was mainly mechanical decay in the form of spalling and grain disaggregation caused by the algae.

Young (1997) showed that in general the diversity of biological growths was greater in rural rather than urban areas. Young (1997) focused on algae, and identified mainly unicellular or colonial forms on the sandstone, whilst filamentous forms were found in areas that are persistently damp. The most common species of microorganisms were the genii *Chlorococcum* and *Pleurococcus*. Young (1997) also suggested that the architectural complexity of the buildings plays a large factor in the distribution, stating there was little algal colonisation on plain unornamented facades.

Suihko et al. (2007) also undertook a study of microbes present on Scottish stone using rRNA as previously outlined in section 1.2.8 and identified pigmented bacterial species such as *Arthrobacter* and *Bervundimouas*, and fungi *cladosporium* and *penicillum*. However, they did not evaluate how their presence on the sandstone may affect the weathering process of its surface.

As shown, very limited work has been conducted on Glasgow sandstones in particular apart from a few overviews of chemical and microbial work.

As stated previously it is fundamental to understand the primary product which is being weathered. Therefore, the next section will detail the diagenetic history of the Glasgow sandstones and provide a brief introduction to the predominant mineralogy of the sandstones found in the Glasgow region.

1.4 Geology of the Glasgow Region

Sandstone is a naturally durable material and is abundant in the west of Scotland and for these reasons, was used extensively to construct local monuments and buildings.

Sandstone is still used in modern construction, both new and when replacing damaged blocks in older buildings. The buildings surveyed in this study are all approximately 150 years old and built within the Glasgow district using blond sandstone, which were acquired from numerous small local quarries within the Glasgow district (Figure 1-8). Therefore, it is important to understand the diagenetic history and mineralogy of the sandstones used so that it is possible to distinguish between products of diagenesis and of weathering post-construction.

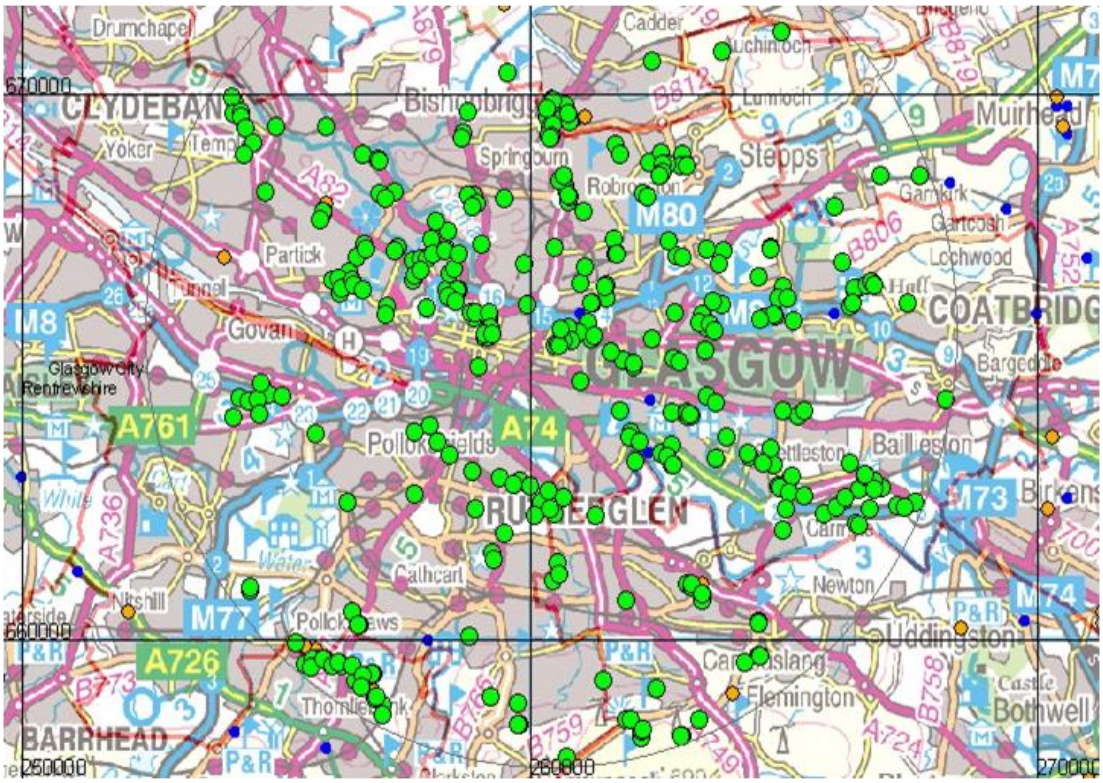

Figure 1-8: Image of historic quarries within the Glasgow region.
Each green dot highlights an individual quarry, all map rights reserved to ©NERC.

The Glasgow region and therefore the main source of building material, is dominated by two sandstone groups: the Clackmannan Group (CKN) and the Scottish Coal Measures Group (SCMG) (Figure 1-9), which are both Carboniferous in age (Figure 1-10).

The description by Browne et al. (1999) provides the main reference used in the geological descriptions below.

The Clackmannan Group (CKN) is the main geological unit covering the north, west and south of the Glasgow region. The CKN includes the Lower Limestone Formation, Limestone Coal Formation, Upper Limestone Formation and the Passage Formation

(Browne et al., 1999). The group is predominantly Namurian in age (335 Ma to 315 Ma) and was deposited in a fluviodeltaic environment (Woodcock and Strachan, 2000). Sandstone occurs in all of the Formations in small quantities but is most common in the Passage Formation. The Passage Formation sandstone alternates between fine and medium-grained lithologies and the dominant clay within them is illite (Wilson et al., 1972). These sandstones are generally off-white to grey in colour.

The Scottish Coal Measures Group (SCMG) dominates the east of Glasgow and contains the Lower, Middle and the Upper Coal Measures, which are Westphalian in age (315-306 Ma). The SCMG was deposited within a large array of environments ranging from alluvial to lacustrine, however the thickest sandstone units were deposited in river and delta distributary channels (Browne et al., 1999). The sandstone units may be both upward fining and upward coarsening, with colours ranging from grey to off-white and vary from fine to medium grained. The main clay found within these is kaolinite (Wilson et al., 1972). Sedimentation of these sandstones was dominated by episodic progradation and abandonment of delta lobes which had sediment supplied from both the north east and west (Browne et al., 1999). The SCMG sandstones are generally seen to be moderately sorted and quite mature with quartz, feldspar and mica as the main constituents.

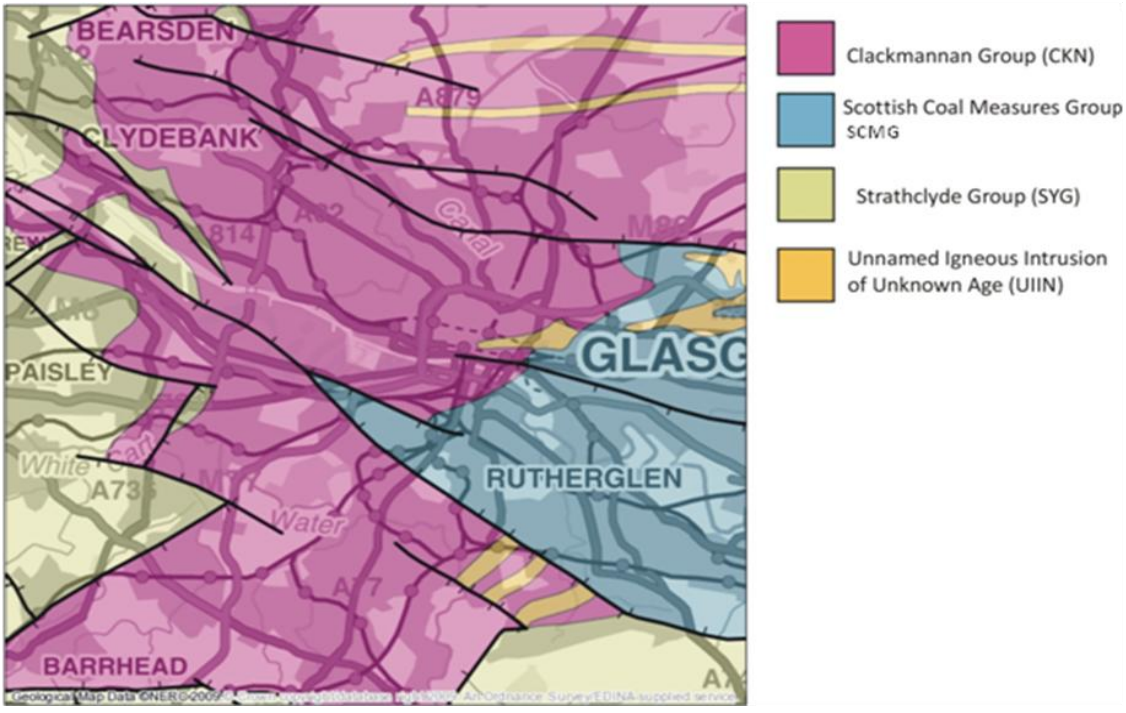

Figure 1-9: Map of the geology underlying the Glasgow region. Modified from Browne et al. (1999).

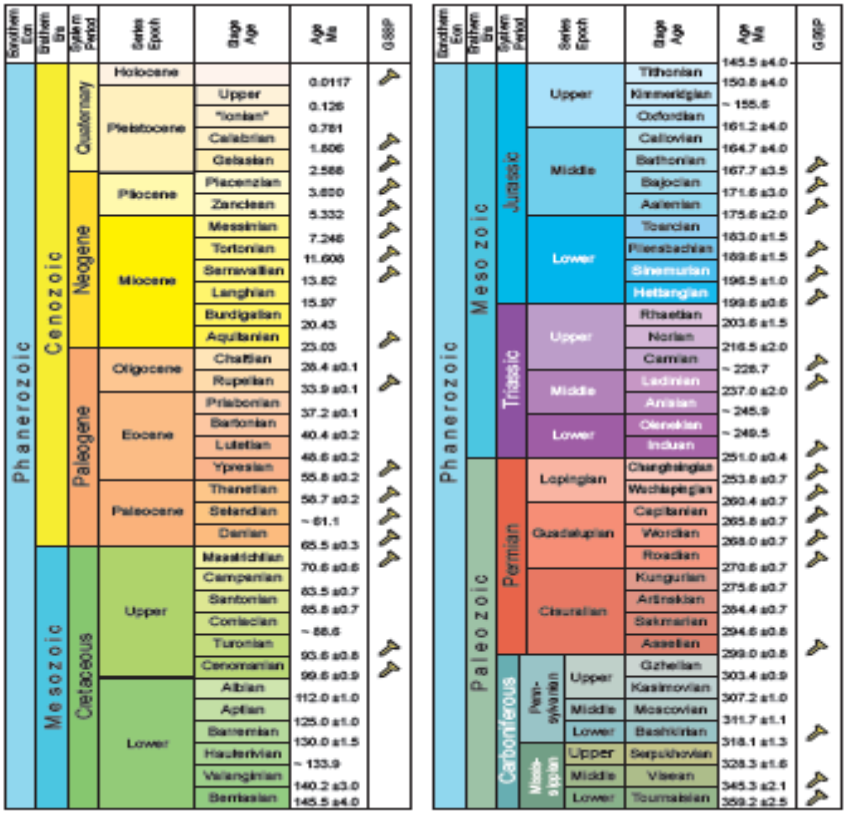

Figure 1-10: Stratigraphic column.
Column taken from the international commission on stratigraphy (2010).

1.4.1 *Mineralogy of Glasgow Sandstones*

Bluck and Porter (1991b) first described the mineralogy of sandstones that were used to construct the infrastructure of Glasgow. These were general observations, comparing blond and red sandstone. In 2004, Scottish Enterprise Glasgow (SEG) commissioned the British Geological Survey (BGS) and the Scottish Stone Liaison Group (SSLG) to undertake a two-part study of Glasgow's stone built heritage. This was prompted by concerns about the health of Glasgow's buildings, due to factors such as: 1) their age; 2) air pollution (legacy of industrial and domestic coal burning); 3) inappropriate repairs, such as plastic surface repairs, mechanical and chemical cleaning; 4) the use of incompatible replacement stone. Hyslop et al (2006) also noted that climate change was an additional problem, and conducted a visual survey complimented by examination of sandstone samples using optical microscopy. Through this work, they proposed the main decay processes on uncleaned sandstone to be crust formation, granular disintegration (particularly on lower facades enhanced by de-icing salts), biogenic soiling and the saturation of pore space within the sandstone by water. Bluck and Porter (1991b) and Hyslop et al. (2006) both also noted that scaling on blond sandstone is a much greater

problem compared to the red sandstones due to mineralogy, as the blond sandstones contain variable proportions of carbonates, iron oxides and clay minerals, which can enhance disintegration. In addition to effects of the detrital and authigenic minerals, the blond sandstone buildings are also generally older than those made from red sandstone, as red sandstone was imported later with the advent of railways. Although many blocks are face bedded (identified by the alignment of micas) this does not seem to be a primary reason for stone decay, but it may exacerbate the scaling issues (Hyslop et al., 2006). There are 24,349 stone buildings in Glasgow, of which 60% are constructed from blond sandstone, and will require 293,787 tonnes of stone for repairs (each facade requiring on average 20.11 tonnes of stone). This is twice as much repair required than for the red sandstone facades (Hyslop et al., 2006).

Hyslop et al. (2006) classified Glasgow blond sandstone based on their basic mineralogy of quartz, potassium feldspar and mica, as well as using their porosity values. They collected samples from 112 buildings within Glasgow and the sandstone were characterised into six sub groups these were named B1, B2, B2a, B3, B4, and B5. Each is described below, in accordance with the observations of Hyslop et al. (2006) and Hyslop and Albornoz-Parra (2009). Also noted are the currently available stone types that may be used for replacement.

1.4.1.1 Blond Sandstone Descriptions

B1: This is a uniform medium-fine grained quartz arenite, containing quartz and minimal clays and carbonates. The fresh surfaces appear pale to white in colour (Figure 1-11A). As the B1 sandstone (Craigleith) is no longer available, Clashach and Cullalo sandstones are now used for replacement. Prestigious buildings were often built using Craigleith and, therefore, a good replacement sandstone is essential.

B2: A medium-grained quartz arenite, with a small proportion of feldspar. B2 contains iron oxide, carbonates and clay minerals in varying quantities, but in total comprise ~20%. Fresh surfaces are pale in colour (Figure 1-11B) but, during weathering, the carbonate is altered and stained by the iron oxides producing an orange-brown appearance. Original sources are no longer available, so Scotch Buff and Blaxter sandstones are commonly

used for repair and replacement, but these normally have a more intense colouration as they contain a larger proportions of iron oxides.

B2a: These are medium-coarse grained sandstones but show greater variability in grain size. Quartz accounts for the largest proportion of the sandstone's mineralogy but significant amounts of iron oxides are present (3-7%) and give a speckled appearance (Figure 1-11C). During weathering, the iron oxides progressively change the stone to an orange colour. Replacement sandstones with similar characteristics are Blaxter, Dunhouse Buff and Stainton.

B3: This is a poorly sorted immature sandstone containing a higher proportion of clays and iron oxides compared to other Glasgow blond sandstones. Due to a relatively low porosity, it is quite dense (Figure 1-11D). As the main diagnostic characteristic is variable grain size, there are several main alternatives available for replacement when decayed such as Blaxter, Blaxter High Nick, Black Pasture, Stainton, Witton Fell and Stanton Moor.

B4: This is a fine-grained sandstone with an open pore structure. Internal layers are composed of dark iron oxides (12%), carbonaceous material and mica giving the sandstone a "wispy" look (Figure 1-11E). Due to the striking appearance of this sandstone, a similar stone is difficult to identify but Scotch Buff, Darney and Spynie have the same open pore structure whilst being fine grained, but do not exhibit the "wispy" appearance.

B5: This is a poorly sorted coarse grained stone with variable bedding (however the thickness of the bedding is not stated in Hyslop et al., 2006) and appears "gritty" (Figure 1-11F). Other such coarse-grained sandstones are Bearl, Catcastle, Course Buff and Peak Moor.

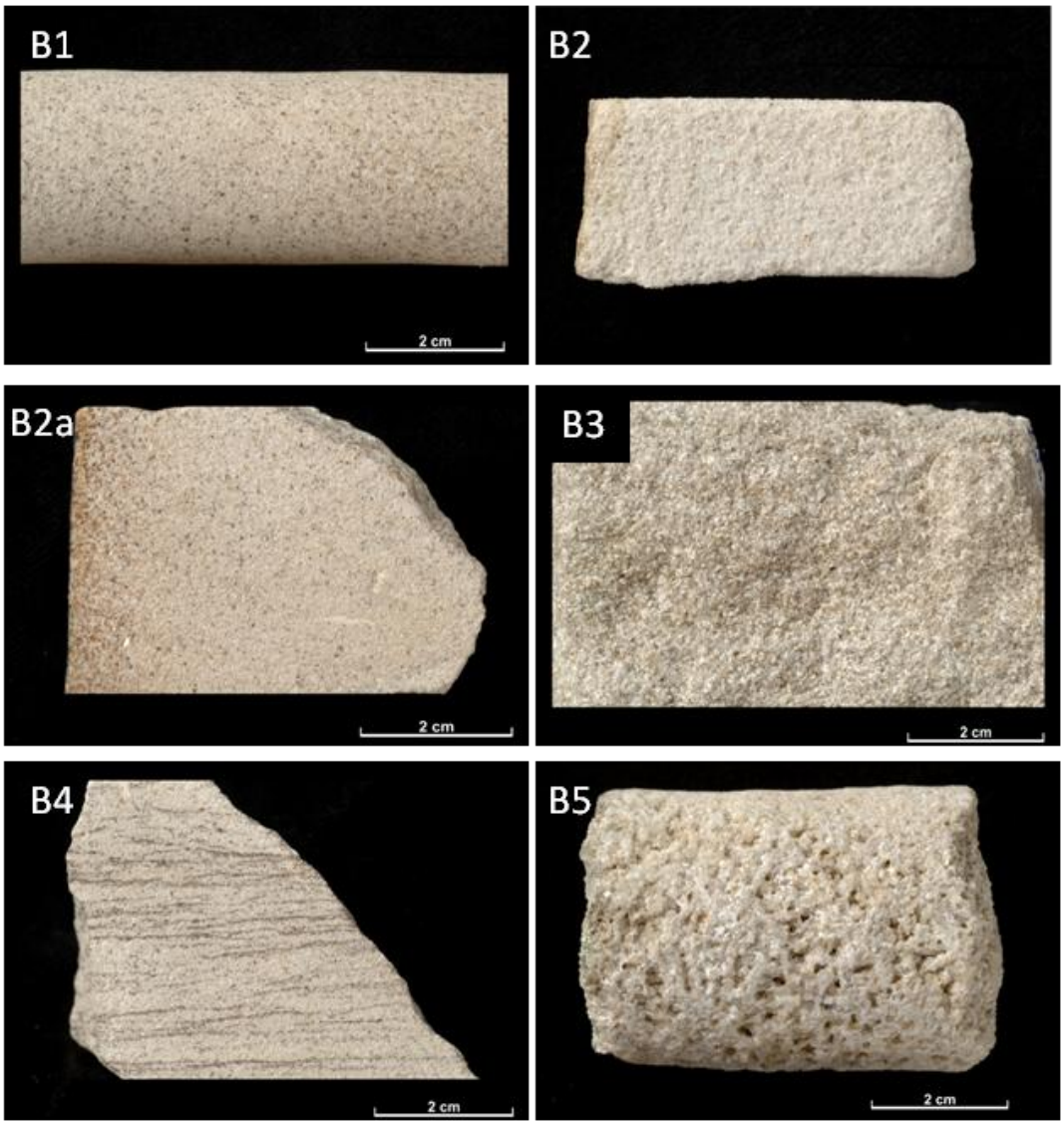

Figure 1-11: Images showing the typical appearance for each blond sandstone group. Modified image from Hyslop et al., 2006.

1.5 Glasgow's Past Climate

To fully understand the weathering that has taken place on the buildings sampled, it is necessary to consider the local environmental conditions within which they have been residing. Data from Springburn Park (NS 609 686) and Glasgow University (NS 569 666) weather stations (Figure 1-12) were analysed, spanning a time frame of 109 years between 1886-1995. The data from these two weather stations were provided courtesy of the Meteorological Office Scottish archive. These weather stations were chosen due to their close proximity to the current weather data collection point at the University of Glasgow weather station (NS 559 667; Figure 1-12) and for the range of the records they provide. Data between June 1920 and 1937 for Springburn Park are unavailable due to the station being decommissioned during this period. Three weather parameters were

analysed to give an overall view of the climate, and they may play an important role in understanding historical (and future) weathering: temperature, rainfall and hours of sunshine.

Figure 1-12: Location map of weather stations.

1.5.1 *Temperature*

Mean temperature data were plotted using the weather station in Glasgow University to cover the period from 1886 to 1913, and then Springburn Park data was used from 1914 to 1994 (Figure 1-13 andFigure 1-14). In the winter months (December, January and February as defined by the UKCIP02 report) there is generally a shift to cooler monthly averages over the time-period (Figure 1-13). This is confirmed by the mean temperature for the first 20 years (1868-1888) compared to the mean value for the last 20 years (1975-1995). The mean temperature in January decreases from 3.5°C to 3°C, a change of 0.5°C, which is in accordance with results from February, which decreases from a mean of 4.1°C to 3.2°C, a change of 0.9°C. Overall, in winter, there has also been an increase in the frequency of cold average temperatures compared to the absolute means. Between 1868 and 1919 (51 years), only three years show evidence of the January monthly average temperature being less than 2°C below the absolute mean whilst in the 55 years between 1939 and 1994 this has doubled to six, and is also observed in February's data.

Summer (June, July and August as defined by the UKCIK02 report) shows the opposite trend. June and July (Figure 1-14) show a marginal increase in average temperature, and the August data, when first and last 20 year average temperatures were compared show a rise in temperature of 0.6°C.

When the deviation from the absolute mean for August is analysed it shows that a 2°C deviation from the absolute mean occurs once in the first 50 years but four times in the latter 50 years. These events have changed to a lesser degree for June and July (Figure 1-14).

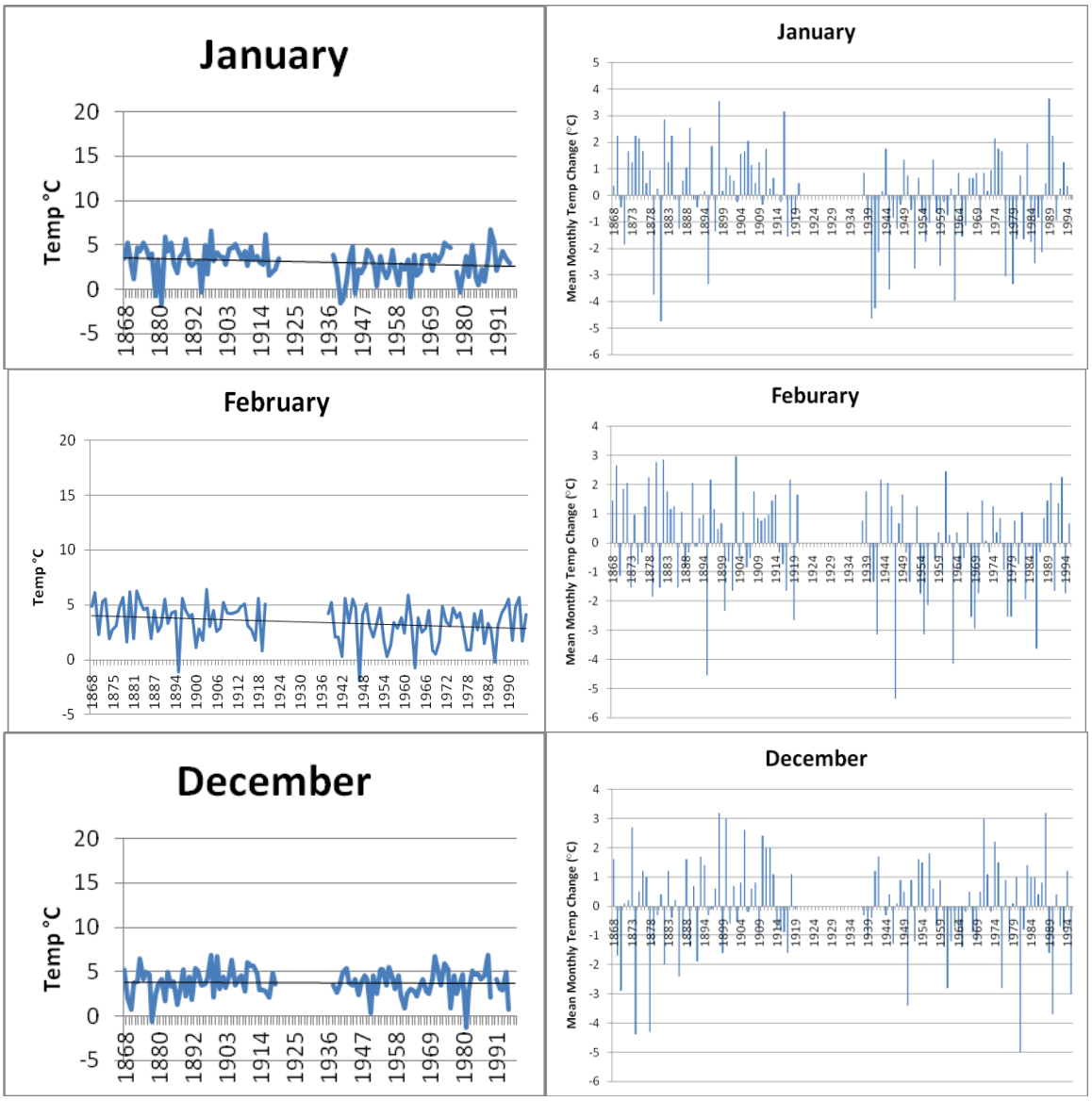

Figure 1-13: Left) Absolute winter temperature values from 1868 – 1994 with linear trend line, Right) Offset in temperatures from the absolute mean.

January mean = 3.1°C, February mean = 3.4°C, December mean = 3.7°C.

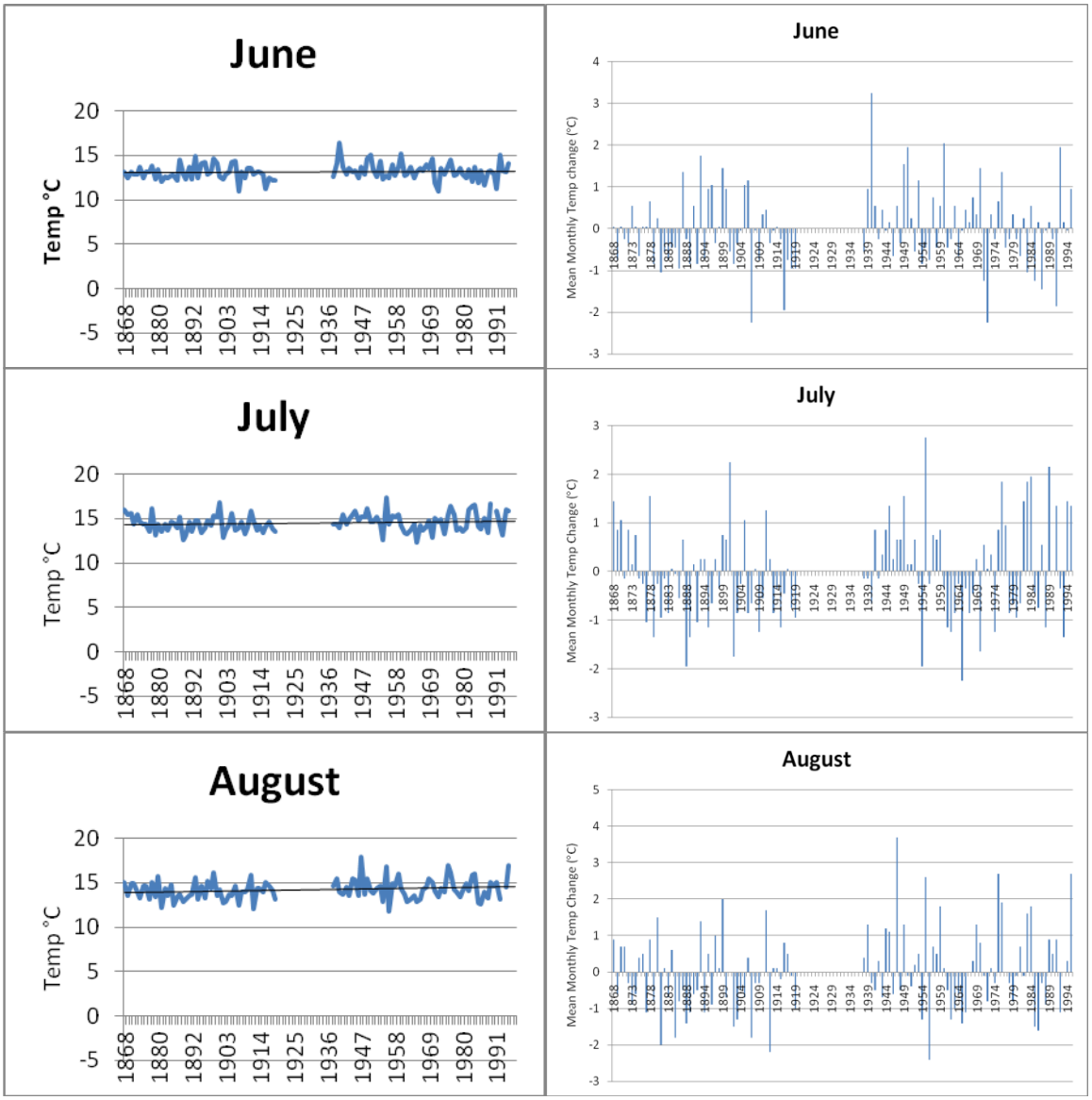

Figure 1-14: Left) Absolute summer month temperature values from 1868 – 1994 with linear trend line, Right) Offset in temperatures from the absolute means.

June = 13.1°C, July = 14.5°C, August = 14.2°C.

The temperature results indicate that the mean winter temperature is becoming cooler whilst there is no immediately obvious meaningful change in the summer average temperature.

1.5.2 *Rainfall*

Rainfall was recorded at the Glasgow University weather station between 1886 and 1910 and the Springburn Park weather station between 1911 and 1990. No overall winter seasonal change in rainfall patterns can be easily seen in the data (Figure 1-16). On a monthly scale, January and December show no clear patterns, although February data show a strong decreasing trend in the mean amount of rainfall. In February, the mean

rainfall for the first 20 years data (1886-1906) is 85.8 mm, decreasing to 66.8 mm between 1970 and 1990. Taking the summer data as a whole, there is also no obvious seasonal change in the amount of rainfall. However, June, when analysed in isolation, indicates a slight decrease in average rainfall between the first and last 20 years average of 70 mm to 58 mm. However, there are no other significant changes apparent in this data set.

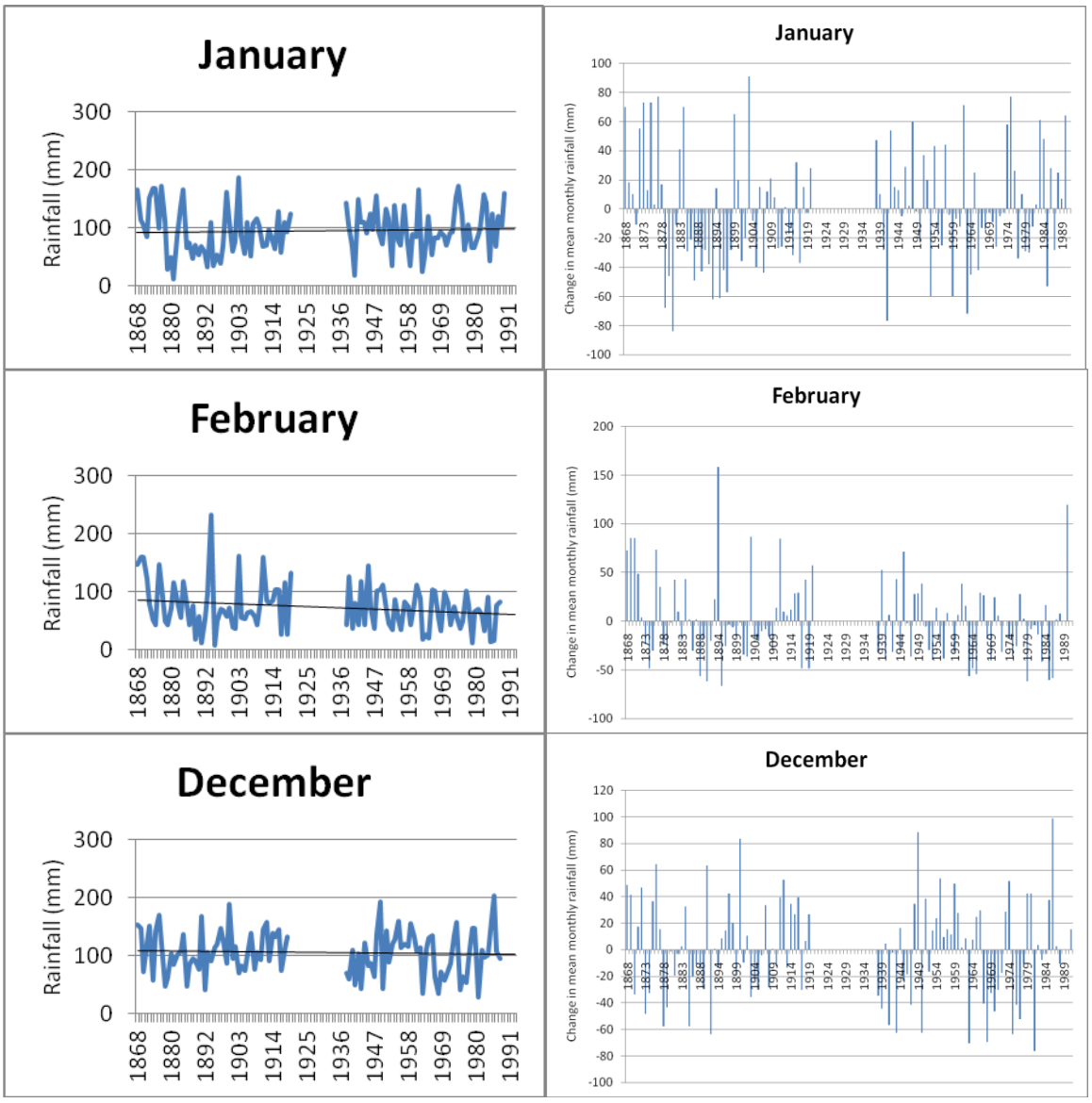

Figure 1-15: Left) Absolute winter month rainfall values from 1866 – 1990 with linear trend line, Right) Offset in rainfall from the absolute mean.

January = 96 mm, February = 74 mm, December = 102 mm.

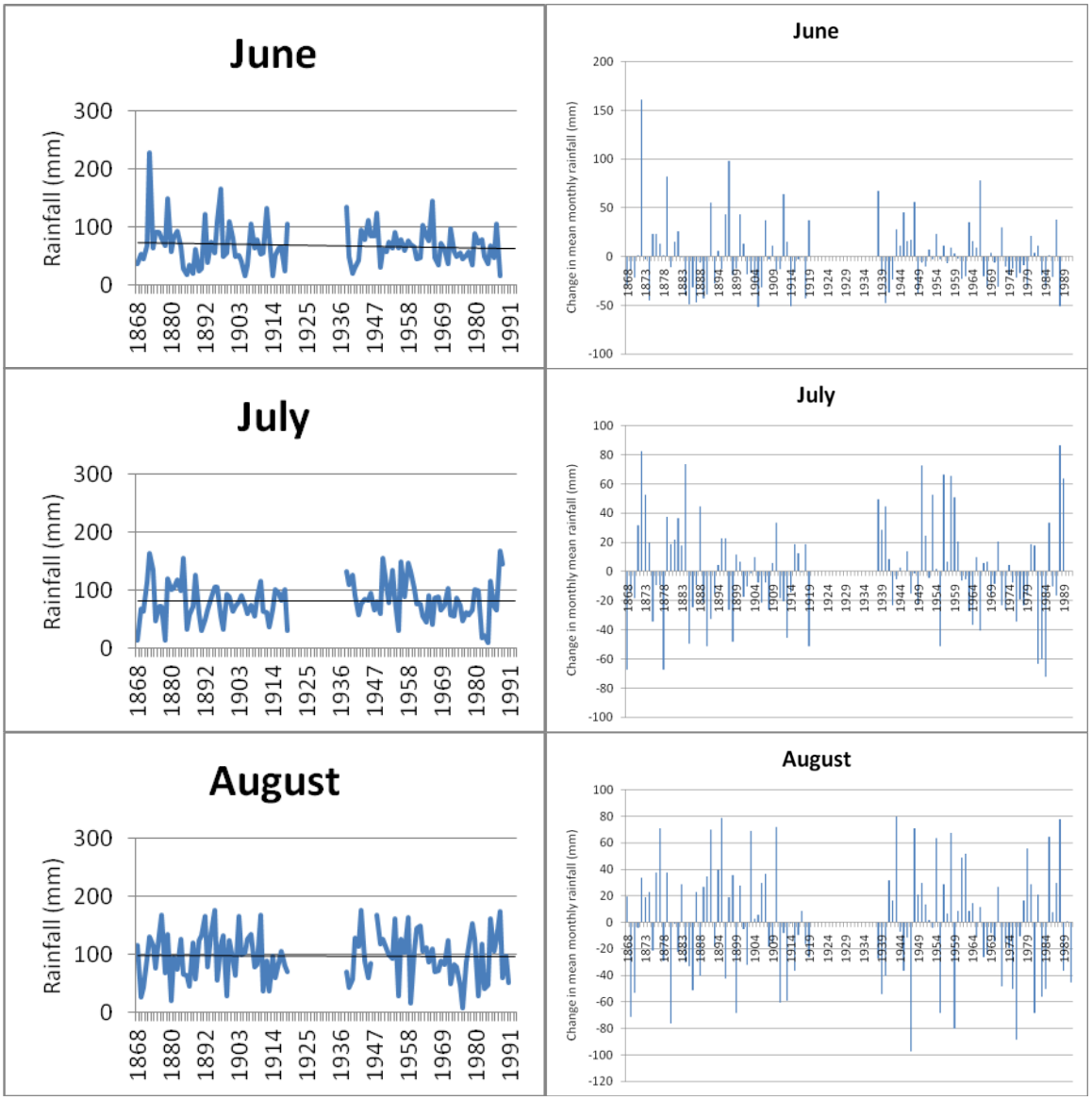

Figure 1-16: Left) Absolute summer month rainfall values from 1866 – 1990 with linear trend line, Right) Offset in rainfall from the absolute mean.

June = 68 mm, July = 82 mm, August = 97 mm.

Rainfall data indicates that although no seasonal trends are apparent on a monthly scale, there is definite evidence for drying occurring in both February and June.

1.5.3 *Sunshine*

Hours of sunshine were measured at the Glasgow University station between 1881 and 1988. The meteorological office used a Mk2 sunshine recorder (previously named the Campbell-Stokes sunshine recorder; Figure 1-17) until ~1969 when they were replaced by the Mk3C, which was specifically designed to be used in latitudes between 45° and 65° north or south of the equator and are still being used today. These are glass spheres that concentrate the sunshine and leave a burn imprint on the specially treated card beneath

the glass sphere. During less intense periods of sunshine, e.g. sunrise and sunset, a brown scorch mark will be produced. As the rays become more intense they will burn through the card. On days of broken sunshine, typical in Glasgow, hours of sunshine are complicated to measure as the scorch is not a fine line but a broad burn (~3 mm wide) which exaggerates the duration of short bursts of sunshine, and allowance must be made for this. Care has to be taken when calculating the total sunshine hours within a particular day, as there will be rounded ends due to "burn spread", therefore measuring is preformed between points half way between the centres of curvature. Although the recorders are very sensitive, a thick veil of high cloud such as cirrus-stratus seen on hazy days may stop recording. This information has been derived from the Meteorological Office Observer's Handbook (Third edition) HMSO 1969.

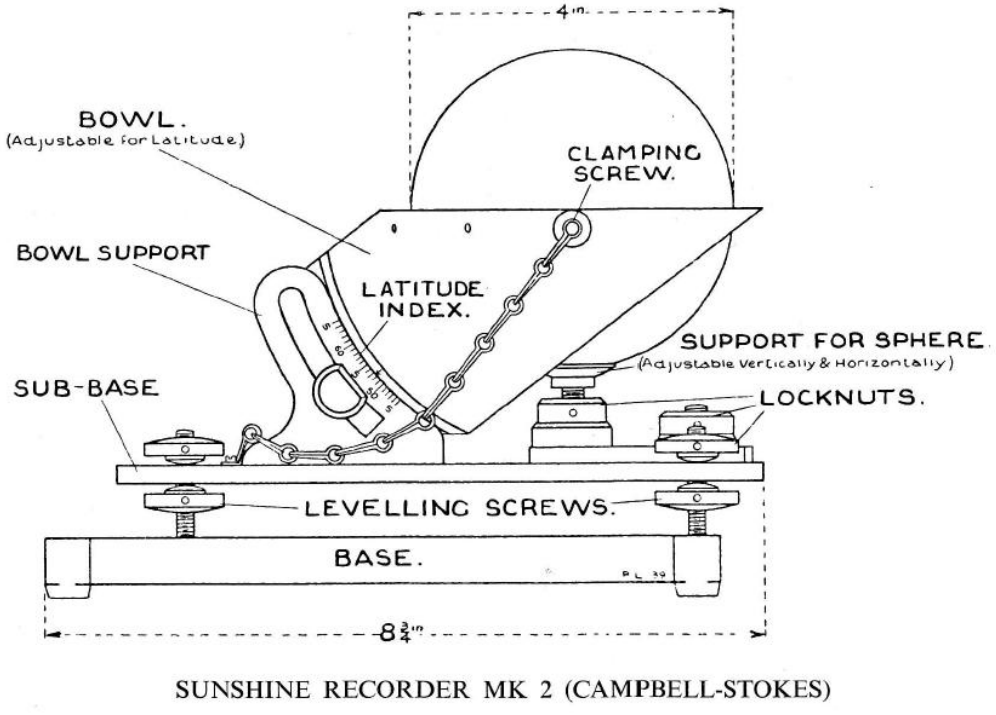

Figure 1-17: Sketch diagram of the MK2 sunshine recorders.
Taken from the Meteorological Office Observer's Handbook (Third edition) HMSO 1969.

Despite the above caveats leading to slight inaccuracies and imprecision, a clear trend in monthly sunshine hours over the measured period does emerge. The winter months show a dramatic increase in the hours of sunshine, although the summer months show no variation over the period 1881-1988 (Figure 1-18). The mean for the first 20 years compared to the latter 20 years in February show that the sunshine hours for the month have risen by 19 hours, whilst December data shows a rise from 17 to 33 hours for the month (Figure 1-18). This large increase in sunshine hours during the winter is probably

an outcome of the Clean Air Act 1956 and a reduction in the amount of open fires in homes within Glasgow, with the associated burning fuel throughout the winter months, which has led to a decrease in the amount of smog in winter, thus increasing the sunshine levels.

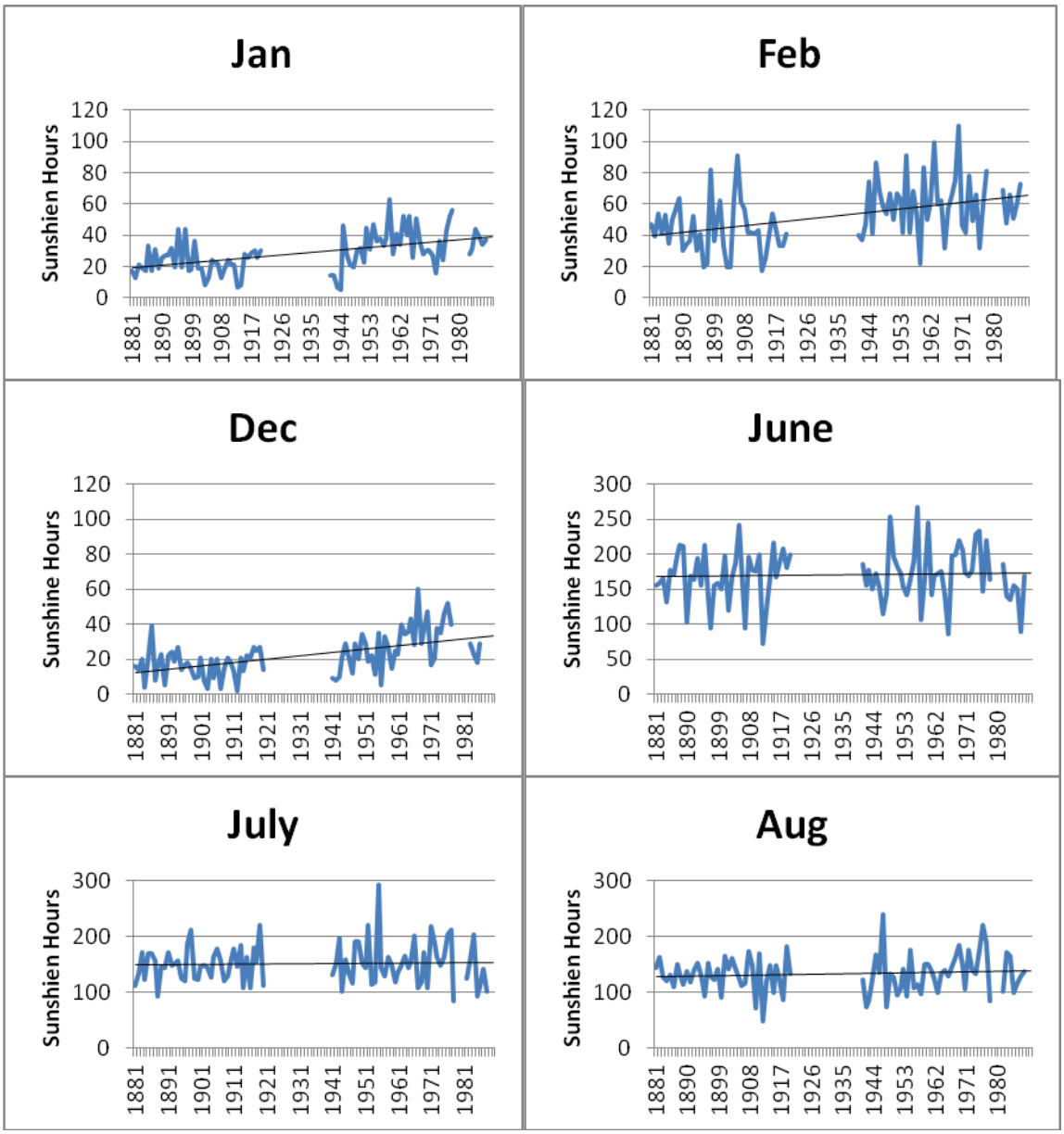

Figure 1-18: Total number of sunshine hours in each month.
For summer and winter from 1868 – 1988, with trend line.

1.5.4 *Discussion*

These data, particularly the mean temperature and the average rainfall, must be viewed with caution and objectively. Glasgow has a highly variable climate throughout the year. The winter weather is heavily affected by the North Atlantic Oscillations, whilst the summer weather is affected by the Atlantic Meridinal Oscillations. These control the

climate throughout the west of Scotland and small changes in these, and the heat that they bring heavily impacts the local climate. Therefore, due to the relatively short period of time analysed in this study, it is difficult to say whether or not these are overall significant climatic trends. The gap in the data also leads to complications with statistical analysis required to verify the trends.

The Glasgow sandstone buildings were constructed 200-150 years ago, when the winter months were, in general, slightly milder with higher rainfall, combined with limited daylight due to higher levels of cloud/smog in comparison to the present conditions. However, the summer climate has remained relatively stable. This change in the winter climate would have meant that, in the past, there was less solar heating of sandstone and there would have been less light to penetrate into the sandstone. These are likely to causing any microbes present to live at shallower depths, and may also have changed the species of microbes which inhabit the building surfaces. The milder climates during winter will also have meant less need for de-icing salts in the past, while the actions of freeze thaw, would have been more limited than at present due to the warmer winters.

1.6 Detailed Aims of the Present Study

As described in this chapter, the blond sandstone local to Glasgow, contains varying proportions of diagenetic minerals shown by Hyslop et al. (2006) due to the fluviodeltaic environment in which it was deposited and as a result, it is much more susceptible to weathering in comparison to the local red sandstone, which is mineralogically much simpler than the blond. For this reason, blond sandstone was used as the main sample type within this study.

The blond Glaswegian sandstones have been sub divided into a range of classifications in previous studies but, whilst being useful for tasks such as stone matching, do not quantify how the accessory minerals (such as iron oxides and the clay minerals present) may alter the internal structure and decay response of the stone.

There is an abundance of knowledge on how sandstones weather throughout the world (with particular relevance to Mediterranean climates). However, there is a general lack of information on how Scottish sandstones respond to the cool, wet environment, they are

exposed to, with the only available model produced by Bluck and Porter (1991b). Weathering processes acting on the sandstone (past and present) will be explored within the context of chemical and microbial decay in an attempt to understand the future weathering processes.

However, the Glasgow environment is set to alter in the future due to climate change, which will modify the weathering processes.

This study therefore sets out to combine present understanding of stone properties from the geological knowledge with reference to the past weathering procedures and environment to predict which weathering events or mechanisms will be acting upon the buildings in 2080.

The three main research questions are:

- What weathering processes have occurred historically and are at work presently on the blond sandstones of Glasgow?
- How will current weathering cycles alter with climate change?
- Which buildings are most at risk and how can we mitigate against these degradation processes?

The objectives of this study are to:

- To characterise the sandstone, in terms of its mineralogy and permeability.
- Detail the internal environment of the blond sandstone, in relevance to its temperature, relative humidity and liquid water.
- Understand how the external conditions affect the syrface and internal conditions of the sandstone.
- To model how the future climate will alter present day decay processes.

- To observe and identify the microbes which exist on and within the sandstone.
- To determine the amount of microorganisms living on and within the sandstones.
- To deduce the amount of light, which can pass through the surface of blond sandstones.
- To determine the effectiveness of produces designed to mitigation against sandstone decay.

These issues will be investigated using a multitude of experiments and technology ranging from chlorophyll-a assays to Raman spectroscopy, combined with unique datalogging techniques.

2 Methods and Materials

A suite of procedures and samples were used to answer the questions previously outlined. This chapter provides a comprehensive description of all the materials used and an in depth review of each procedure and the techniques applied, together with a detailed review of the experimental design.

2.1 Methods

The first half of this chapter will detail the experiments conducted.

2.1.1 *SEM Techniques*

Initially, before any SEM analysis could be undertaken, the samples had to be prepared first. Both rough surface fragments and polished block samples were examined within the SEM. The polished blocks were produced by embedding the sample in Buehler epoxicure epoxide resin, within a vacuum, to ensure maximum penetration of the resin into the sandstones pore space. Once the resin hardened, the standardised procedure to prepare polished blocks was followed. Excess resin was ground away through a series of decreasing roughness sandpapers (80P to 4000P,where P = the grit size) and then the sample was polished through 6 µm to 0.3 µm diamond paste, to leave a highly polished surface which could then be imaged by SEM. Many SEM techniques were utilised within this study and these will be outlined, in detail, in turn. However, these techniques were conducted on two different SEMs and these machines are described below.

The first SEM used was the Quanta 200F field-emission environmental SEM (from herein known as the FEG-SEM). This SEM can operate in high, low and environmental modes. The X-ray chemical microanalysis was undertaken using the EDAX Genesis software system and a panchromatic detector was used for cathodoluminescence (CL) imaging.

The second SEM used was the Zeiss Sigma field-emission analytical SEM (although also a FEG-SEM, from herein will be referred to as the ZS-SEM to differentiate between the SEMs). The ZS-SEM can operate in high and low vacuum conditions and the X-ray

chemical microanalysis is undertaken using an Oxford instruments X-Max system, with INCA software.

High vacuum conditions are preferable within the chamber as this means that particles will not interfere with the electron beam, providing a higher quality image.

Low vacuum conditions can be used to help eliminate charging effects as it allows samples to be imaged without coating (discussed next) and without the loss of natural contrast caused by the coating, but are unable to achieve the resolution attainable by conventional SEMs with coated specimens.

Both these systems are typically operated at 20 kV in all conditions and modes. Of the two SEMs, the FEG-SEM was used most frequently.

As stated, the SEMs can be used in many operating modes and conditions to obtain varying information. However, for the SEMs to provide maximum information, it is necessary to eliminate charge on the polished block samples, meaning they have to be prepared with differing coatings, dependent on the mode. These are outlined in Table 2-1. A gold coat was applied as a very thin (few tens of nanometers) veneer onto the surface of samples using an Agar Sputter Coater B7340 and is most often used when the topography of a sample (Table 2-1) is being studied in high vacuum. The carbon coat was applied using two different machines: an Agar Carbon Coater B7367 and an Edwards Model 306 Evaporation Carbon Coater. These both have advantages and disadvantages. Whilst the Edwards evaporation carbon coater provides a more even spread of carbon onto the surface of the samples, it is also very time consuming with the higher vacuum needed taking a long time to obtain. The Agar carbon coater is quicker but the coat is uneven and less conductive and therefore 2-3 coats may be required to adequately prepare the whole sample. These coatings stop the incident electrons from building up on the sample surface, which would cause it to become negatively charged.

Table 2-1: Coating and operating conditions required for the various operating modes. Applicable for both the FEG-SEM and the ZS-SEM. All at 20 kV and variable beam current.

Operating conditions	Coating	Operating mode
High Vacuum	Gold	SE (topography)
($7x10^{-5}$ Pa)	Carbon	CL
	Carbon	X-ray microanalysis
	Carbon	BSE imaging
Low Vacuum (60 Pa)	None	SE (topography)
		BSE imaging
Environmental (660-800 Pa)	None	SE (topography)

2.1.1.1SEM Imaging

The SEMs image samples in two modes: secondary electron (SE) and backscatter electron (BSE). SE images are generated from a very small area around the point of contact between the primary electron beam and sample (Figure 2-1), which makes this imaging ideal for surveying the topography of a sample. BSE images are generated from signals returned from much deeper into the sample (Figure 2-1), when the backscattered electrons are produced by interaction of the primary beam with the nucleus of sample atoms. They provide images with atomic number contrast, which can be obtained in high or low vacuum operating conditions (Table 2-1), although best results are obtained in high vacuum mode with a carbon coat. The detectors for these rays within the FEG-SEM chamber are shown in Figure 2-2.

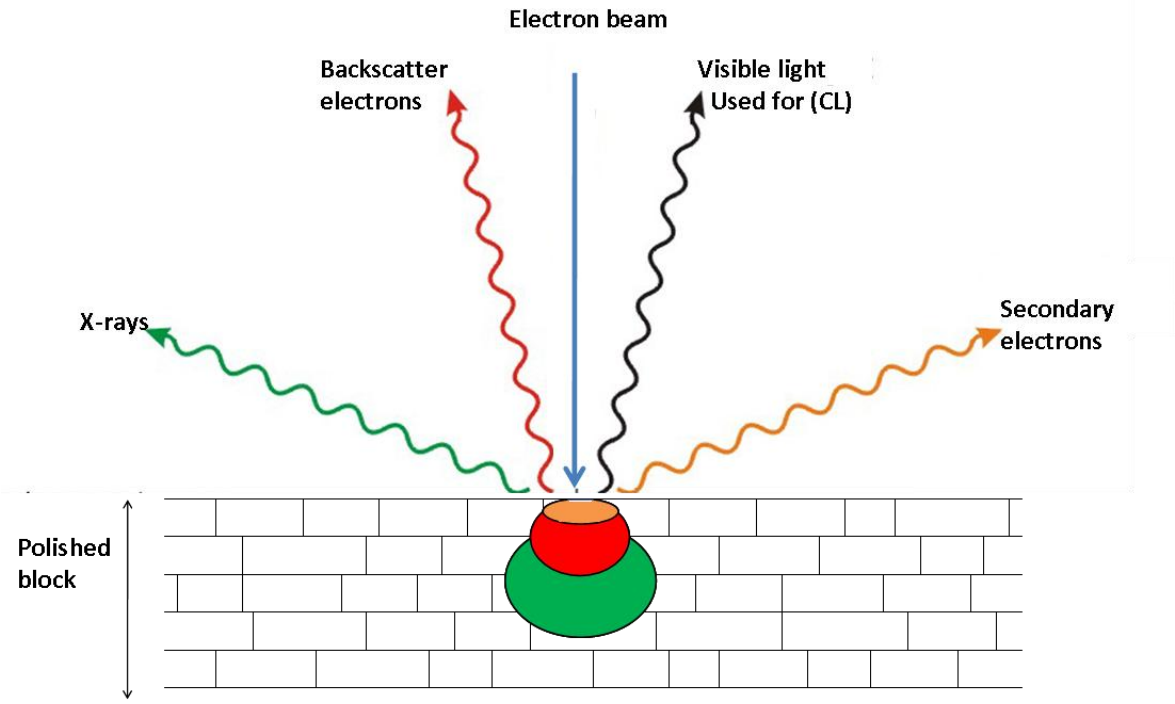

Figure 2-1: Schematic diagram of where signals are generated within a sample, when viewed under SEM conditions.

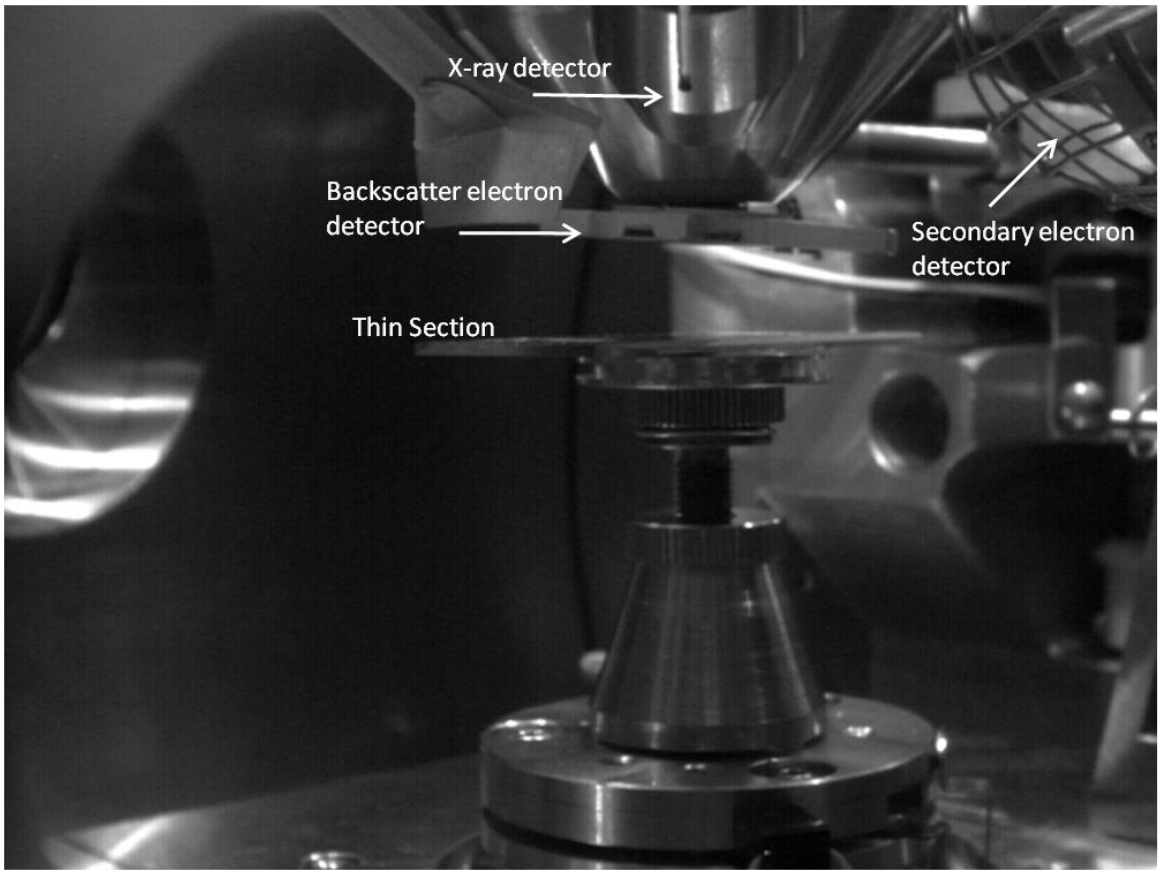

Figure 2-2: Position of detectors within the FEG-SEM.

2.1.1.2 Point Counting and Grain Size

Point counting was performed on all samples using the FEG-SEM to quantify porosity, mineralogy and any mineralogical changes within the weathering profiles. This provided a volume measurement of the mineralogy and porosity. Point counting was undertaken in BSE mode at 1000 times magnification, and a distance of 300 µm was moved each click and the area at the centre of the cross hairs on screen was noted. This was chosen because the geological review of the area (section 1.4) stated that most sandstone's within the Glasgow region are fine to medium-grained. Therefore, the distance was just slightly smaller than the Plas and Tobi (1965) rule that "the point counting distance chosen should be larger than the largest grain fraction that is to be included in the analysis." Point counting was performed in a series of 1 mm wide strips (between 150 and 350 points) parallel to the outermost surface with a millimetre gap between each strip (Figure 2-3). A millimetre gap was left so that a clear systematic grid pattern could be used on all samples to provide a control as to where sample analysis was preformed. Also, this helped to identify any small variations in the mineralogy as the point-counted zone edges did not become blurred.

The point counting data was then used to make ternary plots so that the relative proportion of main rock-forming minerals could be determined and analysed. Quartz, feldspar and muscovite ternary plots were used, as when analysis was undertaken no rock fragments were identified therefore these plots provided a better representation of the main rock-forming minerals. In addition kaolinite, Fe-oxide and ankerite plots were produced to show the minor mineral proportions.

According to Dryden (1931), when conducting point counting, 300 grains should suffice for most ordinary work. However, when Van Der Plas and Tobi (1965) undertook more statistical analysis, their chart suggests that when small mineral percentages are being analysed, a greater number of total points need to be counted in order to validate the accuracy of the results. However, owing to the limitations on the samples used in this study, as well as the size of the resin blocks, the amount of total points counted varies between each sample, but are generally less than ~300 points. Nevertheless, the Van Der Plas and Tobi (1965) method of calculating uncertainty in point counting was used within

this study, because it was deemed sufficient for the purpose of understanding the possible uncertainties associated with the research.

Grain size for quartz was calculated using the XT Doc software on the FEG-SEM. Approximately 30 quartz grains were measured against the long axis, and an average was calculated for each sample.

Pore size was calculated by printing BSE images of the sandstone and measuring the width of pores (in mm), which were seen as black areas of resin between grains. The pores were measured on a series of parallel lines, parallel to the outermost surface, superimposed onto the digital print outs. These measurements were then converted into microns. The amount of pores counted was dependant on the porosity of the sandstone and ranged between, 30-100 pores.

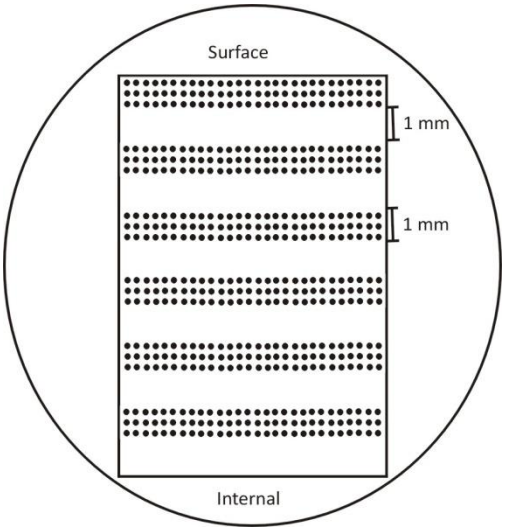

Figure 2-3: Schematic diagram illustrating point counting procedure.
Images show outline of a sandstone block within resin mould. Dots indicate the location of points that were counted.

2.1.1.3 EDS Maps

Both SEM machines were used to obtain Energy Dispersive Spectroscopy (EDS) maps which revealed the sandstone elemental compositions and therefore mineralogy. Because EDS maps were produced using INCA hardware and software on the ZS-SEM, as well as EDAX hardware and software on the FEG-SEM, comparison EDS maps were run on the same area within the same sample, which allowed resolution and colour blending to be compared. Also the optimum frame size was calculated so that image quality was not

lost due to a decrease in dwell time. The FEG-SEM maps were obtained at resolutions of: 1024-800, 512-400 and 256-200 pixels (Figure 2-4) using the set up outlined in Table 2-2. The high resolution (1024-800 pixel) map takes a longer time to obtain whilst 512-400 pixel maps are much quicker without losing the depth of information gained. The 256-200 pixel maps are very quick but the images are very pixillated and less informative. Therefore the majority of maps used the 512-400 pixel resolution.

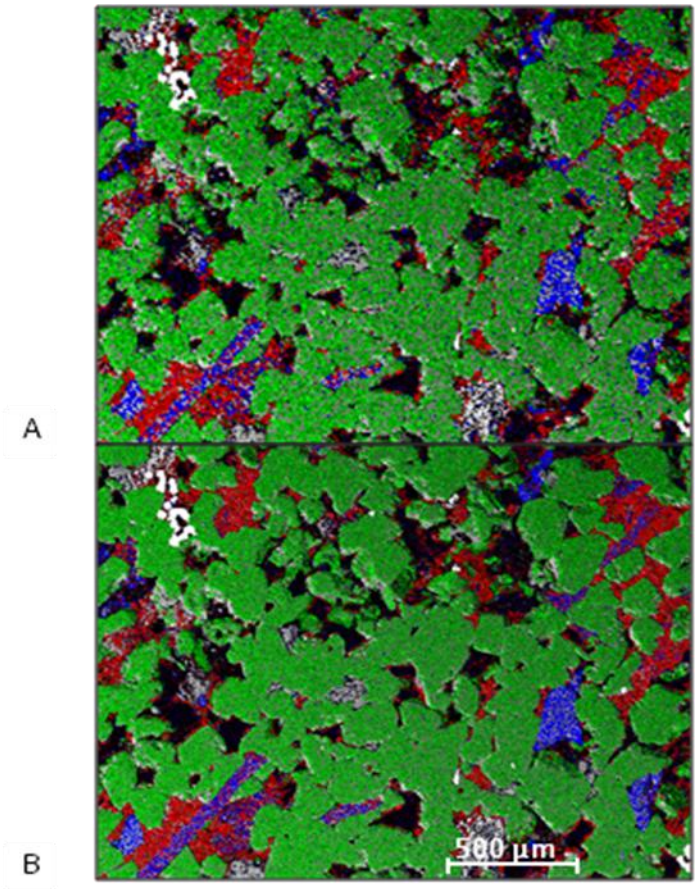

Figure 2-4: Comparison of optimum acquisition conditions for EDS maps on the FEG-SEM. Sample area within CS4, A) 256x200 pixel resolution, B) 514x400 pixel resolution. Green = Silicon, Red = Aluminium, Blue = potassium.

Table 2-2: Set up used on ZS-SEM and FEG-SEM to compare EDS maps.

Property	FEG-SEM (high vacuum)	ZS-SEM (high vacuum)
kV	20	20
Spot	5	Not measured
Aperture	40 µm	60 µm
Magnification	150x	124x
Counts	102,000 /sec	100,000 /sec
Working Distance	11.5 mm	8.2 mm

2.1.1.4 Cathodoluminescence Imaging

Cathodoluminescence (CL) imaging works by gathering the light generated by the electron beam striking the sample (Figure 2-1) in high vacuum conditions. This technique can provide information on the different generations of the same mineral. This is because it identifies small variation in trace element chemical composition and helps to infer any mechanically induced defects within the mineral lattice. CL imaging was conducted on carbon coated samples using the FEG-SEM. This process was carried out on a variety of samples to help understand their diagenetic history in great depth and, in particular, to see whether quartz overgrowths were breaking off in the weathered region.

2.1.1.5 X-ray Microanalysis Under High and Low Vacuum

Comparisons were conducted to evaluate the differences between X-ray spectra acquired under high and low vacuum conditions, both using the FEG-SEM. This is important because the primary electron beam disperses as it collides with water molecules in the chamber. A prominent sub-micrometer tin-copper-nickle sulphide particle from rough sample EE1 was used for the experiment. The FEG-SEM configuration was 20 kV, spot size 3, working distance 11 mm, 6000 counts/sec, 50 sec count time, 0.53 Torr in low vacuum and $5x10^{-5}$ Torr in high vacuum. The resultant spectra (Figure 2-5) show that, under low vacuum conditions, a decrease in the concentration of silicon (Si) is recorded, compared to high vacuum conditions. Also, high vacuum shows an increase in sulphur (S), indicating that the S is liberated from within the particle rather than the surrounding region. The low vacuum analysis detected increased levels of iron (Fe), which must be from the surrounding minerals (Figure 2-5). It was concluded that, although spot analysis can be conducted in low vacuum conditions, analysis with superior spatial resolution is performed in high vacuum.

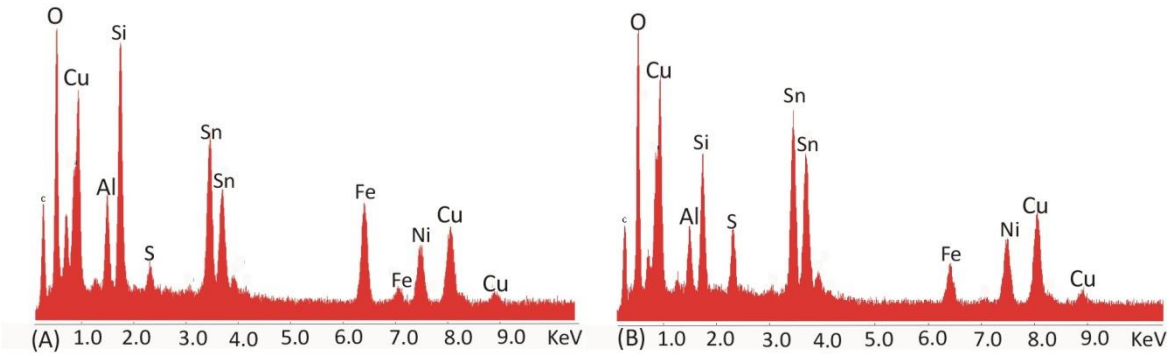

Figure 2-5: Low and high vacuum comparison within FEG-SEM.

Compassion conducted on a Cu-Ni-Sn sulphide particle in EE1, A) low vacuum spectrum, B) high vacuum spectra. A) Shows a greater quantity of both silicon and iron, reflecting 'contamination' of the spectrum by scattering of incident electrons.

2.1.1.6 Quantitative EDX

The ZS-SEM was used to conduct quantitative energy-dispersive X-ray spectrometry (EDX), which can determine mineral chemistry. Although qualitative X-ray microanalysis can provide chemical compositions, it does not allow specific concentrations of elements to be determined within the minerals, so quantitative EDX was used.

Two sample preparation methods for the EDX were tested to help understand the limitations of this quantitative analysis. Sample preparation method one (SP1) reused the polished blocks previously prepared for the other SEM methods (see section 2.1.1 for full detail on how these were produced). However, when analysed, SP1 produced excessive charging due to the block's size (1.5 x 3 cm) and topography caused by the high percentage of porosity within the sandstones.

Sample preparation method two (SP2) involved using small amounts of crushed sandstone from the interior of the sample which were then embedded into resin to produce grain mounts. This provided a much smoother surface after polishing as this eliminated porosity which causes topography on the surface. Due to the smoother surface, electrons were much easier to disperse over the surface and less charging of the sample occurred.

To test whether the charging seen in SP1 skewed the analytical results, kaolinite, muscovite and carbonate grains prepared by both methods were analysed under the same conditions using the ZS-SEM (Table 2-3). Results from the two preparation methods

show that SP1 was quite accurate despite the charging although a larger spread in the results were seen compared to that seen in SP2, which produced tightly clustered results for all the minerals (Figure 2-6 Figure 2-7 and Figure 2-8), full results are seen in chapter4. However, the main conclusions were that a larger difference was seen in the carbonate results, and that SP2 should be employed in future analytical work for coarse sandstones.

Mineral standards were used to calibrate the ZS-SEM before analysis was undertaken, the main minerals used for this was cobalt, pyrite, periclase, rhodonite, calcite, jadite, rutile, kyanite and orthoclase. The kaolinite and muscovite results were produced in element percentage, whilst the results for ankerite were gained as weight present element and then converted to mole percentage so that they could be analysed. The full formula is on the electronic appendix.

Table 2-3: ZS-SEM set up used during quantitative EDX, on the silicate, phylosilicates and the carbonate minerals.

Property	Silicates and Phylosilicates	Carbonate
Process Time	5 sec	5 sec
Live Time	30 sec	30 sec
Dead Time	40 sec	40 sec
Acquire Time	50 sec	50 sec
Beam Current	1.1 nA	1.1 nA

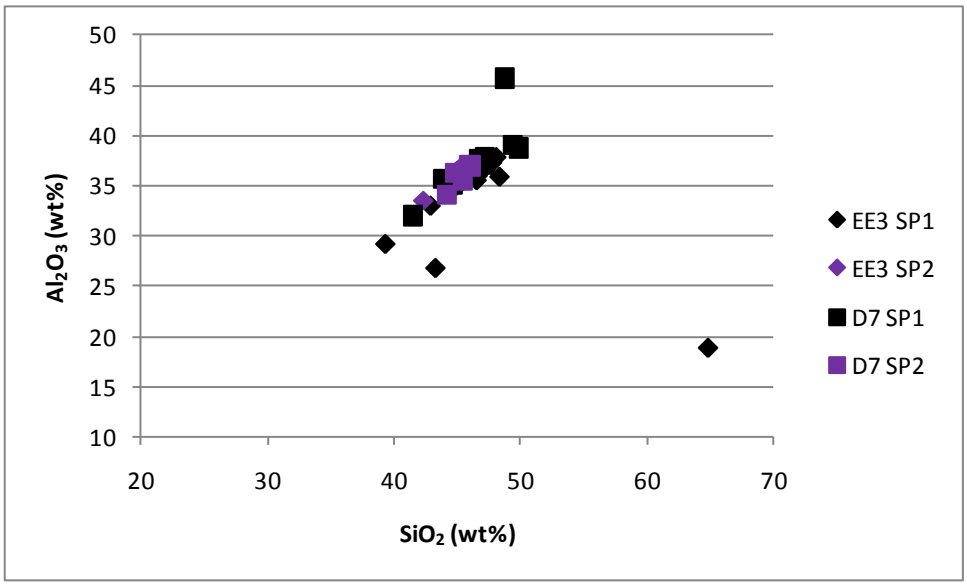

Figure 2-6: Quantitative EDX comparison of kaolinites.

Within EE3 and D7 using the SP1 and SP2 methods outlined, showing tighter clustering of the SP2 results.

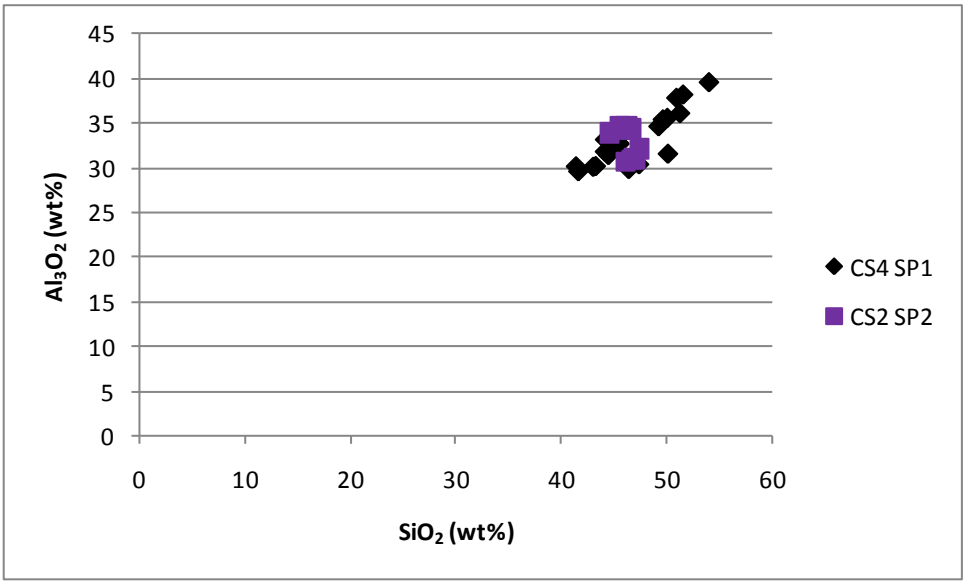

Figure 2-7: Quantitative EDX comparison of muscovites.

Within CS4, using the SP1 and SP2 sample methods outlined, showing tighter clustering of the SP2 results.

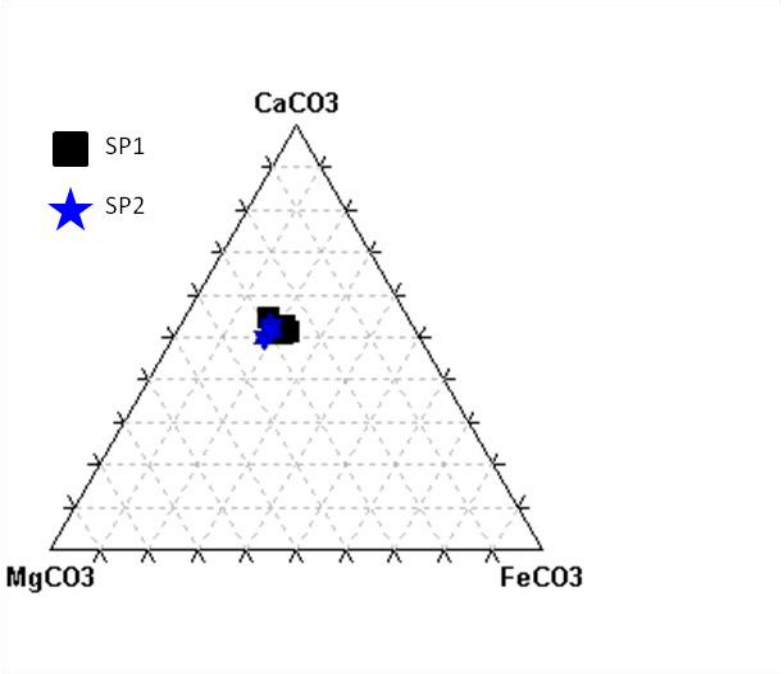

Figure 2-8: Quantitative EDX results from carbonates.

Plotted on a Ca, Mg, Fe ternary plots, comparing SP1 and SP2 in EE3, data expressed as moles % carbonate.

2.1.2 *Permeability*

Permeability tests were undertaken to help understand the flow of water through the various different rock types, because high permeability coupled with high porosity could accelerate weathering issues.

The permeability tests were undertaken at Aberdeen University with help from Professor John Parnell. Large sample blocks were provided so that multiple cores (~5) with a diameter of 2.5 cm and maximum length of 6 cm could be taken to conduct repeat experiments on each sandstone. This requirement limited the sandstones that could be examined, so a selection of six suitable sandstone types was tested: UE2, UN2 (both University samples), Dunhouse Buff (fresh quarry stone), EE3 and CS4 (both St Vincent Street samples). These samples provide a representative cross-section of the sandstones examined in this research. The procedure used is described in detailed by Parnell et al. (2010), whereby a gas pereameter was used to inject nitrogen into each core at a known and controlled pressure. The core is held in a Hassler sleeve and is plugged to stop leakage of gas around the samples. The pressure difference at the two ends is then used to calculate the permeability, which is quantified in millidarcies.

2.1.3 *Raman Spectroscopy*

Raman spectroscopy was conducted using a Renishaw InVia Raman microscope. It works using the principle of a single beam of laser light which is diffracted through a series of mirrors, before reaching the sample. The Raman scattered light produced is then gathered and focused back to the detector (Figure 2-9).

The Raman affect has been understood since 1928 but only in the 1960's, when laser technology had improved sufficiently, could it be established as a viable method to characterise materials. Raman works on the principle that monochromatic light will pass through matter, although a small proportion will be scattered. The measurement of this scatter reveals information about the bonds between the atoms.

X-ray microanalysis only provides information on which elements are present in a sandstone mineral grain, not how the elements are bonded. Therefore, Raman was used here to further understand the mineralogy of the samples, and to determine whether any changes could be seen in the molecular structure of those minerals nearest the weathered outer stone surface compared to the interior. Raman spectroscopy was chosen rather than Fourier Transform Infrared Spectroscopy (FT-IR) (which it is closely related to), as Raman has better spatial resolution and sample preparation is minimal, but a full list of differences are outlined in Table 2-4.

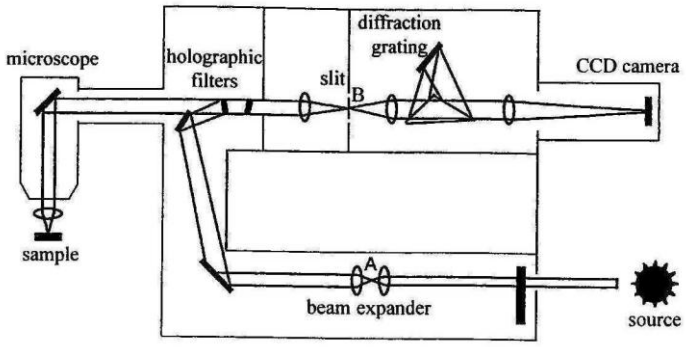

Figure 2-9: Diagram of laser pathway through the Raman microscope.
Image taken from Leng (2008).

Table 2-4: The characteristic advantages and disadvantages of FT-IR and Raman micro spectroscopy.

Property	FT-IR	Raman
Phenomenon	Absorption	Scattering
Sample Preparation	Required	None
Accessories	Multiple	Single
Data Collection	Fast	Slow
Sensitivity	Good	Fair
Water interference	Strong	Very weak
Spatial resolution	$\geq 10\ \mu m^2$	$\geq 1\ \mu m^2$
Signal-to-Noise	High	Low
Fluorescence	None	Overwhelming
Heat destruction	None	Strong
Mapping/imaging	Yes	Yes
Light	Infrared	Monochromatic & infrared

Data modified from Lin et al. (2007).

The minerals studied by Raman spectroscopy were those suspected to be most susceptible to weathering within the sandstone: muscovite, kaolinite, carbonates and Fe-oxides. The layered microstructure of muscovite and its complex elemental composition produces an array of bonds that results in mica having a intricate Raman spectrum, with peaks occurring at 160, 195, 220, 240, 270, 640, 654, 702, 715 and 1058 cm^{-1} (Tlili et al., 1989). As kaolinite is a much simpler compound than muscovite, it has only four main peaks at 3620, 3652, 3669, 3697cm^{-1} (Frost et al., 2001). The type of carbonate cement within these sandstones was also determined by the use of Raman spectroscopy.

Iron oxides are complex and difficult to distinguish by SEM, as the ferric oxyhydroxides exist in several forms which X-ray microanalysis cannot distinguish. However, due to their different crystal structures, Raman spectroscopy can be used to discriminate between the

iron minerals. Some of the main iron oxides which can develop within sandstone are: goethite, akaganeite, lepidocrocite, haematite and maghemite (Dapples, 1967). These ferric oxyhydroxides and their expected band positions are outlined in Table 2-5.

Table 2-5: Raman band positions of various oxides and oxyhydroxides of iron.

Formula	Mineral	Band Position (cm^{-1})
α-FeOOH	Goethite	393, 307[A]
		299, 387,554[C]
β-FeOOH	Ankaganeite	400, 680[B]
γ-FeOOH	Lepidocrocite	257 393[A]
		250, 379,525, 650[B]
α-Fe_2O_3	Haemitite	222, 296, 406[A]
		293,299,412,613[C]
γ-Fe_2O_3	Maghemite	380, 500, 700, 670, 720[B]

Data from [A] = Johnston (1990), [B] = Neff et al. (2006), [C] = Larroumet et al (2007).

2.1.4 *Protein and Chlorophyll-a assay*

Protein assays were conducted to quantify the mass of protein on the surface of the sandstone samples. This was used as an indication of biomass from all organisms inhabiting the surface of the sandstone. In contrast, the chlorophyll-a assays were used to determine the mass of photosynthetic organisms on the stone surface. Samples for both procedures were obtained by scraping the outermost surface of the block (no deeper than 1 mm) using a stainless steel spatula on an area of a known size. When cores were used, half of the outermost surface was used for each procedure, although the surface area was highly dependent on the sample.

The protein assay used was a modified Lowry protein assay from Peterson (1977) and Phoenix et al. (2001). The Lowry method (Lowry et al., 1951) does not involve heating the samples and is also not so good at distinguishing small sample quantities of protein compared to the modified Lowry protein method which has that advantage. In addition, the modified version is better at absorbing thicker celled wall organisms such as cyanobacteria and algae (Peterson, 1977), hence why the modified version was implemented.

For the protein assay, four different reagents were employed:

Reagent A: 2 g Na_2CO_3 in 100 ml deionised water + 0.1 M NaOH,

Reagent B: 0.1 g $CuSO_4.5H_2O$ in 20 ml% (w/v) sodium tartrate,

Reagent C: A mix of 50 ml of A with 1 ml of B,

Reagent D: Folin's reagent.

The samples were washed with deionised water and centrifuged for six minutes at 4000 rpm. 2.5 ml of 1 M NaOH was added to the sample, and heated to 120°C for 15 minutes. Samples were then centrifuged at 4000 rpm for six minutes again before adding 1 ml of supernatant to 5 ml of reagent C. This was subsequently mixed and left to stand for ten minutes at room temperature, before adding 0.5 ml of reagent D and being left to stand for 30 minutes. An absorbance reading was taken using a HACH/LANGE DR 5000 UV/VIS spectrophotometer at 750 nm. The reading was then calibrated with the graph in Figure 2-10, before being converted to mg/cm^{-2} using Equation 1.

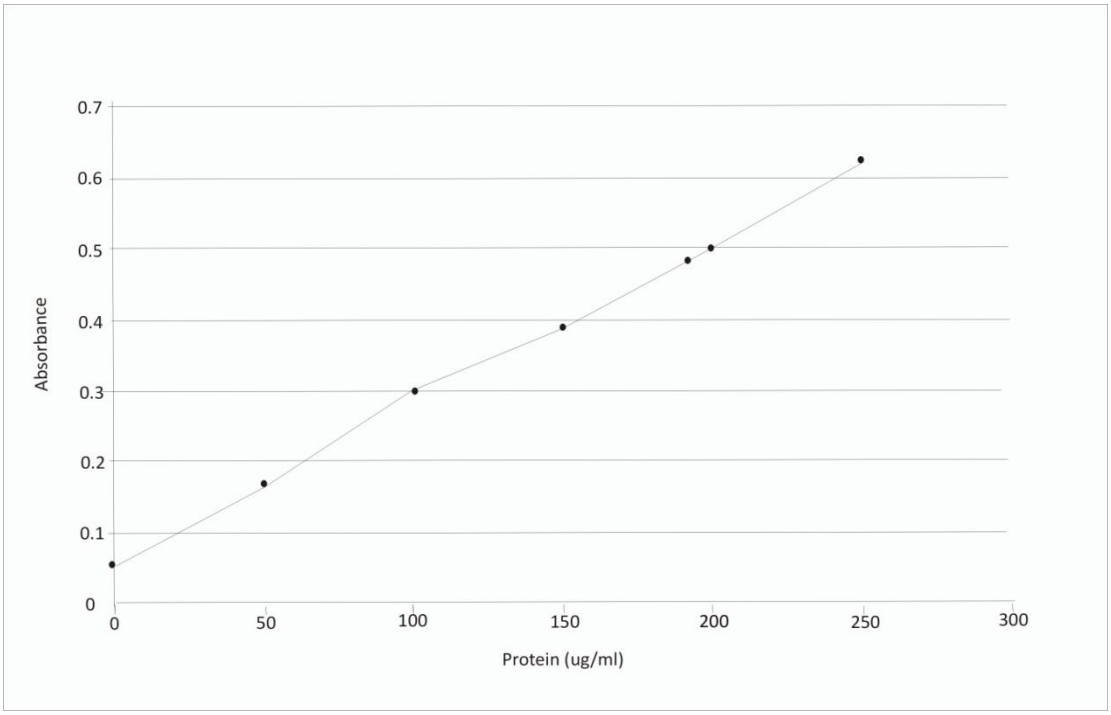

Figure 2-10: Protein calibration graph.

$$\frac{\mu g/ml \times 2.5}{area} = \mu g\ protein/cm^2$$

Equation 1: Protein assay conversion equation.

Chlorophyll-a assay samples were washed with 50 ml of deionised water before being centrifuged at 4000 rpm for six minutes. The deionised water was decanted off before 5 ml of 90% methanol was added to the solids. Samples were left in the dark for one hour before a second centrifuge. The supernatant was pipetted into cuvettes for testing in the HACH/LANGE DR 5000 UV/VIS spectrophotometer at 665 nm. Chlorophyll-a concentrations were then calculated using Equation 2.

$$\frac{(A_{665} \times 13.9) \times 5}{Area} = mg/Cm^2$$

A = Absorbance reading at 665 nm, Area = cm^2

Equation 2: Chlorophyll-a assay conversion equation.

2.1.5 *Osmium Stained Polished Blocks*

To identify biological communities within stone, osmium stained polished blocks were prepared. The osmium only attaches itself to lipids within organic material (Adams, 1960) and its high atomic number simplifies the identification of stained organic matter when using backscattered electron SEM imaging. This technique was adapted from Omelon et al (2006a).

Osmium staining of sandstone consists of three steps. 1) The cells were fixed by cross-linking the proteins using glutaraldehyde (fixer); 2.5% of the fixer was prepared to neutral pH in 0.05 M HEPES Buffer. The samples were then submerged in the glutaraldehyde liquid for a minimum of 24 hours, after which they were washed using a pH neutral 0.05 M HEPES Buffer three times for a minimum of four hours each time. 2) For osmium staining of the samples a 1% solution of osmium tetroxide was used. Samples were submerged in the osmium tetroxide for three hours before being washed three times with distilled water. 3) Samples were dehydrated through a graded ethanol series (30%, 50%, 70%, 90%, 100%, 100%, 100%), each step lasting a minimum of two hours with the third 100%, lasting 12 hours.

Once the staining procedure was completed, the samples were embedded in London white resin (LR), within a vacuum, to ensure maximum penetration of the resin into the

sandstone pore space. LR white was used as it is less harmful to the microbial cells in comparison to other resins. Once the resin had hardened the same procedure are described in section 2.1.1 was undertaken.

2.1.6 *Optical Light Transmission*

For cryptoendolithic photosynthetic organisms to be able to live, light has to penetrate into the sandstone. Therefore, the depth at which they inhabit is controlled by depth of light penetration (Nienow et al., 1988). The optimum light levels required are 50 - 500 µmol $m^{-2}s^{-1}$, but microbes can survive with conditions as low as 5 µmol $m^{-2}s^{-1}$ (Litchman et al., 2003; Phoenix et al., 2006). If light levels are greater than the optimum the microorganisms will suffer photo-oxidative damage, whereas insufficient light equates to no photosynthetic communities being viable.

The optical light transmission (OLT) protocol for experimentation in this study was adapted from Phoenix et al. (2006) and Hall et al. (2010). The aim of these experiments was to determine how surface weathering, as well as stone type, might affect the depth of light transmission. The experiment was set up using a hand held Macam Q203 Quantum Radiometer pyronometer (spectral range 400-700 nm) and a desk lamp. The pyronometer was placed directly under the light source with a constant distance of 14 cm between the light source and the pyronometer (Figure 2-11). Sandstone samples were then attached to a glass slide using Lakeside resin. This meant that 1 mm slivers could be removed from the bottom of the sample without any damage occurring to the surface of the sandstone occurring (Figure 2-11). The glass slide and dry sandstone samples were then placed over the sensor (glass slide facing upwards) and the reading was noted. To minimise any external light the experiments were conducted in a dark room and all sides of the sample were sealed with black insulating tape so that only light travelling through the topmost horizontal surface was recorded.

The data collected in these experiments were extrapolated and coupled with the macroclimate data gathered using the fixed CMP3 pyronometer (spectral range 310 - 2800 nm) located at the University of Glasgow weather station. When combined this information then provides data on how deep microbes can live within buildings situated in the environment local to Glasgow. It is understood that water saturation of porous

matter such as sandstone can affect the behaviour of light (Nienow et al., 1988), although only minimally, and therefore, this experiment was conducted on dry sandstone only. A selection of sandstones were used with varying degrees of weathering on the surface, ranging from clean to thick black crust.

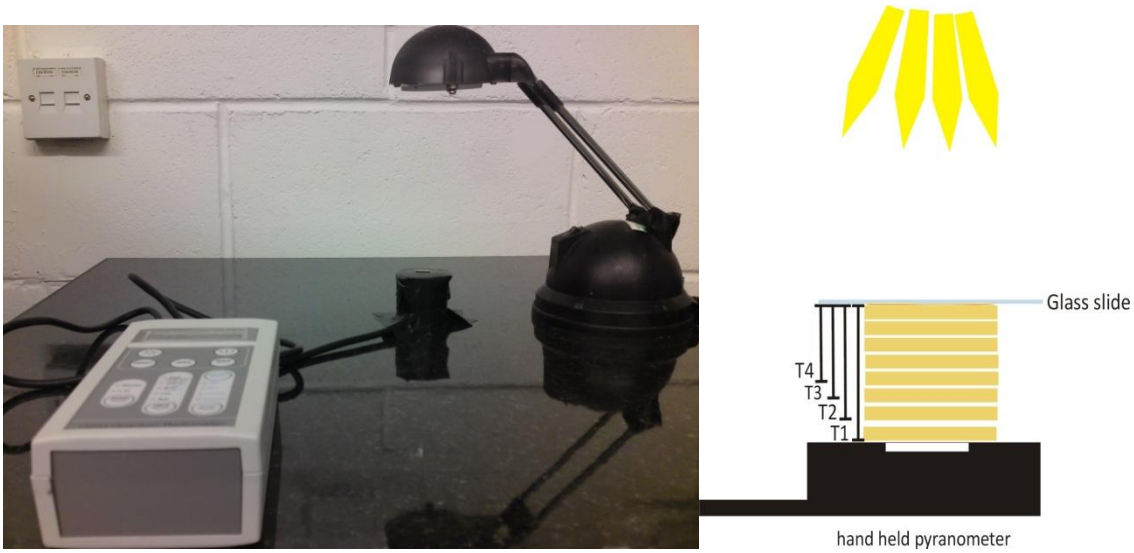

Figure 2-11: Image and sketch of optical light transmission experimental design. Left) actual set up, right) sketch diagram of sandstone sample thickness, T1 = whole thickness T4 = T1-(T1-T2)-(T2-T3)-(T3-T4).

As this experiment has many components and has a unique design there are many sources of uncertainty to consider. The manufacturers of the Macam Q203 Quantum Radiometer state an error of 1% whilst the CMP3 operator' manual state an error of 2.5%. The average amount of light emitted from the lamp was 116.49 ± 3.8%. In addition to these, the amount of light in which the lakeside glue stops form travelling through was calculated to be 20 ± 6.5 µmol $m^{-2}s^{-1}$. Whilst the samples were cut on the Buehler IsoMet 5000 precision low speed saw, which has an error of ±5 µm.

2.1.7 *Chamber Experiment*

As the literature review shows a variety of environmental chambers have been used in previous studies of stone decay to simulate effects such as salt weathering (Mcgreevy and Smith, 1985; Warke et al., 2006), pollution (Ausset et al., 1996) and thermal weathering (2003; Prikryl et al., 2003; Smith et al., 2008a). To examine how changes in the climate may affect the weathering processes and the microorganisms present on Glasgow sandstones, a simulation experiment was set up in a Sayno Fitotron Plant Growth chamber located in the workshop of Historic Scotland, Edinburgh. The environmental

chamber replicates a preset range of temperatures, relative humidity and light settings. This control over the set up of the chamber and the cycling of programmed conditions means that future climate conditions for Glasgow (as predicted by the UKCIP02) can be run within the chamber and on many samples simultaneously.

Six blond sandstones were used in this experiment: Bearl, Blaxter, Clashach, Cullalo, Dunhouse Buff and Scotch Buff (full mineralogical description of each stone is given in section 2.2.5). This sample set represents one commonly used replacement sandstone for each of the blond sandstone categories identified by Hyslop et al (2006). These sandstones were chosen as the majority of original quarries are now disused, leaving no present-day source for sampling of the stones. In addition, these are the stone types that are expected to be used for the majority of future constructions and repairs.

Each stone type was prepared by cutting it into three 9x9x9 cm cubes. During sawing of the blocks, oil was used as a lubricant, then washed with water. However, a few samples were left with small amounts of oil residues on the surfaces, which were later abraded off. In more extreme circumstances, where oil had penetrated into the sample, the top 3 mm of the affected surface was sawn off using only water as a lubricant. An unaffected face of the block was then used for the experiment.

After the blocks were cut, three stainless steel screws were drilled into the same surface of each block in a triangular pattern. Stainless steel screws were chosen as they would not corrode over time and thus could then be used as reference points for monitoring stone surface degradation. The screws should not interact with the block as plastic casings (raw plugs) were placed in first to restrict contact between the sandstone and the metal. Using a Konica Minolta Vivid 9i laser scanner, each block was scanned before being installed (02/08/2008) in the environmental chamber and rescanned at the end of the experiment on the 26/01/2010. The manufacturer's specifications state that for the Konica Minolta Vivid 9i scanner it has a precision of 0.008 mm with an accuracy of 0.05 mm. Within the chamber, the blocks were divided into three sets, which each comprised of one block of each stone type. The three sets were comprised of an inoculated set, water only set and a chamber set (Figure 2-12). These sets were then arranged on one level within the chamber (Figure 2-13).

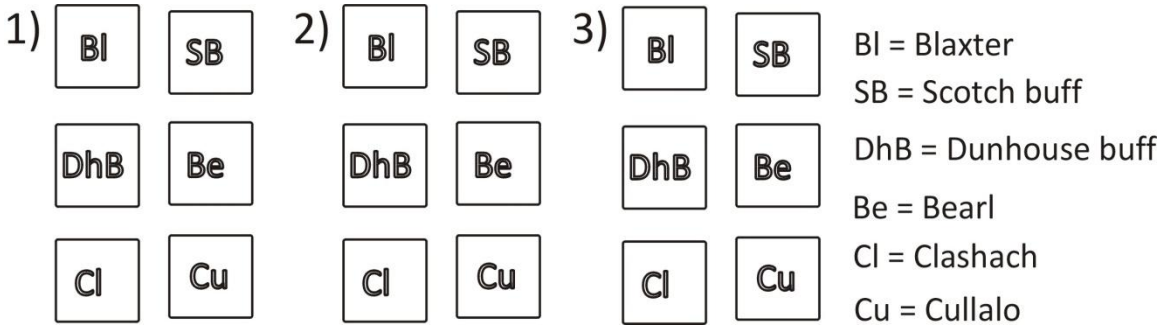

Figure 2-12: Plan view of environmental chamber set up.
1) Inoculated set, 2) water set, 3) chamber set.

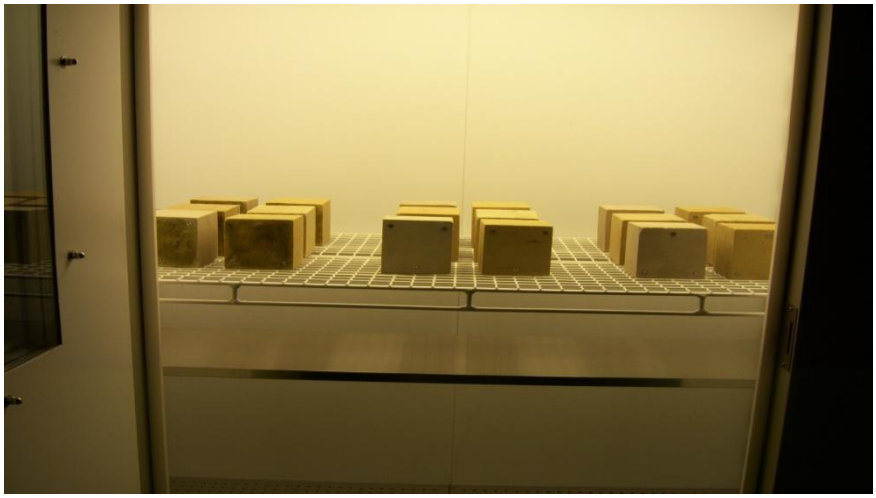

Figure 2-13: Internal view of the environmental chamber.

The inoculated blocks involved using a variety of microbes, sampled from six different areas of typical weathering on blond sandstone surfaces from the West End of Glasgow. These were collected from walls surrounding properties within the Dowanhill area of Glasgow. The microbes gathered were combined and thoroughly mixed before being equally divided up into seven 0.2 g samples. The microbe mixture was applied within one week of collection into the rock surface using droplets of water to help it bind, one portion was retained for visual identification of the microbes. Visual identification was undertaken using a Zeiss Axioplan microscope, and three main species were identified. The first has an elongated form with a green to brown coloured internal configuration, contained within a clear outer structure. This microbe is morphologically consistent with the algae *Hyalotheca* (Figure 2-14 A and B). The second main microbe has a morphology consistent with the fungi *Rhizopus,* which has previously been observed living within sandstone (Burford et al., 2003). *Rhizopus* has two distinct parts: the fibrous stolons and clusters of brown sporangium (Figure 2-14C and D). The third microbe has a plant-leaf-like structure (Figure 2-14E), but is yet to have been formally identified, although the

most likely option is for it to be a lichen or algae due to its size and form. Artificial rain water (composition in Table 2-6) was sprayed onto these inoculated blocks twice a week when in the chamber so that free water was available for the growth of microbes.

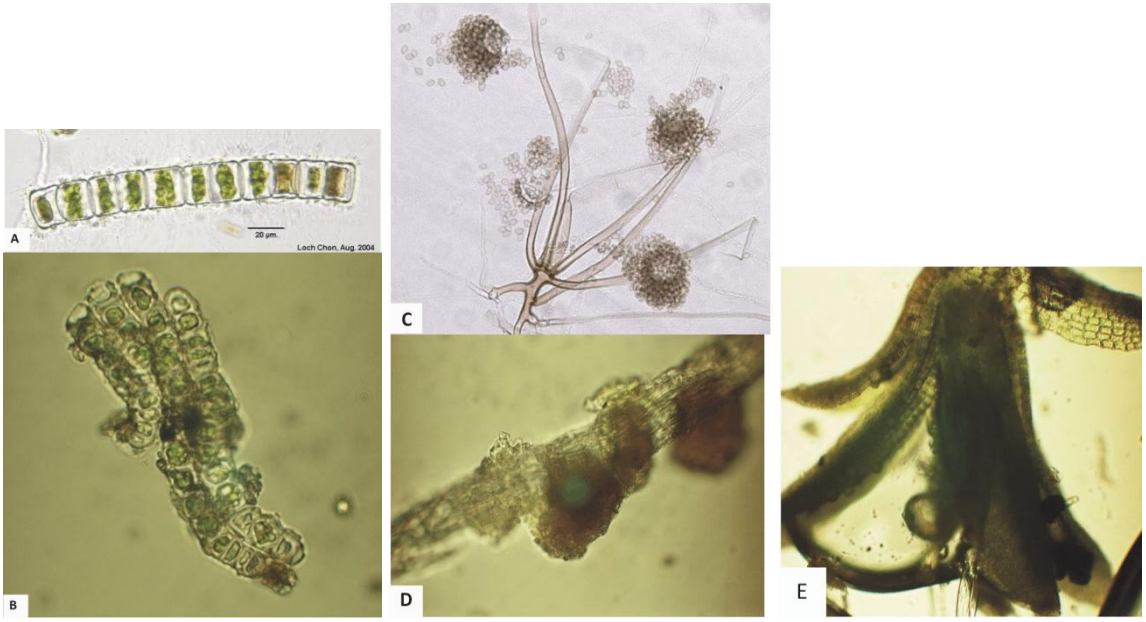

Figure 2-14: Comparison images of microbes seen and its morphological consistent image of suggested microbe.

A) typical *Hyalotheca*, (http://www.algalweb.net), B) microorganism seen in the mixture, C) a typical *Rhizopus* (http://www.doctorfungus.org), D) microbe seen in the mixture, E) unidentified lichen.

The water-only set of blocks had no microbes present but required additional artificial rainwater sprayed onto their surface, in conjunction with the standard environment chamber set up, to imitate an increase in high magnitude events which are linked with heavy rainfall events, defined as 5 ml per minute (Svensson and Jakob, 2002). A spray bottle was used to distribute the artificial rainwater and tests were conducted to see how many sprays were required to deliver the right amount of water. Results showed that one spray equated to ~1.3 ml of water, therefore four sprays were used in each set of blocks (full detail of results are found on the electronic appendix).

The chamber set of blocks experienced only the internal conditions within the environmental climate chamber rather than being subjected to extra weathering processes, such as microbial action or wetting.

Artificial rainwater was used as the chamber could not run at the high humidity levels required, so this water helped to achieve the correct RH for the experiment. Artificial rainwater was preferred rather than collected rainfall so that its elemental composition

could be precisely controlled (shown in Table 2-6), using a formula modified from (Wakefield et al., 1996).

Table 2-6: Chemical composition of artificial rain water.

Chemical	Moles	g per l
NaCl	0.28	16.4
$MgSO_4$	0.016	1.9
KNO_3	$8x10^{-3}$	0.8
$CaSO_4$	$8m10^{-3}$	1.1

Used in environmental chamber experiments.

Once the blocks were placed in the chamber, conditions were set to mimic summer and winter seasons. The chamber was set to simulate two weeks of summer and then two weeks of winter.

Summer and winter cycles were chosen as the predicted changes to these seasons are better constrained within the UKCIP02 report as changes to spring and autumn are often stated to be within "natural" variability. Therefore, using these seasons, allowed us to clearly observe the changes in the decay process due to seasonal conditions. Also, summer and winter were used so that the extremes of weathering within Glasgow could be identified.

Summer months were defined as June, July and August within the UKCIP02 report whilst winter months were defined as December, January and February. These will be the standard throughout this study.

The summer set up is shown in Table 2-7 and is repeated 14 times in each cycle. The winter set up again is run 14 times in each cycle and is shown in Table 2-8. The temperature reduction after six hours in both cycles was to compensate for the heat produced by the fluorescent tubes and incandescent lamps within the environmental chamber. The amount of light produced also varied by 25% from the centre (605.9 µmol m^2s^{-1}) to the back right corner (455.8 µmol m^2s^{-1}) of the chamber, which was measured using a hand held Macam Q203 Quantum Radiometer pyronometer.

Table 2-7: Environmental chamber set up for summer cycle.

Time	Temperature (°C)	Relative Humidity (%)	Light Setting
6 Hours	18.2	78.6	On
6 Hours	16.2	78.6	On
12 Hours	18.2	78.6	Off

Table 2-8: Environmental chamber set up for winter cycle.

Time	Temperature (°C)	Relative Humidity (%)	Light Setting
6 Hours	8	87.8	On
6 Hours	6	87.8	On
12 Hours	8	87.8	Off

Due to a breakdown of the environmental chamber from September 2008 to January 2009, the blocks were transferred to the University of Glasgow's Gregory building where they were placed in a laboratory on the 4th floor and faced a southerly directed window. This was to allow them to receive natural light whilst in a controlled environment. While being located at the University of Glasgow regular artificial rain continued to be sprayed on. Once returned to the chamber, to compensate for the reduction of time within the chamber, the cycles were shortened to ten days of summer and winter, to help maximise the amount of "years" the blocks experienced. The full cycle experienced by the sandstone blocks over the two year period are schematically represented in Figure 2-15. To monitor the actual temperature and RH that the blocks experienced throughout the whole experiment, an IButton datalogger (detailed latter in section 2.1.8) was kept with the blocks at all times to record these parameters on an hourly basis. A sample of the results from the IButton is shown in (Figure 2-16). A large range was seen in the recorded temperature and RH as the environmental chamber tries to regulate the conditions and establish an average.

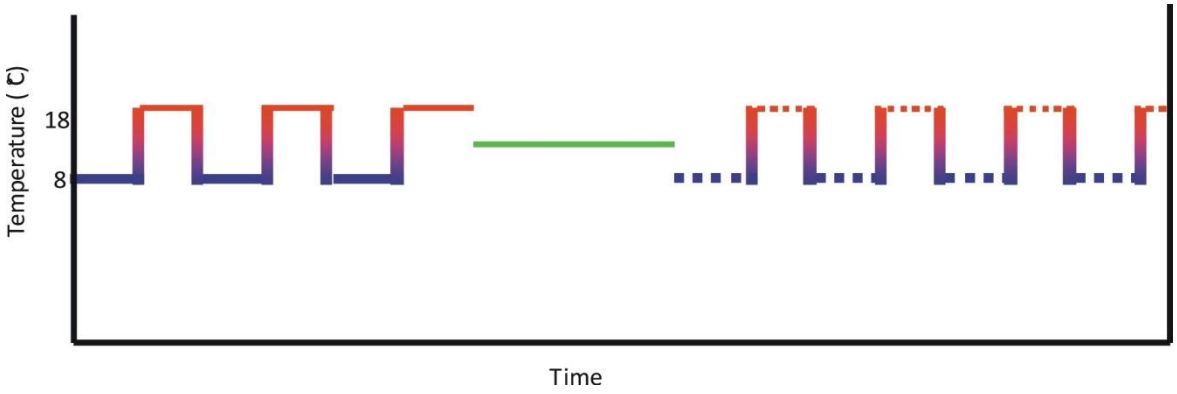

Figure 2-15: Sketch graph of cycles experienced by chamber blocks.

Blue) winter cycle, red) summer cycle, green) time out of chamber. Solid lines = two week cycles, dotted lines = 10 day cycle.

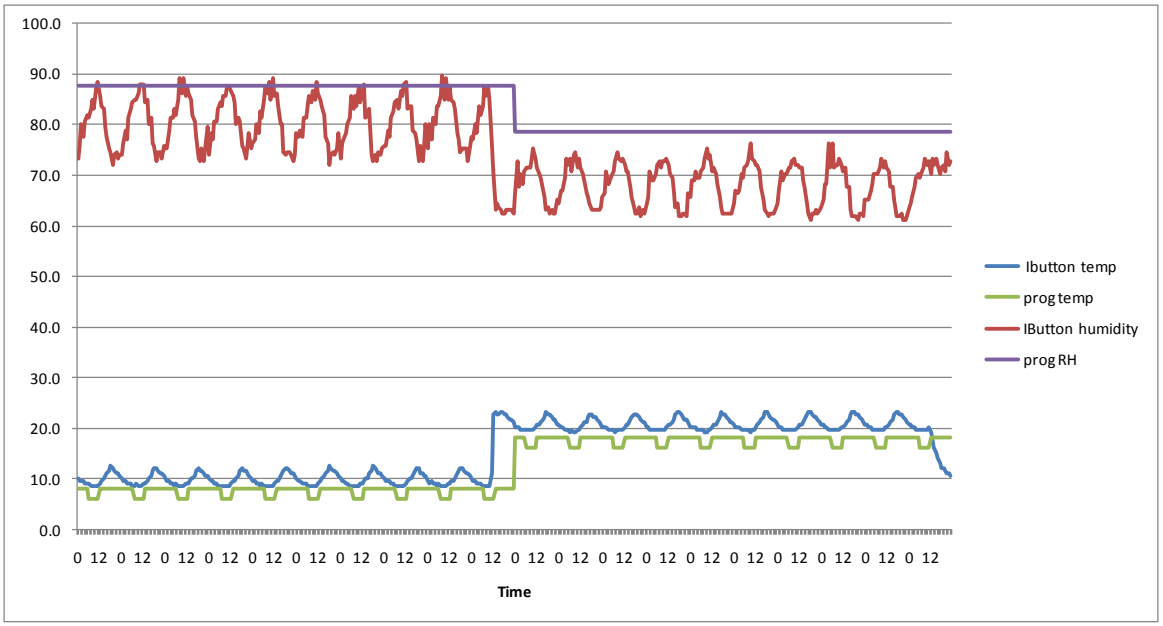

Figure 2-16: Data from environmental chamber showing the programmed conditions against data recorded by the IButton.

Graph shows a 10 day cycle of both summer and winter, Y-axis in °C for temperature and % for RH.

2.1.7.1 Prediction of Future Climate Conditions

The temperature and RH settings used in the climate chamber experiment were determined using the average present day values for summer and winter seasons. These data were derived from the archive data collected by the University of Glasgow weather station over the summer months of 2003-2007 and winter months of 2004-2007 to estimate the conditions experienced in the Glasgow area. Then, using the United Kingdom Climate Impacts Program 2002 (UKCIP02) report (Hulme et al., 2002) which outlined various emission paths and indicated how these scenarios may affect the climate. The outlined scenarios are: **low** (525 ppm CO_2 by 2080s), **low to medium** (562

ppm CO_2 by 2080s), **medium to high** (715 ppm CO_2 by 2080s) and **high** (810 ppm CO_2 by 2080s) (Table 2-9). More up-to-date predictions (UKCIP09 report) have been published but were not available when experiments for this study were designed. The UKCIP09 report is on a 25 Km grid plot, whereas the model from the UKCIP02 report is of comparatively poorer spatial resolution, (plotted on a 50 Km grid) but still sufficient for the needs of this study. The UKCIP02 calculations are reported on a map of the UK in a colour code fashion. The area used to represent Glasgow and the surrounding area is shown in Figure 2-17. Calculations presented later are based on the "medium to high" scenario, as this is believed to be the most likely (Anderson and Bows, 2008).

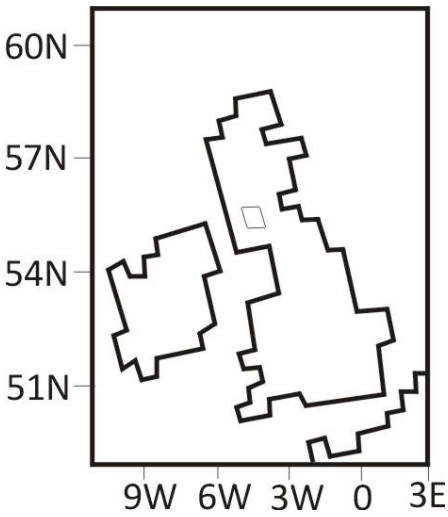

Figure 2-17: A replica of the UK maps used in the UKCIP02 report.
The grey square represents the area used to predict the Glasgow changes.

These average values for present day conditions were then extrapolated out using the data for the 2080 conditions in order to predict the climate of the Glasgow region in a medium-to-high scenario (Table 2-9). The year 2080 was used as this is the model limit that the UKCIP02 report covers.

Table 2-9: UKCIP02 report figures for the four climate change scenarios.

Scenario	2020s CO_2 (ppm)	2050s CO_2 (ppm)	2080s CO_2 (ppm)
Low Emissions	422	489	525
Medium-Low Emissions	422	489	562
Medium-High Emissions	435	551	715
High Emissions	437	593	810

Data retrieved from Hulme et al. (2002).

2.1.8 *Observatory Wall Microclimates*

This particular experiment was used to evaluate the microclimatic conditions within the sandstone. The parameters recorded were temperature and RH, in order to understand how they differ between the external conditions. The data collected could then be extrapolated and combined with climate predictions for 2080.

To enable this, test blocks (Figure 2-18) were erected at the University of Glasgow's Garscube complex at 55° 54' 8.29'' N, -4° 18' 25.93'' E (see Figure 1-12), where the experiments ran from May 2008 to April 2010. The blocks were placed at the Garscube complex so that the external condition in which the internal conditions were compared to were collected at the same site, less than 10 m away from the experiment.

Four different sandstone blocks were studied to evaluate how variations in porosity, grain size and building aspect may affect the heat and RH within the sandstones. The sandstones used were: 1) Dunhouse Buff, a very fine-grained sandstone with a porosity of ~16.5%; 2) Bearl, a very coarse-grained sandstone with a porosity of ~14%; 3) A Dalry primary school block with well established black crust. These were positioned to face south, whilst 4) Blaxter sandstone (similar in properties to Dunhouse Buff) was positioned to face north. IButton dataloggers were placed at depths of 3 mm and 6 mm below the stone surface, and were set to record both temperature and RH every hour on the hour. The north facing block only had one IButton embedded within it, at 6 mm depth. Whilst the Bearl, Dunhouse Buff and North block recordings were from a vertical facade, the recordings from the Dalry block were from an angled surface (Figure 2-18).

The Maxima IButton dataloggers are 5 mm thick and 17 mm in diameter (Figure 2-19). Each IButton has a data contact (called the 'lid') and a ground contact (called the 'base'), which are connected to the silicon chip inside. The lid is the top of the datalogger and the base forms the sides and the bottom of the datalogger. Data are stored and then downloaded from the IButton manually, using a PC 1-wire connection, which has a USB port attached to an IButton port, from which the stored information can then be transferred to the computer. Before being secured into the sandstone, the accuracy of the IButtons was calibrated over a 24 hour period. During this time, all IButtons were left within a laboratory to record the temperature and RH on a 10 min interval and

demonstrated the precision between IButtons. The temperature readings had a standard deviation of 0.2°C, whilst the manufacturers state an accuracy of 0.5°C. RH readings had a standard deviation of 0.6%, however the manufactures guidelines state that they should have accuracy within 5%. To embed the logger into the sandstone block a small hollow was drilled into the surface of the sandstone to a known depth and marginally wider than the IButton. The IButtons were then placed into the hollow with the 'lid' facing outwards and then a stone cap (taken from the original core) was placed over the hollow and grouted into place using Polycell weather proof polyfilla to form a secure seal while trying to minimise the alterations to the sandstone properties.

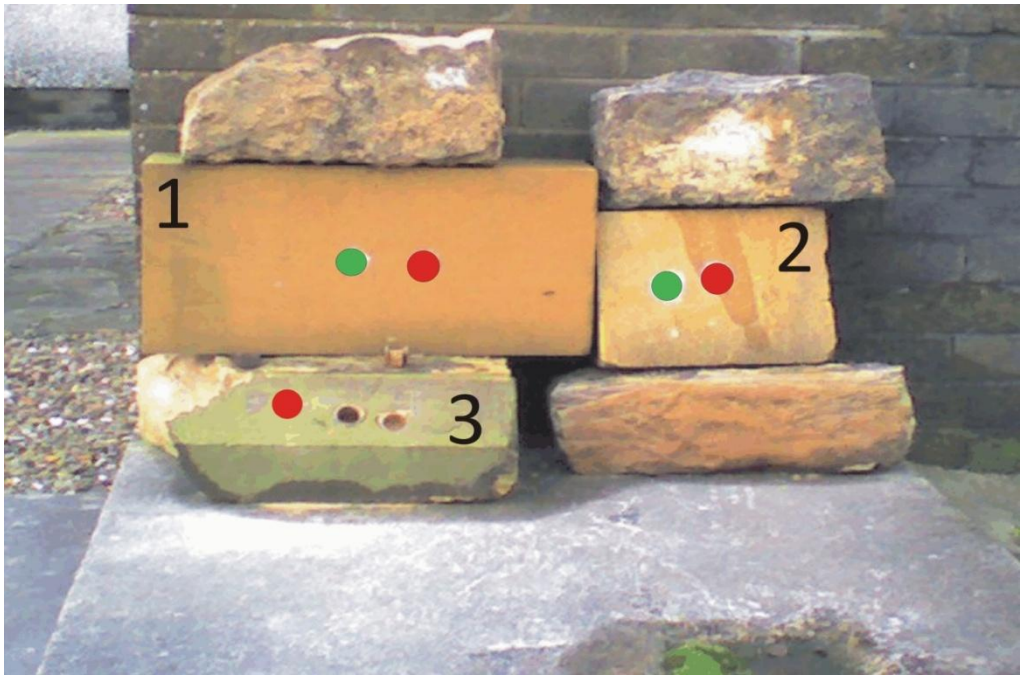

Figure 2-18: Test blocks situated at Garscube campus (University of Glasgow).

1) Dunhouse Buff, 2) Bearl, 3) Dalry primary school block (unknown sandstone), green circles = 3 mm depth IButton, red circles = 6 mm depth IButton.

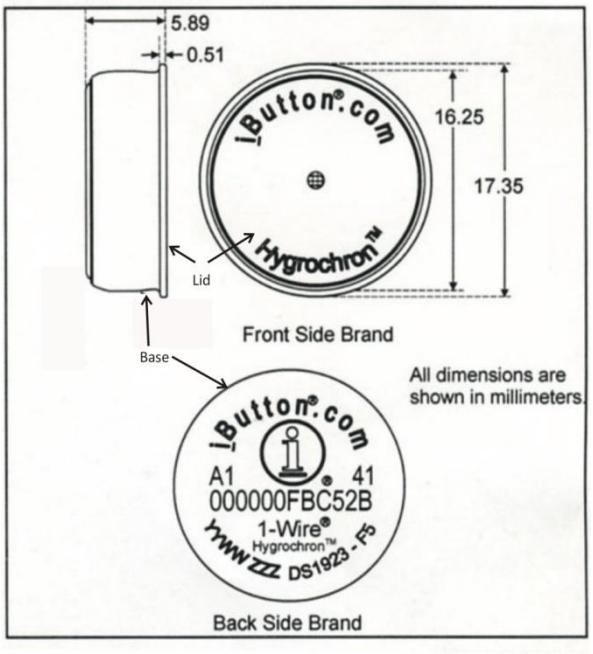

Figure 2-19: IButton dimensions.
A modified sketch of the IButtons taken from the manufacture guidelines.

2.1.9 *Thermal Imaging*

Thermal imaging cameras are often used as a non-invasive data collection technique on historic buildings, to gather information on the physiochemical behaviour of conservation treatments such as stone cleaning and repair mortars (Avdelidis and Moropoulou, 2003a) and also to monitor heat flow through building materials (Griffith and Arasteh, 1999). Thermal imaging in this instance is used to determine exact stone surface temperatures to correlate with the internal data. This provides spatially and temporally accurate data on the surface of the sandstones. Temperature measurements of the stone surfaces were collected on both a representative summer and winter day. An image of each sandstone block (Bearl, Dunhouse Buff and Dalry sandstones) was taken on the hour between 9 am and 4 pm to correlate with the data being collected by the IButtons; images were captured using a Flir ThermaCam B400. The Flir ThermaCam B400 has a thermal sensitivity of <0.05°C and an IR resolution of 320 X 240 pixels.

The value set for the emissivity is very important to gain accurate and correct results (Avdelidis and Moropoulou, 2003b). As the emissivity is the ability of a surface to emit radiant energy compared to that of a black body at the same temperature with the same area, this emitted heat value has to be therefore compensated for so that accurate

surface temperatures can be gained. As only one material was being imaged this matter was simplified and a value of 0.9 was used for the sandstones.

2.1.10 *Calibration of Decagon Dataloggers*

To test whether free water was trapped within stone, Decagon Leaf Wetness Sensors were used. Leaf Wetness Sensors (LWS) measure only the amount of free water on the sensor (rather than RH for the IButtons). The LWS was originally designed to measure water densities on leaves for botany research and therefore has dimensions similar to leaves (Figure 2-20). However, here they were used to measure free water whilst encased within sandstone.

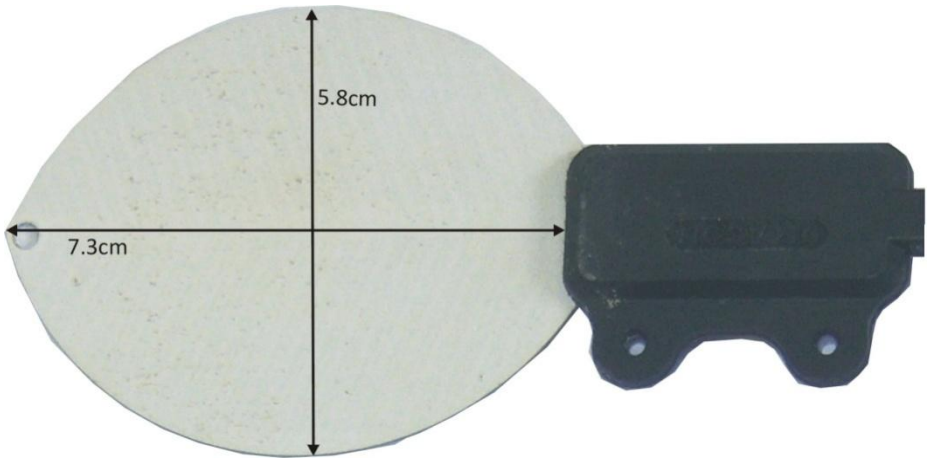

Figure 2-20: Image of leaf wetness sensor with dimensions (actual size).

As the LWS loggers had not been constructed for use in sandstone, instead for use in exposed natural environments, they had to be calibrated specially for this purpose.

To calibrate and deduce the errors on the LWS, a beaker was filled with sand and the two LWS sensors (LWS1 and LWS2) were placed within the sand. 10 ml of water was then added at five minute intervals until 100 ml of water had been added in total. This experiment was run three times to ensure reproducibility. The procedure was then repeated but the time interval between water addition was increased to ten minutes and again run three times. The minimum and maximum counts in which the LSW records were also tested. Between each test, the sand was oven dried for a minimum of five hours at temperatures between 47 and 50°C. These calibration experiments revealed

that LWS2 recorded at a slightly elevated level compared to LWS1 (for 100 ml of water LWS1 recorded 692 counts whilst LWS2 recorded 773 counts). Over the three five minute tests the error in LWS1 ranged from 9.4-18.2 counts which is smaller than the error range in LWS2 (2.3-30.1 counts) (Figure 2-21 andFigure 2-22). The minimum count was 445 when recording in air and 1023 counts when submerged in water, these are in accordance with the manufactures guidelines. The calibration graph for LSW1 is shown in Figure 2-23, showing a confident R^2 value of 0.95.

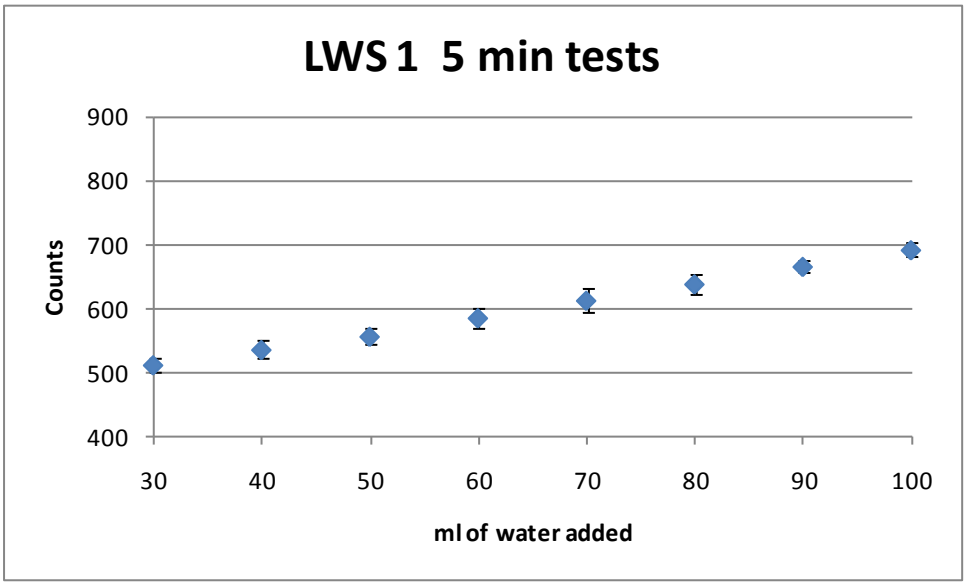

Figure 2-21: Calibration graph for LWS1.
Where 10 ml of water was added every five minutes, with error bars.

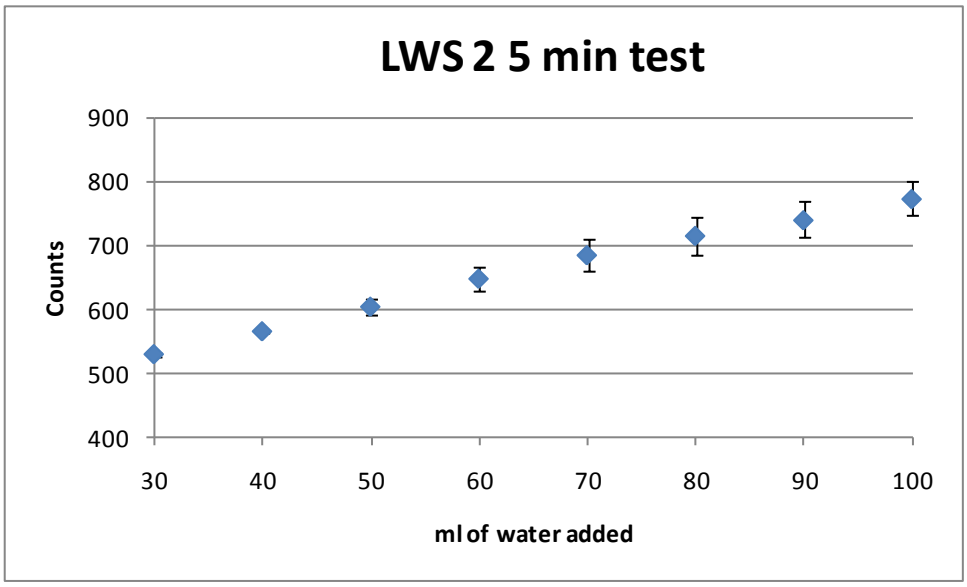

Figure 2-22: Calibration graph for LWS2.
10 ml of water was added every five minutes, with error bars.

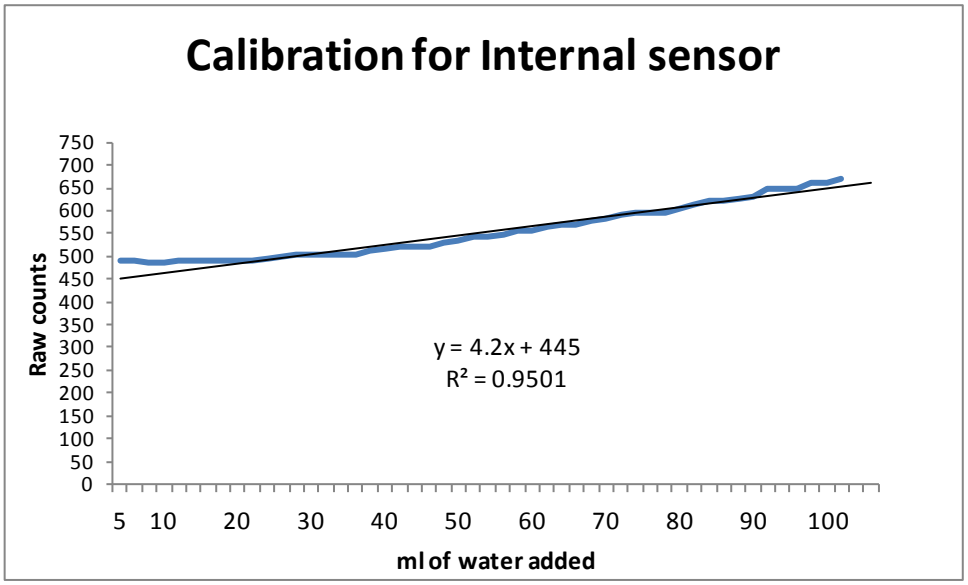

Figure 2-23: Calibration graph used for LWS1.

2.1.11 *Internal Moisture Experiments*

Blaxter sandstone was used in this experiment (full mineralogical details found in section 2.2.5.2).

The block was 9x15x17 cm in size and the sensors were placed into a notch 0.5 wide was cut 6 mm from the vertical face of the block.

The sides of the notch were then sealed using a waterproof silicon sealant. The sensor LWS1 was placed as close to the front of the notch as possible.

The sandstone sliver originally cut from the block was ground to form sand and it was this material which was compacted around the sensors and then the top was also sealed with silicon sealant to ensure it was watertight (Figure 2-24). Although some sand will have come between the sandstone and sensor this was restricted as much as possible so that the sand grains did not affect the properties of the sandstone, as the sand grains will have a different affect on the capillary action of the water.

The experiment was placed at the University of Glasgow's observatory beside the observatory microclimate experiment (section 2.1.8), with stones surrounding all sides so that only the vertical face was directly exposed, to try and mimic the outermost surface of a building facade.

LWS2 was placed unprotected at the University of Glasgow's observatory facing the same direction so that comparisons could be made between the external and the internal sensor readings.

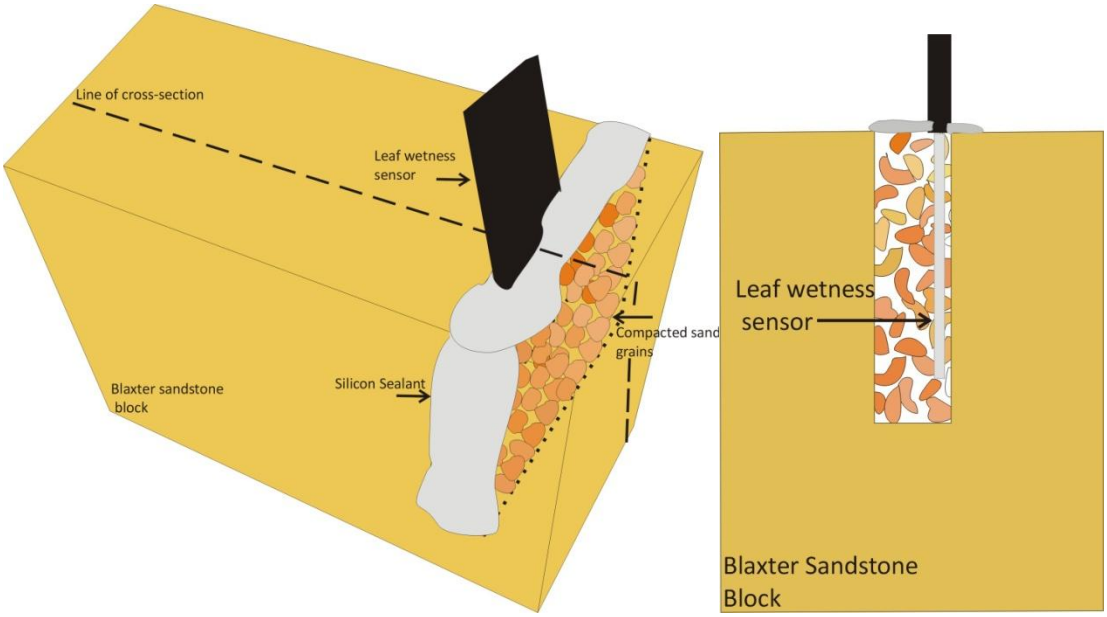

Figure 2-24: Apparatus set up for internal free water experiments.

Left) is a sketch diagram of the internal free water block set, Right) cross-section images along indicated line.

2.1.12 *Mitigation Experiments*

With the weathering damage increasingly visible on sandstone, many conservation companies are now designing products that they suggested will increase the life of masonry. One of the most common mitigation products are water repellents for masonry. Therefore, tests were conducted on some of the sandstone water proofing sealants available. These were: Kingfisher Extreme Climate - Next Generation Water Seal and Thompson's water seal. These were painted on blocks of the Scotch Buff sandstone (quartz = 77% and porosity =21%) in accordance to the manufacturers instructions. A blue dye was dissolved into each sealant so that the flow of sealant could be tracked under the microscope when thin sections were prepared, which has a standard procedure (Casadio and Toniolo, 2004; Cnudde et al., 2007). The dissolution of the blue stain crystals was examined before being applied to the sandstone to make sure that its presence would not affect the viscosity of the sealant. One coat of water repellent was applied onto the vertical surface of the sandstone and left to dry. A cross section from

both the top and bottom of the vertical block was then made into a thin section so that depth of penetration could be observed.

Un-dyed Kingfisher sealant was also applied to the Bearl and Dunhouse Buff sandstone blocks situated at the observatory, to avoid changing the characteristics of the sandstone to much. Sealant was applied in accordance to the manufacturers instructions in April 2010 and the experiment ran until October 2010. Therefore, prior to application, the blocks were taken inside and dried out for a week to remove excess moisture and then the dust and dirt particles were cleaned off the surface to which the sealant was being applied. As the IButtons within these blocks have established well defined temperature and RH patterns over the previous two years, any changes within these patterns will therefore be due to the presence of the water sealant on the surface.

2.2 Background to all Sandstone Samples

Within this section, an overview of all the samples used during this project will be supplied. In addition the location of the building studied or the quarry location will be given (shown in Figure 2-25).

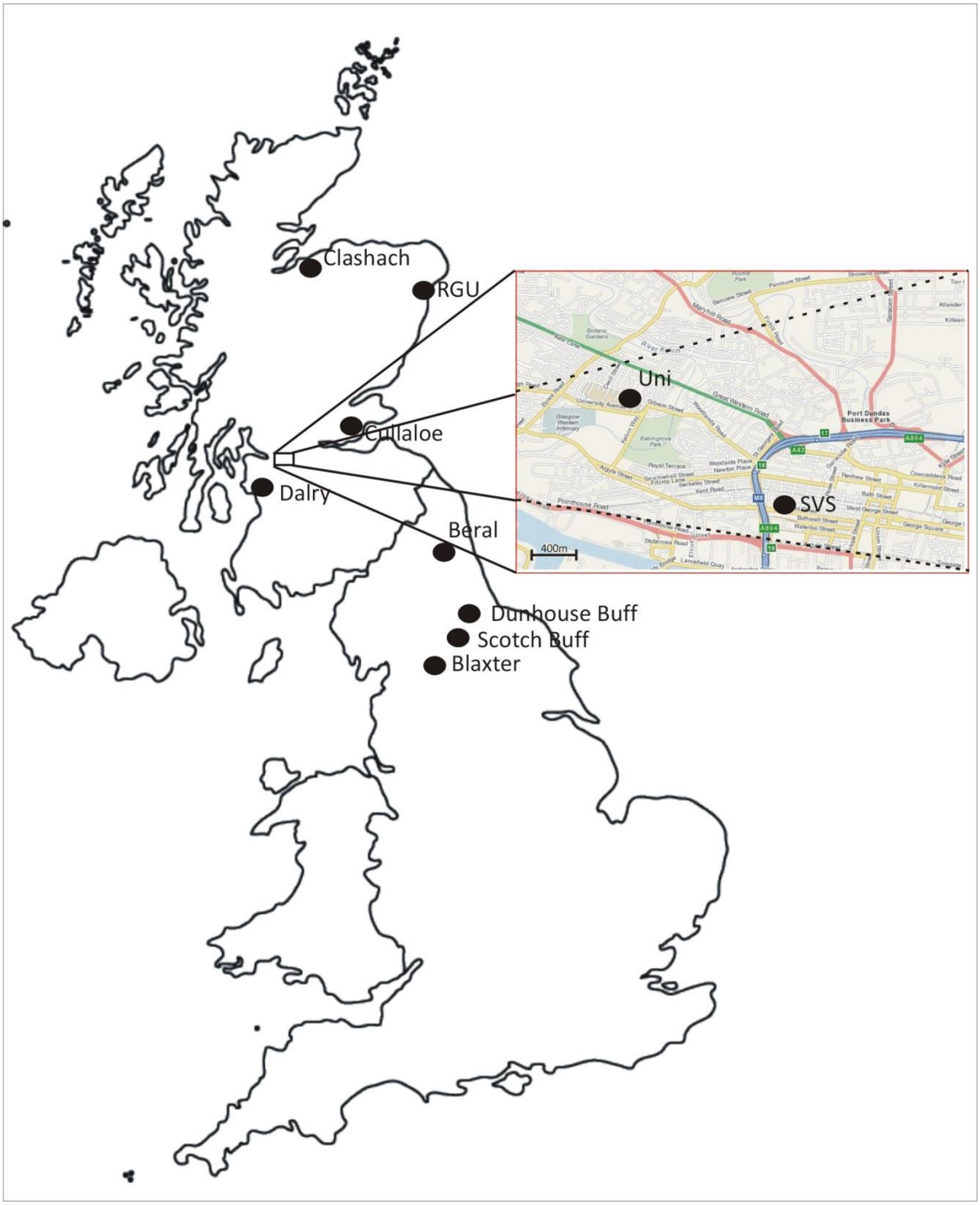

Figure 2-25: Location of the buildings and quarry's of the sandstone samples used in this study.

Within enlarged map of Glasgow region: Uni = University location; SVS = St Vincent Street location.

2.2.1 *Dalry Samples*

The Dalry samples were obtained from a disused primary school on Sharon Street located in the village of Dalry, 25 miles south west of Glasgow (Figure 2-25). Given the location of the village and the low through-flow of traffic (Figure 2-26), the sandstones here are

presently experiencing low levels of pollution, although, from the 1840's to 1980's coal mining was common in the area. This building was constructed in 1863 and sampled for this study in 2007, prior to its demolition, meaning the sandstones had been exposed for approximately 145 years. Cores with a 6 cm diameter and 7-8 cm depth were acquired using a 110v Makita electric drill in dry conditions, and were taken from both the northeast facing facade (Figure 2-27) and southeast facade (Figure 2-28). Sampling strategies were focussed on the four main weathering types observed on multiple sides of the building (Table 2-10). The whitened zones were areas which seemed to have been kept clean, due to run-off water flowing over the surface. The vertical surface of the sills was tested as they had an easily visible dark greenish surface. Cores were taken from a sandstone block which had suffered general weathering. The mullions were tested as they had a uniform block colouration over their surface.

The sandstone used in construction is currently unidentified, although a variety of local lithologies may have been used.

Table 2-10: Weathering zone type and corresponding sample identification for Dalry School.

Weathering Zone	NE Facade	SE Facade
Whitened zone	D1	D7
Sills	D2	D5
General black weathering	D3	D6
Mullion	D4	D8

Figure 2-26: Google satellite image of Dalry village.

Plan view of Dalry with the primary school located in the centre of image.

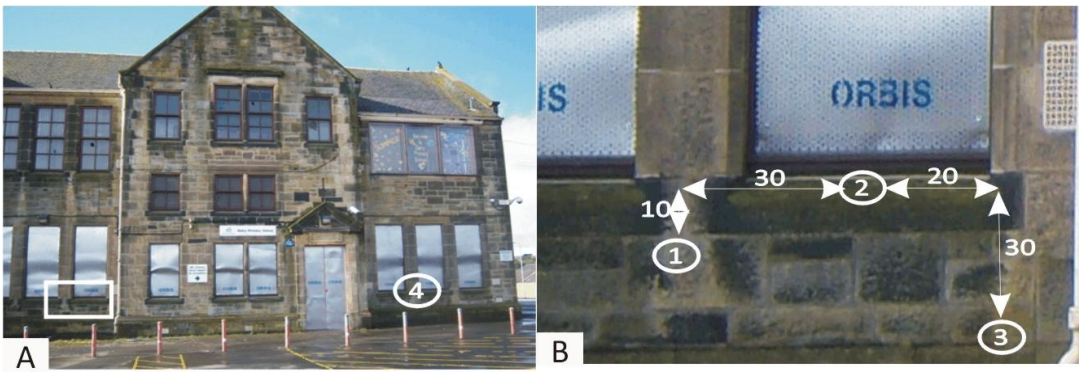

Figure 2-27: Northeast facing facade of Dalry school.

A) Whole of the northeast facing facade front of building. White rectangle shows area of (B). B) Location of cores 1-3, dimensions in centimetres. Circled numbers represent from where cores were taken. Core 2 was taken from the vertical surface of the sill.

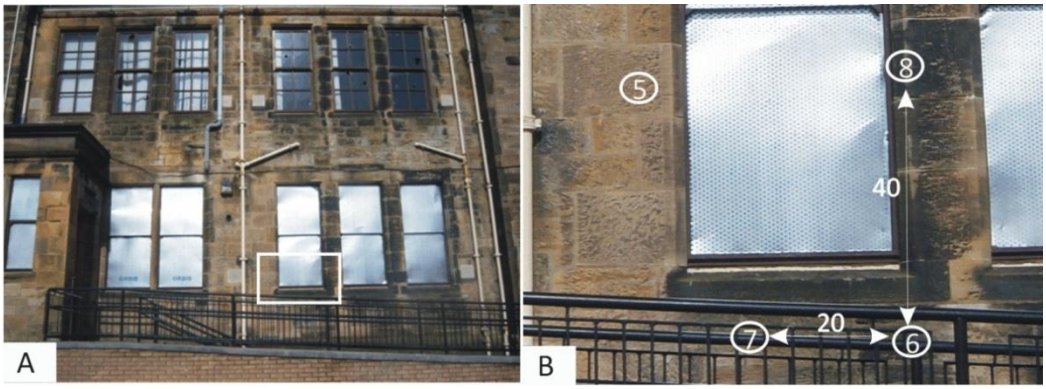

Figure 2-28: Southeast facing facade of Dalry school.

A) Whole of the southeast facing facade front of building. White rectangle shows area of (B). B) Location of cores 5-8. Dimensions in centimetres. Circled numbers represent from where cores were taken on the wall behind the railing.

2.2.2 *RGU Samples*

The "RGU" samples were obtained from test walls built on the Garthdee campus of the Robert Gordon University (RGU), Aberdeen (Figure 2-25). The test walls are located within a courtyard area (Figure 2-29) and are south facing. Due to their semi-enclosed location, the samples have experienced little direct traffic pollution whilst also being sheltered from the full force of the weather. Five test walls were constructed in 1997, through a partnership between RGU and Historic Scotland. Four of these walls are to assess the effectiveness of various consolidates and water repellents whilst the fifth wall is used as a control; samples were therefore obtained from this fifth "control" wall. The walls are built from a variety of sandstones and granites frequently used as replacement stones throughout Scotland (Figure 2-30). Core samples were taken from six rock types on the 26th of March 2009, using a 110v Makita electric drill with a 6 cm diameter diamond tipped core bit to a depth of 7-8 cm in dry conditions. The core collected were Leoch granite, Cat Castle Sandstone, Stainton Sandstone, Locharbriggs Sandstone, Unknown Stirling Sandstone and Clashach Sandstone. However, the blond sandstone samples were predominantly used in the experiments.

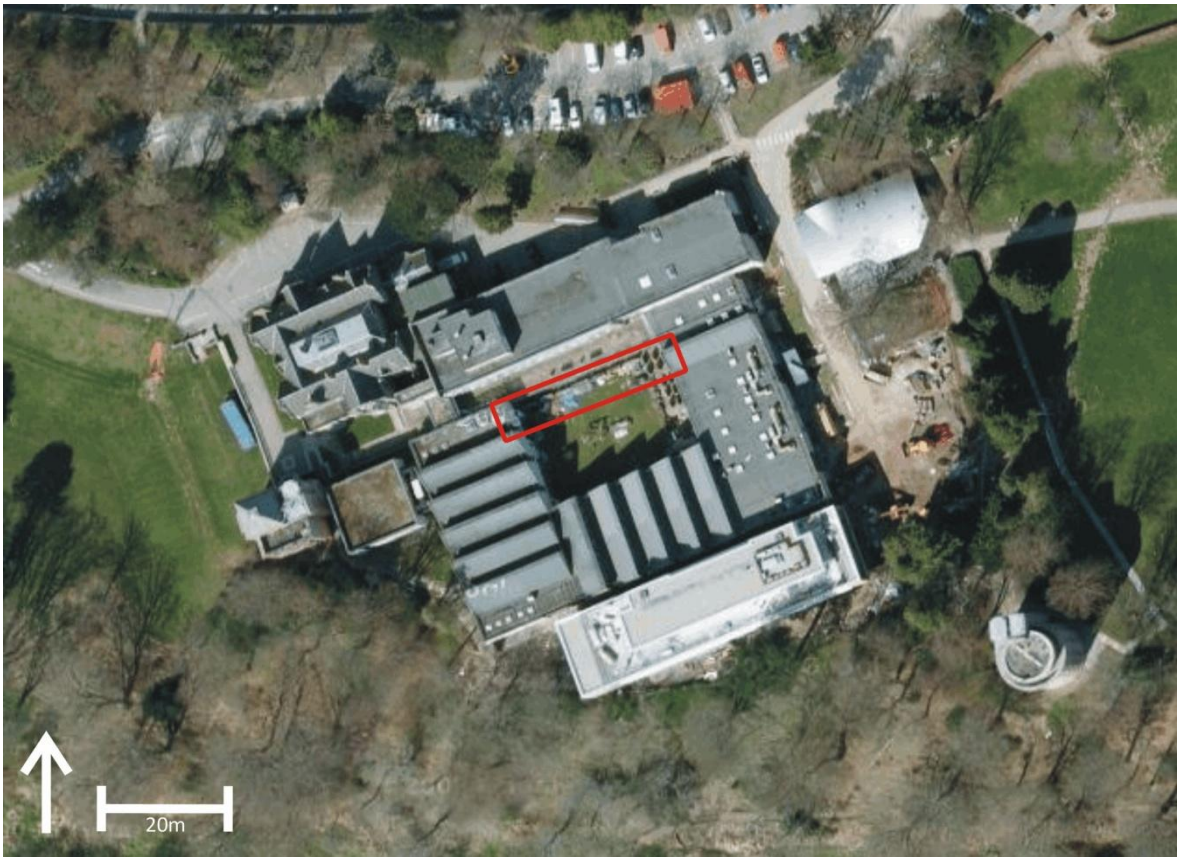

Figure 2-29: Google satellite image of Garthdee campus of RGU.

RGU samples taken from the test walls located within red rectangle.

Figure 2-30: Image of test wall situated at RGU.

1) Leoch granite, 2) Cat Castle Sandstone, 3) Stainton Sandstone, 4) Locharbriggs Sandstone, 5) Unknown Stirling Sandstone, 6) Clashach Sandstone.

2.2.3 *University Samples*

South Park Terrace was built in 1862, meaning the samples had been in place for 147 years before being sampled in 2009. The building is located on South Park avenue (Figure 2-31), within the main Gilmorehill campus of the University of Glasgow in the west end of Glasgow (Figure 2-25). Built in a renaissance style, they were originally used as three-storey housing before being converted into university offices in 1984. The stone type and origin used in the construction are unknown at present. Samples were taken during stone replacement work from the east-south-east and north-north- east face's of the building (Figure 2-32, Table 2-11). At present, traffic emissions within the area are at a medium level due to the location in the centre of the campus. However, the building may have been subjected to pollution from the heavy industry in Glasgow during the 1900's. The exact location of the sample retrieval is unknown but, the location of the fresh replacement blocks (as seen in Figure 2-32) suggests they are most likely from both sills and mullions, at heights above ground level, exceeding 2 m.

Table 2-11: Facade where sample was collected from and sample identification.

East-South-East facade	North-North-East facade
UN1	UE1
UN2	UE2
UN3	UE3
	UE4

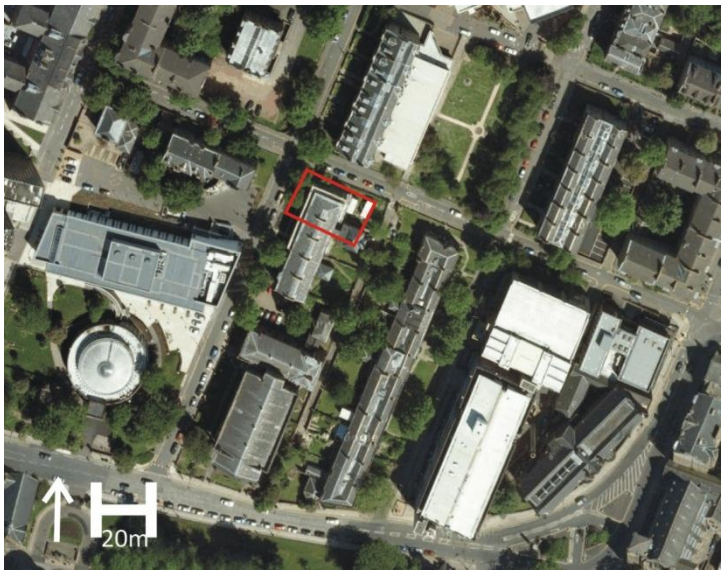

Figure 2-31: Google satellite image of South Park Terrace.
Red box indicates sample building.

Figure 2-32: Image of South Park Terrace.
East south east (ESE) and North north east (NNW) facades post-stone replacement.

2.2.4 *St Vincent Street Samples (SVS)*

The St Vincent Street (SVS) samples came from the Free Church of Scotland on St Vincent Street, Glasgow, which is a major route through the city centre, leading towards the M8 motorway (Figure 2-34). The church is located at the west end of the street (Figure 2-25). Traffic pollution within this region is high at present (Kent et al., 2010) and has been in the vicinity of heavy industry (e.g. steelworks and coal mining) in the recent past (200-100 years ago). The church was built in 1859 by Alexander Thomson and sampled in 2009, 150 years later. The building style is based on his personal interpretation of Greek revival (Figure 2-33) and was constructed using Giffnock sandstone, known through his investments into the quarry. Samples were taken from the east elevation (EE numbered samples) and the northwest corner (CS (corner section) numbered samples) during conservation work (Figure 2-34). Exact locations for each sample are unknown; all that is known is that the samples were taken from the upper regions of the church and some samples are associated with surface mortar repairs.

Figure 2-33: Image of St Vincent Street church.

Image taken from the south west, viewing both the north and west facing facades of the building.

Figure 2-34: Google satellite image of St Vincent Street church.

Church is located (within large white rectangle), white triangle) CS sample, white rectangle) EE samples.

2.2.5 *Replacement Samples*

Fresh, unweathered sandstones were used in a variety of experiments within the study, such as the environmental chamber and in datalogging experiments. Fresh sandstones were also used to evaluate the impact of climate change on the sandstone's weathering characteristics and for predicting how they might perform if used as a replacement stone. The sample set contains six of the most common replacement stones used in the Glasgow region, and each was characterised by point counting using the SEM. These sandstones are:

2.2.5.1 Bearl

Bearl is quarried in Stockfield, Northumberland (Figure 2-25); is a medium-grained Carboniferous sandstone (Figure 2-35A) and has a porosity of ~14% (Table 2-12). This sandstone is moderately sorted and contains a significant proportion of kaolinite, mica and K-feldspar, and the quartz grains are rounded. The feldspar grains show partial dissolution and the kaolinite pre-dates any quartz overgrowths observed (Figure 2-35B).

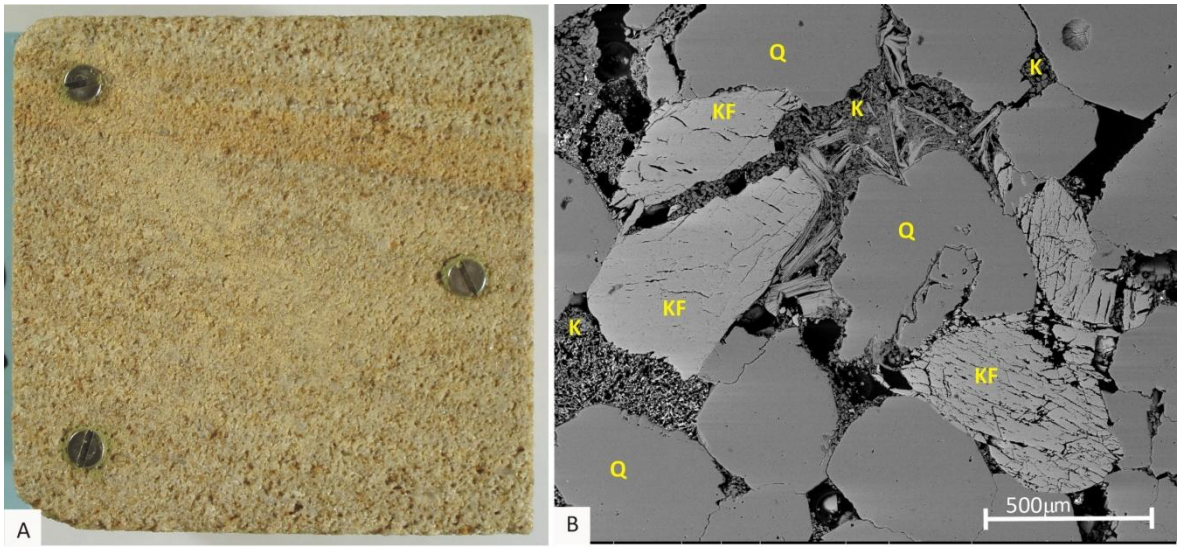

Figure 2-35: Images of Bearl sandstone.

A) Image of hand specimen 9x9 cm, B) FEG-SEM BSE overview image at 150 magnification. Q = quartz grains, KF = K-feldspar grains, K = kaolinite.

2.2.5.2 Blaxter

The Blaxter sandstone is quarried in Otterburn, Northumberland (Figure 2-25) and is Lower Carboniferous in age with a fine-medium grained texture. Porosity is generally

quite low in this sample, ~12% (Table 2-12). Blaxter is poorly sorted, containing significant volumes of kaolinite, mica and K-feldspar. The quartz grains are sub-angular with well developed overgrowths. The K-feldspar grains in this sample are fresh and show minimal alteration, while many iron oxides are present giving it a soft yellow colouration in hand specimen (Figure 2-36A and B).

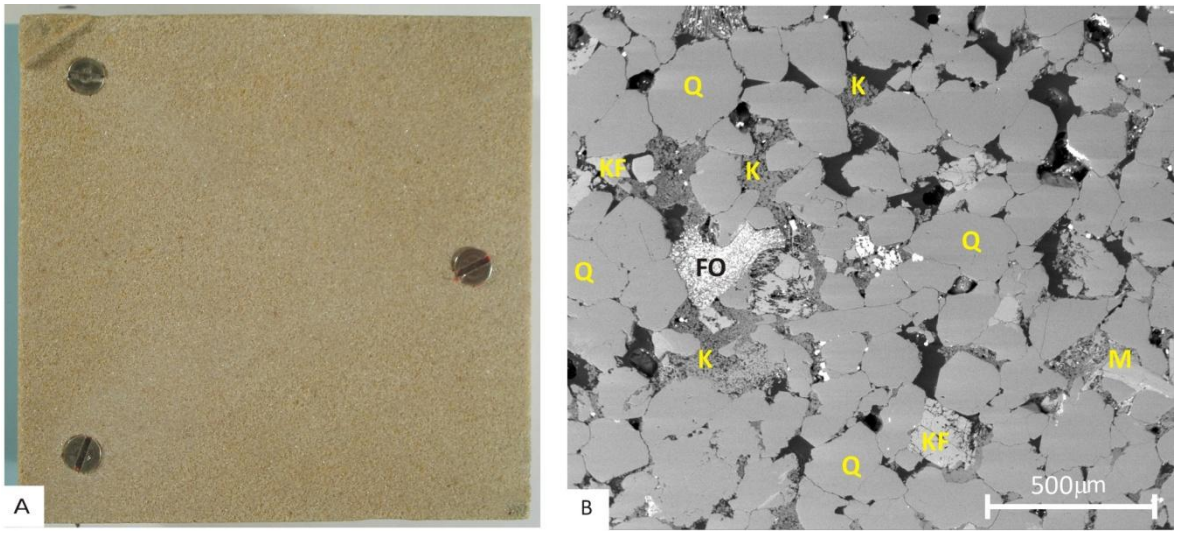

Figure 2-36: Images of Blaxter sandstone.

A) Image of hand specimen 9x9 cm, B) FEG-SEM BSE overview image at 150 magnification. Q = quartz grains, KF = K-feldspar grains, FO = Fe-Oxides, K = kaolinite grains, M = Muscovite.

2.2.5.3 Clashach

Clashach sandstone is quarried from the Moray Firth coast (Figure 2-25), is Permian in age and medium-grained. This sample has high porosity values: up to 19.8% (Table 2-12). This sample has relatively low quantities of feldspar, mica and iron oxides, therefore meaning that Clashach is very clean and a well sorted sandstone. Both the quartz and feldspar crystals show coarse overgrowths making the grains sub-rounded (Figure 2-37A and B).

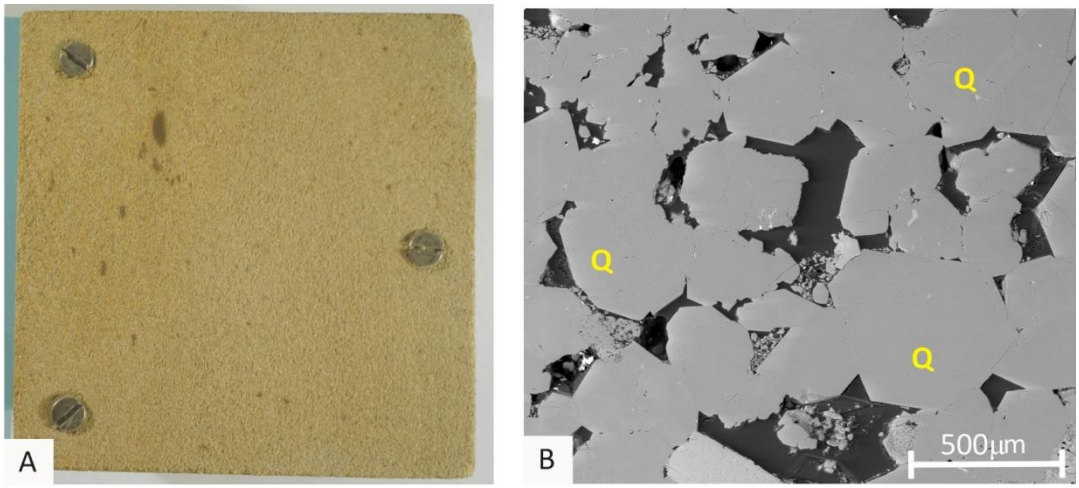

Figure 2-37: Images of Clashach sandstone.

A) Images of hand specimen 9x9 cm, B) FEG-SEM BSE overview image at 150 magnification. Q = quartz grains.

2.2.5.4 Cullalo

Cullalo is a Carboniferous sandstone quarried at Burntisland, Fife, and has a very fine-grained texture. This sandstone is very well sorted with trace amounts of fine-grained kaolinite (Figure 2-38), whilst the quartz grains are also well rounded. The low proportions of iron oxides, gives the sandstone a cream colour (Figure 2-38).

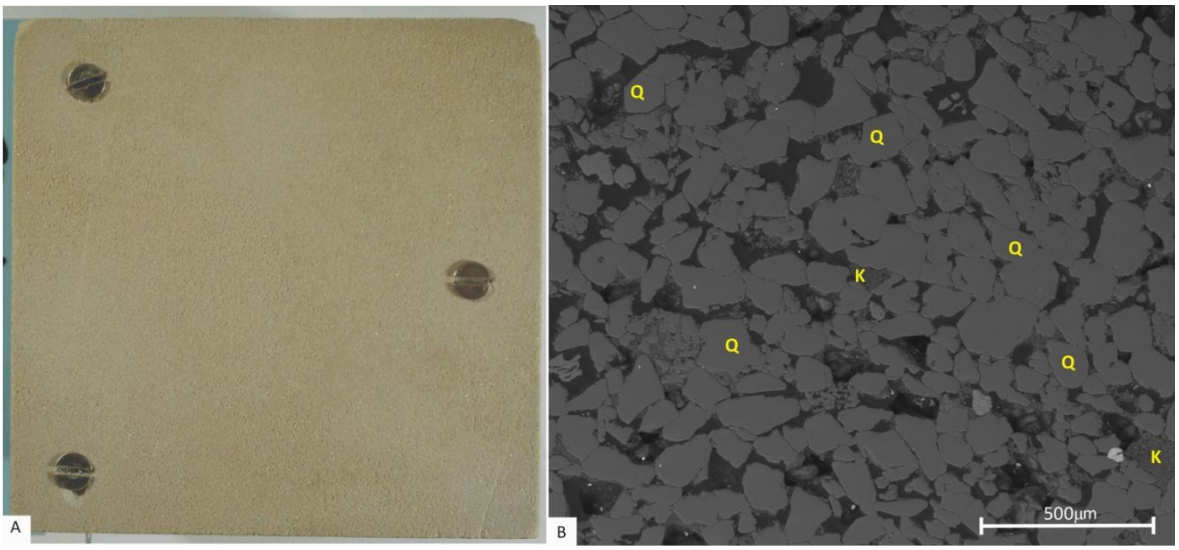

Figure 2-38: Images of Cullalo sandstone.

A) Images of hand specimen 9x9 cm, B) FEG-SEM BSE overview image at 150 magnification. Q = quartz grains, K = kaolinite.

2.2.5.5 Dunhouse Buff

Dunhouse Buff is quarried in Darlington (Figure 2-25), is Carboniferous in age is a fine-grained, well sorted sandstone. Dunhouse Buff has a mean porosity of ~16.5% (Table 2-12) and the sub-rounded quartz grains have well developed overgrowths. Both the K-feldspar and mica grains present have undergone dissolution. There is a significant quantity of goethite which gives the stone an orange buff colour (Figure 2-39).

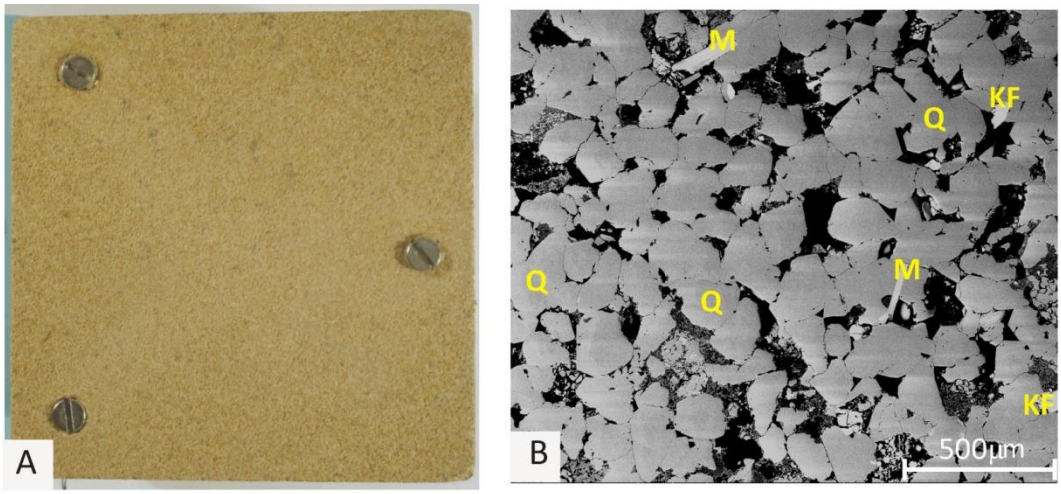

Figure 2-39: Images of Dunhouse Buff sandstone.

A) Image of hand specimen 9x9 cm, B) FEG-SEM BSE overview image at 150 magnification. Q = quartz grains, KF = K-feldspar grains, M = Muscovite.

2.2.5.6 Scotch Buff

Scotch Buff sandstone is quarried near Scotch Corner in Richmondshire (Figure 2-25), is of Carboniferous age and medium-grained. It has a very pure, well sorted mineralogy, containing only well rounded quartz and kaolinite (Figure 2-40) but with a high porosity of ~20% (Table 2-12).

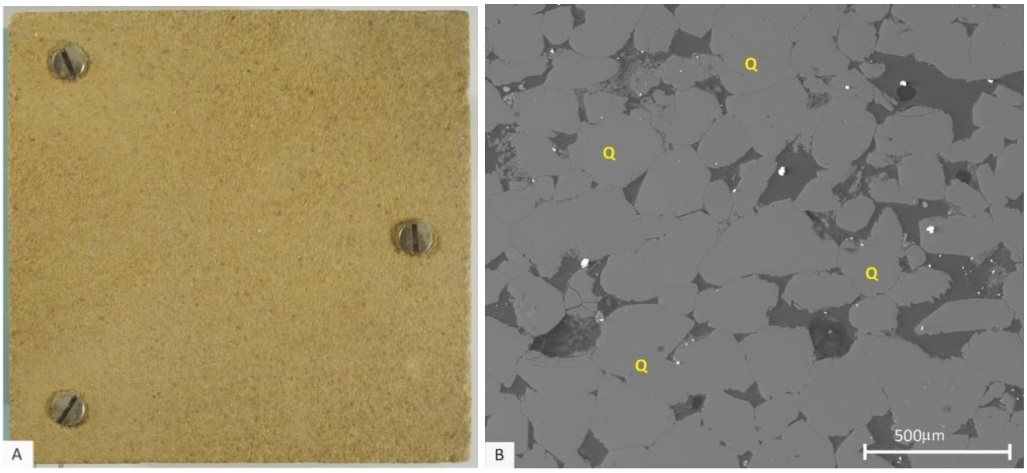

Figure 2-40: Images of Scotch Buff sandstone.

A) Image of hand specimen 9x9cm, B) FEG-SEM BSE overview image at 150 magnification.

Q = quartz grains.

Table 2-12: Mineralogical properties for the replacement sandstone.

Mineral	Bearl (%)	Blaxter (%)	Clashach (%)	Cullalo (%)	Dunhouse Buff (%)	Scotch Buff (%)
Quartz	71.0	69.9	72.8	83.1	70.0	77.0
Porosity	14.3	11.9	19.8	13.5	16.5	20.7
Kaolinite	7.8	7.7	4.3	--	5.0	2.1
Mica	1.4	3.1	--	--	1.7	--
K-feldspar	4.6	4.7	1.2	3.5	4.5	--
Fe-oxide	1.0	2.1	1.6	--	1.7	--
Total Points	217	193	257	261	242	280

Values determined by SEM point counting, -- denotes when mineral is not present.

3 Description of External Crust and the Structure of Weathering Layers

Buildings constructed from sandstone are often found with coatings and accretions, which mar the surface; the outermost layer has been classified as the crust layer within this study. However, these crusts on the outermost surface are only one layer in the weathering profile, and therefore a cross-sectional view has to be examined. Four questions relating to the crust and internal layering were posed:

- What is the composition and origin of the crust?
- Is there any stratigraphy to the internal structure?
- How long do these crusts and layers take to form?
- Are the crusts having a positive (protective) affect or negative (damaging) affect?

These questions will be answered using cross-sectional views under light microscopy, which was undertaken on all samples to examine the thickness of the surface crust and to identify any other layers and structures formed within the sandstone at depth. For all samples, an in-depth analysis was undertaken by examining rough crust surfaces of the samples in low vacuum conditions, using the FEG-SEM as well as BSE imaging of polished blocks.

3.1 Dalry School

3.1.1 *Light Microscope Observations.*

The Dalry polished block samples were viewed under an Olympus SZX7 light microscope, which showed that over half of the samples have a dark weathered crust on the surface (Figure 3-1B, C, D, E, F and H). In most circumstances they are very thin (<10 µm), however D4 exhibits a 1 mm thick crust. The stones in Figure 3-1A and G have a very light coloured outermost surface in comparison to the other samples. Weathering profiles are difficult to define visually, although D2 and D4 (Figure 3-1B and D) are the only samples to have a light weathered zone (layer 1) beneath its outer surface, presumably caused by a depletion of iron oxides. D7 (Figure 3-1G) is the only sample with a thick red layer (layer 2) beneath the crust, which is presumably an iron oxide rich layer.

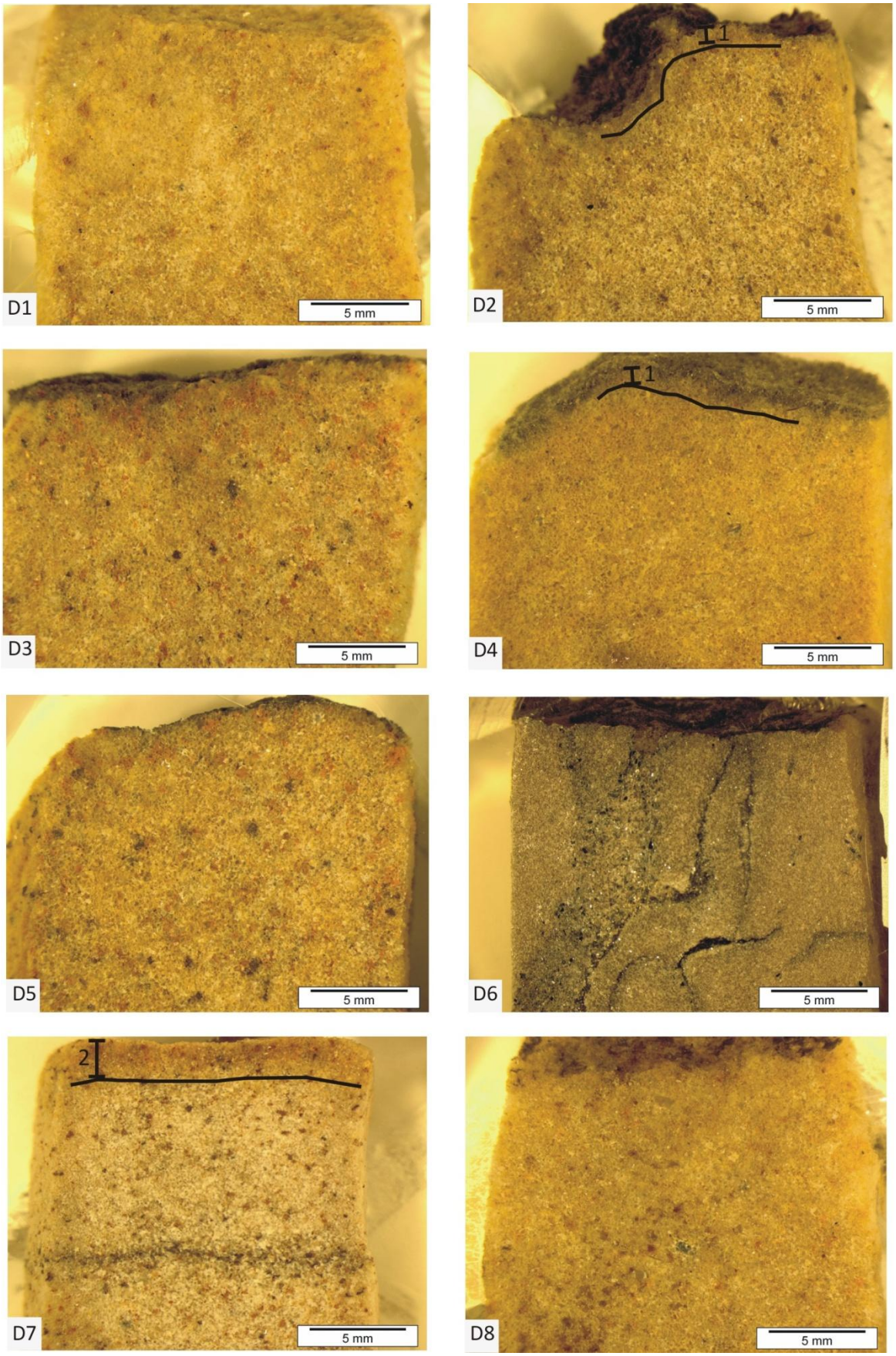

Figure 3-1: Light microscope images of Dalry school polished block samples.

Outermost surface of each block is at the top of each image. 1 = bleached layer, 2 = rusty red layer. Black line denotes the separation between layers.

3.1.2 *SEM Imaging of Outer Surface*

FEG-SEM analyses of rough samples of the outermost stone surface as well as polished blocks were conducted. Samples D1-D4, D6 and D7 have ordinary black accretions which, in these samples, are dominated by mineral fragments littering the surface and infilling depressions (Figure 3-2). These are combined with possible atmospheric debris which produces the black coloration. No salt crystals were seen however, as the fine nature of this debris may have hindered visual identification of any salt.

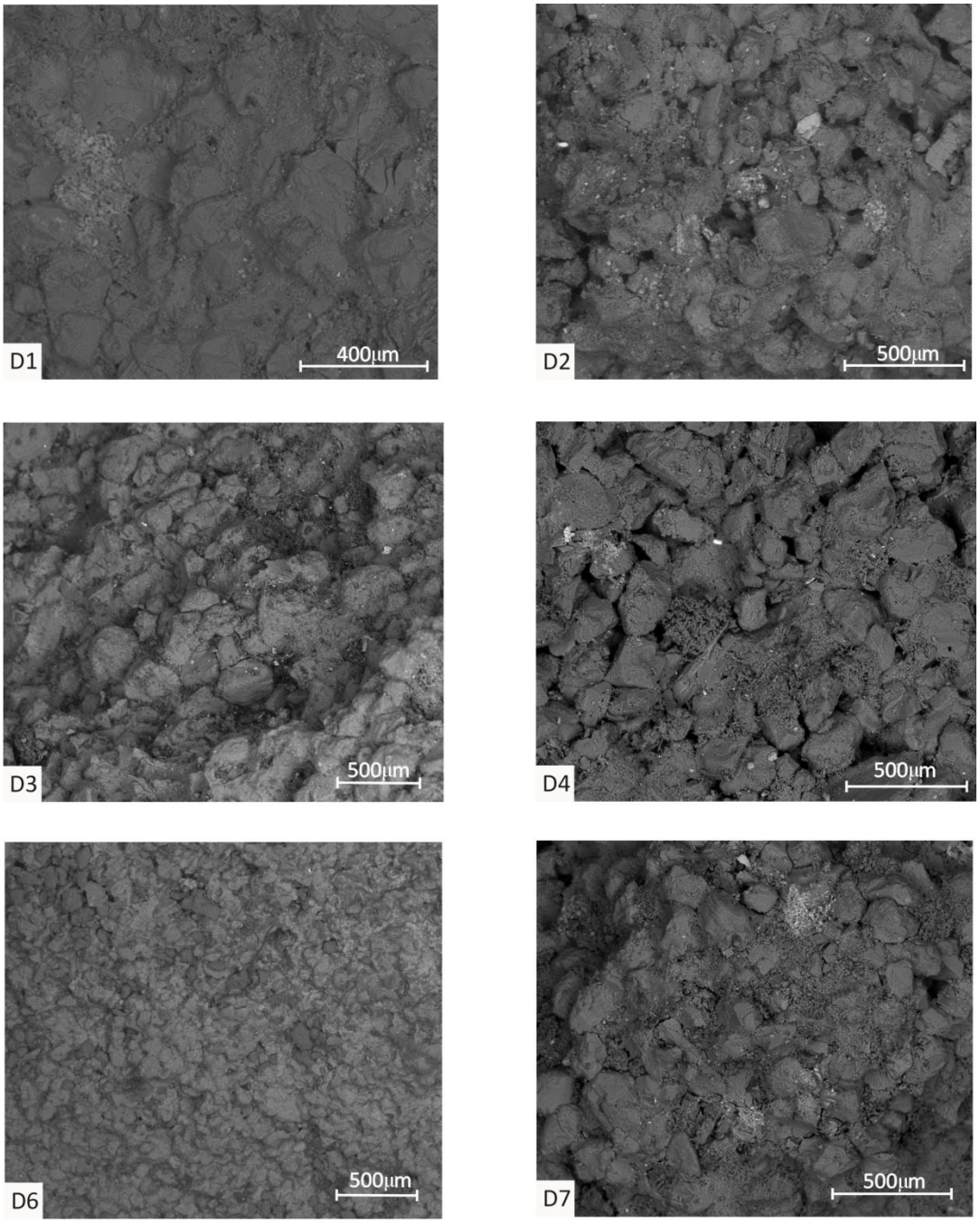

Figure 3-2: FEG-SEM SE rough surface overview images of Dalry samples D1-D4, D6 and D7.

The detrital sandstone minerals at the outermost surface of D5 (sill) have a thick film coating their surface. Under SEM conditions, it shows that the coating is smoothing the surface and therefore making the grain shape beneath less pronounced (Figure 3-3A). In cross-section this coating has a layered structure (Figure 3-3B). Layer one is densely packed and has a continuous thickness of ~25 µm, with a smooth surface. Layer two has a much looser structure with greater porosity and chemical analysis shows it contains higher abundances of barium and lead (Figure 3-4) in comparison to layer 1 (Figure 3-4). Layer two's thickness varies as it infill's topography between the grains, ranging from ~10 µm to ~75 µm.

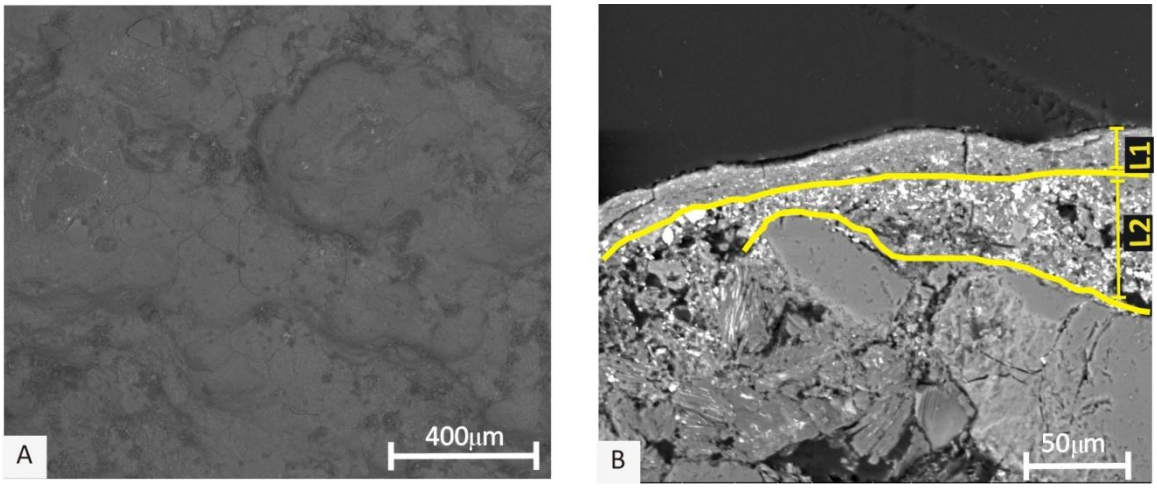

Figure 3-3: Images of D5.

A) FEG-SEM SE image of rough surface, B) FEG-SEM BSE cross-sectional image of polished block outermost surface. Yellow lines represent boundaries between the two layers: L1: layer 1; L2: layer 2.

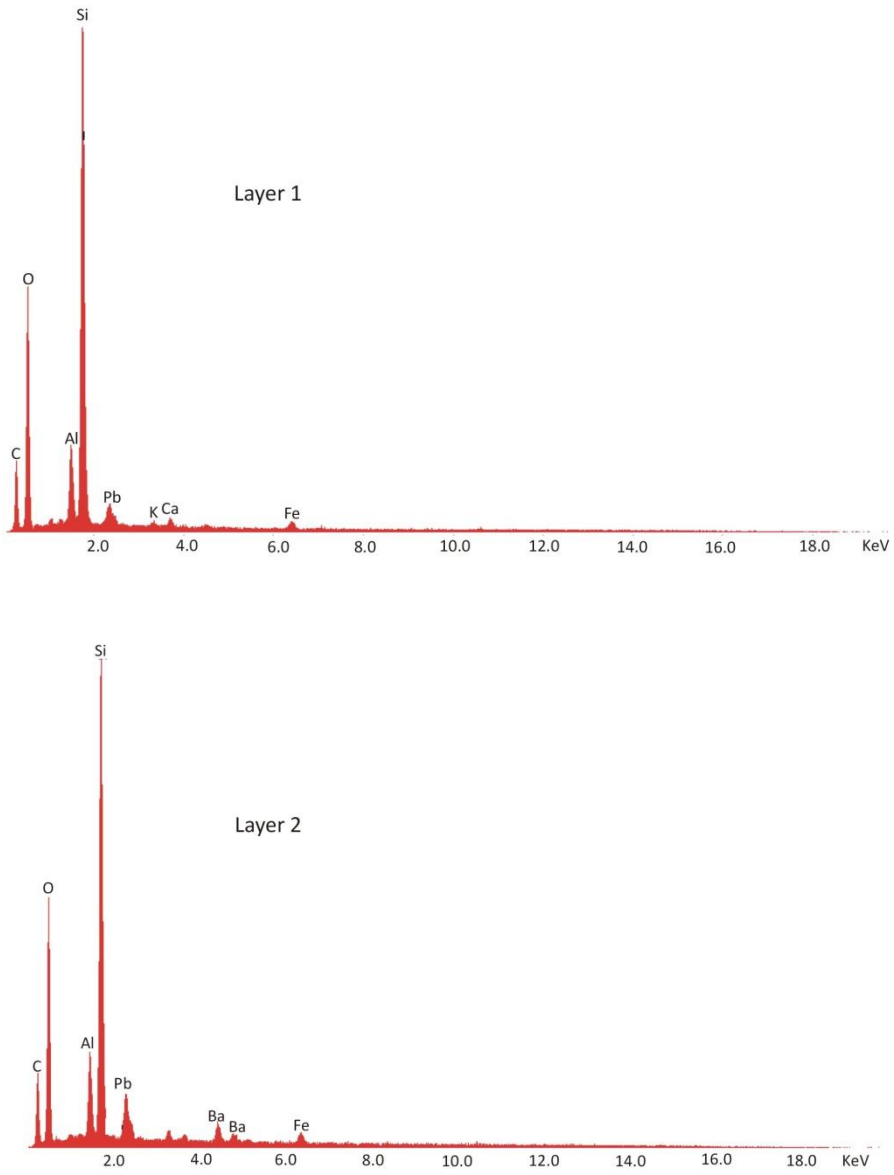

Figure 3-4: FEG-SEM raster spectra for layer 1 and 2 in D5.
These show increased amounts of barium and lead in layer 2 compared to layer 1.

The D8 (mullion) sample also has a film covering grains at the stone surface, which appears white under BSE (Figure 3-5A), suggesting it contains elements with a high atomic number. However, the grains beneath this are much more pronounced (compared to D5), suggesting that this crust is much thinner than on D5. The cross-section view confirms this as the coating appears as an intermittent <10 µm thick veneer (Figure 3-5B).

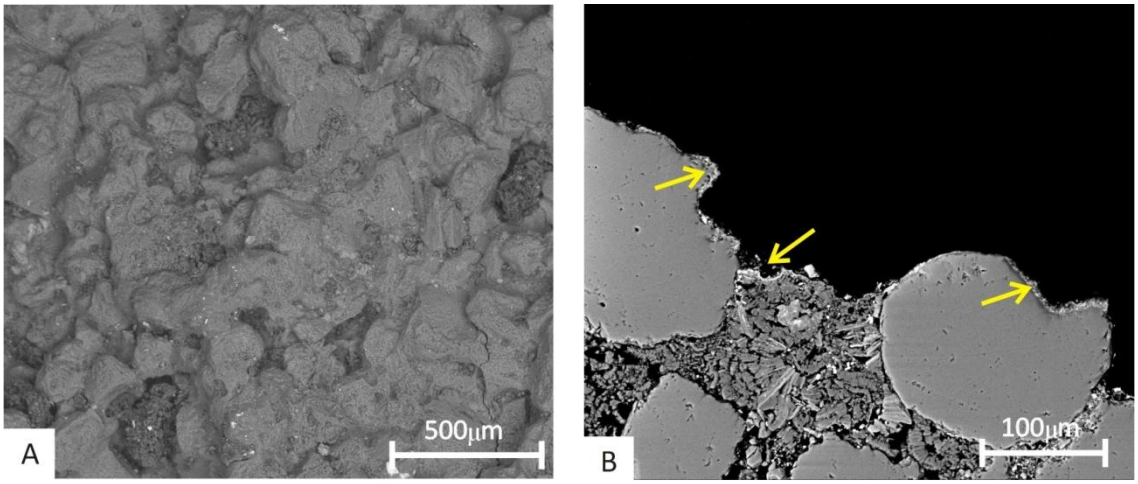

Figure 3-5: FEG-SEM images of D8.

A) SE plan view of fracture surface, B) BSE cross-sectional view of the polished block outermost surface, yellow arrows indicating the surface layer.

Due to the placement of these sandstones on the building (D5 sill and D8 mullion), these samples may have been contaminated with paint from wooden window frames. Paint is suggested due to the spot X-ray analysis detecting traces of both barium and lead in the compound. However, the hand specimens of these samples do not show coloured paint on the surface rather a black surface similar to all the other samples. D5 may have been contaminated to a greater extent as it was lowest, whereas D8 (mullion) could have benefited from the effects of rain wash and gravity which may have lessened the extent of contamination.

A few of these surfaces also contain a proportion of organic material and these will be discussed later in chapter 5. However, as can be seen, the majority of surfaces (six out of eight) on Dalry school stones are dominated by a fine grained mineral black crust. Beneath these crusts no clear layering can be defined. Also, the presence of possible paint on the surface does not seem to have caused any obvious damage to the sandstone situated below it, or caused any preferential internal layering.

3.2 RGU Samples

3.2.1 *Light Microscope Observations*

Polished blocks of RGU2, RGU3, RGU5 and RGU6 were studied using the Olympus SZX7 light microscope, as these were the blond sandstones in the sample set. The only sample to have any surface coating is RGU2 where the crust is extremely thin and has a very light

coloration. No clear layering could be identified in the cross-sectional view within any of these samples (Figure 3-6A). Banding is seen in RGU6, although this is inferred to be bedding within the sandstone, given the thickness, depth and angle of the layers (Figure 3-6D). Organic matter was highlighted in RGU2 at a depth of 3 mm by its green colouration, although this occurred in small patches and so did not represent a continuous microbial layer within the sandstone (Figure 3-6A).

Neither the rough fracture surface sample nor the polished blocks, when viewed within the FEG-SEM, showed crust formations on the surface. Microbial matter was seen but this will be discussed in chapter 5. The lack of crusts and internal layering is most likely a factor relating to their age, having been exposed to the environment for less than 15 years in a relatively unpolluted area.

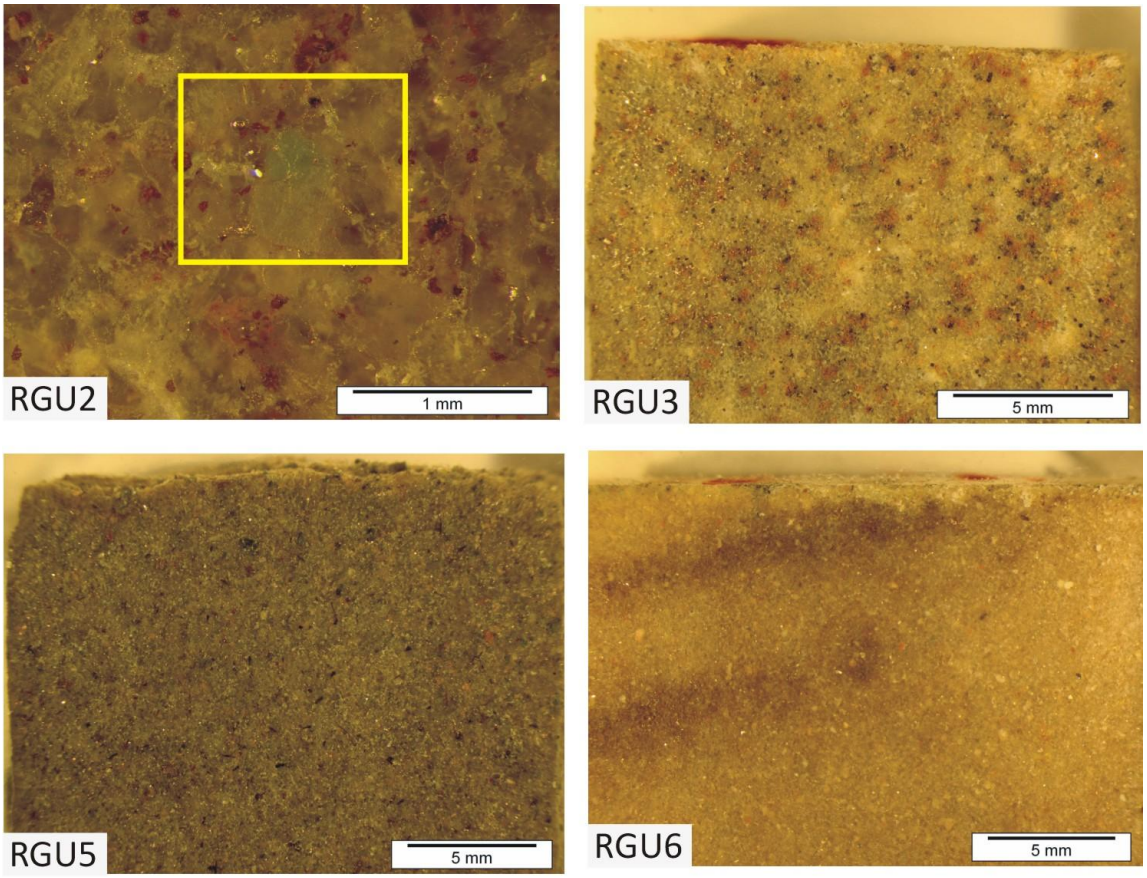

Figure 3-6: Light microscope images of RGU samples.

The yellow box within RGU2 at a depth of 3 mm beneath the surface is highlighting microbes within the sandstone. Outermost surface of the sample is at the top of each picture.

3.3 University Samples

3.3.1 *Light Microscope Observation*

Visually, black crust formations could be identified on all samples with the exception of UN1, although not all samples show a well developed weathering profile (Figure 3-7).

The main internal layers identifiable are: layer 1) a pale bleached layer, which ranges in thickness from 0.25 – 2.5 mm; layer 2) a speckled red rusty layer, which is generally the thickest layer seen ranging from 2.5 - 5 mm, where the colour of the layer is dependent on the amount of iron oxides available, which are presumably causing the coloration; layer 3) a darkened zone, although it is unknown what is causing this layer to occur. Samples UE1 and UE2 (Figure 3-7A and B) show a well developed weathering profile comprising all three layers, whereas UE3, UN2 and UN3 only contain layer 2 (Figure 3-7C, F and G). Samples UE4 and UN1 show no visible weathering profiles (Figure 3-7D and E). The red rusty layer is the most common layer (found in five out of seven samples, and dominates the sample due to its relative large thickness (~5 mm). There is no specific order in which the layers occur, however, if layer 2 is present, it is found deepest within the sample (Figure 3-7). The weathering style does not differ depending on the facade. This would agree with the Dalry samples which also show varying orders of internal layers on both facades. However, the internal layers on the university samples are much more developed in comparison to the Dalry samples.

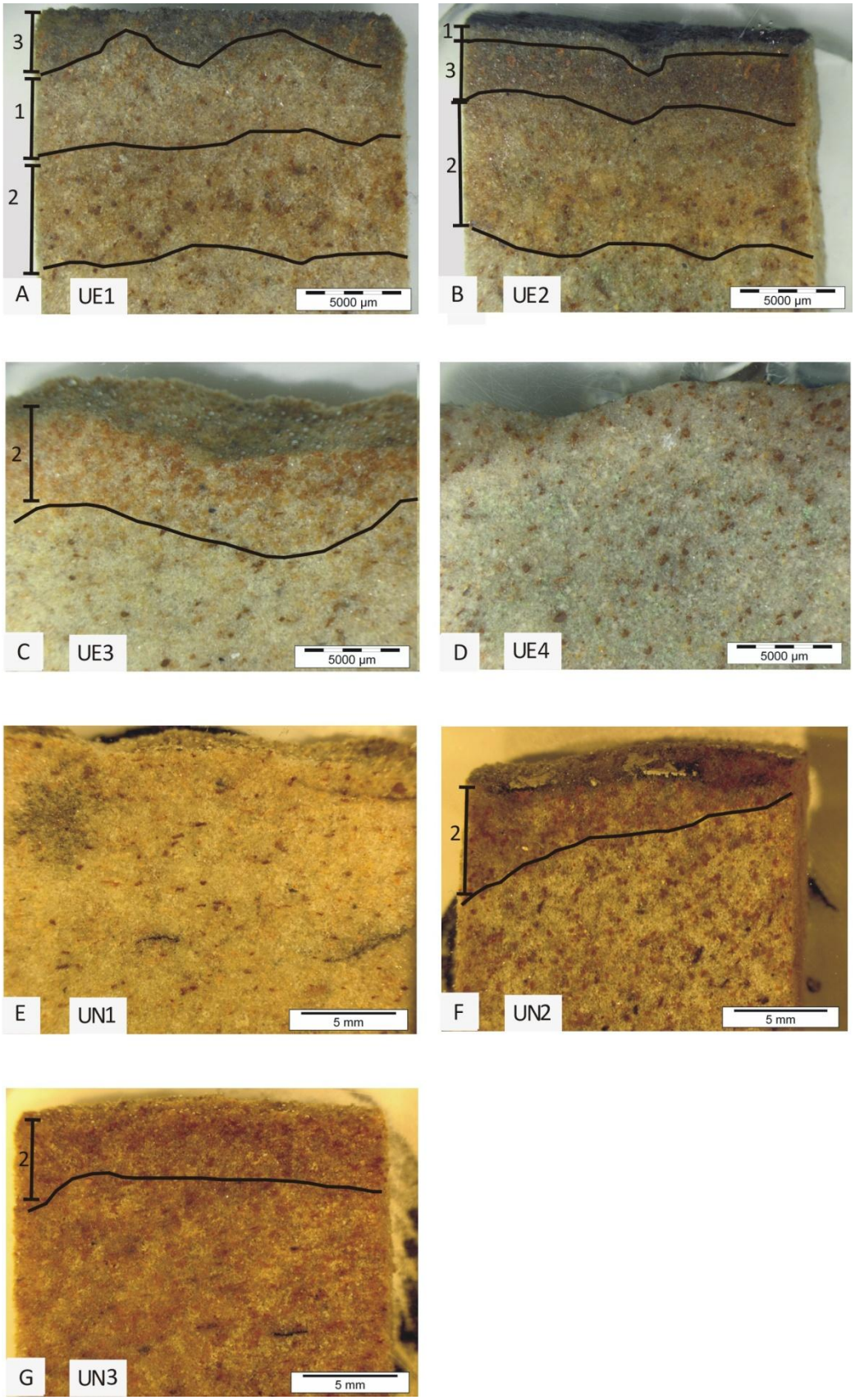

Figure 3-7: Light microscope images of University samples.

Layers: 1) Bleached zone; 2) red rusty layer; 3) darkened layer. A) UE1, with well developed weathering profile, with all layer occurring, B) UE2, same as UE1, C) UE3 only layer 2 present, D) UE4, no weathering layers evident, E) UN1 no weathering layers evident, F) UN2, thick dark crust with layer 2 present, G) UN3 layer 2 evident.

3.3.2 *SEM Imaging of the Outer Surface*

FEG-SEM analyses were conducted on both the rough samples of the outermost surface and polished blocks. Rough surface analysis shows that the majority of samples (UE3, UE4, UN1 and UN3) have "typical" black crusts, similar to those seen on Dalry school samples where quartz grains can be identified with small fragments of kaolinite, quartz and other debris amalgamating in depressions between grains (Figure 3-8). When these samples are viewed in cross-section, this debris is not identifiable as a distinct layer.

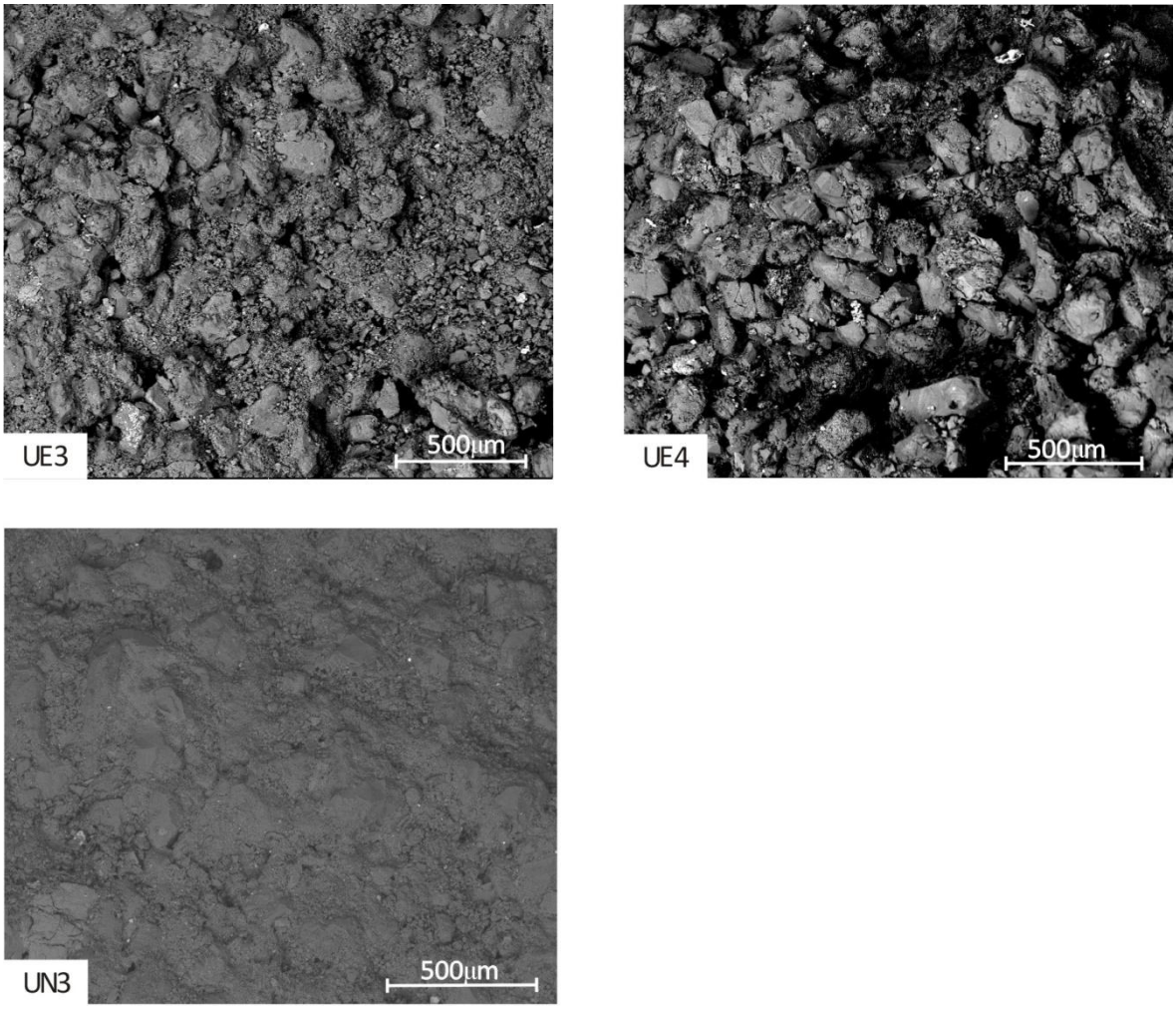

Figure 3-8: FEG-SEM SE rough surface images of University samples.

Within the University sample set, the fracture surface images of the outermost parts of UE1 and UE2 are very similar. On some regions of the surface a thin film is present, the film covers the raised surfaces of the quartz grains (Figure 3-9 A and B). It is identifiable by the much whiter coloration compared to the quartz in SE mode, it therefore must

contain elements with a higher atomic number. The X-ray spot analysis produces a spectra with high quantities of silicon, sulphur, aluminium and iron (Figure 3-10).

This crust was then examined in the polished blocks. In cross-section, the film is seen at the edge of the quartz grains and is less than 10 µm thick, as the fracture images show (Figure 3-9C). The covering is not laterally continuous and these combined factors made identification difficult in some regions.

To investigate this crust further Raman spectroscopy was also undertaken. The spectra gained from these investigations into the crusts were identified as quartz. Considering all the data gathered, it was concluded that a silica glaze was present on these samples. Five types of silica glaze are found on sandstone and, from the properties found in this study, it is most like a "type three" alumina-iron rich silica glaze (Dorn, 1998). The formation of these glazes is poorly understood and the most common idea in the literature is that silica glaze is a product of the chemical precipitation of monosiliciic acid ($Si(OH)_4$) through complexing with organic matter (Dorn, 1998). This may have happened in the past but, at present, no organic material was found on the surface of these samples.

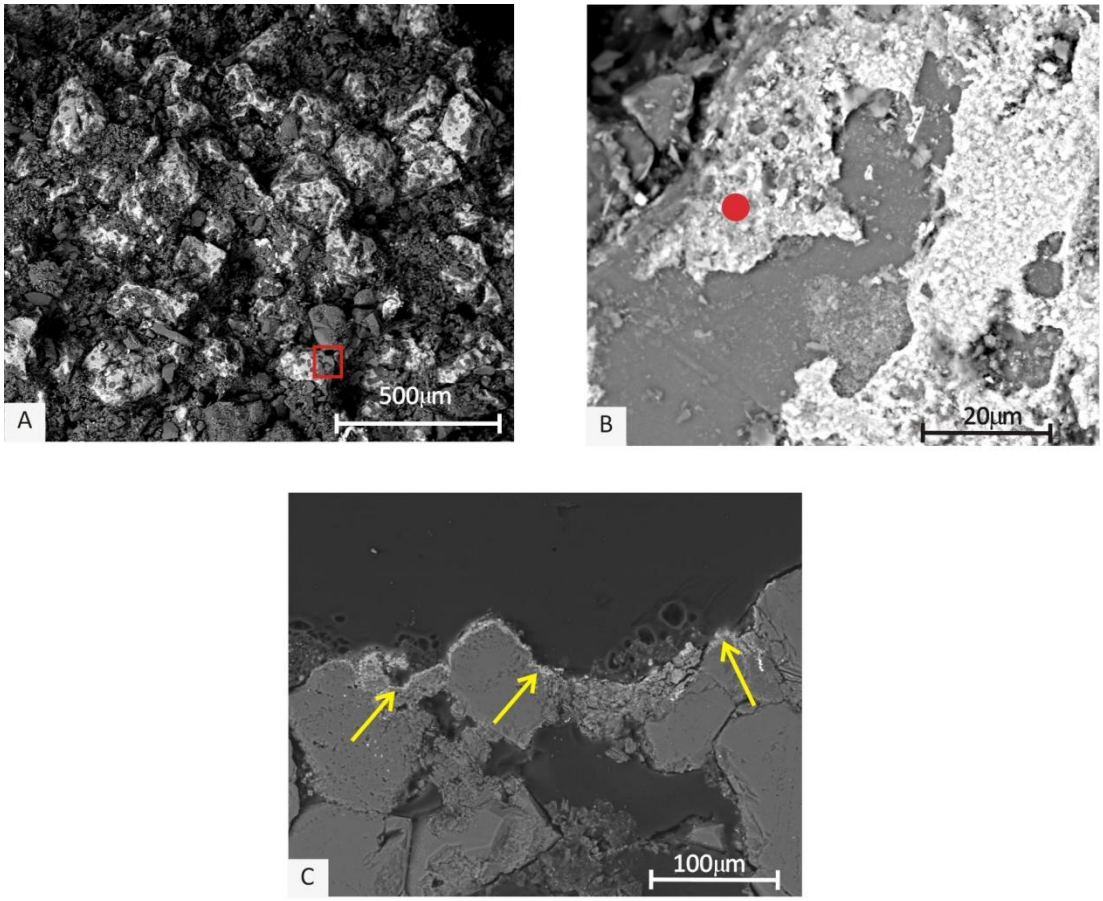

Figure 3-9: Images of UE2 surface.

A) FEG-SEM SE overview image of fracture surface, red square shows area of image B, B) magnified image of (A) showing the film covering quartz grains, red spot indicates area of X-ray spectra, C) FEG-SEM BSE image of polished block, showing a cross-section view of the surface coating. Yellow arrows denoting surface coating.

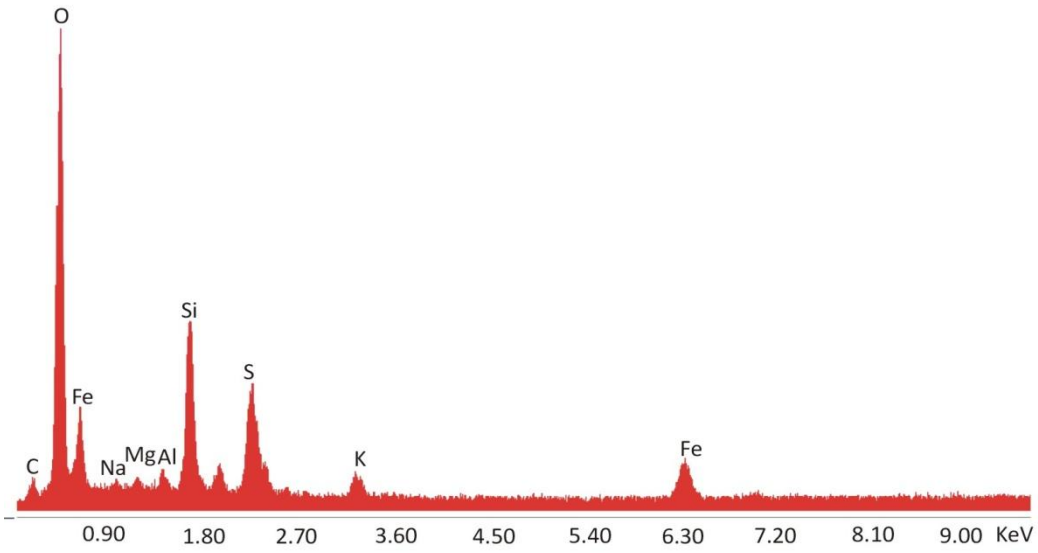

Figure 3-10: FEG-SEM X-ray spectrum.

Spectrum is from the visually white areas on the rough surface image.

The surface of UN2 is smooth, obscuring the grains beneath it (Figure 3-11A). The coating is thick (300 µm) and infill's the spaces between grains (Figure 3-11B), while it has a barium and sulphur-rich composition (Figure 3-11C), pointing towards a paint origin. However, the coating is not laterally extensive over the surface, therefore this may have been deposited onto the surface from a painted source near the sandstone sample. The light microscope image (Figure 3-7F) shows lighter areas on the outermost surface mixed in with darker areas and so are not easily identifiable as possible paint.

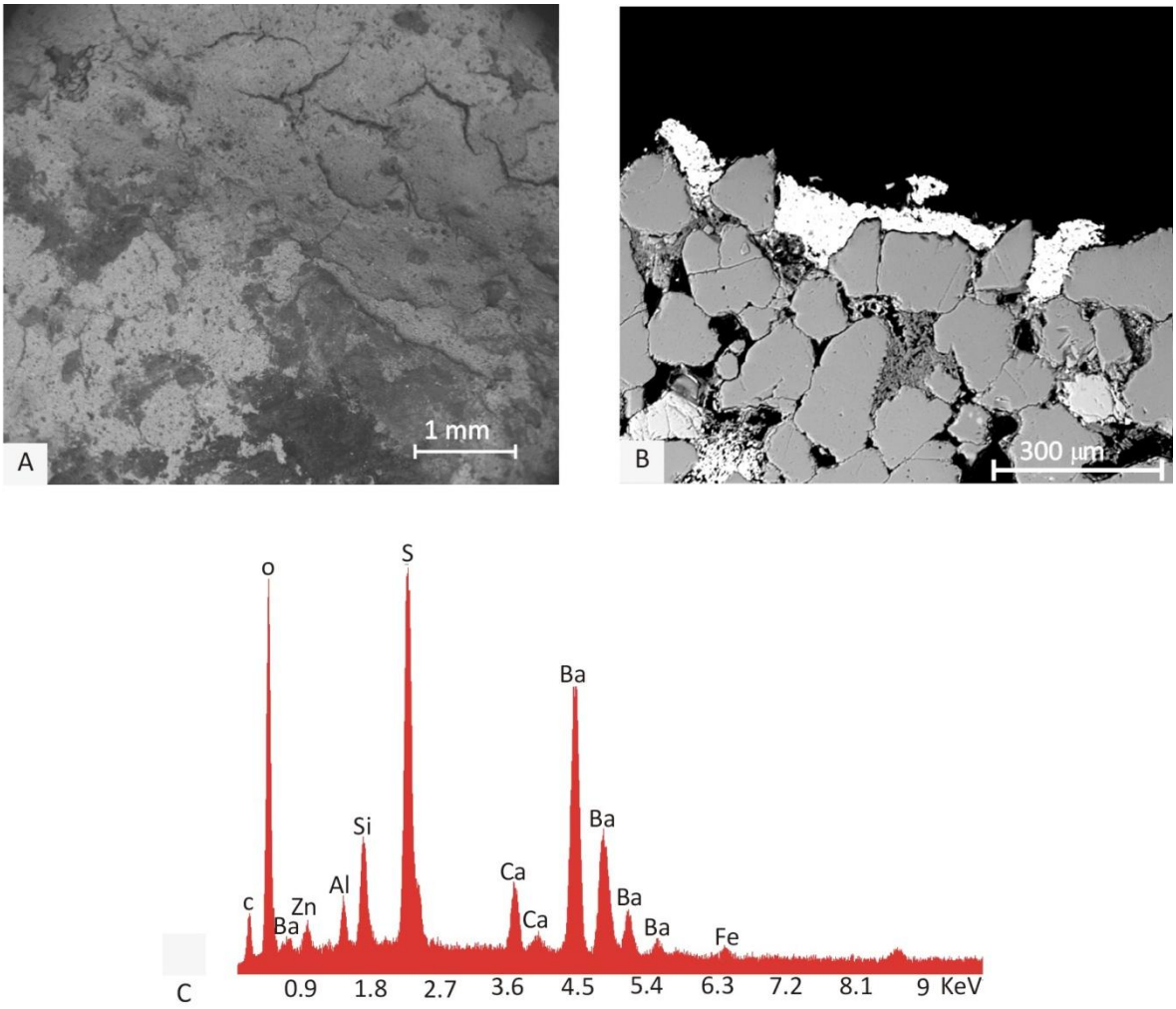

Figure 3-11: FEG-SEM images and X-ray spectrum from UN2.

A) SE overview of fracture surface, B) BSE image of polished block cross-section of outermost surface, C) X-ray spectrum from possible paint substance, showing large quantities of barium and sulphur.

3.3.3 *Summary*

These samples have a large variety of crusts including probable silica glazes, which occur on the south facade. As samples have a high likelihood of a lintel setting (see Section 2.2.3) these sandstones may have been contaminated by paint from the windows, but most other samples also have a fine-grained mineral black crust. Well defined layering has occurred within the samples and the mineralogical expression of these internal layers will be investigated later in the study.

3.4 St Vincent Street Samples

3.4.1 *Light Microscope Observations*

This study concentrated on sandstone samples which had not previously been repaired, or cleaned, to remove the effects of weathering caused by these processes. However, due to the constraints on the samples obtained, a proportion of the SVS samples had mortar repairs associated with them. For these reasons, only CS4, EE1, EE3 (no mortar) and EE4 (which had a partial covering of mortar) were analysed in these experiments. Under light microscopy, CS4 shows a thin black surface crust with layer 2 (red rusty layer) directly beneath it, which is presumed to be rich in iron-oxide minerals. This layer is highly variable in thickness across the sample, ranging from 1 mm to 6 mm (Figure 3-12A), whereas EE1 layer 2 has an almost constant thickness (Figure 3-12B). Furthermore, a very thin layer 1 (bleached layer) is present at the surface of CS4 above layer 2. Although crusts are evident on EE3 and EE4, there are no observable weathering layers present beneath them. The internal weathering pattern on the SVS samples is difficult to define due to the use of mortar on the surface of the building, and therefore only a small proportion of samples could be analysed.

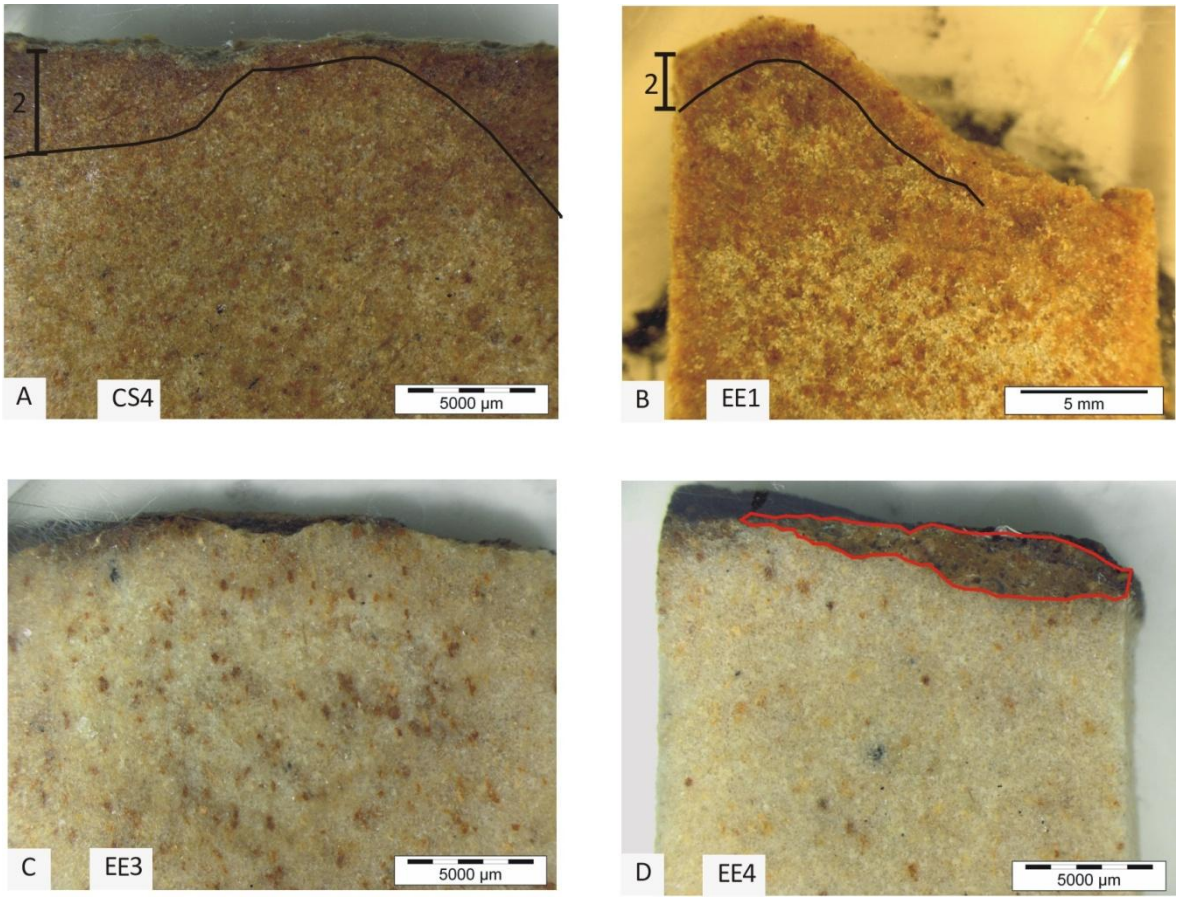

Figure 3-12: Light microscope images.

Black line represents depth of weathering within layer 2 (rusty red layer). On EE4 the red enclosed area defines the extent of mortar present.

3.4.2 *SEM Imaging of the Outer Stone Surface*

Outer surface fragments were analysed using the FEG-SEM. The surfaces of EE1 and EE3 are very similar. They are densely packed with fine grained mineral shards, which distort the shape of the detrital grains beneath (Figure 3-13). The surface of EE1 is also combined with carbon rich material, identified by spot analysis. The carbon rich material is seen coating mineral grains on the surface making identification of these particles difficult (Figure 3-13).

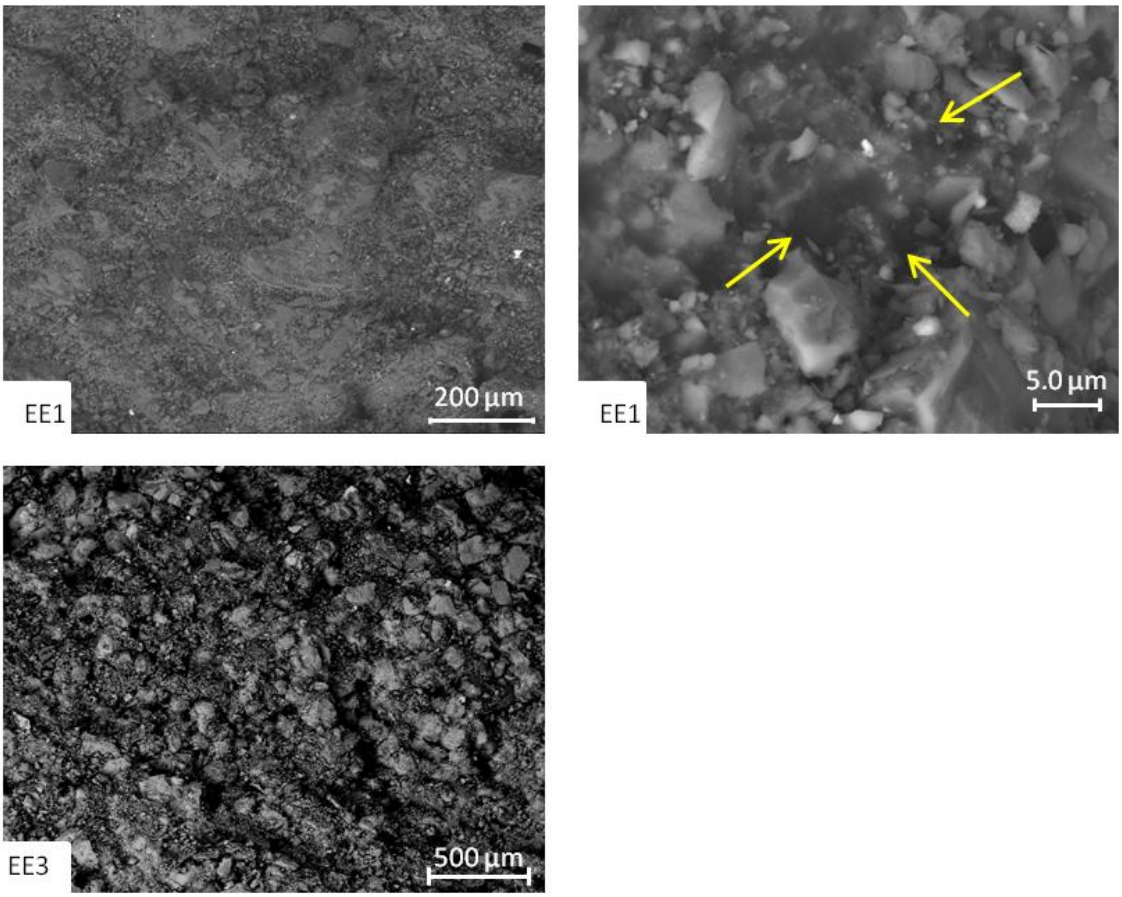

Figure 3-13: FEG-SEM SE images of the outermost surface of EE1 and EE3. The yellow arrows on EE1 are indicating the carbon rich material.

The surface of CS2 (mortar covering) has a "salt accretion" black crust formation on its surface, where salt crystals (mainly gypsum, identified by the chemistry and thin platy crystal shape) have combined with presumably atmospheric particulates to produce the black coloration of the crust. In general, the gypsum has formed in a chaotic manner over the surfaces although, in some areas, the crystals have some alignment and are found surrounding quartz grains (Figure 3-14). These thin platy crystals are also apparent on the surface of CS4 mixed with mineral fragments in an unorganised fashion.

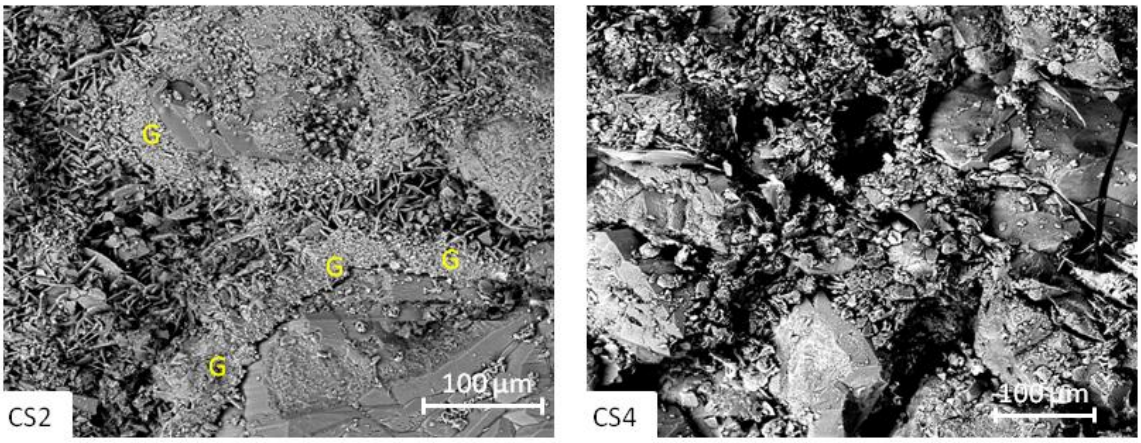

Figure 3-14: FEG-SEM SE images of the outermost surface of CS2 and CS4.
Yellow G = Gypsum crystals surrounding quartz grains.

When polished block cross-sections of the outermost surfaces were viewed no black crust could be identified. This may have been due to damage during the sample preparation procedure. The surface of EE1 does appear to be slightly more densely packed with fragmented minerals occupying space between quartz grains. However this is difficult to distinguish as an individual layer.

3.4.3 *Summary*

Only a red rusty layer is detailed as an internal structure. The black crusts found on the surface are quite difficult to fully understand due to the mortar coverings which have possibly enhanced the production of salt crystals.

3.4.4 *Discussion*

Although the vast majority of samples surveyed have an outermost black crust, only a few have any defined internal layering profiles. Three main types of crust are evident: The first are crusts which are composed of a layer of small mineral fragments infilling all indentations on the stone surfaces and enveloping the detrital grains. The fine mineral detritus on the surface is most likely composed of kaolinite and quartz, which are most likely to have been transported from the interior of the stone (Cnudde et al., 2009). The black colour seen on the surface is most likely due to the mineral detritus combining with a proportion of atmospheric particulates of metal, such as Al, Cd, Cr, Cu, Fe, Mn, Ni, Pb and Zn as collected in a study of Glasgow's atmosphere by McDonald and Duncan (1979), as well as some salt crystals. The salts are difficult to identify due to the quantity and size

of the matter being observed. Crystals of gypsum are evident in the SVS samples, although these are the only sample set which had mortar repairs associated with it. Mortar acts as a large store of calcium which could provide the source of the calcium ions to form salts. The black crusts are the most commonly occurring formation (Table 3-1). They are normally less than 1 mm thick and are difficult to distinguish in cross-section, but this may be due to damage by the sample preparation methods. However, as this was consistent throughout all sample sets, it is unlikely to be wholly a preparation artefact.

The role the crusts play in weathering is difficult to determine, as the proportion of atmospheric pollutants is unknown. However, by restricting the pore space at the surface, they seem to provide a layer that is limiting water flow deeper into the sandstone and a limited supply may therefore protecting the sub-layers.

The second crust is the “silica glaze”, which appears only on UE1 and UE2 (Table 3-1) and is an extremely thin (~10 μm) veneer which leaves the block with a black and slightly glossy lustre. Dorn (1998) states that the presence of a silica crust on the surface will protect and strengthen the sandstone beneath.

The third main surface crust found was paint (Table 3-1). Paint on the surface of sandstone provides an impermeable layer, and therefore has a detrimental effect on the sandstone beneath as any water which becomes trapped behind this layer cannot evaporate from within. However, the paint seen on these samples is often not laterally extensive and probably has caused minimal harm to the sandstone below.

The internal layers identified beneath the crust formations were: layer 1) a pale bleached zone which is normally very thin (<1 mm) and, in most situations, is formed just below the crust; layer 2) a red, rusty speckled zone which ranges widely in thickness from 1 mm to 6 mm and is most likely formed by the oxidation of any iron compounds present and layer 3) a darkened region, generally 3-4 mm thick. The process of formation for this third layer is as yet undetermined. The weathering profiles have no reoccurring pattern and only two samples show evidence of all three layers (Table 3-1). The most common layer is layer 2 and occurs in eight out of the ten samples which have any weathering layers present therefore appearing to be the most dominant weathering process in these

Scottish sandstones. To determine if the colour changes seen are due to mineral proportions point counting data was acquired, for all the cross-sections and will be discussed in greater depth within chapter 4. However, results show that those samples that develop a red rusty layer do not show larger quantities of Fe-oxide, or a loss of Fe-oxides from the internal regions. Nevertheless, very small amounts of strongly coloured minerals, such as iron oxides, can impart a strong colour on the rock.

Within the time frame of 150 years, a well developed crust has adhered itself to the surface of most of the sandstones, whether it be a mineral fragment crust or a silica glaze. Although internal layers were found in many samples, well-developed internal stratigraphy is much more rarely seen, suggesting that it takes a longer time frame to develop. Layer 2 (Fe-oxide rich layer) may be the first to establish as it is the most widely found.

Whether the crusts identified have a positive or negative effect on the decay of sandstone beneath is not easy to determine from these results. However, once chemical analysis has been undertaken on the minerals beneath the crust, this can maybe be resolved.

Table 3-1: Key facts concerning the crusts and weathering profiles.

Sample	Weathering profile layers	Crust/no crust	Silica glaze	Mineral fragment crust	Salt	Paint residue
D1	---	---	--		--	--
D2	1	Yes	--	Yes	--	--
D3	---	Yes	--	Yes	--	--
D4	1	Yes	--	Yes	--	--
D5	---	Yes	--		--	Yes
D6	---	Yes	--	Yes	--	--
D7	2	Yes	--	Yes	--	--
D8	---	Yes	--		--	Yes
RGU2	---	Yes	--	Yes	--	--
RGU3	---	---	--	--	--	--
RGU5	---	---	--	--	--	--
RGU6	---	---	--	--	--	--
UE1	3, 1, 2	Yes	Yes	--	--	--
UE2	1, 3, 2	Yes	Yes	--	--	--
UE3	2	Yes	--	Yes	--	--
UE4	---	Yes	--	--	--	--
UN1	---	---	--	--	--	--
UN2	2	Yes	--	--	--	Yes
UN3	2	Yes	--	Yes	--	--
CS4	1, 2	Yes	--	Yes	Yes	--
EE1	2	Yes	--	Yes	Yes	--
EE3	---	Yes	--	Yes	--	--
EE4	---	Yes	--	Yes	--	--

Table represents all samples analysed. --- denotes not present.

4 Mineralogical and Chemical Results

Chemical decay is one of the many processes active in weathering sandstone, and the blond sandstones of Glasgow due to the presence of carbonate cement, are potentially highly susceptible. Therefore, to understand the processes and quantify the magnitude of chemical decay in the net weathering cycle, detailed large scale whole rock investigations were undertaken to quantify the properties of each sample. Any mineralogical changes at the outer surface could then be identified as caused by weathering rather than being a diagenetic feature of the sandstone. Once whole rock analysis was completed, mineral specific chemical and molecular analyses were also undertaken.

This chapter aims to answer the following questions:

- What is the mineralogy of the sandstone and what is the variability both intra-and-inter-building?
- Which minerals are most reactive?
- How do these minerals decay?
- What is the spatial scale of decay?
- Can a rate of decay be determined?

The methods used to answer these questions include a variety of SEM techniques (e.g. mapping, point counting and CL), Raman spectroscopy and permeameter measurements.

4.1 Dalry School

4.1.1 *Sandstone Mineralogy, Porosity and Grain Size*

Eight samples (D1 to D8) were collected in cores from the outer walls of Dalry primary school (Table 4-1, pages 144-146). Point counting was conducted on all samples, using the method outlined in section 2.1.1.2, and the mineralogical compositions of the sandstones were then plotted on a ternary diagram (Figure 4-1; where, as describe in section 2.1.1.2 quartz, feldspar, mica and kaolinite, Fe-oxide, ankerite plots were used). To avoid any weathering-related anomalies and ensure a true representative 'bulk rock' value, an average value of the data from the innermost 4 mm of the sample was plotted. The ternary diagrams show that quartz arenite sandstones were used to construct the school (Figure 4-1A). Figure 4-1B shows that accessory minerals occur in all samples, mainly in the form of clays, which range in volume from 3% in D1 to 23% in D7. Oxides are found in much smaller percentages, with D5 having the largest proportion at 4%, whereas D4 has only trace quantities. Carbonates are not seen in any samples with the exception of core D7, which has a small fraction (<2%) of carbonate cement (identified as ankerite, as discussed later in this chapter). All point counting data are presented in Table 4-2.

These sandstones are mainly medium-grained (quartz mean = 207 ± 14 µm for D1, D2, D3, D4, D5 and D8) with the exceptions of D6 and D7 which are fine-to-medium grained (quartz mean = 141.3 ± 24 µm) as represented in Figure 4-2A. The quantities of quartz and porosity occur within a relatively small range within the eight samples: quartz = 58.4 - 66.5%, porosity = 17.0 - 26.7%. The pores have a mean diameter generally less than 124 µm (Figure 4-2B). The largest feldspar proportion is seen in D7 (3%), whilst D4 and D8, have none at all. These samples are quartz arenites and consistent with the Hyslop et al. (2006) description of B1 sandstones (see section 1.4.1.1). Due to the similarity in their mineralogical properties, the samples are assumed to have been derived from one quarry source.

Table 4-1: Weathering zone and corresponding core sample identification for Dalry School samples.

Weathering Zone	NE Facade	SE Facade
Whitened Zone	D1	D7
Sills	D2	D5
General Black Weathering	D3	D6
Mullions	D4	D8

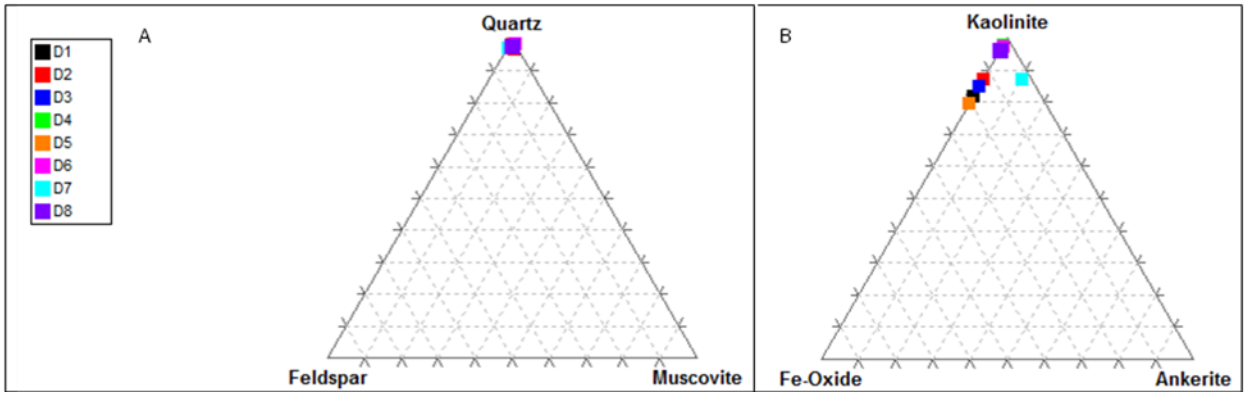

Figure 4-1: Ternary plots of the Dalry sandstone cores.

A) Quartz, K-feldspar and muscovite plot, B) kaolinite, Fe-oxide and ankerite plot. Ternary plots reveal that samples have a quartz arenite composition containing limited ankerite.

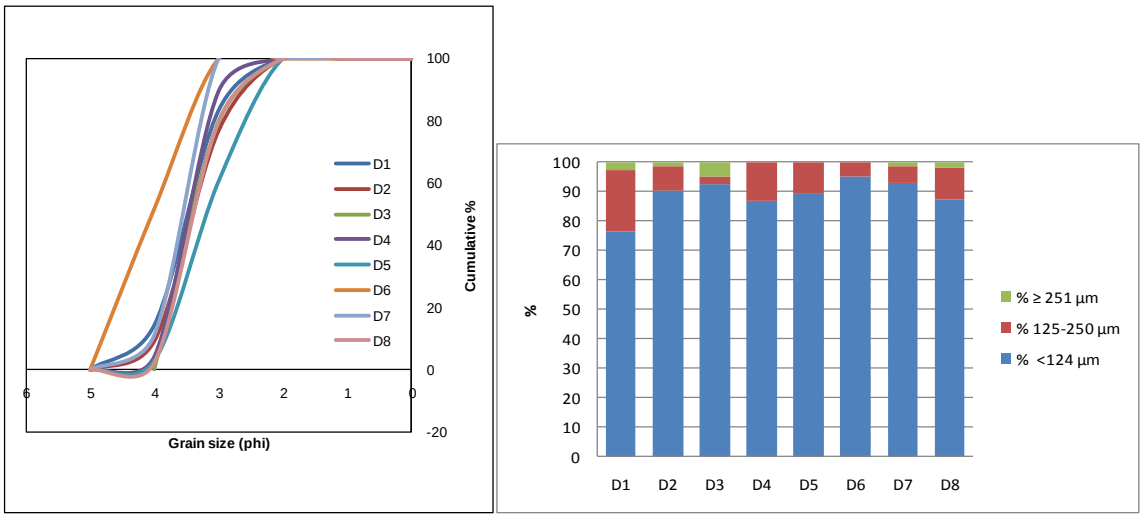

Figure 4-2: Cumulative grain size frequency chart for quartz (right) and pore size fraction graph for the Dalry samples (left).

4.1.2 *Mineralogical Impact of Decay on the Minerals*

Point counting was also conducted to identify small changes to mineralogical composition and porosity between the internal and outermost regions of the core samples. Therefore, as each sample was compared with itself, any changes seen could be attributed to effects of weathering. All point counting data is in Table 4-2.

Between the surface and a maximum depth of 5 mm, a high percentage of quartz occurs in comparison to the average bulk quartz percentage for the stone interior. Of the eight samples six, show evidence in the first 3 mm (Table 4-2). Five of the eight samples have a high quartz percentage between 0 - 1 mm before recording a comparative low between 2 – 3 mm depth (Figure 4-3). The high and low value is relative to the "bulk rock percentage", which is an average of the data from the innermost 4 mm of the sample.

Although the average porosity is the same for the outermost and innermost 6 mm, a porosity low is clearly identifiable in most samples within this first 6 mm; although D6 is an exception (Figure 4-3, Table 4-2).

The kaolinite results show that, within the outermost 5 mm of the samples, an area of low kaolinite concentration occurs (Table 4-2). Other kaolinite "percentage lows" may be seen further into some samples but are sporadic in their occurrence and so no other clear and conclusive trends are identifiable. This low relative proportion often occurs between 0-1 mm depth, which is followed by a sharp increase in the amount of kaolinite recorded at 2-3 mm depth (seen in samples D3, D5, and D7; Figure 4-3)

Between depths of 2 to 5 mm below the outermost surface, many of the samples show a high in Fe-oxide abundance compared to directly above and below this region (Figure 4-3).

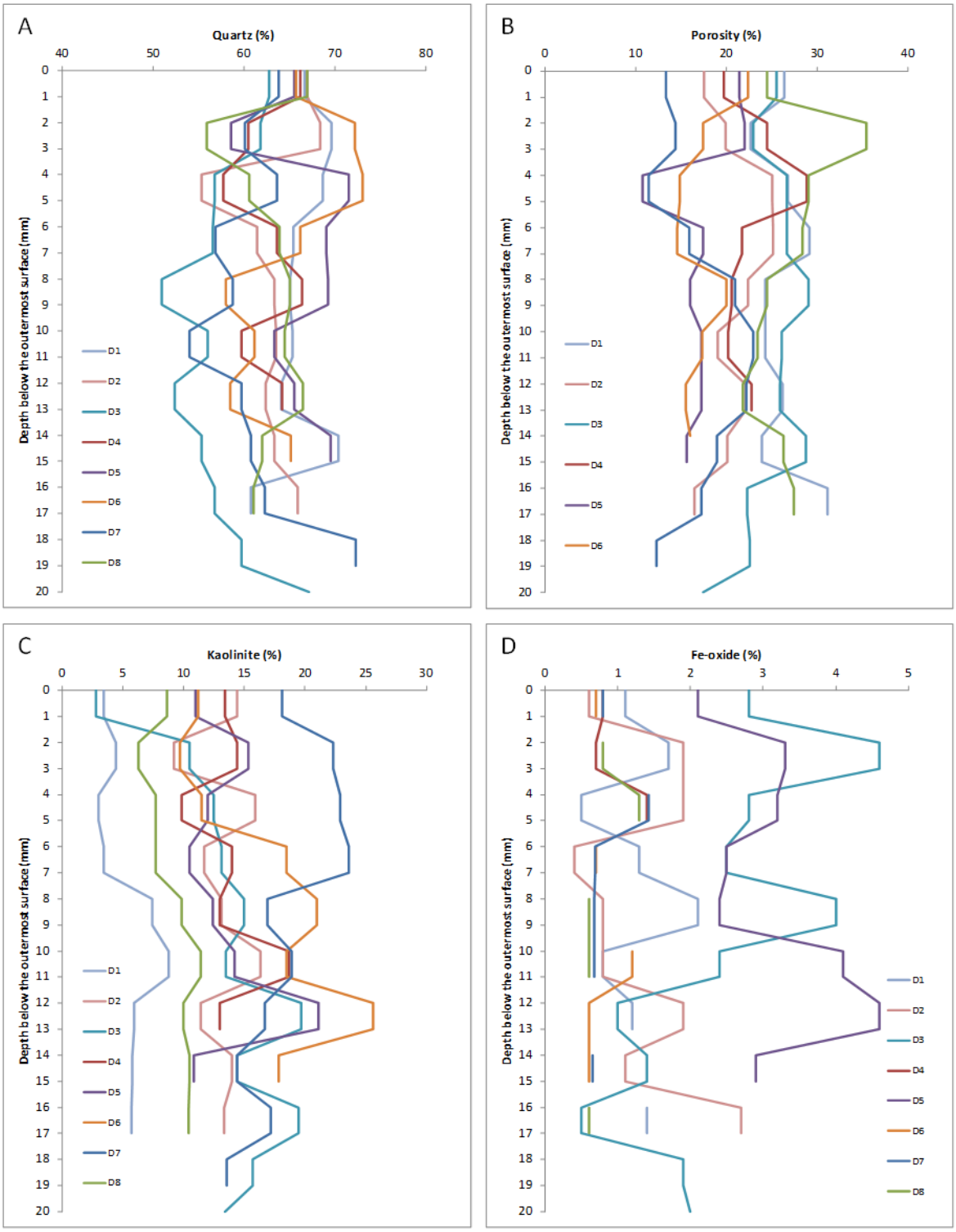

Figure 4-3: Depth against sandstone constituent proportion graphs for Dalry samples. A) quartz, B) porosity, C) kaolinite, D) Fe-oxides. Data obtained by point counting.

4.1.3 *Physical Weathering Evidence*

The outermost regions of each core (surface to 2 mm depth) were studied using a FEG-SEM in BSE mode to help identify any physical features that may be indicative of chemical weathering. However, most samples show no obvious physical evidence of weathering

features. Quartz grains are intact with no visible pitting or cracking. The K-feldspars are fractured but this is also seen at much greater depths within the sandstone, and so is likely to be a sample preparation artefact or a process which has occured pre-quarring. A cracked layer is evident on the surface of D5, but this is not a weathering product as it has been identified as a paint layer (see section 3.1.2). Beneath this layer in D5, there is no evidence of weathering affecting the detrital quartz and K-feldspar grains. The presence of Fe-oxide pseudomorphs in D5 show that ankerite has been dissolved away: However, as these pseudemorphs are seen all the way through the sample (Figure 4-4), it is difficult to know whether they are a diagenetic feature or have been caused by extensive weathering post-construction. D7 also contains evidence for dissolution of ankerite, and a systematic weathering profile is observed: 0-2 mm depth shows no evidence of any ankerite or Fe-oxide psuedomorphs; 2-6 mm depth shows skeletal Fe-oxides and hydroxides; and intact ankerites are observed at depth exceeding 7 mm from the surface (Figure 4-5).

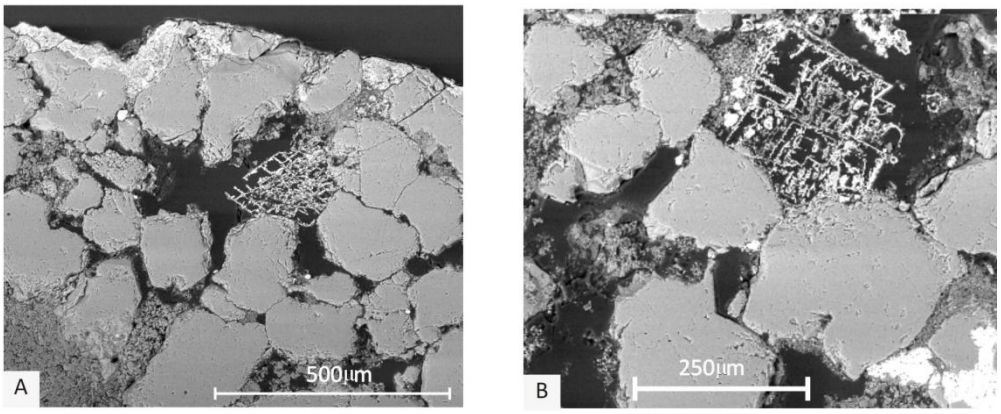

Figure 4-4: FEG-SEM BSE images of D5 polished blocks.

A) Surface of D5 showing Fe-oxide pseudomorphs of ankerite crystals (left of centre) below the crust surrounded by unaffected detrital grains. B) 23 mm beneath the outer surface showing Fe-oxide pseudomorphs of ankerite (located in the upper middle of image).

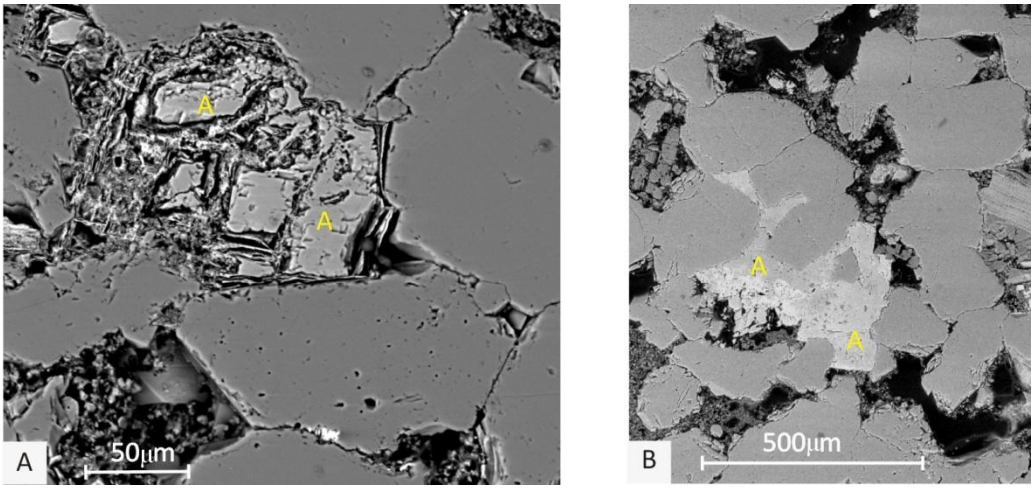

Figure 4-5: FEG-SEM BSE images of D7 polished blocks.

A) Partially dissolved ankerite at 4 mm depth. B) Unweathered ankerite at a depth of 20 mm. Ankerite crystals denoted by yellow A.

4.1.4 *X-ray Mapping*

False colour EDS maps of the surface of the block as well as an interior section (normally half way through the block) were produced to examine the mineral distribution throughout samples. This distribution should help to identify any variation between the outermost surface and the interior (Figure 4-6). The images show kaolinite being distributed evenly throughout the samples, although the outermost surfaces of D2, D4 and D8 seem to have a diluted proportion of clay compared to greater depths in those samples (Figure 4-6G and H).

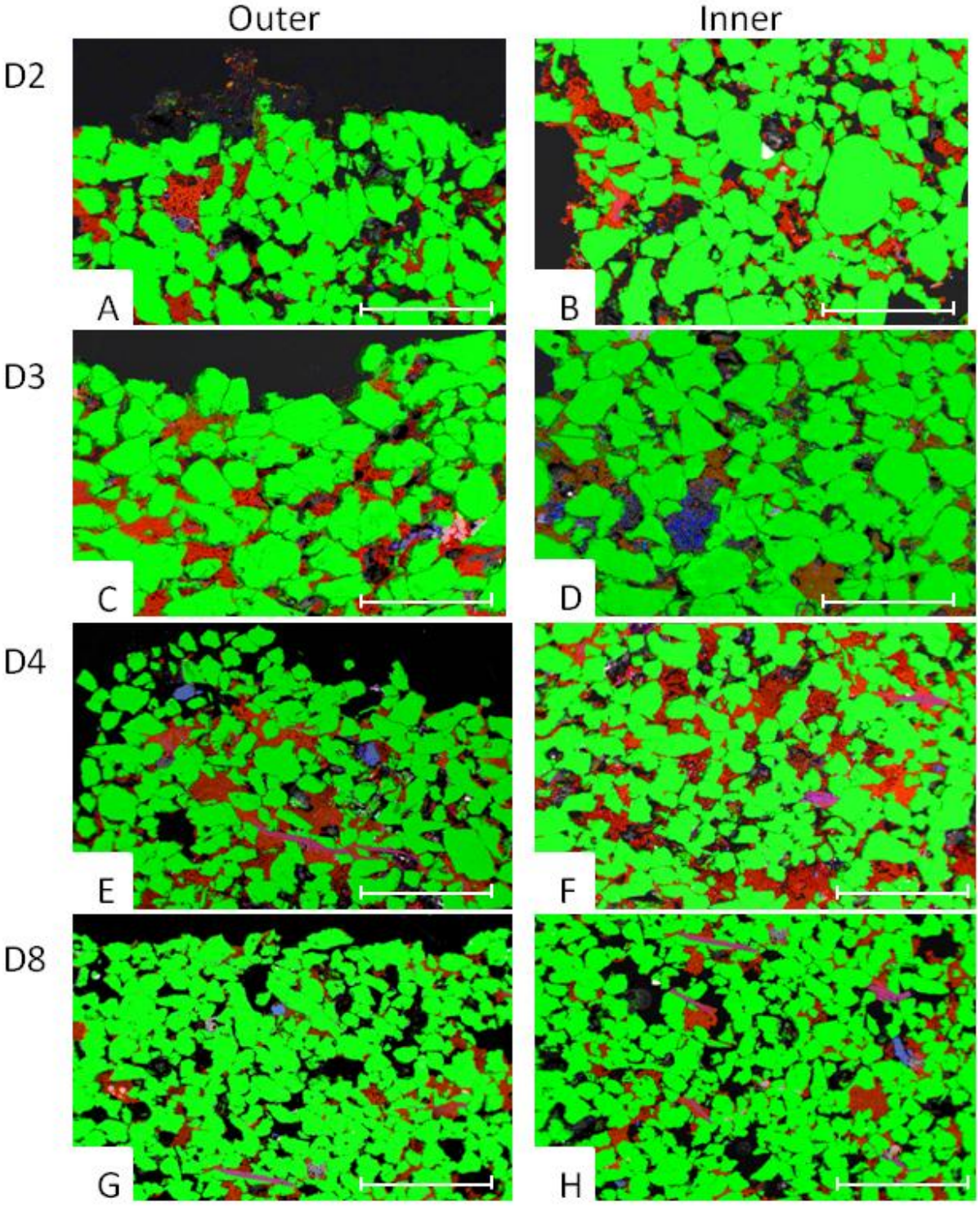

Figure 4-6: A selection of EDS maps of Dalry samples produced on the FEG-SEM.

A and B) D2; C and D) D3; E and F) D4; G and H) D8. Each set is complied of one outer surface and one inner map, and the scale bar is 500 µm long. Green = silicon, red = aluminium, blue = potassium. Inner images are from 12 mm below the outermost surface.

4.1.5 ***Summary***

The Dalry stones produce clear evidence of chemical alteration. Where carbonate cements are present, such as in D7, intact ankerite crystals occur below depths of 6 mm. However, above that level, only Fe-oxide/hydroxide pseudomorphs are observed, which suggests that they were once present in this zone. For the samples that lack diagenetic ankerite, the magnitude and depth of weathering proves much harder to identify. The point counting data shows some mineralogical layers to occur in the outermost 5 mm of the samples. Loss and gain of minerals has taken place in these near surface regions, producing a Fe-oxide enriched layer and a kaolinite depleted layer, whilst a peak of quartz abundance and a porosity low also occur in the outermost 6 mm (Figure 4-3).

The trends seen in each mineral within the sandstone are easily identifiable, although when combining the data for all the minerals appears more tricky.

Common patterns are shown schematically in Figure 4-7 and these layers combine to produce a possible 'case hardened' layer at the surface of (or within) the sandstone. Figure 4-7A and B show a Fe-oxide abundant layer at 4-5 mm depth, while the porosity low always occurs at the surface. Of these scenarios 'A' shows a greater argument for case hardening, as the quartz high and porosity low both occur at the same depth unlike 'B'. Figure 4-7C indicates that case hardening is occurring at deeper levels within the sandstone, with a Fe-oxide high, quartz peak and porosity low all being located at the same depth. In these circumstances, the placement of the kaolinite low is difficult to precisely define. These patterns have no preferred facade orientation. These are the average overall trends and not all samples show each of these features and, as can be seen, are highly variable which makes one general trend difficult to isolate within the data.

The average porosity for the outermost 2 mm is generally slightly higher than the interior (1-2%). Curiously though, in D7, which has experienced ankerite dissolution, the porosity is significantly less at the outermost dissolved region than internally (13.1% to 17.5%).

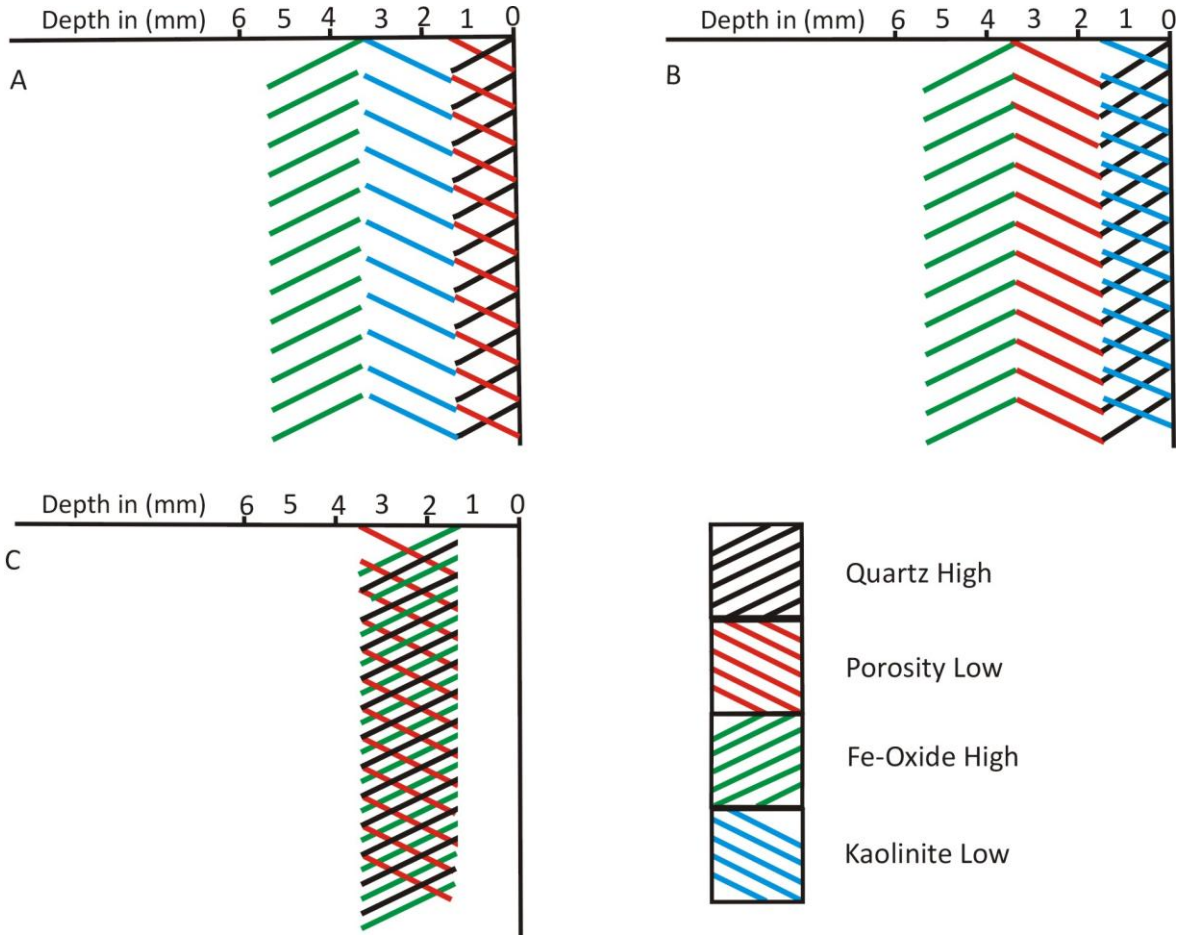

Figure 4-7: Schematic models for the mineralogical trends observed in the Dalry school samples using point counting.

The three models were produced using the patterns observed in the point counting data. The main differences are in the position of the porosity low and quartz high position.

Table 4-2: Volumetric proportions (in %) of minerals and porosity in Dalry sandstones.

Sample	Mineral	0-1 mm	2-3 mm	4-5 mm	6-7 mm	8-9 mm	10-11 mm	12-13 mm	14-15 mm	16-17 mm	18-19 mm
D1	Quartz	66.7 ± 11	69.6 ±10	68.7 ± 9.5	65.4 ± 9.5	65.0 ± 9.9	65.3 ± 10	64.1 ±9	70.4 ± 8.5	60.8 ± 11.5	n/a
	Pore	26.4 ± 26	22.7 ± 28	26.8 ± 28	29.1 ± 24	24.3 ± 23	24.3 ±23	23.9 ±20	31.1 ± 20	23.9 ± 24	n/a
	Kaolinite	3.4*	4.4*	3.0*	3.4*	7.4*	8.8*	5.9*	5.8*	5.7*	n/a
	K-Feldspar	1.1*	0.6*	0.5*	--	--	0.4*	1.2*	--	0.5*	n/a
	Mica	1.1*	1.1*	0.5*	0.9*	1.2*	0.4*	1.6*	--	0.5*	n/a
	Ankerite	--	--	--	--	--	--	--	--	--	n/a
	Fe-oxide	1.1*	1.7*	0.5*	1.3*	2.1*	0.8*	1.2*	--	1.4*	n/a
	N.O of points Counted	174	181	198	234	243	251	256	243	212	n/a
D2	Quartz	66.9 ±11	68.4 ± 9.5	55.3 ± 13	61.4 ± 9	63.3 ±10	63.5 ± 10	62.4 ±10	63.3 ±10	65.9 ± 10.5	n/a
	Pore	17.5 ± 34	19.9 ± 29	25.0 ±24.5	25.1 ±24	22.4 ±24	19.1 ±26	22.1 ± 24	20.1 ±25	16.5 ± 31	n/a
	Kaolinite	14.4 ± 40	9.2*	15.9 ±32	11.7 ±41	13.1 ± 49	16.3 ± 30	11.4 ±38	14.0 ±31	13.3 ± 40	n/a
	K-Feldspar	0.6*	--	1.0*	0.9*	0.4*	--	0.8*	1.1*	--	n/a
	Mica	--	0.5*	1.0*	0.4*	--	0.4*	1.5*	0.4*	1.6*	n/a
	Ankerite	--	--	--	--	--	--	--	--	--	n/a
	Fe-oxide	0.6*	1.9*	1.9*	0.4*	0.8*	0.8*	1.9*	1.1*	2.7*	n/a
	N.O of points Counted	160	206	208	223	237	252	263	264	188	n/a

Sample	Mineral	0-1mm	2-3 mm	4-5 mm	6-7 mm	8-9 mm	10-11 mm	12-13 mm	14-15 mm	16-17 mm	18-19 mm	20-21 mm
D3	Quartz	62.8 ± 13	61.8 ± 13	56.8 ± 14	56.6 ± 13	51.0 ± 14.5	56.0 ± 12.5	52.4 ±12.5	55.3 ±12	56.8 ± 11.5	59.7 ±12	67.1 ± 11
	Pore	25.5 ±30	23.0 ±30	26.7 ±26	26.7 ± 24	29.0 ± 22	26.1 ±24	25.9 ±24	28.8 ±23	22.3 ±24.5	22.6 ±20	17.4 ± 33
	Kaolinite	2.8*	10.5 ± 49	12.5 ±45	13.1 ±40	15.0 ± 36	13.5 ±36	19.7 ± 28	14.4 ±40	19.5 ± 27	15.7 ± 36	13.4 ± 44
	K-Feldspar	0.7*	--	0.6*	1.0*	0.5*	1.4*	0.5*	--	0.9*	--	--
	Mica	--	--	0.6*	--	0.5*	0.5*	0.5*	--	--	--	--
	Ankerite	--	--	--	--	--	--	--	--	--	--	--
	Fe-oxide	2.8*	4.6*	2.8*	2.5*	4.0*	2.4*	1.0*	1.4*	0.5*	1.9*	2*
	N.O of points Counted	145	152	176	198	200	207	208	215	220	159	160
D4	Quartz	66.1 ± 13.5	60.4 ± 14	57.8 ±15	63.6 ± 14	66.4 ±13	59.7 ±14.5	64.2 ± 13.5	n/a	n/a	n/a	n/a
	Pore	19.7 ± 39	24.5 ± 30	28.9 ± 27	21.7 ± 34	20.6 ± 34	20.2 ± 34	22.8 ± 32	n/a	n/a	n/a	n/a
	Kaolinite	13.4*	14.4 ± 42	9.9*	14.0 ± 48	13.0 ± 48	18.7 ± 35	13.0 ± 49	n/a	n/a	n/a	n/a
	K-Feldspar	--	--	--	--	--	--	--	n/a	n/a	n/a	n/a
	Mica	--	--	2.1*	0.8*	--	1.5*	--	n/a	n/a	n/a	n/a
	Ankerite	--	--	--	--	--	--	--	n/a	n/a	n/a	n/a
	Fe-oxide	0.8*	0.7*	1.4*	--	--	--	--	n/a	n/a	n/a	n/a
	N.O of points Counted	127	139	142	129	131	134	123	n/a	n/a	n/a	n/a
D5	Quartz	65.5 ± 12	58.6 ± 14	71.5 ± 10	69.0 ± 10.5	69.2 ± 10.5	63.3 ± 12	65.5 ± 11	69.5 ±10.5	n/a	n/a	n/a
	Pore	21.4 ± 32	22.0 ± 30	10.8 ± 50	17.4 ± 35	16.0 ± 36	17.2 ± 34	17.2 ± 34	15.6 ±40	n/a	n/a	n/a
	Kaolinite	11.0 ± 49	15.3 ± 41	12.0 ± 49	10.5 ± 49	12.4 ±48	14.2 ± 41	21.1 ± 30	10.8 ± 49	n/a	n/a	n/a
	K-Feldspar	--	--	1.9*	0.6*	--	--	0.5*	--	n/a	n/a	n/a
	Mica	--	0.6*	1.9*	--	--	1.2*	--	--	n/a	n/a	n/a
	Ankerite	--	--	--	--	--	--	--	--	n/a	n/a	n/a
	Fe-oxide	2.1*	3.3*	3.2*	2.5*	2.4*	4.1*	4.6*	2.9*	n/a	n/a	n/a
	N.O of points Counted	145	150	158	161	169	169	174	167	n/a	n/a	n/a

Sample	Mineral	0-1 mm	2-3 mm	4-5 mm	6-7 mm	8-9 mm	10-11 mm	12-13 mm	14-15 mm	16-17 mm	18-19 mm
D6	Quartz	65.7 ± 13	72.2 ± 14.5	73.0 ± 14.5	66.2 ± 11.5	58.0 ± 14	61.1 ± 13	58.5 ± 13.5	65.1 ± 11	n/a	n/a
	Pore	22.4 ± 32	17.4 ± 36	14.9 ± 41	14.6 ± 41	20.0 ± 32	17.3 ± 36	15.5 ± 40	16.0 ± 36	n/a	n/a
	Kaolinite	11.2*	9.7*	11.5 ± 49	18.5 ± 30	21.0 ± 32	18.5 ± 36	25.6 ± 28	17.8 ± 35	n/a	n/a
	K-Feldspar	--	--	--	--	--	--	--	--	n/a	n/a
	Mica	--	0.7*	0.7*	--	0.6*	1.9*	--	0.6*	n/a	n/a
	Ankerite	--	--	--	--	--	--	--	--	n/a	n/a
	Fe-oxide	0.7*	--	--	0.7*	--	1.2*	0.6*	0.6*	n/a	n/a
	N.O of points	134	144	148	151	157	162	164	169	n/a	n/a
D7	Quartz	63.8 ± 14	60.1 ± 12	63.6 ± 12.5	56.8 ± 15	58.8 ± 14	54.1 ± 15.5	59.7 ± 13.5	60.8 ± 13.5	62.3 ± 12.5	72.3 ± 10.5
	Pore	13.4 ± 49	14.1 ± 30	11.4 ± 49	15.9 ± 41	21.0 ± 32	23.0 ± 31	22.2 ± 31	19.0 ± 32	17.2 ± 36	12.3 ± 46
	Kaolinite	18.1 ± 39	22.3 ± 28	22.9 ± 31	23.6 ± 31	16.9 ± 39	18.9 ± 33	16.7 ± 40	14.4 ± 42	12.2 ± 46	13.6 ± 46
	K-Feldspar	3.5*	2.7*	0.7*	1.4*	2.0*	2.0*	0.7*	3.9*	2.7*	--
	Mica	--	0.5*	--	--	0.7*	--	--	--	--	--
	Ankerite	--	--	--	1.4*	--	1.4*	0.7*	1.3*	--	1.9*
	Fe-oxide	0.8*	--	1.4*	0.7*	0.7*	0.7*	--	--	--	--
	N.O of points	127	188	140	144	151	144	150	150	151	155
D8	Quartz	66.9 ± 12	55.9 ± 12	60.6 ± 13.5	63.9 ± 12	65.0 ± 11	64.5 ± 12	66.5 ± 11	62.0 ± 12	61.0 ± 12.5	n/a
	Pore	24.5 ± 22	35.4 ± 24	29.0 ± 25	28.4 ± 26	24.5 ± 28	23.4 ± 30	21.8 ± 30	26.3 ± 27	27.4 ± 26	n/a
	Kaolinite	8.6*	6.3*	7.7*	7.7*	9.8*	11.4 ± 48	10.0 ± 48	10.5 ± 48	10.4 ± 50	n/a
	K-Feldspar	--	--	--	--	--	--	--	1.2*	--	n/a
	Mica	--	1.6*	1.3*	--	--	--	1.8*	--	0.6*	n/a
	Ankerite	--	--	--	--	--	--	--	--	--	n/a
	Fe-oxide	--	0.8*	1.3*	--	0.6*	0.6*	--	--	0.6*	n/a
	N.O of points	139	127	155	155	163	158	170	171	164	n/a

Data determined by point counting, -- denotes not present. n/a indicates data was not available. Uncertainty calculated using Figure 1 of Plas and Tobi (1965), * denotes the uncertainty data points are outside the bounds on the Plas and Tobi (1965) chart, where uncertainty is greater than 50%.

4.2 RGU Samples

4.2.1 *Sandstone Mineralogy, Porosity and Grain Size*

The mineralogy of the blond sandstone samples within the RGU set are very different to each other (Figure 4-8A and B), as they have been sourced from quarries throughout Scotland and England. Figure 4-8A is a quartz, feldspar, muscovite ternary plot (discussed in section 2.1.1.2) illustrating the sandstone classification for each sample. Figure 4-8B is a kaolinite, Fe-oxide, ankerite ternary plot, highlighting the accessory mineral quantities within each sample. RGU2 (Cat Castle) is a medium-grained quartz arenite sandstone with kaolinite and Fe-oxides, accounting for a small proportion of the mineralogy, whilst carbonates are absent. RGU2 has an average quartz grain size of 414 ± 105 μm (Figure 4-9A) and pores are generally small, i.e. less than 124 μm in size (Figure 4-9B). RGU3 (Stainton Sandstone) has a quartz arenite composition and kaolinite is the main accessory mineral (~6%) but contains minimal Fe-oxide and no carbonates. The grain size of RGU3 is an average of 180 ± 42 μm and, therefore, classified as fine-to-medium grained (Figure 4-9A). Pores are mainly small in diameter, with a low proportion (5.4%) of medium to large pores (Figure 4-9B). RGU5 is an unknown Stirling Sandstone with a litharenite composition where feldspar contributes ~25% and there are small proportions of kaolinite and Fe-oxides with trace amounts of ankerite. RGU5 is medium grained (mean quartz = 194.5 ± 71 μm) (Figure 4-9A) with no accessory minerals observed apart from a tiny proportion of kaolinite (<1%), while pores are mainly small (average = 65.3 μm) (Figure 4-9B). Sample RGU6 is a Clashach Sandstone, which is medium-grained and with quartz grain diameters averaging 205.9 ± 63.8 μm (Figure 4-9A), and has the highest proportion of medium and large pores in this sample set (Figure 4-9B).

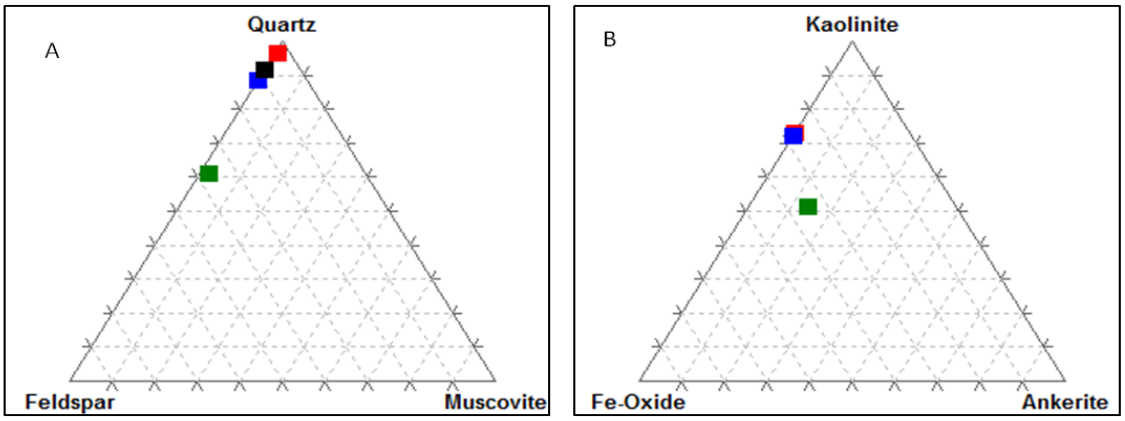

Figure 4-8: Ternary plots of the RGU samples.

A) quartz, feldspar, muscovite plot, B) kaolinite, Fe-oxide, and ankerite plot. RGU2 = red, RGU3 = blue, RGU5 = green, RGU6 = black.

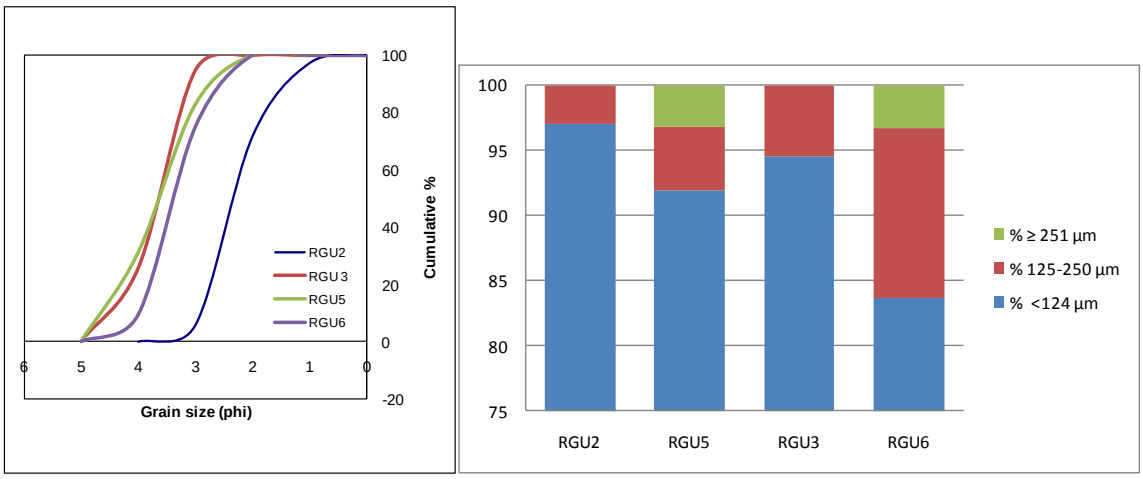

Figure 4-9: Cumulative grain size frequency chart for quartz (left) and pore size fraction chart (right) for each RGU sample.

4.2.2 *Mineralogical Impact of Weathering on the Minerals*

Although there is a range of sandstone types within this sample set, the point counting data, showed that quartz consistently has a peak abundance at 4-5 mm depth in samples RGU2, RGU3 and RGU5, whilst sample RGU6 has a peak between 2-3 mm depth (Figure 4-10). All point counting data are in Table 4-3 (pages 153-154).

Porosity lows and highs were both evident in these samples. The high occurs immediately beneath the surface of each sandstone, whilst the low generally coincides with the quartz peak area.

In those samples which contain kaolinite, a relative low in kaolinite abundance occurs, at 4- 5 mm below the outermost surface. This coincides with the high abundance of quartz

seen. In RGU2 and RGU3 a relative high proportion of kaolinite is seen occurring above this (2-3 mm depth). The Fe-oxide point counting results, however, show no conclusive patterns (Figure 4-10).

These results indicate that the formation of a hardened layer (lower porosity plus quartz high) at a depth of 4 -5 mm below the surface may be the first step in the weathering process.

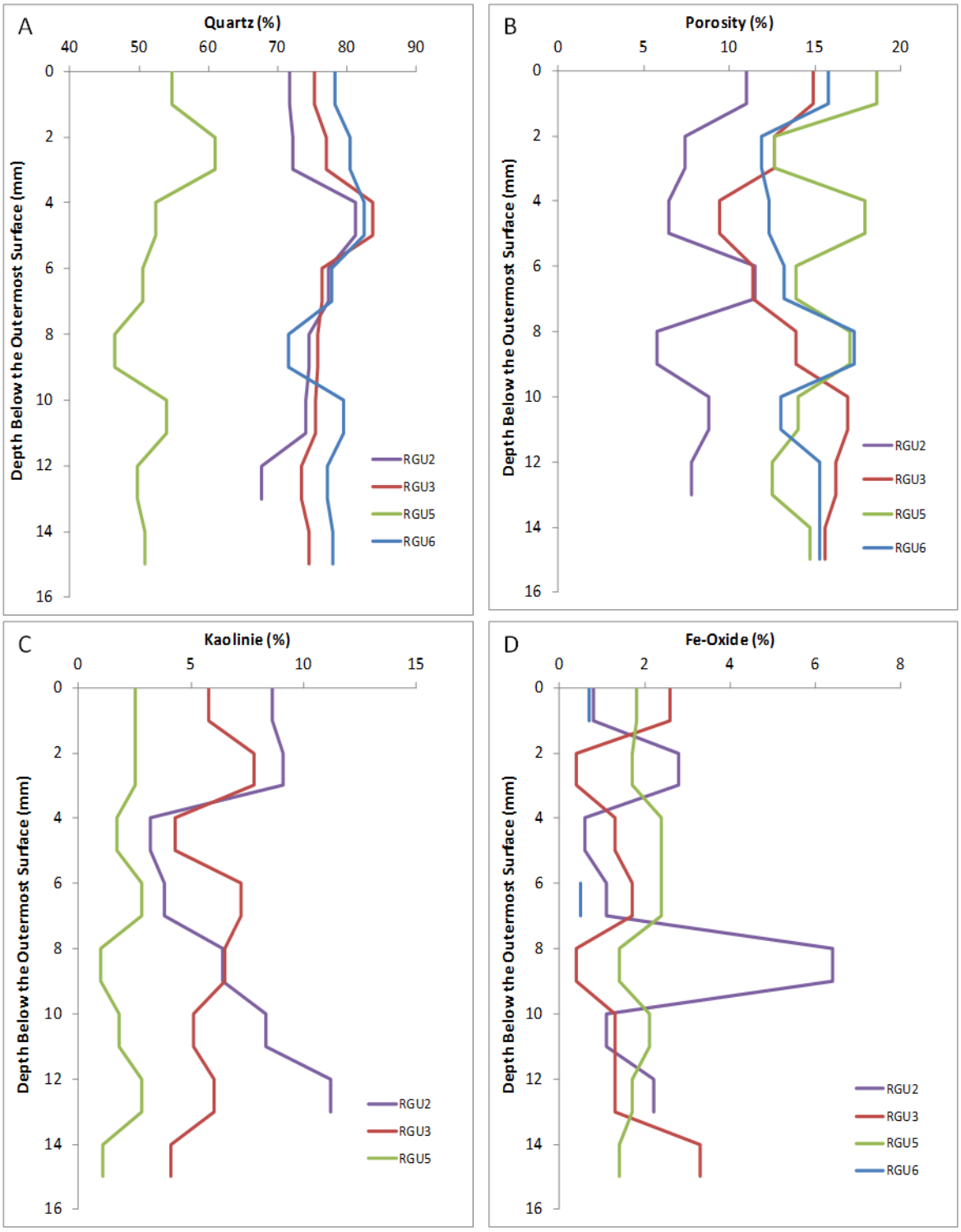

Figure 4-10: Depth against mineral proportion graphs for RGU samples.

A) quartz, B) porosity, C) kaolinite, D) Fe-oxides proportions. Data obtained through point counting.

4.2.3 *Physical Weathering Evidence*

Samples were imaged in BSE mode using the FEG-SEM to determine whether any chemical modification could be seen on either the detrital or diagenetic minerals. RGU2, RGU5 and RGU6 show no clear physical decay features on the minerals within the

outermost regions of the samples. RGU3 contains Fe-oxide pseudomorphs of carbonate cement beneath the surface but, as these are present throughout the whole sample (Figure 4-11), it is unknown whether they are a diagenetic feature or a weathering product. Due to the RGU's samples having a very short duration of exposure (10 years), it is unlikely that the pseudomorphs are purely a weathering product. Instead diagenetic dissolution may be the most likely process to have created the pseudomorphs.

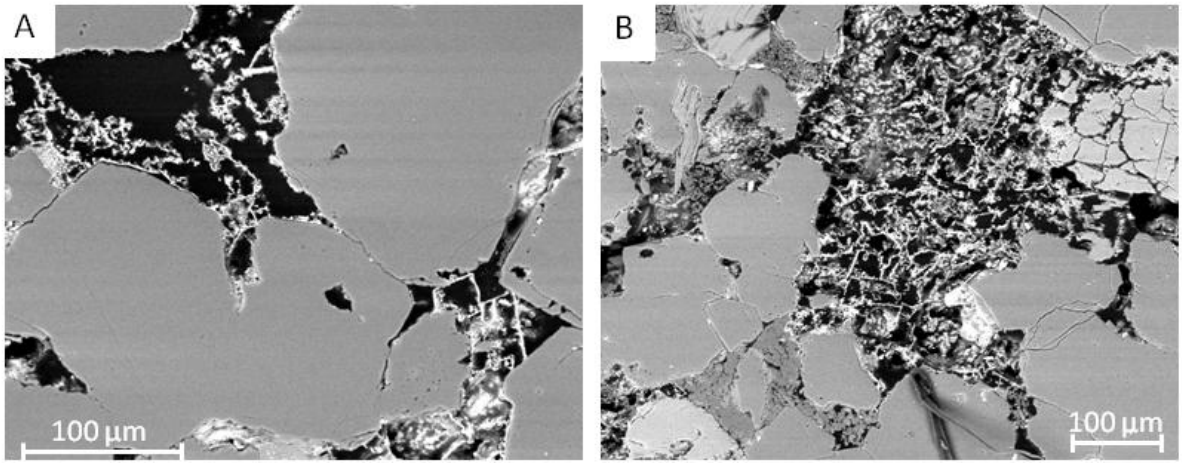

Figure 4-11: FEG-SEM BSE images of RGU3.

A) Image from 1 mm beneath the outermost surface, B) image from 21 mm beneath the outermost surface. Both images show Fe-oxide pseudomorphs replacing areas of carbonate cement.

4.2.4 *Summary*

These samples provide insight into the early stages of weathering once placed into a construction environment and indicate that case hardening at depth may be the first step in chemical weathering, and that processes such as the mobilisation of Fe-oxides take a greater time to develop. They also confirm that dissolution of ankerite can occur pre-construction.

In this sample set, a developed weathering profile is seen in both RGU2 and RGU3, where a relative porosity low, quartz high and kaolinite low occur together at a depth of 4-5 mm. These, circumstances are also partially, seen in RGU5 and RGU6, producing case hardening at depth, whilst the surface is relatively soft due to the high porosity values observed in all samples (Table 4-3). Although there is a high level of uncertainty within the point counting data, the consistency of the data throughout the samples validates the trends seen. However, this consistency in the decay trends is surprising due to the

variation in the original mineralogy and their limited exposure time. The mineralogical variation found, could possibly be an artefact of the sample collection process, where the vibrations of the drill may have caused movement of the minerals. This damage caused by drilling has not been reported before, but cannot be ruled out as a possibility. If not, a sampling artefact, these data indicate that chemical weathering develops and, affects sandstone very quickly after initial exposure to the environment.

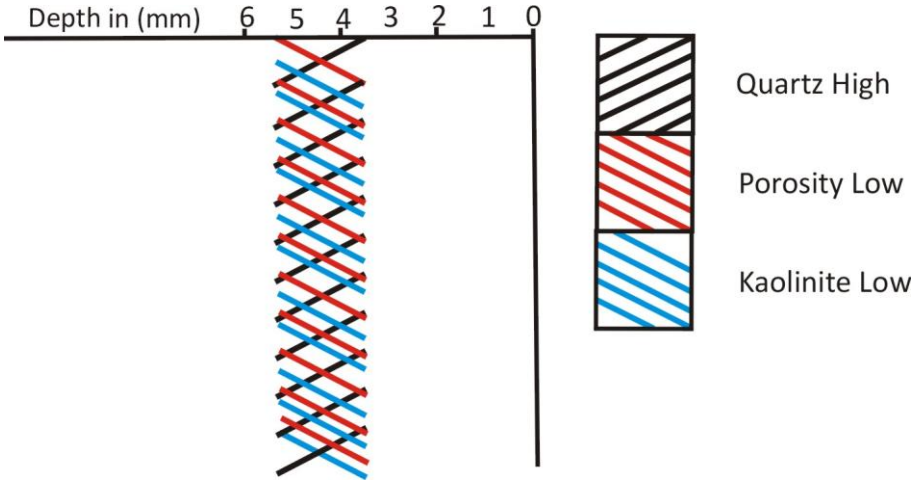

Figure 4-12: Mineralogical patterns identified in the RGU2 and RGU3.

Table 4-3: Volumetric proportions (in %) of minerals and porosity in RGU sandstones.

Sample	Mineral	0-1 mm	2-3 mm	4-5 mm	6-7 mm	8-9 mm	10-11 mm	12-13 mm	14-15 mm
RGU2 Cat Castle Sandstone	Quartz	71.7 ± 11.5	72.2 ± 10	81.3 ± 8	77.3 ± 8	74.6 ± 9	74.0 ± 8.5	67.6 ± 10	n/a
	Pore	11.0 ± 50	7.4*	6.5*	11.5 ± 48	5.8*	8.8*	7.8 ± 50	n/a
	Kaolinite	8.6*	9.1 ± 49	3.2*	3.8*	6.4*	8.3*	11.2 ± 44	n/a
	K-Feldspar	5.5*	5.1*	7.7*	2.2*	6.9*	5.0*	8.9*	n/a
	Mica	--	--	--	--	--	--	--	n/a
	Ankerite	--	--	--	--	--	--	--	n/a
	Fe-oxide	0.8*	2.8*	0.6*	1.1*	6.4*	1.3*	2.2*	n/a
	Na-feldspar	2.4*	3.4*	0.6*	4.3*	--	2.8*	2.2*	n/a
	N.O of points counted	127	176	155	185	173	181	179	n/a
RGU3 Stainton Sandstone	Quartz	75.3 ± 9	77.1 ± 7.5	83.8 ± 6	76.4 ± 7.5	75.8 ± 7.5	75.5 ± 7.5	73.5 ± 8	73.6 ± 8
	Pore	14.9 ± 42	12.6 ± 36	9.4 ± 44	11.4 ± 38	13.9 ± 32	16.9 ± 30	16.2 ± 30	15.6 ± 31
	Kaolinite	5.8*	7.8*	4.3*	7.2*	6.5*	5.1*	6.0*	4.1*
	K-Feldspar	1.3*	1.3*	2.6*	3.0*	2.6*	1.3*	2.6*	1.6*
	Mica	--	0.4*	--	--	0.4*	--	--	0.4*
	Ankerite	--	--	--	--	--	--	--	--
	Fe-oxide	2.6*	0.4*	1.3*	1.7*	0.4*	1.3*	1.3*	3.3*
	Na-feldspar	--	1.3*	--	0.4*	0.4*	--	0.4*	0.4*
	N.O of points counted	154	231	234	237	231	237	234	244

Sample	Mineral	0-1 mm	2-3 mm	4-5 mm	6-7 mm	8-9 mm	10-11 mm	12-13 mm	14-15 mm
RGU5 Unknown Stirling Sandstone	Quartz	54.8 ± 11	60.9 ± 11	52.4 ± 11.5	50.5 ± 12	46.5 ± 13	54.0 ± 11.5	49.8 ± 12	50.9 ± 12
	Pore	18.6 ±25	12.6 ± 35	17.9 ± 25	13.9 ± 30	17.0 ± 27	14.0 ± 30	12.5 ± 31	14.7 ± 30
	Kaolinite	2.5*	2.5*	1.7*	2.8*	1.0*	1.8*	2.8 *	1.1*
	K-Feldspar	21.0 ± 24	22.3 ± 24	23.8 ± 22	27.2 ± 20	28.1 ± 20	21.8 ± 23	26.5 ± 20	24.9 ± 21
	Mica	0.4*	--	0.3*	1.0*	0.7*	1.1*	2.1*	2.5*
	Ankerite	--	--	--	--	--	0.4*	0.7*	0.7*
	Fe-oxide	1.8*	1.7*	2.4*	2.4*	1.4*	2.1*	1.7*	1.4*
	Na-feldspar	--	0.4*	1.4*	2.1*	5.2*	4.9*	3.8*	4.2*
	N.O of points ccounted	272	238	290	287	288	285	287	285
RGU6 Clashach Sandstone	Quartz	78.3 ± 8.5	80.5 ± 7	82.5 ± 6	77.8 ± 7.5	71.6 ± 9	79.5 ± 7	77.2 ± 7.5	78.0 ± 7.5
	Pore	15.8 ± 38	11.9 ± 40	12.3 ± 36	13.2 ± 36	17.3 ± 30	13.0 ± 36	15.3 ± 32	15.3 ± 32
	Kaolinite	--	--	--	--	--	--	--	--
	K-Feldspar	5.3*	7.6*	5.2*	8.5*	11.1 ± 48	7.4*	7.4*	6.7*
	Mica	--	--	--	--	--	--	--	--
	Ankerite	--	--	--	--	--	--	--	--
	Fe-oxide	0.7*	--	--	0.5*	--	--	--	--
	N.O of points counted	152	214	210	211	212	208	215	215

Data determined by point counting, -- denotes not present. n/a indicates data was not available. Uncertainty calculated using Figure 1 of Plas and Tobi (1965), * denotes the uncertainty data points are outside the bounds on the Plas and Tobi (1965) chart, where uncertainty is greater than 50%.

4.3 University Samples

4.3.1 *Sandstone Mineralogy, Porosity and Grain Size*

The samples and their source locations are listed in Table 4-4 (on pages 163-165). Point counting was conducted on all samples using the method outlined in section 2.1.1.2**.** The bulk compositions of the sandstones, using the average of the innermost 4 mm of point counting data (to any avoid decay effects) are plotted on ternary diagrams. These plots show that the University samples have a quartz arenite composition (Figure 4-13A), with widely ranging diagenetic mineral abundances (Figure 4-13B) with all samples being fine-to-medium grained (mean 176.9 ± 10.4 µm) (Figure 4-14A). The pore size of these samples is generally small (71.6 µm), but ~20% of the pores within each sample are medium to large (Figure 4-14B).

Quartz quantities are very similar in all samples, ranging from 61.9% - 70.5%. The Fe-oxide proportions are also consistent between samples. However, the abundance of kaolinite has the largest proportional range, varying from 6.4% in UE1 to 12.3% in UN3. Carbonate cement is present in all samples apart from UE1, and is in the form of ankerite (discussed later) and occurs throughout the whole sample, apart from UE2, which only shows evidence of carbonates below 12 mm depth. These overall similarities in mineralogy indicate that the stone used to construct this building was sourced from one quarry. The mineral characteristics for the samples are consistent with the Hyslop et al. (2006) description of B2 sandstone (section 1.4.1.1).

Cathodoluminescence (CL) images were obtained from the outermost layer of the samples and the interior regions to provide information on the diagenetic history of the sandstone, and to assess if any effects of weathering can be diagnosed. As the similarity of the mineralogy of the samples suggests one quarry source, only some samples were chosen for analysis using CL (UN2, UE2 and UN3). Their diagenetic histories are quite similar; moderate compaction has occurred causing point contacts between grains (Figure 4-15). Quartz overgrowths are generally <20 µm in width, although slightly thicker in UE2 (Figure 4-15C and D). In all three samples, there is evidence that fracturing of quartz

grains occurred prior to cementation, as quartz overgrowths material is seen infilling fracture space. The overgrowths are non-luminescent and are presently seen intact in the outermost regions of the sandstone.

Table 4-4: Sample identification and facade for University samples.

East South East Facade	North North East facade
UN1	UE1
UN2	UE2
UN3	UE3
	UE4

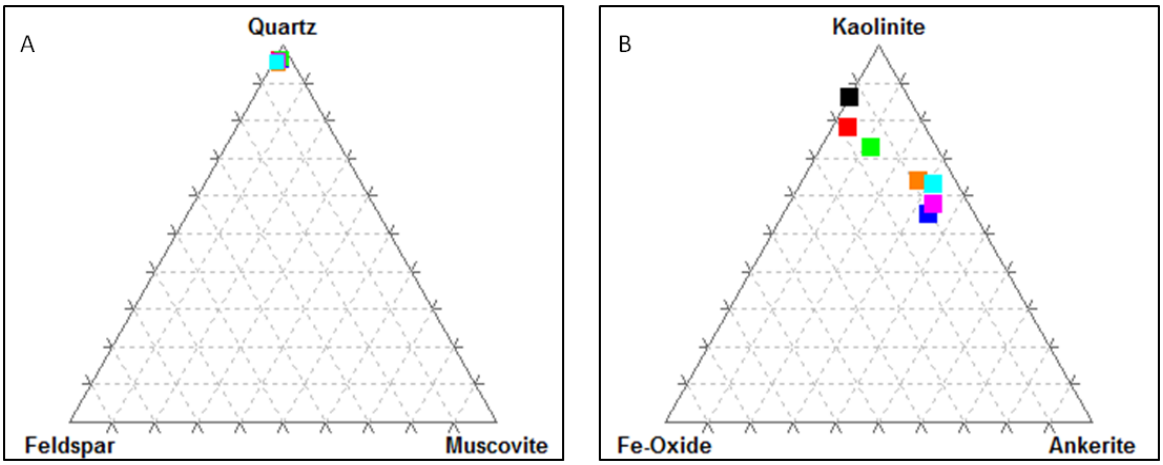

Figure 4-13: Ternary plots of all the University samples.

A) quartz, feldspar, mica plot, B) kaolinite, oxide, ankerite plot. UE1 = black, UE2 = red, UE3 = blue, UE4 = green, UN1 = pink, UN2 =orange and UN3 = light blue. Data obtained by SEM point counting.

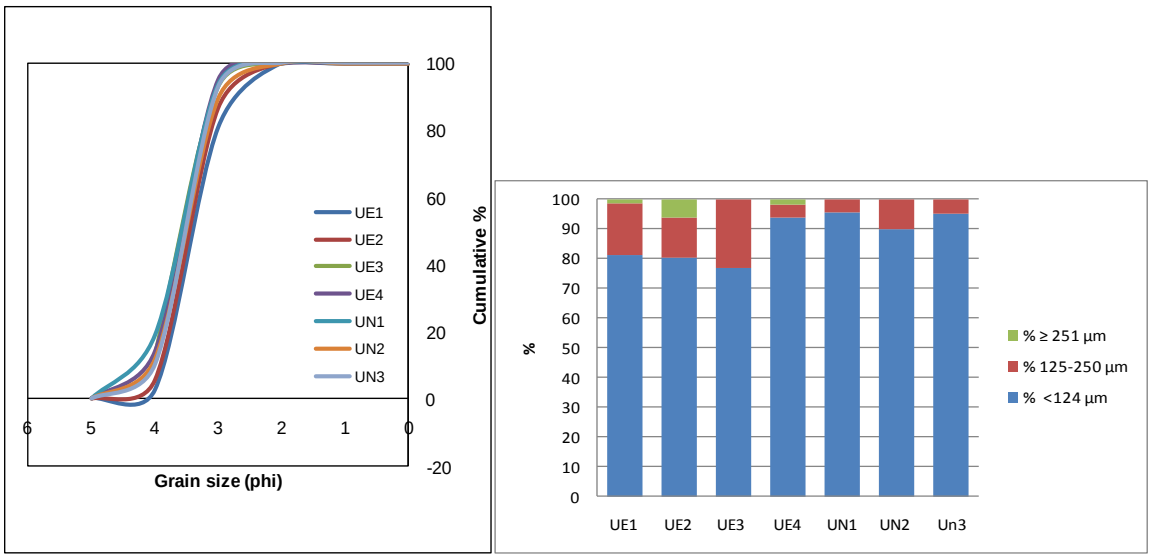

Figure 4-14: Cumulative grain size frequency chart for quartz (left) and pore size fraction graph (right) for the University samples.

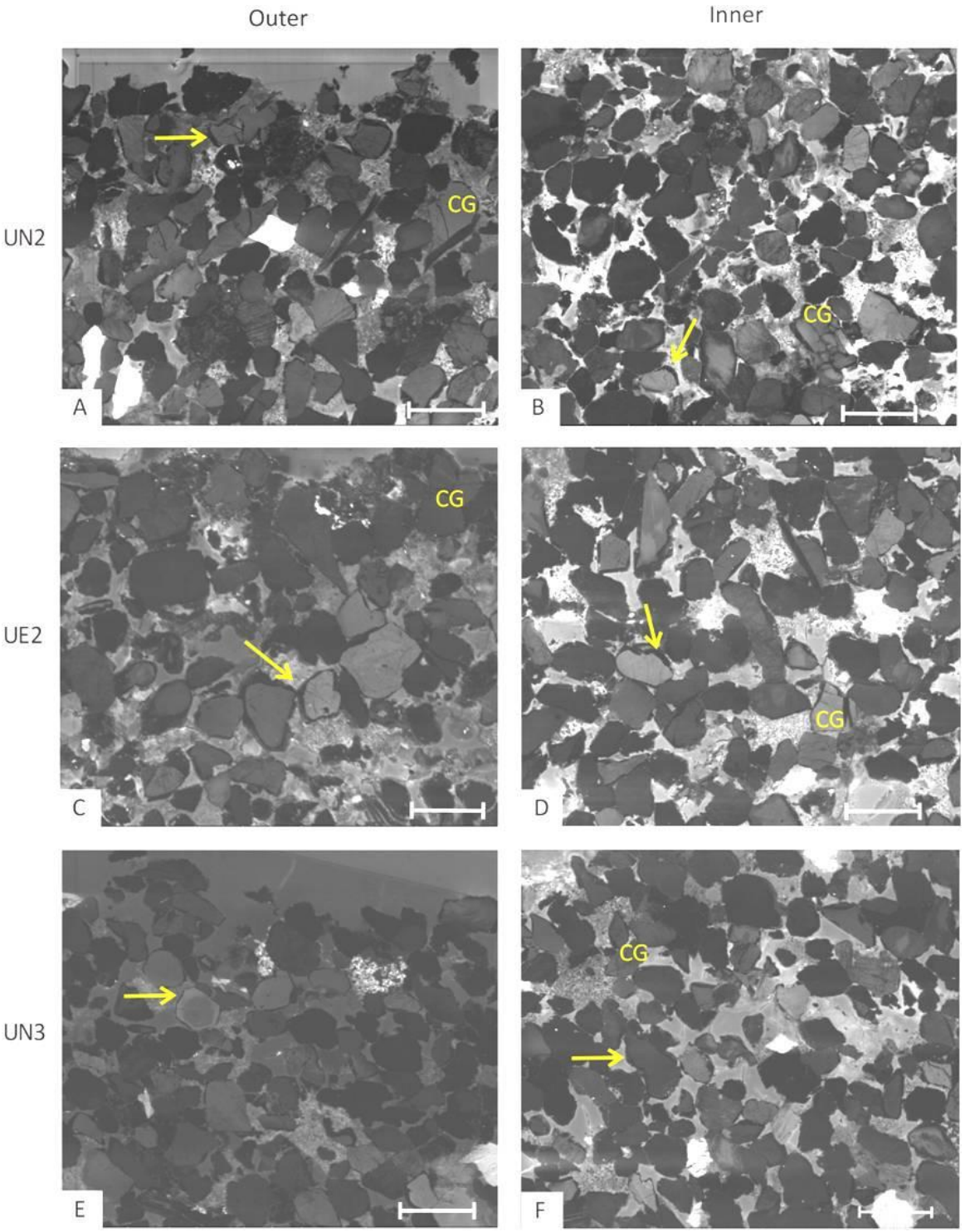

Figure 4-15: FEG-SEM CL images of University samples.

A and B) UN2. C and D) UE2. E and F) UN3. Inner images from 12 mm depth. Scale bars are 3 mm long, CG indicates cemented grains and arrows indicate quartz overgrowths. Lighter gray between grains represents the resin.

4.3.2 *Mineralogical Impact of Weathering on the Minerals*

Point counting was also conducted to assess any weathering related variations in mineral abundance and porosity between the surface and the internal part of each sample; all this data can be found in Table 4-5.

The University samples show no particularly obvious patterns within the quartz.

When any low porosity values are recorded, they occur at 2-5 mm below the outer surface and the average porosity for the outermost 6 mm is 1-2% greater than the innermost 6 mm. In UE2, where the ankerite has been lost at the surface, the porosity has been increased by 1% (Table 4-1). These porosity average values are comparable to those seen within the Dalry results.

Five of the seven University samples (UE2, UE3, UE4, UN2 and UN3) show a depleted quantity of kaolinite situated at a depth of 2 -3 mm below the surface. These generally coincide with a high proportion of clay observed at the surface of the sample (Figure 4-16).

Five out of seven samples also show Fe-oxides to be absent within the first millimetre below the surface (Figure 4-23). Generally, deeper than this, there is a high proportion of Fe-oxides. The high and low values are relative to the “bulk rock percentage”, which is an average of the innermost 4 mm of point counting data.

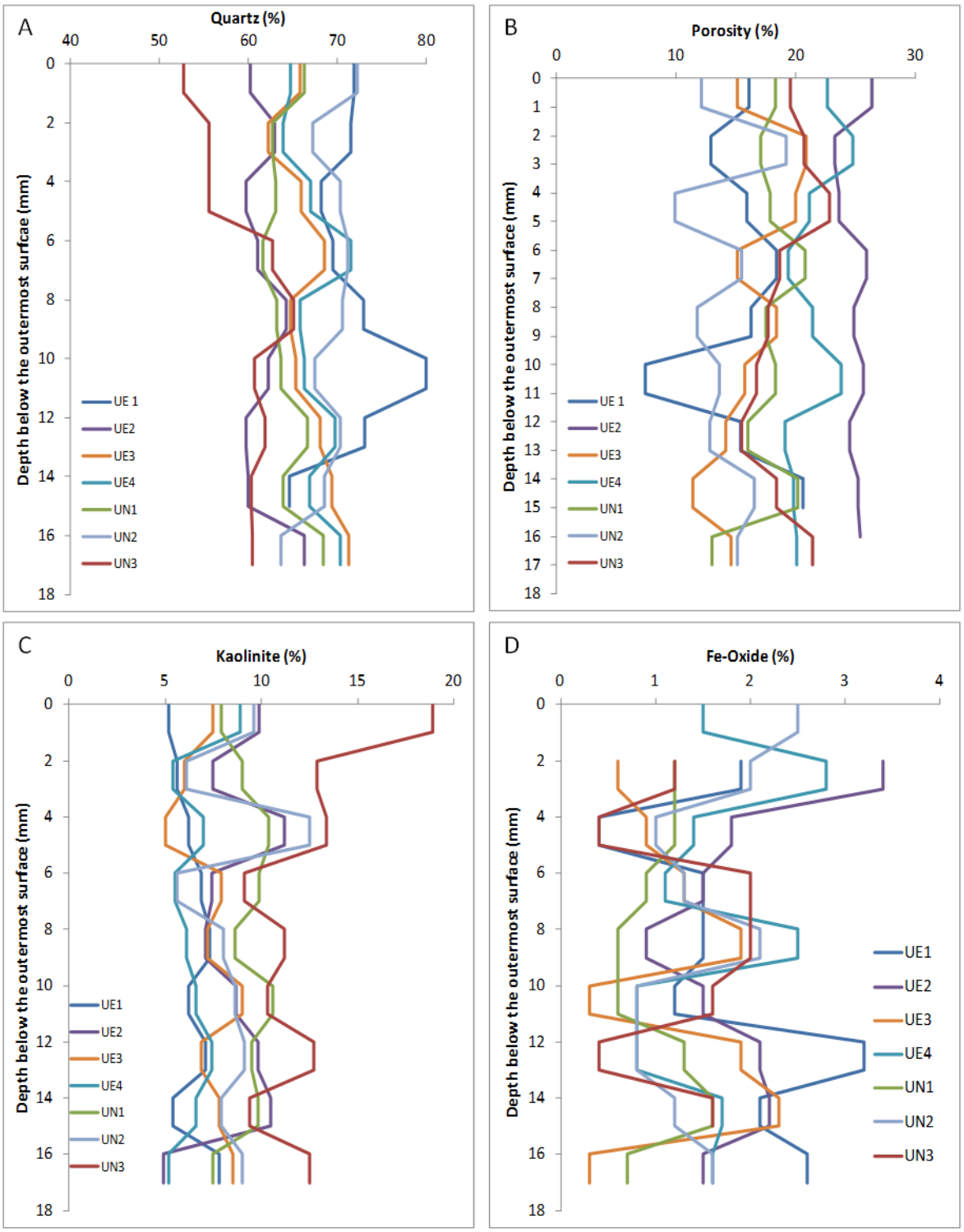

Figure 4-16: Depth against mineral proportion graphs for University samples.

A) quartz, B) porosity, C) kaolinite D) Fe-oxides, proportions within the University samples. Data obtained by point counting.

4.3.3 *Physical Weathering Evidence*

The upper regions of the polished blocks were viewed in BSE mode using the FEG-SEM, to aid identification of any physical features associated with weathering. Samples UE1, UE3,

UE4, UN1, UN2 and UN3 do not show any weathering effects on any detrital or diagenetic minerals near the surface. The carbonate cement crystals are intact and only a few show signs of slight dissolution within the outermost 2 mm. However, the carbonate minerals are affected to a much greater depth within UE2. Pristine ankerite crystals occur at 12 mm whereas, above this depth, only Fe-oxide and hydroxide pseudomorphs are found (Figure 4-17 A and B). Therefore there is good evidence for weathering to a depth of 12 mm for carbonate cements in UE2.

Despite UN2 having possible paint deposits on its surface (section 3.3.2), their presence does not seem to have increased the rate of chemical decay and, damaged the minerals beneath.

The depth of chemical weathering is generally difficult to identify within this set, apart from UE2 as it contains sequential degradation of the carbonate minerals.

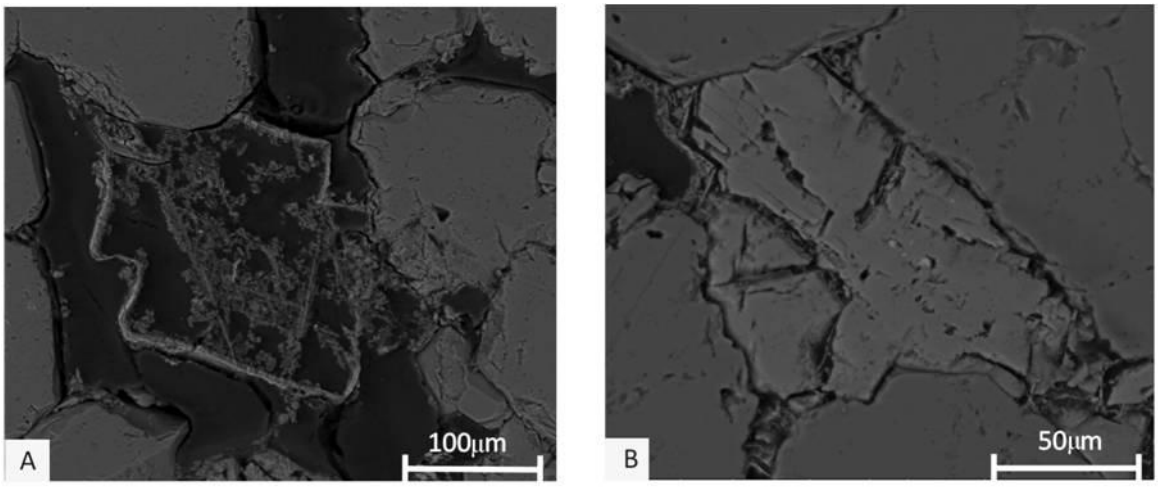

Figure 4-17: BSE FEG-SEM images of UE2.

A) UE2, Fe-oxide pseudomorph of ankerite at 3 mm beneath the weathered surface, B) UE2, partially ankerite crystal at a depth of 20 mm within the sample.

4.3.4 *X-ray Mapping*

False colour X-ray maps were made for a selection of the University samples. These images detail the surface of the blocks and highlight the quantity and extent of carbonate minerals present at the surface of the sandstones.

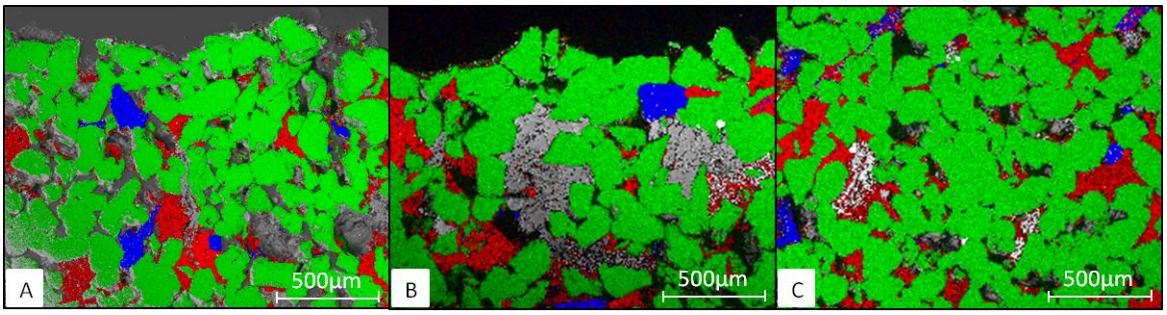

Figure 4-18: EDS false coloured maps for University samples.

Images were produced on the FEG-SEM. A) UE2 and B) UE3 at their outermost surface. C) UE4, image taken at a depth of 1 mm from the outermost surface. Green = silicon, red = aluminium, blue = potassium, light gray areas (particularly prominent in B) are carbonate minerals.

4.3.5 *Summary*

The outermost 6 mm of these samples contains the greatest evidence for chemical decay, through the loss and gain of minerals which causes a change to the original mineral proportions at various depths. However, a general weathering profile is harder to define when combining all the mineral trends. Nevertheless, two general models were produced from the evidence, which are schematically represented in Figure 4-19. Both Figure 4-19A and B show Fe-oxide rich and porosity low zones at 2-3 mm depth, with a kaolinite high directly below this. Any pattern of quartz abundance variations proves more difficult to constrain. Four samples out of the six lack any Fe-oxide in the outermost layer but are enriched below. This may indicate that the Fe-oxides are very mobile within the sandstone, forming an enriched layer before being 'washed away'. The occurrences of these patterns have no preference for orientation on the building.

Analysis of UE2 shows chemical weathering to be active in the outermost 6 mm in the form of mineral enrichment and depletion, but also shows the weathering of the carbonate cement occurs to a depth of 12 mm. It therefore has two 'levels' of chemical weathering occurring within the sample.

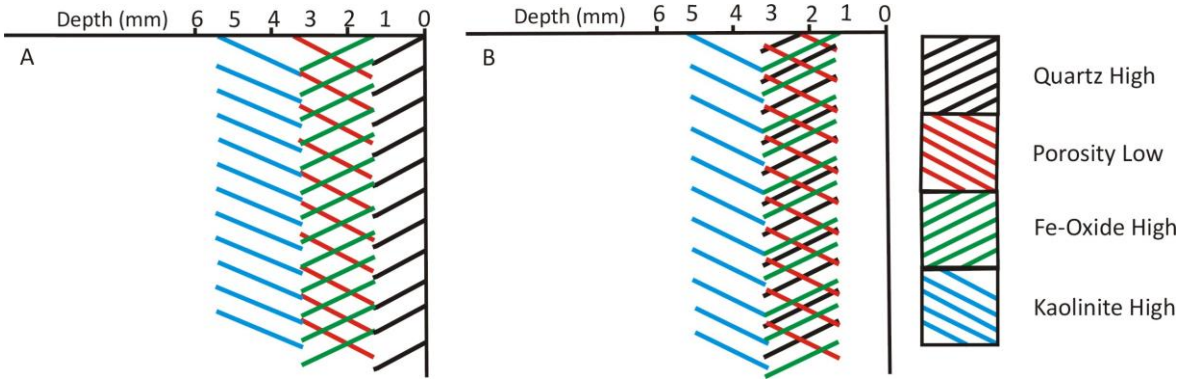

Figure 4-19: Models for the weathering profiles observed in the University samples.

Models were produced using the trends observed in the point counting data. A) has a quartz high at the surface whilst in B) the quartz high is 2-3 mm depth.

Table 4-5: Volumetric proportions (in %) of minerals and porosity in the University samples.

Sample	Mineral	0-1 mm	2-3 mm	4-5 mm	6-7 mm	8-9 mm	10-11 mm	12-13 mm	14-15 mm	16-17 mm
UE1	Quartz	71.9 ± 9	71.5 ± 10	68.2 ± 11	69.5 ± 14	73.0 ± 7.5	80.0 ± 7.5	73.1 ± 9	64.6 ± 11	n/a
	Pore	16.1 ± 32	12.9 ± 41	15.9 ± 36	18.4 ± 32	16.3 ± 28	7.4 ± 50	15.4 ± 38	20.6 ± 24	n/a
	Kaolinite	9.5 ± 46	12.4 ± 41	11.8 ± 48	7.5*	7.2 ± 41	6.3*	10.3 ± 48	10.3 ± 48	n/a
	K-Feldspar	0.5*	1.2*	3.5*	3.4*	1.5*	4.8*	1.1*	2.3*	n/a
	Mica	--	--	--	1.5*	0.4*	--	--	1.1*	n/a
	Ankerite	--	--	--	--	--	--	--	--	n/a
	Fe-oxide	2.0*	1.2*	0.6*	--	1.5*	1.7*	--	1.1*	n/a
	N.O of points counted	199	170	170	174	263	175	175	175	n/a
UE2	Quartz	60.2 ± 9	63.0 ± 9	59.8 ± 9	61.1 ± 9	64.3 ± 9	62.2 ± 9	59.8 ± 9	60.0 ± 9	66.3 ± 8
	Pore	26.4 ± 20	23.3 ± 21	23.6 ± 21	25.9 ± 20	24.9 ± 20	25.7 ± 20	24.5 ± 20	25.2 ± 20	25.4 ± 20
	Kaolinite	9.9 ± 36	7.5 ± 30	11.2 ± 32	7.4 ± 36	7.1 ± 36	8.7 ± 35	9.8 ± 35	10.5 ± 32	4.9*
	K-Feldspar	2.2*	1.9*	2.7*	3.1*	2.2*	1.9*	2.8*	1.5*	1.5*
	Mica	1.3*	0.9*	0.9*	0.9*	0.6*	--	0.3*	0.3*	--
	Ankerite	--	--	--	--	--	--	0.6*	0.3*	0.3*
	Fe-oxide	--	3.4*	1.8*	1.5*	0.9*	1.5*	2.1*	2.2*	1.5*
	N.O of points Counted	314	322	331	324	325	323	326	325	327
UE3	Quartz	65.8 ± 10.5	62.3 ± 9	65.9 ± 8	68.6 ± 7.5	64.8 ± 8.5	65.3 ± 8	68.1 ± 7.5	69.4 ± 7	71.3 ± 7
	Pore	15.1 ± 32	20.9 ± 23	20.0 ±22	15.1 ± 27	18.4 ± 24	15.8 ± 28	14.2 ± 27	11.4 ± 30	14.6 ± 30
	Kaolinite	7.5 ± 50	6.0 ± 46	5.0 ± 48	7.9 ± 41	7.2 ± 38	9.0 ± 34	6.9 ± 42	7.8 ± 38	8.5 ± 36
	K-Feldspar	5.0*	2.5*	2.2*	1.9*	2.2*	2.5*	3.1*	0.9*	0.9*
	Mica	0.5*	0.9*	0.9*	0.9*	0.6*	0.6*	0.9*	1.4*	1.2*
	Ankerite	6.0*	6.6 ± 45	5.0 ± 48	4.4 ± 50	5.0 ± 48	6.5 ± 46	4.7 ± 50	6.4 ± 46	3.0*
	Fe-oxide	--	0.6*	0.9*	1.3*	1.9*	0.3*	1.9*	2.3*	0.3*
	N.O of points counted	199	316	320	318	321	323	317	319	328

Sample	Mineral	0-1 mm	2-3 mm	4-5 mm	6-7 mm	8-9 mm	10-11 mm	12-13 mm	14-15 mm	16-17 mm
UE4	Quartz	64.7 ± 9.5	63.9 ± 8	67.0 ± 7.5	71.5 ± 7	65.8 ± 8	66.3 ± 7.5	69.8 ± 7	66.9 ± 7.5	70.4 ± 7
	Pore	22.7 ± 23	24.8 ± 20	21.2 ± 21	19.4 ± 21	21.4 ± 21	23.8 ± 20	19.1 ± 22	19.8 ± 22	20.1 ± 22
	Kaolinite	8.9 ± 40	5.4 ± 46	7.0 ± 40	5.5 ± 46	6.1 ± 41	6.6 ± 40	7.4 ± 36	6.6 ± 40	5.2 ± 41
	K-Feldspar	1.1*	1.7*	2.0*	0.8*	2.8*	1.0*	1.6*	1.7*	1.6*
	Mica	--	0.8*	0.8*	0.6*	0.3*	--	0.3*	1.9*	0.5*
	Ankerite	1.1*	0.6*	0.6*	1.1*	1.1*	1.4*	1.1*	1.4*	0.5*
	Fe-oxide	1.5*	2.8*	1.4*	1.1*	2.5*	0.8*	0.8*	1.7*	1.6*
	N.O of points counted	269	355	358	361	360	362	367	363	368
UN1	Quartz	66.3 ± 10	62.7 ± 8.5	63.1 ± 8.5	61.7 ± 8.5	63.2 ± 8.5	63.7 ± 9	66.7 ± 8	63.9 ± 9	68.4 ± 8
	Pore	18.3 ± 20	17.1 ± 24	17.9 ± 24	20.8 ± 22	17.5 ± 24	18.3 ± 24	16.0 ± 28	20.2 ± 23	13.0 ± 33
	Kaolinite	7.9 ± 48	9.0 ± 33	10.4 ± 32	9.9 ± 33	8.6 ± 38	10.6 ± 33	9.5 ± 36	9.8 ± 36	7.5 ± 36
	K-Feldspar	2.1*	3.1*	1.8*	2.0*	3.1*	1.6*	2.0*	1.6*	3.5*
	Mica	1.3*	0.6*	1.2*	1.2*	2.5*	2.3*	0.3*	0.3*	2.3*
	Ankerite	4.2*	6.2*	4.5*	3.5*	4.6*	2.9*	4.2*	2.6*	4.6*
	Fe-oxide	--	1.2*	1.2*	0.9*	0.6*	0.6*	1.3*	1.6*	0.7*
	N.O of points counted	240	322	336	342	326	311	306	307	307
UN2	Quartz	72.2 ± 8.5	67.2 ± 10	70.3 ±9.5	71.2 ± 8.5	70.6 ± 8.5	67.5 ± 9	70.4 ± 8.5	68.5 ± 9	63.7 ± 10.5
	Pore	12.1 ± 40	19.2 ± 29	9.9 ± 45	15.5 ± 32	11.8 ± 40	13.6 ± 32	12.8 ± 32	16.6 ± 30	15.1 ± 32
	Kaolinite	9.6 ± 45	6.1 ± 50	12.5 ± 40	5.6 ± 50	8.0 ± 44	8.6 ± 45	9.1 ± 42	7.9 ± 45	9.0 ± 42
	K-Feldspar	3.0*	4.0*	1.6*	3.4*	3.4*	3.7*	3.3*	0.4*	2.9*
	Mica	0.5*	1.5*	2.1*	1.3*	1.3*	0.8*	--	0.4*	1.2*
	Ankerite	--	--	2.6*	1.7*	2.9*	4.9*	3.7*	5.0*	6.5*
	Fe-oxide	2.5*	2.0*	1.0*	1.3*	2.1*	0.8*	0.8*	1.2*	1.6*
	N.O of points counted	198	198	192	233	238	243	243	241	245

Sample	Mineral	0-1 mm	2-3 mm	4-5 mm	6-7 mm	8-9 mm	10-11 mm	12-13 mm	14-15 mm	16-17 mm
UN3	Quartz	52.7 ± 12	55.6 ± 11.5	55.6 ± 12	62.7 ± 10	65.1 ± 9.5	60.7 ± 10.5	61.9 ± 10	60.4 ± 10.5	60.5 ± 10.5
	Pore	19.6 ± 32	20.7 ± 26	22.8 ± 24	18.7 ± 28	17.7 ± 28	16.7 ± 30	15.5 ± 30	18.4 ± 28	21.4 ± 23
	Kaolinite	18.9 ± 33	12.9 ± 33	13.4 ± 33	9.1 ± 42	11.2 ± 36	10.3 ± 38	12.7 ± 33	9.4 ± 50	12.5 ± 33
	K-Feldspar	6.1*	2.9*	1.7*	2.0*	2.0*	3.2*	3.2*	1.6*	2.0
	Mica	2.0*	2.5*	0.9*	0.4*	0.8*	0.4*	0.4*	0.4*	0.8
	Ankerite	0.7*	4.1*	5.2*	5.2*	5.2*	7.1*	6.0*	8.2*	2.8
	Fe-oxide	--	1.2*	0.4*	2.0*	2.0*	1.6*	0.4*	1.6*	--
	N.O of points	148	241	232	252	249	252	252	245	248

Data determined by point counting, -- denotes not present. n/a indicates data was not available. Uncertainty calculated using Figure 1 of Plas and Tobi (1965), * denotes the uncertainty data points are outside the bounds on the Plas and Tobi (1965) chart, where uncertainty is greater than 50%.

4.4 St Vincent Street Samples

4.4.1 *Sandstone Mineralogy, Porosity and Grain Size*

Four samples were analysed from the SVS set: EE1, EE3 and EE4 from the east elevation of the building and CS4 from the northwest corner. The mineralogical compositions of the sandstones (using an average of the deepest 4 mm point counted to eliminate anomalous results due to weathering) were plotted onto ternary diagrams (Figure 4-20A and B) to represent the bulk composition. All the point counting data can be seen in Table 4-6 (pages 172-173). The ternary diagrams show that all samples from this building have predominantly a quartz arenite composition (Figure 4-20 A). They are medium-grained (mean = 170.5 ± 3.4 μm) (Figure 4-21A). Pores are generally small, with EE4 exhibiting the largest variation in pore size, ranging from 291.6 – 8.3 μm (Figure 4-21B). The accessory minerals are quite wide ranging in their proportions (Figure 4-20B). The clay minerals vary from 4.7% in EE1 to 12.7% in EE3, although little variation in the quantities of Fe-oxides occurs. The proportion of carbonate within stone from the two facades is quite different. The east elevation (EE) samples show an average of 6%, ranging up to 10.5% in EE4, whilst the average carbonate content for the northwest corner (CS) samples is markedly different at 1.5%, with the highest abundance only reaching 2.8%. Based on the diagenetic minerals present, these samples correspond to the Hyslop et al. (2006) description of the B2 sandstone category, and historical records indicate that the sandstones are all from the Giffnock quarry, located on the outskirt of Glasgow. Therefore, the difference in proportion of carbonate cement proportions on the differing sides of the building may be a characteristic of the sandstone and so an artefact of where the stone was taken from within the quarry.

The FEG-SEM was used to obtain CL images, which were taken from the outermost layer of the sample as well as the interior to provide information on the diagenetic history of the sandstone. CL imaging may also provide information on whether the outermost layer has been affected by weathering since being placed within a building. As mineralogical and historical evidence suggests one quarry source, only CS4 and EE4 were analysed within this set and both show very similar features. The images of the sandstone show that they have suffered moderate compaction with point contacts between the quartz

grains, and only thin non-luminescent quartz overgrowths present (Figure 4-22). Both samples show evidence of quartz fracturing occurring prior to cementation, as the overgrowths infill fractures (Figure 4-22). The overgrowths at the surface of the sandstone appear unaffected by weathering.

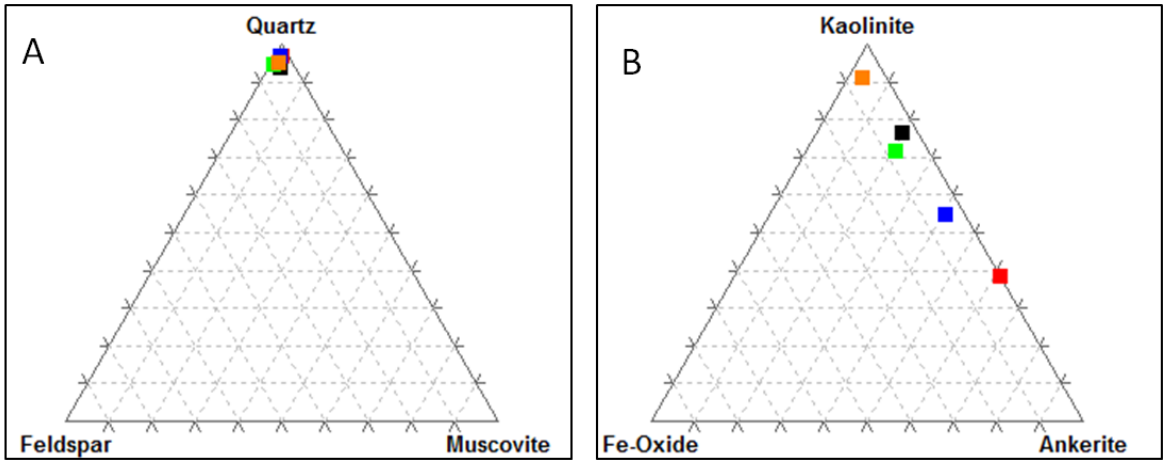

Figure 4-20: Ternary plots of the St Vincent Street samples.

A) Quartz, K-feldspar and muscovite plot, B) kaolinite, Fe-oxide and ankerite plot. EE3 = black, EE4 = red, EE1 = blue, CS2 = green and CS4 = orange.

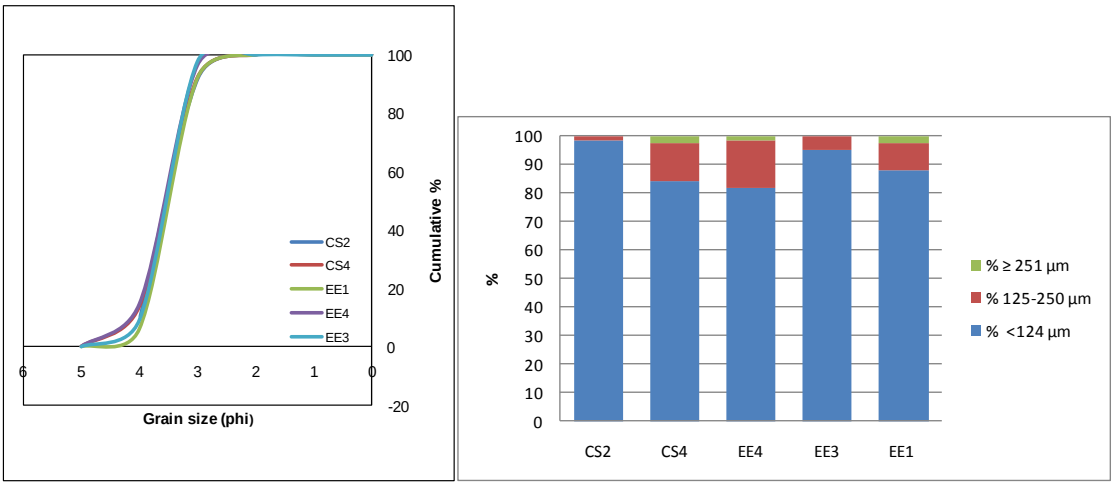

Figure 4-21: Cumulative frequency chart for quartz size (left) and pore size fraction (right) for each SVS sample.

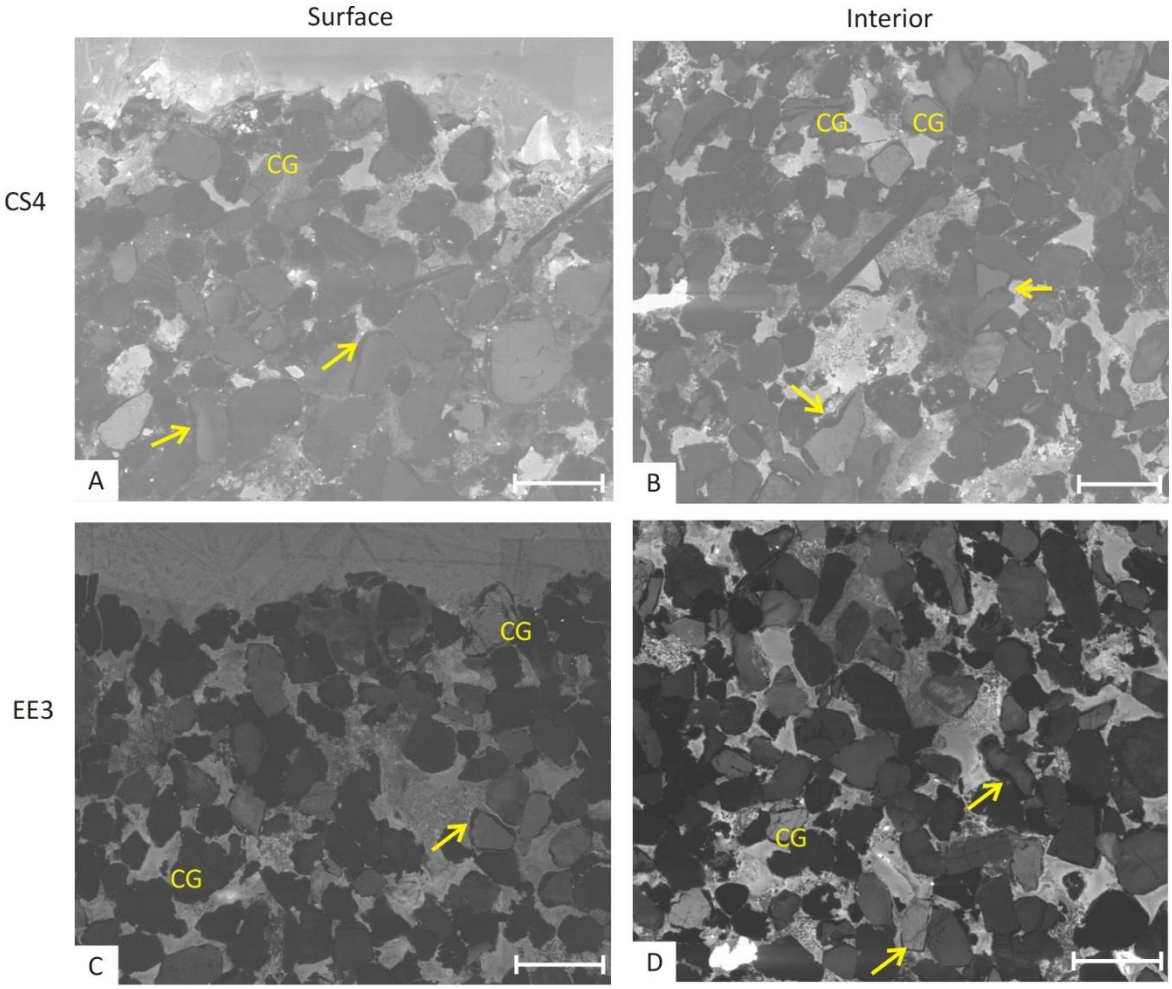

Figure 4-22: Series of CL images taken on the FEG-SEM of CS4 and EE3.

A and B) CS4. C and D) EE3. Scale bars are 3 mm long. CG = carbonate grains, arrows indicate quartz overgrowths. Gray between quartz represents resin.

4.4.2 *Mineralogical Impact of Decay on the Minerals*

Point counting was also conducted to investigate any small alterations and/or repeating patterns in the mineralogical composition between the surface and the internal part of the core, potentially caused by weathering. All data is in Table 4-6.

The highs and lows in mineral abundance are compared with the bulk average which was taken from the innermost 4 mm of point counting data.

Some samples (EE1, EE4 and CS4) show a high abundance of quartz occurring at the surface and, directly below this is a low in abundance relative to the internal average (Figure 4-23). EE3 gives an anomalous result, as the observed low quartz abundance occurs at 4 – 5 mm below the outermost surface.

The porosity results show that a high in quartz is recorded alongside a low in exists, and vice versa (Figure 4-23).

The kaolinite point counting data shows a consistent low at a depth between 2-5 mm below the sandstone surface in each sample (Figure 4-23).

CS4 exhibits a relatively enriched layer of Fe-oxides between 8-9 mm depth, which is followed by a dramatic decrease in the Fe-oxide at 10-11 mm depth, while only a small proportion of Fe-oxide is recorded at deeper levels. This pattern is also seen in EE3 but each stage is seen a millimetre deeper than in CS4 (Figure 4-23).

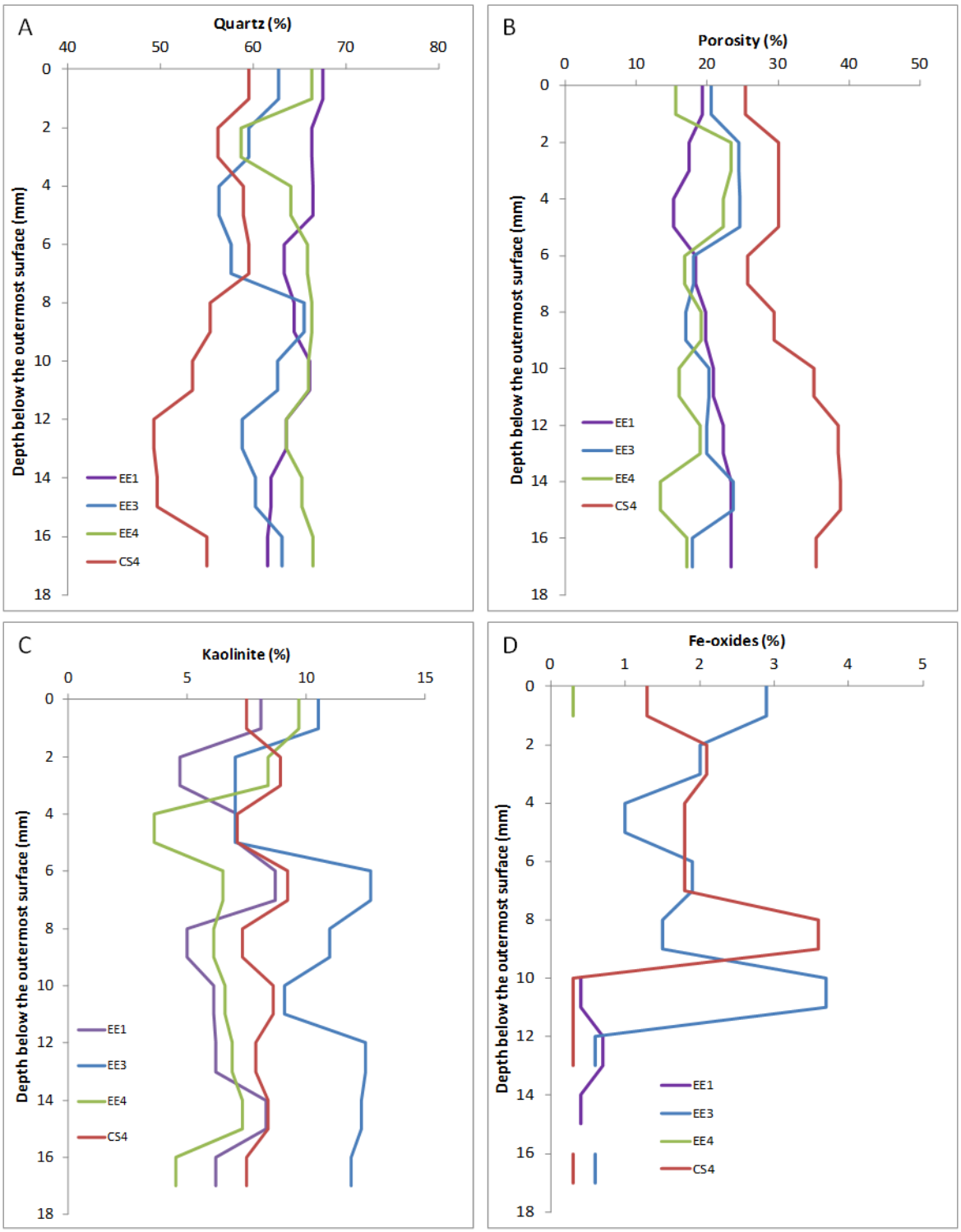

Figure 4-23: Depth against mineral proportion graphs for SVS samples.

A) quartz, B) porosity, C) kaolinite D) Fe-oxides, proportions within the SVS samples. Data obtained by point counting.

4.4.3 *Physical Weathering Evidence*

The upper regions of each block were studied in BSE mode using the FEG-SEM, to help identify any physical features which may be linked to decay. Samples CS4, EE1, EE3 and

EE4 were analysed in this section. Both CS4 and EE3 show no weathering features within the quartz grains and there is no dissolution of the carbonate minerals as they remain intact at the very surface of these samples. Whole ankerite crystals are present at the surface of EE1, although kaolinite is infilling the regions between the quartz grains on the surface (Figure 4-24A). The surface of EE4 is half covered in mortar, while the half with no mortar shows kaolinite crystals infilling the gaps between the detrital quartz and K-feldspar grains at the surface. The quartz grains are highly fractured at the surface (Figure 4-24), which is not thought to be an artefact of sample preparation because such extensive fracturing is not observed on any other side of the sample. Whole ankerite crystals at the surface can also be seen in EE3 and EE4 (Figure 4-25).

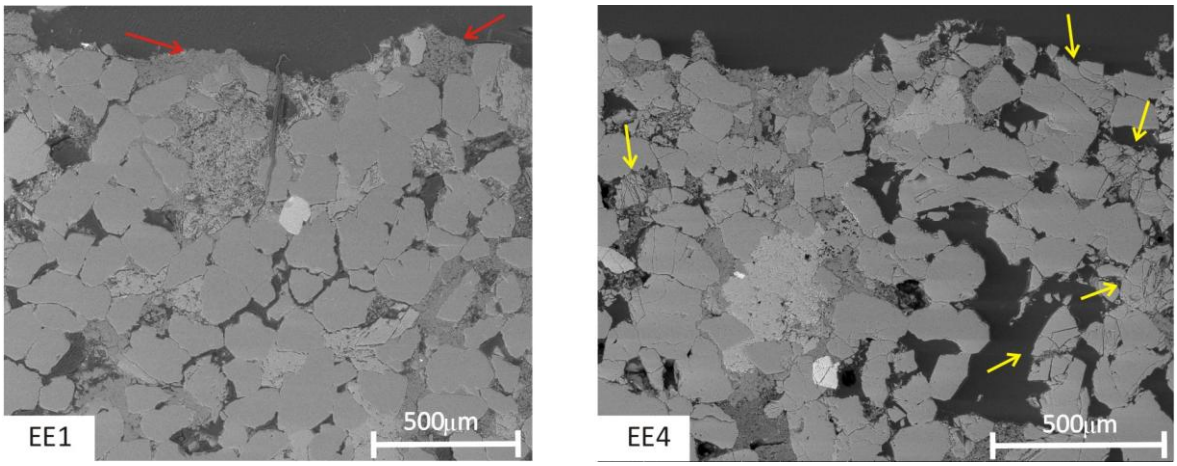

Figure 4-24: BSE FEG-SEM images of SVS polished blocks.

A) EE1, showing kaolinite dominating regions between quartz grains on the surface (red arrows). B) EE4, showing cracked and broken quartz grains at the surface (yellow arrows).

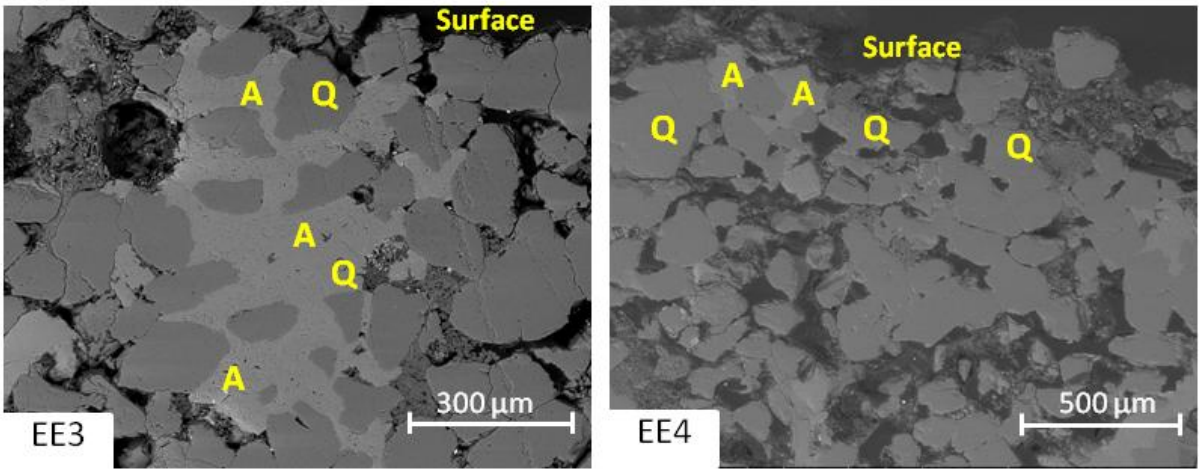

Figure 4-25: FEG-SEM BSE images of ankerite minerals within EE3 and EE4.

A = ankerite, Q = quartz, both images from the outermost surface.

4.4.4 *Summary*

The carbonate cements in these samples appear totally unaffected by chemical weathering, with intact carbonates occurring at the outermost surfaces. This could be because a new surface has recently been exposed, but the samples show a dark crust on the surface which dismisses this possibility.

The main effects of weathering are again symbolised by the loss and gain of minerals within the outermost 6 mm of the sandstones (Figure 4-26). Although the uncertainty associated with point counting is high, clear trends are still identifiable. Generally, the outermost millimetre has a quartz and Fe-oxide peak accompanied by a porosity low. The clays are likely being lost from 4-5 mm depth and brought to the surface to cause a high abundance in the outermost layer (Figure 4-26). This may be the evidence of chemical weathering, causing the surface of the sandstone to become case hardened.

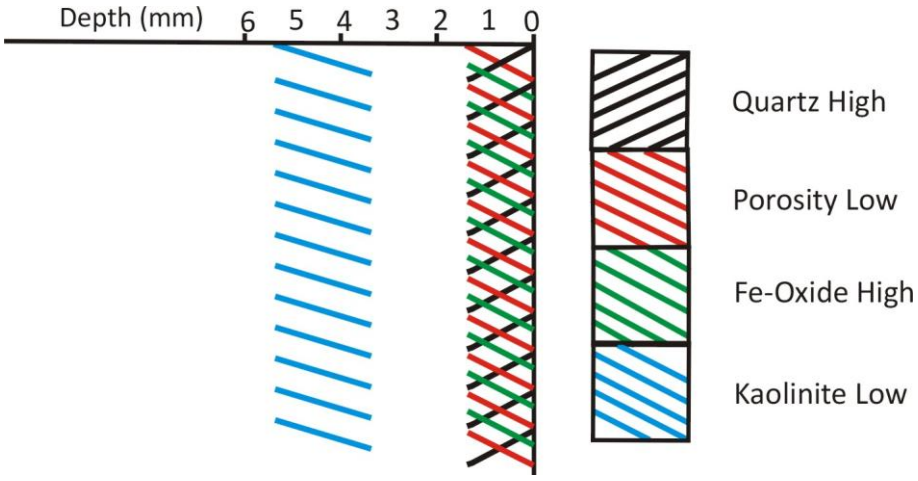

Figure 4-26: Models for the weathering profiles observed in the SVS samples.

Models were produced using the trends observed in the point counting data. Due to Quartz and Fe-oxide high at surface case hardening may be forming.

Table 4-6: Volumetric proportions (in %) of minerals and porosity within the SVS samples.

Sample	Mineral	0-1 mm	2-3 mm	4-5 mm	6-7 mm	8-9 mm	10-11 mm	12-13 mm	14-15 mm	16-17 mm
EE1	Quartz	67.5 ± 10	66.3 ± 9.5	66.4 ± 10	63.4 ± 8.5	64.4 ± 10	66.1 ± 8.5	63.6 ± 9	61.9 ± 10	61.5 ± 10.5
	Pore	19.3 ± 29	17.4 ± 28	15.2 ± 32	18.4 ± 24	19.7 ± 27	20.9 ± 24	22.3 ± 23	23.4 ± 30	23.3 ± 23
	Kaolinite	8.1 ± 49	4.7*	7.1 ± 48	8.7 ± 38	5.0*	6.1 ± 46	6.2 ± 44	8.3 ± 40	6.2 ± 48
	K-Feldspar	1.5*	3.9*	2.8*	1.9*	1.7*	0.7*	1.4*	1.4*	1.2*
	Mica	--	1.6*	0.9*	--	1.3*	1.1*	0.3*	0.7*	1.2*
	Ankerite	3.6*	6.2 ±48	7.6 ± 48	7.4 ± 39	7.9 ± 44	4.7*	5.5*	3.2*	6.6*
	Fe-oxide	--	--	--	--	--	0.4*	0.7*	0.4*	--
	N.O of points counted	197	258	211	309	239	277	291	278	257
EE3	Quartz	62.7 ± 10.5	59.5 ± 11.5	56.3 ± 13	57.6 ± 12	65.5 ± 10.5	62.6 ± 11.5	58.8 ± 13	60.2 ± 11	63.1 ± 12
	Pore	20.6 ± 31	24.5 ± 24	24.6 ± 25	18.0 ± 30	17.0 ± 32	20.3 ± 29	20.0 ± 30	23.7 ± 24	17.9 ± 36
	Kaolinite	10.5 ± 40	7.0 ± 48	7.0 ± 48	12.7 ± 39	11.0 ± 44	9.1 ± 47	12.5 ± 40	12.3 ± 36	11.9 ± 46
	K-Feldspar	1.3*	1.0*	5.5*	2.9*	1.5*	0.5*	3.1*	1.7*	1.8*
	Mica	0.4*	0.5*	0.5*	2.0*	1.0*	0.5*	--	--	1.8*
	Ankerite	1.6*	5.5*	5.0*	4.9*	2.0*	3.2*	5.0*	2.1*	2.4*
	Fe-oxide	2.9*	2.0*	1.0*	1.9*	1.5*	3.7*	0.6*	--	0.6*
	N.O of points counted	228	200	199	205	194	187	160	236	168
EE4	Quartz	66.3 ± 9	58.7 ± 9	64.0 ± 7.5	65.9 ± 7.5	66.3 ± 7.5	66.0 ± 7.5	63.6 ± 8	65.2 ± 10	66.5 ± 9.5
	Pore	15.6 ± 30	23.4 ± 20	22.3 ± 20	16.8 ± 22	19.1 ± 21	16.1 ± 24	19.0 ± 22	13.4 ± 32	17.1 ± 28
	Kaolinite	9.7 ±38	8.4 ± 36	3.6*	6.5 ± 40	6.1 ± 40	6.6 ± 38	6.9 ± 36	7.3 ± 44	4.5*
	K-Feldspar	1.0*	1.4*	1.4*	0.8*	1.6*	0.8*	1.1*	2.0*	0.4*
	Mica	0.3*	0.9*	0.3*	0.5*	0.3*	1.6*	0.6*	1.6*	0.8*
	Ankerite	6.6 ± 48	7.2 ± 40	8.3 ± 38	9.5 ± 32	6.6 ± 40	9.0 ± 32	8.8 ± 34	10.5 ± 41	10.6 ± 41
	Fe-oxide	0.3*	--	--	--	--	--	--	--	--
	N.O of points counted	288	346	358	369	377	379	363	247	245

Sample	Mineral	0-1 mm	2-3 mm	4-5 mm	6-7 mm	8-9 mm	10-11 mm	12-13 mm	14-15 mm	16-17 mm
CS2	Quartz	64.7 ± 8	67.7 ± 7.5	68.1 ± 11.5	n/a	n/a	n/a	n/a	n/a	n/a
	Pore	22.3 ± 21	15.3 ± 26	15.3 ± 32	n/a	n/a	n/a	n/a	n/a	n/a
	Kaolinite	7.3 ± 48	9.6 ± 32	8.7 ± 44	n/a	n/a	n/a	n/a	n/a	n/a
	K-Feldspar	1.7*	4.2*	3.5*	n/a	n/a	n/a	n/a	n/a	n/a
	Mica	0.6*	0.3*	0.4*	n/a	n/a	n/a	n/a	n/a	n/a
	Ankerite	2.8*	2.0*	2.6*	n/a	n/a	n/a	n/a	n/a	n/a
	Fe-oxide	0.6*	0.8*	1.3*	n/a	n/a	n/a	n/a	n/a	n/a
	N.O of points counted	354	353	229	n/a	n/a	n/a	n/a	n/a	n/a
CS4	Quartz	59.5 ± 9	56.2 ± 8	58.9 ± 10	59.5 ± 9.5	55.4 ± 9	53.4 ± 11	49.3 ± 11.5	49.7 ± 14	55.0 ± 10
	Pore	25.3 ± 23	30.0 ± 18	30.1 ± 18	25.7 ± 21	29.5 ± 20	35.0 ± 16	38.4 ± 15	38.7 ± 18	35.4 ± 15
	Kaolinite	7.5 ± 48	8.9 ± 40	7.1 ± 41	9.2 ± 41	7.3 ± 41	8.6 ± 40	7.9 ± 37	8.4 ± 46	7.5 ± 40
	K-Feldspar	4.0*	1.4*	1.4*	1.8*	1.0*	1.4*	2.1*	1.8*	0.9*
	Mica	1.3*	1.4*	0.4*	1.4*	2.3*	1.0*	1.4*	0.9*	0.6*
	Ankerite	0.9*	--	0.4*	0.7*	0.5*	0.3*	0.7*	0.4*	0.3*
	Fe-oxide	1.3*	2.1*	1.8*	1.8*	3.6*	0.3*	0.3*	--	0.3*
	N.O of points counted	225	292	282	284	193	292	292	225	322

Data determined by point counting, -- denotes not present. n/a indicates data was not available. Uncertainty calculated using Figure 1 of Plas and Tobi (1965), * denotes the uncertainty data points are outside the bounds on the Plas and Tobi (1965) chart, where uncertainty is greater than 50%.

4.4.5 *Discussion of Overall Decay Patterns*

Once the mineralogy and porosity values have been well established for each sample, it is easier to distinguish the diagenetic features from the weathering features. As previously described, chemical weathering can occur in many different forms, such as the movement of minerals through reprecipitation, complete dissolution of particular minerals and the chemical and physical alteration of minerals. All samples analysed in this study show chemical weathering occurring, but to varying degrees.

The easiest samples to identify evidence of chemical weathering in are those that show a progressive degradation of carbonate cement from the interior to the exterior of the sample (e.g. D7 and UE2). The depth of carbonate weathering is expressed as the depth to where altered carbonate minerals are seen, beyond which the carbonate crystals remain unaffected and whole. D7 has a carbonate weathering depth of 6 mm whilst, within UE2, it is as deep as 12 mm. Carbonate cement is expected to dissolve rapidly in comparison to other minerals (Price, 1995; Lasaga, 1998) and their dissolution is common-place in limestone (Evamy, 1967; Al-Hashimi and Hemingway, 1973; Frank, 1981) and sandstone (Wang, 1992), which is believed to produces secondary porosity. However, Lee et al. (2006) conducted one of the few studies that have discussed the dissolution of carbonate cement as a viable weathering process in sandstone buildings. The present study, together with Lee et al. (2006), shows that porosity within the dissolved carbonate region of the stone was reduced, rather than the expected increase. This contradicts the previous studies mentioned, where dissolution was believed to cause secondary porosity. The two main possibilities for this contradictory result are: 1) due to the weakened structural integrity at the surface, the remaining minerals have collapsed inwards onto themselves to reduce porosity; 2) the presence of increased void space could allow atmospheric debris to penetrate, blocking the pores and reducing the porosity. Carbonate cement is observed in many of the samples occurring at the outermost surface, where it appears as whole intact crystals, although it is unknown why this ankerite is unaffected by decay. These crystals may contain trace elements which are causing the ankerite to be resilient to decay. Alternatively, the overlying black crust may have formed quicker than the initialisation of dissolution of the cement, therefore acting

as a protective layer. The last hypothesis may be that the rain water solution is not as efficient at dissolving these carbonates.

Chemical and physical weathering is also expressed through the abundance and reduction of minerals within layers, in the outermost ~6 mm of the sandstone, which can occur at a rapid rate. The RGU samples indicate a well defined weathering structure, despite their very short duration of exposure to the environment and their range of original compositions.

The main weathering layers observed in the building stone samples are:

- quartz abundance/quartz reduction
- Fe-oxide abundance/ Fe-oxide reduction
- porosity reduction
- kaolinite abundance/kaolinite reduction

Due to the variability in the original composition of the differing sample sets, it is difficult to incorporate all the data gathered into a general model, However, the most common trends are shown in Figure 4-27A and B.

The features worked into the models are the quartz high, porosity low and Fe-oxide high. However, as a consequence of enrichment of a mineral in one layer, a depleted instance of that mineral will form in another layer. Kaolinite concentrations do show significant enrichment and depletion in layers within the outermost 6 mm. However, the precise location of these layers is less well defined and, therefore, harder to incorporate into the generalised models.

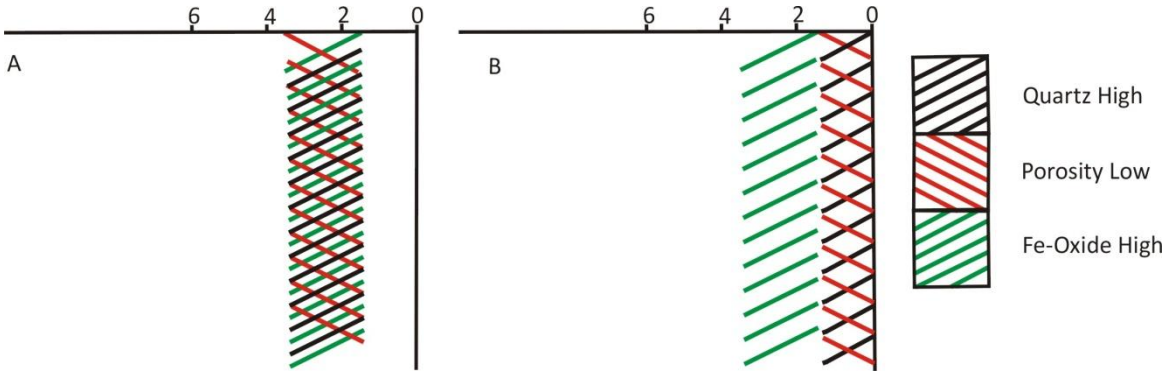

Figure 4-27: Most common internal structures seen throughout all the samples. Measurements are in mm.

Internal layers within sandstone have been previously described and discussed extensively, although these studies are normally in association with microbial activity (Friedmann, 1982; Gómez-Alarcón et al., 1995; Omelon et al., 2006b, 2007). In these studies, the weathering layers are defined by colour, and the only mineralogical change discussed is the depletion and enrichment of Fe-oxides caused by the mobilisation and activity of microorganisms, as the layers are caused by large mats of microbial matter. As detailed further in the chapter 5 (microbial results), no extensive layers of cryptoendolithic microbes were identified during the present study. Therefore, it is unlikely that the layering seen in these samples are an outcome of microbe assisted movement of minerals.

A few previous studies focus only on chemical changes which cause a mineralogical stratification within sandstone. Jefferson (1993) and Bluck and Porter (1991a and b) both suggest that the ingress and later egress of water will dissolve the slightly unstable Fe-oxides and clay minerals at depth, then redeposit them at the outermost surface, which will consequently produce a porosity low due to the influx of kaolinite. Price (1995) acknowledges that chemical weathering occurs within sandstone and that minerals will be transported to shallower levels due to water movement, although does not provide further detail regarding any layering structures this may cause.

The model presented by Bluck and Porter (1991a) has three layers beneath the crust: 1) an enriched layer, 2) a light brown patina and 3) a depleted layer. However, no scale is given on the thickness and placement of each layer and only vague details of their compositions are provided. Lee et al. (2006) identifying, one layer within the blond sandstone located at a depth of 8-10 mm which is characterised by the production of Fe-

oxides and hydroxide by ankerite dissolution. There is no mention of regions abundant in kaolinite and quartz.

Results from the present study also indicate that case hardening may be an important process on the surface of the sandstones. A case hardened crust consists mainly of host rock with a fine-grained cement and kaolinite, and is 0.5-5 mm thick (Conca and Rossman, 1982). Results from the Glasgow stones show that a layer abundant in quartz, Fe-oxide and kaolinite is evident in most samples near or at the outermost surface, which also coincides with a porosity low (~1 mm thick). Comparable layers have been seen on other sandstones of similar ages (Mcalister et al., 2003) and case hardening is a common feature found on many different sedimentary rock types including sandstone. Case hardening can be caused by entirely physical and chemical processes, but it has been suggested that micro-organisms may play an important role in the hardening of rock (Viles and Goudie, 2004), although the specific role microbes may play is still uncertain. As the least exposed samples (RGU), show case hardening at a depth beyond possible microbe habitation (detailed later), it is unlikely the microorganisms have significantly altered these sandstones. Instead, it may be that case hardening gradually progress towards the surface, rather than occurring on the surface on the sandstone and progressing inwards.

In the present study, no weathering related physical alterations are seen on the detrital grains. Although some were identified on K-feldspar by Kamh (2005b), the results from the present study disagree instead showing that the dissolution of K-feldspars is a pre-construction feature, because partially dissolved K-feldspar minerals are evident throughout the depth of each sample and in all the sets. It has also been suggested that quartz overgrowths may spall off (Wright 2000) as a form of weathering. The CL-SEM results showed that overgrowths are fully attached to the quartz mineral substrate. Therefore, the detachment of overgrowths does not seem to be significantly affecting these sandstones. Wright's (2000) study was a laboratory based experiment and the spalling of overgrowths may not have established on these relatively young case study sandstones.

4.5 Permeability

The porosity and permeability of a sandstone determines the movement of water within the rock, and so permeability tests were undertaken on representative samples of the sandstones studied, to further understand the characteristics. Not all samples could be tested due to the constraints on the volume of material needed for the experiment (section??). The samples analysed were: UE2, UN2, UN3 (all from the University set), Dunhouse Buff (DH; a fresh quarry stone), EE3 and CS4 (both from St Vincent Street). These were chosen to represent the large variety of sandstone used to construct the buildings sampled and also those used during replacement. Permeability tests were completed by the University of Aberdeen using the method outlined by Parnell et al. (2010) and is discussed in methods section 2.1.2. Repeat tests were carried out on the samples and their average permeability was plotted against the samples' mean porosity, (taken from the inner most 4 mm of the sample) (Figure 4-28). The data shows that increased porosity leads to increased permeability with UN2, UN3, DH and EE3 showing a good correlation. The exceptions are CS4, which shows a very high porosity but lower permeability and UE2, which only has a marginally higher porosity but much greater permeability than the other samples.

The standard deviations for permeability range widely within each sample (1.7 in Dunhouse Buff to 35.2 in UE2) and, therefore, can be discounted as a reason for the skewed results. However, CS4 shows the highest standard deviation for porosity, CS4 (5.1), compared to the others which range from 1-2.9 for porosity. Therefore, given this high standard deviation, the porosity values for CS4 may be underrepresented, causing the result to be 'out of sync' with the others. Although this does not explain UE2's result, UE2 does contain the highest proportion of large pores (10% are >251 μm) within the tested samples. This large pore size distribution can alter the porosity permeability ratio (Sperl and Trckova, 2008) and therefore may explain the skewed result. Overall, all the sample data are in agreement with other porosity/permeability results for sandstones compiled by Tucker (1981), indicating that CS4 and UE2 are not highly unusual.

Although these findings show that the data is 'normal' in the context of sandstone, the data also highlights the variability in the porosity/permeability ratio within the sandstone used to construct one building. Figure 4-28 shows that UE2 has a much higher

permeability compared to the other University samples. Whilst the SVS samples have similar permeability values, their porosity values differ by 10%. These spatial variations within a type of sandstone used on one building may, in some part, explain why a 'patchwork' of weathering appears on the surface of the sandstone.

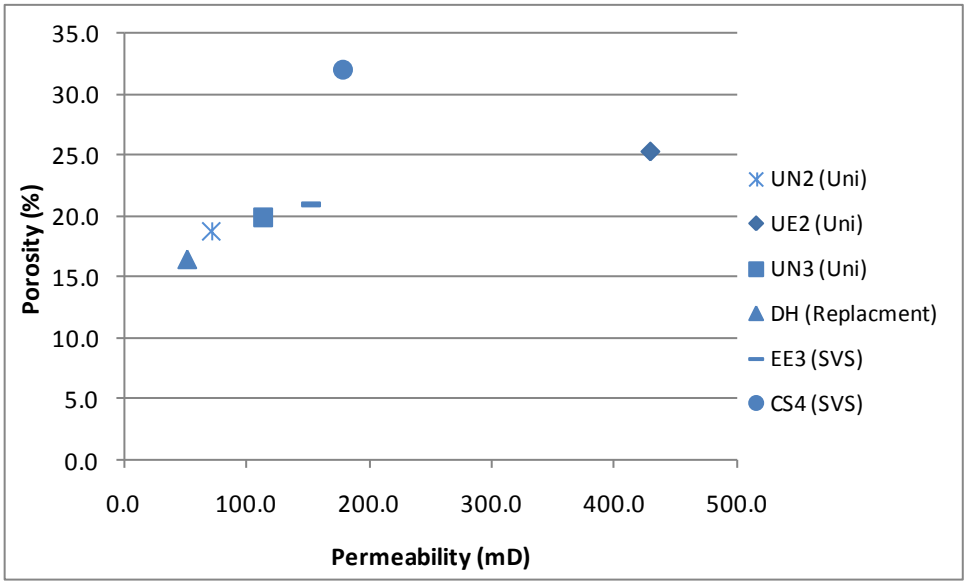

Figure 4-28: Sample permeability plotted against porosity, for selected samples. Samples tested were from a selection of sandstones used within the present study.

4.6 Chemical and Structural Damage to Individual Minerals

Minerals within the sandstones were also investigated using Raman spectroscopy. This was to determine whether decay had caused any structural deformation, by chemical or mechanical means, to those minerals at the stone's outermost surface, compared to minerals situated internally. This work was complimented by quantitative energy dispersive X-ray spectroscopy (EDX) using the ZS-SEM; both these techniques are outlined in sections 2.1.1.6 and 2.1.3. The quantitative chemical analysis can be used to identify the elements and their relative proportions within the minerals. When these techniques are combined, any changes seen in the Raman spectra from the outermost regions can then be determined as a result of structural or composition modifications to the mineral.

Due to the time frame of weathering under consideration (maximum 150 years), the only minerals likely to dissolve and be subjected to chemical change are the carbonate cements as calculated by Lasaga (1998), whose results are shown in Table 1-3**,** section

1.2.5. Therefore, the carbonate cements were analysed to constrain their composition and to see whether any chemical differences between the sample sets could be observed. Carbonates were also investigated to identify any possible leaching of elements from within the crystals, which may be the first step in their dissolution and breakdown. As the Fe-oxides within the sandstone are often reprecipitated through water movement, these techniques were also used to assess whether different generations of Fe-oxides could be identified. The other minerals within sandstone which may be susceptible to weathering are muscovite and kaolinite. Their sheet structure may act as a weak plane for chemical weathering to exploit, although these minerals should not be dissolved away in the relatively short lifetime of the buildings. However, small precursors to decay may still be evident by analysing the results.

4.6.1 *Kaolinite*

Kaolinite is the most common clay found in the samples studied, but trace amounts of illite are sometimes also present. Kaolinite ($AlSi_2O_5(OH)_4$) is present within every sample, although sometimes in very small quantities. However, small proportions of Fe and K may be substituted into the platelet structure (Piffy, 1979).

4.6.1.1 EDX Microanalysis of Kaolinite

EDX analyses of kaolinite were taken from: D7 (Dalry School), UN3 (University sample), CS4 and EE3 (SVS samples), as these contained plentiful amounts of kaolinite. A comparison of the effects of sample preparation methods was firstly undertaken (SP1 = polished blocks, SP2 = grain mounts; full details in section 2.1.1.6).

When the ratio between the main constituent elements (SiO_2 and Al_2O_3, which have not been normalised) are compared, both sample preparation methods (SP1 and SP2) agree generally that most of the EDX analyses lie within a well constrained region, although SP2 results showing slightly tighter clustering (Figure 4-29A and B).

All analyses are low in aluminium (SP1 range = 32.01 – 38.99, SP2 range = 33.43 – 37.25) in comparison to the standard kaolinite plotted (Figure 4-29). The standard kaolinite ratio for Al and Si were derived from Jepson and Rowse (1975), who conducted an electron

microscope microprobe study on English kaolinites which were derived from the best available materials in terms of mineralogical purity. These were then plotted by Deer et al (1992). However, a few spectra are also relatively low in silicon concentrations (SP1 range = 41.46 – 49.86%, SP2 range = 44.19- 47.18%) in comparison to the majority of kaolinite analysed (Figure 4-29). A few factors may have affected the results: 1) a ~5x5 μm raster area was used, although this area will include empty space due to the sheet structure of the kaolinite, where electron beams may have entered, reducing the X-ray signal; 2) much of the kaolinite has been produced through the breakdown of muscovite which has been visually identified within various samples (Figure 4-30). This will increase the proportion of trace elements such as potassium while decreasing the amount of Al and Si, although only small amounts of trace elements were recorded. All data can be seen within the electronic appendix. As stated, all these results have a low Al content compared to the standard muscovite plotted. This is true for both the sample preparation methods and is therefore most likely an indicative feature of kaolinite within Scottish sandstones.

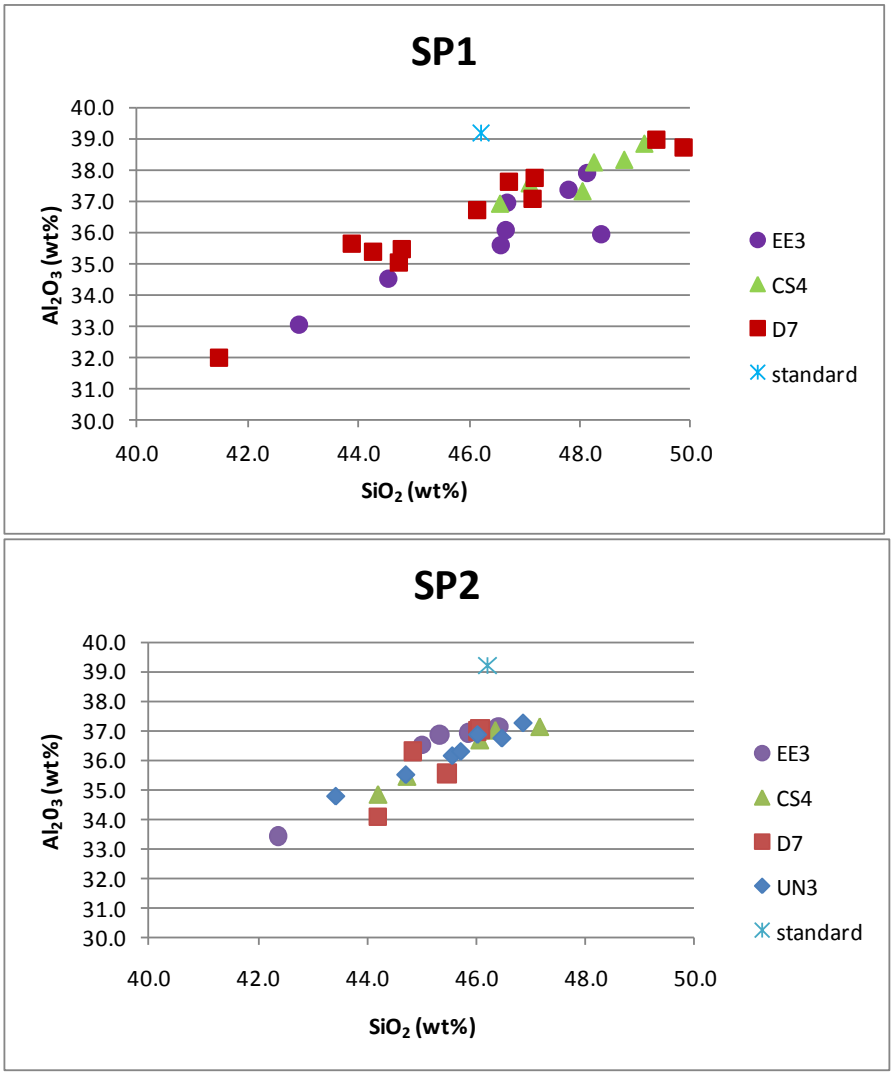

Figure 4-29: Quantitative EDX results for preparation methods when tested on kaolinite.

These are Al_2O_3 against SiO_2 plots, SP1 shows a greater range within the results. The standard data for kaolinite is from Deer et al. (1992).

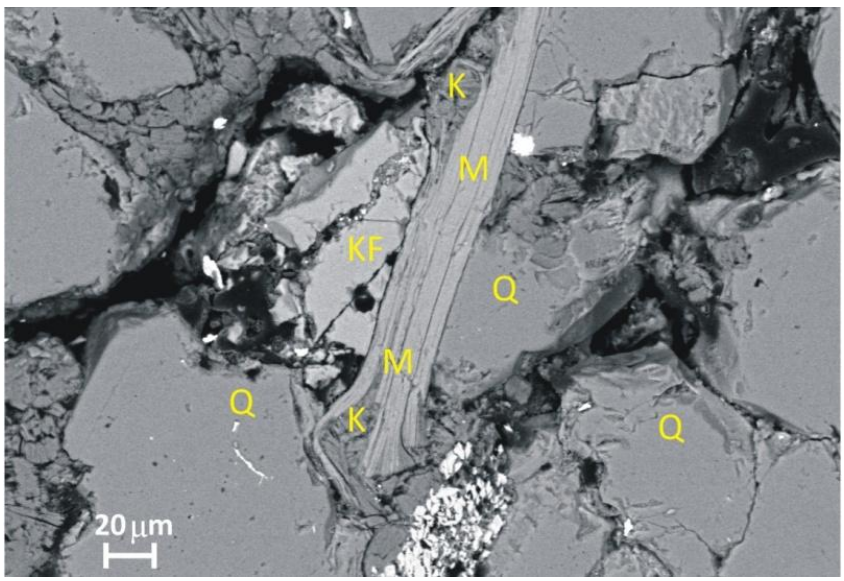

Figure 4-30: BSE ZS-SEM image of Mica grain within CS4.

Image shows the mineral edges of the mica being broken down into kaolinite, confirmed by EDS chemical analysis. Q = Quartz, KF = K-feldspar, K = kaolinite and M = mica.

Kaolinite minerals were then sampled in D7 and CS4 from the weathered region at the outermost surface and as well as the interior. These samples were chosen due to their high abundance of kaolinite, whilst the kaolinites sampled were chosen to provide a cross-section of the kaolinite population within the sample (i.e. small and large platelets). The ratio between the Si and Al was compared and results show that the compositions of the kaolinites are similar in both regions of the samples (Figure 4-31). SP1 (polished blocks) was chosen for this as it means the exact location of the mineral within the sample is known. The kaolinite samples in both sets of data (as shown in Figure 4-31) have an average of 46 wt% SiO_2, although D7 has a much greater range of SiO_2 (41.5 – 49.9 wt% SiO_2) compared to CS4 (46.5 – 49.2 wt% SiO_2). No conclusive difference in chemistry can be seen between those kaolinite crystals at the surface and internally. All kaolinite EDX data can be found in the electronic appendix.

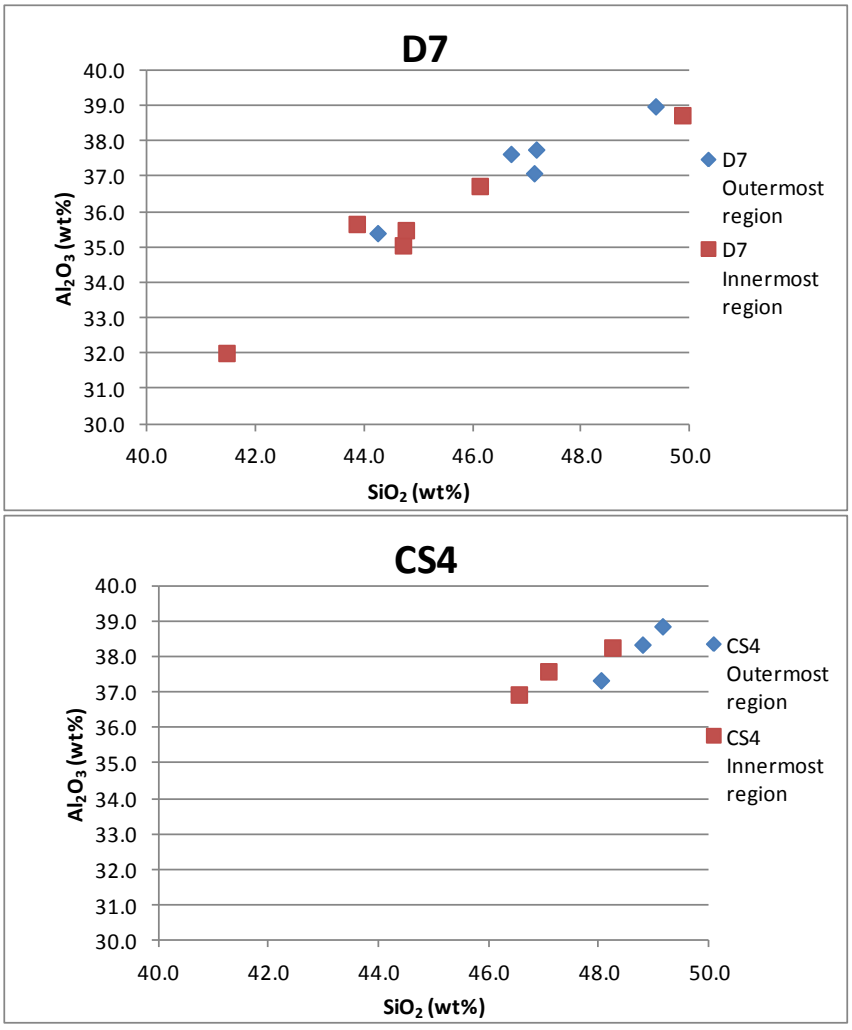

Figure 4-31: Quantitative EDX results for kaolinite at the surface and interior of D7 and CS4. Al_2O_3 against SiO_2 plots, D7) left and CS4) right, comparing crystals from the outermost 2 mm to those within the innermost 2 mm.

4.6.1.2 Raman Spectroscopy of Kaolinite

Kaolinite has four main peaks, known as the inner surface hydroxyl group (OuOH), which includes bands V_1, V_2 *and* V_3 whose centres are at 3697, 3669 and 3652 cm^{-1}, and the inner hydroxyl group V_5 situated at 3620 cm^{-1} (Frost et al., 2001). Kaolinite was examined in samples D7, D6 (Dalry school), CS4, EE4 (St Vincent Street), UE3, UN1 (University) and RGU5, an unknown Stirling sandstone. These samples were chosen to represent a cross-section of the material studied and, where possible to correlate with samples used in EDX analysis. Raman spectra taken from kaolinite were collected from the surface to a depth of one millimetre and from the bottom millimetre of the sample (i.e. an innermost region of the sandstone) in order to identify any weathering related differences in the spectra.

Of the peaks, V_5 (3621 cm^{-1}) and V_1 (3695 cm^{-1}) are the most important in this study as they are most clearly related to changes in the kaolinite crystal structure (Frost 1995, 1998). Spectra of kaolinite in UN1, EE4, RGU5 and UE3 show no clear changes between the top and the bottom of each polished block. The spectra from the top samples often show the V_5 band as having a lower peak height but, as peak height is strongly dependent on crystal orientation relative to the laser beam (Frost et al., 1998), this feature cannot be confidently ascribed as, purely a product of weathering.

Spectra collected from the top of D7 and D6 are very similar to those from the bottom region of each. However, a few kaolinite crystals in the outermost regions do show a shift in the position of V_1 from 3697 to 3707 cm^{-1} and V_5 from 3621 to 3623 cm^{-1} (Figure 4-32). These band shifts are related to changes in the inner surface hydroxyl group and the inner hydroxyl group, and indicate that the kaolinite has transformed into dickite (Frost et al., 1998). Dickite is chemically identical to kaolinite but its layers are arranged in a two layered cell unlike kaolinite, which is a single layer cell. When the OH bonds within kaolinite are stretched, its single layer cell is transformed into this two layered structure of dickite. Dickite has four main peaks: the inner hydroxyl group InOH = V_4 = 3622 cm^{-1} and the outer hydroxyl group OuOh = V_1 V_2 V_3 at 3708, 3655 and 3643 cm^{-1} (Frost et al., 1998). No other sample sets show the presence of dickite within the top millimetres or indeed any other region.

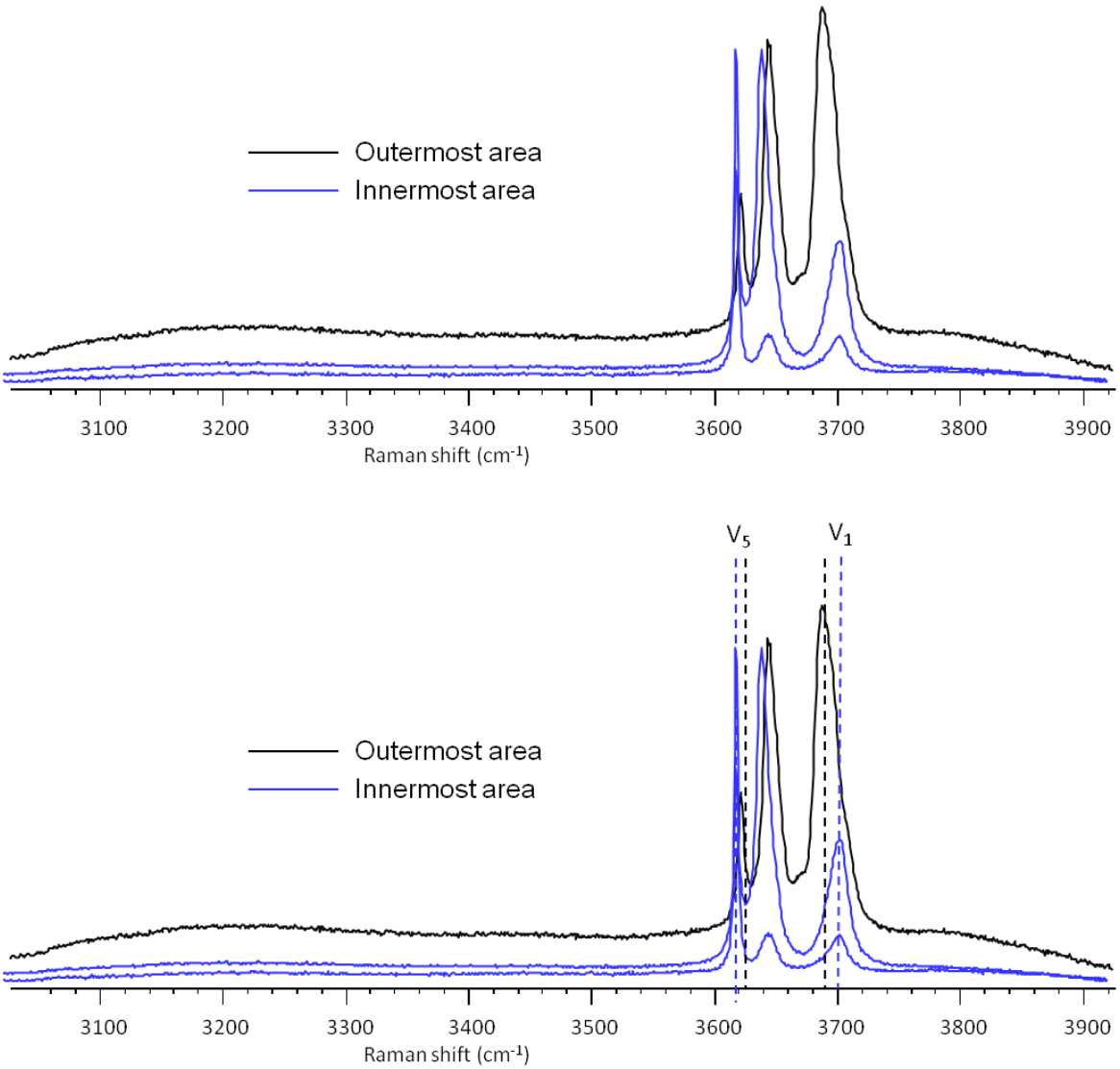

Figure 4-32: Raman spectra of kaolinite within D7.

Spectra are from the outermost surface and internally regions showing the shift in the V_1 and V_4 position. Dashed lines on the second image signify the centre of the peak V_1 and V_4 for the internal and outermost spectra.

The CS4 sample also shows an alteration of the V_5 band in some kaolinite crystals at the sample surface. Spectra from the bottom show an average placement for V_5 at 3621 cm^{-1}, whereas the top spectra show an average centre of 3623 cm^{-1} (Table 4-7). No other peak movement is associated with these shifts. The shift in peak V_5 is thought to be due to the kaolinite being less crystalline. As shown by Frost, (1995), crystalline kaolinite has a V_5 peak nearer 3620 cm^{-1} whilst, in less well crystalline minerals there is a shift to 3624 cm^{-1}. This V_5 shift could occur because the kaolinite at the top is starting to be broken down or is undergoing the first step in becoming dickite.

Table 4-7: Table of Raman data on where the centre of V_5 occurs for kaolinite minerals within CS4.

Peak Centre of V_5 (cm^{-1})	
Outermost area	**Innermost area**
3623	3622
3622	3622
3623	3621
3623	3621

4.6.1.3 Summary

The kaolinite results show that, although no chemical differences could be identified between minerals at the surface and internally using EDX, a few structural differences were identified by Raman spectroscopy. In D7 and D6 from the southeast facade of Dalry School, dickite crystals are found in the outermost region of the samples. These do not seem to be original as they are not located at any other depth within the samples. A kaolinite to dickite transformation is also seen on sandstone taken from St Mary's Cathedral, Sydney (Australia) (60 - 68% quartz with up to 25% clay); this was identified using FTIR spectroscopy (Ip et al., 2008) and attributed to weathering. Sample CS4, from the northeast facade of St Vincent Street, also shows a change in the form of the crystals becoming less crystalline in the outer regions of the sample compared to the interior. This may indicate the breakdown of the crystal caused by weathering. Chemical weathering is therefore affecting the kaolinite within the outermost regions of the sandstone samples.

4.6.2 *Mica*

The phyllosilicate minerals occur throughout all samples studied. Its chemical composition is $KAl_2(Si_3Al)O_{10}(OH,F)_2$ and this mineral is constructed from layers of silicate and gibbsite. Elements such as potassium within the structure have been shown to be leached by lichens (Prieto et al., 1994; Wierzchos and Ascaso, 1996) meaning their sheet structure may be susceptible to chemical weathering over the timescale of building stone decay.

4.6.2.1 EDX Microanalysis of Muscovite

For every mica crystal studied, triplicate spectra on a ~5x5 µm raster area were taken so that an average composition could be determined. The raster size was chosen so that a large sample area could be analysed without having interference from crossing mica layers. Minerals from D7 (Dalry school), UN3 and UN1 (University), CS4 and EE3 (SVS) were analysed. The results using SP2 (outlined in section 2.1.1.6) for the muscovites are shown in Figure 4-33. As these are grain mounts from crushed samples, it is harder to constrain where precisely the minerals came from; although crushed rock only from the lower region of the sample was used. The SiO_2 varies from 42.5% to 47.7% and a larger variation is seen in Al_2O_3, ranging from 25.0% to 36.0%. Micas from D7 and EE3 have the largest compositional spread whereas UN3 micas have a particularly low proportion of SiO_2 compared to CS4 micas which have a particularly high concentration of SiO_2. The compositions of the micas in comparison to the literature standard are a few percent lower in SiO_2 but generally also have a greater proportion of Al_2O_3. The comparison muscovite is from low-grade psammitic schist from the Inverness region of Scotland (Deer et al., 1992). The minor elements, potassium and iron, were then analysed and show that EE3 has the closest values to those of the literature mica, with the rest tightly clustered and containing a significantly smaller proportion of Fe in contrast to the standard mica plotted (Figure 4-34).

It is possible that the chemical analyses were influenced by the sheet structure, with the incident electrons being channelled between sheets to yield micas with lower apparent element concentrations. Care was taken to eliminate this problem by taking triplicate results and avoiding areas with obvious cracks. Therefore, as all micas, appear to follow this pattern, it is possible that mica within Glasgow region sandstones typically have a composition different to that obtained from literature.

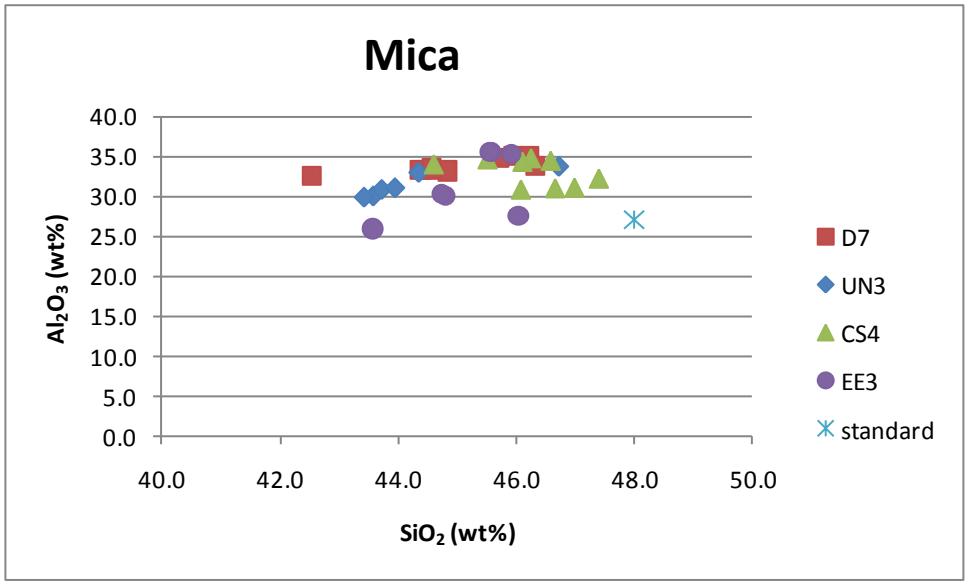

Figure 4-33: Quantitative EDX results for the micas major element ratios, for a range of samples.

Samples are plotted as SiO_2 against Al_3O_2 and compared with a standard (Deer et al., 1992). Results obtained using SP2 method.

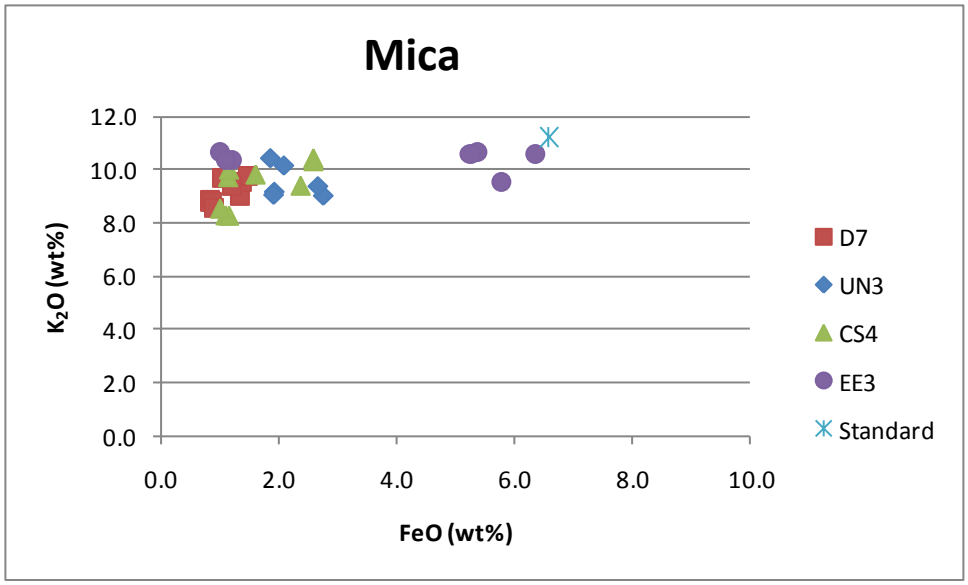

Figure 4-34: Quantitative EDX results for the micas minor elements, for a range of samples.

Samples are plotted as FeO against K2O and compared with a standard (Deer et al., 1992). Results obtained using SP2 method.

Micas from the outermost region and from internal regions of the sandstone were then compared to investigate any differences potentially caused by decay within this region. Figure 4-35 shows that, in the two samples studied there is little difference in the element ratios between the outermost and innermost regions. These were performed using SP1, which has a slightly greater potential error than SP2, but does provide an accurate mineral position within the sandstone. No clear difference is seen in the Si and Al ratios between the top and bottom, whilst data from UN1 is tightly clustered.

The minor element composition was then examined for the same micas used in Figure 4-35. Within these there does seem to be a slight variation in the element quantities between the outermost regions and the inner regions. For both the CS4 and UN1 micas, those at the surface have a fractionally smaller quantity (~1.5%) of potassium (Figure 4-36). In addition, the micas from the top in CS4 also have a smaller proportion of iron, although this is not seen in the UN1 sample (Figure 4-36). All mica EDX data can be found in the electronic appendix.

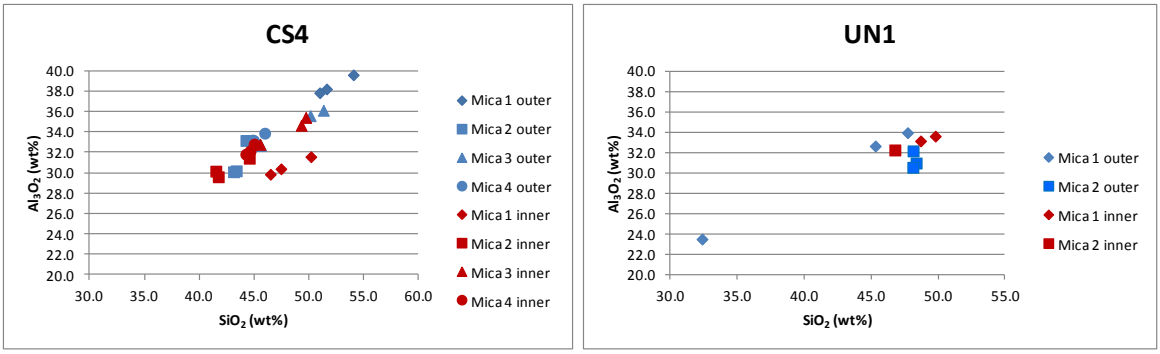

Figure 4-35: Quantitative EDX results for SiO_2 v Al_3O_2 within muscovite.

Compositions between outermost surface and interior regions within CS4 and UN1, prepared using the SP1 method.

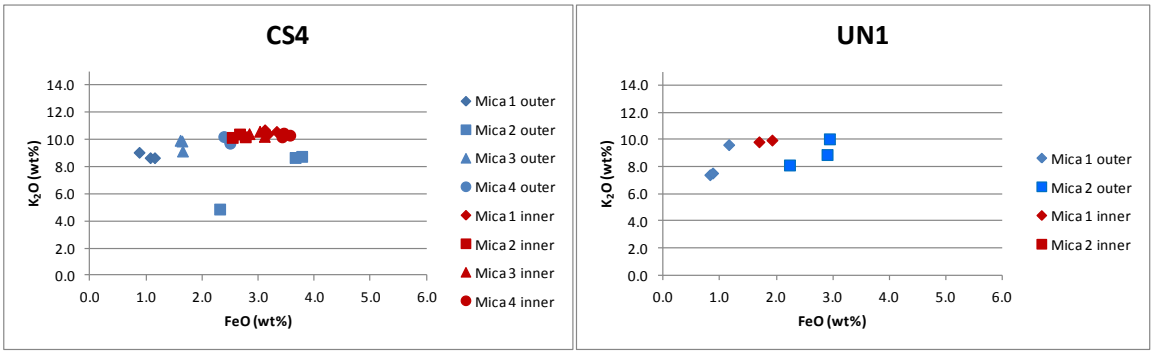

Figure 4-36: Quantitative EDX results for ratio of K_2O to FeO within muscovite.

Compositions between outermost surface and interior regions within CS4 (left) and UN1 (right), prepared using the SP1 method.

4.6.2.2 Raman Spectroscopy of Muscovite

Raman spectroscopy was undertaken to determine whether any changes to the crystal structure of the mica had occurred within the outermost region (2mm) of the sandstone. The phyllosilicate minerals show a range of peaks between 50-1250 cm^{-1}; for simplification these have been divided into two main sub-categories. The low wavenumber region is 50-300 cm^{-1}, and includes peaks at 100, 160, 195, 220, 240 and 270 cm^{-1} which have been assigned to vibrations involving the interlayer cation (Tlili et al.,

1989). The second sub category is from 300-1250 cm^{-1} and includes peaks at 640, 654, 702, 715, 1058 cm^{-1} and a wide shoulder between 400- 435 cm^{-1}; these peaks are assigned to vibrations of the Si_2O_5 layers (Tlili et al., 1989). A third set of peaks were also identified between 3600-3750 cm^{-1} and are attributed to the stretching of the OH bonds (Wang et al., 2002). In this study, only peaks between 50-1250 cm^{-1} were analysed in order to minimise confusion due to the large array of peaks within the micas. In addition, owing to the variety of phyllosilicates and therefore range of possible bonds not all of the peaks will be of equal strength and in some cases may be absent (Tlili et al., 1989).

Raman spectra were taken from phyllosilicates in samples CS4, UN1 and UE3 and, where possible, from the same micas as chemically analysed by EDX. Spectra were obtained from crystals in both the outermost two millimetres and the innermost two millimetres of the sample with a minimum of four micas being analysed in each region. For each mineral grain analysed, a minimum of two spectra were acquired so that an average spectra could be determined, as the spectra may change over the length and breadth of crystals due to their complex layered structure and potential zoning.

The spectra collected are mostly consistent with the dioctahedral phyllosilicates muscovite and paragonite. Spectra collected from the internal parts of each sample consistently show peaks at 195, 262, 270, 408, 464, 702, 750 and 1058 cm^{-1}, but an additional peak at 220 cm^{-1} is frequently masked by the more prominent 195 cm^{-1} peak. The strongest peak is at 270 cm^{-1}. Of the two analyses taken from each mineral grain within the internal section, one spectrum shows a very clear correlation to muscovite. This is in contrast to minerals in the outermost region of the sample where much weaker spectra were obtained and in most cases no clearly defined muscovite spectra were collected, an example of this is shown in Figure 4-37.

Furthermore, internal spectra show a peak at 1058 cm^{-1} which is absent in the spectra from the outermost region of the sandstone. This feature is prominent in UN1 and CS4 and could be due to a loss of one of the SiO bonds. The 220 cm^{-1} peak is much more obvious in the outermost surface spectra as the 195 cm^{-1} peak is much weaker and is therefore not over shadowing it.

During analysis, a few weak spectra were acquired from the micas from within the interior of the samples. These few weak spectra from within the "unweathered" region of the sample may be a relic of the original diagenetic history. In contrast, the lack of any strong defined muscovite spectra from the top regions of the samples shows that this is a product of later weathering, i.e. post-construction.

These results show that there is a very clear difference between grains in the outermost parts of samples and the internal muscovite observed in both CS4 and UN1, and indicate that SiO_2 and the interlayer cation bonds are being broken down to produce weakened Raman spectra. Spectra from UE3 show a few high quality muscovite spectra within the surface region and at 2 mm depth (Figure 4-38) and may indicate that the micas within this sample have experienced less weathering in comparison to the other sample. The lack of weathering evidence is possibly a product of the microenvironment surrounding the University building.

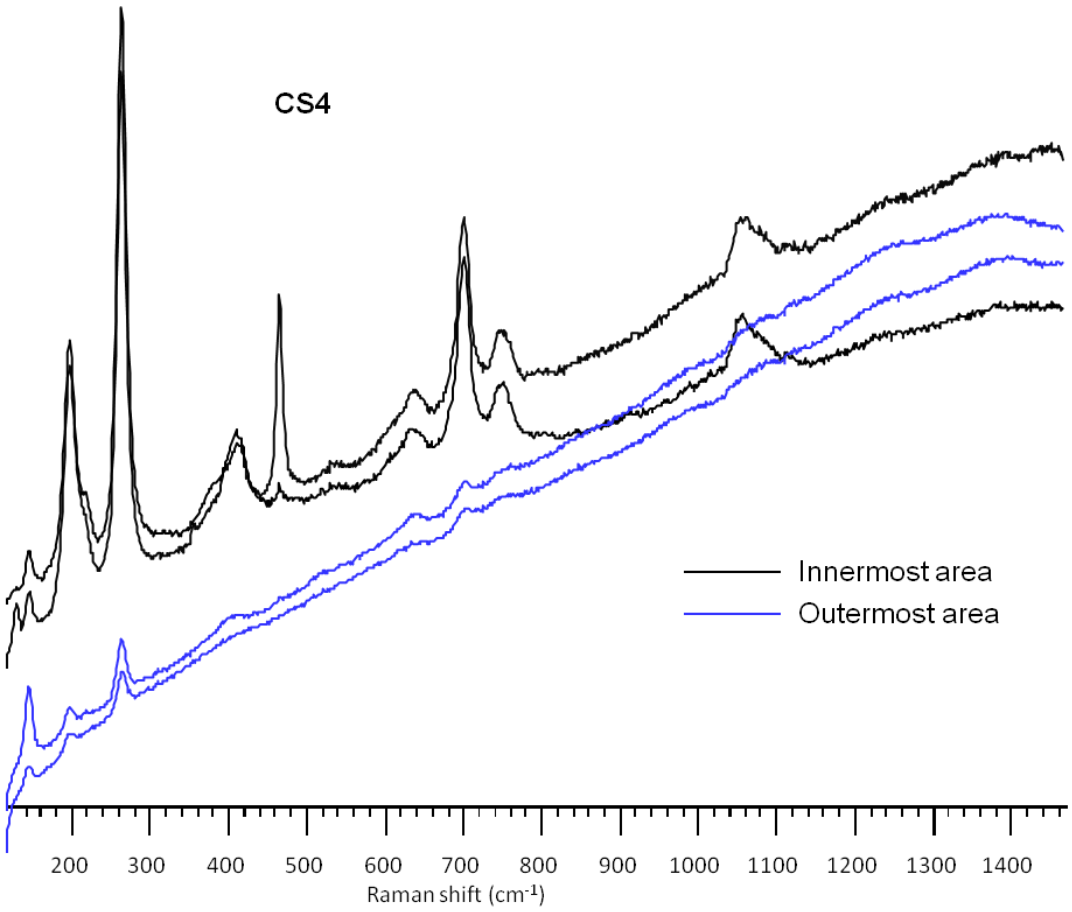

Figure 4-37: Raman spectra from muscovite at surface and interior within CS4.

Black: two spectra from one mica grain at a depth of ~20 mm, blue: two spectra from one mica mineral at a depth of 0.1 mm from the surface.

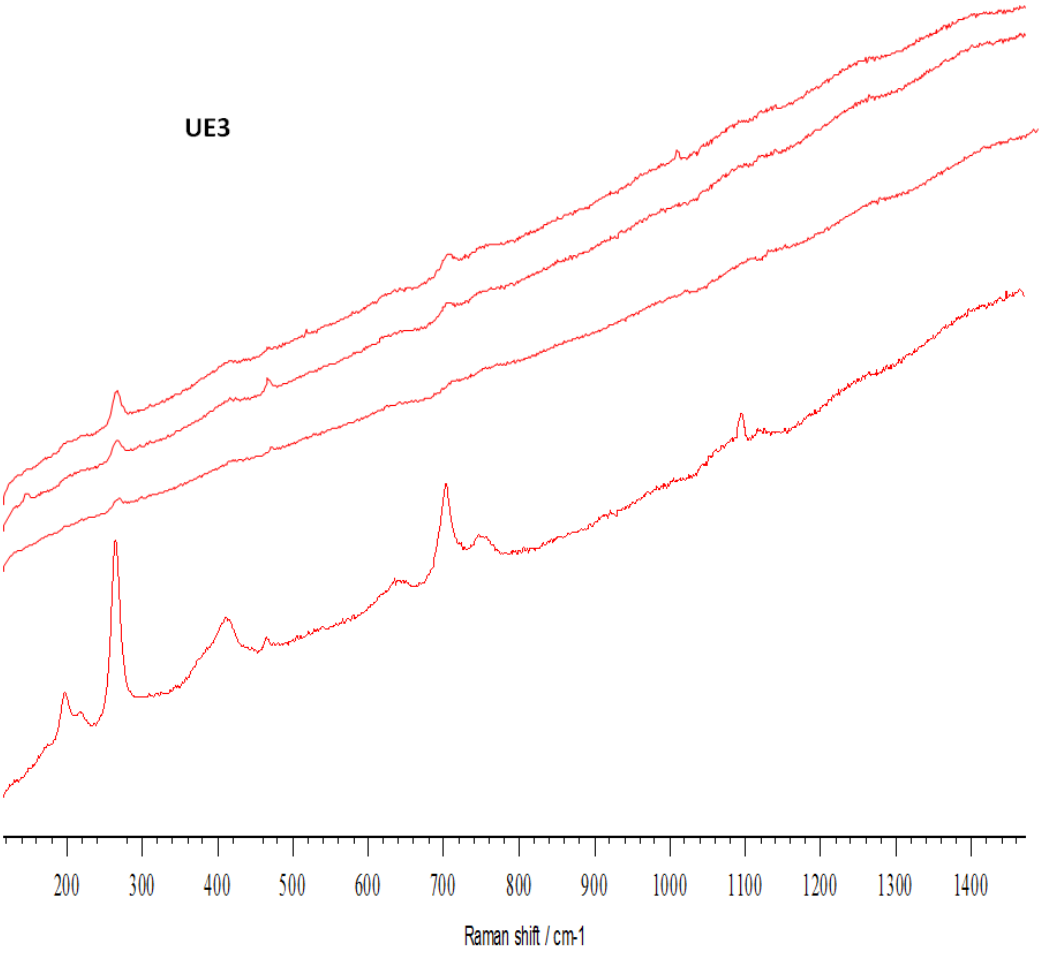

Figure 4-38: Raman spectra from UE3.
All spectra taken from the outermost 2 mm of the sample.

4.6.2.3 Depth Profile Using Muscovite

Due to the clear difference between Raman spectra from its interior and exterior regions, UN1 was used to investigate whether muscovites could be used to define and quantify a weathering profile within the sample. For this study, a ~2 mm wide section through the middle of the sample was investigated from the surface to the interior and each mica grain within this cross-section was analysed, and its depth from the sample surface was recorded. Three spectra were taken from each grain to compensate for any anomalous results that may have been caused by the sheet structure. A total of 26 micas were recorded, and their Raman spectra show very good correlation with depth. Until a depth of 12.6 mm from the surface, none of the 14 micas analysed show a significant Raman spectrum. However, the next mica examined at a depth of 14.6 mm shows weak spectra and, between 14.6 mm and 21 mm, intermediate defined spectra are located in the sample. Once a depth of 21 mm is exceeded, all micas analysed (five in total) showed high-quality spectra with well defined peaks; a representative selection of these results is

shown in (Figure 4-40). With this evidence it can be concluded that there is a weathering profile for mica minerals located at a depth between 14.6 mm to 21 mm in the UN1. To test the consistency of these results, the same procedure was conducted on CS4 and similar results were found, although it was not until a depth of 12- 16 mm from the outermost surface that unmodified and strong mica spectra were identified; a representative selection of results are shown in Figure 4-39.

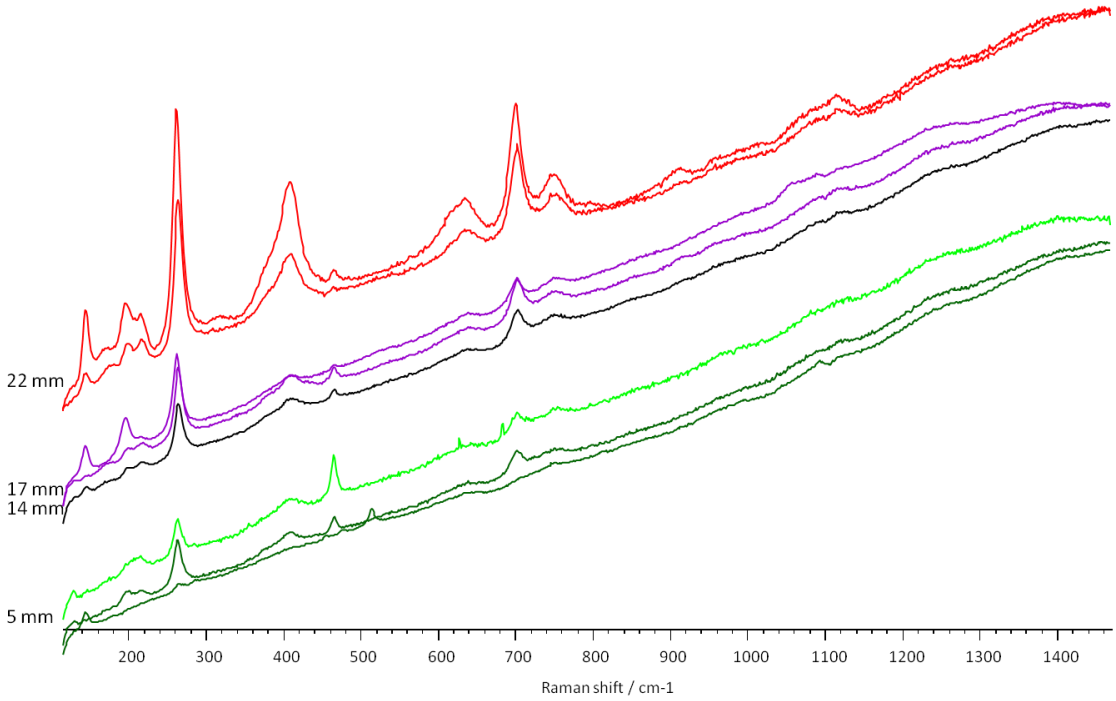

Figure 4-39: A selection of Raman spectra for micas from UN1.

A selection of spectra was chosen to highlight the main Raman trend within the sample. Dark green: 4.1 mm from surface; green: 5 mm from surface; black: 14.6 mm from surface; purple: 17.2 mm from surface; red: 21.9 mm and 22.4 mm from surface.

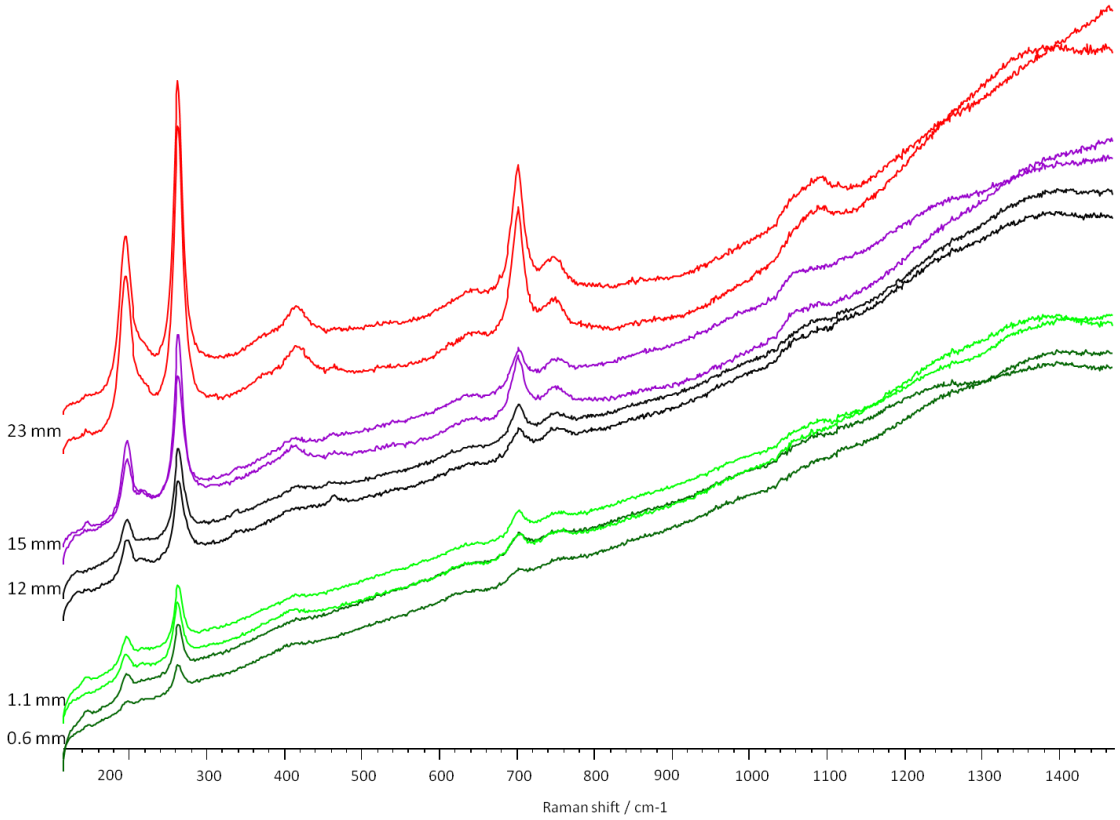

Figure 4-40: Raman spectra for micas within CS4.

Dark green: 0.6 mm from outer surface; green: 1.1 mm from surface; black: 12.4 mm surface; purple: 15.2 mm from surface; red: 23.8 mm from surface.

The use of Raman spectroscopy in locating weathered minerals is a completely new technique, which enables identification of weathering in sandstones and, in particular, those which are carbonate poor. It can accurately show the spatial weathering as well as the intensity of weathering the sandstone has experienced and this process also shows the power of Raman spectroscopy in identifying modifications to minerals undetectable by other techniques.

4.6.2.4 Summary

These results indicate that micas are affected strongly by chemical weathering and these effects are seen in less than 200 years. Although the EDX analysis does not indicate any change in the major element compositions of the micas with depth, there is a small shift in the potassium concentration between those at the surface and those internally. This coincides with the breakdown cycle of muscovite and biotites where the first stage of weathering involves the replacement of potassium ions by water molecules (Mitchell and Taka, 1984). Thus, this first stage in breakdown may be reflected in the EDX results.

Furthermore, when the same mica crystals were analysed by Raman spectroscopy, it shows clearly that micas at the outermost surface are being strongly affected and producing spectra that are not easily distinguishable as muscovite. Therefore, although ions are present (shown by the EDX results), the bonds between them are being broken to leave an "ionic slurry" and most probably it is the potassium bonds which are being affected. This leaves the mica minerals susceptible to attack from lichens and other microorganisms scavenging for nutrients as well as chemical weathering by dissolution. The weathering depth profiles show that the breaking of bonds in muscovite is happening down to depths greater than ~12 mm from the exterior surface. Therefore these micas have suffered a great deal of weathering within a short time frame (150 years).

4.6.3 *Carbonate cement*

Each sample set contains a minimum of one block with a carbonate cement. Using BSE imaging with SEM equipment often leads to difficulties in distinguishing the type of carbonate minerals present, as small variations in the proportions of Ca, Fe or Mg will change the classification of the carbonate. Therefore, EDX and Raman spectroscopy techniques were conducted to constrain the cement present within each sample set.

4.6.3.1 EDX Microanalysis of Carbonate

As the structure and composition of these minerals is completely different to the phyllosilicates, a new EDX set up was used (as outlined in section 2.1.1.6). The main alterations regarding this set up are that oxygen is measured, while carbon is added stoichometerically. Again, the two sample preparation methods (SP1 and SP2) were compared. For each sample, numerous EDX spectra were acquired from the carbonate throughout the sample. Although the preparation method is a very important consideration, results from SP1 and SP2 are found to be very similar. SP2 does, however, produce a slightly tighter clustered set of data (Figure 4-41A and B), suggesting a lower error within the results.

The EDX results were collected as weight percent element, which was then converted to weight percent carbonate. The atomic weight of the molecule could then be used to finally convert the original data into moles percent, the results of, which are presented in

the following ternary diagrams. Full details about the formula used for the ankerite data can be found in the electronic appendix.

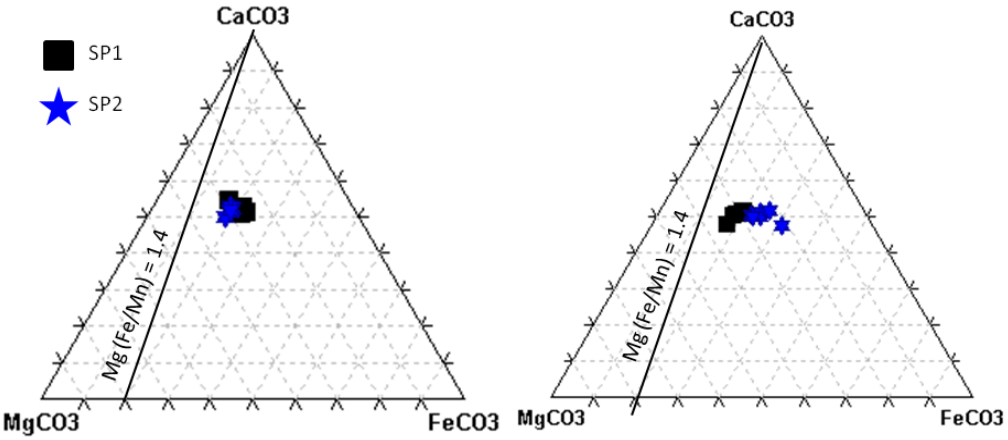

Figure 4-41: Quantitative EDX results from carbonates plotted on a Ca-M-Fe, ternary plots, comparing SP1 and SP2.

Left) EE3; Right) CS4. Data are expressed as mole % carbonate. Black line represents the cross over from dolomite to ankerite with all plots on the ankerite side of the division.

As SP2 produced a tighter cluster of results in comparison to SP1, these data were used for all sample sets and results are plotted in Figure 4-42. All data points plot in the ankerite segment of the ternary diagram, with CS4, EE3 and UN3 having very similar compositions whereas D7 has a slightly higher Fe content (Figure 4-42), although it is still categorised as ankerite. The average amount of each constituent for the samples are shown in Table 4-8. All carbonate EDX data can be found in the electronic appendix.

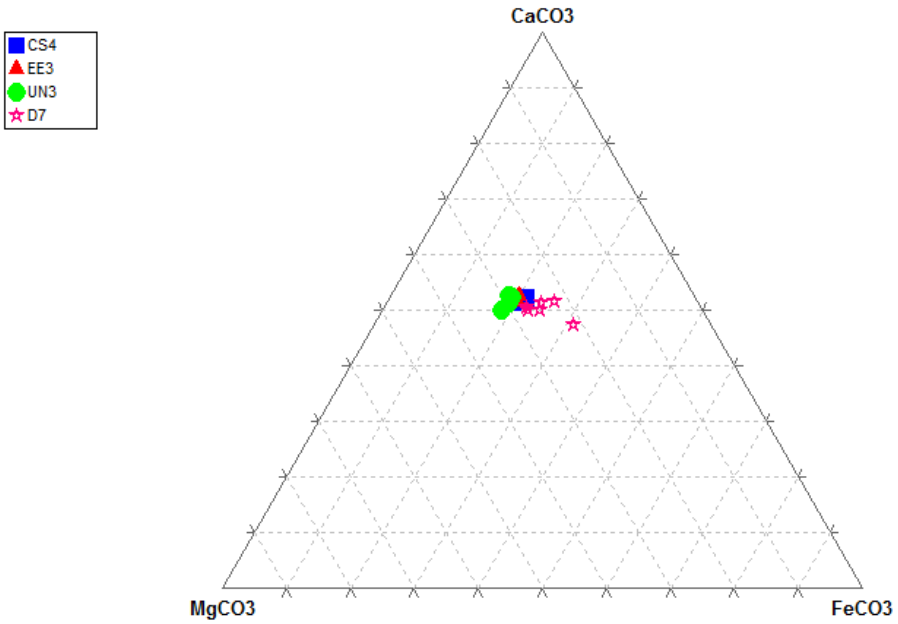

Figure 4-42: Quantitative EDX results plotted on Ca-Mg-Fe, ternary plot for ankerites. Chemical analyses have been obtained from samples which were prepared using SP2; data are expressed as mole % carbonate.

Table 4-8: The average amount of each constituent within the ankerite expressed as moles percent, with the standard deviation.

Sample	$CaCo_3$	$Mg\ CO_3$	$FeCO_3$
CS4	50.2 ± 0.4	32.1 ± 1.2	17.2 ± 0.7
EE3	50.4 ± 0.4	32.9 ± 0.7	16.2 ± 0.4
UN3	49.9 ± 1.1	33.9 ± 1.2	15.6 ± 0.2
D7	49.1 ± 1.4	28.8 ± 2.6	21.3 ± 2.9

4.6.3.2 Raman Spectroscopy of Carbonate

EDX results confirmed the carbonate cement to be ankerite, but greater insight into the identity and properties of the carbonates was provided by Raman spectroscopy. The peaks unique to ankerite are at 165, 290, 720, 1095 cm^{-1} (Bernard et al., 2008), although their positions are not allocated to specific bonds. The internal regions of samples, UN1, UE3, UN3 (University), EE4 and CS4 (SVS) were analysed. In these samples, the majority of spectra show the three longer wavenumbers bands (290, 720 and 1095 cm^{-1}), although the 165 cm^{-1} peak was absent. However, most spectra also show a peak at 170±1 cm^{-1} (Figure 4-43). Some of the spectra show all the main ankerite peaks but, below ~200 cm^{-1}, there are a variety of extra peaks, which may be due to contamination by kaolinite or Fe-oxides. Analyses were then taken from ankerite located in the outermost region and the deepest internal region of EE4 for comparison. The 170±1 cm^{-1} peak is seen in both the top of the sample and in its lower regions (Figure 4-44) and therefore is

not believed to be an effect of weathering. However, a small shift has occurred in the position of the major peak at 1095 cm^{-1}, and this feature may be a product of weathering. However, as previously stated, it is unknown what bond within the sample this represents.

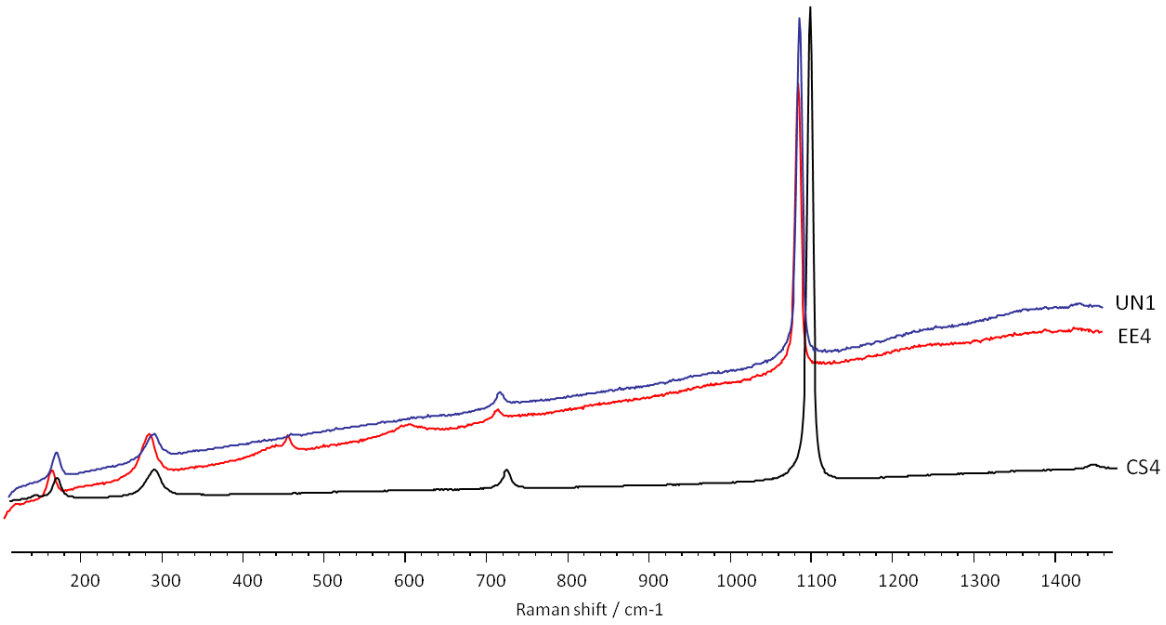

Figure 4-43: Raman spectra for ankerite.

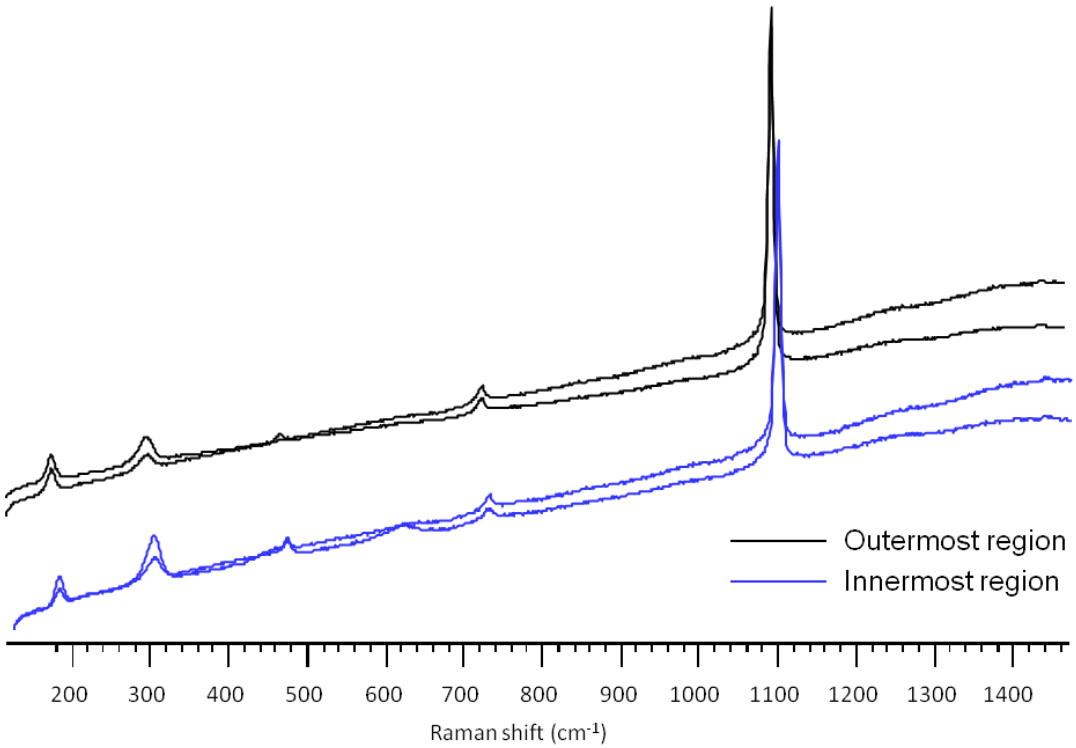

Figure 4-44: Raman spectra from ankerite within EE4 only.

Black) two ankerite spectra from the sample outer surface, blue) two ankerite crystal spectra from internal regions.

4.6.3.3 Summary

All sample sets contain ankerite with a similar chemical composition, rather than a unique composition per set (no trace minerals were indentified), which may have helped identify the quarry from which the original sandstone was excavated. In EE4, a slight shift in the main peak position has occurred, which may be an effect of weathering however, the particular bond that has been changed is unknown.

4.6.4 *Oxides*

As Fe-oxides and hydroxide minerals are composed of the same two elements they are difficult to distinguish by EDS and EDX alone. Raman spectroscopy was also used as it should detect the differences in the structure of the bonds and hence help identify different generations of Fe-oxide produced by decay.

4.6.4.1 Raman Spectroscopy of Oxides

Raman spectroscopy was undertaken on Fe-oxides in samples D7 (Dalry School), RGU2 and RGU5 (Unknown Stirling sandstone) and UN1 and UN3 (University). As the structure is highly variable within the Fe-hydroxides and oxides, considerable research has already been conducted into them using Raman spectroscopy ((Johnston, 1990; Neff et al., 2006; Larroumet et al., 2007); their results are listed in Table 4-9.

Table 4-9: Raman band positions of various iron oxides and oxyhydroxides.
Data taken from, [A] = Jonston (1990), [B] = Neff et al (2006), [C] = Williams and Smith (2007).

Mineral	Formula	Band Positions (cm^{-1})
Goethite	α-FeOOH	393, 307[A]
		299, 387,554[C]
Ankaganeite	β-FeOOH	400, 680[B]
Lepidocrocite	γ-FeOOH	257, 393[A]
		250, 379,525, 650[B]
		250, 376[C]
Haematite	α-Fe_2O_3	223, 296, 406[A]
		293, 299, 412, 613[C]
Magnetite		380, 500, 700, 670, 720[B]
	$Fe(OH)_3$	303, 387, 698[C]

The most commonly occurring spectra belongs to goethite, which was detected in D7, RGU2 and RGU5 (Figure 4-45). This is not wholly unexpected, as goethite is one of the most common Fe-oxides. The wide range in peak position for each Fe-oxide/hydroxide makes identification very difficult, as the spectra may also be variations of structures which are in different states of weathering. The Fe-oxides and hydroxides may also be contaminated by ankerite, as many are produced through this weathering process. However, haematite may be present in RGU5 and possible rhodochrosite, which has been previously found in other Glasgow sandstone (Hughes and Tennent, 2008), although further investigations would be necessary to clarify this.

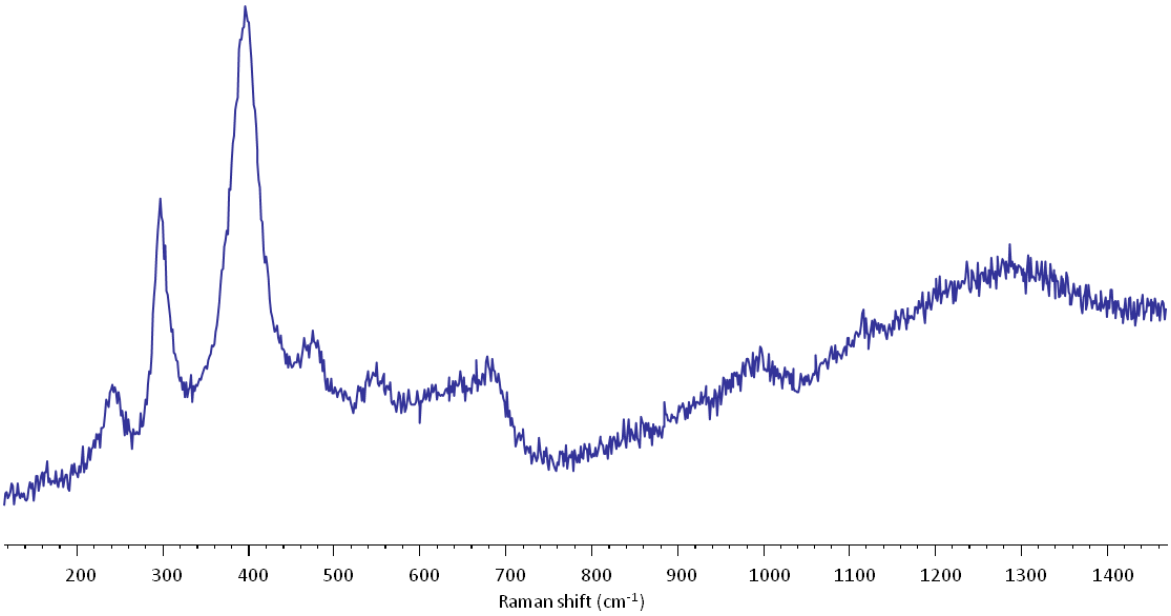

Figure 4-45: Raman spectra of goethite from 1 mm depth from the surface within RGU2.

4.6.4.2 Raman and EDX results discussion

Raman spectroscopy indicates that there are differences between the kaolinite and muscovite crystals at depth, compared to those in the outer ~2 mm of the sandstone. Raman results suggest dickite to be present in the outer regions of samples D6 and D7 and, as this mineral is not found elsewhere within the samples, its presence indicates a kaolinite to dickite transformation has occurred. In addition, kaolinite was less crystalline at the outermost surface of CS4 in comparison to the internal region, shown by a shift in the V_5 position. Less crystalline varieties of kaolinite were also detected by mid- and far-infrared studies in the weathered section of Maroubra Sandstone from Sydney (O'connor et al., 2001). Raman spectroscopy also reveals a “weakened” mica structure in the outer

regions of samples showing increasingly diluted spectra, suggesting that many bonds are being broken down simultaneously rather than one specific bond. Within this study, this process has been identified in the Dalry, University and SVS samples. CS4 (St Vincent Street) is the only sample where both mica and kaolinite are affected. However, unlike mica weathering, the changes in the kaolinite Raman spectra are much more subtle and, if both a wider set of samples and more kaolinite minerals were analysed, more kaolinite changes may have been identifiable. The chemical changes shown by Raman spectroscopy and EDS are summarised in Figure 4-46.

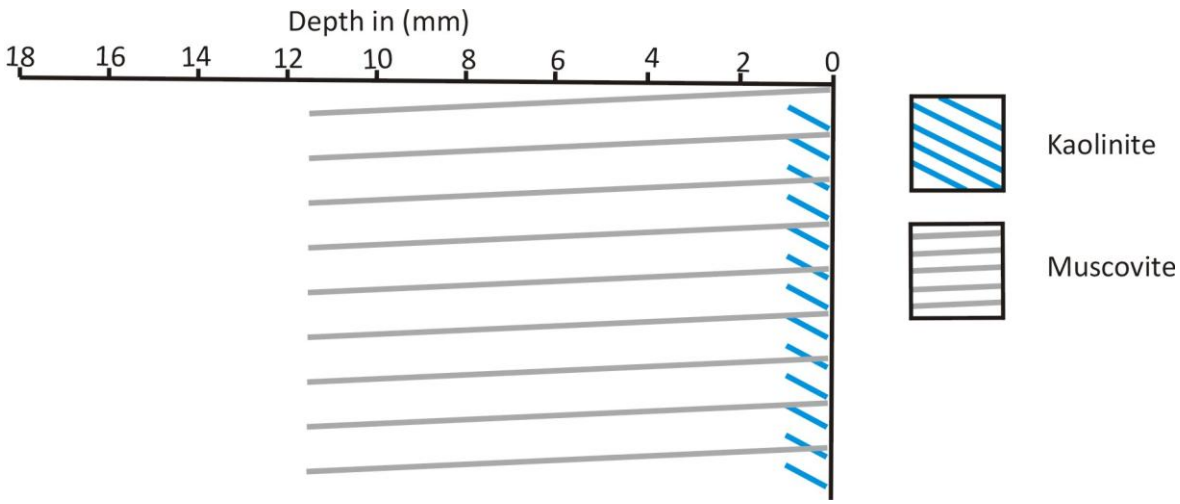

Figure 4-46: Sketch of chemical weathering for muscovite and kaolinite depths identified by Raman spectroscopy in CS4.

4.6.5 *Chemical Weathering Discussion*

All the sandstone used in the Glasgow buildings studied originate from the Scottish Coal Measures Group, which is known to have kaolinite as the main clay present suggesting that the sandstones were laid down in rivers, delta distributaries and channel environments (see section 1.4). These depositional environments have been found to produce sandstones with inherent weak petro-physical properties leading to greater rates of decay (Weber and Lepper, 2002). The sandstones in this study have also been shown to have rapid rates of decay, and the associated weathering processes observed are discussed next.

The results from the detailed point counting, EDX and Raman spectroscopy, show that many forms of chemical weathering are identifiable in the sandstone, affecting both detrital and diagenetic minerals. The formation of a hardened layer is evident in most

samples, whether it is at the outermost surface or a few millimetres below. Case hardening is caused by a quartz-rich layer in comparison to the overall quartz proportion and is normally seen in conjunction with a porosity low and a layer enriched in either Fe-oxide or kaolinite. This process seems to occur rapidly after the initial placement into the building. The RGU samples, which have only been weathered for 12 years and already have a wide ranging original composition, show the formation of this layer at a depth of 4-5 mm from the outermost surface. The permeability results indicate that the samples tested (UE2, UN2, UN3, DH, EE3 and CS4) have a very normal porosity to permeability ratio, therefore the rate of water transport is within the expected range for the sandstones used to construct many of Glasgow's buildings. The movement of the Fe-oxides and kaolinite are associated with the transport of water. The production of a quartz rich layer at depth has not previously been described because it is normally seen as a surface feature (Conca and Rossman, 1982; Viles and Goudie, 2004). However, the buildings studied by those authors are much older than the ones used in the present study. Therefore, the hardened layer may form at depth and progressively move to the outermost surface as seen in the older sample sets as the sandstone becomes weathered, producing a typical case hardened surface.

As previously discussed, the carbonate cement, in rare cases, was altered through chemical weathering to form Fe-oxide and hydroxide pseudomorphs, showing a clear depth profile of weathering. However, the majority of samples which contain carbonate contain unreacted carbonates. Raman and EDX results both indicate that ankerites in both reative and unreactive sample sets has a very similar composition. Therefore, we can assume that the composition of the carbonate cement is not rendering it unreactive. Possibly the black crust on the surface is protecting the ankerites from dissolution, as the crust may have formed more rapidly than the cement could breakdown.

Kaolinite and muscovite have also experienced chemical weathering. Kaolinite experiences two types of transformation: 1) a less crystalline form seen at the weathered surface and 2) a kaolinite to dickite reaction. These both occur within the outermost 2 mm but with no evidence of deeper transformations.

There is evidence of muscovites being altered at a much greater depth; ~12 mm within the samples. The bonds within the muscovite are being broken down, rather than the

depletion of a specific element, as EDX results indicate invariant ratios of elements in the outermost and interior minerals. Interestingly, the processes affecting the kaolinite and micas are seen within samples where the ankerite has remained unreactive, such as CS4. This may mean the initial stages of muscovite weathering can occur much more rapidly than ankerite (i.e. before the protective crust can form) and/or that the muscovites are much more reactive than first thought.

As outlined above, several minerals have experienced various forms of chemical weathering, but these results reveal no visual evidence of physical weathering affecting any mineral grains besides the ankerite. The CL-SEM results indicate intact quartz overgrowths, whilst BSE imaging shows no pitting or cracking of the quartz grains. Although secondary porosity is seen within the K-feldspars, this is a feature present throughout the whole sample depth and so is very unlikely to purely be a weathering effect.

This is surprising as the dissolution rate of K-feldspar is so slow that, even in the most acidic solutions, only a few micrometres of material will be lost per century (Lasaga, 1998; Duthie et al., 2008). Thus, contrary to Kamh (2005b), we propose that feldspar dissolution is not an important decay process in building sandstones.

In conclusion, these results indicate that, within the ≤150 year life time of these buildings, chemical weathering is definitely taking place. Kaolinite and muscovite, which may have previously been thought to be unaffected by weathering, are primarily being broken down. The bonds present are disintegrating, leaving the structure weakened and more likely to be affected by subsequent weathering processes. Chemical weathering is predominantly affecting samples to a depth of 6 mm but, in many sandstones sampled, the effects of chemical weathering can be seen to a depth of ~12 mm within the carbonate and muscovite grains.

5 Microbial Results

Microorganisms are found inhabit rock in almost all environments from polar extremes (Friedmann, 1982; Hughes and Lawley, 2003; Omelon et al., 2007) to hot desserts (Potts and Friedmann, 1981; Schlesinger et al., 2003; Davila et al., 2008). This research has also shown their presence to be damaging to the substrate. Microbial activity is particularly harmful to free standing monuments and buildings, as highlighted in section 1.2.8, although little work has been conducted within Scotland's built heritage.

This chapter aims to answer the following questions:

- Where do the microorganisms inhabit, surface or internal?
- Which microorganisms are present, and in what quantities do they occur?
- What is the rate of colonisation?
- What impact does the external climate have on the microbial communities?
- What impact do microbes have on stone properties and what impact do stone properties have on microbes?
- Finally, how do microorganisms impact on the rates and mechanism of sandstone decay?

These topics will be examined using a variety of techniques such as protein and chlorophyll-a assays, osmium stained polished blocks and optical light transmission experiments.

5.1 Dalry School

Eight samples were taken from two facades of the Dalry school building, as listed in Table 5-1. An in-depth mineralogical description of each sample can be found in section 4.3.1.

Table 5-1: Sample identifiers and corresponding sample sites for Dalry.

Sampling Area	NE Facade	SE Facade
Whitened zone	D1*	D7
Sills	D2	D5
General black weathering	D3*	D6
Mullions	D4	D8

Where * appears it indicates multiple core samples were taken.

5.1.1 *Protein and Chlorophyll-a Assays*

Protein and chlorophyll-a assays were undertaken as outlined in section 2.1.4. For this set of experiments, approximately half of the core's surfaces were sampled for each assay.

Protein assay results are shown in Figure 5-1A. The modified Lowry protein assay results show that all cores sampled do have protein present on their surfaces. Cores D2 and D5 (from sills) have the highest concentrations of proteinaceous material (257 μg/cm^2 and 104 μg/cm^2 respectively), whilst D4 has the smallest amount (4.1 μg/cm^2) within this set (Figure 5-1A). The three D1 cores (1A, 1B, 1C) were taken from a block with an area of 25 x 40 cm, the results have a relative standard deviation (RSD) of 50.4%, whilst the D3 cores (3A, 3B, 3C) taken from a similar sided area as D1 have a RSD value of 45.8%. This shows a large degree of spatial variability in the location and amount of proteinaceous matter on the surfaces of these samples.

Chlorophyll-a assays confirmed the presence of photosynthetic material on the surface of all cores (Figure 5-1B) with the exception of D6 and D1A. D7 (whitened zone) shows the highest concentrations of chlorophyll-a, peaking at 0.97 mg/cm^2, whilst the rest of the samples range from 0.05 - 0.5 mg/cm^2. Triplicate chlorophyll-a assays were undertaken on D1 and D3 cores. The chlorophyll-a on the D1 core has a RDS of 88.9% whilst the RSD of the D3 cores is 23.1%.

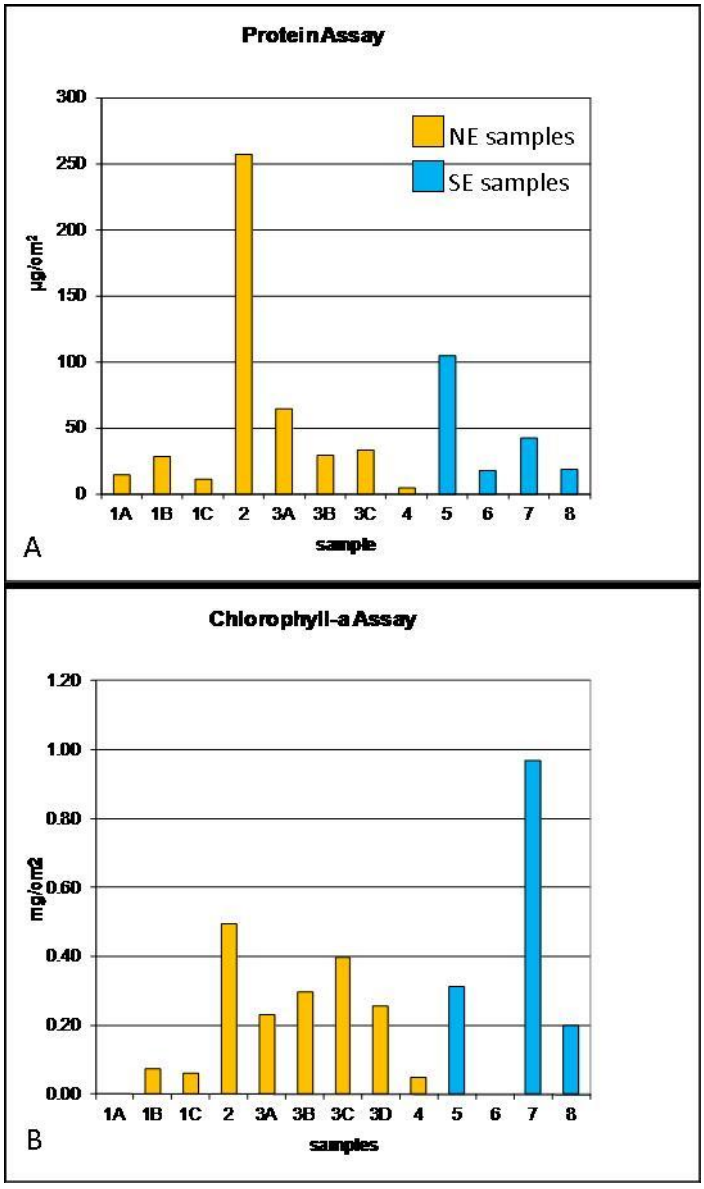

Figure 5-1: Protein and chlorophyll-a assay's for Dalry samples.

A) Protein assay, which is positive on all samples, B) chlorophyll-a assay, which shows it is present on all samples except D6 and D1A.

These results indicate that both photosynthetic and non-photosynthetic microorganisms inhabit the surface of the sandstone. The types of microorganisms present do not show a particular preference towards either side of the building, with D2 (NE facade), D5 and D7 (both SE facade) showing the largest quantities of protein and chlorophyll-a within this sample set. The zero chlorophyll-a result for D6 could either be because all protein detected is from a non-photosynthetic source or due to the variability of photosynthetic material that was sampled. The results show that the spatial variation of protein and chlorophyll-a is very high within these samples, as there is a high variability (protein = 50.4% and chlorophyll-a = 88.9% over a small area (25 x 40 cm).

5.1.2 *SEM Imaging of the Outer Surface of the Stones*

Small fragments of the outermost surfaces of each stone block were broken off and examined using the FEG-SEM in low vacuum conditions, in order to image and identify the microbes present.

The surface of D1 (whitened zone) shows quartz grains surrounded by fragments of kaolinite, quartz and unknown particulates possibly atmospheric dust which may include pollutants (Figure 5-2). Dehydrated extracellular polysaccharides (EPS) are seen in oval crevices between larger grains. These have a honeycomb appearance (~250 µm in length), and the gel-like EPS has trapped small mineral fragments (Figure 5-2). There are some possible filamentous cyanobacteria with a similar morphology to that of *Phormidium* (Rippka et al., 1979). These are unbranching and appear smooth, while the filaments are only a few microns thick. Calcium oxalates are also present on the surface of the sample (Figure 5-2) and were identified through spot X-ray chemical analysis in the SEM (location of spot analysis is illustrated on Figure 5-2).

On the surface of D2 (sill) large quantities of filamentous cyanobacteria with a morphology similar to *Ossillatoria* or *Scytonema* (Rippka et al., 1979) are seen. These microbes are ~10 µm thick and no internal cell structure can be seen in the FEG-SEM (Figure 5-2). Calcium oxalates were identified but, due to the "dirty" appearance of the surface (caused by the abundance of small mineral fragments and likely atmospheric dust debris), dehydrated mats of EPS could not have been seen even if they were present.

The surface of D3 (general back weathering) shows large quantities of the dehydrated EPS, occurring within depressions on the sample surface, as well as communities of possibly both the filamentous *Phormidium* and *Ossillatoria/Scytonema*. Thicker and thinner strands are both present and resemble a web-like network covering the sandstone (Figure 5-2).

The surface of D4 (mullion) had a large mass of kaolinite and quartz fragments and possibly contains fly ash and soot particles (Figure 5-2) (as these are typical Glasgow pollutants; McDonald and Duncan, 1979), infilling the space between larger detrital

grains. It was therefore difficult to draw any conclusions about whether organic matter was present, as this debris may have obscured microbial matter.

The minerals on the surface of D5 (sill) have a possible thick paint coating distorting the grain shape beneath (discussed section 2.1.1.6). However, on top of this surface and sitting within depressions are areas of dehydrated EPS (Figure 5-3) up to 150 µm in diameter.

D6 (general black weathering) has a similar surface to D4 (Figure 5-3).

The surface of D7 (whitened zone) has an abundance of calcium oxalates in small (20 µm) patches. These calcium oxalates have the same honeycomb texture as the dehydrated EPS (Figure 5-3), although no EPS was identified on this sample.

D8 (mullions) has a film covering the grains at the surface, which is white under the SEM in BSE imaging mode (i.e. has a high atomic number Figure 5-3) and is discussed extensively in section 3.1.2. However, dehydrated EPS is seen on the surface but is restricted to crevices, which are normally oval in shape and 150 - 250 µm in length (Figure 5-3).

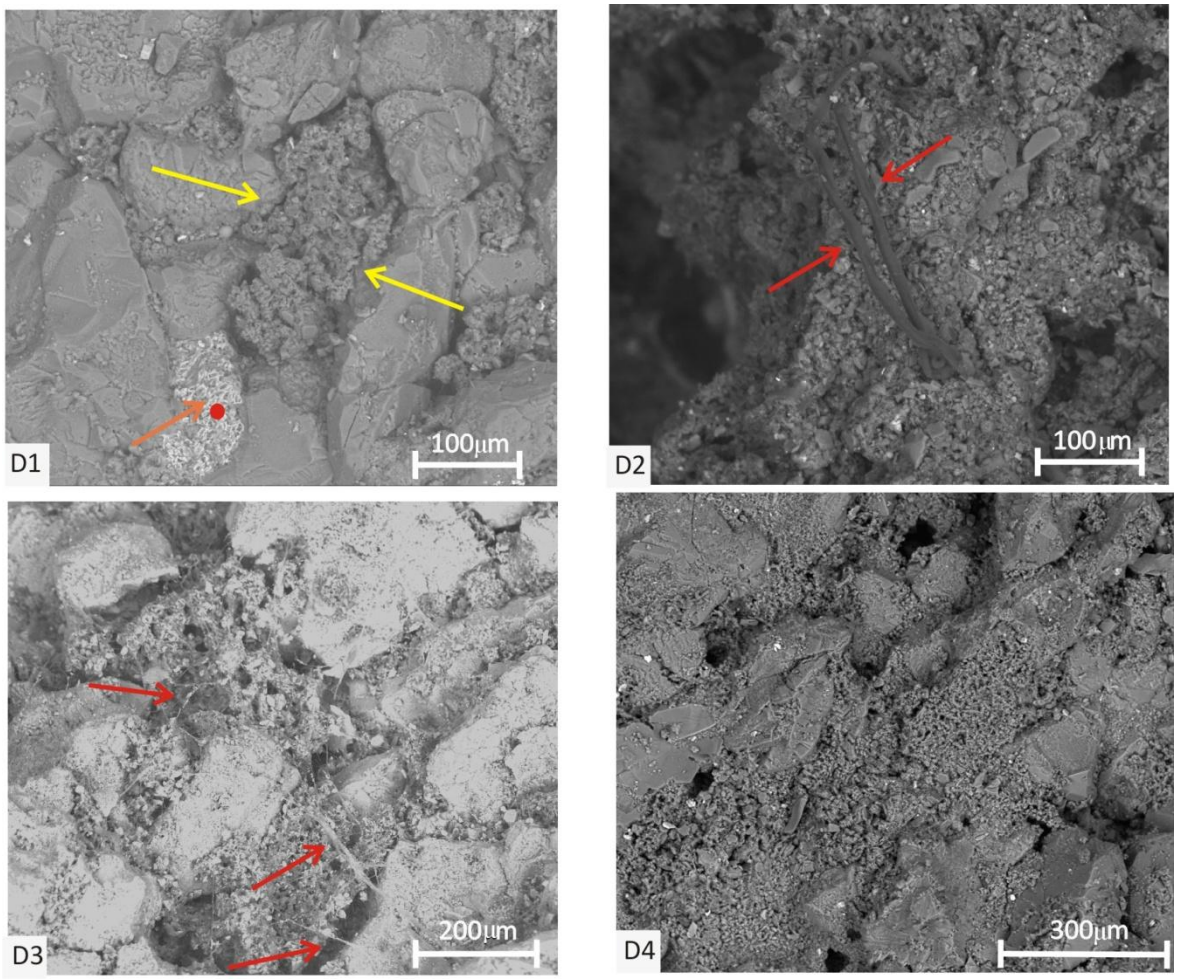

Figure 5-2: FEG-SEM SE images of Dalry outer surfaces fragments D1-D4 (note varying scales on images).

Yellow arrows = dehydrated EPS, orange arrows = Ca oxalates, red arrows = filamentous cyanobacteria, D1) Ca oxalates and dehydrated EPS within a crevice, spot indicates area of spot analysis for the Ca oxalates, D2) filamentous cyanobacteria, D3) mat of filamentous cyanobacteria, D4) undistinguishable surface with large amounts of small fragment on surface.

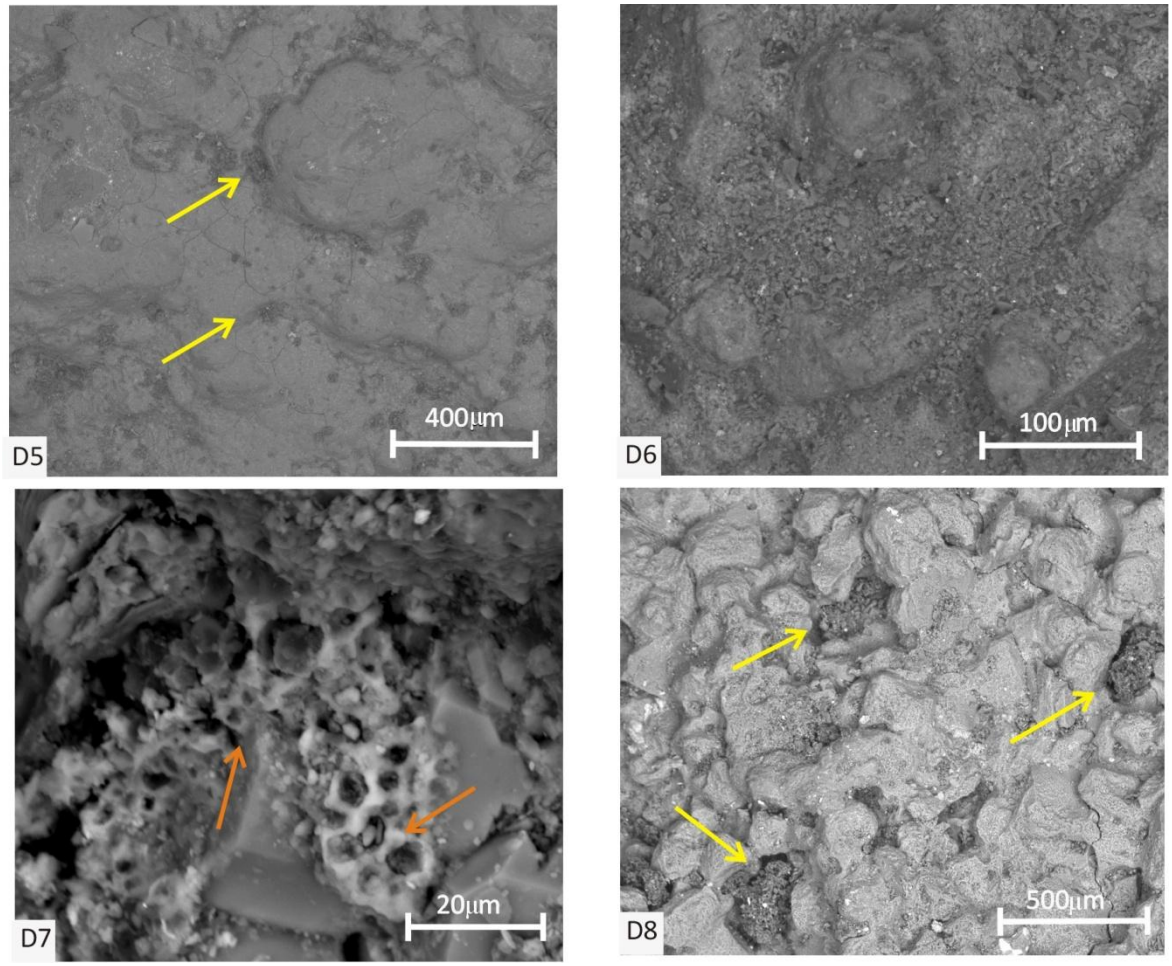

Figure 5-3: FEG-SEM SE images of Dalry outer surfaces fragments D5-D8 (note varying scales on images).

Yellow arrows = dehydrated EPS, orange arrows = Ca oxalates, D5) smooth surface with EPS forming in hollows, D6) undistinguishable surface with large amounts of debris, D7) Ca oxalate with honeycomb structure of the dehydrated EPS below, D8) hollows filled with dehydrated EPS.

5.1.3 *Osmium Stained Cross-Sections*

An osmium stained polished block was made for each sample to show a cross-section of the core, from the outermost surface to internal regions. As osmium has a high atomic number and preferentially stains organic material, it highlights any cryptoendolithic communities within the sample (detailed in section 2.1.5). Of the eight samples studied, only four showed any osmium stained organics within the sandstone, and these were the samples from the SE facade (cores D5, D6, D7 and D8). Core D7, taken from the whitened zone, was most abundant in organics within this set whilst core D8, retrieved from the black weathered mullions, had the least. The organisms present in D5, D7 and D8 have a morphology consistent with cyanobacteria *Gleocaspsa* (Rippka et al., 1979). These are globular cells generally less that 5 µm in diameter within large expanses of EPS (Figure

5-4). These microbes were found to a depth of 2 mm, with the highest concentrations occurring between grains at the sample surface. Some filamentous cyanobacteria, or a fungus, are seen in D6. It has thin hyphens and was found at a greater depth within the sample (up to 13 mm beneath the surface) exploiting a fracture infilled with a highly organic-rich substance (Figure 5-4), a high abundance of carbon was identified by spot X-ray chemical analysis. These are likely to be fungi rather than cyanobacteria due to the light requirements for photosynthesis (see later discussion). However, no globular cyanobacteria were present in D6.

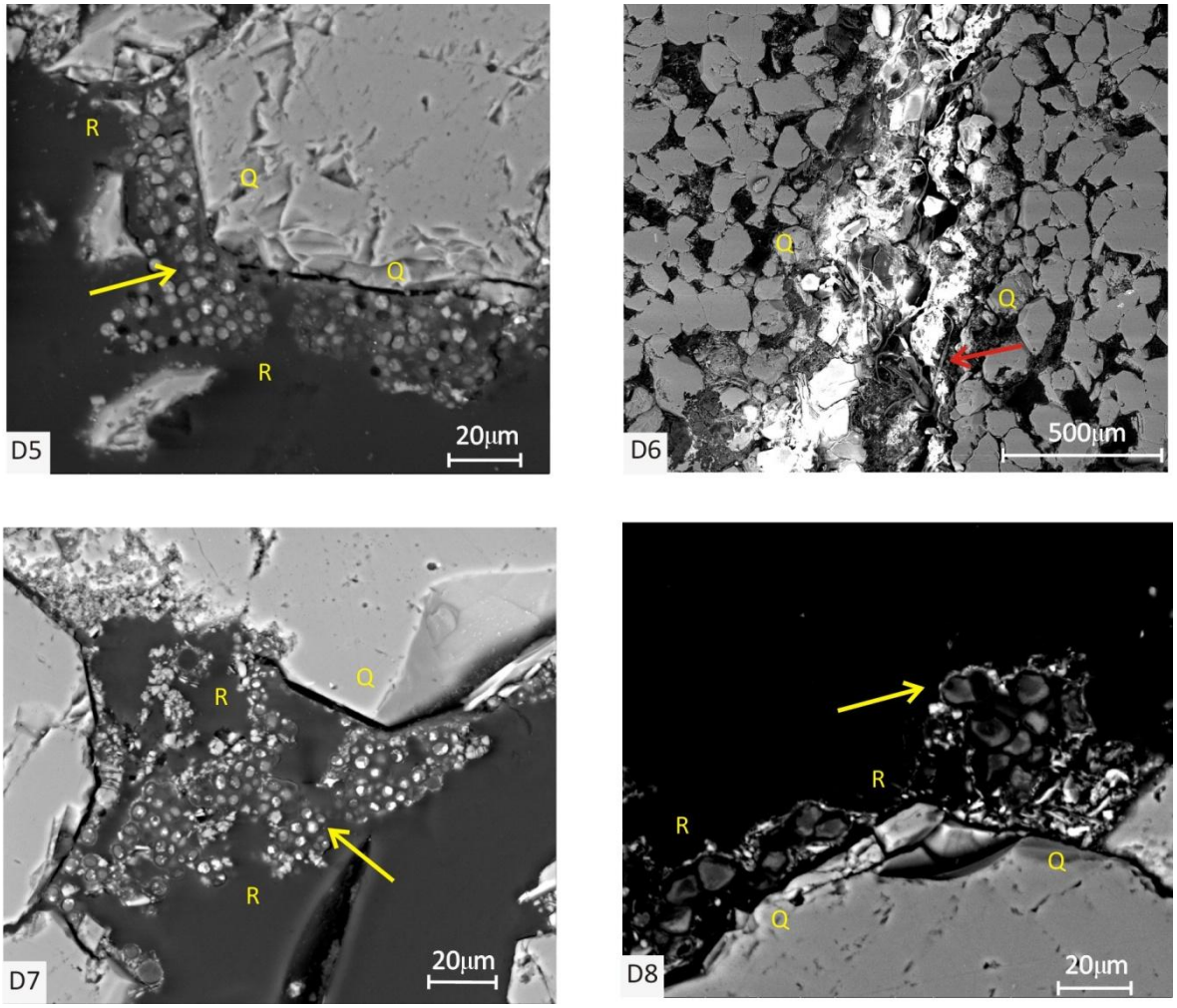

Figure 5-4: FEG-SEM BSE images of osmium stained polished blocks of Dalry stones.

Q = quartz grain, R = resin, yellow arrows indicate globular cyanobacteria, red arrow indicates filamentous cyanobacteria. D5) cyanobacteria on the surface between quartz grains, D6) filamentous cyanobacteria within organic rich area of the sample, D7) cyanobacteria infilling a pore space 2 mm beneath the surface, D8) shows minimal cyanobacteria on the surface of the sample.

5.1.4 *Dalry Summary*

Results from the FEG-SEM analysis of the outer stone surface and the protein and chlorophyll-a assays generally correlate very well. Those samples that displayed a high protein and chlorophyll-a assay results also show an abundance of microorganisms, which were easily identifiable under the SEM. The only surface which does not show a clear relationship is D2, as only a small amount of microbial matter was identifiable on the outer fracture surface, whereas the assays suggests much more should be present.

Dehydrated EPS has been identified on both facades of the building and is the most widespread organic material recognised on the surface of these samples. Calcium oxalates are also prevalent on both sides of the building and are often seen to be mimicking the honeycomb texture of the dehydrated EPS. In the case of D7 where no EPS is directly seen, the presence of the Ca-oxalates in a honeycomb formation provides evidence that microorganisms within the EPS may have once been present on this surface. Significantly, the filamentous cyanobacteria seen on the stone surface are restricted to stone surfaces on the northeast facade whilst only minimal evidence for surface colonisation by microbes was found on the southeast facade. However, when the osmium stained polished blocks were analysed, no subsurface (cryptoendolithic) communities were observed in the northeast face, but large communities of globular cryptoendolithic were seen in the southeast facade. Results are summarised in Table 5-2.

Two species of filamentous cyanobacteria were identified on the surface of the sandstones and these had morphologies consistent with *Phormidium* and *Oscillatoria/Scytonema,* whilst the cryptoendolithic cyanobacteria have a bulbous form consistent with *Gleocapsa*.

Table 5-2: General microbial observations from the Dalry School samples.

Facade	Surface	Interior	Type
NE	✓	X	filamentous cyanobacteria
SE	X	✓	globular cyanobacteria

5.2 RGU Samples

Six cores were acquired from the RGU test walls, but only four of these were blond sandstones: Cat Castle (RGU2); Stainton (RGU3); unknown Stirling sandstone (RGU5); and Clashach (RGU6). Core one is Leoch granite (RGU1) and core four is Locharbriggs red sandstone (RGU4) and, as these were not blond sandstone, they were not analysed in all experiments. In addition, a loose block of Blaxter (blond) sandstone was retrieved from RGU.

5.2.1 *Protein and Chlorophyll-a Assays*

Protein assays were conducted on all samples with the exception of the Blaxter sandstone block and RGU6, where the fine-grained texture and thick quartz overgrowths of Clashach meant that no scrapings could be collected from its surface. Protein was found on all surfaces, generally ranging from 4.2 $\mu g/cm^2$ to 15 $\mu g/cm^2$ (Figure 5-5A). The RGU4b result is much higher (78.1 $\mu g/cm^2$) than the other results, as the sample was taken from an area which had a patch of moss growing on it.

Chlorophyll-a assays were conducted on the same samples as the protein assays. However, the results are much sparser with only RGU4 and RGU5 showing any chlorophyll-a: RGU4a = 0.23 mg/cm^2 and RGU5 = 0.28 mg/cm^2 whilst RGU4b is much higher again due to the moss (Figure 5-5B). The lack of chlorophyll-a in RGU1, RGU2, and RGU3 indicate that the protein found on their surfaces was from non-photosynthetic sources, such as fungi or bacteria, whilst RGU4 and RGU5 contain either purely photosynthetic microorganisms or a mixed community.

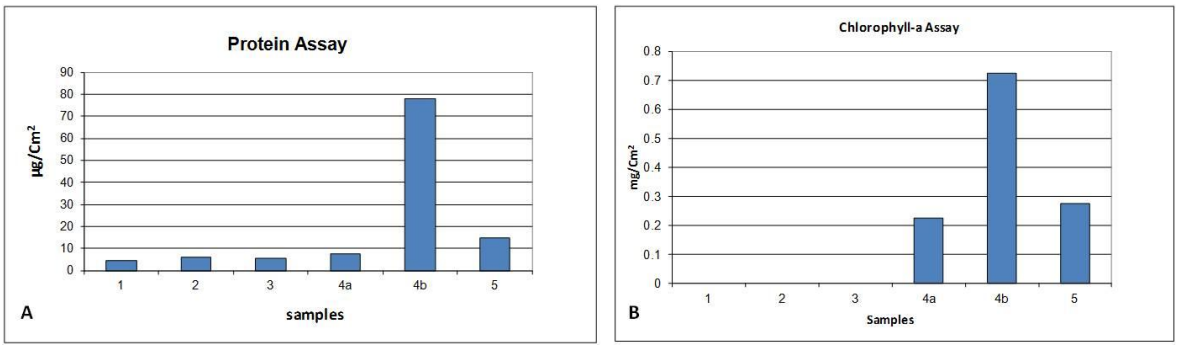

Figure 5-5: Protein and chlorophyll-a assays for RGU samples.

A) Protein assay, B) chlorophyll-a assay. These results show that although protein is present on all sample surfaces, it is not always from a photosynthetic source.

5.2.2 *SEM Imaging of the Outer Surfaces of the Stones*

Only the blond sandstone samples were examined in these experiments (RGU2, RGU3, RGU5 and RGU6). Small fragments of the surface were broken off and observed using the FEG-SEM in BSE mode. The fracture surface of RGU2 is speckled with dark clusters of deflated pods; each pod is 10-20 µm in size, indicating an algal species. These colonies of algae live within hollows on the surface (Figure 5-6). There is no evidence of any other organic material on the RGU2 surface, although it may be obscured by the kaolinite and quartz fragments found littering the surface and infilling depressions. The surface of RGU3 shows no microbial communities living on its surface, although small quantities of dehydrated EPS with a honeycomb structure are seen, with Ca-oxalate encrusting the surface and taking on the form of the EPS (Figure 5-6). Large quantities of a filamentous cyanobacteria <5 µm thick, with no identifiable internal structure, were found on the surface of RGU5 and have a morphology consistent with *Phormidium* (Rippka et al., 1979; Phoenix et al., 2006). The inter-locking webs of filaments have gathered mineral fragments and atmospheric particles, binding them together on the surface of RGU5 (Figure 5-6). RGU6 has scattered dehydrated EPS which has decreased in size in the hollows where it occurs (Figure 5-6). These regions of dehydrated EPS mats are ~200 µm in diameter, which is consistent in size with other EPS mats on Dalry samples but no calcium oxalates were found on RGU6.

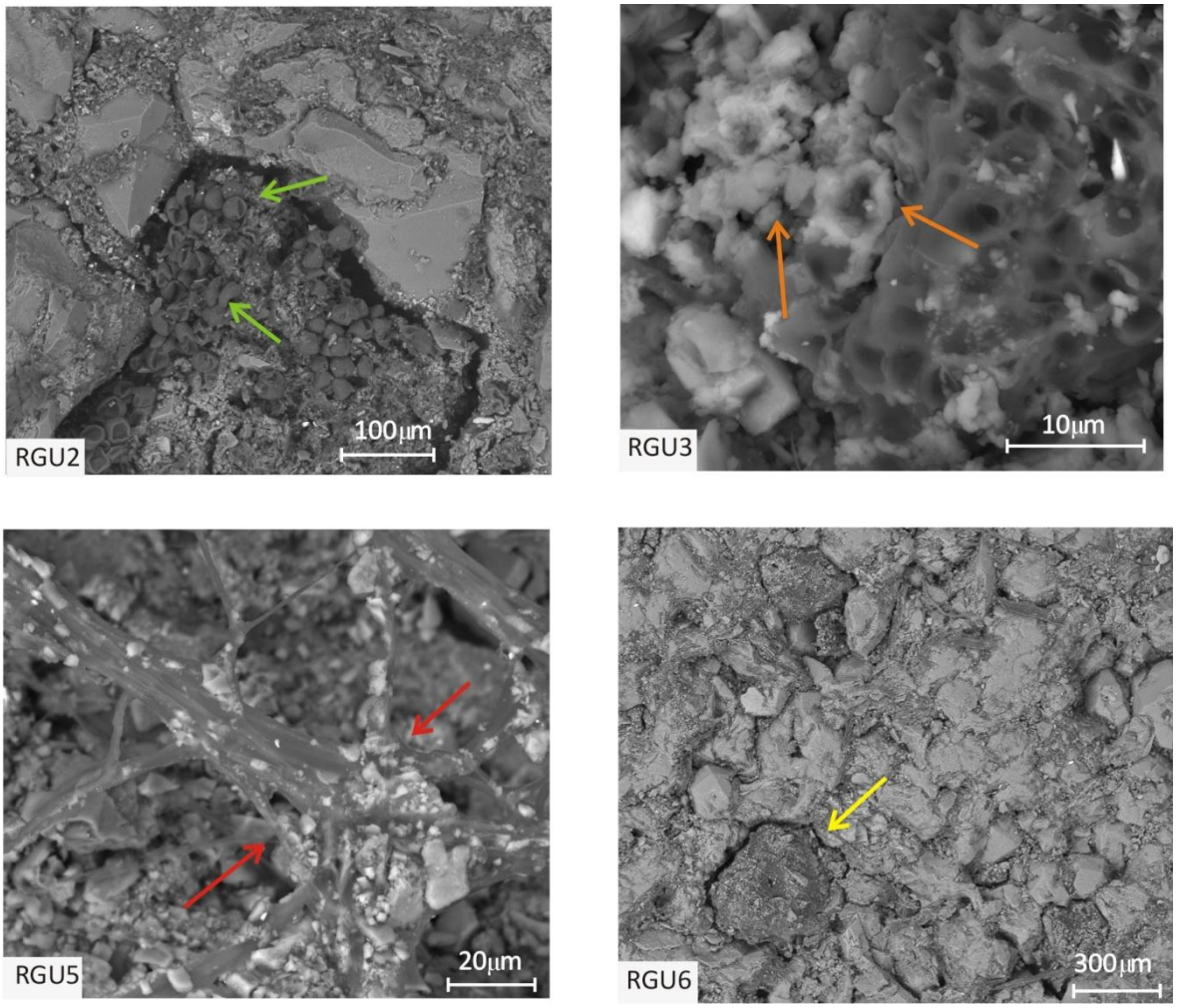

Figure 5-6: FEG-SEM SE images of outer surface samples from RGU samples. Note varying scale bar on images.

Yellow arrows = dehydrated EPS, orange arrows = Ca-oxalates, red arrows = filamentous cyanobacteria, green arrows = algal pods. RGU2) algal pods within a hollow, RGU3) calcium oxalates forming on dehydrated EPS, RGU5) showing *Phormidium* binding rock fragments, RGU6) shrunken dehydrated EPS within hollows.

5.2.3 *Osmium Stained Cross-Sections*

The blond sandstone cores (RGU2, RGU3, RGU5 and RGU6) and the loose block of Blaxter sandstone were all used for the osmium staining experiments. This technique did not show any stained microbes to be present within RGU2 and RGU5, but stained organic material does occur in RGU3, RGU6 and the Blaxter block.

In RGU3, communities of bulbous microbes, which are comprised of 1-4 cells surrounded by gelatinous EPS, are found to a depth of 2 mm. There, they form communities which can be seen infilling pore spaces with dimensions of ~1.5 x 1.5 mm (Figure 5-7); each unit is ~5 µm in diameter. This microorganism is morphologically consistent with the

cyanobacteria *Gleocaspa* (Rippka et al., 1979). The communities at the surface are dominated by EPS and are less densely populated than the internal communities (Figure 5-7). Small quantities of filamentous cyanobacteria material were also identified to a depth of 2 mm.

RGU6 results show an abundance of microbial matter that lives between the surface and 2 mm depth. At the surface, large expanses of EPS with a low density population are seen infilling gaps between grains (Figure 5-7) whilst, at depth, semi-rounded cells (~2 µm in diameter with no internal structure) are infilling pores ~1.5 x 0.5 mm in size. A smaller quantity of EPS is seen to surround these cells, in comparison to those at the surface and seen in RGU3, and are an unknown species at present.

The microorganism communities found within Blaxter show a highly developed structure throughout the sample. On the surface, only a few globular cyanobacteria are found (Figure 5-8A) but, at depths of 2-3 mm, dense populations of the same cyanobacteria are observed (Figure 5-8B) and these appear morphologically consistent with *Gleocaspa*. Deeper than this, the densely packed communities of cyanobacteria become sparser and are replaced by filamentous organisms at a depth of 7 mm (Figure 5-8C). These branching filaments are only 2 µm thick and appear translucent under the FEG-SEM. Due to their depth within the sandstone, they are likely to be fungus rather than filamentous cyanobacteria, given the light requirements for photosynthesis (see later discussion).

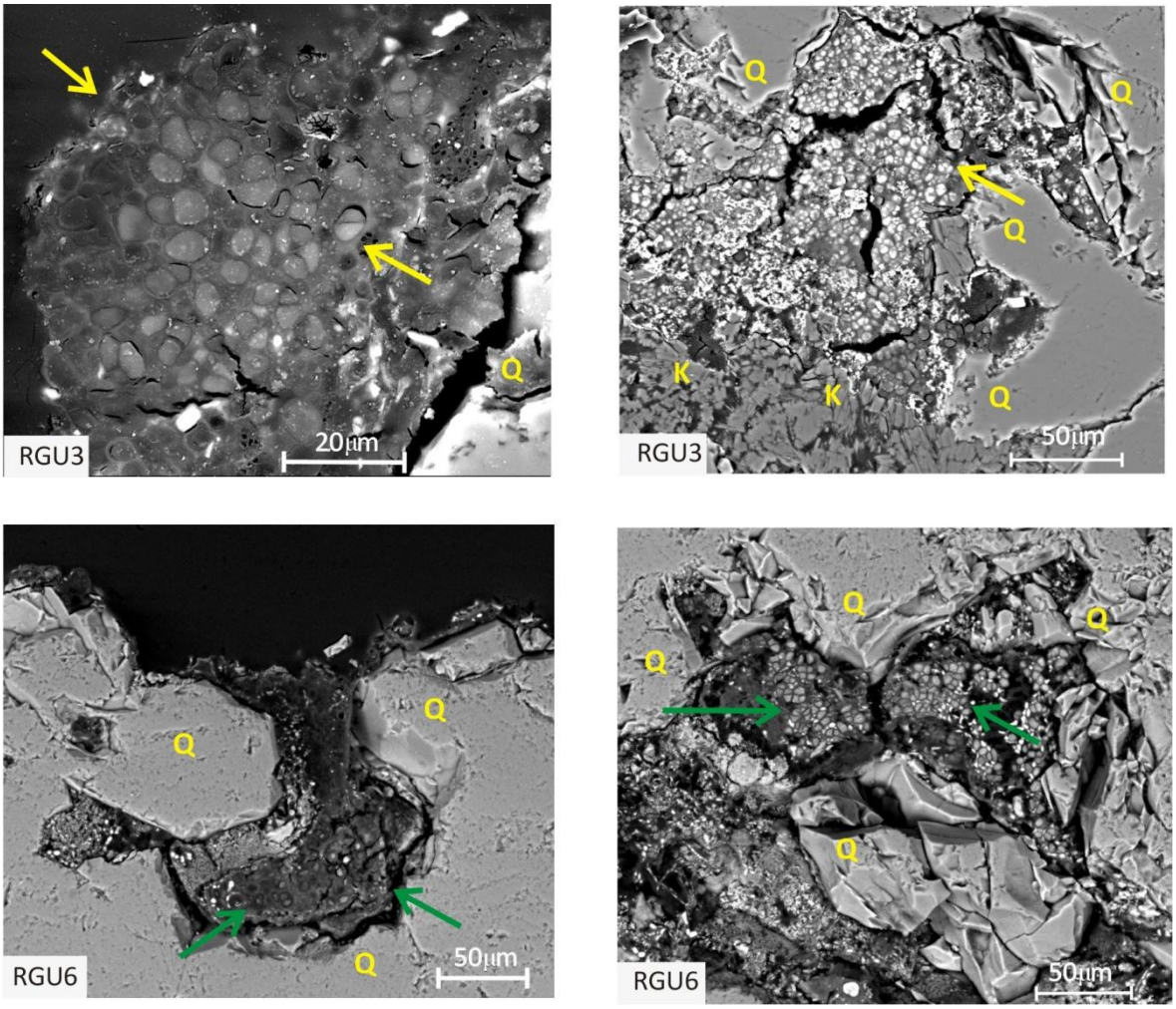

Figure 5-7: FEG-SEM BSE images of RGU polished blocks.

RGU3 and RGU6, both samples show cyanobacteria and EPS engulfing pore space within the sandstone. Q = quartz, K = kaolinite, yellow arrows = *Gleocapsa* cyanobacteria, green arrows = unknown globular cyanobacteria. Both RGU3 and RGU6 show sparser populations on the surface with larger denser communities at 2 mm depth.

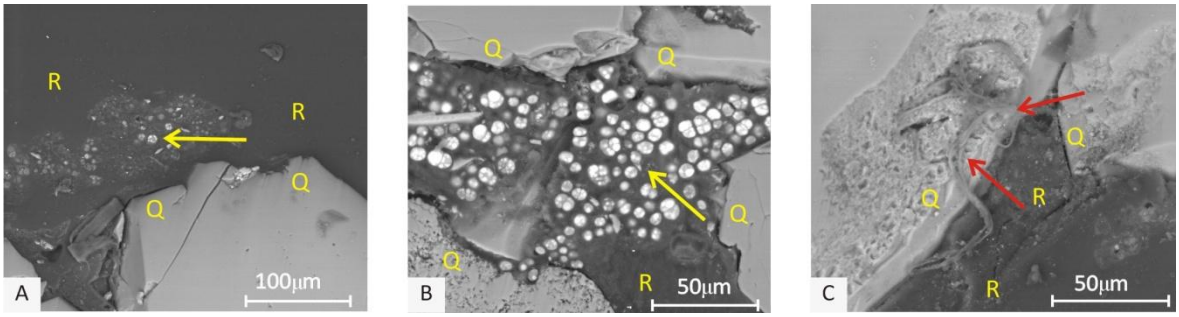

Figure 5-8: FEG-SEM BSE images of Blaxter polished block.

R = resin, Q = quartz, yellow arrows = globular cyanobacteria, red arrows = filamentous cyanobacteria. A) Surface image of the cyanobacteria, B) dense community of cyanobacteria beneath the surface, C) fungus at a depth of 7 mm

5.2.4 ***Summary***

Results from the surface protein and chlorophyll-a assay are consistent with the FEG-SEM observations of the rough surface. The only inconsistency arises in evidence from RGU2,

where the chlorophyll-a assay detects nothing whereas the SEM images show large communities of algae living on the surface. This may be due to them living within hollows and so were protected during sample collection, or the algae seen could possibly have contained chlorophyll 'b' or 'c' which were not tested for.

Results for the blond RGU samples show a divide between the sandstones that have surface dwelling microbes in comparison to the cryptodendolithic microbial communities. Microbes seem to preferentially live on the surface of RGU2 (Cat Castle) and RGU5 (unknown Stirling sandstone), whereas microbial communities are cryptoendolithic in RGU3 (Stainton) and RGU6 (Clashach). A reason for this may be the translucency of the sandstones, with those containing cryptoendolithic communities having considerably smaller proportions of all other minerals besides quartz. RGU3 and RGU6 have less than 10% of these whilst RGU2 and RGU5 have 17.7% and 26.3%. The purer quartz sandstones will allow more light to penetrate, supporting cryptoendolithic cyanobacteria (detailed further in later discussion).

5.3 University Samples

The samples for the University set were obtained from Southpark Avenue, University of Glasgow (a compositional review is in section 4.3.1). Two facades of the building were sampled for microbial work, as listed in Table 5-3**.**

Table 5-3: Sample identifier and associated facade for University set.

East South East Facade	North North East Facade
UN1	UE1
UN2	UE2
UN3	UE3
	UE4

5.3.1 *Chlorophyll-a Assay*

The chlorophyll-a assays show that all the samples have a proportion of photosynthetic material on the surface (Figure 5-9), ranging from 0.03 mg/cm^2 to 0.41 mg/cm^2. The largest amount within these samples is found on UE3. The amount of chlorophyll-a found

on these samples is marginally lower than that on the RGU and Dalry samples. However, two groups emerge from this data: UN1, UE1 and UE2 (0.03 mg/cm^2 to 0.05 mg/cm^2) have similar proportions of chlorophyll-a, whilst UN2, UN3, UN4 and UE3 have slightly higher levels (0.29 mg/cm^2 to 0.41 mg/cm^2) within this data set (Figure 5-9).

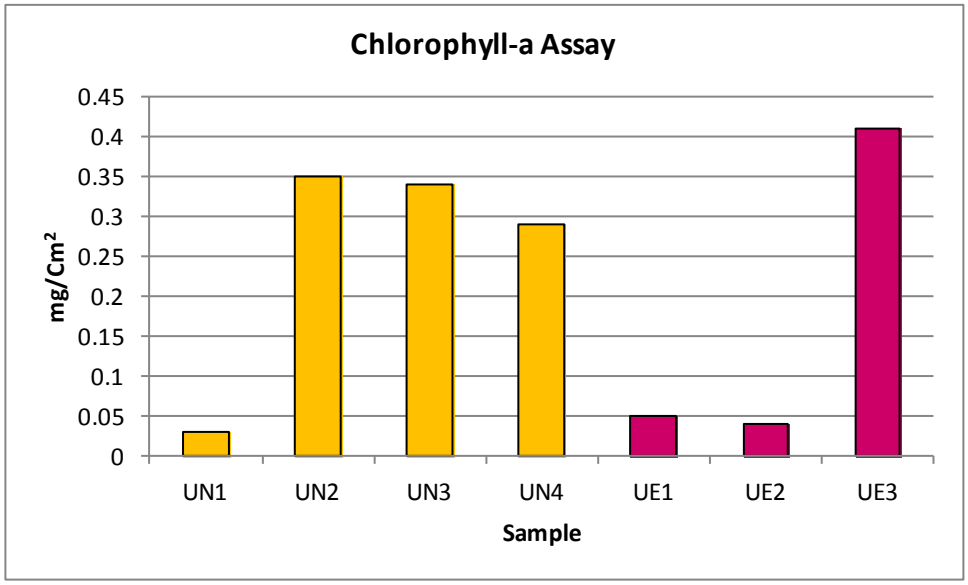

Figure 5-9: Chlorophyll-a graph for University samples.

Protein assays were also conducted, but all samples returned with zero results. This is theoretically impossible, as chlorophyll-a assays show that some photosynthetic microbes are present. Therefore, it may be that the experimental procedure was not conducted properly. However, due to limitations of the size and number of available samples these experiments could not be repeated.

5.3.2 *SEM Imaging of the Outer Surface of the Stones*

Outer surface fragments from these samples were broken off and imaged using the FEG-SEM, to determine whether any organic material could be identified on the surface, but none was observed on any sample. Large quantities of kaolinite, quartz, other mineral fragments, and possibly atmospheric dust, lie on the surface and these particles have infilled depressions on UN3, UE3 and UE4 (Figure 5-10). Therefore, organic matter may have been obscured and hidden by the debris. Samples UE1 and UE2 had surfaces similar in nature, where the quartz grains had a thin film coving them (discussed further in section 3.3.2). The surface of UN2 is also discussed in section 3.3.2. These surfaces with coverings did not show any evidence of inhabitation by microorganisms either.

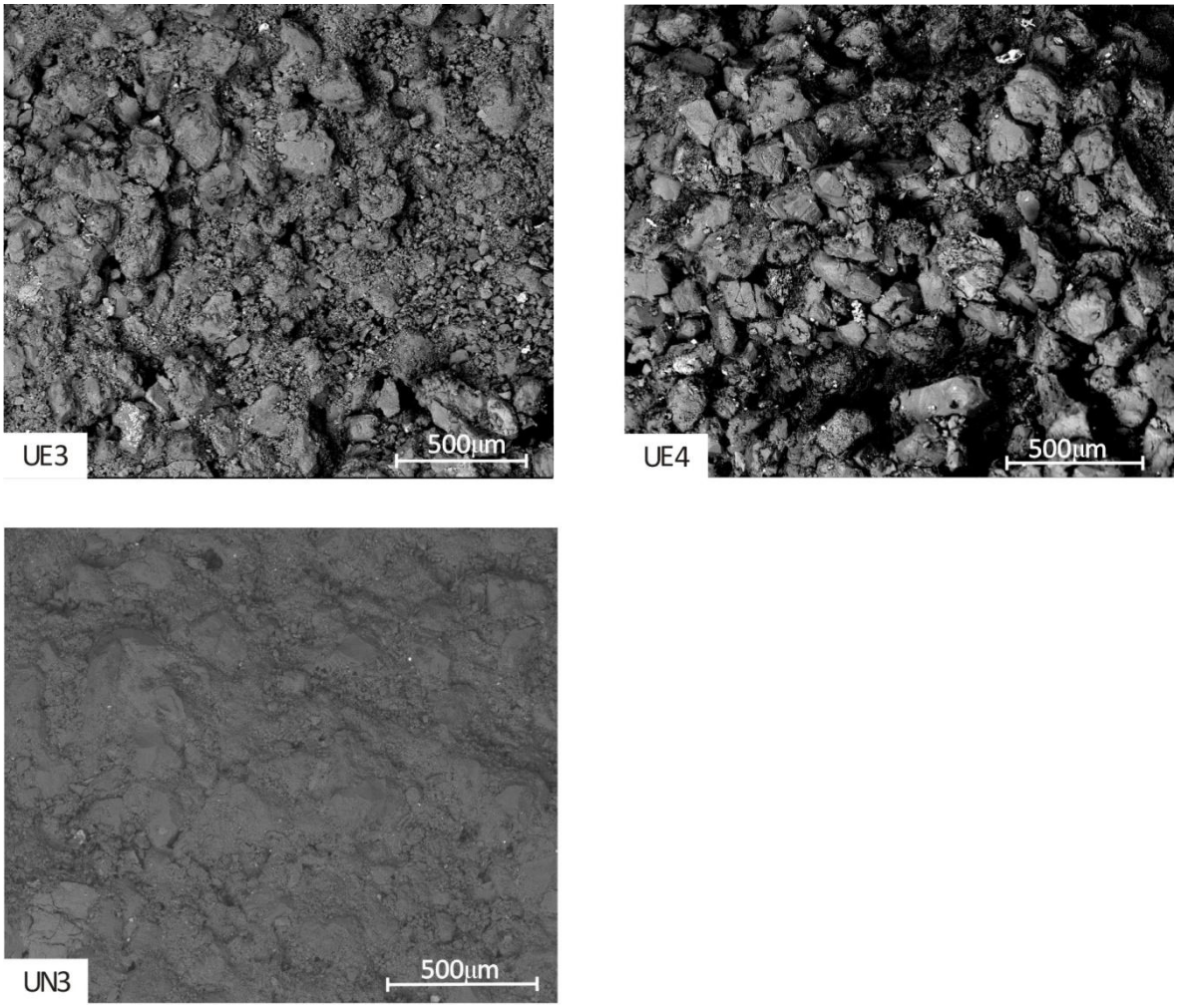

Figure 5-10: FEG-SEM SE images of outer most surface of University samples. Samples UE3, UE4 and UN3, highlighting the particle-rich surfaces of the blocks.

5.3.3 *Osmium Stained Cross-Sections*

The osmium stained blocks from the University sample set were studied using the FEG-SEM and prepared as outlined in section 2.1.5. Of all the University samples studied, UE2 is the only one that contains any stained microbial matter. Microorganisms were found in abundance at the surface and to a maximum depth of 2 mm. These microbes consist mainly of spherical cyanobacteria or algae with complex internal structures situated largely around the edge of the cell. Cells range from 2-10 µm in size and are occasionally seen to be dividing (Figure 5-11). These microbes are found within large expanses of EPS, colonising pore spaces and attaching themselves to mineral surfaces (Figure 5-11). However, no fungi or filamentous cyanobacteria were observed.

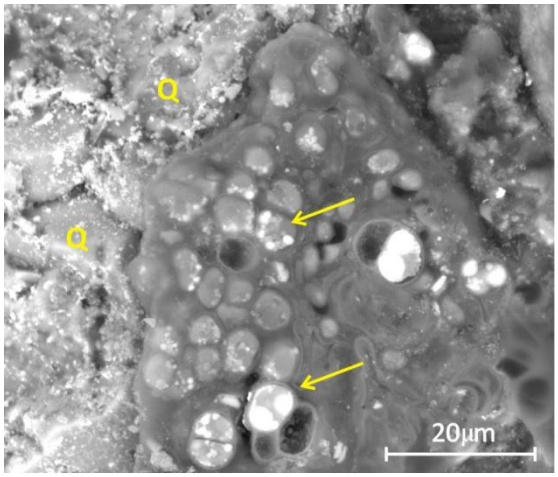

Figure 5-11: FEG-SEM BSE image of UE2 polished block.
Q = quartz grain, yellow arrows = spherical microorganism within EPS.

5.3.4 *University Summary*

The FEG-SEM images of surface fracture samples indicate that the sandstones have been very poorly colonised by microorganisms, with only minimal identification possible. However, the chlorophyll-a assay shows all the University building samples to be positive, with an average of 0.22 mg/cm^2 of chlorophyll-a on the surface. This is marginally lower than the averages for RGU (0.25 mg/cm^2) and Dalry (0.26 mg/cm^2). All these samples have a crust formation, whose presence may be obscuring and covering the microbes.

When osmium stained polished blocks were examined, the results showed that only UE2 contained osmium stained microorganisms living cryptoendolithically. The only major difference between UE2 and the rest of the University samples was the lack of ankerite crystals at its surface.

5.4 St Vincent St Church Samples

All samples obtained from the St Vincent Street Church, Glasgow, are listed in Table 5-4. Some of these blocks have a mortar covering on the surface, and so not all were used in each experiment.

Table 5-4: Sample identifiers for St Vincent Street church samples.

East facade	North-west corner
EE1	CS1 (mortar)
EE2	CS2 (mortar)
EE3	CS3 (mortar)
EE4 (mortar)	CS4

Those with a mortar covering are indicated.

5.4.1 *Chlorophyll-a Assay*

The samples used for the chlorophyll-a assays were EE1, EE2, CS1, CS3 and CS4 and all tested positive for chlorophyll-a on the surface. The results range from 0.07 to 0.42 mg/cm^2; CS1 has the most, peaking at 0.42 mg/cm^2 (Figure 5-12), which is consistent with chlorophyll-a assay data from other sample sets.

Protein assays were also conducted, but all samples returned with no results. In common to the University results, this may be because the experiment procedure was not conducted properly but, due to sample size limitations, repeat experiments could not be carried out to validate the data preparation method.

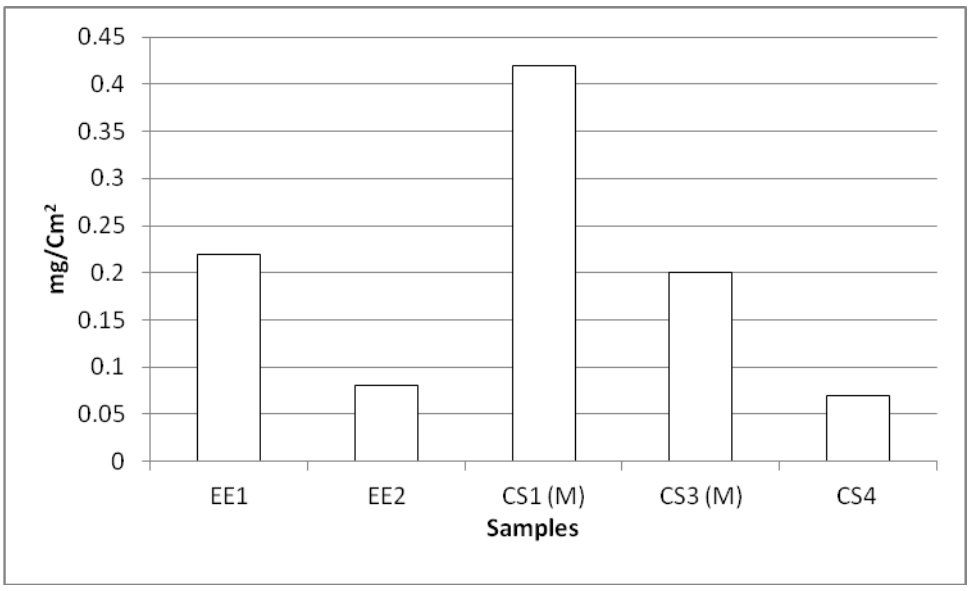

Figure 5-12: Chlorophyll-a graph for SVS samples.

5.4.2 *SEM Imaging of the Outer Surface of the Stones*

Surface fragments were collected from CS4, EE1, and EE3 (those without mortar) and studied using the FEG-SEM in BSE low vacuum conditions. The surface of EE1 is covered in fine-grained debris, comprised of fragments of kaolinite, quartz, and possible atmospheric particulates, as discussed in section 3.4.2. However, some strands of filamentous cyanobacteria were detected, which are ~10 µm thick and appear semi-transparent in SEM imaging; no internal structure could be seen due to the filaments gathering debris (Figure 5-14A). These are akin to cyanobacteria *Oscillatoria* or *Scytonema*. Figure 5-14A demonstrates the difficulty in identification when debris coats the filaments, thus hampering classification.

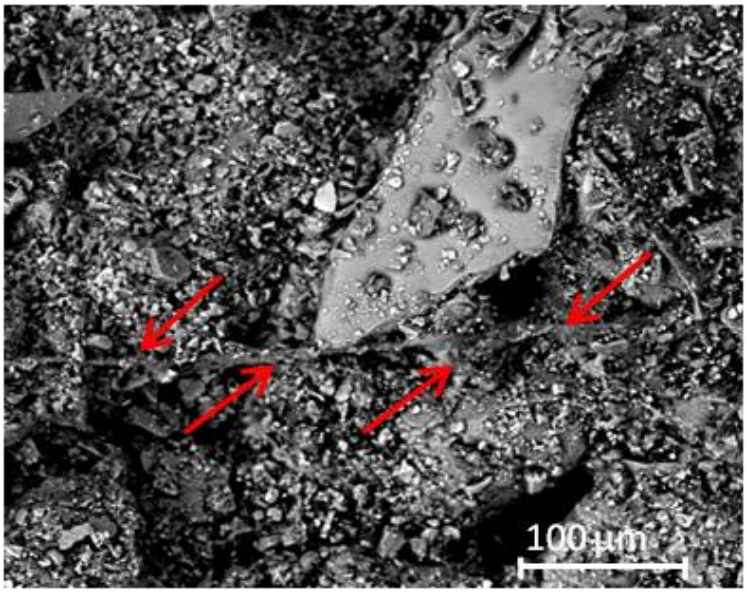

Figure 5-13: FEG-SEM SE images of EE1's outermost surface.
Red arrows highlight *Oscillatoria*/Scytonema strands.

The surface of EE3 and CS4 (Figure 5-14B) are both very similar to EE1 with a coating of fine-grained fragments although no other organics were identified (Figure 5-14). However, no microbial matter was identifiable.

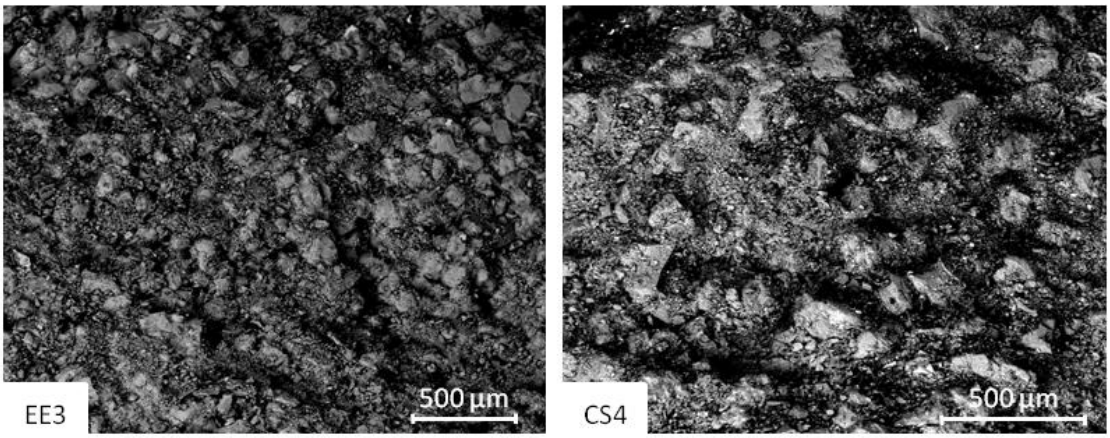

Figure 5-14: FEG-SEM SE images of outermost fracture surfaces of SVS samples EE3 and CS4.

No identifiable microbial matter was seen on these surfaces.

5.4.3 *Osmium Stained Cross-Sections*

When the SVS samples were osmium stained, all blocks tested negative for organic material with the exception of CS4 (this is also the only non-mortar covered sample from this facade). A cyanobacterium consistent with the morphology of *Gleocapsa* was found and in association with EPS. It was seen bridging quartz grains at the outermost surface (Figure 5-15). However, the microbes were only seen to a maximum depth of 0.5 mm.

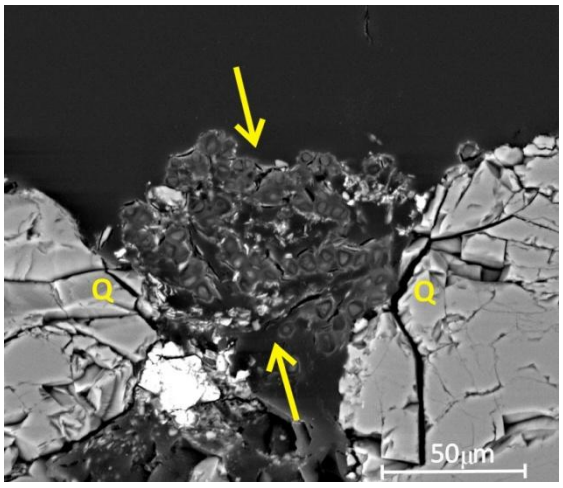

Figure 5-15: FEG-SEM BSE image of CS4 polished block.

Cyanobacteria surrounded by EPS between quartz grains on the surface. Q = quartz grains, yellow arrows = cyanobacteria.

5.4.4 *Summary of SVS Samples*

A clear view of the microbes living on the sandstone surfaces of these samples was particularly difficult to obtain due to the presence of mortar on the surface of many of

the samples, although the sandstone samples did seem to have a low bioreceptivity. Filamentous cyanobacteria are present, on the surface of EE1 and, internally on CS4 small proportions of globular cyanobacteria are also distinguishable. These samples have a black crust on their surfaces which contains gypsum crystals (see section 3.4.2) and this crust is likely to be hindering the growth of microorganisms because the salt creates a hostile acidic environment on the surface.

5.5 Discussion

To examine microbial colonisation on the outer surface of the sandstones two techniques were employed: 1) protein and chlorophyll-a assays on surface scrapings and 2) FEG-SEM SE imaging of rough outer surfaces. However, discrepancies between the two methods did arise for the D2, University and RGU2 samples.

In the case of D2, the second highest chlorophyll-a measurement of any samples was recorded, but very little evidence of microorganisms was found through imaging of the surface.

This discrepancy may be a product of spatial variation in colonisation, because the scrapings (for proteins and chlorophyll-a assays) and surface fragments (for SEM) were produced from different regions of the same core. The triplicate results from D1 and D3 also show that a large amount of spatial variation can occur on these stones, for both protein (RSD 47%) and chlorophyll-a (RSD ranging from 21-81%).

The poor correlation in the University results, where chlorophyll-a was detected but no microbes were seen, may be due to the nature of the stone surface. The samples were littered with loose mineral fragments and debris, potentially obscuring the identification of microbial matter. Moreover, the surface filamentous cyanobacteria on other samples were seen to have mineral fragments caught within their structure, which could also hinder the identification of microbes on the University samples.

In observations from RGU2, it was the chlorophyll-a assays which were negative whereas the SEM imaging clearly reveals algal matter inhabiting the surface of the sandstone. The first possible reason for this contradiction is that only chlorophyll-a is analysed in the

experiments, whilst the algae may have contained chlorophyll 'b' or 'c'. However, this is unlikely as chlorophyll-a is much more abundant within algae, especially those identified on Scottish buildings (Urquhart et al., 1995). Therefore, it is much more likely, that during collection, the algal microbes were not sampled, as they inhabit depressions protecting them from surface scraping (see Figure 5-7C).

These methods, in general, complimented each other but highlight the benefit of combining the techniques as each procedure when conducted in isolation, has some limitations.

The main surface microbes identified were filamentous cyanobacteria, with two main morphologies: 1) A thin (2 μm wide) unbranching cyanobacteria similar to *Phormidium;* and 2) a thicker variety (10 μm wide) which is also unbranching, but closer resembling *Oscillatoria* or *Scytonema*. Calcium oxalates were also present on the surface of some samples, and these suggest that microbes were once present. The calcium oxalates occur as a by product of reactions between microorganisms and calcium carbonates (Del Monte et al., 1987).

The osmium staining results show that a third of all sandstones analysed had cryptoendolithic microbial communities and they occur within all the sample sets. All internal microbes identified are globular cyanobacteria or algae, with up to three different morphologies identified, with the exception of D6, where filamentous microorganisms were observed, (Table 5-5). One of the globular cyanobacteria seen could be *Gleocapsa,* whilst the other cyanobacteria is unknown but may be *Gleocapsa* at a different stage of growth/dehydration. The globular cells in UE2 are thought to be algae due to their complex internal structure and large size.

Surface and subsurface species identification have both been undertaken using visual criteria only. To provide more precise classification, DNA testing such as 16s rRNA, could be used on the microbes.

However, *Gleocapsa* has previously been found on Scottish sandstones (Young, 1997) and, although *Phormidium* and *Osillatoria* have not been found inhabiting Scottish sandstone, they have been shown to live on and within sandstone in environments as

different as Antarctica (Omelon et al., 2006b) and the Mediterranean (Ortega-Calvo et al., 1991; Macedo et al., 2009).

The Dalry samples, which are composed of the same sandstone on both facades, highlight the fact that facade orientation may influence which type of microbe is dominant. In these samples, the SE facing set has abundant internal (cryptoendolithic) globular cyanobacteria, whereas the NE facade has plentiful surface filamentous cyanobacteria. The summary in Table 5-5 shows that this is also generally true for the other sample sets. The surface microorganisms tend to be more concentrated (although not always present) on sheltered facades of the buildings such as the northeast and east, i.e. where the impact of solar radiation is less. The cryptoendolithic microbes generally coincide with south facing facades, although this is not always the case (e.g. samples RGU2, RGU5 and UE1, UE3). Therefore, a second control on their presence must influence the placement of organisms, possibly the sandstone's mineralogical composition influencing the areas that become colonised by affecting porosity or light penetration.

A second common mineralogical feature corresponding to the location of globular cryptoendolithic microbes congregating is the ankerite content of the sample. Samples that have suffered depletion of ankerite at the surface or samples in which ankerite has always been absent have globular cyanobacteria (samples D7, RGU5 and UE2).

The paucity of microbes identified on the University building and SVS samples could be a combination of many factors. One factor could be that the sandstone used to construct these buildings has a very low bioreceptivity to microbial colonisation. Most sandstone types have a reasonably high bioreceptivity in comparison to other rocks such as limestones or granites; bioreceptivity is normally closely related to the porosity of the material (Miller et al., 2006). The University samples have a mean porosity of 19.5% in the outermost regions (surface to 4 mm depth) while porosity is ~22.4% in the SVS samples. However, this is similar, to the porosity found within the Dalry cryptoenolithic bearing sandstones (21.4%) which contain more microbial matter. Consequently, porosity cannot single-handedly explain the poor bioreceptivity of the University and SVS samples. The other main control on the bioreceptivity of stone is its chemical composition (Miller et al., 2006). However these sandstones are mineralogically similar to the other sandstones which test positive for microbial communities. Consequently,

there must be a third factor, reducing the bioreceptivity of the University and SVS samples, although this is unknown at present.

Table 5-5: Summary of microbial communities and their placements within or on the samples.

Sample set	Aspect	Surface (SEM Identification)	Type	Internal (SEM identification)	Type
Dalry 1	NE	YES	Filamentous	NO	
2	NE	YES	Filamentous	NO	
3	NE	YES	Filamentous	NO	
4	NE	NO		NO	
5	SE	NO		YES	Globular
6	SE	NO		YES	Filamentous
7	SE	NO		YES	Globular
8	SE	NO		YES	Globular
RGU 2	S	YES	Algae pods	NO	
3	S	NO		YES	Globular
5	S	YES	Filamentous	NO	
6	S	NO		YES	Globular
Blaxter	S	---		YES	Globular
Uni UN1	SES	NO		NO	
UN2	SES	NO		NO	
UN3	SES	NO		NO	
UE1	NNE	NO		NO	
UE2	NNE	NO		YES	Globular
UE3	NNE	NO		NO	
UE4	NNE	NO		NO	
SVS EE1	E	YES	Filamentous	NO	
EE3	E	NO		----	
EE4	E	----		NO	
CS2	NW	NO		YES	Globular
CS4	NW	NO		NO	

The previous reasons help explain why the filamentous and globular cyanobacteria are found on different sandstones, but Table 5-5 also indicates that both epilths and cryptoendolithic microbes are never found on the same sample, with no exceptions to this rule. Most likely is that the internal microbes were established first and later migrated to the surface. As the *Phormidium* may be more tolerant to solar radiation and the extreme weather experienced at the surface causing, the dominant species to change from *Gleocapsa* to *Phormidium* as the microbial communities move towards the surface. The change in dominant species may be due to the changing environmental conditions or the surface or the sandstone's surface, changing colour and or texture (discussed further later in this chapter).

5.6 Light Penetration into Sandstone

Photosynthetic organisms need light to survive and therefore, to support cryptoendolithic communities, light has to be able to penetrate into the sandstone. The optimum amount of light (photosynthetically active radiation (PAR) intensity) needed for photosynthetic communities to thrive is between 50 and 500 µmol $m^{-2}s^{-1}$ (Litchman et al., 2003; Phoenix et al., 2006). Too little light means microbes will not be active and communities cannot be maintained, although some species will survive with the minimum requirements of 5 µmol $m^{-2}s^{-1}$ of PAR (Nienow et al., 1988; Phoenix et al., 2006). Yet, too much light will result in photo-oxidative damage to the cells, hindering and ultimately stopping microbial activity. This need for light to fuel metabolic activity, along with the requirement of protection from intense sunshine (which in Glasgow can reach over 1000 µmol $m^{-2}s^{-1}$ regularly), dictates the depth at which the photosynthetic organisms present can penetrate and inhabit the sandstone. To quantify this, a series of optical light transmission (OTL) experiments were undertaken, as outlined in section 2.1.6.

Five samples were used, which all showed differing degrees of surface weathering, to provide a representative cross-section of crusts seen on Glasgow buildings. A fresh, unaltered sample of Bearl sandstone (quartz = 71%, porosity = 14%) was used to represent the optical penetration in cleaned or new constructions. Samples UE2 from the south facade of the University (quartz = 62%, porosity = 25%), EE3 from the east facade of the SVS samples (quartz = 61%, porosity = 21%) and CS4 from the northwest corner of the SVS samples (quartz = 49%, porosity = 32%) were used to represent Glasgow's buildings and these have varying degrees of weathering crusts in the surface. Furthermore, a uniform black crust was present on UE1 from the University sample set (quartz = 72%, porosity = 15%). The samples used are shown in Figure 5-16.

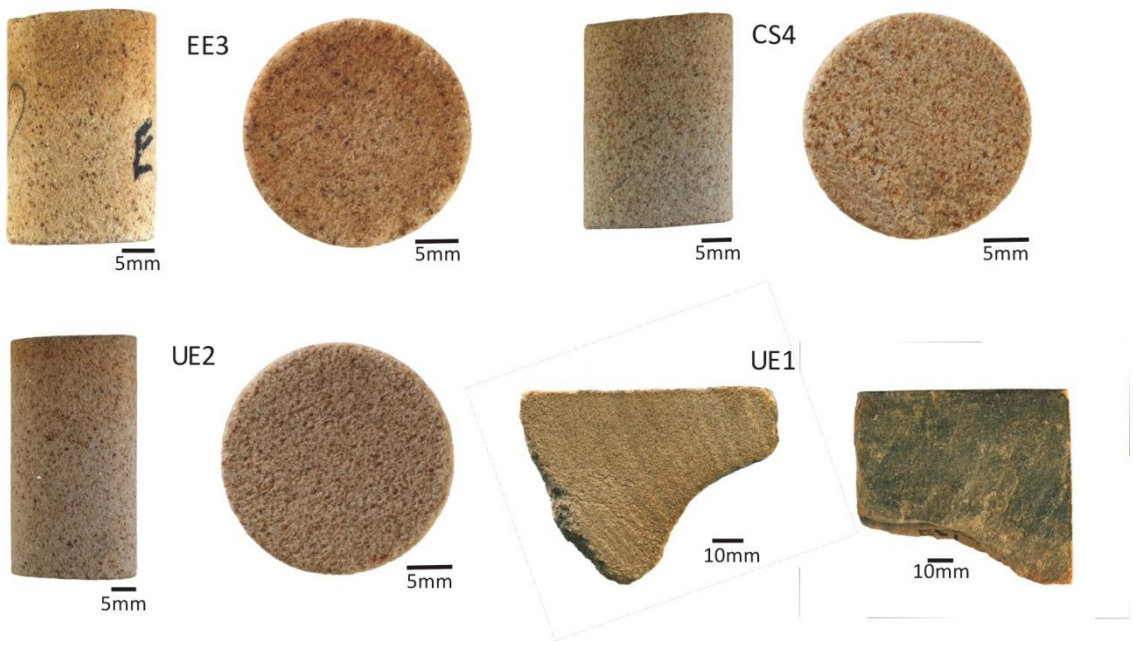

Figure 5-16: Images of cross-sectional and plan views of samples used in the OTL experiments.

Outermost surface of the core is at the top of the image.

During the experiment, a minimum of five measurements were taken to allow an average to be calculated for each sample, and help to quantify the repeatability, and so reliability of the results.

To ensure that the experimental data (collected by a Macam Q203 Quantum Radiometer pyrometer, measuring in µmol $m^{-2}s^{-1}$, known as the Hp) could be compared with daily pyrometer data (gathered at the University of Glasgow weather station by a Kipp and Zonen CMP3 pyranometer (Op) measuring in Wm^{-2}), a conversion was calculated. On the 06/06/2010, the Hp pyrometer was used to simultaneously gather data at the weather station site. These data were plotted against the weather station pyrometer results to provide a conversion graph (Figure 5-17). Although the weather during this day was a mixture of sunshine and showers, a linear correlation can be seen between data collected from the two pyrometers (Figure 5-17).

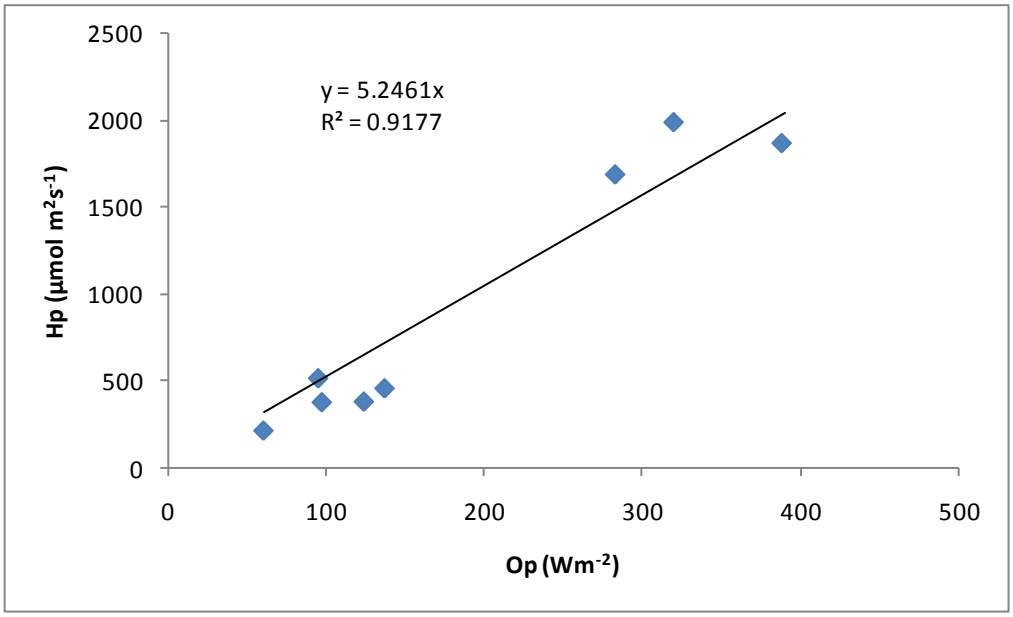

Figure 5-17: Conversion graph for the Hp to Op pyrometer.

Hp) hand held pyrometer, Op) the outside fixed pyrometer at Glasgow University weather station.

The experimental light penetration data was combined with the observatory solar radiation data to determine the actual amount of sunlight reaching a given depth at a given time interval (Equation 3). As the observatory units were in Wm^{-2}, these needed to be converted to µmol $m^{-2}s^{-1}$ using the conversion in Figure 5-17. This was done because µmol $m^{-2}s^{-1}$ are more meaningful when considering the light impact on microbes (i.e. µmol $m^{-2}s^{-1}$ are more commonly used in the literature and so allow greater comparison).

$$((L_I \div L_O \times O_P) \times 5.246 = L_{DO})$$

Equation 3: Amount of light at depth

L_1 is the amount of light penetrating a given thickness of rock.

L_0 is the amount of light incident on the rock surface during the experiments

L_{DO} is the amount of light at a specified depth in concordance with the H_p pyrometer (µmol $m^{-2}s^{-1}$).

O_p is the results from the University of Glasgow's pyronometer.

This equation was used to convert various data sets, to produce models for both summer and winter for light penetration into sandstones through a variety of surfaces, both weathered and unweathered. A detailed outline of the errors concerned with these results are given in section 2.1.6. The first data discussed are from a "typical" Glasgow

summer's day of sunshine and cloud cover, taken from 06/06/2010 (the conversion data day). As 5 µmol $m^{-2}s^{-1}$ is the minimal amount of PAR needed for cyanobacteria activity, it is used as a base amount throughout these experiments.

Bearl with its fresh clean surface is the most translucent of the samples, with a maximum of 77 µmol $m^{-2}s^{-1}$ PAR penetrating to a depth of 1 mm. At 1 mm depth, PAR measurements greater than 5 µmol $m^{-2}s^{-1}$ are seen throughout the day from 8 am to 3 pm. At a depth of 1.5 mm the amount of light transmitted is a third of that at 1 mm, with the maximum PAR measurement recorded at 1.5 mm being 26 µmol $m^{-2}s^{-1}$. By a depth of 4 mm from the surface only a 20^{th} of the light at 1 mm is able to penetrate, with a maximum of 3.8 µmol $m^{-2}s^{-1}$ (Figure 5-18).

Of the weathered surface samples (CS4, EE3 and UN2), EE3 is the only sample able to transmit over 5 µmol $m^{-2}s^{-1}$ of light to a depth of 1 mm. EE3 reaches a maximum of 7.4 µmol $m^{-2}s^{-1}$ PAR at 1 mm depth, and could sustain cyanobacteria life at a depth of 1 mm between the hours of 12 to 2 pm, on this "typical" Glasgow's summer day. Within the CS4 and UN2 samples a maximum light penetration of 1.5 µmol $m^{-2}s^{-1}$ is achieved (Figure 5-18). The UE1 sample with black crust shows only negligible amount of light at 1 mm beneath the surface.

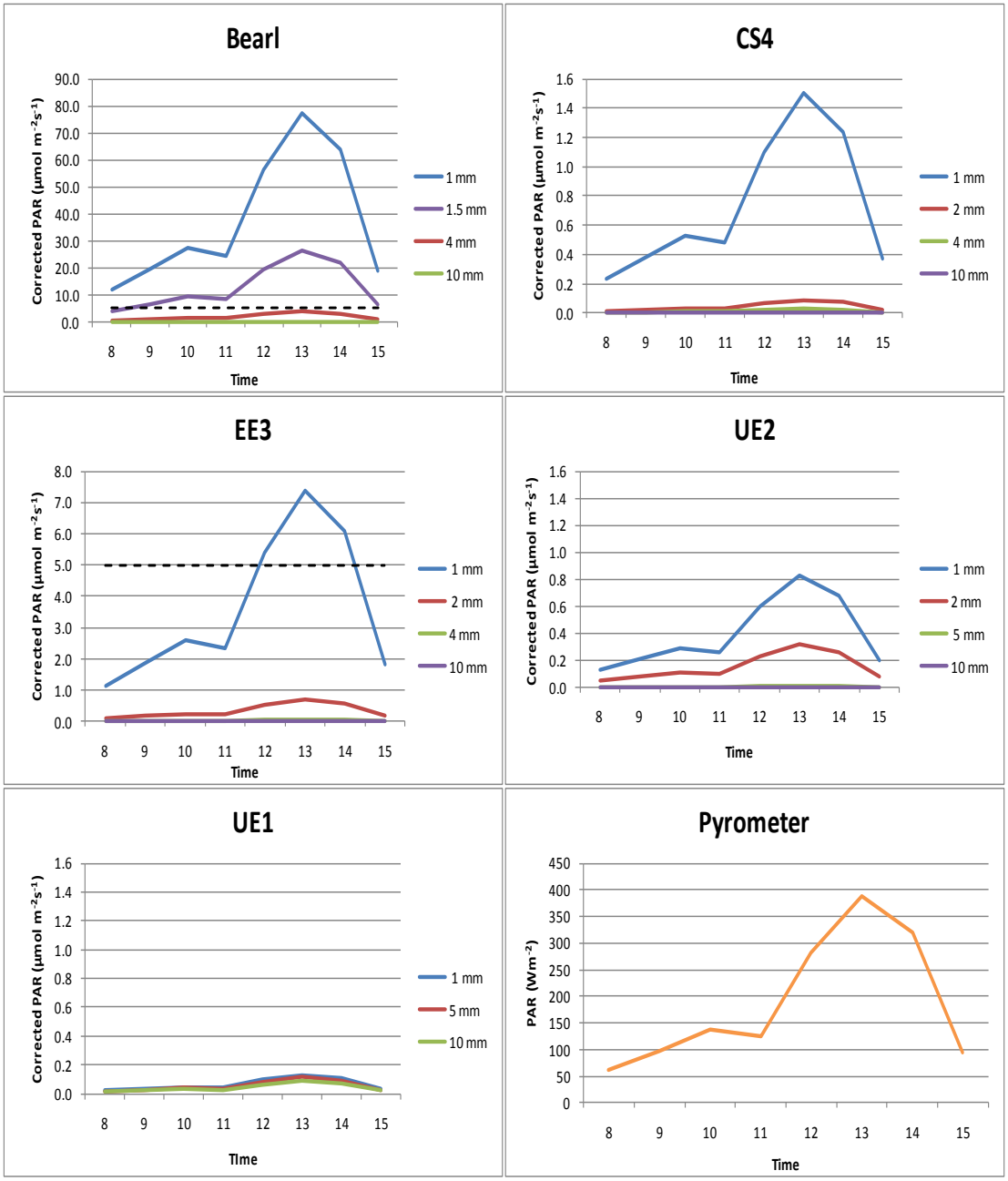

Figure 5-18: Plot of the amount of light at specific depths from the surface against time of day on the 06/06/2010, within each sample.

Data obtained on a "typical" summer's day with sunny spells. Observatory readings for the same time period are also plotted in the pyrometer graph. Note different scales on Y axis. Dashed line denotes 5 µmol m-2s-1, the cut-off for microbial activity.

These experiments were repeated for a sunny and hot summer's day, i.e. when the temperature was greater than the average Glasgow summer temperature, 15.2°C and no rain fell. To comply with these, models were produced for the 29/07/2010 as the air temperature was greater than 15.2°C between 9 am and 9 pm and reached a maximum temperature of 19.3°C, while no rain fell. Bearl shows the greatest transmission of light, with a maximum of 189 µmol $m^{-2}s^{-1}$ PAR occurring at 1 pm at 1 mm depth. PAR of > 5 µmol $m^{-2}s^{-1}$ at 1 mm occurs between the hours of 7 am and 7 pm. At a depth of 4 mm,

enough light to support photosynthetic activity penetrates between the hours of 12 and 5 pm (Figure 5-19). In the weathered crust samples, only EE3 allows sufficient light to penetrate to a depth of 1 mm in order to support photosynthesis. Here, a maximum of 18.2 µmol $m^{-2}s^{-1}$, enough light to activate photosynthetic microbes, penetrates between 9 am and 6 pm at a depth of 1 mm. Light penetration at 2 mm is half of the value at 1 mm depth, but the lower light levels nevertheless can still support photosynthesis between 10 am and 5 pm, but no deeper in EE3 (Figure 5-19). CS4's peak intensity is just below the 5 µmol $m^{-2}s^{-1}$ cut-off for sustaining photosynthetic microbes (3.7 µmol $m^{-2}s^{-1}$). Insufficient light for photosynthesis is transmitted to 1 mm depth in the UE2 and UE1 samples (Figure 5-19).

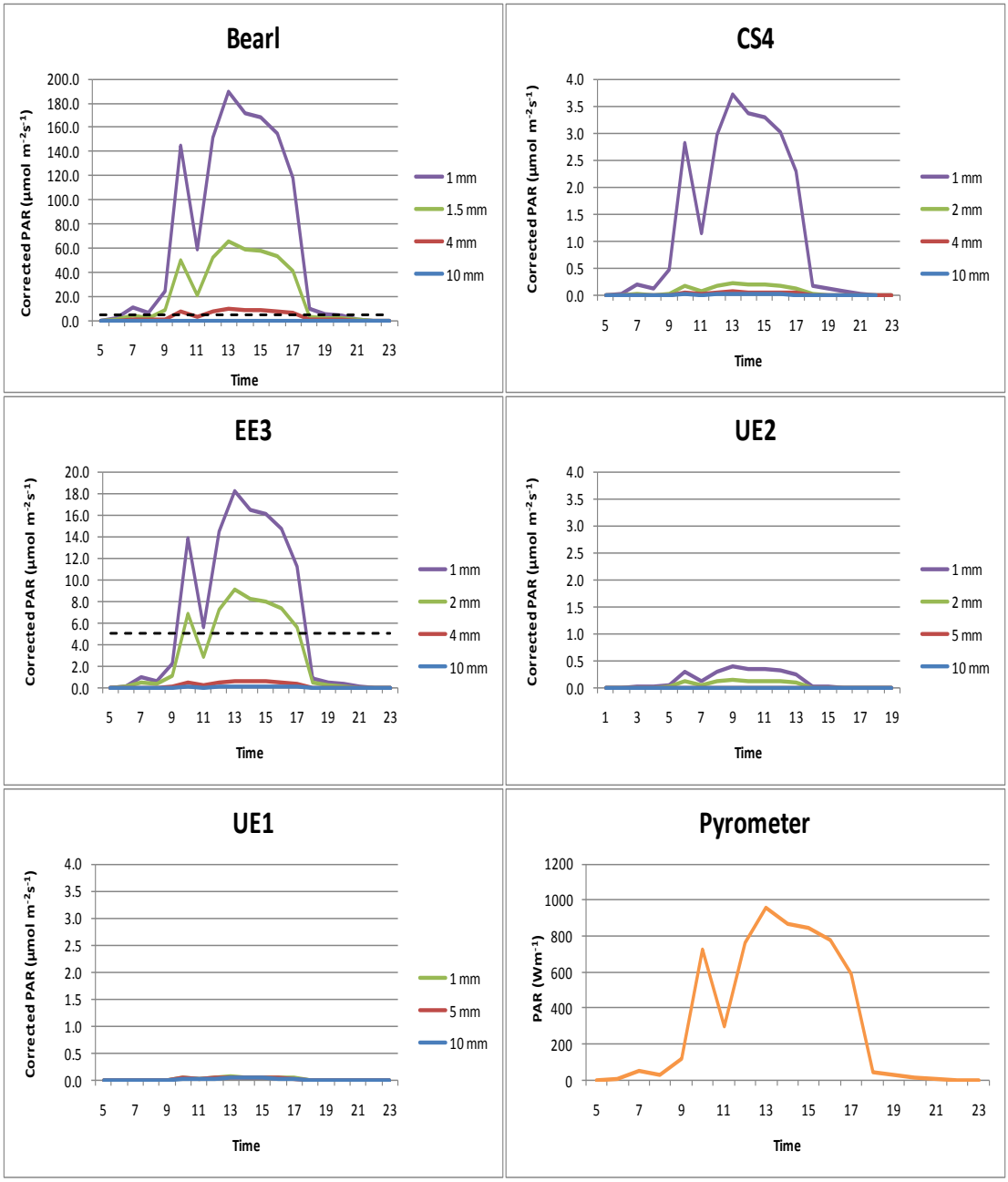

Figure 5-19: Plot of the amount of light at specific depths beneath the surface against time, within each sample, on a hot sunny day.

Data used from a hot summer's day (29/07/2010). The observatory readings for same time period (pyrometer graph) are also included. Note that different scales are used on the y-axis. Dashed line denotes 5 µmol m-2s-1, the cut-off for microbial activity.

The models were further repeated for a sunny and cold winter's day (i.e. when the temperature was below the average for winter, 5.6°C). To adhere to this, the 07/01/2010 was chosen to model the winter results, as the day was sunny with air temperatures below 0°C all day with no rainfall. The samples follow a similar pattern to the "typical" and hot summer's day data. Light can penetrate into the top 1 mm of the fresh Bearl sample, with a maximum PAR of 46.8 µmol $m^{-2}s^{-1}$ occurring at 1 pm. Light levels at 1 mm depth are above 5 µmol $m^{-2}s^{-1}$ from 11 am to 4 pm and between 12 pm and 3 pm at 1.5

mm depth (Figure 5-20). In all other samples, the amount of PAR transmitted to a depth of 1 mm is insufficient to uphold growth of photosynthetic microbes (Figure 5-20).

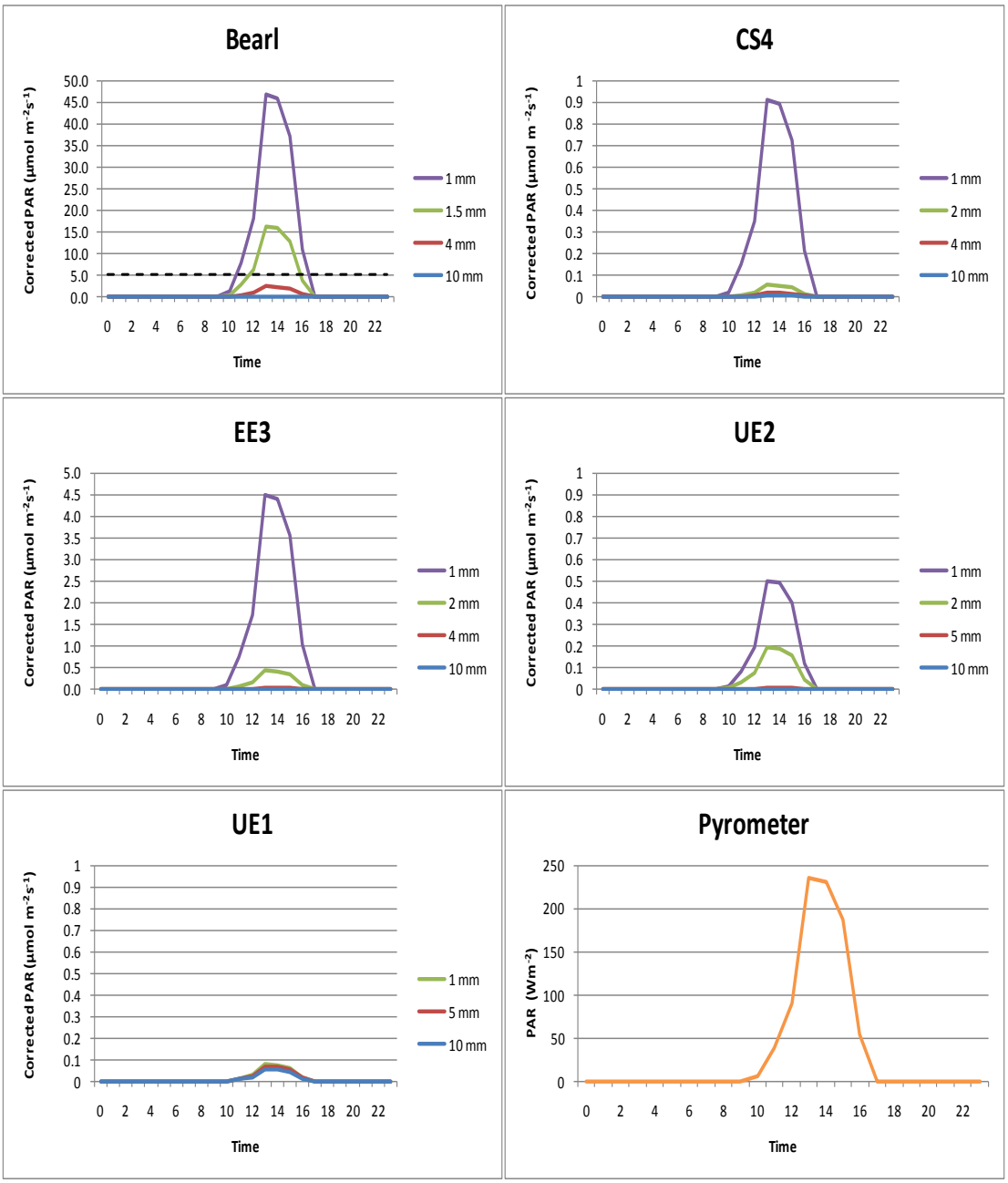

Figure 5-20: Plot of the amount of light at specific depths beneath the surface against time, within each sample, on a winter's day.

Data used from a hot summer's day (29/07/2010). The observatory readings for same time period (pyrometer graph) are also included. Note that different scales are used on the y-axis. Dashed line denotes 5 µmol m-2s-1, the cut-off for microbial activity.

To fully understand the depth to which light can travel into these rocks, at particular times of the day, graphs were constructed which display the amount of PAR against depth in the early morning (8 am) and at midday on the hot sunny summers day (Figure 5-21). A second set of graphs were then constructed to show the same information, but instead showing the cold winters day data (Figure 5-22). However, these graphs only show

midday data as sunrise in winter is later, and hence no pyrometer data was gathered for 8 am.

These results show that, at 8 am on a hot sunny day during the summer, the PAR intensity is only high enough to enable microbial activity in the Bearl sandstone and to a maximum depth of ~1.2 mm. However, by midday, over 5 µmol $m^{-2}s^{-1}$ is reaching a depth of 3 mm and may reach a depth of 4 mm within Bearl (Figure 5-21). Also at midday, enough light is penatrating to a depth of 1.7 mm within EE3. However, PAR cannot penatrate deep enough into any other sandstones for microbial growth to occur (Figure 5-21).

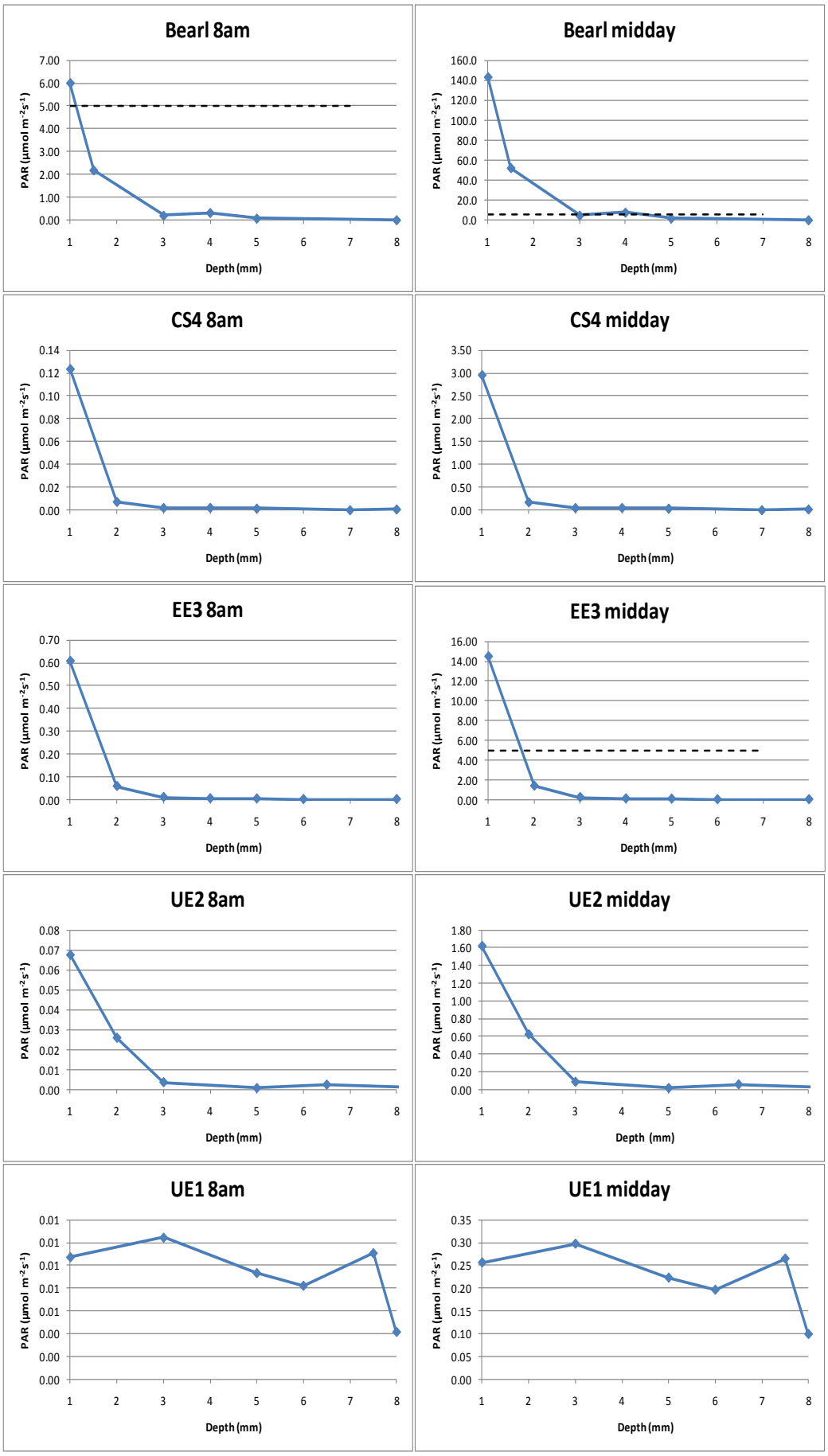

Figure 5-21: Light penetration against depth beneath the stone surface, at 8 am (31.9 PAR) and 12 (762 PAR) on a hot summer's day.

Note different scales on the y-axis. Dashed line denotes 5 µmol $m^{-2}s^{-1}$ cut-off.

The winter results show that, at noon, 16 µmol $m^{-2}s^{-1}$ of PAR is transmitted to 1 mm in Bearl. In addition 5 µmol $m^{-2}s^{-1}$ penetrates to a maximum depth of 1.7 mm within the Bearl sandstone (Figure 5-22), whereas the other sandstones transmit negligible amounts of light (Figure 5-22).

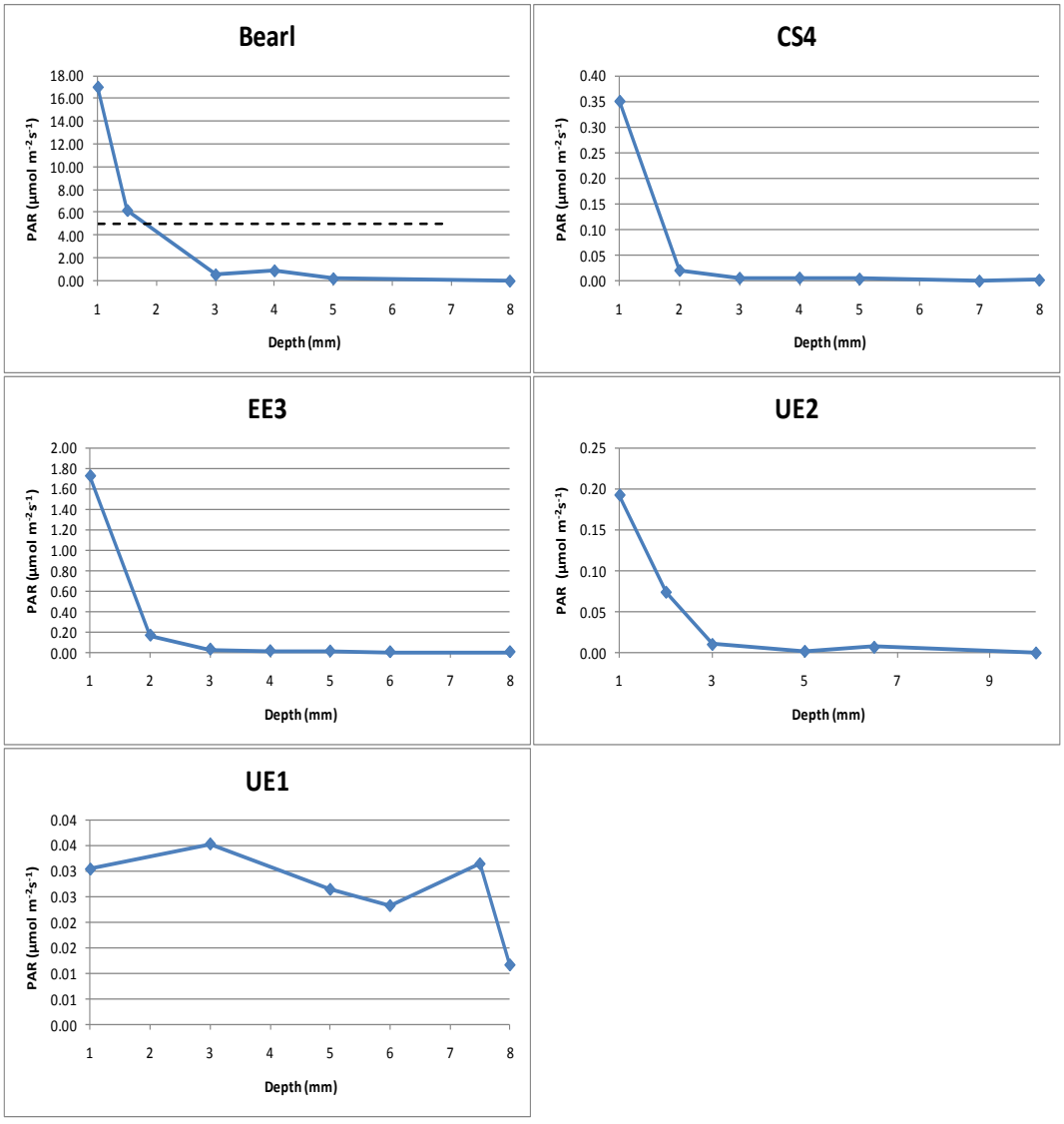

Figure 5-22: Light penetration against depth. At 12 on a cold sunny winter's day the PAR was 90.4 µmol $m^{-2}s^{-1}$.

Note the different scales on the y-axis and dashed line denotes 5 µmol $m^{-2}s^{-1}$ cut-off.

5.6.1 *Discussion of OLT Experiments*

The amount of solar radiation which initially travels into the sandstones varies widely between different stone types (Table 5-6) and seems to be dictated by the amount of weathering crust on the surface. The fresh sandstone surface allows the greatest proportion of light to be transmitted through the surface (20% at 1 mm) (Table 5-6). The

weathered surface on the samples dramatically decreases the light transmitted into the rock, with only 2% of the solar radiation reaching a depth of 1 mm in EE3, and this is even lower in CS4 and UE2 (Table 5-6). The graphs for sample UE2 (weathered crust) and UN1 (black crust) show a slight increase of light nearer the surface, although this is very slight. Furthermore, the hot day results indicate there will never be enough solar radiation (at least in Glasgow) to penetrate beneath the surface, making subsurface phototroph colonisation impossible beneath these heavily weathered crusts.

Once the light enters the sandstone, the amount that penetrates to deeper levels also varies. Bearl (unweathered) sandstone observations show that the light intensity levels drop exponentially whereas, in EE3, the trend is more linear (Figure 5-23). Therefore, by 2 mm in Bearl light has decreased by 87.5% whilst only by 50% in EE3, suggesting that the two sandstones behave differently when transmitting light to depth**.** When the total amount of nontransmissive minerals (i.e. feldspar, mica, Fe-oxide, kaolinite and ankerite) were calculated the totals within the two sandstones were very similar, (Bearl = 14.7%, EE3 = 16.7%). However, a large difference is seen in the porosity between the samples (Bearl = 14.3%, EE3 = 20.6%). This variation in porosity is, therefore, more likely to be responsible for the differences in light transmission patterns (Figure 5-23)**.**

Table 5-6: Percentage of light which travels through the sample.

	Bearl	**EE3**	**CS4**	**UE2**	**UN1**
1 mm	20	1.9	0.4	0.04	---
1.5 mm	6.9				---
2 mm		0.95	0.02	0.02	---
4 mm	1	0.07	---	---	---

Where dashed lines appear (---) it represents that less than 0.01% of light is transmitted.

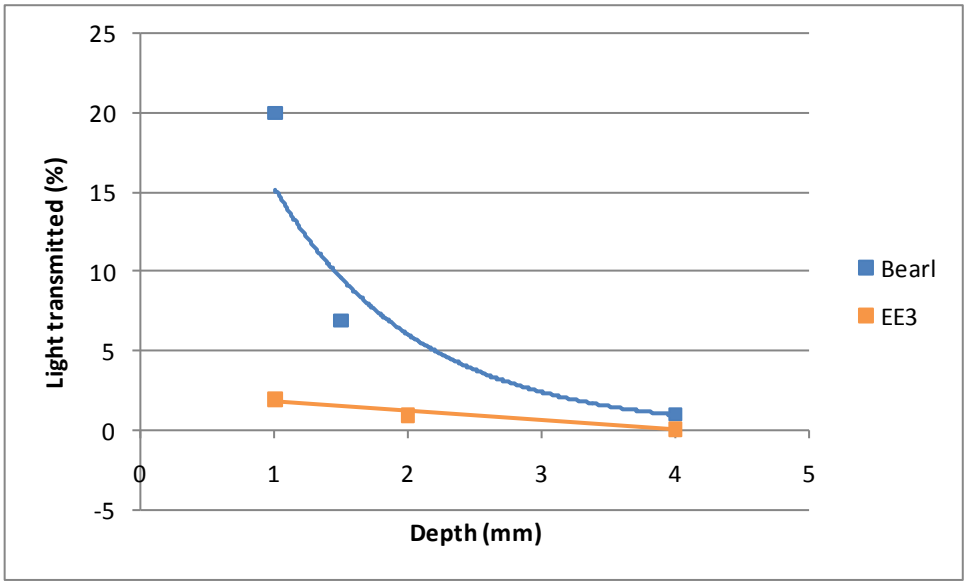

Figure 5-23: Percentage of light transmitted within sandstones.

Bearl shows an exponential decrease in the light being transmitted, whilst the decrease is more linear within EE3.

The amount of solar radiation available to penetrate the sandstone is highly dependent on the season and, therefore, annual variation in solar radiation may alter phototroph activity.

During the summer months, ambient daily PAR levels within Glasgow regularly exceed 500 µmol $m^{-2}s^{-1}$ (the threshold above which photoxidative damage occurs). In July 2010, 10% of daylight hours exceeded this level, therefore surface dwelling photosynthetic microbes may experience some photo-oxidative damage and consequently seek shelter and protection (either by gliding or growth migration) within the sandstone. The (OTL) results show that photosynthetic microbes can obtain enough light to survive to a depth of 3 mm in unweathered sandstone and to a depth of 2 mm in some circumstances where a weathering crust is present.

Also during summer, sunlight shines for a maximum of 17 hours within Glasgow, which equates to eight hours of sufficient PAR at a depth of 2 mm to activate photosynthetic microbes in some weathered crust samples. The internal length of day within a sample is increased when nearing the surface and especially in samples with a cleaner surface. The light levels within these sandstones then provide an environment in which cryptoendolithic photosynthetic communities can be sustained.

During the winter months, the amount of solar radiation is much less than that of the summer, with the 500 µmol $m^{-2}s^{-1}$ PAR threshold never being exceeded in December 2009 and January 2010. Therefore, during the winter months, microbial activity at the surface may be much more prevalent as they can gain large amounts of energy without incurring photo-oxidative damage. This is coupled with a reduction in the number of sun light hours (November only has a maximum total of 8 hours of sunlight). This means that these light levels can only support cryptoendolithic photosynthetic communities within the fresh unaltered sandstone as the intensity of light is too low to penetrate the weathered surfaces. These factors combine to ensure that sandstones with weathered surfaces cannot support cryptoendolithic microbes during the winter. Therefore as the microbes are restricted to the surface of the sandstone, this is where they will cause most damage by releasing chelting agents and acids.

However, the amount of light available may affect different species of photosynthetic microbes in different ways. *Phormidium* (possible surface filamentous cyanobacteria) has shown that it has the lowest growth efficiency under short day length situations (6:18 hours light : dark) in comparison to other species of cyanobacteria and algae such as *Nitzschia* and *Sphaerocystis* (Litchman et al., 2003). This light ratio is similar to the winter months within Glasgow, suggesting that the surface damage potential is limited if *Phormidium* is present. Thus, although this organism appears to be suited to the surface growth, its slow metabolic activity during short-day cycles means it, fortuitously, will cause less damage to the sandstone than the other cyanobacteria.

The presence of water within the sandstone can change the optical properties of the stone by enhancing the absorption of light by ~3% (Phoenix et al., 2006), although this is a minimal amount and, therefore, the use of dry wafers in this experiment should not have affected the depth estimations.

These results indicate that, regarding cryptoendolithic bacteria, most damage is likely to occur on unweathered buildings rather than those with a prominent weathering crust. As crusts form on these previously unweathered sandstones, the microbial communities will be forced nearer the surface. The general conclusion is that summer conditions will support cryptoendolithic microbes which may cause damage to the subsurface whilst, in

winter, the epilith microbes may be activated on the surface and cause harm to the outermost surface of the sandstone.

5.7 Discussion and Conclusions of Microbial Results

The depth to which microbes are seen in the osmium stained polished blocks is consistent with the light penetration results. The majority of osmium stained samples indicate that microbes were found no deeper than 2 mm. The OTL results show that in those sandstones with weathered crusts, light can only penetrate sufficiently for photosynthesis to a maximum of 2 mm.

When the Blaxter from RGU block was examined, cyanobacteria were found at a depth of 5 mm, but this was a fresh unaltered sample (when placed outside 10 years ago) and the OTL results show that light penetration is much deeper in unaltered sandstones and may explain the evidence of microbial communities at 5 mm depth. Microbes were also found in the Blaxter samples between 6-7 mm and were classified as fungi, as the light could not penetrate to that depth to sustain filamentous cyanobacteria. For this reason, the microbes found at a depth of 13 mm within D6 were also classified as fungi.

When previous investigations have been conducted on microbial colonisation of building sandstones, the research has predominantly been restricted to the surface, with little or no emphasis on cryptoendolithic communities and, even when these are mentioned, no depth of penetration is stated. However, colonies of cryptoendolithic photosynthetic cyanobacteria have been found between 3-7 mm depth within halite crusts in the Atacama Desert (Davila et al., 2008) and at 5 mm within sandstone from Ellesmere Island, Canada (Omelon et al., 2006a, 2007); both sets of results were from vertical rock exposures. Each of these studies show cyanobacteria much deeper than the majority of the Glasgow samples (i.e. < 2 mm deep). A few reasons could account for this: 1) the samples used by Davila et al. (2008) and Omelon et al. (2006a, 2007) have much simpler mineralogy, compared to the Glasgow sandstones, which are only ~70% quartz, with significant proportions of other detrital and diagenetic minerals hindering the transmission of light. 2) The grains within the sandstones and crusts may have been larger, reducing the impact of light scattering and increasing the depth of light penetration (De et al., 1992). 3) The Glasgow sandstones have been exposed to an

environment that is much “dirtier”, with atmospheric pollution from heavy industry in the past and vehicle derived pollutants at present, affecting the surface of the sandstone and adding the formation of dark crusts. The halite and sandstones of the Atacama Desert and Ellesmere Island are in areas of minimal population and hence minimal atmospheric pollution, reducing the formation of surface crust and, as the OTL experiments show, dark crusts reduce light penetration, and therefore limit the depth cyanobacteria can occur at.

In the RGU Blaxter block, which shows deeper cyanobacteria communities, in comparison to the RGU3 and RGU6 samples which also contain subsurface microbes, the one major difference to all other samples examined is that its surface was horizontal rather than vertical. This surface will therefore receive a larger proportion of solar radiation striking it compared to the vertical faces and hence a larger quantity of light can be transmitted inwards, increasing the depth of potential inhabitation. Pyronometer readings taken at the University of Glasgow’s weather station (on the 30/06/2010 and 20/07/2010) show that, in general, the vertical surfaces receive 30% less PAR compared to the horizontal surfaces. This difference can reach a maximum of 50% (in the early morning 7 and 8 am) and as little as 8% at midday.

On vertical faces, the microbial growth within Glasgow samples is restricted to very shallow depths (<2 mm) and this is seen in both the young sandstones (RGU which is 12 years old) and old sandstones (Dalry which is 150 years old). The placement of these communities is restricted by a complex series of factors including:

1) The fine-grained nature of the sandstone increases light attenuation (De et al., 1992; Schlesinger et al., 2003).

2) The high abundance of nontransmissive mineral grains i.e. muscovite and clays which, reduce the penetration of light (Hall et al., 2008).

3) The crust formation on the surface of the sandstone also hinders the penetration input of solar radiation, as shown in the OLT data results.

In ideal circumstances, where large (25 mm thick) single quartz crystals are present in high solar radiation conditions (2200 µmol $m^{-2}s^{-1}$), approximately 2 µmol $m^{-2}s^{-1}$ of solar radiation can penetrate through these quartz pebbles (Schlesinger et al., 2003). As can be

seen, many of the characteristic of the Glasgow sandstones are impeding the penetration of light and therefore the growth of cryptoendolithic communities. However, the macro climatic features such as the amount of solar radiation in the area will ultimately determine the depth of cyanobacteria penetration.

These conclusions, when understood together indicate that only small proportions of microbes live on and within the Glasgow sandstones and at very shallow depths (only 2 mm). Therefore microbial communities may have, in the past, caused more weathering to the sandstones when crust formations were thinner. Their destructive properties are most likely to affect a building in its early years whilst the surface is fresh and light can easily penetrate, causing larger communities to occupy the pore space. As the building ages, and a weathered crust has formed (due the combination of microbes, pollution and salt) the microorganisms become restricted until no light can penetrate to sustain the cryptoendolithic cyanobacteria communities, and they will eventually die out. Then the microbes are restricted to being surface-dwelling and, in the summer, they will be harmed by photo-oxidative damage. Therefore, they are only active in the winter and cause most damage during this period, as the surface is more hospitable for microbes. However, the black crust of Glasgow buildings may be harmful to microbes as suggested by Bluck and Porter (1991b) and, therefore, the few microorganisms that do survive only cause minimal damage in comparison to other processes affecting the sandstone. Moreover, reduced growth of phototrophs on the black crust may diminish the supply of organic matter (dead phototrophs) to fungi and bacteria deeper in the sandstone, which also reduces deeper internal weathering.

Although the microbial weathering cycle is expected to be different for each facade, the likelihood is that the north, east and west facing facades receive conditions much more similar to those during the winter all year and this means that few cryptoendolithic microbial communities are able to survive due to receiving much less solar radiation.

Turning clockwise from the west to east only one sample out of 13 has internal microbes associated with it. However, five of these have surface dwelling microbes (Figure 5-24). Whilst continuing around from southeast to southwest only two of the 12 samples show surface microbes (Figure 5-24), whereas five of these have internal microbes. The

placement of the microbes may be because the conditions are generally too harsh on the surface for microbes to survive.

As the dynamics of the building's mineralogy, crust and environmental conditions changes over time, due to weathering, crust formation and a change in environment, the species of microbe present, their location and the resultant damage caused will continually change and adapt on a seasonal and annual scale. These are discussed further in chapter 7**.**

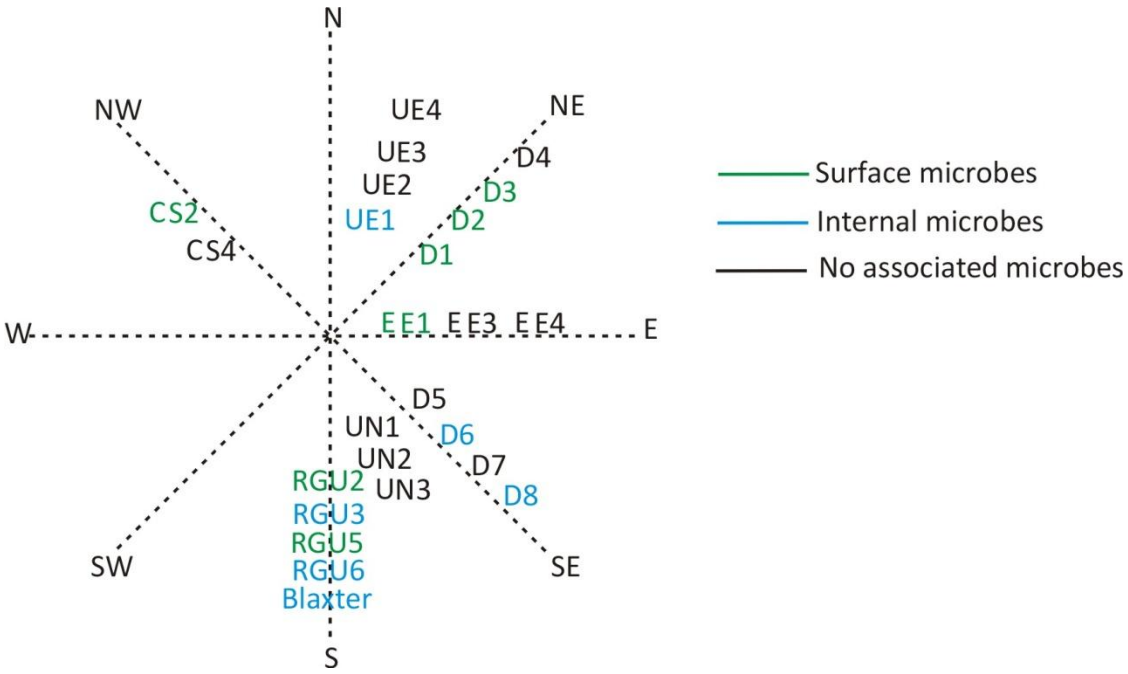

Figure 5-24: Schematic representation of the microbe's position with relevance to facade orientation.

6 Internal Monitoring and Accelerated Weathering Results

Atmospheric pollution, together with the regional climate, has dictated how historic buildings and monuments have decayed during the last 150 years. Equally, the future climate and air quality will remain the driving factor behind stone decay. As the amount of air pollution has decreased due to the clean air act (1956) and the reduction of heavy industry in Glasgow, pollution has and will continue to become less of a factor. However, future climate change predictions suggest ambient conditions will be quite different from the past and present, as discussed in the next section. Furthermore, the response to this in sandstone weathering is unknown and therefore, these questions are posed:

- What will the future climate in Glasgow be in 2080?
- What is the relationship involving the air temperature/RH between the stone's surface and interior conditions?
- What is the impact of changing climate on stone surfaces?
- What is the link between RH and free liquid water within the sandstone?
- What are the implications of changing climate for both the inorganic and organic weathering processes?

To answer these questions, sandstones were subjected to accelerated weathering within an environmental chamber. This was complimented by a variety of datalogging experiments, which were conducted to determine the internal microclimate of sandstone at the present-day, allowing results to be extrapolated to model future scenarios. Therefore, the first step was to determine the future climate conditions.

6.1 Climate Change

Using the method outlined in section 2.1.7.1 the following results for the 2080 climate for Glasgow were produced: The UKCIP02 report states that the temperature over the United Kingdom is expected to rise during both summer and winter. The model for temperature rise in the Glasgow area is shown in Figure 6-1, constructed using the present day values combined with the prediction.

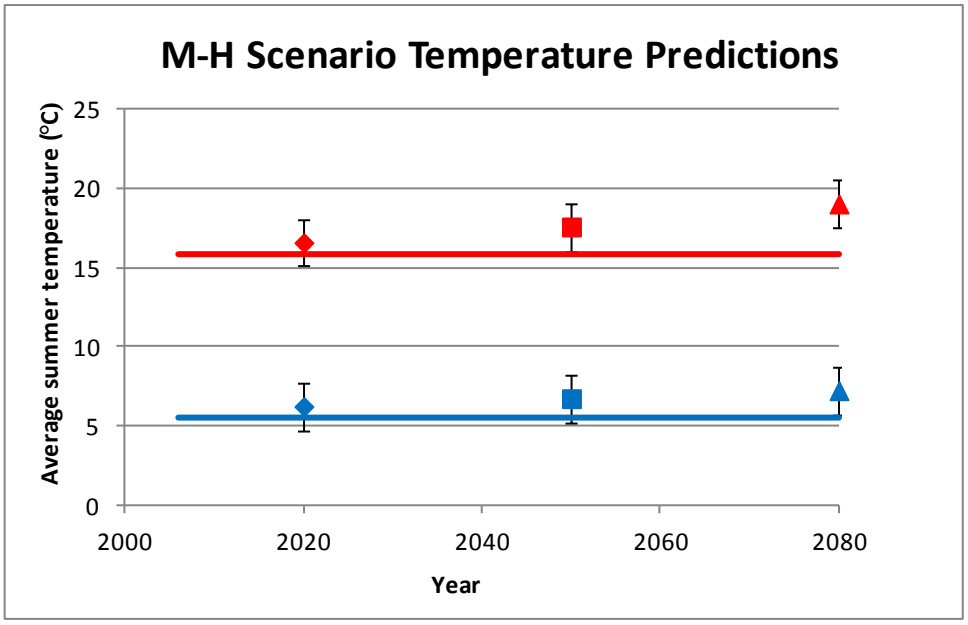

Figure 6-1: Climate change temperature predictions for the Glasgow region in winter and summer.

Blue data) winter, blue line indicates 2004-2008 winter average temperature, Red data) summer, the red line indicates 2004-2008 summer average temperature. Error bars are ±1.5°C as stated in UKCIP02, (Hulme et al., 2002).

Summer temperatures for Glasgow are expected to have risen by 3.25°C ±1.5°C by 2080, whereas the winter temperatures are only expected to rise by 1.75°C ±1.5°C.

The total annual precipitation from 2009 to 2080 is expected to change within “natural variation”, although there will be a modification to the distribution of rainfall throughout the year. Natural variation is defined within Hulme et al. (2002) as one standard deviation of 30 year average climates, estimated from the control models simulations of the HadRM3. In summer, rainfall may decrease by as much as 40% ± 30% over the Glasgow region whereas, in winter by 2080, it may have increased by 20% ± 15% (Figure 6-2).

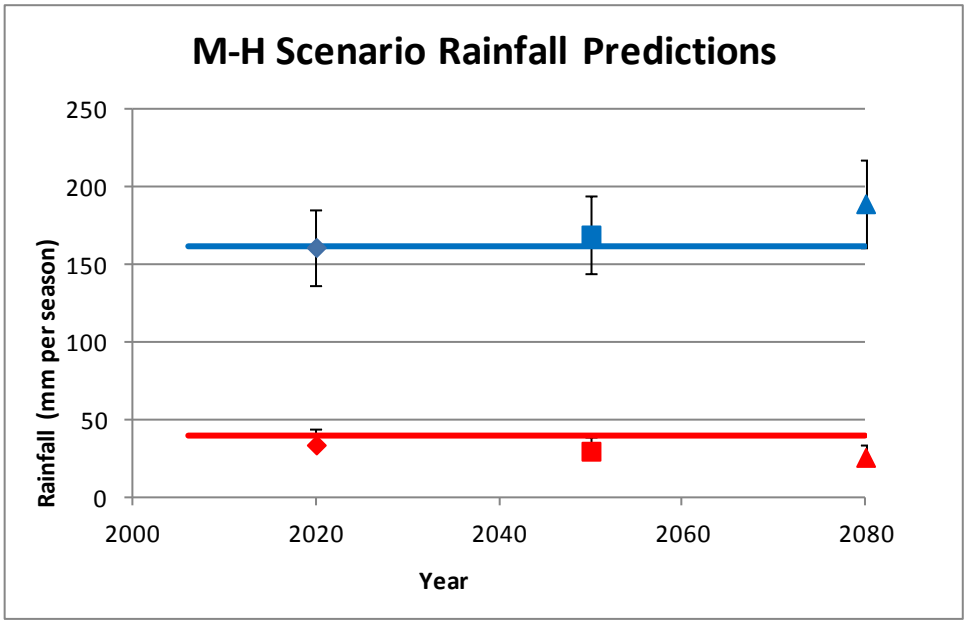

Figure 6-2: Rainfall climate change predictions for Glasgow in winter and summer.

Blue data) winter, blue line indicates 2004-2008 winter average rainfall, Red data) summer, the red line indicates 2004-2008 summer average rainfall. Winter error bars = ±15%, summer error bars = +30% from UKCIP02, (Hulme et al., 2002).

Relative humidity is expected to decrease in both the summer and winter months (Figure 6-3). The decrease in RH throughout winter may still occur despite the predicted increase in rainfall, as the rain is expected to fall in more heavy rainfall events with "dry" (low humidity) periods in between these events.

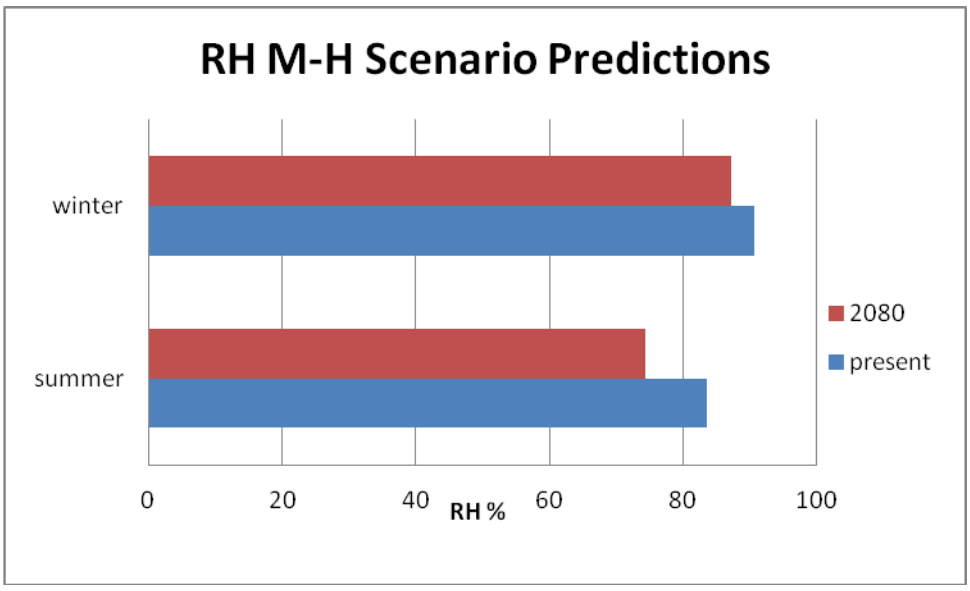

Figure 6-3: RH values comparing 2008 figures to predictions for 2080.

The annual average wind speed is predicted to change, mainly within natural variability by 2080, although wind speed may decrease slightly (-3%) during the summer months in particular. There is no indication in the UKCIP02 report as to whether the prevailing wind

direction will change. Further studies on wind direction and speed were then undertaken by the "Built Environment: Weather Scenarios for Investigation of Impacts and Extremes" report (Hanson and Goodess, 2004), whose results are in agreement with UKCIP02. Hanson and Goodess (2004) indicate that major changes in direction or speed are unlikely and the authors state that, if changes in wind speed do occur, these may only be in the order of ± 0.1ms^{-1}.

Other predictions which, may impact upon sandstone decay includes a decrease in the annual cloud cover (by 3% by 2080) where a greater proportion of this will occur during the summer months and, in addition, the number of depression lows or "storm events" will increase. At present, an average of five depression lows occur during the winter months and, by 2080, this is expected to increase to an average of eight events during winter over the Glasgow region.

All the climate change components outlined so far will have an effect on the decay of sandstone buildings and monuments, although some more so than others. Below are a set of predictions that encapsulate the three most relevant sets of changes.

Winter months with an increase in temperature coupled with higher rainfall:

- May encourage faster chemical reactions thereby increasing the amount of dissolution of relatively soluble carbonate minerals (Smith et al., 2008a).

- Higher winter temperatures will also reduce the number of days where temperature is below 0°C, limiting both the impact on of freeze thaw on stone and also the need for de-icing salts, which can become absorbed into the sandstone and cause mechanical weathering (Hyslop et al., 2006).

- Improved environmental conditions for microbes leading to larger communities within the sandstone, which has already been observed in Northern Ireland (Smith et al., 2008a). These microbes can then produce a greater quantity of organic acids, which will weaken minerals further. Greater densities of microbial communities may then infill more pore spaces, disrupting the natural flow of water through the rock.

Summer months with an increase in temperature coupled with dry periods and heavy rainfall events, may lead to:

- Increased mechanical destruction to the sandstone through microbial shrinking and swelling. It has been shown that cyanobacteria on the surface of stone can expand by 300% when wet (Wakefield et al., 1996) and this process is likely to happen internally.

- Faster rates of chemical decay (Smith et al., 2008a).

- Increased heavy rainfall events may also lead to periodical flushing out of the microbial communities. However, microbes may also play an important bioprotective role, shielding the stone from other decay processes or by holding the sandstone together using a "wire mesh" system of fungi.

Other predicted changes in the climate which have to be considered are the high magnitude events, which may lead to:

- An increased frequency of "storm events", which may promote more frequent bursts of sandstone surface detachment. This is because decay happens as episodic bursts of sandstone detachment rather than continuous detachment (Smith et al., 2008a).

- Other climate elements will also play a part in the decay process but to a much lesser extent. If a change in wind direction occurs, sandstone which was once sheltered will now be exposed to wind blasting, potentially causing an increased decay on a face of the building which had not previously been exposed to the full force of the wind.

6.2 Quantifying the Impact of Future Climate on Stone Surfaces

To examine how sandstone may respond to these predictions, in regards to temperature, RH, and how the current microbial communities may cope, a variety of stones commonly used as replacements in Glasgow buildings were placed within an environmental chamber at the Historic Scotland conservation laboratory, as described in section 2.1.7. Three sets of blocks were placed within the chamber, these being the inoculated, water only and

chamber set. The environmental chamber was set up to simulate 20 years of the predicted 2080 climate conditions. The chamber experienced technical difficulties (full details in section 2.1.7) but the climate conditions that the blocks did endure throughout the full period of the experiments were logged by an IButton (Figure 6-4). The intended programmed climate condition can be seen in section 2.1.7. Before starting the experiments, the blocks were scanned using a Konica Minolta Vivid 9i laser scanner, giving a sub-millimetre accurate model of the stone surface and rescanned when finally removed. Both times the scanning was conducted under the same conditions and at the same resolution. Visually, the majority of blocks appeared unchanged in colour and roughness after the experiments, with the exception of some of the inoculated blocks. However, laser scanning reveals the majority of blocks have undergone various amounts of mass loss and gain to the surface, as shown by compiling the laser scan data into shell to shell deviation images. The shell to shell deviation (SSD) maps were prepared on "Rapidform 2006" software by Colin Muir from Historic Scotland. These are colour-coded pictures to compare the ‘before’ and ‘after’ images, which were then used to calculate the difference in surface height. On the SSD images, dark blue equates to no change, then ranges through light blue, green, yellow, and finally red indicating the largest changes. However the SSD maps do not differentiate whether this is a gain or loss in height change, and are therefore used in conjunction with the initial and final laser scanning images to provide 2D profiles of the vertical surface of the block that was studied.

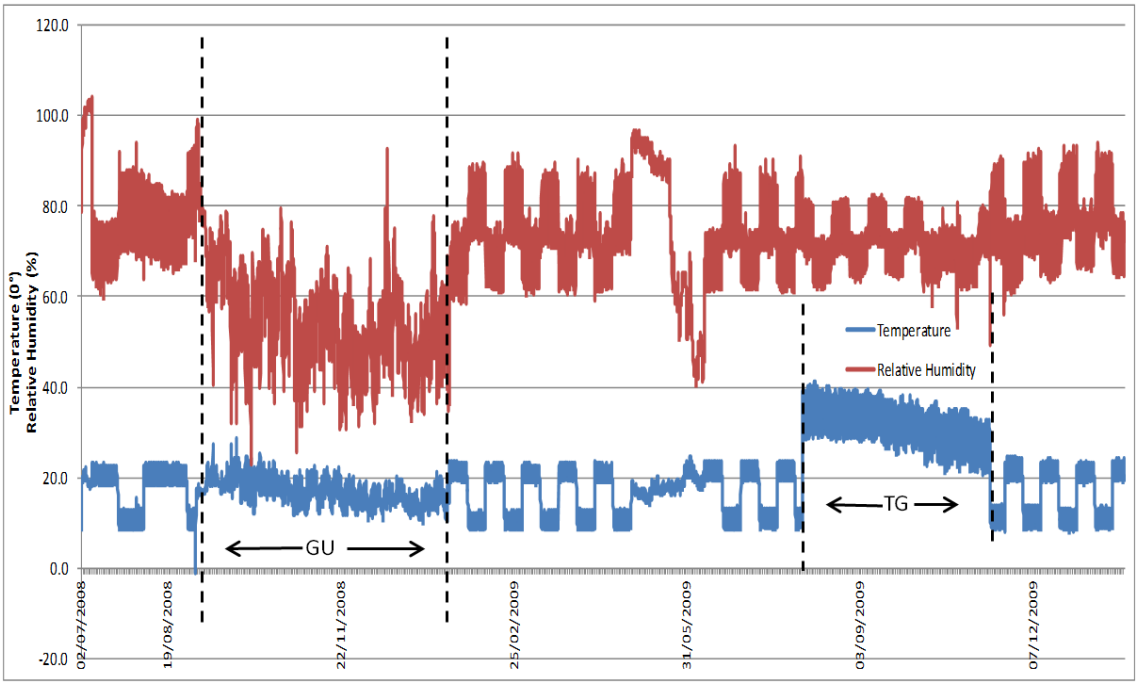

Figure 6-4: Temperature and RH conditions experienced by the test blocks throughout the running time of the experiment.

Measurements were logged by an IButton datalogger. GU = time in the University of Glasgow, TG = temperature gauge broke.

6.2.1 ***Bearl***

Bearl is the coarsest grained sandstone used in this experiment. When these samples were taken out of the chamber, their rough surface texture visually appeared to have been accentuated for both the inoculated and water only blocks. The SSD images show that the average change on the surface of the inoculated blocks is 0.055 mm, the water only block is 0.050 mm, whilst the control block has an average change of 0.038 mm. The maximum change for each block, in the same order, is 0.276 mm, 0.250 mm and 0.183 mm (Figure 6-5,Figure 6-6, and Figure 6-7 and all data is in Table 6-1). The inoculated and water only set show similar amounts of change occurring at the centre of the block, whilst the change occurring on the chamber block was focused around the edge of the face. The scanned images indicate that the changes on these surfaces are predominantly due to surface loss (Figure 6-5Figure 6-6 andFigure 6-7).

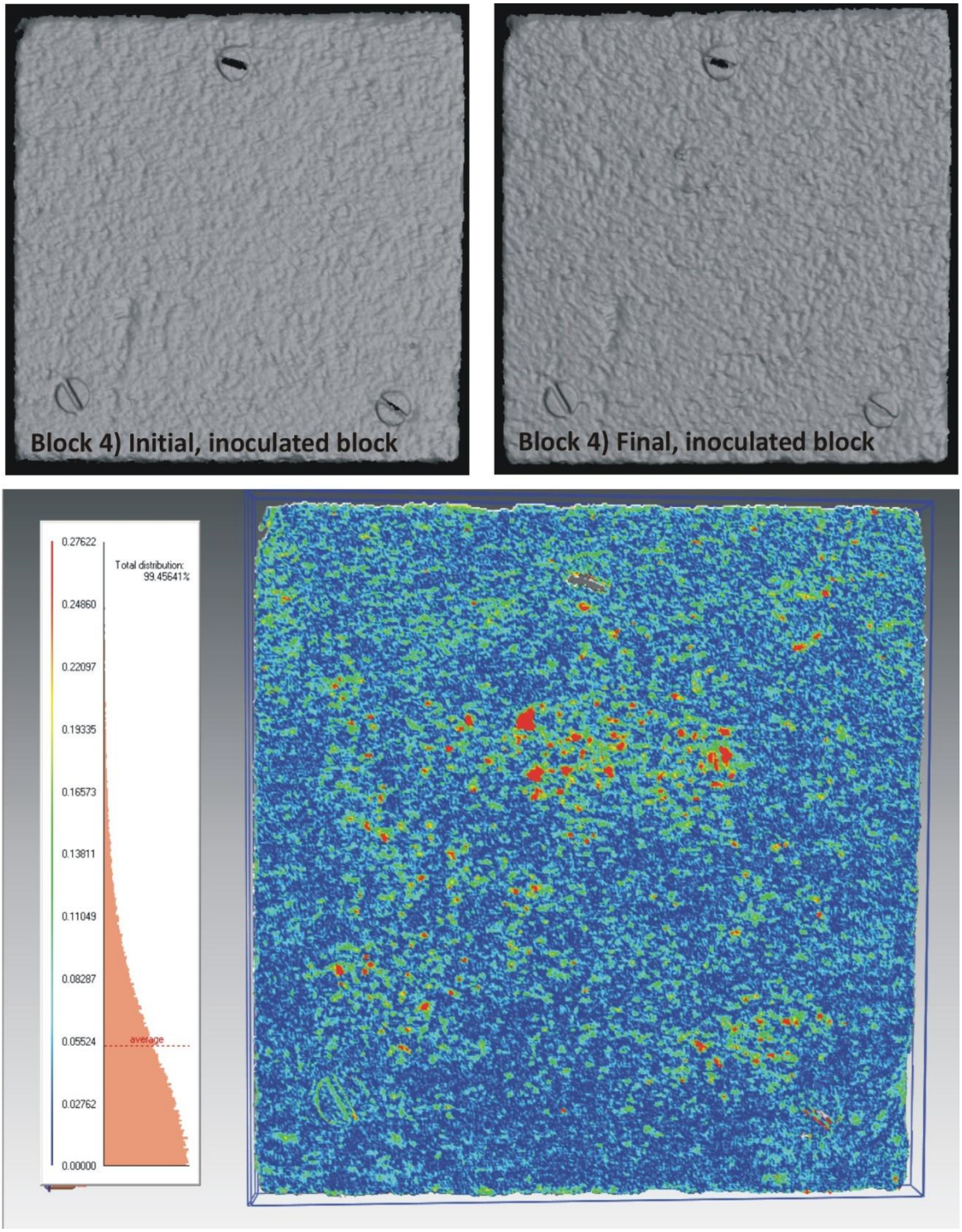

Figure 6-5: Bearl inoculation block, initial and final scan images and coloured SSD image.

Colour scale at the side runs from blue indicating smallest, red indicating largest change. The peach area to the right of the scale represents the amount of area on the surface which has changed by that amount. Significant amount of granular disintegration have occurred over the surface with a large amount taking place in the central region of the face.

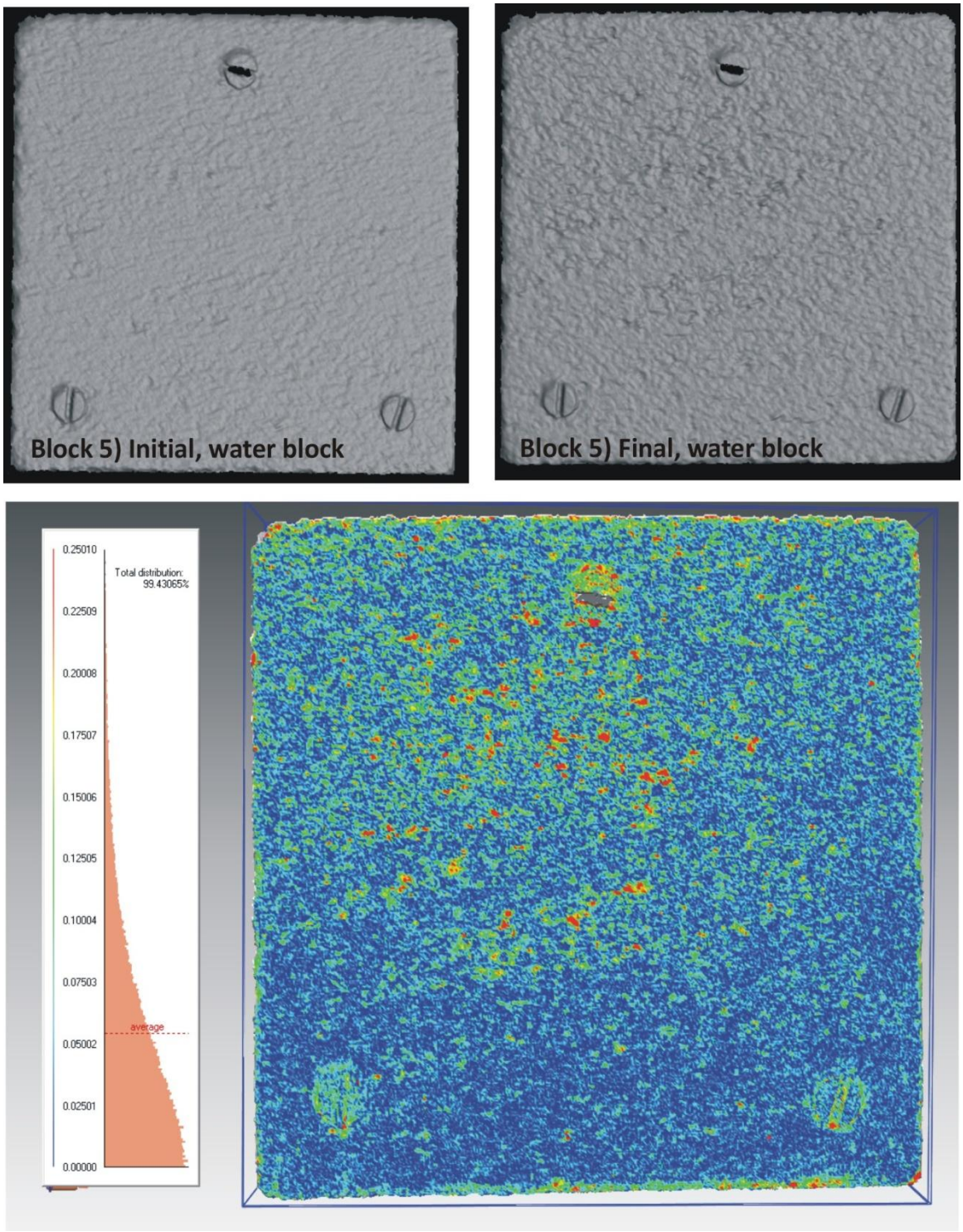

Figure 6-6: Bearl water block, initial and final scan images and coloured SSD image.

For key see Figure 6-5. Granular disintegration has occurred on the surface of the block, with most occurring in the central upper area of the face.

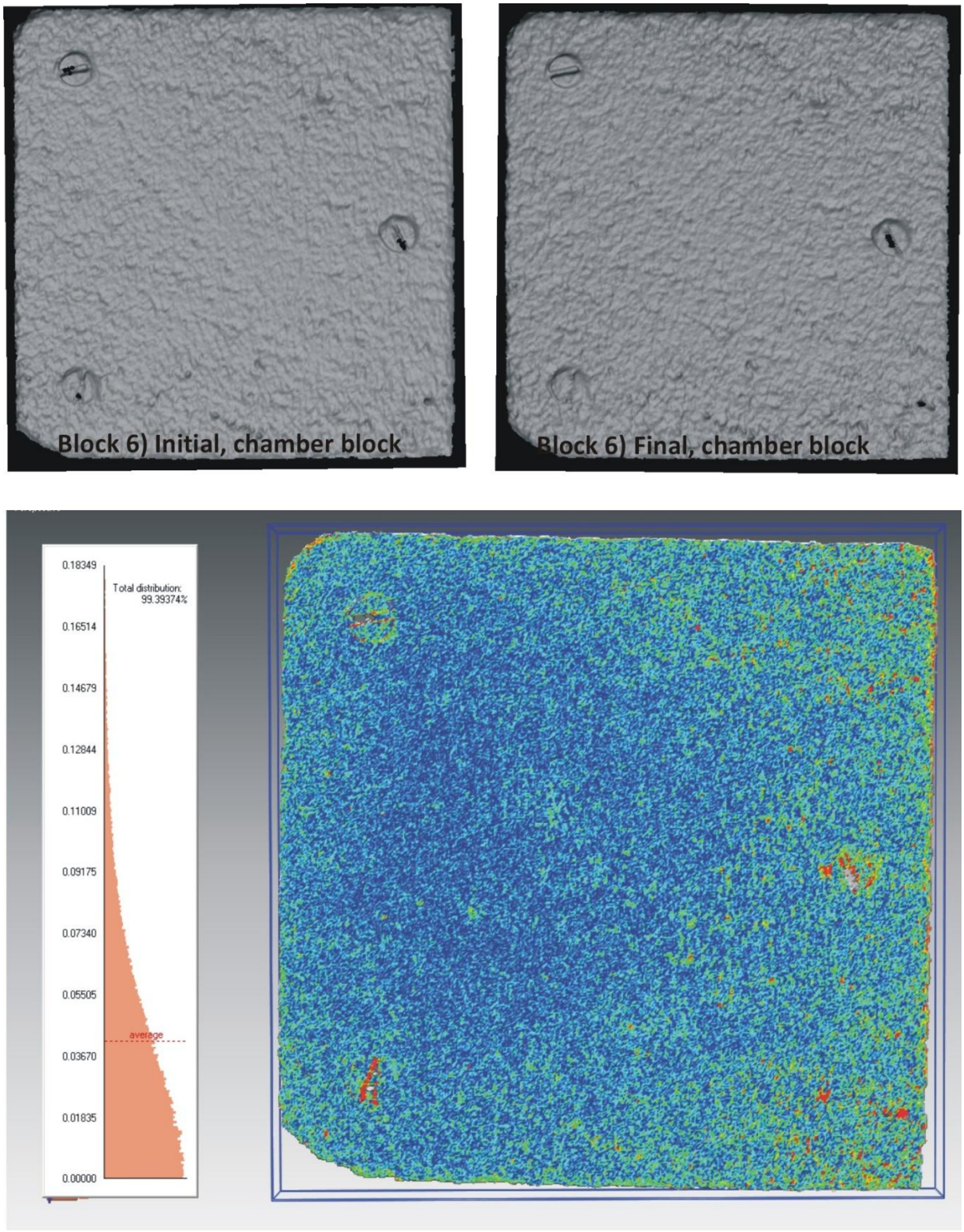

Figure 6-7: Bearl chamber block, initial and final scan images and coloured SSD image.

For key see Figure 6-5. Only small amount of evenly distributed granular disintegration are seen on the sandstone.

6.2.2 ***Blaxter***

The Blaxter blocks visually had a smooth cut surface. The inoculated block surface changed by an average of 0.040 mm, the water only block by an average of 0.038 mm, whilst the chamber block changed by an average of 0.031 mm. The maximum topographic change seen on the inoculated set was 0.325 mm, water only was 0.175 whilst the chamber block maximum change was 0.150 mm (images in Figure 6-8,Figure 6-9, Figure 6-10 and data in Table 6-1).

A large range of measurements are recorded on the inoculated Blaxter block, although the colour scale remains the same. This skews the colour scale in comparison to the other blocks and makes the SSD images predominantly dark blue, which would suggest small amounts of change but due to the skewed scale, it actually records the largest average change (Figure 6-8). The water only block has also experienced significant change (Figure 6-9) whilst the change to the chamber blocks is minimal (Figure 6-10). The modification to the surface of the inoculated block was patchy, whereas it is more evenly distributed over the surface of the water block. All blocks show signs of mass loss as the original smooth surface of the sandstone has become visually rougher. The inoculated block, however, also shows signs of significant mass gain occurring around the inserted screws and in small patches (<1 mm in diameter). The possible mass gain on this block is either a product of microbial colonisation or an accumulation of inorganic debris and will be discussed later.

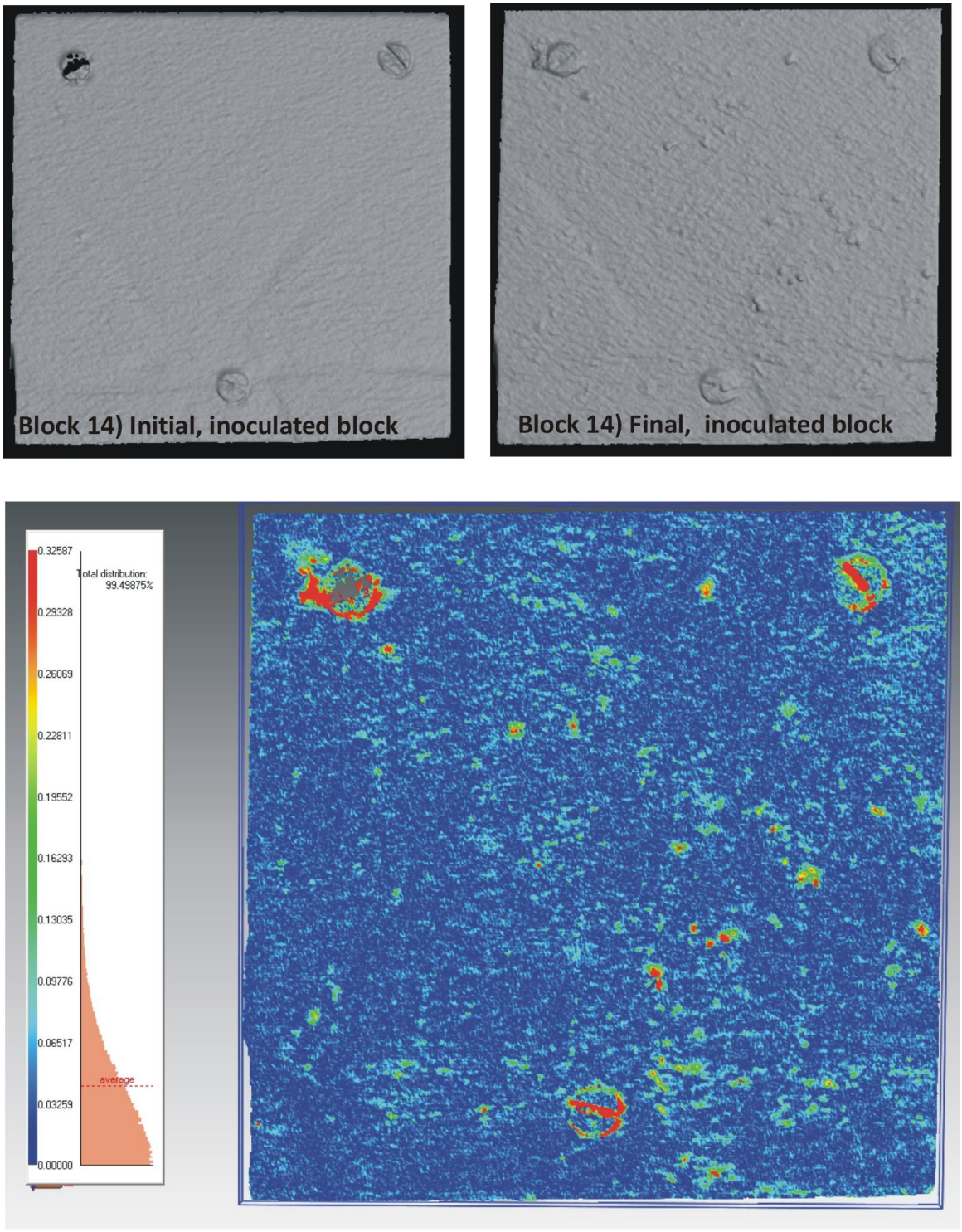

Figure 6-8: Blaxter inoculated block, initial and final scan images and coloured SSD image.

For key see Figure 6-5. The inoculated block shows loss over the surface of the sandstone whilst small patches (<1 mm) of gain occur predominantly on the left-hand of the surface.

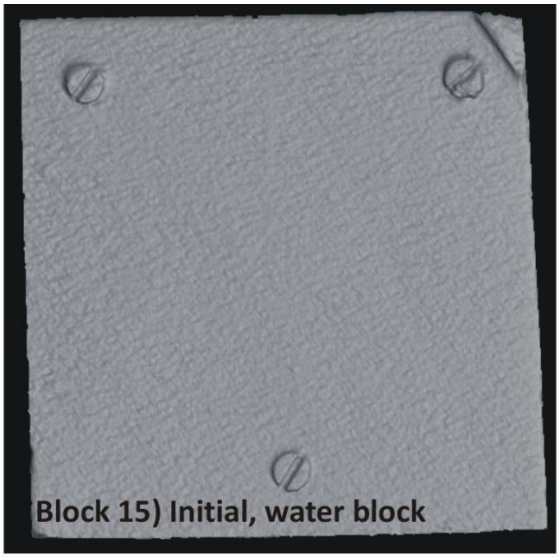

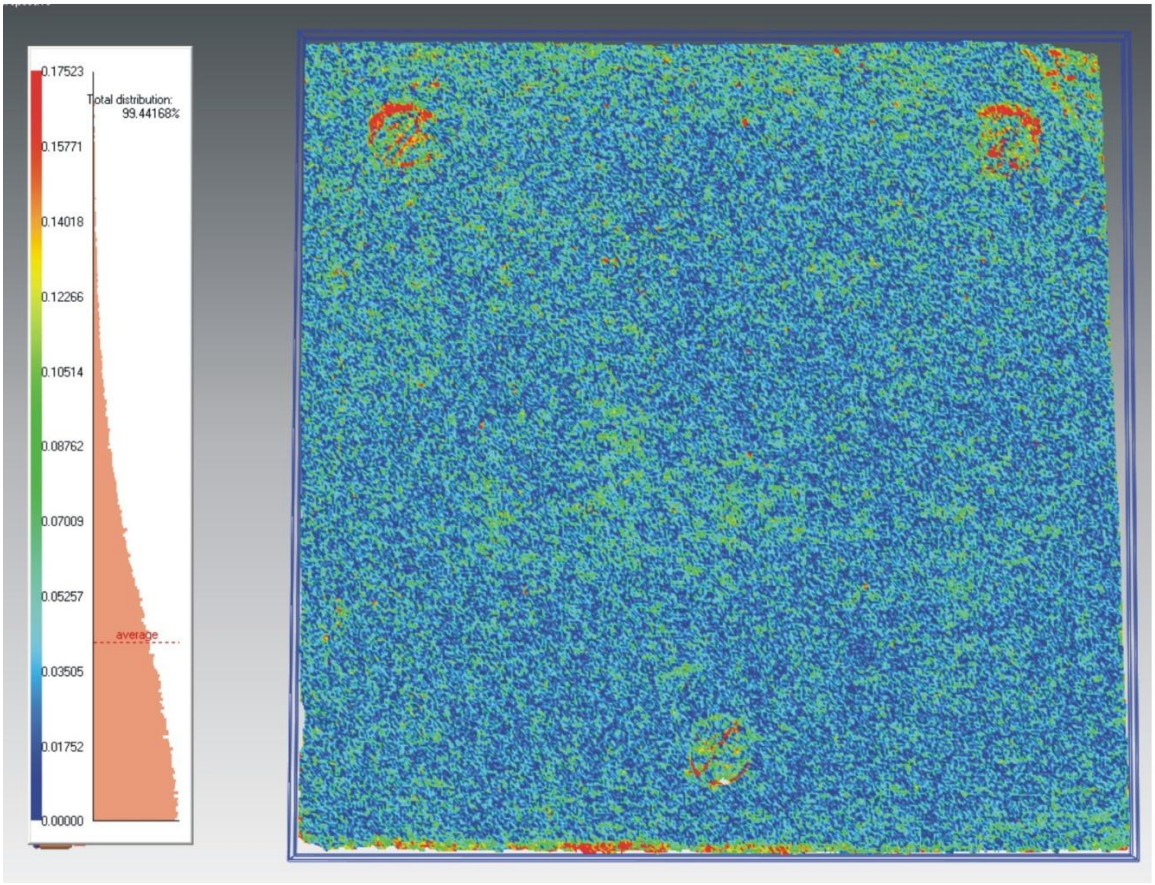

Figure 6-9: Blaxter water only, initial and final scan images and coloured SSD image.

For key see Figure 6-5. Granular disintegration has occurred evenly over the whole surface of the block.

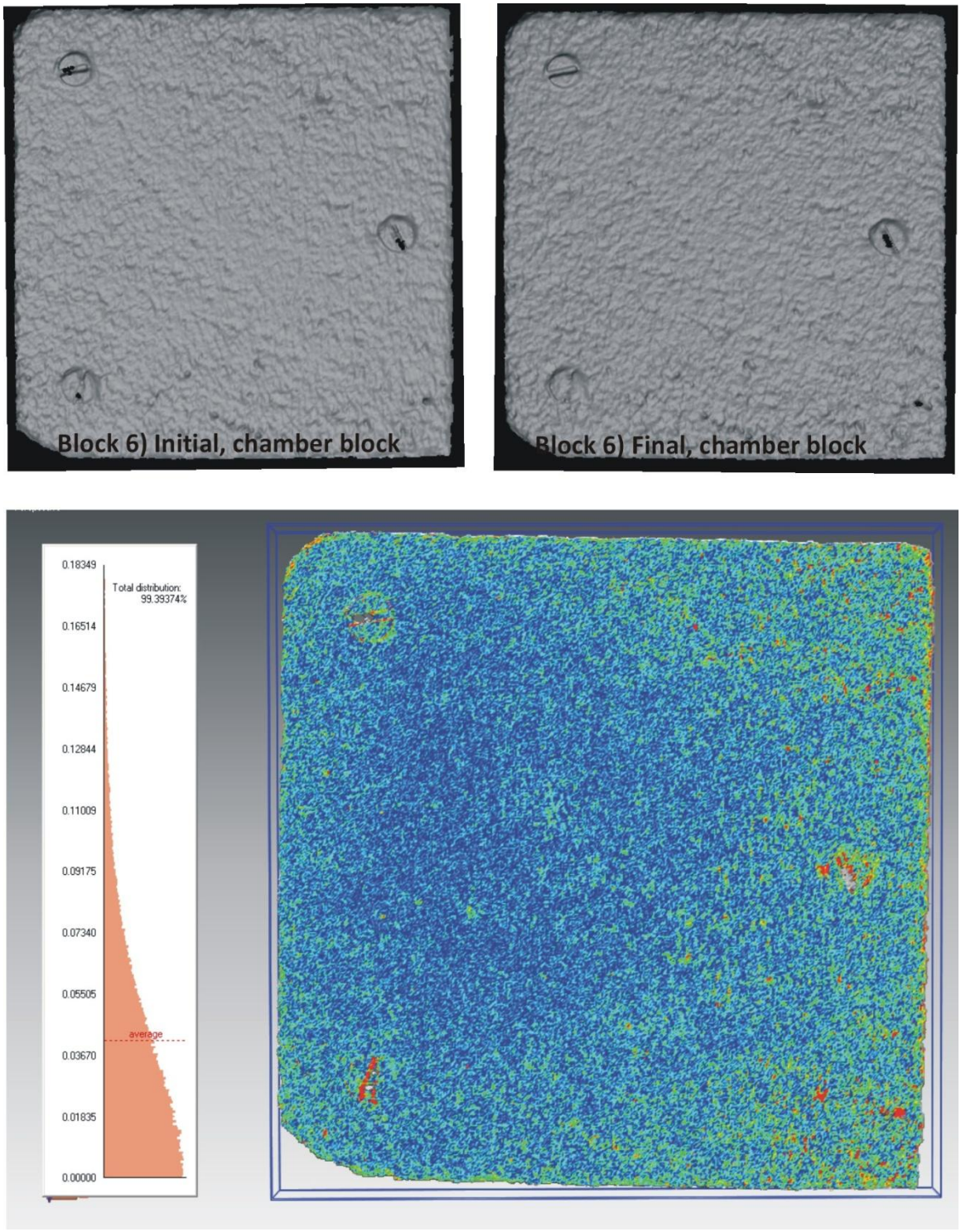

Figure 6-10: Blaxter chamber only, initial and final scan images and coloured SSD images. For key see Figure 6-5. Granular disintegration occurred over the whole surface of the block.

6.2.3 *Clashach*

The SSD data shows that the inoculated block have an average topographical change of 0.039 mm over the surface, and a maximum change of 0.328 mm. The water block has an average change of 0.030 mm and a maximum of 0.163 mm, whilst the control block

has an average change on the surface of 0.024 mm and a maximum change of 0.121 mm (Figure 6-11, Figure 6-12,Figure 6-13 and all data in Table 6-1).

The data range from the inoculated bock results is larger than those from the water and chamber blocks, although they have the same colour chart to represent the data. Therefore, care must be taken when drawing comparisons between areas of similar colours on the different blocks. As a consequence, although the inoculated SSD image looks dark blue which implies that little change has occurred, it has experienced similar amounts of average loss as the water block (Table 6-1). The inoculated block shows evidence of both surface gain and loss. In the top left-hand corner of the final laser image, there is a heightened region which agrees with the SSD image, whilst an originally indented area in the lower left-hand side of the block has been enlarged (Figure 6-11). The water block only shows evidence of loss on the cut surface with enhancement to the rough texture and a depression has also formed in the bottom right hand corner (Figure 6-12). The laser images indicate that original surface features (saw markings) on the chamber block may have been accentuated by the loss of surface material, although the SSD images do not show this to be true (Figure 6-13) and suggest only minimal loss to the surface.

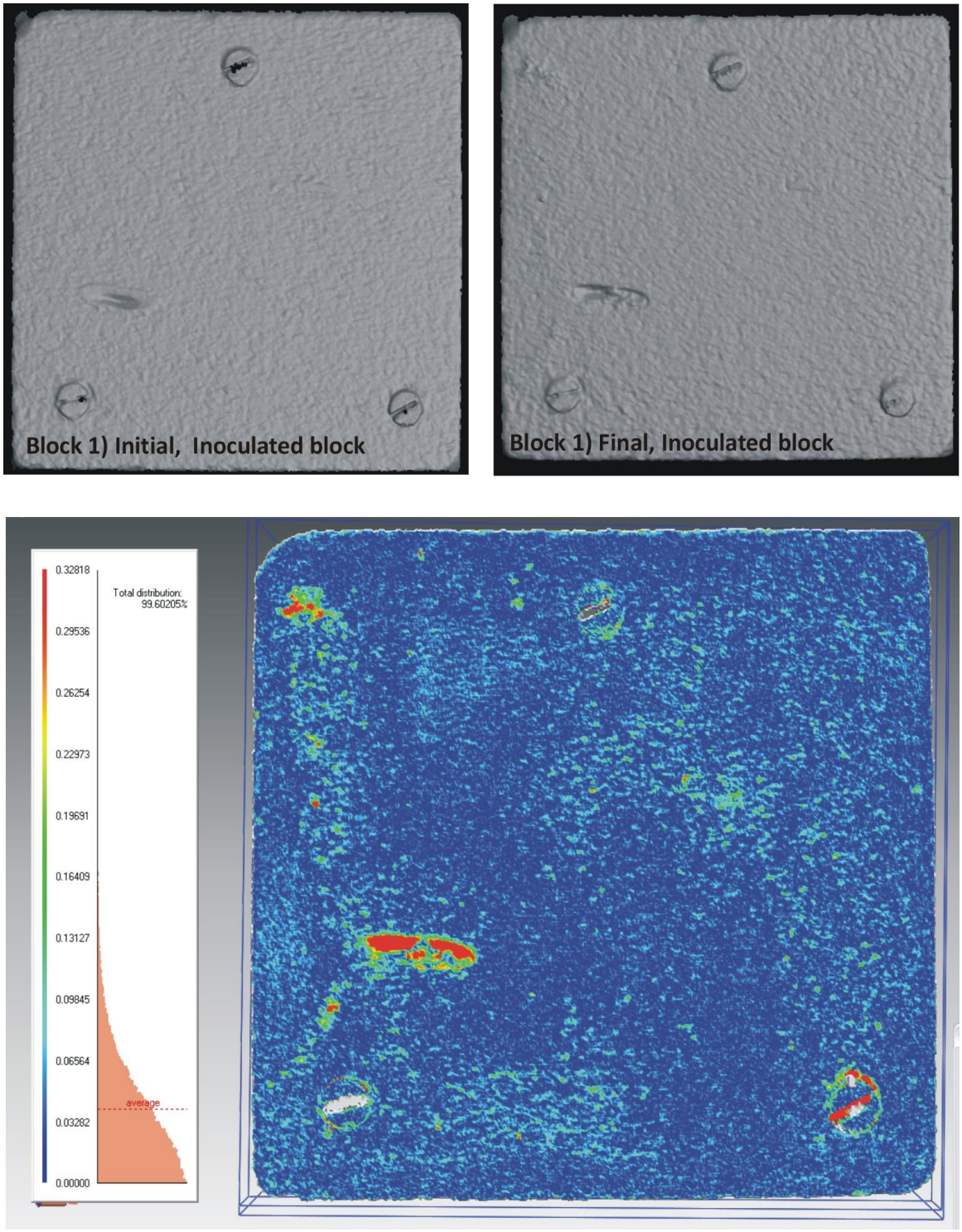

Figure 6-11: Clashach inoculated block, initial and final scan images and coloured SSD image.

For key see Figure 6-5. Both signs of granular disintegration (enlargement of the indentation) and gain (around screws) can be seen.

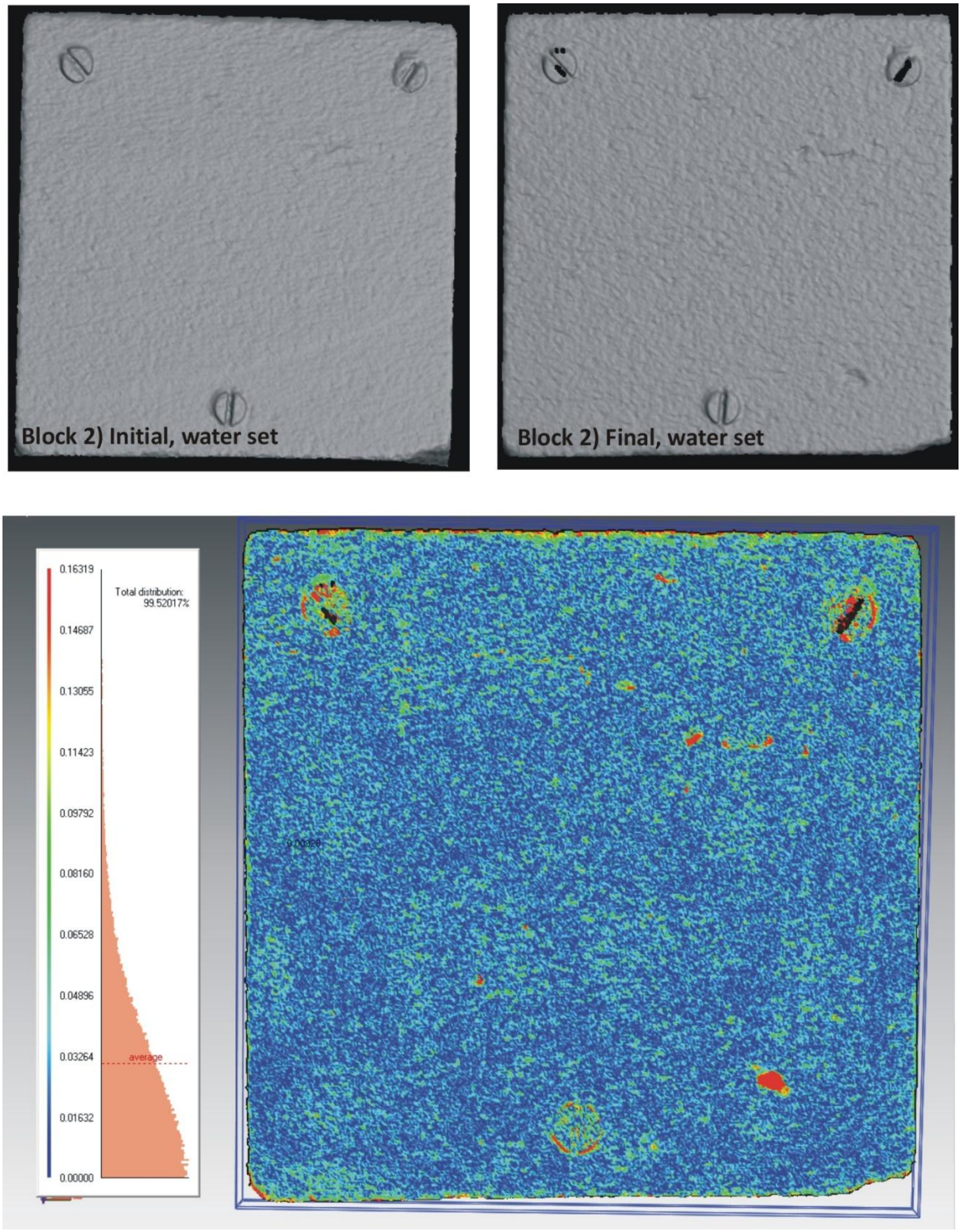

Figure 6-12: Clashach water only block, initial and final scan images and coloured SSD image.

For key see Figure 6-5. Evenly distributed granular disintegration has occurred on the surface of the block.

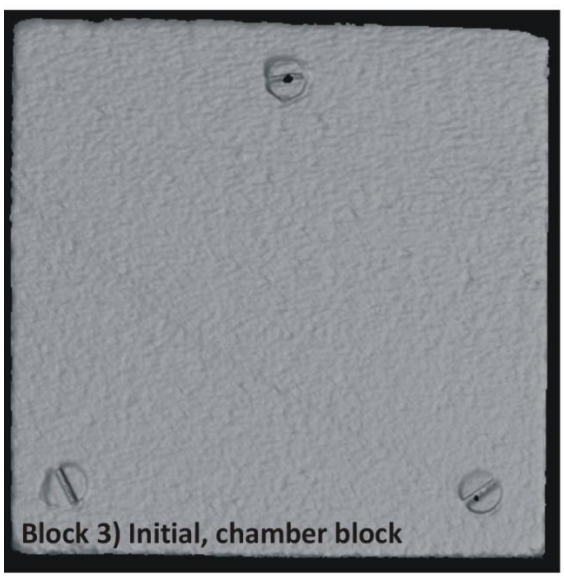

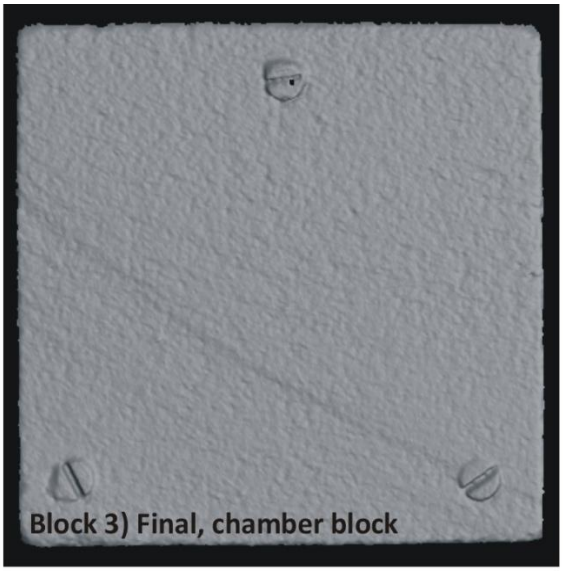

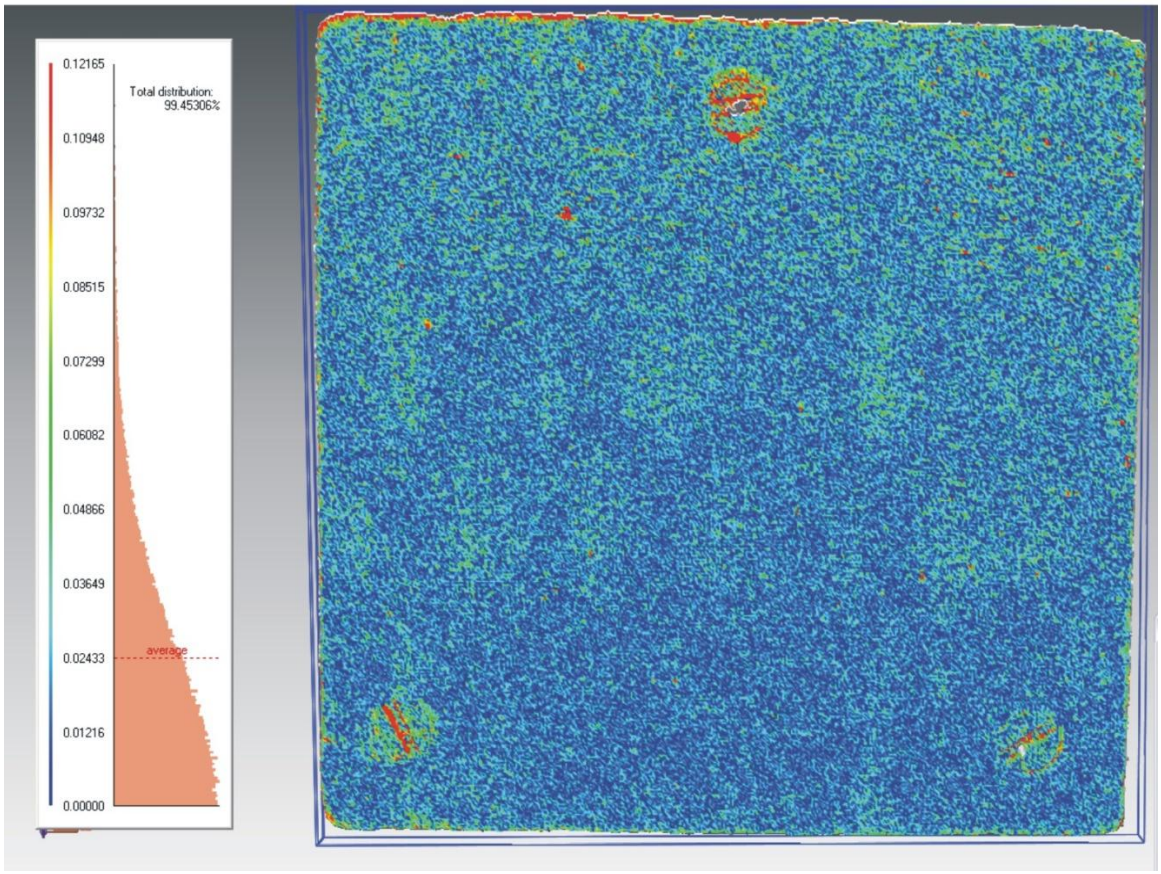

Figure 6-13: Clashach chamber block, initial and final scan images and coloured SSD image. For key see Figure 6-5. Evenly distributed granular disintegration has occurred over the surface of the block.

6.2.4 *Cullalo*

The inoculated block has an average change of 0.040 mm and a maximum change of 0.552 mm. The water block has an average change of 0.030 mm and a maximum change of 0.309 mm. Whilst the chamber block has an average change of 0.020 mm and a

maximum change of 0.180 mm (Figure 6-14,Figure 6-15,Figure 6-16 and Table 6-1). The inoculated Cullalo block has experienced the largest change to its surface within this set. Both loss and gain are identified, gain of matter has occurred predominantly around and in the screws and a patch in the upper left hand corner. The loss identified on the scan is restricted to small areas with a general wide spread loss over the rest of the surface (Figure 6-14). The large maximum change on the water block is caused by an increase in mass around the screws and also a chip on the right edge of the block causing loss. The water only block has also suffered damage to the surface in the form of mass loss, with the surface roughness being increased (Figure 6-15). The chamber block has suffered negligible amounts of damage. The loss of grains from the analysed facade of the water and chamber block is evenly distributed over the surface of the stone (Figure 6-16).

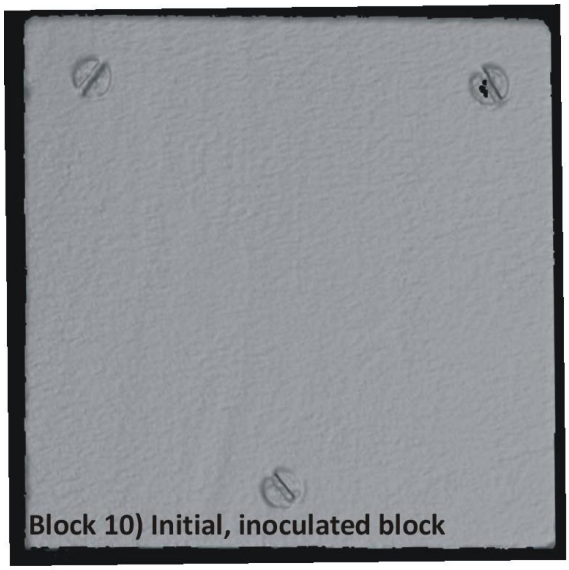

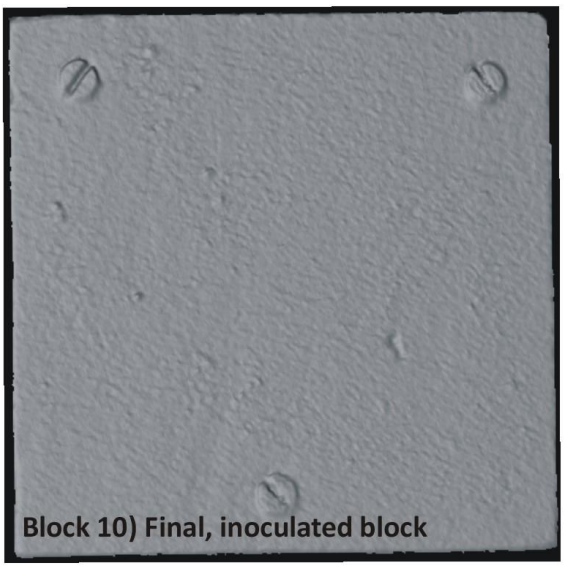

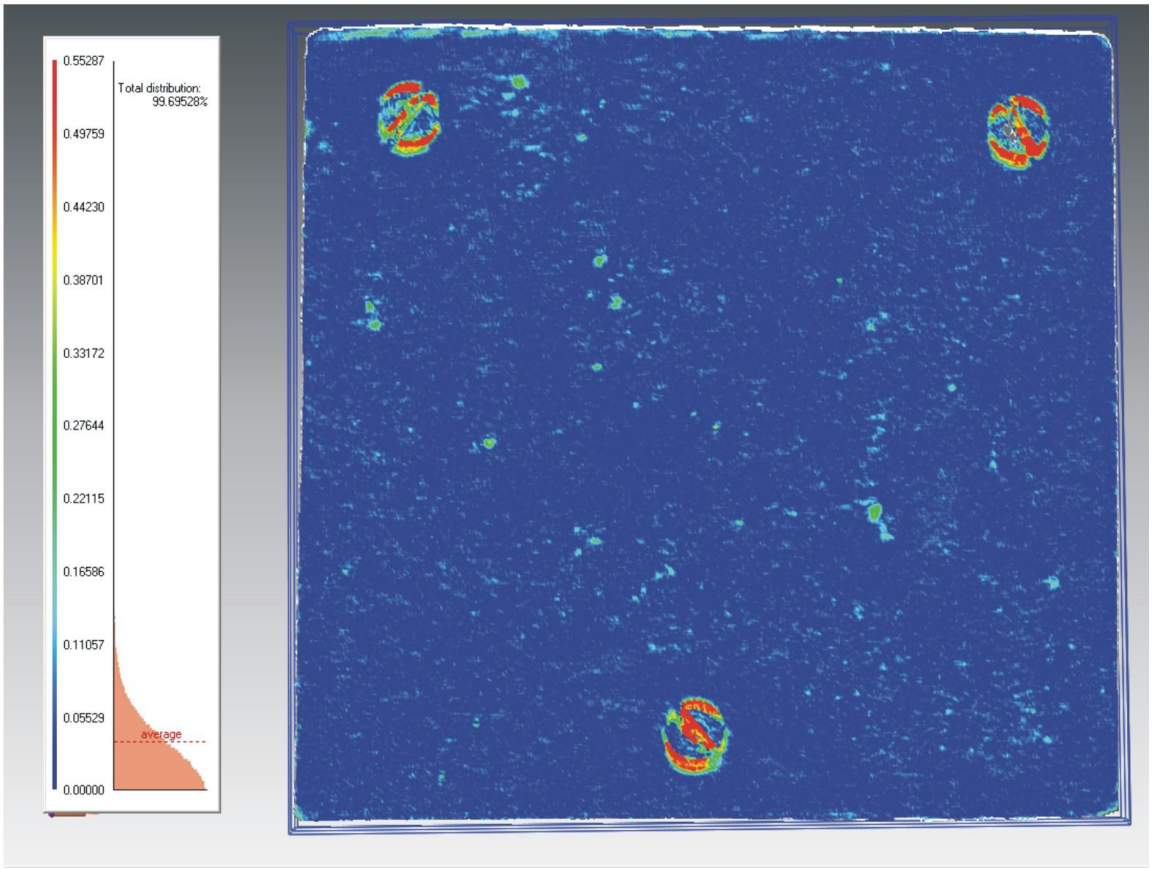

Figure 6-14: Cullalo inoculated block, initial and final scan images and coloured SSD image. For key see Figure 6-5. The areas around the screws are the focus of gain on the block.

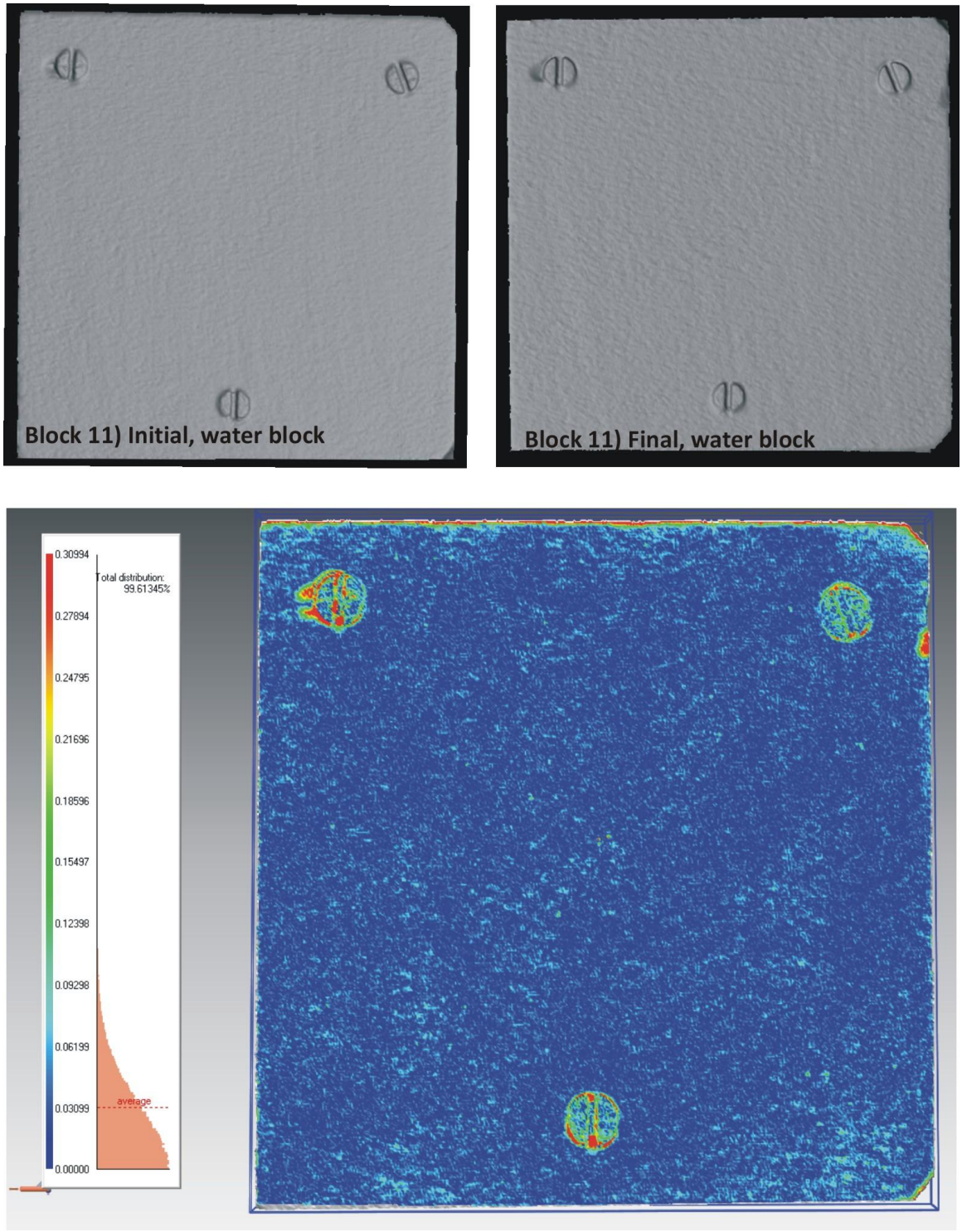

Figure 6-15: Cullalo water only block, initial and final scan images and coloured SSD image.

For key see Figure 6-5. The granular disintegration seen is evenly distributed over the surface of the face.

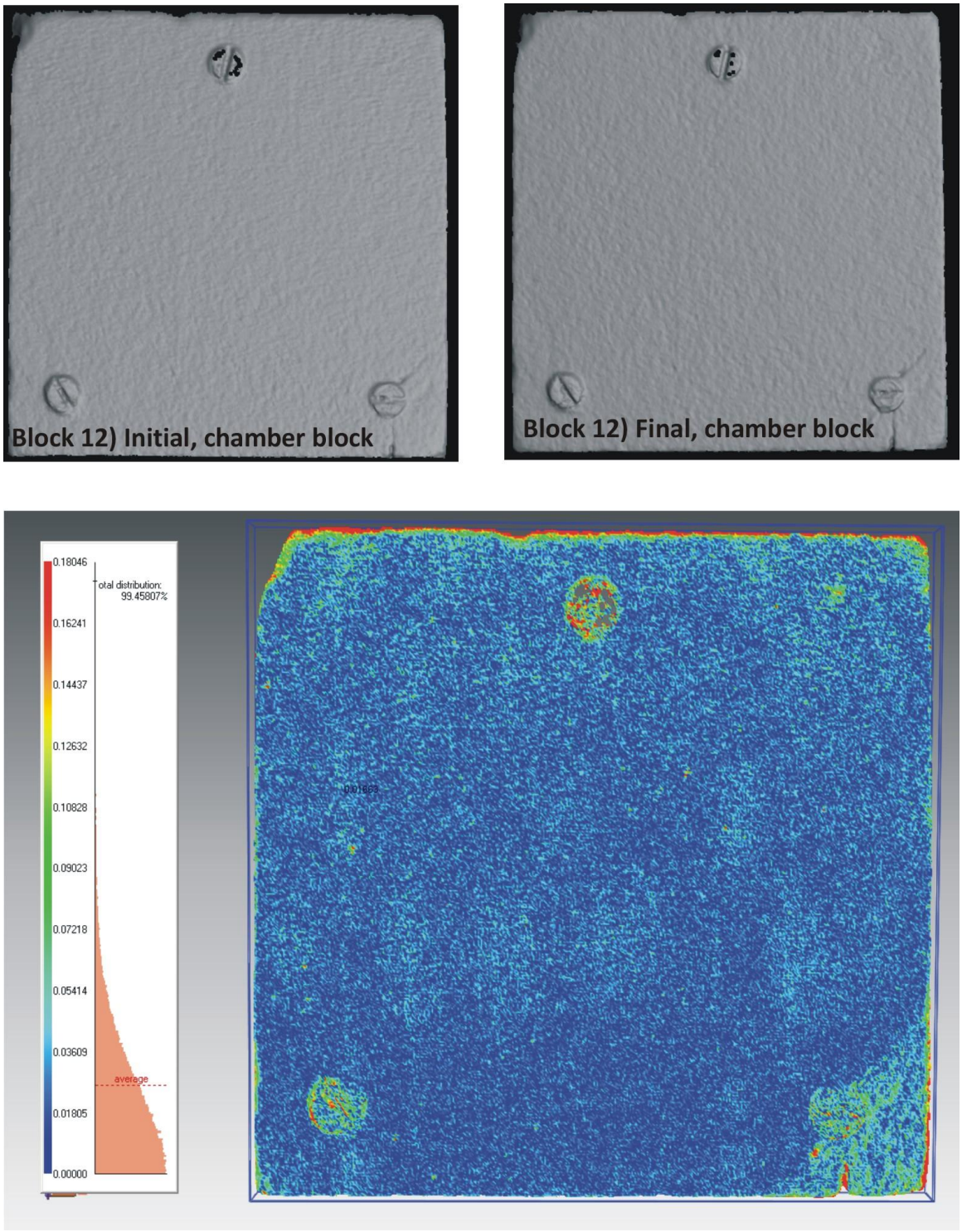

Figure 6-16: Cullalo chamber block, initial and final scan images and coloured SSD image. For key see Figure 6-5. The changes seen over the surface of the face are evenly distributed.

6.2.5 ***Dunhouse Buff***

A small amount of surface change has occurred to the inoculated block with an average of 0.034 mm and a maximum change of 0.184 mm, particularly on the left

hand side and lower centre of the block face (Figure 6-17 and Table 6-1). The water block has an average change of 0.021 mm and a maximum change of 0.147 mm, whilst the chamber block has an average change of 0.029 mm and a maximum change of 0.144 mm (Figure 6-18 Figure 6-19 and all data in Table 6-1). This set shows very similar average and maximum changes, and seems to have reacted similarly under each set of conditions. Loss has been widespread over the surface, rather than in patches and, therefore the original surface features have remained intact (Figure 6-18).

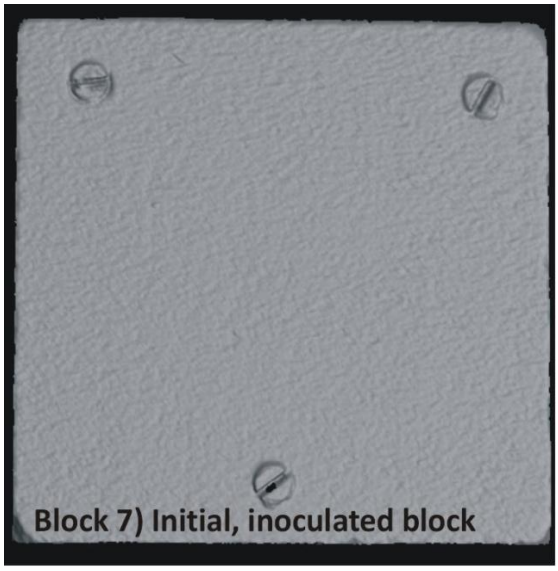

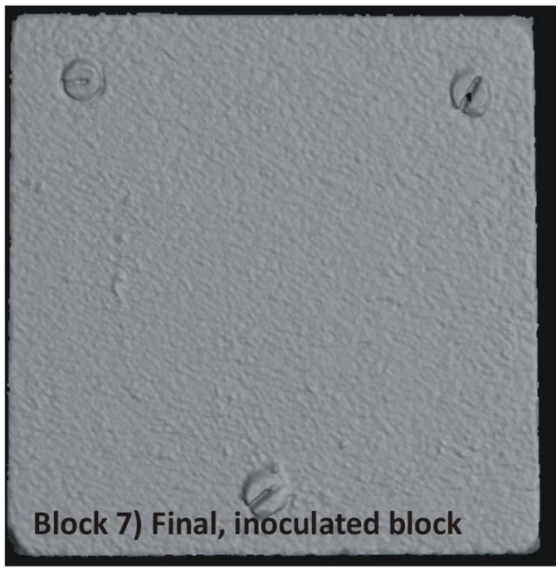

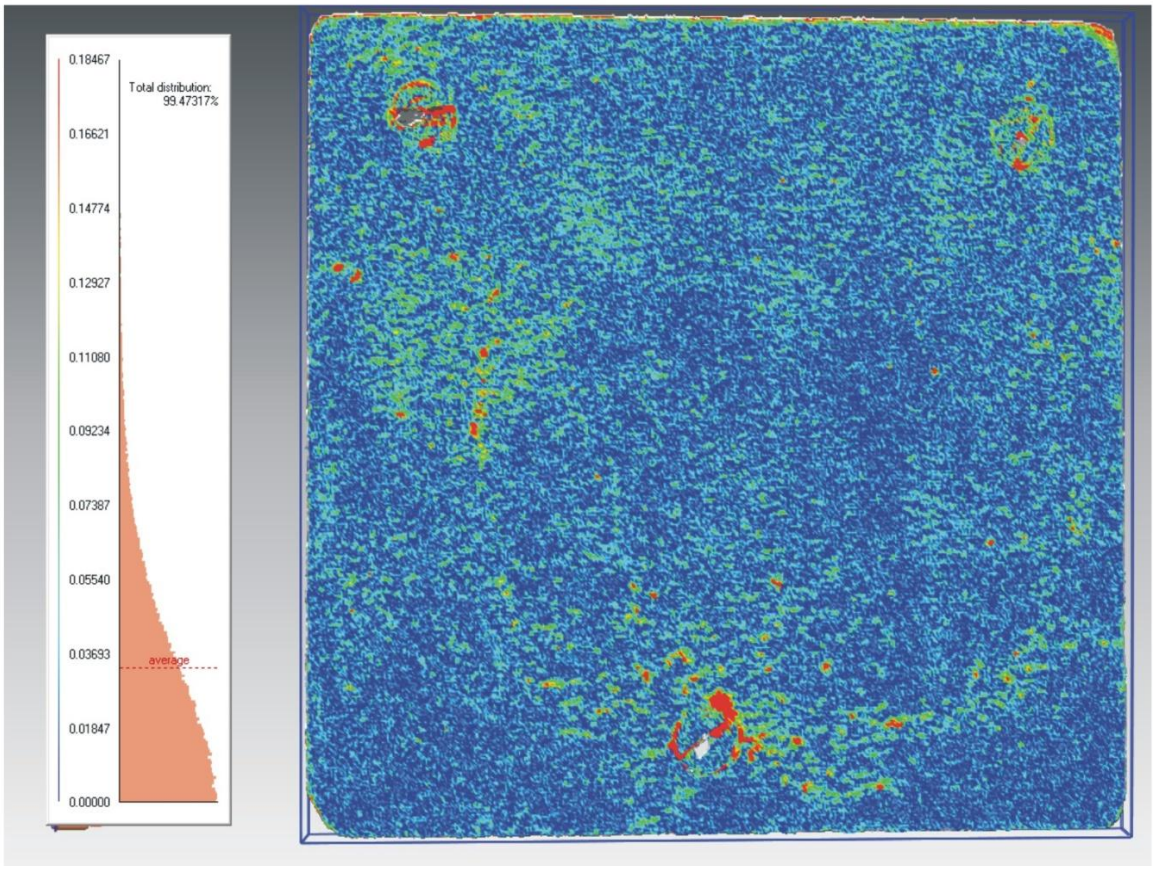

Figure 6-17: Dunhouse Buff inoculated block, initial and final scan images and coloured SSD image.

For key see Figure 6-5. The largest change to this block has occurred in and around the screws.

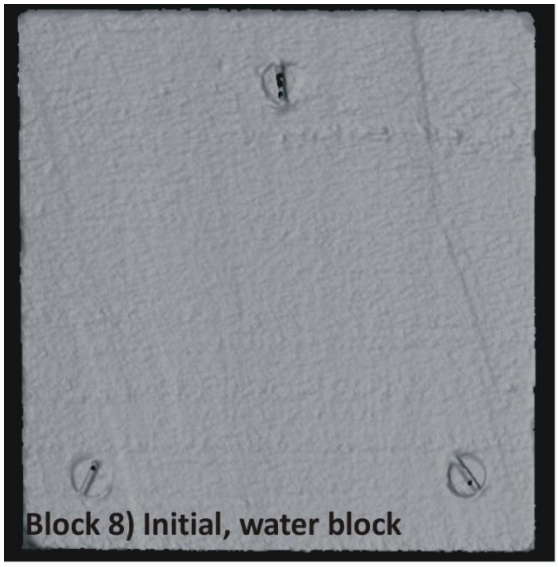

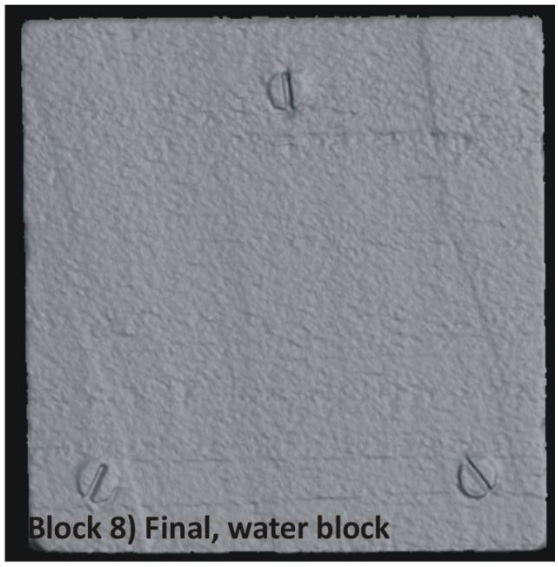

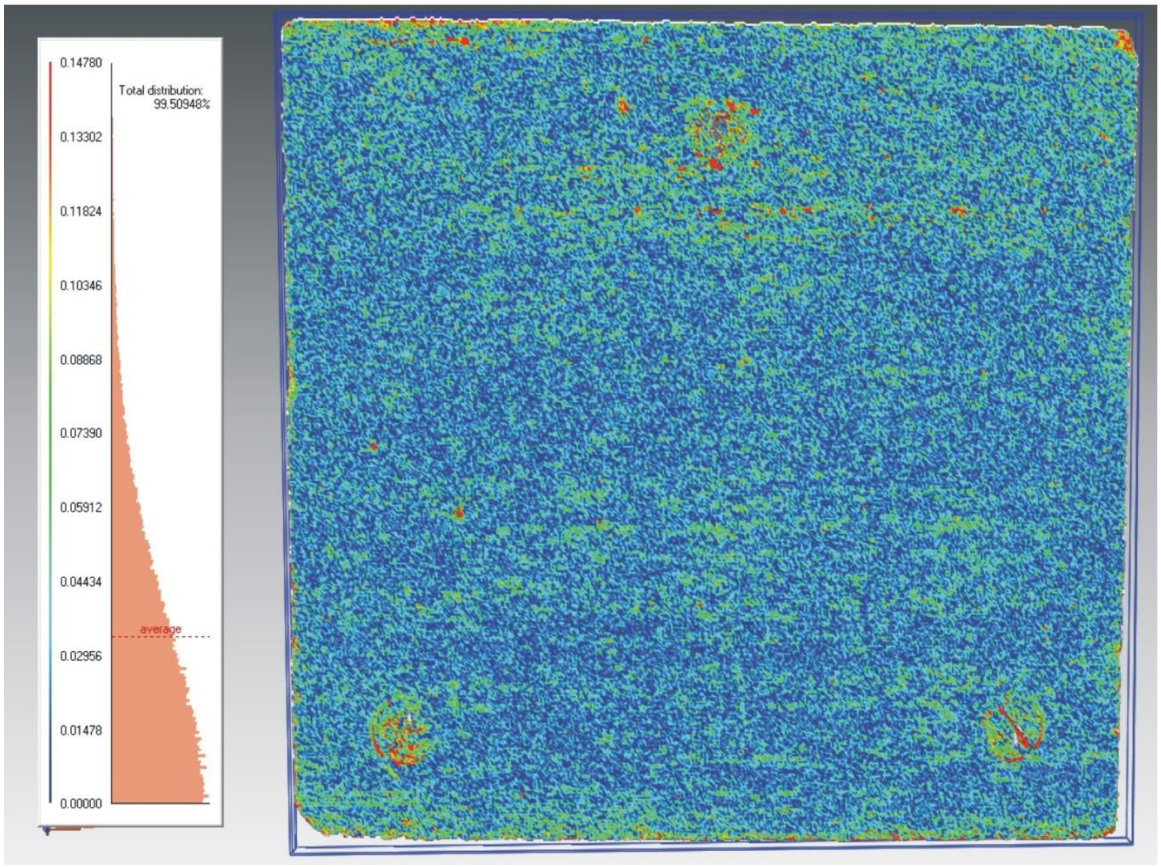

Figure 6-18: Dunhouse Buff water only block, initial and final scan images and coloured SSD image.

For key see Figure 6-5. This image shows that minimal change has occurred, leaving original surface features intact.

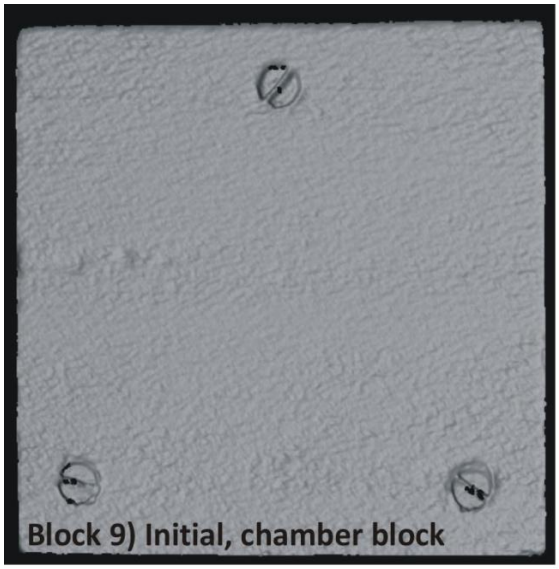

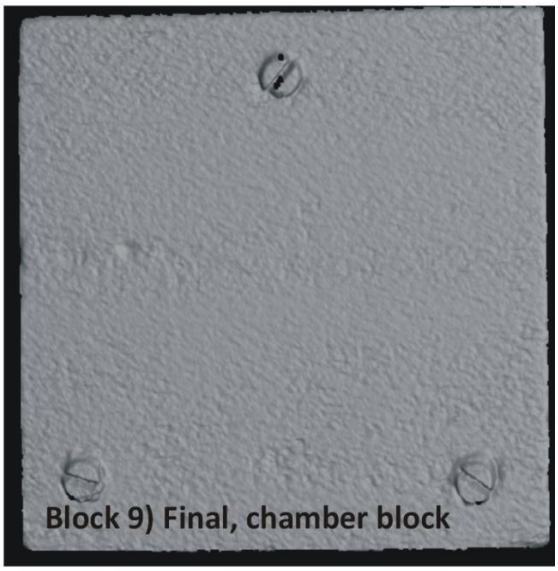

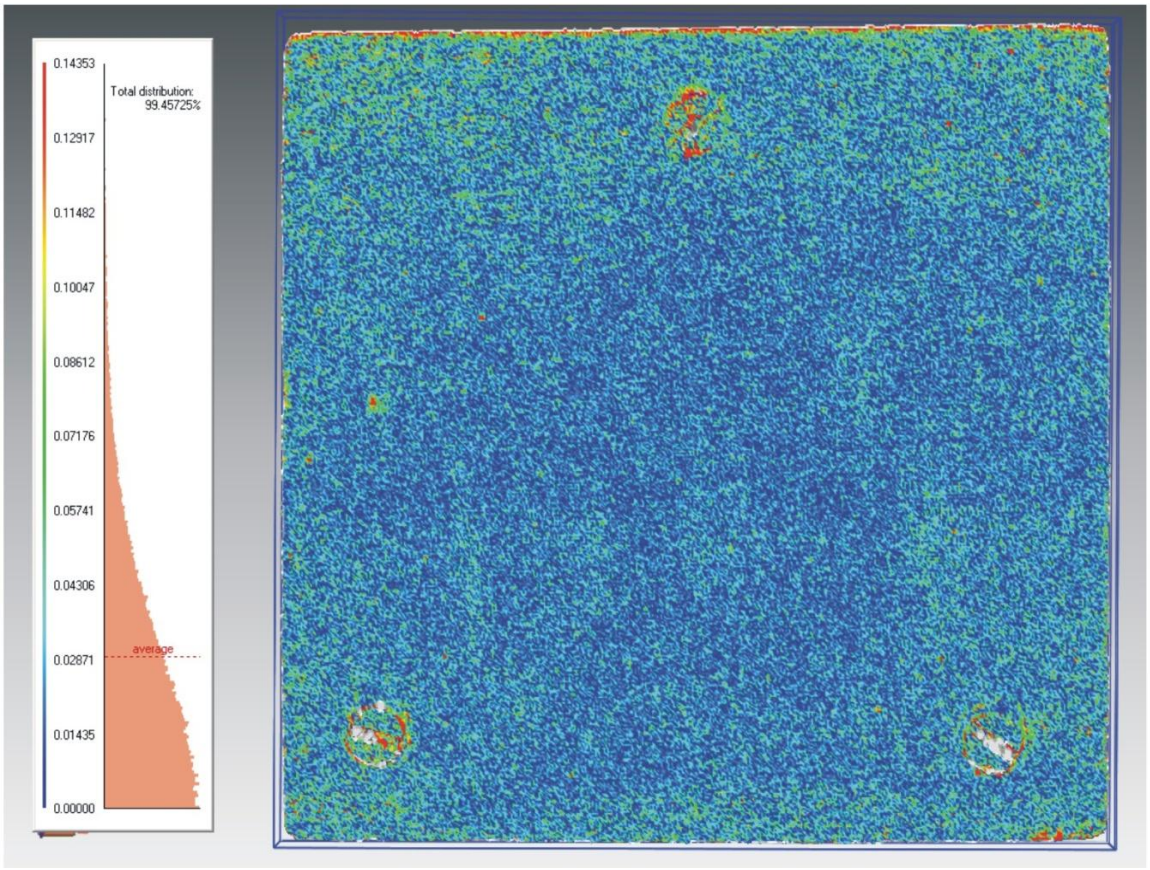

Figure 6-19: Dunhouse Buff chamber block, initial and final scan images and coloured SSD image.

For key see Figure 6-5. The image shows change is minimal and evenly distributed over the surface.

6.2.6 *Scotch Buff*

The inoculated block has an average change of 0.046 mm and a maximum change of 0.231 mm, whilst the water block has an average change of 0.030 mm and a maximum change of 0.136 mm. The control block has an average change of 0.020 mm and a

maximum of 0.118 mm (Figure 6-21,Figure 6-22,Figure 6-22 and Table 6-1). These values indicate that the inoculated block has experienced the greatest amount of change, which is the result of a few small patches of increased height, coinciding with a general loss of grains from the surface making the texture increasingly rough (Figure 6-20). The water only block has also suffered damage to its surface, the final scan indicating a rougher texture with the original saw markings being lost (Figure 6-21) whilst, the main area of decay is on the top edge of the block. This loss at the top edge is reflected in the chamber block SSD image, although in general it has seen lower levels of change (Figure 6-22).

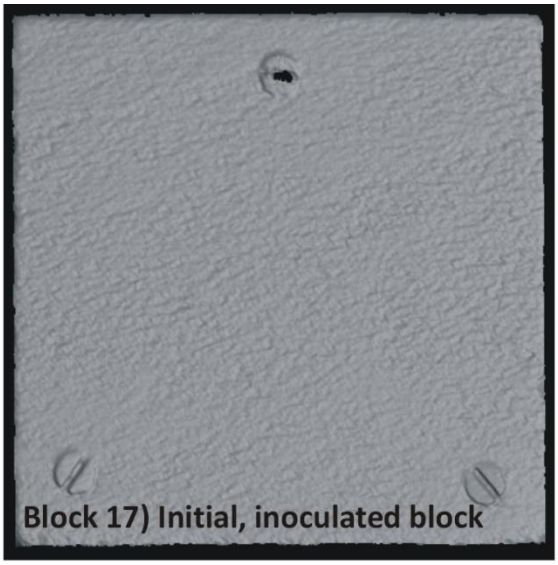

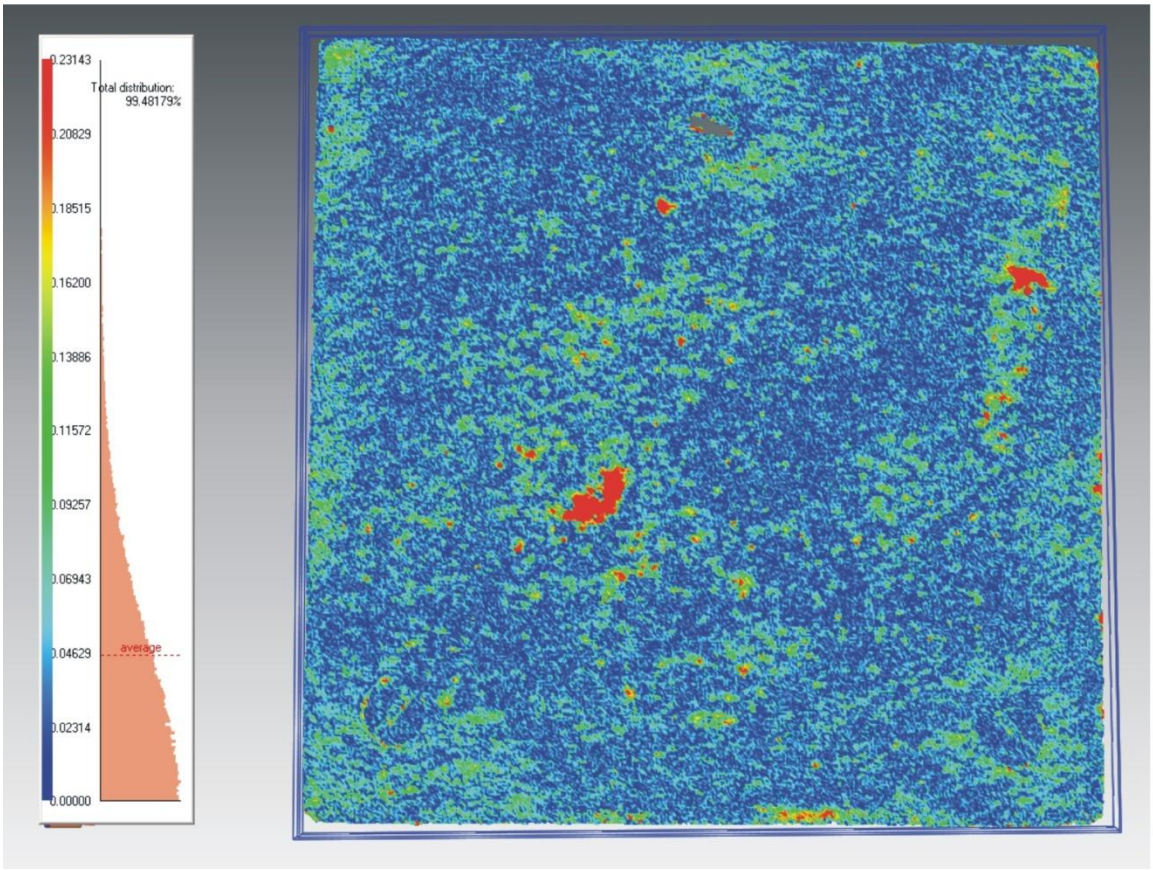

Figure 6-20: Scotch Buff inoculated block, initial and final scan images and coloured SSD image.

For key see Figure 6-5. The image shows overall granular disintegration, whilst patches of gain have occurred.

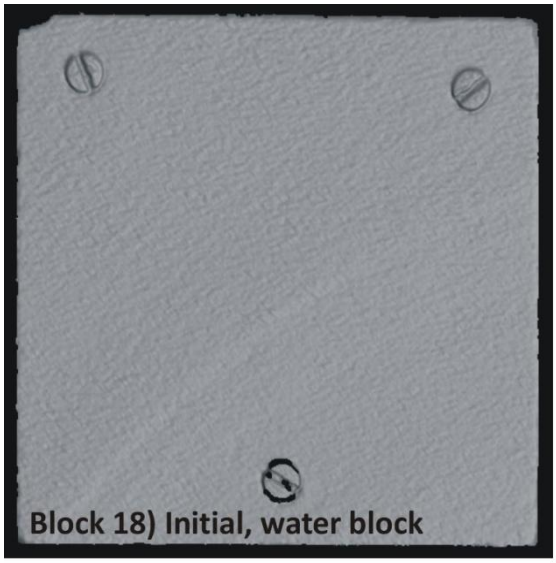

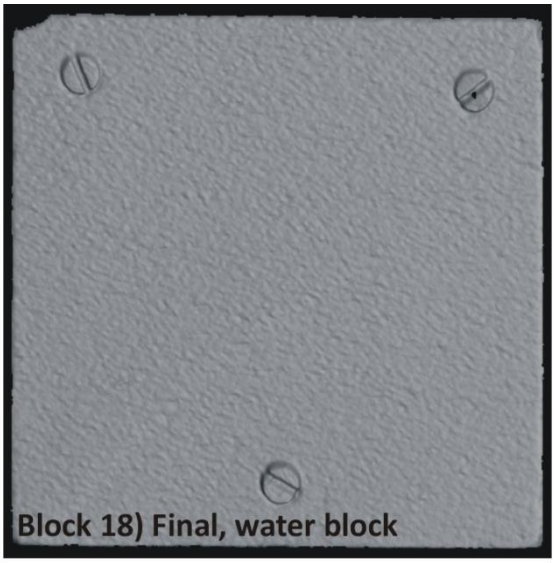

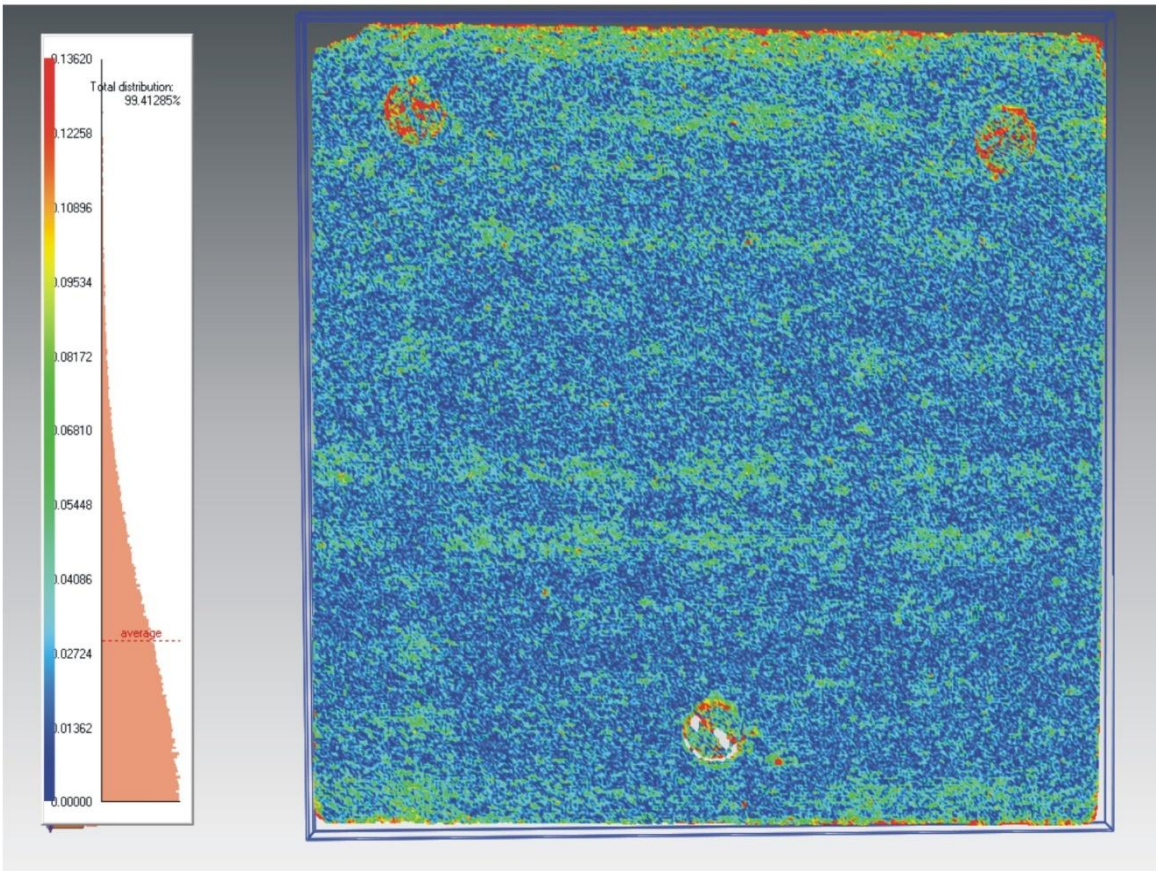

Figure 6-21: Scotch Buff water only block, initial and final scan images and coloured SSD image.

For key see Figure 6-5. The image shows granular disintegration along the top edge of the block face, in addition original markings have been lost.

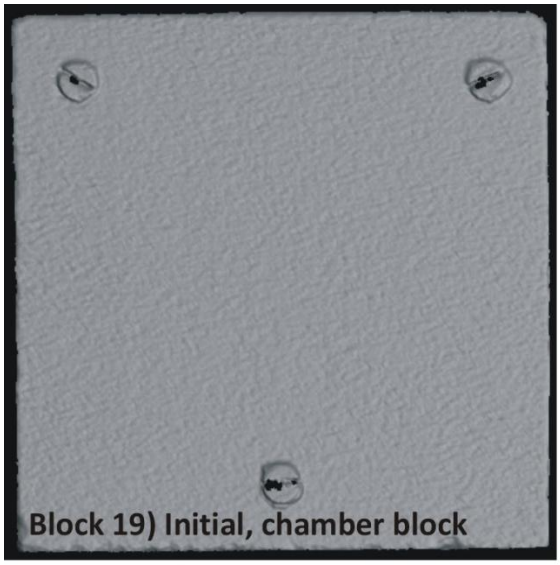

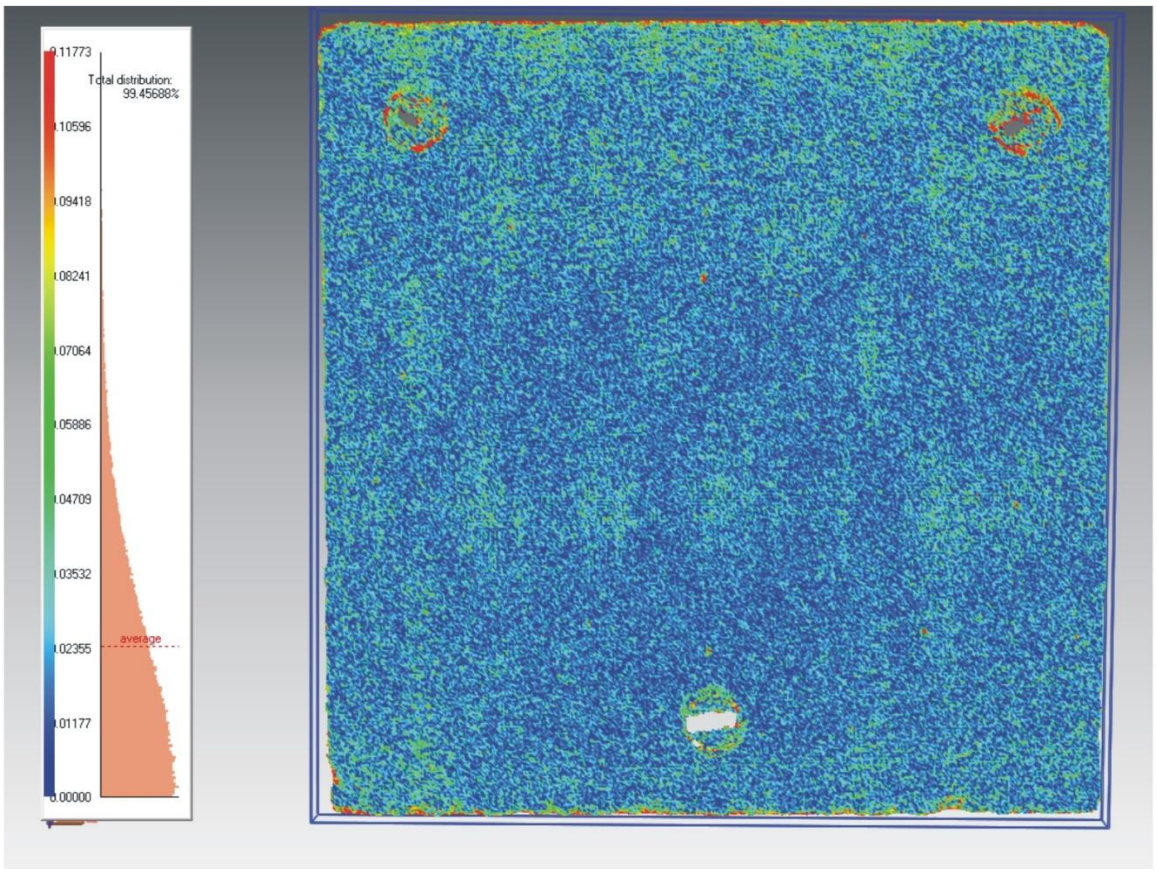

Figure 6-22: Scotch Buff chamber block, initial and final scan images and coloured SSD images.

For key see Figure 6-5. The image shows small amounts of change along the top edge of the face.

Table 6-1: The change recorded on all the blocks within the environmental chamber (mm).

Sandstone	Inoculated		Water		Chamber	
	Av	Max	Av	Max	Av	Max
Bearl	0.055	0.276	0.050	0.250	0.038	0.183
Blaxter	0.040	0.325	0.038	0.175	0.031	0.150
Clashach	0.039	0.328	0.030	0.163	0.024	0.121
Cullalo	0.040	0.552	0.030	0.309	0.020	0.180
Dunhouse Buff	0.034	0.184	0.021	0.147	0.029	0.144
Scotch Buff	0.046	0.231	0.030	0.136	0.020	0.118

The table includes both average and maximums. All results are subject to ±0.05 mm error.

6.2.7 *Discussion*

Most environmental chamber experiments use a much more aggressive configuration of temperature and time period cycles during their running, such as 8 hours at 40°C followed by 8 hours at 10°C (Warke and Smith, 1998). The environmental chamber experiment in this study simulates much more realistic conditions over a prolonged period of time and was therefore much less aggressive. The combination of the use of Rapidform 2006 software and laser scanning is very accurate, detecting the smallest of changes on the investigated surfaces. The greatest alteration was seen on the Cullalo inoculated block, where a maximum change of 0.552 mm had occurred. The average change seen on all the inoculated blocks was 0.042 ± 0.007 mm, the mean change on all the water only blocks was 0.035 ± 0.01 mm, whilst the chamber set had an average change of 0.029 ± 0.007 mm for all the blocks.

The total amount of loss experienced on the sandstone surface was crudely calculated using Equation 4. The average change over the surface was divided by the average quartz diameter for the appropriate sandstone, which then provided an estimate of the amount of grains lost and, therefore, the amount of grains lost per day could be calculated (Table 6-2), however, this assumes that all loss is quartz grains rather than kaolinite, K-feldspar or mica and that the average change was due to loss. To understand the effect of the heavy rainfall the chamber results were subtracted from the water block to gain insight to the effect of the extra water. The results in Table 6-2 are probably over-estimates for the inoculated blocks, because not all topographical change was mass loss (a small proportion was mass gain), but the data are more realistic for the water and chamber blocks, which predominantly experienced mass loss. These calculations indicate that Cullalo had the

highest amount of grain loss per day whilst Clashach has least on both the water block and the chamber block (Table 6-2).

Equation 4: Equation of total loss

$$\frac{Area \times Av\ Change}{Grain\ Size} = Total\ loss$$

Table 6-2: The total and daily number of sand grains lost.

Sandstone	Av Grain size (µm)	Inoculated block	Water block	Chamber block	Water only
Bearl	450.0	992[A]	902[A]	685[A]	217[A]
		1.7[B]	1.6[B]	1.2[B]	0.4[B]
Blaxter	188.7	1723[A]	1637[A]	1335[A]	302[A]
		3[B]	2.8[B]	2.3[B]	0.5[B]
Clashach	394.2	801[A]	616[A]	493[A]	123[A]
		1.4[B]	1.06[B]	0.85[B]	0.2[B]
Cullalo	135.2	2400[A]	1800[A]	1200[A]	400[A]
		4.1[B]	3.1[B]	2.1[B]	1[B]
Dunhouse Buff	163.7	1689[A]	1441[A]	1043[A]	398[A]
		2.9[B]	2.5[B]	1.8[B]	0.7[B]
Scotch Buff	221.3	1685[A]	1099 [A]	733[A]	366[A]
		2.9[B]	1.9[B]	1.3[B]	0.6[B]

Total grains lost indicated by A and the daily loss is indicated by B. These results are equated by assuming all change on the stone surface is loss. The water only column was calculated by subtracting the chamber results from the water block results.

The Cullalo sample may be the most reactive because the petrography results indicate that it has experienced minimal compaction, while there is no carbonate cement to help bind the grains together (section 2.2.5.4).

There is error associated with all these results, when the error is added to these results it shows that all the error bars between the sample blocks overlap. However, the fact remains that the inoculation block, in each set, always shows the highest amount of average change and the chamber block in each set suggests the lowest average change signifies that there is some truth in these results.

The final image scans indicate that all of the inoculated blocks have experienced surface gain (with the exception of Bearl), combined with increased roughness to their surface, which may be due to granular disintegration. The height gain is not uniform over the inoculated blocks, occurring mainly in small patches over the surface, which are generally <2 mm in diameter. The largest patch of gain was seen on Scotch Buff at 10 mm in length. Bearl shows no gain to the surface; if the surface gain is a product of microbial growth

then pore size (Bearl mean = 73 μm) may have impeded the colonisation of microbes. As it has previously been suggested, that the optimum conditions for microbial colonisation are sandstones with a porosity of <14% and small pore size, preferably with diameters between 2 and 20 μm (Warscheid and Braams, 2000). However, all sandstones studied here show a larger pore diameter, ranging from 55.3 μm – 181.4 μm, whilst porosity ranges from 11.9% to 20.7%. Thus, if these height gains are from microbes there is no clear explanation for why Bearl has so few microbes on the surface.

These proposed gains to the surface height on the inoculated block have to be viewed with slight caution, as scanning of the blocks was undertaken before inoculation so the gain of material on the surface may just be an artefact of the inoculation procedure, and later experiments in this study should indicate if this is so. This will be tested by conducting protein and chlorophyll-a assay on the sandstone surface as well as osmium staining, to investigate whether any microbes have managed to penetrate into the sandstones' substrate, to seek an environment less exposed to the environmental chamber conditions.

The water set, which experienced the ambient environmental conditions in addition to artificial rainwater (to simulate increased heavy rainfall), only show signs of loss from their studied surface. The final scan images show a more undulating surface with the loss of original surface features occurring, this is most likely due to minerals being lost. Bearl and Blaxter show the largest amount of average change (0.050 mm and 0.038 mm respectively), whilst Clashach, Cullalo and Scotch Buff all have an average change of 0.030 mm, whilst Dunhouse Buff shows the lowest average change to its surface. Granular detachment has been seen in other studies (Mcgreevy and Smith, 1985; Smith and Mcgreevy, 1988), although these have been in situations where salts were used rather than climatic impacts only and rates of granular detachment were not calculated.

The chamber blocks, which were exposed only to the environmental chamber settings, show the least amount of change to their surface with blocks only marginally increasing in surface topography. The largest average change is seen on Bearl, whilst Cullalo and Scotch Buff show the least. The chamber blocks indicate that, if only an increase of temperature and RH were to take place in the future, then sandstones may be resilient

and therefore other decay processes would be more predominant in weathering the sandstone, such as microbial, chemical and salt processes.

Of the blocks tested, Bearl and Clashach were the most resilient overall. In the case of Clashach this resilience is likely due to its compacted grains and thin quartz overgrowths observed. Bearl sandstone has also suffered compaction during diagenesis and contains thick quartz overgrowths (~ 50 μm wide). As this experiment focused only on change due to climatic events, and was carried out over a long time period, no other studies are available to compare results with.

6.2.8 *Further Chamber Block Experiments*

To investigate the accumulation of material on the inoculated blocks, protein and chlorophyll-a assays were undertaken as outlined in section 2.1.4. These tests were conducted on all blocks within the chamber to check whether cross contamination had occurred. However, all the protein and chlorophyll-a results agreed in detecting no signs of microbes. Therefore, the gain seen on the inoculated surfaces can be assumed to be a product of the inoculation procedure (i.e. dead matter) or accumulations of debris from weathering.

Although no microbial matter was identified on the surfaces, osmium stained blocks were prepared to clarify whether any microbes had migrated (either by gliding or growth migration) to the substrate for protection from the environmental chamber conditions. Osmium stained polished blocks were prepared as outlined in section 2.1.5. The results showed all blocks were in agreement with assay results, where no stained microbial matter was identified.

A few reasons can be suggested to account for why no microbial matter was found on the samples: 1) 0.2 g of microbial matter was placed on the surface during inoculation. This may have been too small a quantity to initiate a thriving community; 2) the microbes were nutrient deprived. Although artificial rain water was used, this did not fully simulate external environmental conditions where sandstone gathers atmospheric debris at an increased rate which provides extra nourishment; 3) Granular disintegration occurred at a greater rate than the microbial inhabitation could occur; 4) Climatic conditions within the

environmental chamber were too harsh for the microbes that were placed on the sandstone surface. However, it is most likely a combination of the first three factors that has inhibited the growth and development of a microbial community on the sandstone surfaces. As microbes survive in much harsher conditions around the world, option four can therefore be discounted.

These results do suggest that slow, long duration, climate chamber experiments can provide useful data on how the sandstone will react to future climate situations. However, there were problems with this new experiment's procedure set up. Therefore, a suggested improved protocol for future work would include a greater proportion of microbial matter to the surface of the sandstone during inoculation and, if time allowed, inoculated sandstones should be exposed to the natural environment for up to a year to increase the probability of microbial communities establishing. These blocks should then be sampled before being placed into the controlled environment to see how the microbial communities react to the new environment. This would help gain more detailed and reliable results.

6.3 Internal Monitoring Results: Part 1

Results from the previous chapter on microbes show that many of the organisms are cryptoendolithic and, in some cases, living to a depth of 6 mm (e.g. the RGU Blaxter block). Therefore, it cannot be simply assumed that they are experiencing the same climatic conditions as those living on the stone surface. The main climatic differences are: solar radiation, temperature and relative humidity conditions. The internal climate will also affect other processes such as chemical decay and freeze-thaw weathering.

To observe these internal conditions IButton dataloggers were inserted into the sandstone blocks (Figure 6-23) as outlined in section 2.1.8. The sandstones above and below the test blocks were placed there to provide some shelter from rain and solar heating. This set-up allowed a comprehensive record of the temperature and RH at a depth of 3 mm and 6 mm beneath the surface, to be recorded. Different sandstone types were tested as well as different aspects. A thermal imaging camera was used to provide spatially and temporally resolved surface temperature of the various stone surfaces over

a daily cycle. Decagon leaf wetness sensors were additionally embedded into the sandstones to measure free water (section 2.1.11). The running time of each datalogging experiment is shown in Figure 6-24.

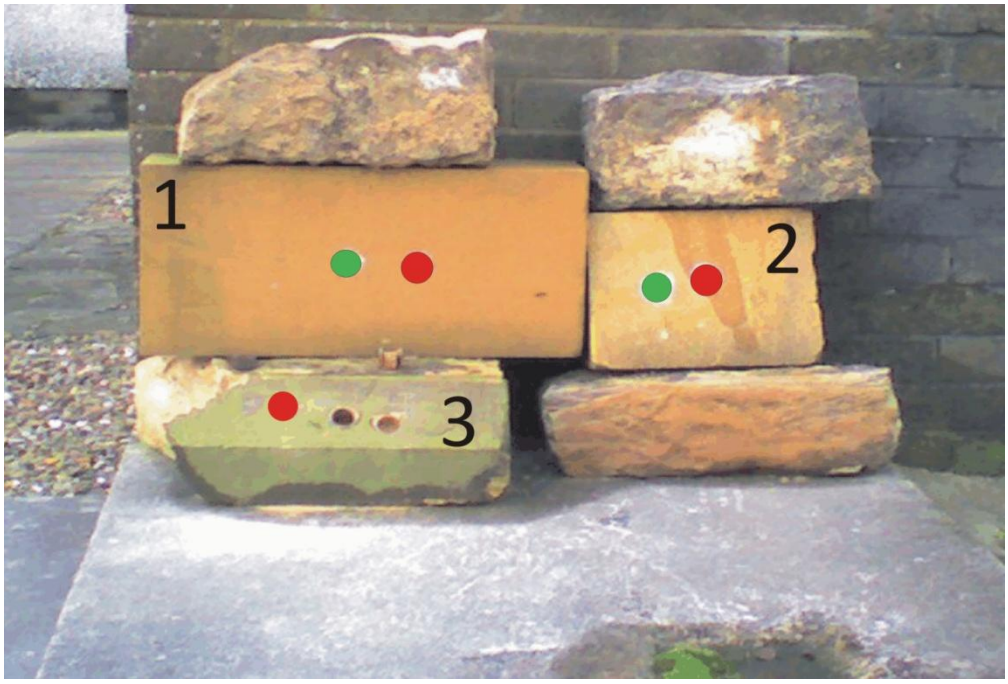

Figure 6-23: Internal climate modelling stones at the Glasgow observatory.

1) Dunhouse Buff, 2) Bearl, 3) Dalry stone, green circles indicate 3 mm deep IButtons, red circles indicate 6 mm deep IButtons.

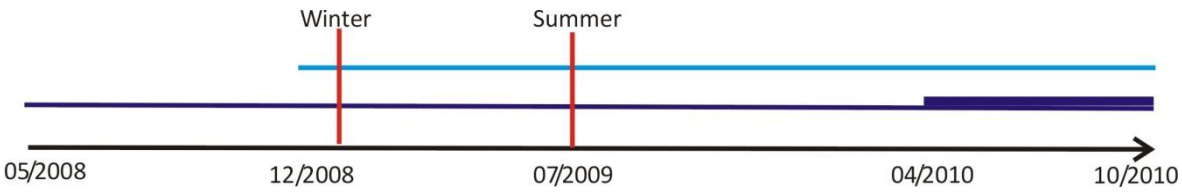

Figure 6-24: Time line of internal datalogging experiments.

Purple line shows IButton experiment using Dunhouse Buff and Bearl, thickened part of line shows when water sealant was applied, blue line shows IButton experiment using Dalry and North blocks, red: thermal imaging days.

A large data set (~118,000 points) was collected over a two year period. This data set is too extensive to examine visually or statistically as one entity, as this may hide subtle features. Therefore, it was broken down to highlight specific features and key trends. The data set was split into “macro” monthly sets and “micro” daily sets; month and day sets for both summer and winter are discussed next.

6.3.1 *IButton Observations "micro": Winter Day (20th Jan 2010)*

6.3.1.1Temperature

The 20/01/2010 was chosen to coincide with the thermal imaging which was also conducted on this day. Thermal imaging data were collected on the hour to compliment the internal IButton collection time. The weather was predominantly overcast all day with drizzle starting at 3 pm. The thermal imaging data, combined with the IButton measurements, show that the three sandstone surfaces (Bearl, Dunhouse Buff and Dalry) behaved in a similar manner over the 9 am to 4 pm period (Figure 6-25). The surface temperatures of the three blocks are very similar until 10 am, when Dalry becomes warmer than the other blocks by an average of 0.3°C. However, all blocks follow the same pattern of warming, with a peak at 11 am and 2 pm. By 4 pm, all blocks are recording similar surface temperatures (Figure 6-25). The internal sensors all follow the same trend rising from 1.5°C at 9 am to 2.5°C by 12, where they become cooler than the surface temperatures. After 12, the Dalry internal sensor records warmer conditions than the Dunhouse Buff and the Bearl sensors. At 1 pm both 3 mm deep sensors show an increase in temperature, whilst the 6 mm deep sensors plateau at 3°C, all with the exception of Bearl 3 mm deep sensors, which reach 3°C by 4 pm, the same temperature as the surface measurements (Figure 6-25). The surface temperatures are not directly reflected internally; surface peaks may have been caused by a burst of solar radiation, because surface temperatures do not follow air temperature either. Air temperature is only exceeded for short periods of time by the surface temperatures of Bearl and Dalry. The only internal sensors which exceed air temperature are those at 3 mm depth and the Dalry sensor, whilst the deeper sensors at 6 mm do not exceed air temperature. The maximum air temperature recorded was 4.2°C; the maximum surface temperature was 3.7°C (Dalry) and maximum internal temperature was 3.5°C (Bearl 3 mm). The surface temperatures for each block at 9 am are all ~1.5°C (Figure 6-25) which may be evidence that, during night time hours, air temperature is heating the blocks whilst during the day, the most dominant force is solar radiation.

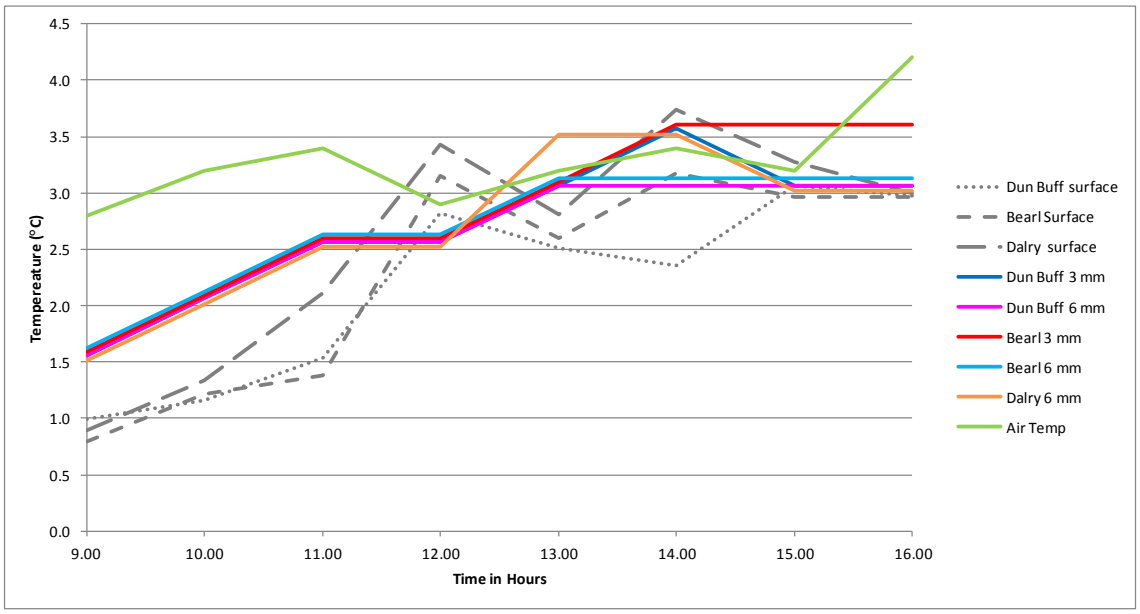

Figure 6-25: Internal, surface and air temperatures on 20/01/2010.

6.3.1.2 Relative Humidity

Relative humidity on this winter day within the stone is almost constant with internal sensors generally recording 110% ± 5% RH (Figure 6-26), with the exception of Dunhouse Buff at 115 ± 5% RH. The IButtons are accurate to 100%, therefore any value recording greater that 100%, the manufactures have suggested, to be due to the presence of liquid water and will be discussed later. The air RH is much lower than internal stone conditions but steady at 90% (Figure 6-26).

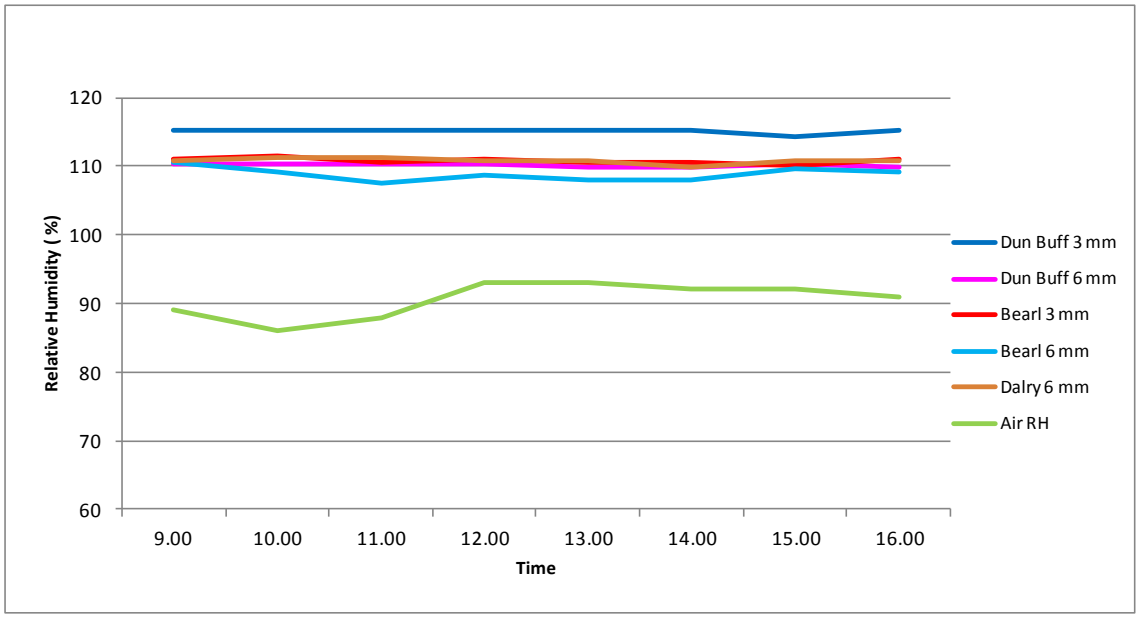

Figure 6-26: Internal and air RH on the 20/01/2010.

6.3.2 *IButton Observations "micro": Summer Day (6th July 2009)*

6.3.2.1Temperature

The 6th of July 2009 was chosen to coincide with the thermal imaging data also acquired on this date. The weather on this day was warm but overcast, with small showers at 11 am and 3 pm. When the thermal imaging data are combined with the ambient air data, they show that the blocks all behave in a similar manner. Internal sensors and surface temperatures of all three blocks exceed air temperature by a considerable margin (Figure 6-27). The surface temperatures at 9 am range between 18-20°C and remain steady until 11 am when they rise to a peak temperature at 12, the surface temperatures then slowly decline until 3 pm when they rise again (Figure 6-27). The surface temperatures of Dunhouse Buff and Bearl are very similar, although Bearl has a slightly warmer surface temperature by an average of 0.4°C, and this difference mainly occurs in the afternoon. During the morning hours, the Dalry surface temperature is higher than the surface temperature of both the other blocks by an average of 1.4°C (with a maximum difference of 3.3°C), until 1.30 pm when the temperature on Dalry's surface decreases and matches the other blocks (Figure 6-27). The internal sensors of Dalry and Bearl 3 mm follow the surface temperatures of their representative block very closely. The other sensors (Dunhouse Buff 3 and 6 mm and Bearl 6 mm) give a maximum temperature one hour before their surface and then have a slower decline in temperature until 3 pm (Figure 6-27). The rain showers indicated seem to have no immediate effect on the temperatures recorded. Internal and surface temperatures are very similar, although all internal temperatures do exceed those of the surface temperatures at some point during the day (Figure 6-27). The maximum air temperature recorded was 17.3°C, maximum surface temperature was 25.3°C (on the Dalry sandstone) and maximum internal measurement was 25.6°C (Dalry sandstone).

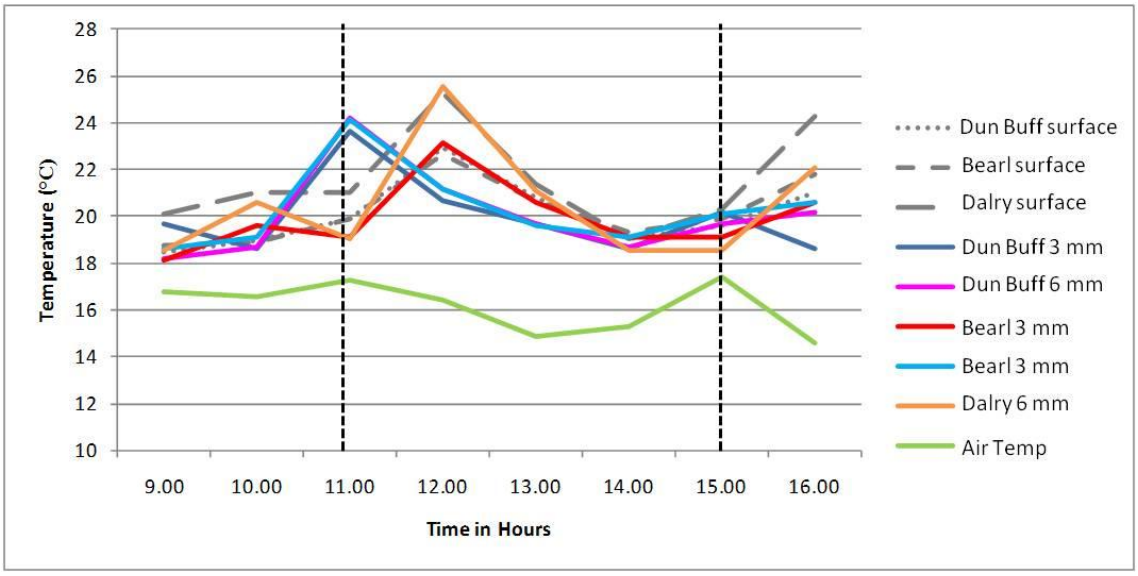

Figure 6-27: Internal, surface and air temperature on the 06/07/2009. Dashed vertical lines indicate timing of rain showers.

6.3.2.2 Relative Humidity

Relative humidity within the stones in this data appears reasonably stable (Figure 6-28). Dunhouse Buff sensors are similar to the air RH then, after midday, the internal RH becomes lower than the air RH, caused by the air RH increasing whilst the Dunhouse Buff remains stable (Figure 6-28). The internal RH of Bearl and Dalry sensors are higher than the air RH (Figure 6-28). The average RH for Dunhouse Buff is 78.5 ±5**%** whilst Bearl's average is 99 ± 5% RH. The range of values at 3 mm depth is much greater than the 6 mm range, (3 mm varying by 17.3% and 6 mm by only 3.2%). When the 5% error is taken into account on the RH data, the Bearl and Dunhouse Buff sandstones only overlap at two points during the day (11 am and 2 pm).

Dalry has the highest and most stable readings (with a range of 2%) and overall never drops below 100%.

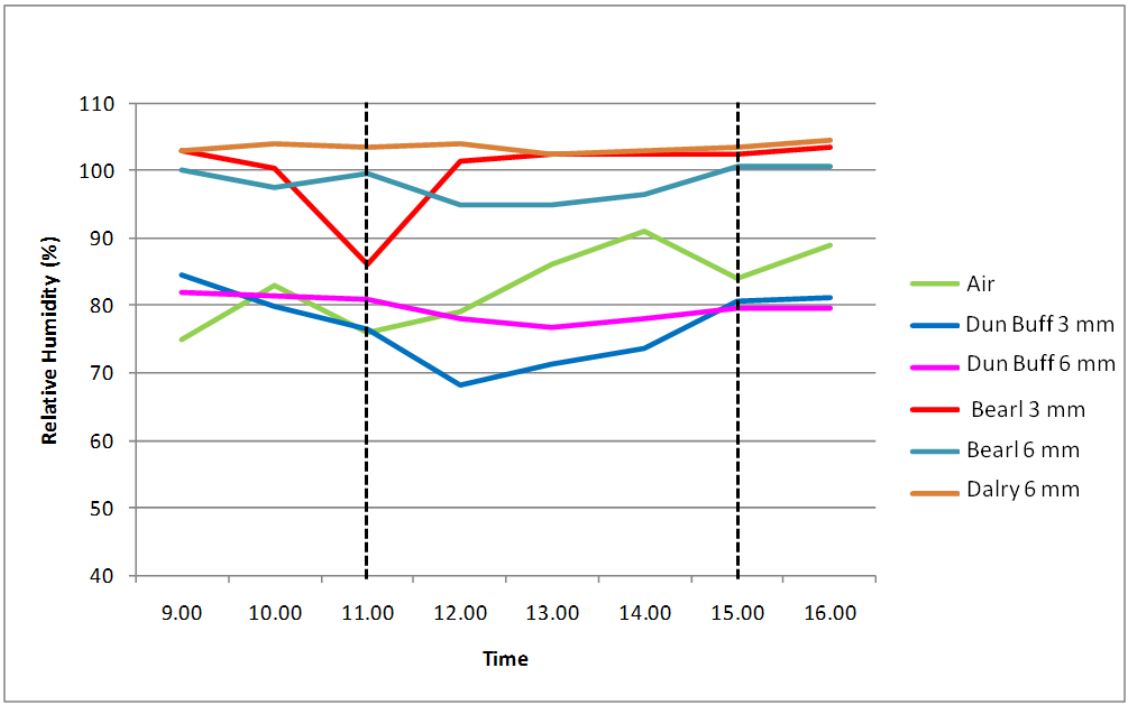

Figure 6-28: Internal and air RH on the 06/07/2009.
Dashed vertical lines indicate timing of rain showers.

6.3.3 *IButton Observations "macro": Winter Cycle (January 2010)*

6.3.3.1Temperature

The month of January 2010 was examined to see whether the daily cycles observed were representative of the monthly data. These data show that the daily trend concurs with the monthly trend (Figure 6-29), with internal sensors recording temperatures close to the air temperature for a large proportion of the month. Only four occasions occur when all internal sensors record temperatures that exceed air conditions by more than 2°C (on the 18th, 29th, 30th and 31st of January). However, during the first ten days of January, where air temperatures were predominantly below 0°C, the internal sensors remained warmer than the air during the extreme cold events (4th, 7th and 8th) (Figure 6-29). The maximum and minimum air temperatures recorded were 9.4°C and -10.2°C, whilst maximum and minimum internal temperature recorded was 14.1°C (Dalry) and -9.0°C (Dunhouse Buff and Bearl 6 mm).

To gain more information on how the air and internal temperatures are linked, the air temperature was subtracted from internal temperature and plotted on a frequency graph to show how often that particular difference between the environments occurs (Figure

6-30). The difference in temperature ranges from the internal conditions being 8.9°C warmer than external temperature to internal temperatures being 6.9°C colder than external temperature. Therefore the latter range of number will appear in the negative area of the graph (Figure 6-30).

The most common difference found to occur is for the internal conditions to be 0.1 to 0.9°C cooler than external temperatures (Figure 6-30). All the sensors show very similar patterns of differences, indicating that they are recording comparable internal environment conditions.

Dunhouse Buff and Bearl record that, 35.9% of the time, the internal temperatures are warmer than the external conditions whilst, the rest of the time (64.1%), it is cooler within the blocks compared to the air temperatures. The Dalry internal temperatures, spend an even larger percentage of time (69.5%) colder than the external conditions.

When the lower limits of the internal temperature compared to external conditions are viewed it shows that there is scatter, the lowest difference for Bearl 6 mm is for internal conditions to be 6 - 6.9°C cooler than the external conditions whilst it is only between 4 - 4.9°C for Bearl 3 mm. All but one sensor, records the maximum internal temperature to be 8 -8.9°C hotter than the external conditions.

The fact that the internal temperatures are spending over half the time recording conditions colder then the air, may correlate with lower amounts of solar radiation in Glasgow in winter, compared to during the summer months.

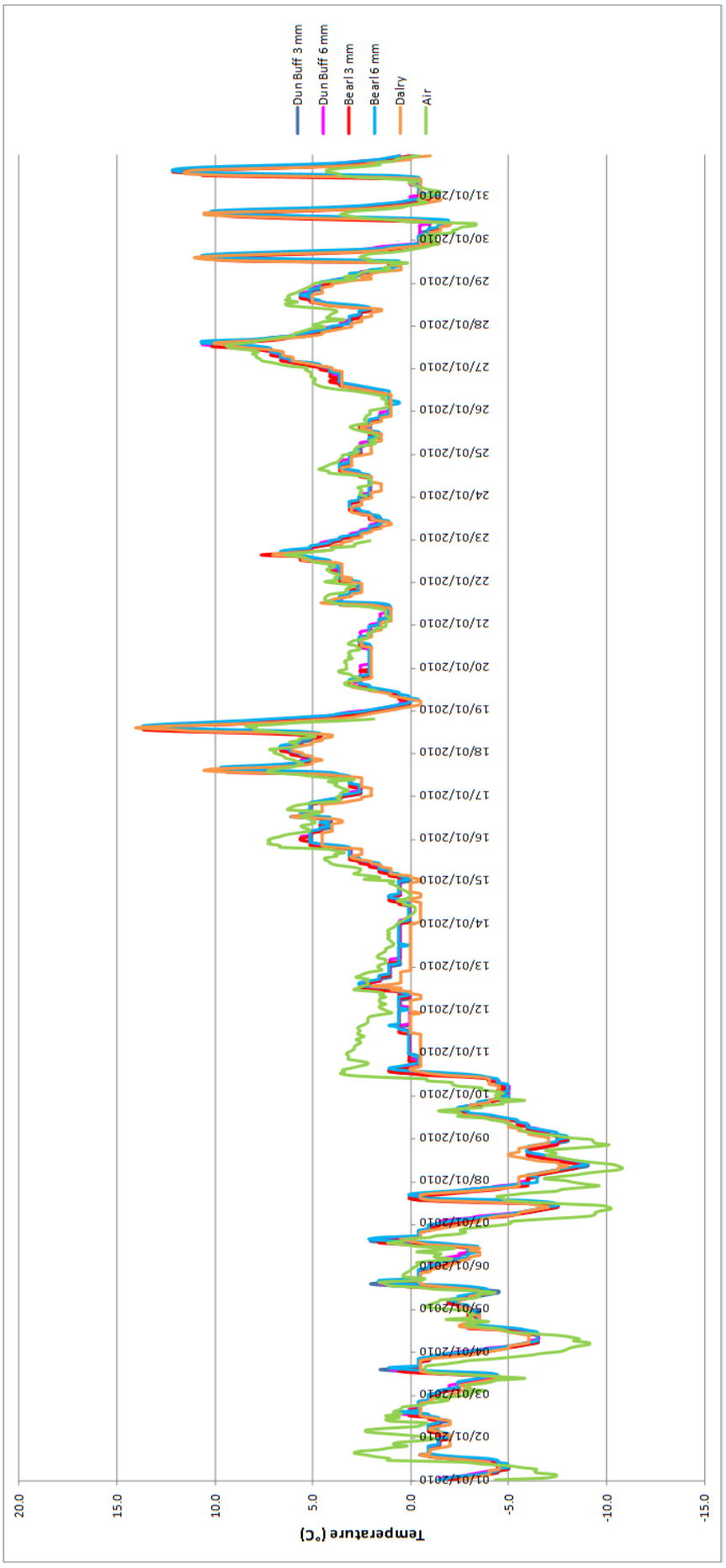

Figure 6-29: January 2010 internal and air temperature data.

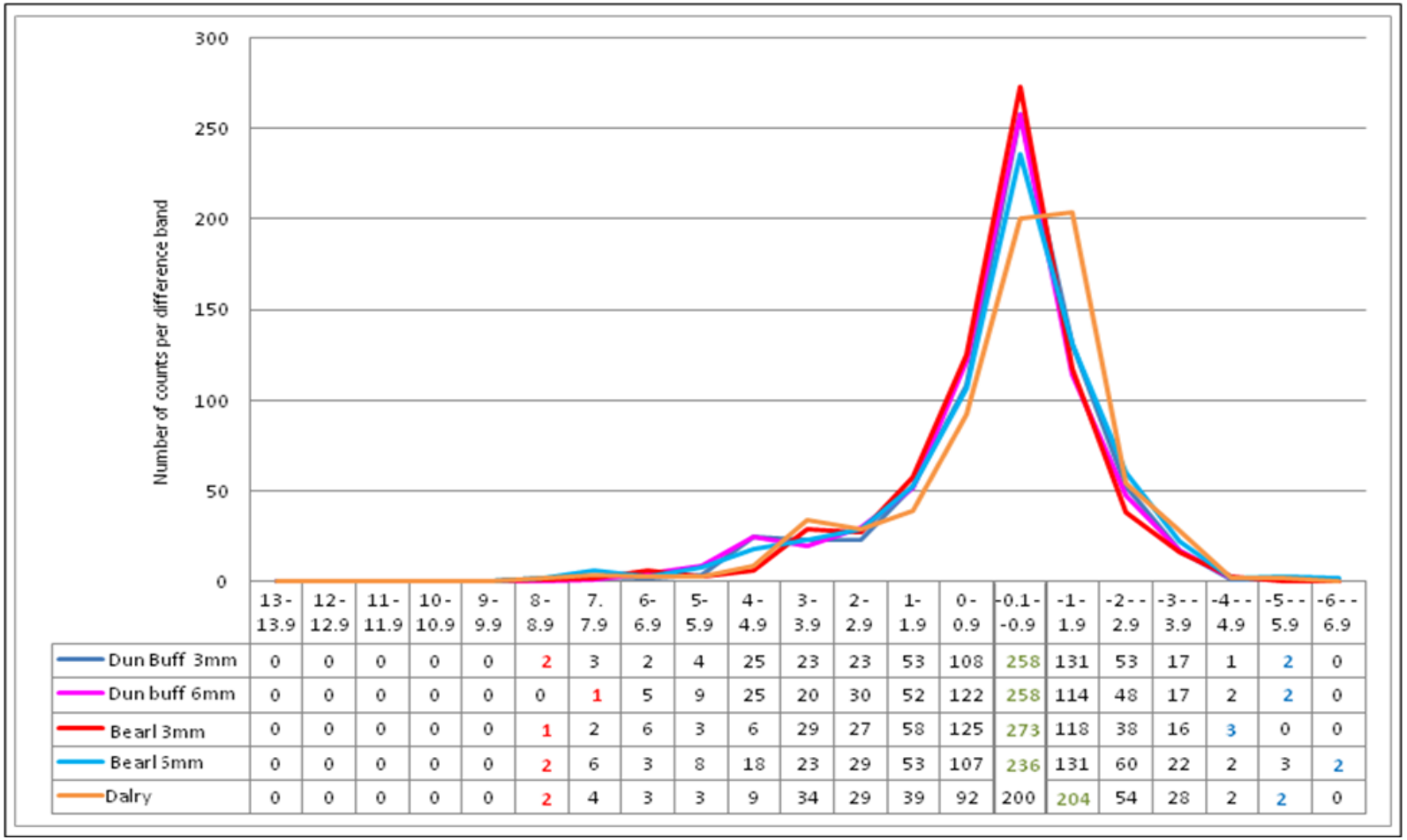

	13-13.9	12-12.9	11-11.9	10-10.9	9-9.9	8-8.9	7.7.9	6-6.9	5-5.9	4-4.9	3-3.9	2-2.9	1-1.9	0-0.9	-0.1--0.9	-1-1.9	-2--2.9	-3--3.9	-4--4.9	-5--5.9	-6--6.9
Dun Buff 3mm	0	0	0	0	0	2	3	2	4	25	23	23	53	108	258	131	53	17	1	2	0
Dun buff 6mm	0	0	0	0	0	0	1	5	9	25	20	30	52	122	258	114	48	17	2	2	0
Bearl 3mm	0	0	0	0	0	1	2	6	3	6	29	27	58	125	273	118	38	16	3	0	0
Bearl 5mm	0	0	0	0	0	2	6	3	8	18	23	29	53	107	236	131	60	22	2	3	2
Dalry	0	0	0	0	0	2	4	3	3	9	34	29	39	92	200	204	54	28	2	2	0

Figure 6-30: Difference graph between internal and air temperature for January 2010.

X-axis is temperature (°C), the table above states the values used to construct the graph. With the table. Red numbers indicate the maximum difference between the internal conditions compared to the air. Green numbers indicate the most common difference. Blue indicate the recording of the internal temperatures colder than the air temperature.

6.3.3.2 Relative Humidity

The January 2010 internal RH data (Figure 6-31) are consistent with the daily winter data. However, the air RH is more variable over the monthly scale compared to the daily scale. All internal sensors record RH measurements above 100%, when values are above 100% it has been suggested an error has occurred due to free water within the sandstone. The maximum and minimum RH recorded for air were 96% and 57% whilst the maximum values for all the sensors were greater than 100%, whilst the minimum RH was 93.7% within Dalry (Figure 6-31). Any variation seen internally does not appear to follow variations in the air.

As the internal sensors always record higher RH conditions than the external RH, there is no opportunity for internal “drying” to occur, i.e. times when the internal RH is lower than the air RH, so that evaporation of internal moisture may occur.

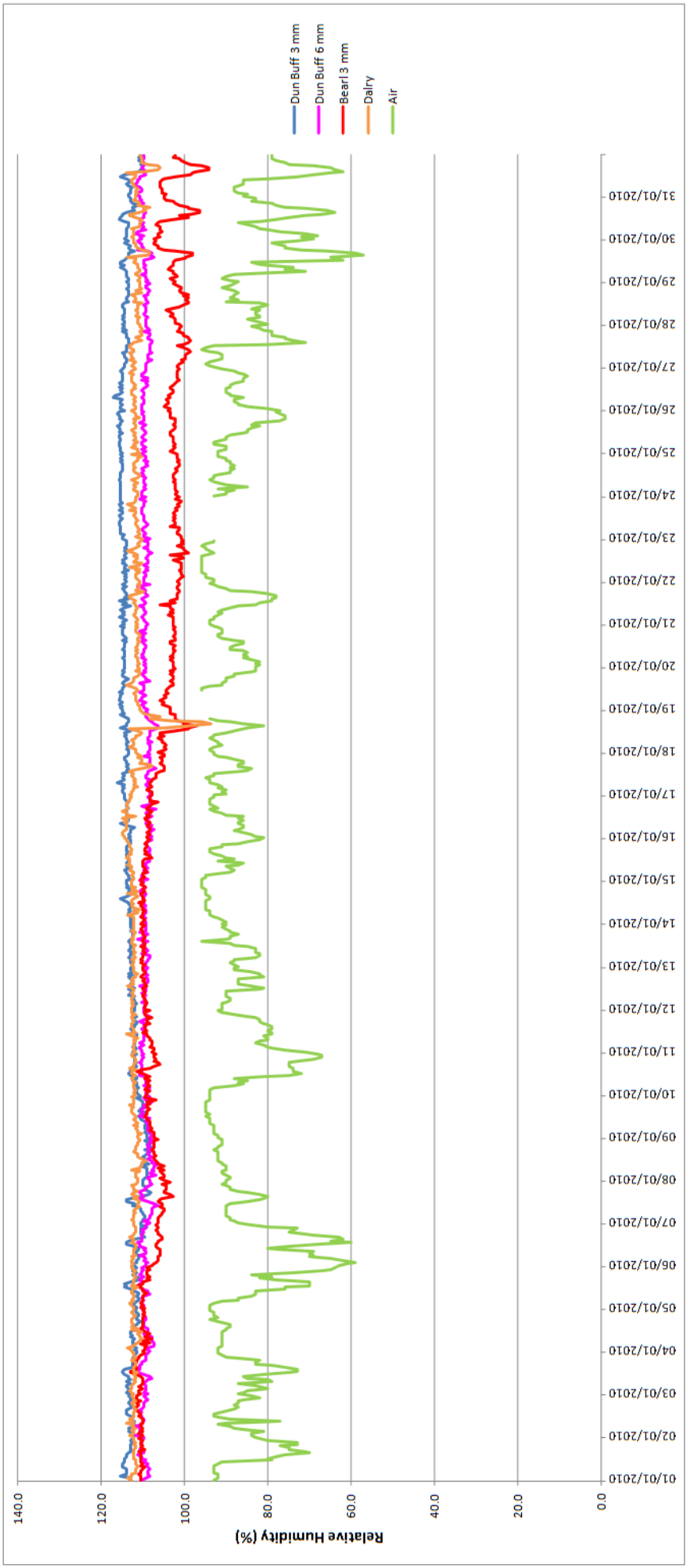

Figure 6-31: January 2010 internal and air RH data.

6.3.4 *IButton Observations "macro": Summer Cycle (July 09)*

6.3.4.1Temperature

July 2009 was examined to identify whether the summer daily cycle observed was representative of the monthly data. The IButton data shows that, during the day, the internal temperatures on all sensors surpass the air temperature by over 2°C on an almost daily basis (Figure 6-32). Then, during the evening and night hours in-stone temperatures fall to similar levels as the air (Figure 6-32). This is the same as the daily scale results. The air maximum and minimum temperatures were 28.3°C and 7.1°C whilst the internal maximum and minimum temperature were 40.1°C (Dalry) and 10.1°C (North).

To gain more information on how the air and internal temperatures are linked, the air temperature was subtracted from internal temperature and plotted on a frequency graph to show how often that difference between the environments occurs (Figure 6-32).

The difference in temperature ranges from the internal conditions being 18.9°C warmer than external temperature to internal temperatures being 4.9°C colder that external temperature (Figure 6-33). Therefore, the latter range of numbers will appear in the negative area of the graph and indicate that the air temperature is greater than the simultaneous internal temperature recorded.

The most frequent difference to occur is for the internal conditions to be 1 to 2.9°C warmer than external temperatures (Figure 6-33).

The temperature difference experienced between the sensors (i.e. at the different depths and within different sandstones) and external conditions are very similar (Figure 6-33).

The south facing blocks show that, internally, the sensors record warmer temperatures compared to the air temperature 95.5% of the time. Therefore, there is only a small percentage of time (4.5%) when it is colder internally compared to the air temperature. In comparison, the North block records more than double the time (11.2%) when it is

colder internally (Figure 6-33). This indicates that the North block is experiencing much less internal heating in comparison to the south facing blocks.

The Dalry block shows the largest differences between the internal and external conditions, where the internal conditions are up to 18°C warmer than the air which occurs four times (Figure 6-33). The Dalry block may be experiencing higher temperatures due to the darker crust on the surface and also due to the surface angle.

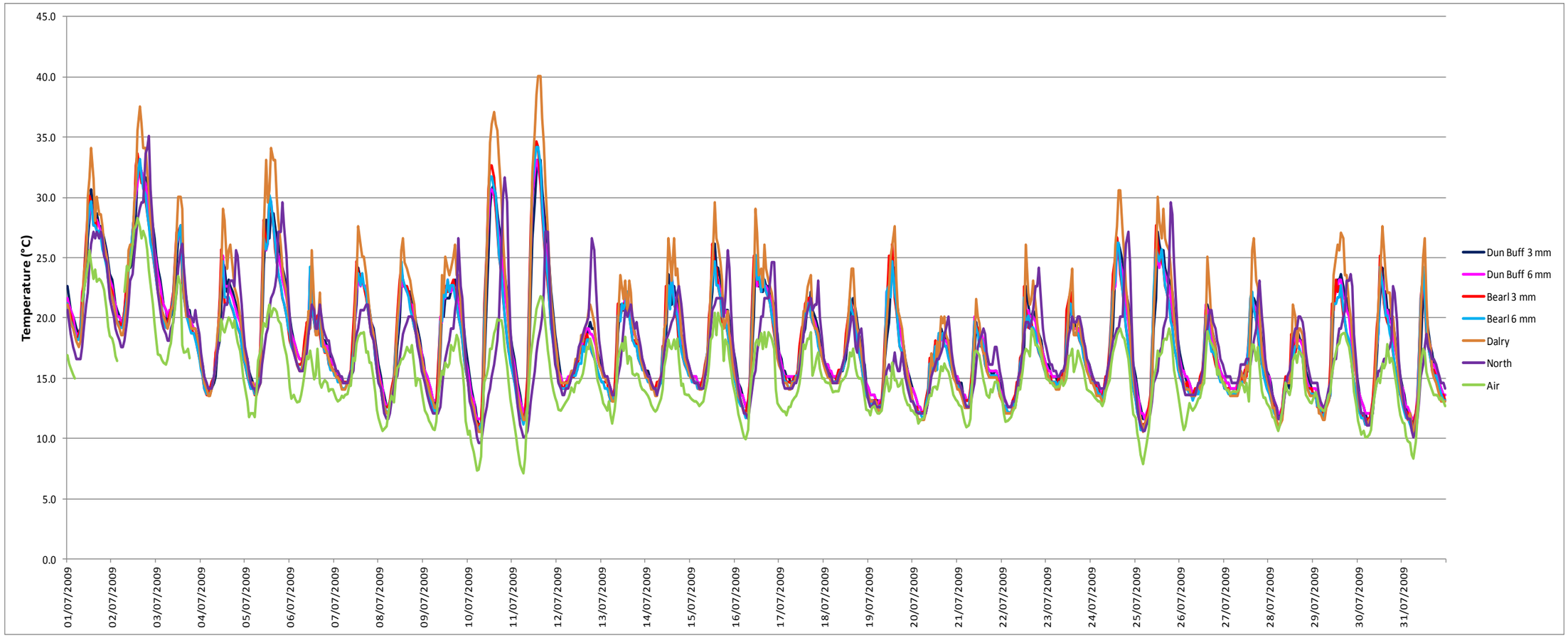

Figure 6-32: July 2009 internal and air temperature data.

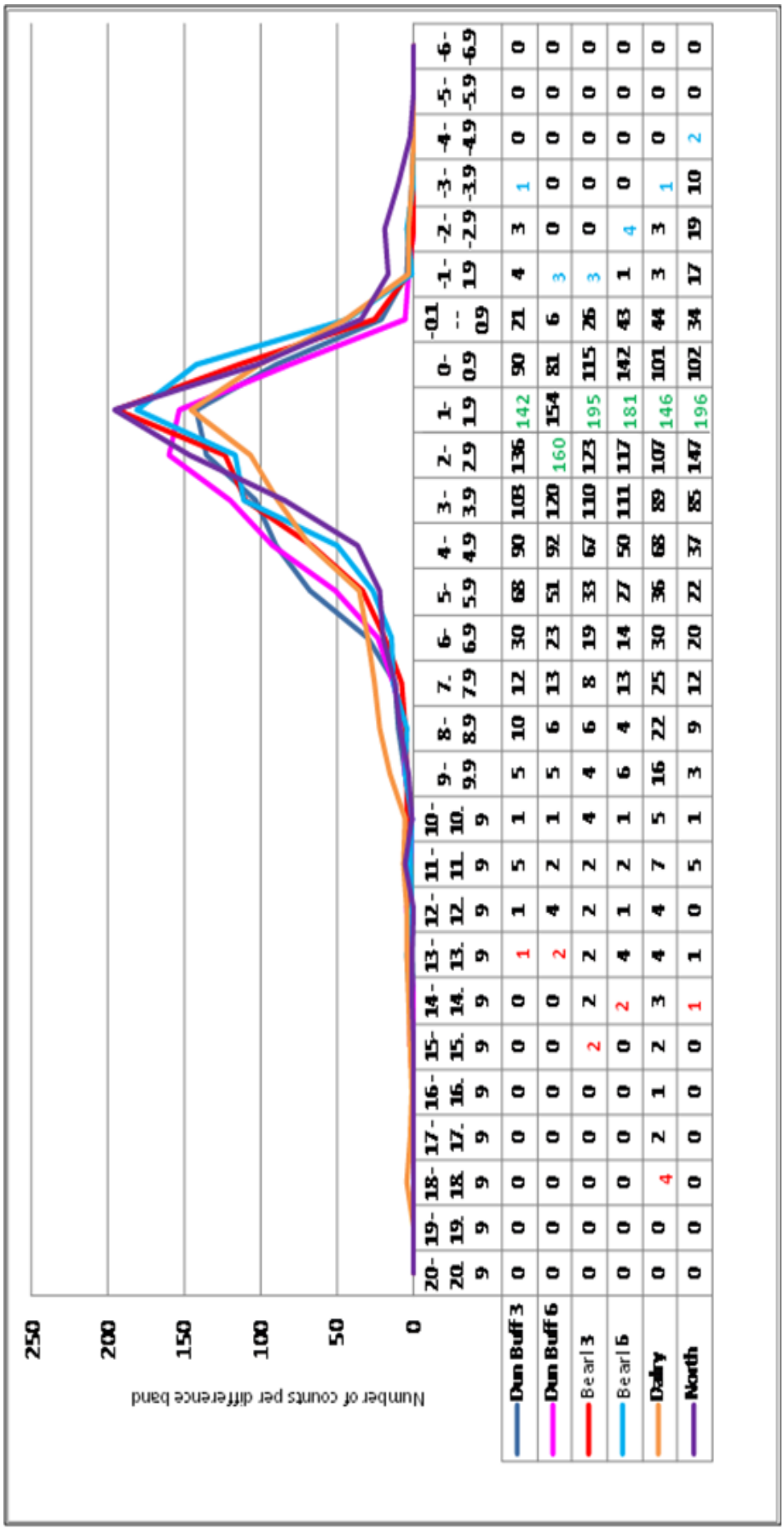

	20-20.9	19-19.9	18-18.9	17-17.9	16-16.9	15-15.9	14-14.9	13-13.9	12-12.9	11-11.9	10-10.9	9-9.9	8-8.9	7.-7.9	6-6.9	5-5.9	4-4.9	3-3.9	2-2.9	1-1.9	0-0.9	-01--09	-1--1.9	-2--2.9	-3--3.9	-4--4.9	-5--5.9	-6--6.9
Dun Buff 3	0	0	0	0	0	0	0	1	1	5	1	5	10	12	30	68	90	108	136	142	90	21	4	3	1	0	0	0
Dun Buff 6	0	0	0	0	0	0	0	2	4	2	1	5	6	13	23	51	92	120	160	154	81	6	3	0	0	0	0	0
Bear 3	0	0	0	0	0	2	2	2	2	2	4	4	6	8	19	33	67	110	123	195	115	26	3	0	0	0	0	0
Bear 6	0	0	0	0	0	0	2	4	1	2	1	6	4	13	14	27	50	111	117	181	142	43	1	4	0	0	0	0
Daisy	0	0	4	2	1	2	3	4	4	7	5	16	22	25	30	36	68	89	107	146	101	44	3	3	1	0	0	0
North	0	0	0	0	0	0	1	1	0	5	1	3	9	12	20	22	37	85	147	196	102	34	17	19	10	2	0	0

Figure 6-33: Difference graph between internal and air temperature for July 2009.

X-axis is RH (%), the table above states the values used to construct the graph. With the table. Red numbers indicate the maximum difference between the internal conditions compared to the air. Green numbers indicate the most common difference. Blue indicate the recording of the internal temperatures colder than the air temperature.

6.3.4.2 Relative Humidity

During July 2009, RH is more erratic than the single day results had suggested (Figure 6-34). The internal and air RH data are highly variable and internal conditions replicate external conditions. Of the south facing blocks, Dalry generally experiences the highest internal RH conditions throughout the month (Figure 6-34). The maximum and minimum air RH was 95% and 44%, whilst maximum and minimum for internal were 108.4% (Dalry) and 32.1% (Dunhouse Buff 3 mm).

To gain more information on how the air and internal RH are linked, the air RH was subtracted from internal RH and plotted on a frequency graph to show how often that particular difference between the environments occurs during the month (Figure 6-35).

The difference in RH ranges from the internal conditions being 59% higher than external RH to internal RH being 29% lower than that of the external RH. Therefore, when the internal is lower than the air, it will appear in the negative area of the graph.

The most frequent difference for the south facing sandstones ranges between being 19% higher than air conditions to 9% lower than the external RH conditions. The North block most frequent difference is between 1% - 29% lower, than the external RH conditions (Figure 6-35). The North block result indicates that it has less moisture trapped internally compared to the south sandstone.

The trends seen between Dunhouse Buff and Bearl blocks are quite different. When the differences between the internal and air RH are examined, it can be seen that, in Dunhouse Buff, a large proportion of the difference counts are located around zero in comparison to Bearl (Figure 6-35). The high proportion of difference counts located in this region, indicates that the Dunhouse Buff internal conditions are more closely related to the external environment. In addition, the Dunhouse Buff block shows many more of the internal RH conditions to be lower than the air conditions, with 44.1% of the time accounting for the internal RH being lower than external RH. This is 4 times more than in the Bearl block, where only 9.55% of the time accounts for the internal conditions being

lower than that of the air RH. The large percentage of time when the Dunhouse Buff block records lower RH compared to the air indicates that the blocks may experience more internal drying compared to the Bearl sandstone.

However, both these blocks record significantly lower internal conditions compared to the Dalry block. During the month Dalry only records 2.1% of the time when internal conditions are lower than the external RH. Therefore almost always records higher internal RH compared to air RH.

The North block, which records the most negative values (64.6%), shows that it experiences the most time when perhaps drying can occur, because internally it has a lower RH in comparison to external conditions.

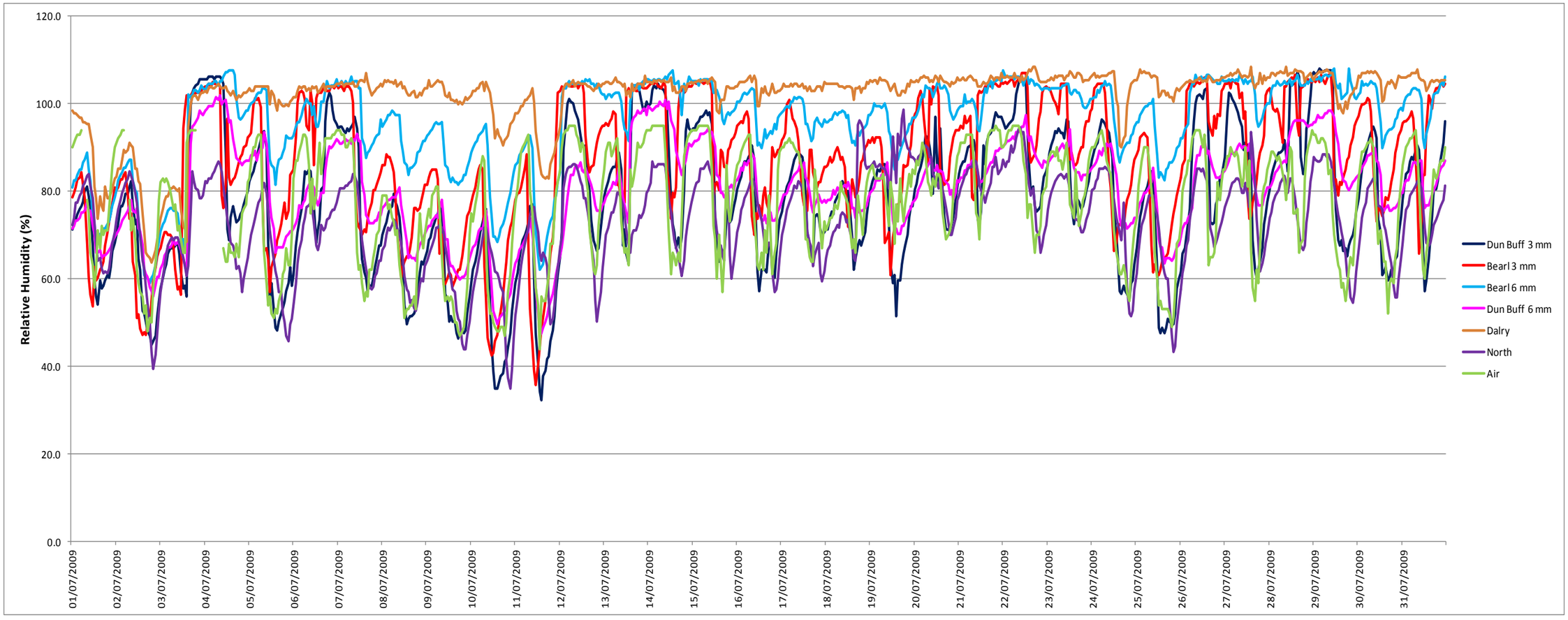

Figure 6-34: July 2009 internal and air RH data.

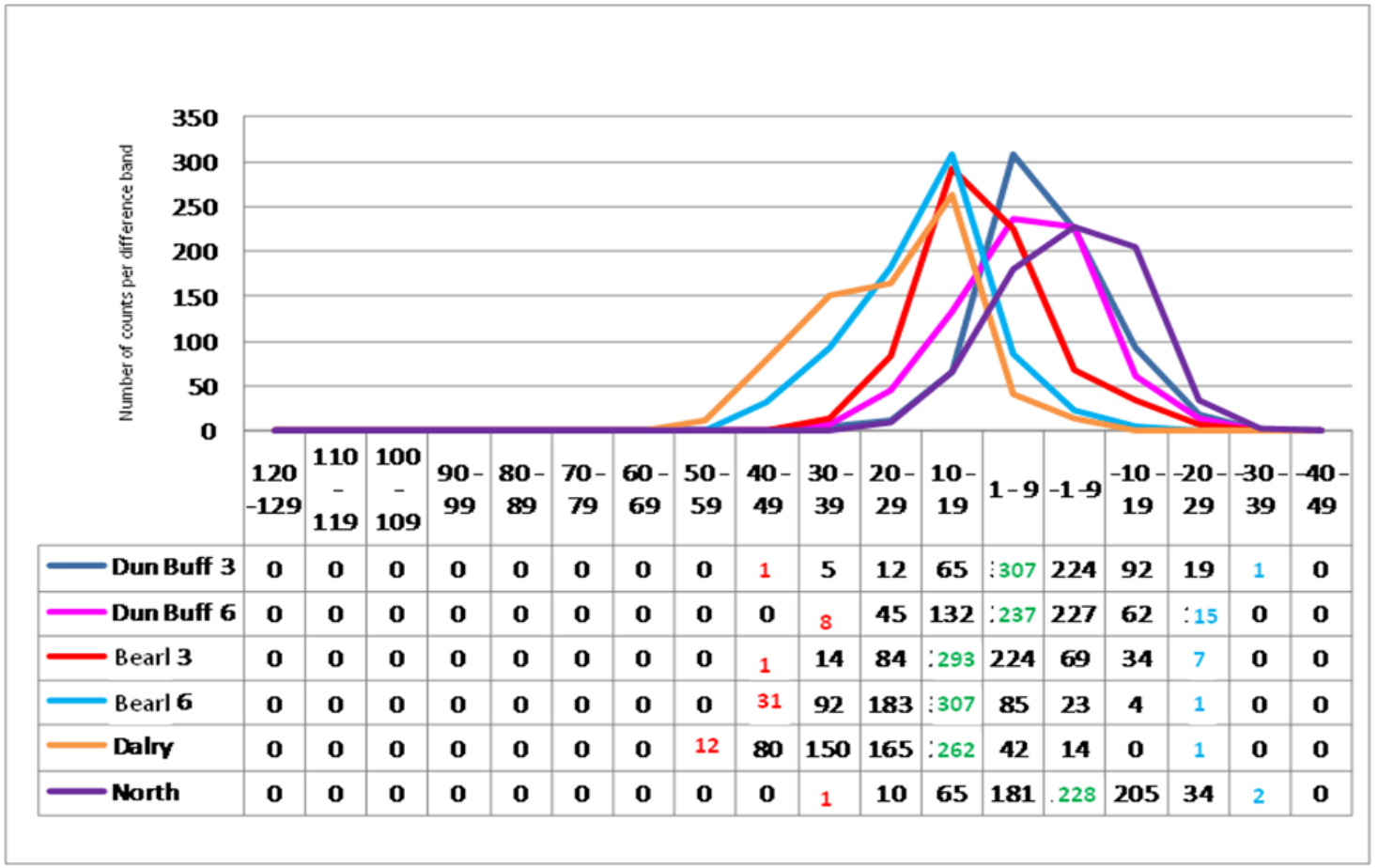

	120 -129	110 - 119	100 - 109	90 - 99	80 - 89	70 - 79	60 - 69	50 - 59	40 - 49	30 - 39	20 - 29	10 - 19	1 - 9	-1 -9	-10 - 19	-20 - 29	-30 - -39	-40 - -49
Dun Buff 3	0	0	0	0	0	0	0	0	1	5	12	65	307	224	92	19	1	0
Dun Buff 6	0	0	0	0	0	0	0	0	0	8	45	132	237	227	62	15	0	0
Bearl 3	0	0	0	0	0	0	0	0	1	14	84	293	224	69	34	7	0	0
Bearl 6	0	0	0	0	0	0	0	0	31	92	183	307	85	23	4	1	0	0
Dalry	0	0	0	0	0	0	0	12	80	150	165	262	42	14	0	1	0	0
North	0	0	0	0	0	0	0	0	0	1	10	65	181	228	205	34	2	0

Figure 6-35: Difference graph between internal and air RH for July 2009.

X-axis is temperature (°C), the table above states the values used to construct the graph. With the table. Red numbers indicate the maximum difference between the internal conditions compared to the air. Green numbers indicate the most common difference. Blue indicate the recording of the internal temperatures colder than the air temperature.

6.3.5 *Discussion*

The “micro” and “macro” data show that the relationship between internal and external temperature and RH is complex and varies on both a daily and seasonally scale. The full extent of these variations are reviewed and discussed below.

6.3.5.1Temperature Summary

The key observations for the data throughout January were that: 1) internal temperatures were similar in each sandstone observed; 2) internal temperatures closely followed the air temperatures throughout both day and night, leading to a narrow range of differences; 3) the 3 mm and 6 mm deep sensors show no significant differences in the temperatures they recorded. Therefore, little internal heating is occurring within the sandstones, and this is the case for all the south facing blocks. However, when air temperature is extremely cold, the sandstone remains internally warmer than air.

During July 2009 the key trends are that: 1) Dunhouse Buff, Bearl and the Dalry blocks exhibit notably higher internal temperatures in comparison to the surrounding air temperature during the day, producing a large range of differences; 2) during the evening internal temperatures fall and follow the air temperature closely; 3) the 3 mm and 6 mm deep sensors record similar temperatures; 4) Dalry internally heats up the most and exhibits the largest temperature differences, compared to Dunhouse Buff and Bearl. This internal heating during daytime causes a wide range of differences to occur between the internal and external data. The North block does warm up internally but not to the same extent as the south facing blocks.

After analysis of all the data recorded during the experiments (June 2008 to March 2010), two defined “seasons” of sandstones internal microenvironments, based on temperature cycles could be identified. The “summer” cycle between May and September and the “winter” cycle between October and March (all data sets can be found on the electronic appendix). These were based on the key trends observed, outlined above. April and September are cross-over months and can be defined as either summer or winter dependant on the external weather conditions. Jenkins and Smith (1990) alluded to

varying winter and summer weathering regimes, but did not allocate specific months to these seasons and failed to detail how they differ.

The thermal imaging data provided information on the temperature of the outermost surface of the blocks and show that the surface can have an erratic rise and change in temperature throughout the day, whereas the internal temperature rises and changes at a steadier rate. These erratic surface temperatures may be due to weather events such as gusts of wind cooling the surface, or periods of cloud cover causing momentary shading, as the level of direct solar radiation is reduced (Jenkins and Smith, 1990; Smith et al., 2008b). However, results indicate that these short periods of loss of direct sunshine do not penetrate to deeper levels, which is in agreement with Jenkins and Smith (1990) who state that short duration temperature fluctuations are restricted to a thin layer at the surface, which these results show to be <3 mm.

In order to investigate solar heating further, the colour of the sandstones was tested using a Konica Minolta CR-400 chromo meter, which produced colour results on the Hunters lab colour space scale L* *a** *b**. The L* data measures the brightness level on a scale of 0% (black) to 100% (white). The *a** values run from green to magenta, where negative values signify green while positive values specify magenta, whilst *b** indicates blues and yellows, where negative values indicate blue and positive values equate to yellow. An average of 30 measurements were taken over the surface of the blocks and the mean values and standard deviation are listed in Table 6-3.

Table 6-3: Colour of sandstone blocks using Hunters lab colour space scale, including SD.

Block	L*	*a**	*b**
Dunhouse Buff	53.73 ± 3.87	6.48 ± 0.58	26.26 ± 1.28
Bearl	61.12 ± 7.47	4.12 ± 1.35	20.49 ± 3.10
Dalry	40.22 ± 2.23	0.30 ± 0.59	11.20 ± 0.89

These results indicate that Bearl is the lightest coloured sandstone whilst Dalry is much darker with the lowest L* value (due to this being a previously weathered sandstone, having a well formed black crust). As all *a** values are positive the sandstone blocks are redder in colouration with Dunhouse Buff containing the largest proportion of red and Dalry has almost no red or green pigment (Table 6-3). The results of the *b** also show that Dunhouse Buff and Bearl have a significant yellow proportion providing the buff colouration (Table 6-3).

These colours are then directly proportional to the albedo of the sandstone. The dark crust of the Dalry sandstone absorbs a greater percentage of light wavelengths, giving it a low albedo. This light energy is then transformed into longer wavelengths, which equates to lower energy infrared heat. As the Dunhouse Buff and Bearl sandstone have a lighter colouration they therefore have a higher albedo, meaning a smaller percentage of wavelengths are absorbed and therefore less heat can be produced.

Although many people use this theory to state that the dark rocks will heat up more than light coloured rocks (Small, 1972; Ahnert, 1998; Bland and Rolls, 1998) these are all assumptions with no evidence. A few studies have recorded field evidence of darker rocks having higher surface temperatures (Kelly and Zumberge, 1961; André, 1992), however, these studies contain significant variability between exposures used and physical properties of the samples. Using advanced dataloggers and concrete blocks within one environment, Hall et al. (2005) investigated the link between colour and heat. Hall et al. (2005) applied paint with varying reflectance properties to concrete blocks and monitored surface temperatures. They found that in general the black block is warmer than the white block but, in some exceptional circumstances, this is not true. When the block's temperatures were equal to or cooler than air temperature, then the black surface recorded the coolest temperatures. However, as stated, this is only on the surface and does not explain how coloration may affect the deeper internal temperatures which this study has predominantly been monitoring.

The idea that dark coloured rocks heat up more at the surface, and that heat can be transmitted to depth to a greater extent than light coloured rocks, can be said to be true for these result during summer, as the Dalry block is generally hotter at depth than the Dunhouse Buff and Bearl sandstones. However, during the winter, the Dalry sandstone had a very similar internal temperature to those recorded within Dunhouse Buff and Bearl. Therefore, a second factor is controlling how much heating can take place and affecting the sandstone this may be the amount of solar radiation available.

The average solar radiation recorded in January 2010 was 39.8 W/m^2 whilst the maximum was 283.1 W/m^2; this is much lower than the 2009 July average of 197.4 W/m^2 and maximum of 1073.0 W/m^2. This difference in available solar radiation is why during the summer data shows considerably higher internal heating occurring on the south facing

blocks compared to the winter months. As the sun never directly illuminates the North block at any point within the year, much less internal heating takes place as it is only the ambient air temperature which is going to affect the surface and internal heat of the sandstone.

Therefore, the two factors controlling the internal heating of these sandstones are the amount of solar radiation available and the colour of the surface (which directly relates to its albedo). Peel (1974) and Kerr et al. (1984a) suggested that thermal conductivity will affect the amount of heating which can occur. However, as the mineralogy and porosity of these sandstones is similar (see chapter 4), thermal conductivity will probably only act as a minimal factor between each of the sandstones studied.

Previous studies on internal heating of sandstone outlined in section 1.2.7 are difficult to correlate with the results gathered in these experiments, as often they are oven based tests or have been conducted in a climate and latitudes unlike that of Scotland, such as Morocco (Kerr et al., 1884a) or Death Valley (Warke and Smith, 1999). However, these studies may help to provide an insight on how temperature regimes may change with the warming Scottish climate.

6.3.5.2 Relative Humidity Summary

The key trends for RH during January 2010 are: 1) Dunhouse Buff, Bearl and Dalry blocks all record internal RH values that are notably higher than the ambient air RH; 2) that this trend is prevalent throughout the whole month, producing a very narrow range of differences; 3) the largest differences between internal and external RH are caused by a lowering of the external RH (rather than a change to internal conditions); 4) the Dalry block continually records the highest values. Glasgow's average RH during January 2010 was 86% RH and ranged between 100% and 56%. The averages recorded by the internal sensors were all above 100%; this high RH within the sandstone suggests the presence of liquid water during the entire month. Throughout January 2010, the RH internally was never lower than the external conditions and, therefore, no periods occurred when potential internal moisture loss could take place. This is due to the already present high RH for air in the Glasgow region in the winter giving the sandstone no opportunity to lower its internal moisture content.

The key trends for RH during July are: 1) within all the sandstones RH is highly variable, reflecting the high variability of external conditions; 2) Dalry, in general, has the highest RH. Dunhouse Buff records the lowest humidity loss internally at both its 3 mm and 6 mm sensors. Of the sensors at 3 mm depth, Dunhouse Buff records the most internal RH below that of the air and, of the 6 mm depth sensors, Dunhouse Buff again records the most internal RH below that of air. The average air RH during July 2009 was 74%, although it ranged between 96% and 43%. During the summer, there is a larger proportion of time where the internal sensor records a lower RH than air (in comparison to the winter), which indicates periods when internal drying may be occurring. There is a larger range of RH at 3 mm in comparison to the 6 mm sensors, illustrated schematically in Figure 6-36.

The discussed months above were then compared to all the other data recorded (June 2008- March 2010) and two internal microclimate cycles have been identified based on these RH trends. These are a summer cycle during May to late August and a winter cycle between September and April (full data set can be found on electronic appendix), which were deduced from the above characteristics for January and July.

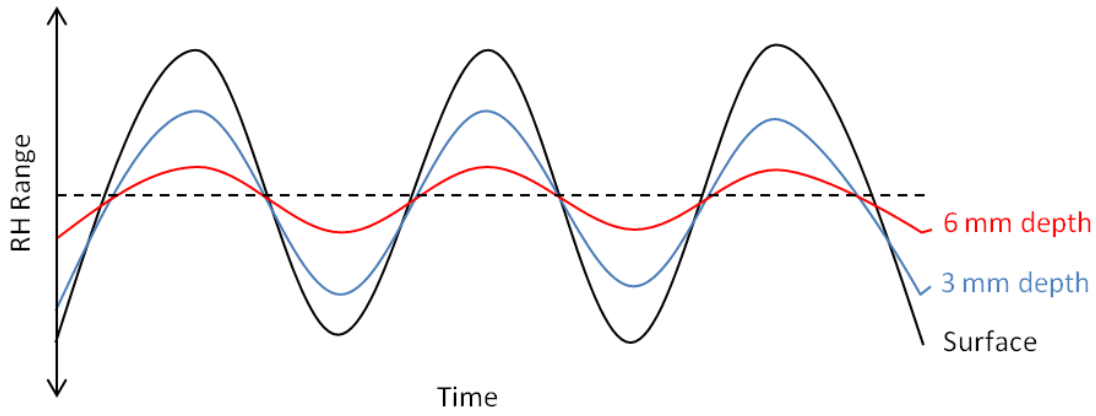

Figure 6-36: Schematic diagram of the range or variations experienced at different depths within sandstones.

These internal RH cycles are completely dictated by the external conditions. The RH within Glasgow during the winter is very high, limiting any internal moisture loss. However, the lower ambient RH, which occurs for longer periods of time throughout summer, allows periods where significant loss of moisture can occur.

The Dalry data show that, internally, it retains the highest RH values throughout the year. This suggests that the black crust may be acting as a barrier for the evaporation of water whilst still allowing inward penetration of water. It also may be a product of being situated on the concrete ground.

The North block records the most time when internal RH is lower than the external conditions, which may be due to the block receiving lower amounts of rainfall on its surface in comparison to the south blocks.

When internal datalogging of building stone has been undertaken by previous studies, most only focus on the internal temperature rather than also monitoring the internal RH of sandstone. This is because, in the past, the technology has not been adequate to quantify RH rather than liquid water and, therefore, only the internal temperature has been considered.

When both the temperature and RH cycles are combined, their timings correlate well. The cycles include the summer cycle (May to late August), which is characterised by all the internal sensors recording higher day time temperatures compared to air temperature, with a maximum difference of 15.3°C. The RH during summer is erratic within these months and internal moisture loss will occur, as internal RH drops below external RH frequently. The winter cycle (September to April) is recognized by internal temperatures closely following the air temperatures and only diverging to either side of it by a few degrees (average difference is 0.1°C). The internal RH is higher than the air RH but, during the winter cycle, there are minimal “drying events”, and the range in differences is much smaller (maximum range 35.4).

6.4 Internal Monitoring Results: Part 2

The IButton dataloggers were used to measure RH within sandstone, although the values obtained frequently surpassed 100% RH in summer and for prolonged periods of time in winter. This indicates an error with the measurements as RH cannot exceed 100%. The manufacturers (Maxima) of the IButtons state that they should be accurate to ±5% RH and work between 0 - 100% RH. These errors, as suggested previously, may be caused by free water within the sandstone block. To test this theory, Decagon leaf wetness sensor

(LWS) were enclosed in a block of Blaxter sandstone (quartz = 70%, porosity = 12%) at a depth of 6 mm as detailed in section 2.1.11. Blaxter sandstone was chosen due to its similar properties to Dunhouse Buff (quartz = 70%, porosity = 14%), where RH was recorded above 100%. As the LWS were originally designed to be used in the open air, a new calibration for their use in sandstone was undertaken, as outlined in section 2.1.10. The LWS only records free water on the surface of the sensor and will therefore confirm whether or not water is present within the sandstone at 6 mm and is therefore causing errors in the IButton data. One LWS (LWS-INT) sensor was embedded into the block whilst the other was placed in open air (LWS-EXT) next to the block facing the same direction, so that direct comparisons could be made between internal and external data gathered by the loggers. After an initial two week trial period, the sandstone block was placed outside with sensors facing south for a four month period from the 30/04/2010 – 17/08/2010.

6.4.1 *Leaf Wetness Sensor Results*

The LWS works by measuring the dielectric constant on the top of the sensor. The sensor then outputs a mV signal proportional to the dielectric of the sensor area and therefore proportional to the amount of water on the surface.

The LWS-INT was calibrated in sand of different moisture contents as described in section 2.1.10. The calibration profile is shown in Figure 6-37, and this graph was then used to convert the raw data counts recorded by the LWS-INT within the Blaxter sandstone and has a R^2 value of 0.95. However, once converted, the baseline data were found to be consistently 15 ml high, even when first embedded into the dried block and sand. For this reason, 15 was subtracted from the converted data to correct for this offset and then divided by the leaf meter area (30.3 cm^2) to produce a recording in ml/cm^2. As LWS-EXT was being used in the same format as originally designed for (open to the air), Equation 5 was used to convert the raw data into ml/cm^2, this formula was provided by the manufacturer Decagon Devices, and the conversion has an R^2 value of 0.97.

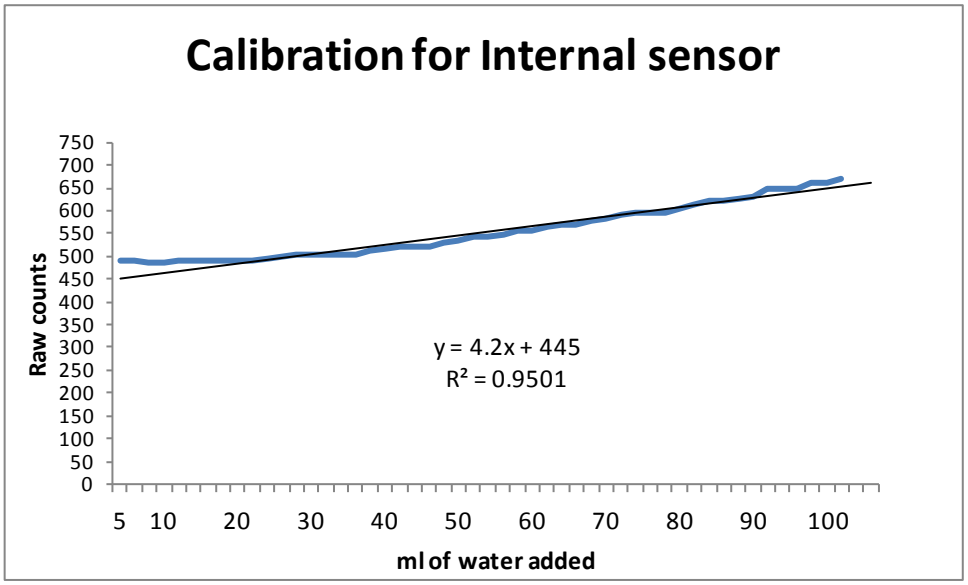

Figure 6-37: Calibration plot for LWS-INT.

$$\frac{(0.004 \times raw\ data) - 20.9}{1000} = ml/cm^2$$

Equation 5: Calibration equation for LWS-EXT

These data are presented in Figure 6-38A and show that the LWS-INT is sensitive to external conditions, recording many of the rain showers detected by the external sensor and the LWS-INT frequently returns to 0 ml/cm^2 between showers. However, between the 25/06/2010 – 23/07/2010, rain fall was frequent and heavy with only small intervals between showers. During this time period, the internal base line increased for LWS-INT to 0.004 ml/cm^2 (Figure 6-38A). This was perhaps because less time was available for evaporation to occur due to the external conditions and therefore the sandstone contained residual moisture throughout the period. However, for long periods of time the internal sensor remained dry despite external rain showers occurring; 10 and 12 dry day periods, are recorded between 21/05/2010 – 31/05/2010 and 14/06/2010 – 26/06/2010 (Figure 6-38A).

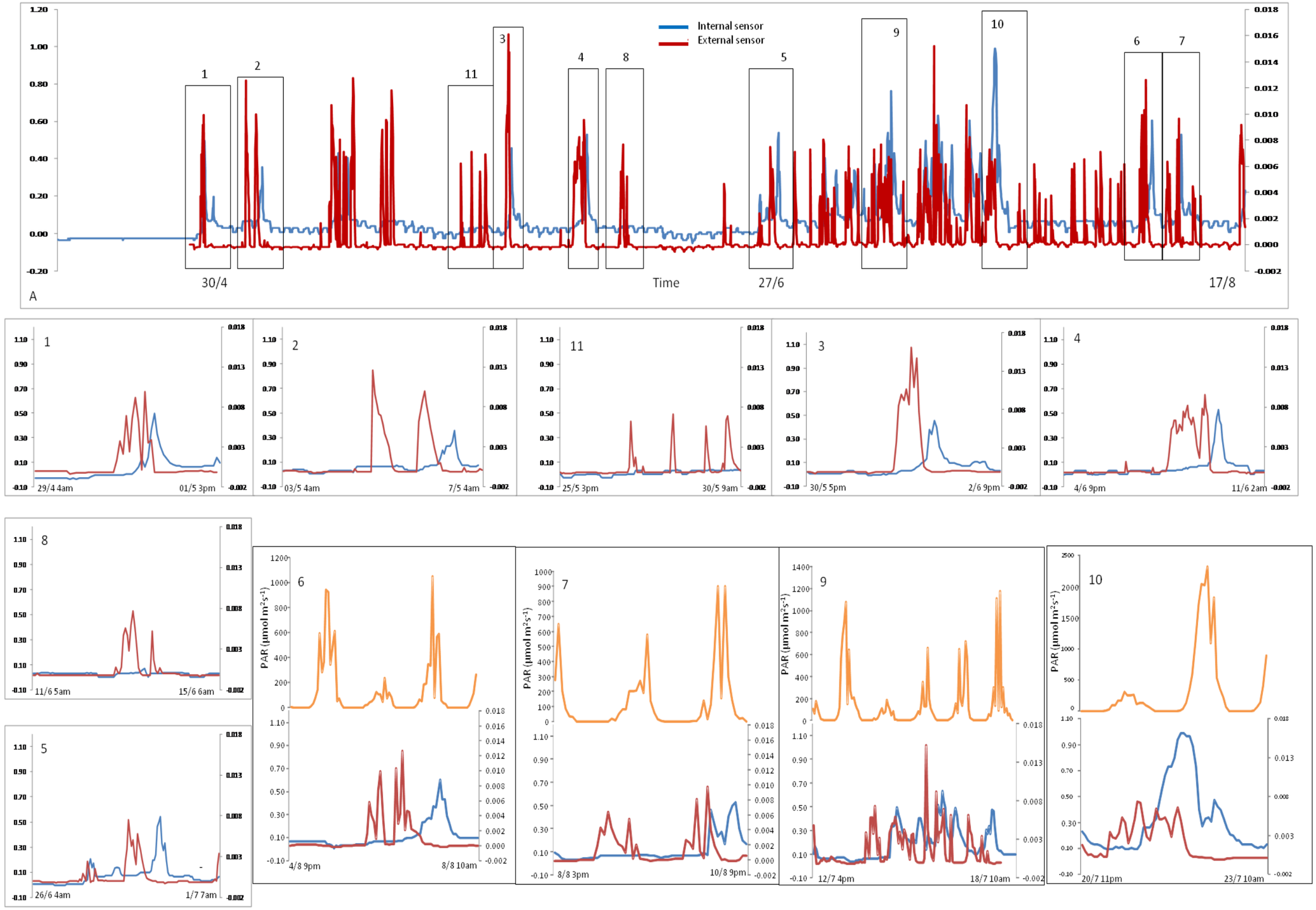

Figure 6-38: Leaf wetness sensor data.

A) The full data set collected. Graphs 1 to 11 represent areas of the large data set. Blue = internal sensor, red = external sensor, orange = PAR readings. LWS-INT on primary axis (ml/cm^2), LWS-EXT on secondary axis ml/cm^2. PAR is in µmol m^{-2}s^{-1}.

A series of 11 individual graphs were produced to highlight the finer details of the large plot (Figure 6-38 1-11). These time periods were chosen due to their relative isolation in relation to other rain showers, making characteristics of the events easier to identify. These individual graphs show four peak profiles sketched in Figure 6-39**.** The profiles of A and B are very similar, although A is a symmetrical profile where the leading edge of the peak is mirrored by the decreasing evaporation edge (Figure 6-39A); these can be seen in Figure 6-38.3, 4 and 5. Profile B differs in that the evaporation side of the peak is curved and a quicker initial decrease of liquid water occurs before the evaporation rate slows down (Figure 6-39B andFigure 6-38.1 and 7). These two peak profiles indicate a similar rate of transport of water to the stone interior but the evaporation rate differs. The C peak (Figure 6-39C) is characterised by having a long slow leading edge rising to the crest of the peak, before the water quickly dissipates (Figure 6-38.2 and 6). In this scenario, the absorption rates are much slower than rates of evaporation. The profile of peak D (Figure 6-39D) is only seen once within the data peaks observed, however its form is similar to that of the C shaped peaks, but has a bulbous curved crest rather than a sharp defined peak (Figure 6-38.10).

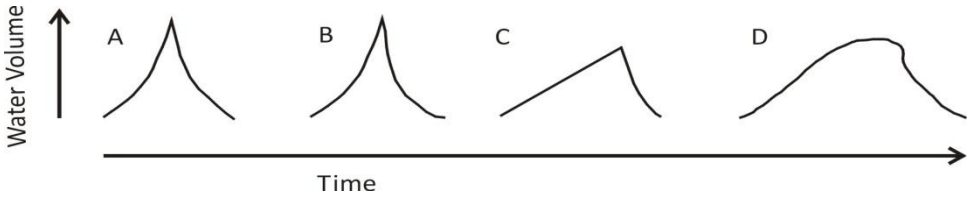

Figure 6-39: Sketch diagrams of LWS-INT peak profiles identified.

Key observations concerning the environmental conditions and the internal peak type are summarised in Table 6-4. It shows that, on occasions when LWS-INT produces A and B shaped peaks (Figure 6-38.1-5 and 7), the lag time between maximum LWS-EXT and maximum LWS-INT recordings are highly variable, ranging from 6 – 20 hours. For the five profiles within this category, two groupings emerge. The first, with a very short lag time of 6-7 hours, and the second, with a very long lag time between 20-22 hours, no obvious reasons are identified for this difference. Of this set, only Figure 6-38.7 has any pyrometer data associated with it and shows sunshine whilst absorption is taking place and darkness during the evaporation leg. The timings of the evaporation and absorption leg were analysed for the rest of the set and they follow the same pattern: absorption = daytime, evaporation = night time. The C and D shaped peaks have a good correlation of 15 hours between maximum LWS-EXT to maximum LWS-INT readings. Solar radiation data are known for Figure 6-38.10 (D peak). The shallow leading edge is in darkness and when the sun begins

to shine the water quickly begins to evaporate giving a drop in the internal water levels. This is not true for the C shaped peaks where the solar radiation information is compatible with the A and B peak formation. These results are summarised in Figure 6-40.

Figure 6-40: Sketch summaries of when the peaks are in daylight and when they are in darkness.

Orange) daylight, dark blue) night time.

Situations also occur where no significant internal peak in water measured occurs, even though external rain is recorded (Figure 6-38.8 and 11). The data in Figure 6-38.8 occurred when very light rain fall ensued over an 11 hours period of time, although Figure 6-38.11 does not follow this pattern. However, these events both occur after a significant dry period (Figure 6-38A). The lack of an internal peak may be caused by a combination of factors such as the rain intensity and volume being too insignificant to penetrate inwards, or evaporation was high at the time, thereby limiting water ingress.

Table 6-4: Table of key observations linked to Figure 6-38 graphs.

Graph	Peak Profile	Length of rair shower (Hours)	Total rainfall (ml)	Lag between ma internal and max external reading (Hours)	Av Temp (°C) during shower	Wind Max[A] Av[B] Av Dir	Sunshine Info
1	B	10	2	7	9	7[A] 2[B] WSW	No
2	C	5	3.75	19	9.7	2[A] 0.09[B] E	No
3	A	14	7.51	6	11	5[A] 0.7[B] SE/SSW	No
4	A	29	11.25	22	11.6	4[A] 1[B] Variable	No
5	A	9	8.29	20	13.8	3[A] 0.2[B] WSW	No
6	C	Over 15h 2 ra events 4 &2	6.78	15	14.7	4[A] 0.5[B] SW	Yes
7	B	9	12.88	7	11.9	5[A] 0.4[B] S	Yes
8	---	11	3	---	10.0		---
9	A and B						
10	D	24	21.9	15	13.4	3[A] 0.1[B] NW	Yes
11	---	5	5.28	---	8.9		---

Where dashed lines appear (--) it denotes not relevant.

To gain further information on the absorption and loss of each peak, these were examined individually.

6.4.2 *Evaporation*

The maximum volume of water detected internally on the LWS-INT is 0.9 ml/cm^2 but the standard maximum is 0.5 ml/cm^2 (Figure 6-41). The majority of peaks (exceptions being 2 and 10) show that it takes 6 to 7 hours for 0.5 ml/cm^2 to dissipate, which means an average of 0.08 millilitres per hour (ml/hr) evaporates. Peak 2 has a rate of 0.06 ml/hr and peak 10 has a rate of 0.05 ml/hr (Figure 6-41). The slow evaporation speed shown by peak 10 may be linked to the fact that it was recorded during a particularly wet period with higher humidity than average for the month (87% compared to 81%). Hall et al.(2011) identified a large

seasonal trend between the potential evaporation (PE) during summer and winter where PE, is defined as the amount of evaporation that would occur if a sufficient water source were available. PE is generally much higher in summer rather than in winter (Figure 6-42), as the amount of PE is highly dependent on external conditions such as temperature, solar radiation and RH (Hall et al., 2011). Although the results from this study are only evaporation rates rather than PE rates, it can be assumed that the evaporation rates calculated are for summer months only. Therefore the evaporation rate in Glasgow during the summer is 0.08 ml/hr. Hall et al.(2011) show that, during winter, London has a lower PE compared to during the summer months (Figure 6-42) following this logic much less evaporation and PE will therefore also occur in Glasgow. In addition, regarding Glasgow, the PE may be even lower due to its higher latitude, reducing the amount of solar radiation further in comparison to London.

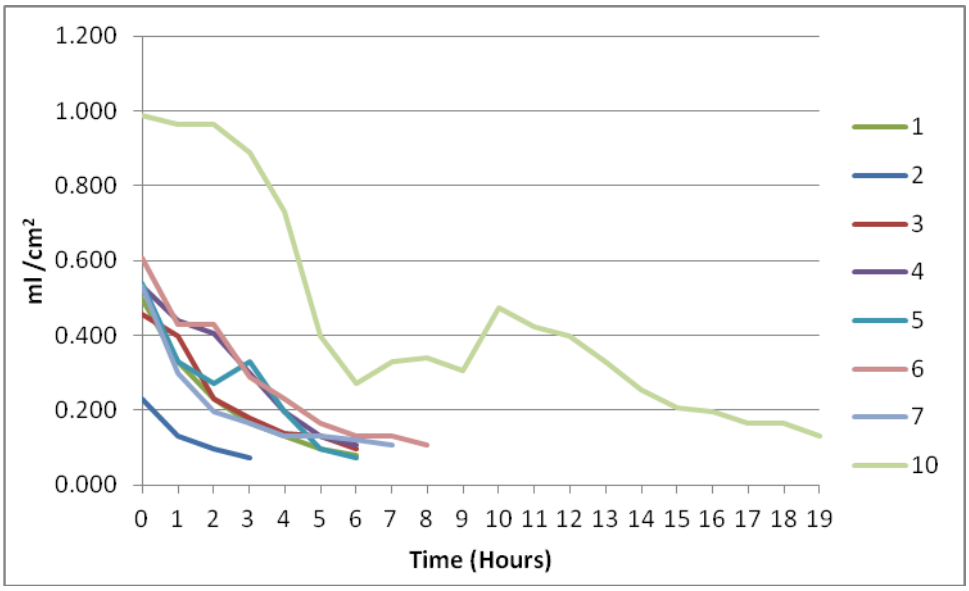

Figure 6-41: Evaporation leg of each peak identified in Figure 6-38. Each line goes from peak ml/cm^2 recording to base of 0.05 ml/cm^2.

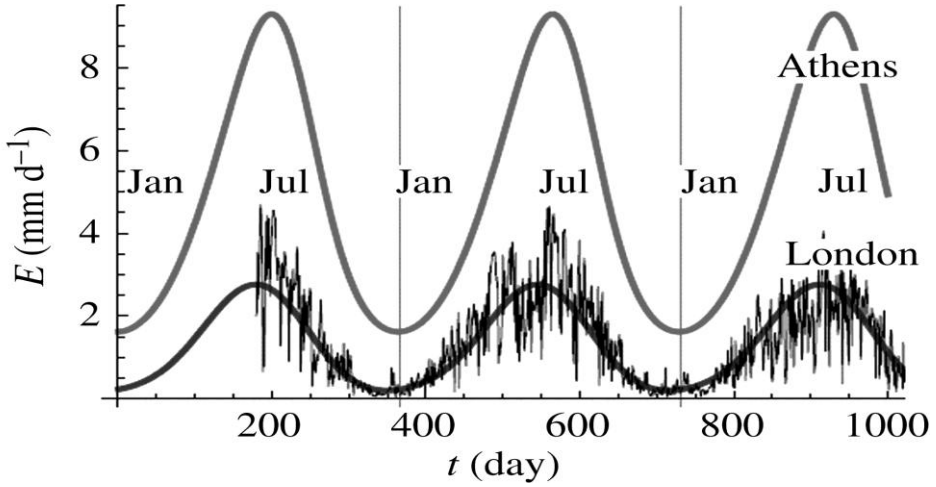

Figure 6-42: Daily potential evaporation graph.

Graph shows raw data for London and superimposed regression curve (solid line) for both London and Athens taken form Hall et al.(2011).

6.4.3 ***Absorption***

Results from the internal moisture sensors indicate that the maximum penetration of water to a depth of 6 mm can take a significant time after the start of rain, in some cases the rain has often stopped falling before any water is recorded at 6 mm depth.

The results from this study for rate of water penetration to depth are shown in Figure 6-43. The absorption values have a much greater range compared to the evaporation. Peak 5 and 6 have an absorption rate of 0.04 ml/hr whereas 1, 3, 4 and 10 have an average rate of 0.08 ml/hr, with peak 2 showing an absorption rate of 0.07 ml/hr. Peak 7 is an unknown as it starts at a higher baseline due to a large internal peak prior to absorption of peak 7 and, therefore, the baseline had not fully recovered (Figure 6-38.7). The data reveals that rate of water ingress is much more difficult to predict (compared to the loss of water), as no obvious differences in environmental conditions are observed.

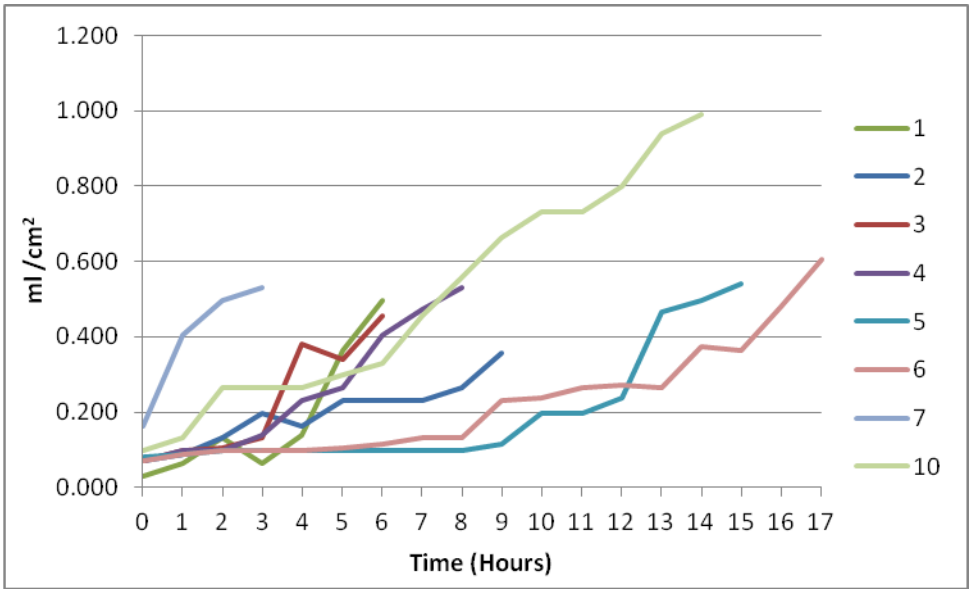

Figure 6-43: Absorption leg of each peak identified in Figure 6-38. Each line goes from base to maximum recording on the LWS-INT.

Many attempts have been made to understand how liquids are absorbed and flow through porous media (Hall, 1977; Gummerson et al., 1980; Wilson et al., 1995; Terheiden, 2008). This process of liquid absorption is complicated by many factors, in addition to the porosity and permeability of the material which also have to be taken into consideration. These are: whether the sandstone is free from salts (if salts are present they will change the flow dynamics of the water); the pore size; the saturation levels within the stone and external conditions such as temperature. However, the studies listed above all focus on absorption by capillary rise ascertained by drying sandstone blocks which are then placed in a tray of water and at various intervals removed and weighed, therefore the water content can be calculated. This is useful in understanding ground water rise in monolithic monuments, but buildings are largely affected by the penetration of rain water, rather than capillary rise which only affects the lower most 2 m of buildings (Hall et al., 2011). To calculate penetration by rain fall, factors such as the angle in which the rain is hitting the surface (which is influenced by the wind speed) and the intensity of rain fall also have to be considered. These variables will all affect the amount of water absorbed and the rate of absorption. Hall and Kalimeris (1982) accounted for these conditions and their results are reported in Table 6-5. In the table, V_o is the rate at which rain is received per unit area of the surface. If the material has high sorpitivity value (more pore space) the surface will take more time to become saturated than a material with low sorpitivity values (minimal porosity) under the same rainfall conditions. This demonstrates that the time for a porous surface to become saturated when exposed to rain depends mainly on the sorpitivity of the

material (sandstone generally have high sorpitivity values at 1 mm $min^{-1/2}$, Hall et al., 2010) and the rate at which rain is received per unit area of the surface. Hall and Kalimeris (1982) only consider the very outermost surface (depth of 1 mm) and do not imply any rate of absorption to depth. Furthermore these results are based on stone at an angle rather than vertical which would cause an increase of rainfall run-off.

As Hall and Kalimeris (1982) indicate in their results, the surface may become saturated quickly. With a rainfall of 75 mm/h onto sandstone with a sorpotivity of 1 mm $min^{-1/2}$, it will take 0.41 of a minute to saturate the surface (Table 6-5) however, the rate of water transportation to depth is a much slower process, as shown by the Glasgow LWS results.

Table 6-5: Table of surface saturation times for different rainfall intensity values.

Sorpotivity mm $min^{-1/2}$	V_O 25 mm/h	V_O 50 mm/h	V_O 75 mm/h
0.50	0.92	0.23	0.11
1	3.69	0.92	0.41
1.50	8.29	2.07	0.92
2	14.75	3.69	1.64

Data taken from Hall and Kalimeris (1982). On an angled surface where gravity is factored in to give a more realistic building surface saturation rates. V_O = intensity.

Other methods which can be used to test the moisture of walls are an adaption of a 2D electrical resistivity survey and the wooden dowel method (Sass and Viles, 2006). The 2D electrical resistivity survey is fast and non-destructive and provides good spatial and temporal resolution. However, this does not provide information on the ingress and evaporation and the rate of movement of the water within the sandstone only providing a snap-shot of where the moisture is within the wall.

6.4.4 *Summary*

The maximum volume of water detected on LWS-INT is generally 0.5 ml/cm^2, with the exception of Figure 6-38.10 showing a much larger amount. However, LWS-EXT (outside) regularly reaches 1 ml/cm^2, which would indicate complete saturation. Therefore, the internal LWS is consistently recording a lower saturation level compared to the external LWS. The lower 0.5 ml/cm^2 recorded by LWS-INT is likely to be internal saturation , as some sand grains will cover the sensor and hinder the amount of surface space on the LWS-INT available for water detected. When the LWS-INT records 1 ml/cm^2 it may be that the pressure of the

water being absorbed has forced the liquid behind the grains onto the sensor and this only occurred during extreme periods of rainfall.

During the experiment, the evaporation of water out of Blaxter sandstone has a consistent value of 0.08 ml/hr, although the absorption is much more variable, ranging from 0.04 – 0.08 ml/hr. The predominance of absorption occurring during daytime may be a factor of Glasgow's rainfall occurring mainly during night time hours and, as absorption is a slow process, taking time to reach 6 mm depth it therefore then occurs during the day. This is in agreement with Svensson et al. (2002), who showed that rain is found to start significantly more often in the first four hours after midnight in Glasgow.

However, when considering the results, some possible sources of error should be acknowledged. Once the water penetrates the sandstone it encounters the impermeable sensor and becomes trapped next to it rather than flowing freely, causing the water to be in contact with the surface of the sensor for a prolonged period of time compared to the external sensor, which is subjected to wind, which may dry the surface much more rapidly. Also, gravity will cause the rain droplets to fall off quicker on the external sensor. Although, even with these complications considered, the results from the LWS dataloggers still provide an important new insight to the flow of water within sandstone in the Glasgow environment. The results provided by the LWS-INT prove the presence of water between the surface and a depth of 6 mm. The evidence of water internally verifies that the IButton data inaccuracies were caused by free water and demonstrate that the sandstone is very sensitive to the external conditions.

6.5 Internal Monitoring and Accelerated Weathering Summary

To understand the impact of climate change on internal microenvironments, and how they influence weathering at present and in the future, these internal monitoring and accelerated weathering experiments were conducted. The long term environmental chamber experiments indicate (on the chamber and water only blocks) that, with a change in temperature and RH, climate will only cause small amounts of change to the sandstone surface predominantly in the form of granular disintegration. Also, the fine-grained sandstones such as Dunhouse Buff (quartz average size = 163 μm) will lose a greater number

of grains compared to the coarse-grained sandstones such as Bearl (quartz average size =450 µm) (Figure 6-44). This suggests that coarse-grained sandstones may be more resilient to granular disintegration. However, the total mass lost is approximately the same (i.e. 2000 fine-grains are the equivalent to the volume of 1000 coarse-grains).

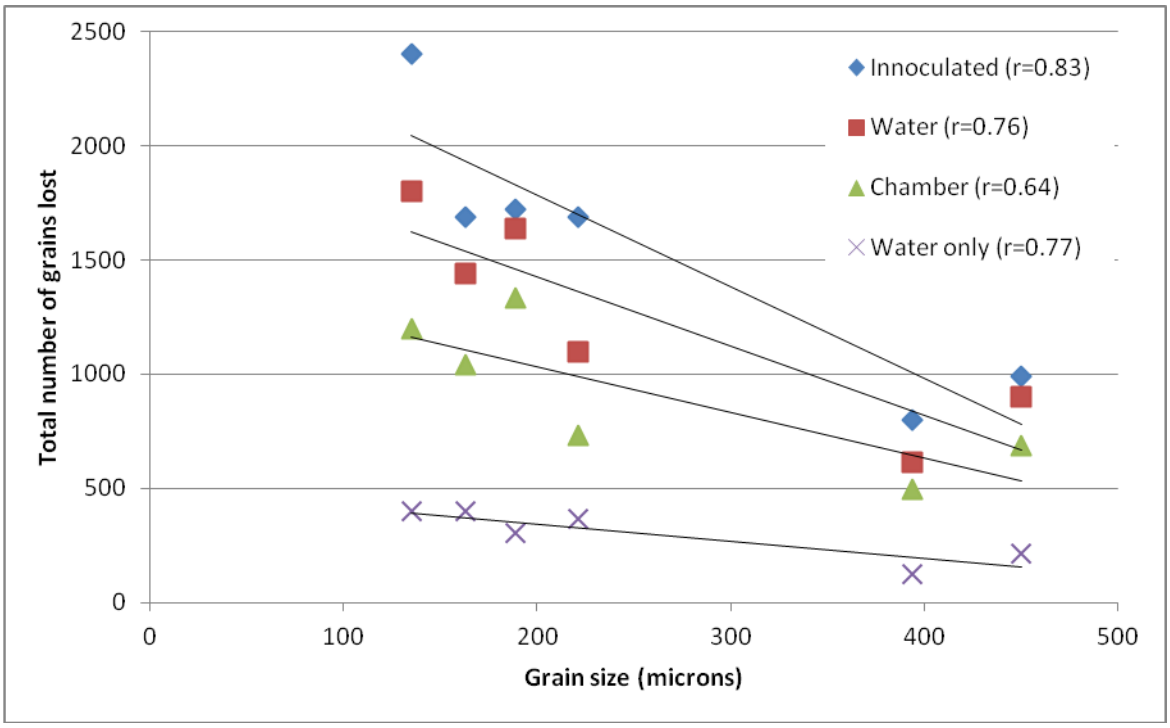

Figure 6-44: Graph of grain size against total number of grains lost.

The internal monitoring results signify that, for almost half of the year, the temperature at 3 mm and 6 mm depth is very different to the external conditions with internal day time temperature readings throughout the summer months much higher than the ambient air temperatures. The likely cause is the higher amount of incident solar radiation during the summer. During winter, solar radiation is much lower and therefore the internal temperature is similar to the air temperature. When these results are extrapolated out to the 2080 medium-high emission scenario, where air temperature is supposed to increase, this will not affect the internal temperature regime on the south facing blocks. The ambient air temperature is not controlling the internal regime within the sandstone; the driving factor instead is the solar radiation. These changes are illustrated in Figure 6-45. An increase in air temperature will only reduce the difference experienced between the internal sandstone and the external conditions. The amount of solar radiation Glasgow receives will be affected by the percentage of cloud cover experienced. UKCIP02 predicts cloud cover to decrease marginally (3%) during the summer months, although this aspect of climate is very difficult to predict. However, if this does happen, then the internal temperature of the south facing

facades will increase. Moreover, an increase in air temperature will have a larger impact on the east, west and north aspect of the building rather than the south facades, because the internal heating on these is dictated directly by the air temperature as no direct solar radiation is striking their surfaces. Therefore, an increase in air temperature will increase the internal temperatures experienced (Figure 6-45).

During the winter months, the internal water content of the sandstones is dominated by liquid water. The UKCIP02 predictions state that RH may decrease marginally during both summer and winter. Internal RH conditions during winter are unlikely to change as internal RH is considerably higher than external RH causing it to continue to have liquid water internally. During the summer, the internal RH, which follows the patterns of the external conditions, will fall and may perhaps cause an increase of periods when loss of internal moisture can occur. In the summer months the rainfall is predicted to be more intense, with heavy showers combined with longer dry spells between these (i.e. no overall change to the amount of rain, more a change to how it falls). These prolonged dry periods, may provide greater opportunities for internal moisture loss to occur.

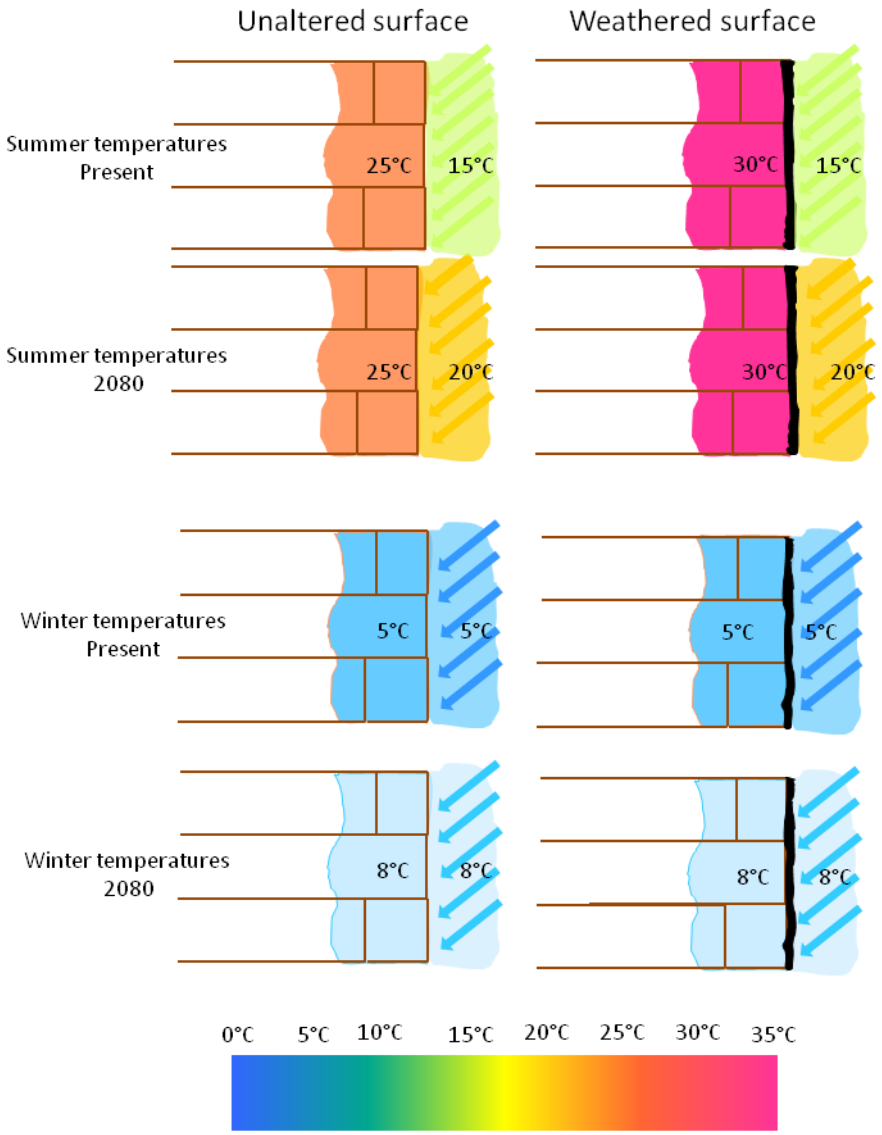

Figure 6-45: Sketch summary of predicted temperature change and the internal impact on the sandstone.

The implications of these climatic changes for both the inorganic and organic weathering processes will be discussed further in the following chapter.

7 Thesis Discussion

So far, the discussion in each chapter has focused on individual aspects of the research. Here I aim to bring together all the results to answer the questions set out at the beginning of the study.

7.1 What weathering processes have occurred historically and are at work presently on the blond sandstones of Glasgow?

To explain how weathering is taking place currently, the seven types of weathering as defined in the literature review will be used to analyses the results. These categories were: pollution; salt crystallization; freeze-thaw; chemical action; clay expansion; thermal heating and biological activity. Although the study focused on a subset of these actions, evidence for all weathering processes was noted. This discussion aims to give a full perspective of internal and surface decay methods.

7.1.1 *Pollution*

The historic buildings of Glasgow display effects of the past clearly on their surfaces as they have become modified through time reflecting the changing urban environment. In particular, many buildings are blemished by black crusts, which have accumulated throughout the industrial period and are at present forming by vehicle-derived pollutants. The FEG-SEM data of crusts are outlined in chapter 3. A synopsis of the results obtained are that, a thin and loosely compacted deposit, mostly composed of mineral fragments, is the most common crust formation, with a few silica glaze crusts evident as well. The mineral crusts only have a small microbial content as indicated by the protein and chlorophyll-a assays. The surfaces of minerals directly below the crust did not show any evidence for pitting or dissolution, and no evidence of enhanced chemical reactions due to its presence was observed. It is unknown whether the crust's presence was causing granular disintegration as the environmental chamber experiments show that this can

occur purely due to the ambient climate (i.e. temperature and RH with and without additional liquid water).

An indirect weathering effect caused by the presence of a black crust on the stone surface is that internal heating is much more effective than in the fresh blond sandstones, whilst also altering the internal RH cycle. The internal IButton datalogging measurements from the Dalry sandstone, (which had a well-formed black crust on its surface) record the highest temperatures and RH values throughout both summer and winter. The crust therefore, seems to be hindering evaporation of moisture, in spite of higher temperatures, leaving the subsurface stone damper. The RH cycle within Dalry could also be a consequence of sitting on a concrete surface. However, the presence of a dark crust is defiantly altering the internal temperatures.

Previous studies have speculated that the occurrence of a black crust may have a positive 'protective' effect by reducing the impact that microbial communities can have on the sandstone (Bluck and Porter, 1991b). Of the ten samples identified as having "mineral fragment black crusts" only three, have microbial matter identifiable within the FEG-SEM (EE1 from SVS, and Dalry samples D2 and D3). In addition, the silica glaze samples also, have no visually identifiable microbial communities associations with them. Therefore, the black crusts could be assessed as reducing the likelihood of microbial colonisation impacting on the stone surface. The reason for this is unknown, although two theories' are that: 1) the crust is toxic to the microbes, 2) the crust is blocking the pore space needed by the microbes to colonise.

With the evidence outlined, it seems that the overall impact of the black crust is not damaging the sandstone beneath; the crust seems to inhibit the growth of microbes and at present the rates of chemical decay are not dramatically enhanced. The biggest effect that pollution has on the Glasgow sandstones is predominantly an aesthetic problem. Therefore, we should not forcefully remove the black crust, and allow it to wear away naturally.

7.1.2 ***Salt***

Results indicate that salts are not prominent within these sandstones. When analysis was undertaken only small quantities of salt were detected residing on the surface, and none were seen internally. Any salts that were present may have dissolved out during sample preparation. Although care was taken to use a dry core bit when sampling (to avoid dissolution by water), the sample preparation into polished blocks may have destroyed any salt crystals present. Although, it is of note that the fractured surface samples which required minimal preparation and no polishing, also, did not show any salt crystals in significant quantities, with the exception of CS4. CS4 (St Vincent St building) shows large deposits of salt on the surface of the sandstone, the main crystal being gypsum ($CaSO_4 \cdot 2H_2O$). However, this sample was taken from an area where mortar repairs had been widespread. As mortar is a combination of putty lime ($Ca(OH)_2$) enhanced with additives such as sand, the mortar was most likely the source of calcium, which then combined with sulphur from pollution in the air to form the gypsum crystals on the sandstone surface. This is an example of the *below* sulphation process detailed in Lefevre and Ausset (2002).

Calcium is found in many other samples analysed, stored in the form of ankerite. The largest quantity of ankerite found was 10.6% in EE4 (SVS). This is a high proportion in comparison to the average of Dalry and RGU samples (0%), and the University samples (3.5%). This much smaller quantity of internal calcium and magnesium, compared to the lime mortar may explain why calcium/magnesium salts have not been produced on, or within the majority of samples. Lack of calcium is the most likely reason, to explain why salt crystals were not present on the stone surface or at depth, but a multitude of factors influence where and when salts will form. Another feature, which may have contributed to the lack of salt crystals in the Glasgow sandstones, is that the saturation levels of salt in the liquid are below that needed for crystallisation. The University and SVS samples (those that contain ankerite) were taken from a height on the buildings where the samples were mainly exposed to rainwater (Hall et al., 2011). Therefore samples are relatively unaffected by the groundwater, which is laden with natural salts and de-icing salts used during the winter months. Kamh (2005a) tested water sources in Chester City (UK) and showed that rainwater has only 94.1 ppm of total dissolved salts whilst snowmelt contaminated with de-icing salts has 225.5 ppm of total dissolved salts.

The data gathered from these samples, suggest that, the presence of salt is only minimally decaying the blond Glasgow sandstones. Where salt crystals do occur, they are not seen penetrating to depth, residing only on the surface. Therefore, the salts are not causing any mechanical damage within pore space through crystallisation or hydration pressures, only attacking the surface of the few sandstones on which they are present.

7.1.3 *Freeze-thaw*

Freeze-thaw as a weathering process was not specifically investigated within this study, due to the difficulties in gathering precise temperature measurements (as continuous datalogging on a 1 minute interval or less is needed to identify the latent heat associated with the freeze-thaw event Hall, 2004). However, the microenvironment climate monitoring shows that the internal temperature at 3 mm and 6 mm occasionally does dip below freezing during the winter months, whilst RH measurements were greater than 100% (i.e. liquid water is present) indicating that conditions are suitable for the process of freeze-thaw to occur. In December 2009, January 2010 and February 2010 this combination happened ~30 times in Dunhouse Buff and Bearl sandstone at each depth, with fewer occurrences in the Dalry sandstone (with black crust). This estimate was calculated using points which crossed 0°C (whilst at 100% RH), but the process of freeze-thaw (microgelivation) can occur between 0°C and -4°C, and colder temperatures, are needed in low porosity rocks (Matsuoka, 2001). These factors suggest that 30 freeze-thaw events are likely to be an over estimate. The low occurrence of freeze-thaw events within the Glasgow sandstones, may be due to extended cold periods of time rather than the external climate hovering around 0°C causing lots of potential freeze-thaw fracturing. Other considerations are that, the Glasgow climate is mild in comparison to other areas in the world. In addition, variables around the building such as broken gutters, elevation and external features such as trees shading the sandstone, will all cause localised changes to the amount of freeze-thaw events in which the sandstone experiences. Furthermore, internal heating of the stone within occupied buildings, will have a significant impact on the number of freezing events, which can occur.

Backscatter electron and CL imaging of the outermost surface, did not show any signs of mechanical defects caused by freeze-thaw, such as physical fracturing of the quartz grains or overgrowth detachment, as no small cracks were seen to be forming either between or

within grains. However, this does not mean that freeze-thaw was not causing micro defects to the mineral structure. However Raman spectroscopy produced standard spectra for the quartz grain at the surface, indicating no change to the minerals.

Freeze-thaw is only potentially operating for a few months of each year within Glasgow (December, January, February and March) making it insignificant in the larger framework of sandstone weathering on these Scottish blond buildings. Furthermore, the effectiveness/ineffectiveness of freeze-thaw (discussed in section 1.2.4) is largely unknown as quantitative analysis has not been undertaken for the natural environment. Thomachot and Jeannette (2002) suggest that after 250 freeze-thaw events no damage had occurred on a German sandstone which had porosities ranging between 4-19%. Therefore, a maximum of 30 freeze-thaw events annually is likely to be insignificant in weathering the Glasgow sandstones.

7.1.4 ***Chemical***

The use of Raman spectroscopy combined with quantitative X-ray microanalysis has produced clear results showing that chemical decay is having a profound effect on the muscovite minerals at the outermost stone surface. More subtle changes also occur in the kaolinite clay. The EDX analysis indicate that muscovite at the outermost surface have chemical compositions close to that of muscovites from the internal regions, with only a slight depletion in potassium. However, Raman spectra are very different from the two regions: at the top of the samples few bonds seem to survive leaving an “ionic slurry”, showing that the micas are being broken down relative to those of the interior, where conclusive mica spectra are recorded. The Raman spectroscopy also shows that the kaolinite is less crystalline at the surface and in some cases has been transformed into dickite through the stretching of bonds, brought about by chemical weathering, (detailed in section 4.6.1.2).

Ankerite minerals were expected to be the most chemically reactive due to their high solubility in comparison to the other minerals present within the sandstone. However, the transformation of ankerite, being dissolved out and leaving Fe-oxide pseudomorphs, is only detected in three out of twelve samples containing ankerite. Many samples have unaffected ankerite crystals directly beneath the outermost surface. This shows that

carbonate cement dissolution is not a weathering process common to all Glasgow sandstones. In addition, the detection of ankerite dissolution in RGU5, which has had minimal exposure to the elements, suggests that this process can also occur pre-construction and may not be a reliable indicator as to how much weathering has occurred, following emplacement into a building. However, when systematic weathering of the carbonate cements does occur within a sandstone, this weakens the internal structure and can be thought of as a significant decay process.

A third form of chemical weathering is also seen in the light microscopy images and is revealed by point counting. Light microscopy results show internal layering defined by colour. The bleached zone seen in samples correlates well with point counting results where no or proportionally low quantities of Fe-oxides occur for that sample. The red rusty layer is much more difficult to correlate with point counting data. However, the data does reveal much more subtle chemical variations within the substrate undetectable by eye. Point counting indicates defined mineral-rich and mineral-poor layers, for kaolinite, quartz and Fe-oxides, including variation in porosity, all occurring in the outermost 6-8 mm zone. Therefore, there is active transport of minerals with the weathering regions changing the original composition of the layers. The transport of minerals particularly Fe-oxides has been assigned two modes of transport, water (Bluck and Porter, 1991a; Jefferson, 1993) and microbial (Gómez-Alarcón et al., 1995; Omelon et al., 2006a, b, 2007). As no microorganisms are seen living at this depth, the main transportation method is through the movement of water (ingression and regress).

The breakdown of micas, coupled with the transport of minerals within the internal regions, are the main chemical weathering processes affecting the sandstone, rather than the dissolution and reprecipitation of minerals.

7.1.5 ***Clays***

Clay weathering is seen within these sandstones, as demonstrated by the Raman spectroscopy and EDX analysis. The kaolinite as discussed is observed to be transforming into dickite and less crystalline forms showing subtle chemical decay process, rather than mechanical damage. As kaolinite is a non-expandable clay, and as no montmorillonite was seen and only very minimal amounts of potential illite were detected (using Raman

spectroscopy), shrinking and swelling of clays has a minimal effect on the sandstone. Although kaolinite is being chemically decayed at the outermost surface, the main weathering process affecting the sandstone is the transportation of the platelets towards the surface. Point counting detected a kaolinite deprived and enriched layer near the outermost surface of the sandstones. This loss and movement of kaolinite may cause the internal structure of the sandstone to become weakened increasing the likely hood of decay, as noted by Sérgio De Melo and César Fonseca Giannini (2007) and Friolo et al. (2003). The leaf wetness sensor shows that there is a very dynamic movement and flow of water within the sandstones. This movement of water is likely to be the main medium of redistribution of the kaolinite. As the kaolinite is transported by water from the deeper regions, a depleted layer is formed and a new enriched layer is created nearer the surface. If the kaolinite enriched layer reaches the surface, it may be washed out of the sandstone completely, or cause a case hardened crust to form.

As a large majority of Scottish sandstones contain kaolinite, and this clay deprived layer was seen in a large cross-section of the samples, it is therefore a significant weathering factor. The transportation of kaolinite also has a knock-on effect to the movement of water within the stone, as it changes the porosity and permeability within the kaolinite enriched and deprived layers.

7.1.6 ***Biology***

Results show microorganisms living on the sandstone surface and cryptoendolithically, but never occurring in both places within any given sample. Of the 23 samples studied, six were found to have surface microbes and eight to have internal microbial communities. An array of microbes was seen including both filamentous and globular cyanobacteria, fungi and algae, but in general, filamentous cyanobacteria were restricted to the surface, whilst globular cyanobacteria was found internally. The vast majority of microbes occur no deeper than 2 mm. The microclimate deeper than 2 mm is not harmful to the microbial communities, with summer conditions of up to 30°C and a healthy supply of free water to aid the microbial activity. The restriction in depth of microbial penetration is a consequence of the poor light conditions recorded within the sandstone. The OLT results show that any form of weathering crust present on the surface hugely reduces the penetration of light. The amount of light penetration also

explains why cryptoendolithic microbes are almost always confined to facades with a southerly facing aspect to their direction, as these are the only facades, which receives enough solar radiation to activate communities at depth. The south face of a building during the summer receives the maximum flux of light and therefore the photosynthetic activated microbes cannot survive on the surface due to photo-oxidation harm (and seek protection within the sandstone). The surface location of the filamentous cyanobacteria is predominantly on the west, north and east facing facades, and again is most likely a product of the available solar radiation.

When observed living cryptoendolithically, the microbes swamp pore spaces, and may be causing mechanical damage to grains during shrinking and swelling episodes. However, as they do not form a continuous layer within the sandstone, unlike the cryptoendolithic microbes of Antarctica (Friedmann, 1982; Omelon et al., 2006a, b, 2007), their mechanical damage potential is patchy. The microbes not only cause mechanical decay to the sandstone but due to the chelating agents and acids that they produce, also chemically corrode the mineral grains within the sandstone. There is possible evidence of this process occurring in UE2, were the quartz grain beneath the EPS and at the edges appears rough and undulating (Figure 5-11). Chemical decay due to microbes may be a more prominent weathering effect internally as only small amounts of microbes were seen living on the surface (supported by the protein and chlorophyll-a results). Therefore, the amount of corrosive damage that these sparsely spread filaments can produce on the sandstone is unknown. However, in addition to these microbes seen it is also possible that bacteria undetectable by eye or osmium staining are living both on and within the sandstones producing acids. 40% of bacterial strains isolated on German sandstone monuments were found to be acid producers (Warscheid et al., 1991). This means that much more chemical weathering could be occurring on and within the sandstone.

In contrast to these negative effects, the filamentous cyanobacteria could also be beneficial to the stone. As the filaments are seen binding mineral fragments together, displaying a wire mesh network over the surface, therefore “holding” the quartz grains in place (Figure 7-1).

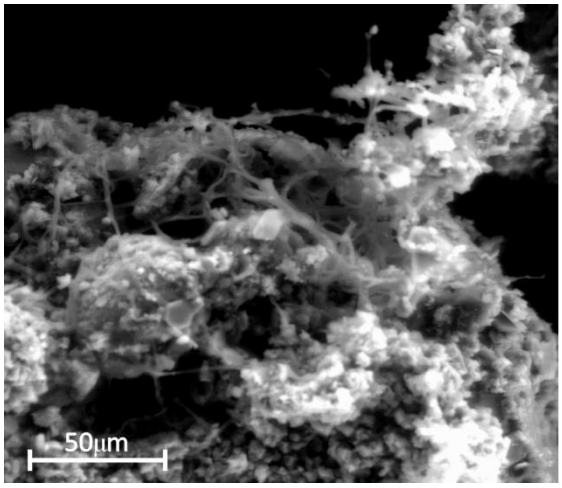

Figure 7-1: FEG-SEM BSE image of a surface scraping.

Quartz grain on the surface of a sandstone being held in place by a network of filamentous cyanobacteria.

For buildings that have crust formation on the surface the microbial results combined with OLT data indicate that during the winter and the summer varying colonisation and potential weathering patterns are taking place. During the summer, microbes will be active on the surface of all facades with the exception of the south where they are in the subsurface. Whilst during the winter microbes will be active on the entire building and at depth on the south facade.

However, on fresh sandstone, the light can penetrate to a maximum depth of 5 mm and the microbial communities are shown to be living at these greater depths (RGU Blaxter). The internal microclimate data indicates that during the summer the microbes are residing in an environment that is much hotter than the ambient air conditions, and this excess heat may stimulate greater microbial activity. The IButton and LWS data shows that a loss of moisture and water is occurring frequently, which would indicate that the microbial communities are shrinking and swelling regularly, potentially causing greater amounts of damage. Therefore, at present those new builds and cleaned sandstone are likely to be suffering from much greater microbial damage, in comparison to the older weathered buildings, when colonised.

The presence of microbes on old buildings with crusts is interpreted as having some positive (protective) effects. However, whether these outweigh the negative (damaging) effects it is unknown, and it would be very difficult to test. Nevertheless, microbial communities are certainly influencing the weathering cycle on sandstone buildings both old and new.

7.1.7 *Thermal heating*

The albedo of the sandstone is certainly having an impact on the internal temperature as data logging shows, that the weathered Dalry block has substantially higher internal temperatures than the fresh cut blocks of Dunhouse Buff and Bearl during the summer months on the south facade. However, albedo is not a weathering process in its own right (as implied by other studies, section 1.2.7) and needs to be combined with solar radiation to make it effective. The albedo of the sandstone was calculated by testing the sandstone's colour which for Dunhouse Buff and Bearl were very similar (see section 6.3.5.1). This when combined with the external conditions do not make albedo a viable weathering concept as the sandstone has a high albedo and the latitude position of Scotland dictates much lower levels of PAR compared to many countries. In addition, the premise of thermal stress occurring due to the differing amounts of heat a mineral grain will absorb, will only have a minimal effect on these blond sandstones. As the minerals present have similar colour qualities, they will absorb similar amounts of heat. Unlike the differences seen between quartz (light) and pyroxene (dark) in granite buildings, where this may have a significant influence on weathering.

Furthermore, the process of thermal heating is an ever changing factor due to the dynamic characteristic of the sandstone surface. Over the last 150 years it is likely that on the Glasgow buildings a green crust formed first due to biogenetic soiling then as weathering progressed this green was slowly replaced by a brown coloration, as the pollutants built up. Which, will suffocate the cryptoendolithic microbial communities of light, and eventually will died out. Eventually this process leads to a black crust, which will then be weathered away to start the cycle again. Therefore, the magnitude of thermal heating is dependent on the surface conditions and colour.

7.1.8 *Summary*

As has been demonstrated, the failure of sandstone within a building at present is a cumulative effect of many reactions occurring within the stone at varying depths, which are ultimately being controlled by the external conditions.

In the introduction section 1.4.1 it was noted that the Hyslop et al. (2006) study of Scottish sandstone, found that the main decay processes active on Glasgow's buildings at present are: crust formation; granular disintegration (particularly on lower facades enhanced by de-icing salts); biogenic soiling and the saturation of pore space within the sandstone by water. The data from the present study supports some of these conclusions. However, crust formation may be less important than suggested by Hyslop et al. (2006) as this study suggests there is no corrosion effect associated with their occurrence. Also, granular disintegration may happen, but the driving mechanism is unclear.

In addition, data from the present study show that the weathering of sandstones on Glasgow's buildings seems to be dominated by chemical decay, breaking down minerals such as muscovite and kaolinite, redistribution of minerals to produce enriched and depleted layers in the outermost 6 mm, and to a lesser extent microbial decay. Biological decay may only have a large impact where lichen or wall climbing plants such as ivy are located on the building facade (Seaward, 1997; Adamo and Violante, 2000), causing large amounts of decay to specific areas of that construction. Nevertheless, the weathered stone used in this research suggested that microbes generally only play a supporting role in the overall weathering process.

The weathering processes contributing to decay at present are summarised in the sketch Figure 7-8, and these are in agreement with Bluck and Porter's (1991b) model (Figure 1-6)but with enhanced detail.

As shown these weathering processes are driven and controlled primarily by environmental conditions, and thus climate change will impact on the summer and winter weathering cycles of buildings in the future. In conjunction with microclimate changes, the weathering cycle will adapt in response to the changes on the surface of the sandstone, which as highlighted, is a forever-changing plane. However, the main question is:

7.2 How will current decay cycles alter with climate change?

As discussed, climate change will alter the weathering cycle of Glasgow buildings. A few studies have addressed the question of "how will climate change affect stone deterioration" from the perspective of historic buildings and monuments cast from sandstone. Cassar (2005) suggests that in the north west of England "fluvial flooding, storminess, extreme winds and rain are of greatest threat" affecting built heritage in the future. However, Viles (2002) and Brimblecombe and Grossi (2007) provide much more in depth predictions for the weathering processes by 2080. The processes highlighted in these papers are discussed alongside the predictions from the present study to evaluate how climate change will alter sandstone decay.

7.2.1 *Pollution*

In the case of pollution, Brimblecombe and Grossi (2007) predict that crusts on buildings will become thinner and richer in diesel-derived carbon and organic material. These elemental carbon particles are responsible for the dark colour of current deposits. They raise the importance of aesthetic considerations and also suggest that biological activity, perhaps, will be supported by an ongoing increase in organic pollutants from deposited diesel emissions.

This study indicates that pollution is not a significant weathering factor at present, therefore its affects should not be detrimental to buildings in 2080. Especially, since the clean air act was enforced and due to the decline of heavy industry, there has been a large reduction of sulphur dioxide (a major component of fly ash and soot particulates) in Glasgow, reducing from 155 $\mu g/m^3$ in 1962 to 25 $\mu g/m^3$ in 2001 (Figure 7-2). Although, Glasgow's population may have swollen by 2080 leading to increased car usage, the fuels of the future are becoming cleaner, making the build up of external crusts increasingly slow and difficult. There is also speculation that buildings may begin to self-cleaning due to heavy rainfall events. Therefore pollution will remain a minimal contribution to the weathering of sandstone and may also become less of an aesthetic problem at the same time (Saiz-Jimenez, 1995; Bonazza et al., 2009). In present-day Mediterranean climates (which by 2080 Glasgow will moving towards), Garcia-Valles et al. (1998) shows that crust

erosion is a more active process than deposition, and that the crusts and patinas tend to disappear from the surface of the monuments.

However, the removal of the black crust (whether by man, rain or both) will have consequences on the sandstone beneath. It may reduce the internal RH, which builds up behind the impermeable layer-potentially reducing weathering. In addition, the reduction of the crust will encourage surface colonisation of microbes, which at present it seems to hamper. It will also let a larger percentage of light to penetrate to depth, increasing microbial communities within the sandstone. These interconnected processes are discussed in detail later in the chapter.

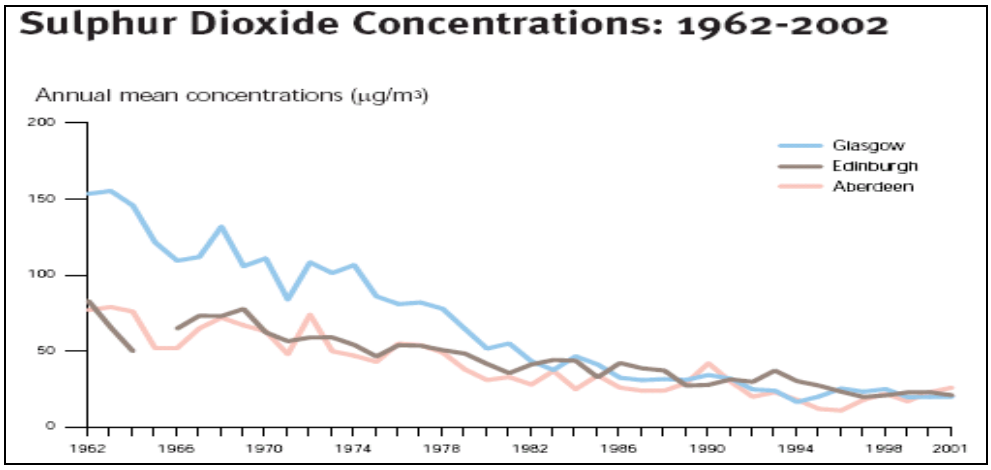

Figure 7-2: Sulphur dioxide concentration for Scottish cities, from 1962-2001

Data shows a general decline in their concentrations. Data from the 'Key Scottish Environmental Statistics Handbook'.

7.2.2 *Salt*

In the case of salt weathering, both Viles (2002) and Brimblecombe et al. (2006) agree that predicting future salt decay is difficult, but suggest that its effects will increase. Brimblecombe and Grossi (2007) use the example of sodium sulphate. Stating that, at higher temperatures, this salt will become increasingly soluble, (e.g. sodium sulphate is only 14% as soluble at 0°C as at 35°C) warming may hinder crystallisation from solution. However, these increased temperatures encourage evaporation, which will promote crystallization through the production of supersaturated solutions. Viles (2002) uses the prediction that "climate is likely to be less humid in the summer months so there will be more frequent transitions across the critical value of RH and this change will lead to more crystallisation-dissolution cycles". Brimblecombe et al. (2006) estimated the annual

number of critical humidity transition for sodium chloride within England, and found that the number of transitions are to increase substantially over the period of 1961-2099 (Figure 7-3). The increase of transitions will exert salt crystallisation and hydration pressures more frequently within the pore spaces.

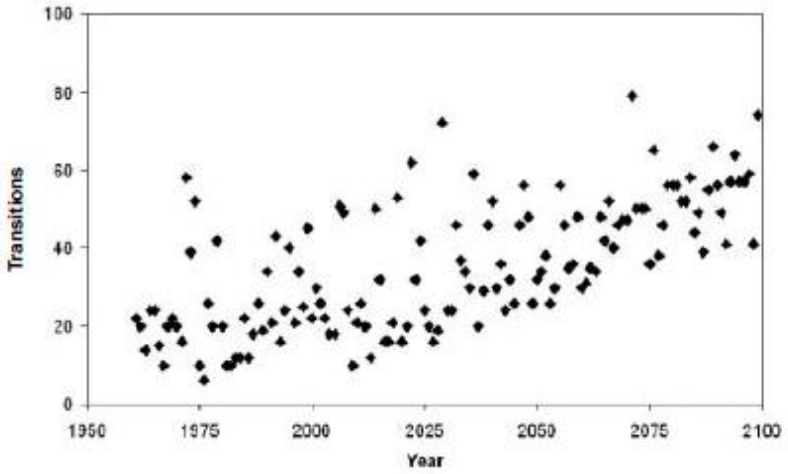

Figure 7-3: The number of transitions each year across the critical humidity (75.5%) for change in sodium chloride in central England.
Data extracted from Brimblecombe et al. (2006).

These phase transitions are likely to increase in Scotland but to a lesser extent due to the annual higher RH and smaller predicted change to the RH in Glasgow compared to England. In addition, the sandstones contained minimal salt content and with less de-icing salts being distributed during the winter months (owing to warmer winters) these factors will keep salt degradation as a minimum effect on Glasgow sandstone decay.

7.2.3 *Freeze-thaw*

The freeze-thaw process is likely to become less of a problem within historic structures due to the increase in temperatures expected for winter, causing fewer freezing events (Viles, 2002; Brimblecombe and Grossi, 2007). Grossi et al. (2007), predict that the number of freeze-thaw cycles per year for London will decrease from the present day of ten to approximately four by 2099. The warming temperatures expected for Glasgow in winter will also decrease the number of freeze thaw events seen, diminishing the present day annual ~30 occurrences, reducing the mechanical decay of freeze-thaw further, as a weathering mechanism.

7.2.4 *Chemical*

In respect to chemical weathering, Viles (2002) suggests that increasing air temperatures and more rainfall will favour and encourage chemical reactions in general, hence, chemical weathering will be of increasing importance. This statement by Viles (2002) agrees with our conclusions, however results from the present study provide an in-depth microscale review of the chemical weathering taking place on Glasgow buildings.

We have concluded that, with increased temperatures, there will be greater rates of chemical dissolution but by how much? To support these predictions, dissolution rates for ankerite, a relatively soluble mineral and feldspar a stable silicate mineral (both commonly found within sandstones), were calculated for 2080 conditions.

Using the work of Golubev et al. (2009) on the dissolution rate of siderite and Gautelier et al. (1999), work on dolomite dissolution rates it was possible to estimate the dissolution rate of ankerite, whose composition lies between these carbonates.

At predicted temperatures of 18°C (predicted summer 2080 temperature) the south facing surface ankerite crystals, at pH4, will have a dissolution rate of 0.09 cm/year (Figure 7-4). However, during the summer months the internal (6 mm depth) temperatures have been shown to be much warmer than the ambient air and surface temperature, frequently reaching upwards of 25°C. This will not change in the future as the internal temperature is controlled by solar radiation rather than air temperature. But these higher temperatures experienced internally will substantially increase the dissolution rate of ankerite to 0.11 cm/year (Figure 7-4). To counteract these very high summer surface and subsurface dissolution rates the cooler temperatures of winter (8°C) both on the surface and internally produce slower ankerite dissolution rates of 0.03 cm/year (Figure 7-4).

These dissolution rates for the ankerite are, as expected very high when compared to feldspar rates. Chen and Brantley (1997) provided dissolution rates for feldspar and show dissolution at the surface (18°C) in acidic conditions (pH3) to be 0.00006 cm/100 year, and this will only increase to 0.00008 cm/100 year when the temperature is raised to 25°C (Figure 7-5) to mimic internal conditions. In winter the rate of feldspar dissolution is

diminished further to 0.00004 cm/100 year (Figure 7-5). Note the difference in the units used for the ankerite and feldspar rates.

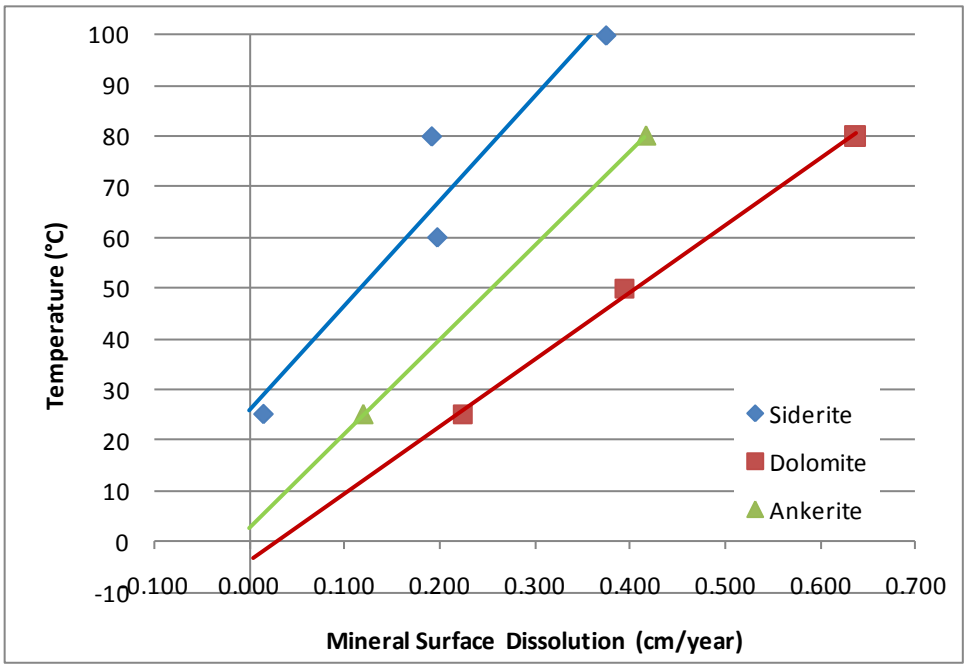

Figure 7-4: Dissolution rates for carbonate minerals

Siderite data from Golubev et al. (2009) and dolomite data Gautelier et al. (1999), with ankerite inferred.

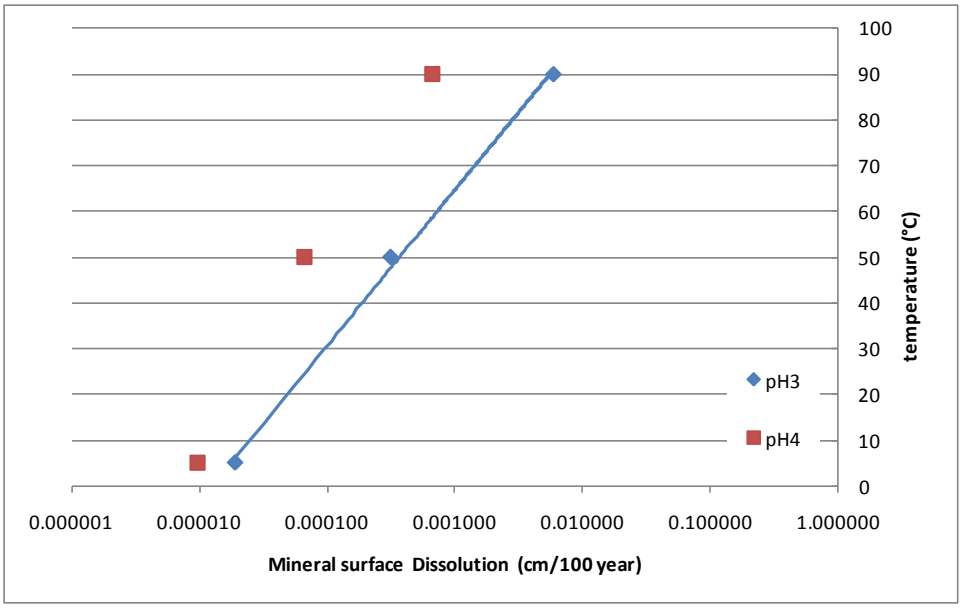

Figure 7-5: Dissolution rate for feldspar.

Data derived from Chen and Brantley (1997).

Furthermore, the data used by Gautelier et al. (1999), Golubev et al. (2009) and Chen and Brantley (1997) are based on the minerals being in saturated conditions continually, whereas the LWS data gathered shows this to be unrealistic. The LWS readings show that between the dates of 30/04/2010 to the 16/08/2010 (a 109 day period in the summer)

the mineral grains at 6 mm depth were only partially or completely saturated for 20% of the time. The IButton data retrieved, however suggests 100% saturation for the mineral grains during the winter.

This information means that the high dissolution rates experienced in the summer by the ankerite and feldspar minerals at depth (6 mm) will be reduced by up to 80%. The revised calculations show that the ankerite will have a dissolution rate of 0.021 cm/year (Figure 7-6), in summer conditions, whilst the feldspar is reduced to the minuscule amount of 0.000005 cm/100 year (Figure 7-7).

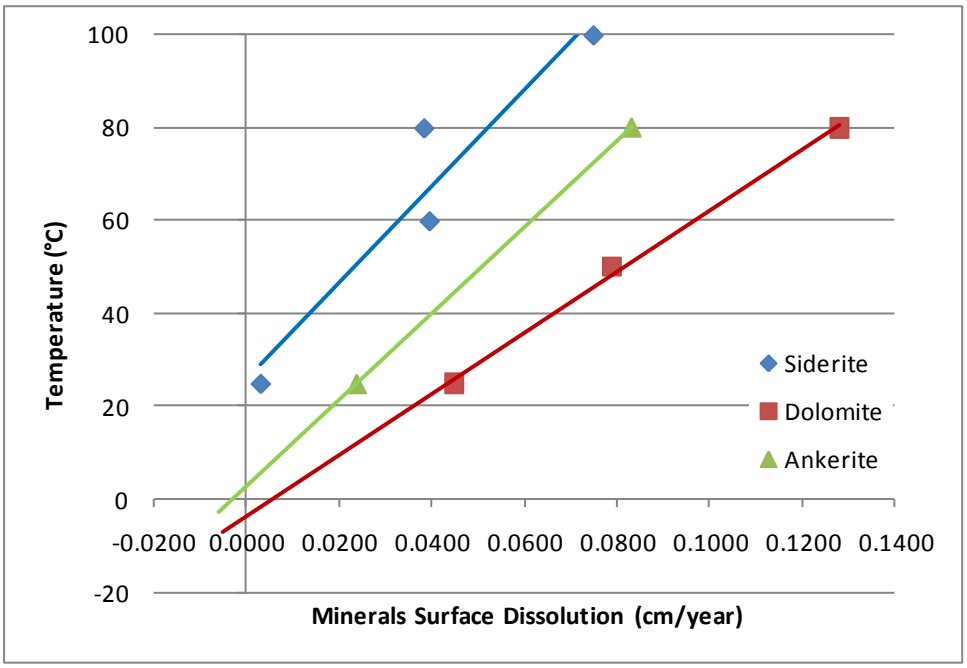

Figure 7-6: Dissolution rate for carbonate minerals at 20% water saturation. Siderite data from Golubev et al. (2009) and dolomite data Gautelier et al. (1999), with ankerite inferred.

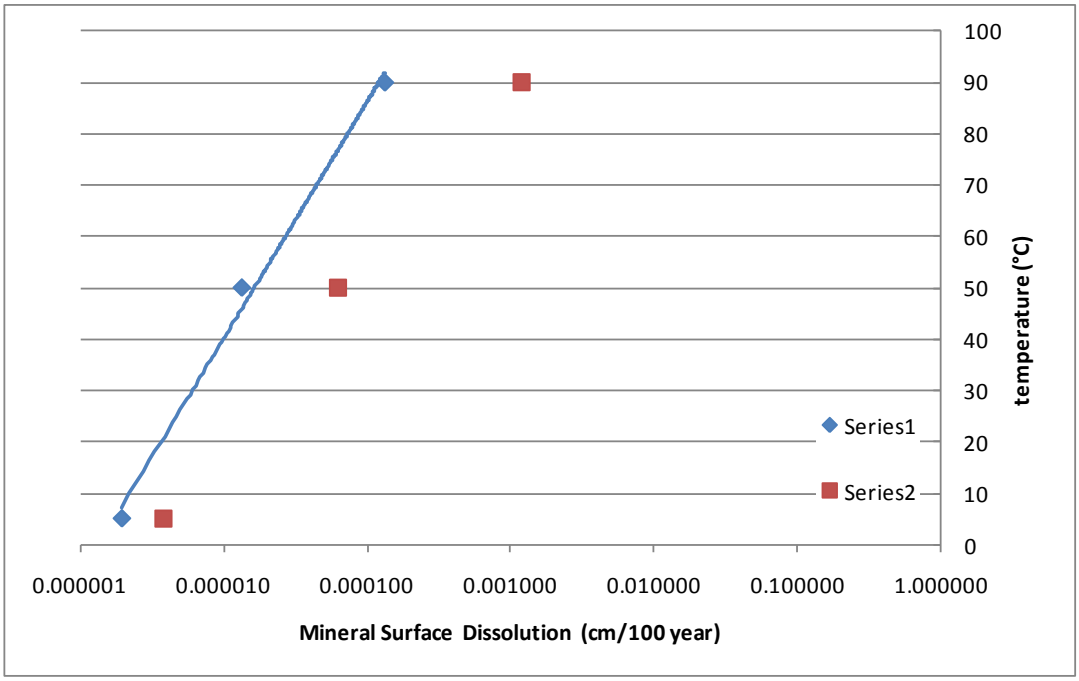

Figure 7-7: Dissolution rate for carbonate minerals at 20% water saturation. Data derived from Chen and Brantley (1997).

Although a seasonal variation is expected in the dissolution rates between the summer and winter (as the summer temperatures are much warmer internally) this is not seen. When the time spent in saturation during summer is considered the rate of decay of ankerite and feldspar crystals is similar in both seasons, thus suggesting a constant dissolution rate throughout the whole year.

These predicted future rates for ankerite dissolution are much greater than the dissolution rates the building sandstones experienced in the past. Using marble gravestones McNeill (1999) found that the average gravestone weathering rate for Scotland was 0.00875 cm/year however higher values of 0.0205 cm/year were found around the Glasgow area. This shows very slow dissolution rates for the carbonate minerals and indicates that the dissolution of carbonate cement in the future will be a much more significant factor compared to the past.

As stated beforehand the internal dissolution rates on these minerals will not increase. However the rates of internal mineral reactions in 2080 will be enhanced if solar radiation does increase as a consequence of a decrease in cloud cover. The UKCIP02 report suggested that over the west of Scotland, cloud cover may decrease by a maximum of 9% during summer which equates to solar radiation increases by up to 30 Wm^{-2} (Hulme et al.,

2002). However this small increase will have a limited impact on the internal dissolution rates.

Although, only the dissolution rates for two minerals have been discussed, this process will also change for the muscovites, kaolinites and Fe-oxides as well.

Physical movement of minerals altering the compositions at the outermost surface will also be affected by the changes to the rainfall patterns forecasted. In winter the total amount of rainfall is expect to increase, however as the sandstones at present are showing signs of being saturated (RH above 100%) the sandstone will not have the opportunity to dry out and for the water to transport minerals. The longer dry spells with intense bursts of rainfall predicted for summer may encourage the ingress and egress of water and encourage mineral transportation. In addition, if the minerals are chemically decaying faster than at present, the grains will become progressively easier to transport and in the long run, will be removed from the sandstone.

These chemical decay factors are combined and summarised in the predictions outlined below. The microclimate data used in the summer predictions are based on an increase in temperature and decrease in rainfall, which occurs as heavy downpours with prolonged dry periods. The winter predictions are based on an increase in both the temperature and rainfall. Both scenarios assume a decrease in the prominence of the crust formations as discussed in section 7.2.1.

South Face Summer: The rate of chemical dissolution of minerals at the surface is likely to increase as the ambient air temperature increases, speeding up the reaction rate occurring on the grains. However, the rate of chemical dissolution of minerals below this depth is likely to stay the same. This is because the internal temperatures during the summer on the south facades are primarily controlled by solar radiation. Therefore all that is going to occur is that the difference between the internal and external temperature is going to decrease (see Figure 6-45). A decrease in the summer rainfall will cause less transportation of minerals within the sandstone. However, as the pattern of rainfall alters to longer dry spells with heavy showers this may cause large irregular movements of mineral causing episodic sandstone failure.

South Face Winter: The rate of chemical dissolution will increase as the ambient air temperature is the controlling factor of both the surface and internal temperatures (due to low solar radiation levels). Therefore, an increase in reactions is set to occur throughout the whole sandstone, and to aid this there will also be larger quantities of available moisture to drive the dissolution process.

North, East and West Facades Summer: The rate of chemical dissolution at the surface and internally, during the summer months is likely to increase as temperatures on this facade are controlled by the ambient air conditions, which are predicted to increase. In addition, the transport of minerals within the sandstone will also increase.

North, East and West Facades Winter: Like the south face, chemical dissolution and transportation of minerals should increase due to the increased ambient air temperature and moisture available.

In conclusion, more chemical decay is likely on all facades during the summer and winter playing an increasingly significant role in the weathering of sandstone.

7.2.5 *Clay*

Neither Viles (2002) nor Brimblecombe and Grossi (2007) refer to clays within sandstone and how these minerals may be affected in the future. However, this study has found that clay plays a significant role in weathering and this is likely to continue.

As the amount of rainfall is only going to increase by a small amount, the pattern in which it falls becomes increasingly important. As discussed, in the west of Scotland heavier rainfall coupled with prolonged dry periods are predicted during the summer, with wetter winters. These sustained wet winters will cause increased transportation of clay minerals within the stone producing thickened enriched and depleted layers. In turn, this will increase the risk of the clay platelets being washed out of the sandstone during the summer heavy rainfall events. This episodic purging of clay will also be assisted by the increased chemical decay reducing the usually large kaolinite platelets (Piffy, 1979) to smaller less crystalline platelets that are easier to mobilise. These processes will leave the interior of the sandstone depleted in kaolinite and hence more susceptible to failure.

7.2.6 *Thermal heating*

Only Brimblecombe et al (2007) refers to thermal heating as an increasingly important factor in future sandstone weathering stating that, “a few degrees in the temperature of monumental heritage is much less important ... however if the annual range between max and min air temperature was to increase, thermal shock could be important”. Thermal shock will not weather sandstone within Glasgow as the temperature range is much less than in other parts of the world where thermal shock may be a significant weathering agent. In addition the main minerals present are similar in colour.

7.2.7 *Biological*

Viles (2002) makes tentative suggestions as to how biological weathering will take place in the future. After stating, that “almost nothing is known about the likely response of most of these organisms to climate change”, Viles (2002) then suggests that the likely impact on biodeterioration is that, as rainfall increases biological growth will also increase. However, the growth will be more benign and less damaging, these suggestions are extrapolated from Viles’ (1995) paper, discussed in section 1.2.8.

However, results of the present study suggest a different conclusion. The season and the facade in question dictate the effectiveness and form of microbial weathering that will take place.

Summer predictions are based on an increase in temperature and decrease in rainfall overall, whilst the rainfall occurs as heavy downpours with prolonged dry periods. Winter predictions are based on an increase in both temperature and rainfall, and both seasons are coupled with a decrease in crust thickness on the surface (it is believed it will naturally wash away as described in section 7.2.1).

South Face Summer: The microbial communities will be able to penetrate to deeper levels due to better optical properties of the sandstone, as the surface of the sandstone is cleansed of the black crust. Also, those microbes living cryptoendolithically will cause more damage through shrinking and swelling as dry periods will become more frequent.

However, the intense light conditions on the surface will remain the same, hindering any growth of surface phototrophs.

South Face Winter: Microbial weathering during the winter months may become more prevalent as the ambient air temperature rises and more moisture is available within the sandstone. This will enable greater microbial activity, increasing the size of the microbial communities on the surface and at depth, enhancing decay due to biofouling.

North, West and East Facades, Summer: During summer the weathering affect of microbes may be felt to a greater level on the north, east and west-facing facades. The warmer temperature and lower rainfall may increase the surface communities. Cryptoendolithic colonies may also have a greater chance to establish as the black crust is washed away. Therefore, the microbes may not be constrained to the surface, however, those on the surface may flourish, producing increased levels of chemical and mechanical decay.

North, West and East Facades, Winter: There may be an increase in surface microbial weathering during the winter months as ambient air temperature rises and conditions in general become milder and wetter. However, the PAR levels are likely to remain too low to support cryptoendolithic communities during the winter on this facade.

Counteracting these increases in microorganism communities the frequency of storms are also predicted to increase. These may periodically wash away microbial communities making it harder for extensive biofilms to establish. The periodical flushing of communities may be particularly prevalent on the south facade, which will be the facade most highly affected by driving rain (Smith et al., 2008).

Whether the species of microbes present will be the same in the future is difficult to predict without rRNA analysis of those identified. In this study the microbes were characterised visually, however, if rRNA results concurred with the morphological analysis it is likely that the same species of microbes will persist in the future. The microbes that have been linked to those seen are very resistant, being identified on both Scottish and Mediterranean buildings. Macedo et al (2009) identifies *Gleocapsa* and *Phormidium* in sandstone substrates within Mediterranean sandstone buildings whilst Young (1995)

observed *Gleocapsa* on Scottish monuments. Therefore, the same microbe can survive under various environmental conditions.

The above statements show that microbial communities may become more prevalent and that an increase in the summer and winter temperatures may lead to greater activity of the microbes already there. It has been shown that the optimum temperature for productivity of *Phormidium* is at 25°C (Vincent and Howard-Williams, 1989). It has also been demonstrated that many species of cyanobacteria will stop activity at 2°C (Seaburg et al., 1981). Therefore an increase in winter temperature will help maintain the growth and production of cyanobacteria species and increase their weathering potential.

This increase in ambient temperature will have knock-on consequences to any microbial chemical processes such as the production of acids. The leaching of acids by microbes will become more rampant due to an increase in the metabolic processes of the microorganisms. Laing et al. (2003) state that the ambient RH is more important than temperature in controlling the amount of microbial activity, with values between 60-70% producing the most intense activity. These results are in contrast to those of Jain et al. (2009) who quotes greater RH values.

Jain (2009) tested how effectively fungi communities could establish themselves on porous material at varying RH levels. Results show that maximum diversity is accomplished at 85% and 96% (i.e. during the winter months more fungal diversity could occur). In contrast, at RH levels lower than 62% no fungal growth occurs (Jain 2009). The average RH in Scotland during summer is very unlikely to reach this low level but a decrease in future RH could produce less diversity and less colonisation within and on the sandstone.

7.2.8 ***Other effects***

Storm events are expected to have increased from five in winter at present to eight by 2080. This could have knock-on effects too many aspects of weathering, results may be that: 1) the black crust is washed away at an increased rate, 2) the extreme rainfall may flush microbes out of the sandstone on a regular basis, making the colonisation by

cryptoendolithic communities difficult, 3) mineral fragments will also be purged on an increased frequency, which will weaken the internal structure of the sandstone.

During storm events, not only will rain play an important part but also the associated wind. Wind may more frequently blast the building causing increased granular disintegration. The general wind direction will also play a vital role in the weathering of sandstone built heritage. If the prevailing wind direction changes, then previously unaffected facades of a building will come under attack from strong winds. The wind will drive rain into previously unexposed areas, which at present only contain a small proportion of liquid water.

Cassar (2005) suggested that fluvial flooding will have a detrimental impact on built heritage in northern England. This does not seem to be the case for Glasgow's heritage. In accordance to the SEPA flood map, Glasgow buildings are quite safe from the impact of flooding and the only minimal risk is in some areas due to river flooding. Therefore, flooding is not a major influence on most historic buildings within Glasgow.

Dependant on the season and facade in question the rate and dominant weathering process is variable. All the data obtained on present-day weathering and how this may alter in the future are summarised in Figure 7-8. The data produced in this study, unlike Brimlecombe and Grossi (2007) and Viles (2005) who look at the macroscale, is specific for Glasgow and is focused on one material type. The data presented show that chemical weathering, clay weathering, mineral reactions and microbial decay are the dominant forces altering and controlling the shape of the exterior of buildings. Some buildings are at more risk than others and now that the mechanisms of decay have been identified the buildings can be protected better, discussed next.

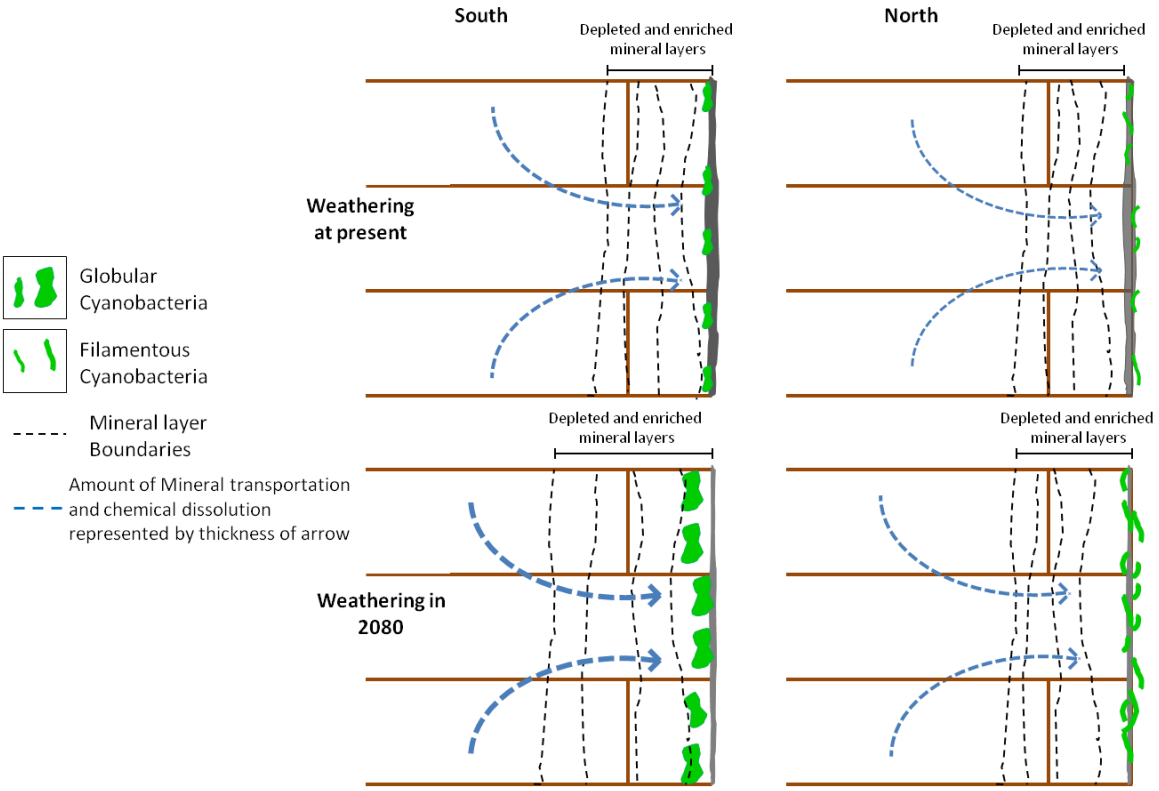

Figure 7-8: Sketch diagram of alterations to the weathering processes due to climate change.

The shading on the surface indicates the amount of crust formation. Changes to the north and south facade include increased depth of chemical decay, increased through flow of chemicals enhancing layering and greater abundance of microbial communities.

7.3 Which buildings are most at risk? In addition, how can we mitigate against these degradation processes?

As one of the main processes working against sandstone integrity is chemical decay, those at risk are the buildings constructed from sandstone that have a significant muscovite and or kaolinite proportion (i.e. the minerals most affected by chemical weathering). As stated, chemical breakdown is suggested to increase in the future, therefore elevating the rate of disintegration. Buildings that have been cleaned, or where sandstone has been used in new constructions or replacements, will be most susceptible to microbial attack. In addition, those buildings constructed from sandstone with a high porosity (~20%) will be resilient. This latter factor is important as the OLT experiments show the light is transmitted to depth more efficiently, in sandstones with lower porosity. The climate chamber results suggest that fine-grained sandstone such as the Dunhouse Buff will lose

more grains due to granular disintegration in comparison to those with a large grain size, for example Cullalo. All factors are listed in Table 7-1.

Table 7-1 Key feature to a resilient sandstone.

Sandstone Feature	Low Resilience	High Resilience
Porosity	<20%	>20%
Grain Size	Coarse-grained	Fine-grained
Kaolinite %	Little	Lots
Mica %	Little	Lots
Surface	Slight weathering	Fresh unaltered

In section 4.6.2.3 it was described how Raman spectroscopy analyses of muscovite may be able to determine how highly weathered a sandstone is, and to what depth it is being affected by this process. These data will be able to provide an overall estimate of how vulnerable a building is to the changing external environment. This process goes beyond the black crust formations on the surface to test whether the sandstone is damaged or not. This method could be used to test whether the sandstone has suffered from chemical decay in almost all Glasgow blond sandstones, and would help construct a database on Glasgow buildings, including their decay statues.

This database of information would help monitor the buildings and in circumstances advice on how best to protect the building from future decay. Maintaining external features on the building, such as guttering, will help reduce the amount of decay. In rural environments, the planting of trees and bushes can be undertaken now, so that in the future the surrounding foliage can provide protection to the buildings from the full force of the weather.

Other measures can be taken to protect the sandstone, such as applying a waterproof sealant. Some preliminary tests on available waterproofing sealants were undertaken as outlined in section 2.1.12. The two experiments undertaken were to first determine the depth of sealant penetration into the sandstone and secondly, to investigate whether the presence of the water sealant affects the internal RH of the sandstone, which would indirectly provide information on the amount of free water. The products used were Thompson's water sealant, which is a combination of hydrocarbon resins and polyoxyaluminium distearate in aliphatic hydrocarbon (mineral) spirit, and Kingfisher

water repellent, which is a solvent based fluorochemical resin. The results from the two experiments proved inconclusive.

Previous studies have suggested that water repellent solutions can penetrate to a wide range of depths, with maximum depths of 15 mm (Zoghlami and Gómez-Gras, 2004; Cnudde et al., 2007) to 1.5 mm (Casadio and Toniolo, 2004) and a minimum of only several tens of micrometers (Domingo et al., 2008). The later study is most similar to the result from this study where no depth of penetration could be visually determined using the Olympus SZX7. Previous experiments were conducted with the sealant applied from above to a horizontal surface or by capillary absorption, potentially providing unrealistically high depth penetrations in comparison to when applied to a vertical face of a building. Young et al (2003) applied a silicon based aliphatic water repellent to vertical faces of building stones and the penetration depth for fresh blond sandstone was a maximum of 12 mm. However, the films that the solution produces around the grains in the treated section are often only 1.5-3 μm thick (Zoghlami and Gómez-Gras, 2004; Domingo et al., 2008) and only minimally reduces the porosity of the sandstone, affecting the microporosity more than the macroporosity (Young et al., 2003; Zoghlami and Gómez-Gras, 2004). This could help explain the lack of sealant seen in this depth penetration experiments. The intrinsic sorpitivity of the water repellents tested may also be less than the other liquids, which have been trialled, as the capillary absorption of a liquid is based on its surface tension and the viscosity (Gummerson et al., 1980).

A very thin film may have been deposited to the surface of the grains unidentifiable with the microscope. This thin layer of water repellent may also explain the moisture results gathered. There seems to be a significant decrease in the moisture reaching the IButton dataloggers in comparison to the previous years during June 2010 signifying that the sealant is working, however little evidence is seen in July and August of this effect. The rainfall data for July 2010 is very high in contrast to the previous years and may have torn and damaged this extremely thin layer of sealant rendering it ineffective, as the sealant did not penetrate to depth on the vertical surface. This damage may be more prominent on the Dunhouse Buff sandstone as its average pore size is smaller (55.3 μm) reducing again the potential depth of penetration leaving the sealant on the surface exposed to damage by the environment conditions. In comparison Bearl, which has a slightly larger

average pore size of 73.2 µm, shows signs of the sealant reducing moisture ingress in August.

These preliminary results indicate that the application of a waterproofing sealant to a building may be an effective form of reducing the infiltration of moisture. However, to compliment this case study a much more in-depth laboratory experiment would need to be conducted to reduce the amount of external factors such as: wind direction, wind speed, rate of rain fall, length of dry periods between rainfall. These factors all change on a daily, monthly and yearly cycle affecting the ingression of water. Also the use of water proofing solutions would need to be investigated further to see whether they cause any secondary weathering processes unidentifiable in this short study, such as freeze thaw. However, Young et al (2003) did indicate that their presence did not seem to affect this cycle. In addition, mitigation procedure should only be undertaken with great care as each sandstone (due to composition and porosity structure) will react in different ways to the application of water repellents and consolidates.

Therefore, the mitigation strategy used for the protection of sandstone constructions needs much more experimentation.

8 Further Work

There are a number of suggested avenues to follow on from this study. The most important, as previously outlined, would be mitigation techniques. In time, the aim is to create widely-applicable procedures to preserve our stone built heritage. There are other aspects of this research which could be examined in further detail. This study focused on blond sandstone buildings in Glasgow which were all ~150 years old. To enhance the conclusions gained from this study, many more blond Glasgow buildings could be examined. In addition, a set of buildings with a broader age range could be investigated, which would provide a more comprehensive knowledge of the dominant decay processes and their rates, helping to identify when particular weathering processes begin to affect the sandstone. Furthermore, it would be of great interest to gain a set of samples from the same height and placement around all four facades of one individual building. This would provide a clearer view of the weathering processes and decay rates for the orientation of each facade of a building.

To complete the understanding of the weathering cycle for Glasgow, the red sandstone buildings should also be subjected to the same scrutiny as the blond sandstone buildings, as 40% of Glasgow's sandstone buildings are constructed from this material.

As, previously shown, one of the major factors which has to be considered whilst studying the decay processes of a construction stone is its primary mineralogy. As each town and city has its own unique local building material source, there will be a variation in the dominant factors behind the decay processes. The other main factor that dictates which decay processes are dominant is the local climatic conditions. Therefore, a comprehensive study of the decay process occurring, similar to this study, could be undertaken in every city within Scotland and the rest of the UK. Comparing the regional variations, whilst understanding the differences in the local environment, could allow correlations to be made throughout the UK and may help to prevent decay process acting as quickly.

These suggestions are quite large scale, although there are some individual features of the present study which could be focused on and in more detail.

One such research area would be to, further investigate the breakdown of the muscovite minerals, possibly through the use of (K-Ar) dating.

This procedure would supply data on whether argon is being lost during breakdown and this subsequently provides information on which bonds are being broken within the mineral, as has been suggested by Michell and Taka (1984).

Potassium-Argon dating would test how much potassium has been lost from the muscovite. Once a 50% loss of potassium has occurred, the potassium will become "stabilised" within the muscovite structure. Once more than 60% has been lost, the grain loses its mechanical strength. If the potassium content could be deduced, then we would understand where in the breakdown process the micas were.

Further benefits may come from expanding the Raman spectroscopy investigation on the Fe-oxides and hydroxides. If additional work were to be conducted into the distribution of the various Fe-oxides and hydroxides, a weathering succession may become identifiable. This would then provide information on how weathered the sandstone had become through analysing the 'generation' of Fe-oxides/hydroxides, which are present. Such work has already been successfully undertaken on archaeological artefacts (Neff et al., 2006). This would also supplying data on the depth of Fe-oxide decay.

The use of organism DNA identification techniques, such as rRNA could be undertaken on the microbes samples, to determine the exact species of microorganism present. This information would help to more accurately predict the microbial weathering cycle at present and for 2080. Experiments could then be run to understand how the species present will react to the change in the climate. Although different species of microbes can survive in a wide variety of environments, each microbial genus has an optimum temperature, RH and light requirements needed to sustain all the processes essential to live and therefore, weathering the sandstone. In addition, if the bacterial communities could be further investigated, then a better idea of the amount of acid corrosion due to microbial communities could be gained. Lead citric tests could be used to determine the bacteria communities (Venable and Coggeshall 1963).

As previously outlined in section 6.2.8 improvements to the climate chamber experiments could be made, such as the protocol undertaken and to the running time of the environmental chamber. These improvements would hopefully produce more accurate and reliable results, reflecting natural weathering better. In addition, the laser scanning of the blocks could be undertaken at more frequent time intervals so that the progression of the granular disintegration could be more closely monitored, to provide information on whether the granular disintegration occurs gradually or in episodic bursts.

Much of the work conducted on sandstone decay has focused on the outermost surface such as the crust which, in reality, is the end product of countless small weathering processes which are taking place at depth, and these need more investigation. Most weathering papers forget to mention or do not even realise that the internal microclimate differs from that of the external and, when it is actually investigated, generally only the temperature has been recorded in detail. In addition, when internal microclimate data is recorded, this is in isolation and is not combined with other weathering processes to see how this “new” climate may affect or alter the established decay processes already occurring. Finally many papers on sandstone weathering wait until the sandstone has suffered failure due to decay, rather than investigating the processes and early warning signs of failure so that precautions can be undertaken to limit weathering before it becomes critical. This work suggests that the ankerite, kaolinite and muscovite minerals can all be used to determine the “health” of the sandstone before the decision to replace the sandstone is made.

References

ADAMO, P., and VIOLANTE, P., 2000, Weathering of rocks and neogenesis of minerals associated with lichen activity: Applied Clay Science. **16**, 229-256.

ADAMS, C. W. M., 1960, OSMIUM TETROXIDE AND THE MARCHI METHOD: REACTIONS WITH POLAR AND NON-POLAR LIPIDS, PROTEIN AND POLYSACCHARIDE: J. Histochem. Cytochem. **8**, 262-267.

AHNERT, F., 1998, Introduction to Geomorphology: London, Arnold.

AL-HASHIMI, W. S., and HEMINGWAY, J. E., 1973, Recent dedolomitization and the origin of the rusty crusts of Northumberland: JOURNAL OF SEDIMENTARY RESEARCH. **43**, 82-91.

ANDERSON, K., and BOWS, A., 2008, Reframing the climate change challenge in light of post-2000 emission trends: Philosophical Transactions of the Royal Society a-Mathematical Physical and Engineering Sciences. **366**, 3863-3882.

ANDRÉ, M.-F., 1992, Plant colonization and geodynamics of slopes in a polar oceanic environment (Svalbard,79° N): Polar Geography and Geology. **16**, 329 - 347.

AUSSET, P., CROVISIER, J. L., DEL MONTE, M., FURLAN, V., GIRARDET, F., HAMMECKER, C., JEANNETTE, D., and LEFEVRE, R. A., 1996, Experimental study of limestone and sandstone sulphation in polluted realistic conditions: The Lausanne Atmospheric Simulation Chamber (LASC): Atmospheric Environment. **30**, 3197-3207.

AVDELIDIS, N. P., and MOROPOULOU, A., 2003a, Applications of infrared thermography for the investigation of historic structures: Journal of Cultural Heritage. **5**, 119-127.

—, 2003b, Emissivity considerations in building thermography: Energy and Buildings. **35**, 663-667.

BALLANTYNE, C. K., and HARRIS, C., 1994, the Periglation of Great Britain: Cambridge, Cambridge University Press.

BENNETT, P. C., ROGERS, J. R., CHOI, W. J., and HIEBERT, F. K., 2001, Silicates, Silicate Weathering, and Microbial Ecology: Geomicrobiology Journal. **18**, 3 - 19.

BERNARD, S., BEYSSAC, O., and BENZERARA, K., 2008, Raman Mapping Using advanced Line-Scanning Systems: Geological Applications: Applied spectroscopy. **62**, 1180-1188.

BLAND, W., and ROLLS, D., 1998, Weathering: An introduction to the Scientific Principles: London, Arnold.

BLUCK, B. J., and PORTER, J., 1991a, Aimes and methods of sandstone cleaning: stone cleaning. **27**, 21-28.

—, 1991b, Sandstone buildings and cleaning problems: Stone cleaning. **26**, 21-27.

BONAZZA, A., MESSINA, P., SABBIONI, C., GROSSI, C. M., and BRIMBLECOMBE, P., 2009, Mapping the impact of climate change on surface recession of carbonate buildings in Europe: Science of The Total Environment. **407**, 2039-2050.

BRIMBLECOMBE, P., and GROSSI, C. M., 2007, Damage to Buildings from Future Climate and Pollution: APT Bulletin. **38**, 13-18.

BRIMBLECOMBE, P., GROSSI, C. M., and HARRIS, I., 2006, The effect of long-term trends in dampness on historic buildings: Weather. **61**, 278-281.

BROWNE, M. A. E., DEAN, M. T., HALL, I. H. S., MCADAM, A. D., MONRO, S. K., and CHISHOLM, J. I., 1999, A lithostratigraphical framework for the Carboniferous rocks of the Midland Vally of Scotland, British Geographical Survey Research report, RR/99/07.

BURFORD, E. P., FOMINA, M., and GADD, G. M., 2003, Fungal involvement in bioweathering and biotransformation of rocks and minerals: Mineralogical Magazine. **67**, 1127-1155.

BUTLIN, R. N., COOTE, A. T., DEVENISH, M., HUGHES, I. S. C., HUTCHENS, C. M., IRWIN, J. G., LLOYD, G. O., MASSEY, S. W., WEBB, A. H., and YATES, T. J. S., 1992, Preliminary results from the analysis of stone tablets from the National Materials Exposure Programme (NMEP): Atmospheric Environment. Part B. Urban Atmosphere. **26**, 189-198.

CASADIO, F., and TONIOLO, L., 2004, Polymer Treatments for Stone Conservation: Methods for Evaluating Penetration Depth: Journal of the American Institute for Conservation. **43**, 3-21.

CASSAR, M., 2005, Climate Change and the Historic Environment: London, University College London.

CHEN, Y., and BRANTLEY, S. L., 1997, Temperature- and pH-dependence of albite dissolution rate at acid pH: Chemical Geology. **135**, 275-290.

CHIN, P.-K. F., and MILLS, G. L., 1991, Kinetics and mechanisms of kaolinite dissolution: effects of organic ligands: Chemical Geology. **90**, 307-317.

CNUDDE, V., DIERICK, M., VLASSENBROECK, J., MASSCHAELE, B., LEHMANN, E., JACOBS, P., and VAN HOOREBEKE, L., 2007, Determination of the impregnation depth of siloxanes and ethylsilicates in porous material by neutron radiography: Journal of Cultural Heritage. **8**, 331-338.

CNUDDE, V., GEERT, S., MATTHIEU, B., JAN, D., BJÖRN, D. S., TOM, S., DENIS, V. L., YONI, D. W., MARLINA, E., LASZLO, V., LUC, V. H., and PATRIC, J., 2009, Multi-disciplinary characterisation of a sandstone surface crust: Science of The Total Environment. **407**, 5417-5427.

CONCA, J. L., and ROSSMAN, G. R., 1982, Case hardening of sandstone: Geology. **10**, 520-523.

COOKE, R. U., and SMALLEY, I. J., 1968, Salt Weathering in Deserts: Nature. **220**, 1226-&.

DAPPLES, E. C., 1967, Chapter 3 Diagenesis of Sandstones, *in* GUNNAR, L., and GEORGE, V. C., eds., Developments in Sedimentology**Volume**: Series Title|: City|, Publisher|. Pages|.

DAVILA, A. F., GOMEZ-SILVA, B., DE LOS RIOS, A., ASCASO, C., OLIVARES, H., MCKAY, C. P., and WIERZCHOS, J., 2008, Facilitation of endolithic microbial survival in the hyperarid core of the Atacama Desert by mineral deliquescence: Journal of Geophysical Research-Biogeosciences. **113**.

DE, B. R., ZABEL, I. H. H., STROUD, D., and NELSON, M. A., 1992, Optical analog of the permeability of sandstones: Physical Review B. **45**, 196.

DE LA TORRE, J. R., GOEBEL, B. M., FRIEDMANN, E. I., and PACE, N. R., 2003, Microbial Diversity of Cryptoendolithic Communities from the McMurdo Dry Valleys, Antarctica: Appl. Environ. Microbiol. **69**, 3858-3867.

DEER, W. A., HOWIE, R. A., and ZUSSMAN, J., 1992, An Introduction to the Rock-Forming Minerals: Harlow, England, Pearson, Prentice Hall.

DEL MONTE, M., SABBIONI, C., and ZAPPIA, G., 1987, The origin of calcium oxalates on historical buildings, monuments and natural outcrops: Science of The Total Environment. **67**, 17-39.

DOMINGO, C., ALVAREZ DE BUERGO, M., SÁNCHEZ-CORTÉS, S., FORT, R., GARCÍA-RAMOS, J. V., and GOMEZ-HERAS, M., 2008, Possibilities of monitoring the polymerization process of silicon-based water repellents and consolidants in stones through infrared and Raman spectroscopy: Progress in Organic Coatings. **63**, 5-12.

DORN, R. I., 1998, Rock Coatings, Elsevier.

DORNIEDEN, T., GORBUSHINA, A. A., and KRUMBEIN, W. E., 2000, Biodecay of cultural heritage as a space/time-related ecological situation -- an evaluation of a series of studies: International Biodeterioration & Biodegradation. **46**, 261-270.

DRYDEN, A. L., 1931, Accuracy in Percentage Representation of Heavy Mineral Frequencies: Proceedings of the National Academy of Sciences. **17**, 233-238.

DUTHIE, L. J., HYSLOP, E., KENNEDY, C., PHOENIX, V., and LEE, M. R., 2008, Quantitative Assessment of Decay Mechanisms in Scottish Building Sandstones, *in* LUKASZEWICZ, J. W.,

and NIEMCEWICZ, P., eds., 11th International Congress on Deterioration and Conservation od Stone, Volume 1: Torun, Poland.

EVAMY, B. D., 1967, Dedolomitization and the development of rhombohedral pores in limestones: JOURNAL OF SEDIMENTARY RESEARCH. **37**, 1204-1215.

FERNANDES, P., 2006, Applied microbiology and biotechnology in the conservation of stone cultural heritage materials: Applied Microbiology and Biotechnology. **73**, 291-296.

FLORES, M., LORENZO, J., and GÓMEZ-ALARCÓN, G., 1997, Algae and bacteria on historic monuments at Alcala de Henares, Spain: International Biodeterioration & Biodegradation. **40**, 241-246.

FRANK, J. R., 1981, Dedolomitization in the Taum Sauk limestone (Upper Cambrian), Southeast Missouri: Journal of Sedimentary Petrology. **51**.

FRANKE, W. A., 2009, The durability of rocks--Developing a test of rock resistance to chemical weathering: Am J Sci. **309**, 711-730.

FRANZEN, C., and MIRWALD, P. W., 2009, Moisture sorption behaviour of salt mixtures in porous stone: Chemie der Erde - Geochemistry. **69**, 91-98.

FRIEDMANN, E. I., 1982, Endolithic Microorganisms in the Antarctic Cold Desert: Science. **215**, 1045-1053.

FRIOLO, K. H., STUART, B., and RAY, A., 2003, Characterisation of weathering of Sydney sandstones in heritage buildings: Journal of Cultural Heritage. **4**, 211-220.

FROST, R. L., 1995, Fourier Transform Raman Spectroscopy of Kaolinite, Dickite and Halloysite: Clays and Clay Minerals. **43**, 191-195.

FROST, R. L., FREDERICKS, P. M., KLOPROGGE, J. T., and HOPE, G. A., 2001, Raman spectroscopy of kaolinites using different excitation wavelengths: Journal of Raman Spectroscopy. **32**, 657-663.

FROST, R. L., TRAN, T. H., RINTOUL, L., and KRISTOL, J., 1998, Raman microscopy of dickite, kaolinit and their intercalates: The Analyst. **123**, 611-616.

GARCIA-VALLÈS, M., VENDRELL-SAZ, M., MOLERA, J., and BLAZQUEZ, F., 1998, Interaction of rock and atmosphere: patinas on Mediterranean monuments: Environmental Geology. **36**, 137-149.

GAUTELIER, M., OELKERS, E. H., and SCHOTT, J., 1999, An experimental study of dolomite dissolution rates as a function of pH from -0.5 to 5 and temperature from 25 to 80°C: Chemical Geology. **157**, 13-26.

GOLUBEV, S. V., BÉNÉZETH, P., SCHOTT, J., DANDURAND, J. L., and CASTILLO, A., 2009, Siderite dissolution kinetics in acidic aqueous solutions from 25 to 100 °C and 0 to 50 atm pCO2: Chemical Geology. **265**, 13-19.

GOLUBIC, S., FRIEDMANN, E. I., and SCHNEIDER, J., 1981, The lithobiontic ecological niche, with special reference to microorganisms: JOURNAL OF SEDIMENTARY RESEARCH. **51**, 475-478.

GÓMEZ-ALARCÓN, G., MUÑOZ, M., ARIÑO, X., and ORTEGA-CALVO, J. J., 1995, Microbial communities in weathered sandstones: the case of Carrascosa del Campo church, Spain: Science of The Total Environment. **167**, 249-254.

GÓMEZ-ALARCÓN, G., MUÑOZ, M. L., and FLORES, M., 1994, Excretion of organic acids by fungal strains isolated from decayed sandstone: International Biodeterioration & Biodegradation. **34**, 169-180.

GÖTZE, J., and SIEDEL, H., 2007, A complex investigation of building sandstones from Saxony (Germany): Materials Characterization. **58**, 1082-1094.

GRIFFITH, B. T., and ARASTEH, D., 1999, Buildings research using infrared imaging radiometers with laboratory thermal chambers: Thermosense Xxi. **3700**, 502-513.

GROSSI, C. M., BRIMBLECOMBE, P., and HARRIS, I., 2007, Predicting long term freeze-thaw risks on Europe built heritage and archaeological sites in a changing climate: Science of The Total Environment. **377**, 273-281.

GROSSI, C. M., ESBERT, R. M., DÍAZ-PACHE, F., and ALONSO, F. J., 2003, Soiling of building stones in urban environments: Building and Environment. **38**, 147-159.

GUMMERSON, R. J., HALL, C., and HOFF, W. D., 1980, Water movement in porous building materials--II. Hydraulic suction and sorptivity of brick and other masonry materials: Building and Environment. **15**, 101-108.

HALL, C., 1977, Water movement in porous building materials--I. Unsaturated flow theory and its applications: Building and Environment. **12**, 117-125.

HALL, C., HAMILTON, A., HOFF, W. D., VILES, H. A., and EKLUND, J. A., 2011, Moisture dynamics in walls: response to micro-environment and climate change: Proceedings of the Royal Society A: Mathematical, Physical and Engineering Science. **467**, 194-211.

HALL, C., and KALIMERIS, A. N., 1982, Water movement in porous building materials--V. Absorption and shedding of rain by building surfaces: Building and Environment. **17**, 257-262.

HALL, K., 2004, Evidence for freeze-thaw events and their implications for rock weathering in northern Canada: Earth Surface Processes and Landforms. **29**, 43-57.

HALL, K., and ANDRE, M. F., 2006, Temperature observations in Antarctic tafoni: implications for weathering, biological colonization, and tafoni formation: Antarctic Science. **18**, 377-384.

HALL, K., GUGLIELMIN, M., and STRINI, A., 2008, Weathering of granite in Antarctica: I. Light penetration into rock and implications for rock weathering and endolithic communities: Earth Surface Processes and Landforms. **33**, 295-307.

HALL, K., LINDGREN, B. S., and JACKSON, P., 2005, Rock albedo and monitoring of thermal conditions in respect of weathering: some expected and some unexpected results: Earth Surface Processes and Landforms. **30**, 801-811.

HALL, K., MEIKLEJOHN, I., SUMMER, P., and AROCENA, J., 2010, Light Penetration into Clarens Sandstone and Implications for Deterioration of San Rock Art: Geoarchaeology-an International Journal. **25**, 122-136.

HANSON, S., and GOODESS, C. M., 2004, Predicting Future Changes in Wind, Climatic Research Unit, University of East Anglia.

HUGHES, J. J., and TENNENT, N. H., 2008, The Petrography of the Giffnock Sandstone from the Interior of the Art Gallary and Museum, Kelvingrove, Glasgow, *in* LUKASZEWICZ, J. W., and NIEMCEWICZ, P., eds., 11th International Congress on Deterioration and Conservation of Stone: Torun, Poland, Nicolaus Copernicus University Press.

HUGHES, K. A., and LAWLEY, B., 2003, A novel Antarctic microbial endolithic community within gypsum crusts: Environmental Microbiology. **5**, 555-565.

HULME, M., JENKIMS, G. J., LU, X., TURNPENNY, J. R., MITCHELL, T. D., JONES, R. G., LOWE, J., MURPHY, J. M., HASSELL, D., BOORMAN, P., MCDONALD, R., and HILLS, S., 2002, Climate Change Scenarios for the United Kingdom: The UKCIP02 Scientific Report: Tyndall Centre for Climate Change Research, School of Environmental Sciences, University of East Anglia, Norwich, UK 120

HYSLOP, E. K., and ALBORNOZ-PARRA, L., 2009, Developing a future repairs strategy for a sandstone city: A petrographic investigation of building stone in Glasgow, Scotland: Materials Characterization. **60**, 636-643.

HYSLOP, E. K., ALBORNOZ, L. J., FISHER, L. C., and HAMILTON, S. L., 2006, Safeguardoing Glasgow's stone built heritage skills and materials requirement: facade surveys and building stone analysis: Glasgow, british Geological survey, p. 1-49.

IP, K. H., STUART, B. H., RAY, A. S., and THOMAS, P. S., 2008, A spectroscopic investigation of the weathering of a heritage Sydney sandstone: Spectrochimica Acta Part A: Molecular and Biomolecular Spectroscopy. **71**, 1032-1035.

JAIN, A., BHADAURIA, S., KUMAR, V., and CHAUHAN, R. S., 2009, Biodeterioration of sandstone under the influence of different humidity levels in laboratory conditions: Building and Environment. **44**, 1276-1284.

JEFFERSON, D. P., 1993, The Weathering of Stone: Stone Industries. **28**.

JENKINS, K. A., and SMITH, B. J., 1990, Daytime rock surface temperature variability and its implications for mechanical rock weathering: Tenerife, Canary Islands: CATENA. **17**, 449-459.

JEPSON, W. B., and ROWSE, J. B., 1975, The composition of kaolinite; an electron microscope microprobe study: Clays and Clay Minerals. **23**, 310-317.

JIMENEZ-GONZALEZ, I., RODRIGUEZ-NAVARRO, C., and SCHERER, G. W., 2008, Role of clay minerals in the physicomechanical deterioration of sandstone: Journal of Geophysical Research-Earth Surface. **113**.

JOHNSTON, C., 1990, In situ laser Raman microprobe spectroscopy of corroding iron electrode surfaces: Vibrational Spectroscopy. **1**, 87-96.

KAMH, G. M. E., 2005a, Mechanism of concave "tafoni" and convex "domal shape" formation on TRIASSIC red sandstone of some old buildings, Chester City, UK, Case Study: Environmental Geology. **48**, 625-638.

—, 2005b, Weathering at high latitudes on the carboniferous Old Red Sandstone, petrographic and geotechnical investigations, Jedburgh Abbey Church, Scotland, a case study: Environmental Geology. **47**, 482-492.

KELLY, W. C., and ZUMBERGE, J. H., 1961, Weathering of a quartz diorite at Marble Point, McMurdo Sound, Antarctica: Journal of Geology.

KENT, A. J., GRICE, S., STEDMAN, J. R., BUSH, T. J., VINCENT, K. J., ABBOTT, J., DERWENT, D., and HOBSON, M., 2010, UK air quality modelling for annual reporting 2005 on ambient air quality assessment under Council Directives 96/62/EC, 1999/30/EC and 2000/69/EC, *in* STEDMAN, J. R., ed.

KERR, A., SMITH, B. J., BRIAN WHALLEY, W., and MCGREEVY, J. P., 1984a, Rock temperatures from southeast Morocco and their significance for experimental rock-weathering studies: Geology. **12**, 306-309.

KERR, A., SMITH, B. J., WHALLEY, W. B., and MCGREEVY, J. P., 1984b, Rock Temperatures from Southeast Morocco and Their Significance for Experimental Rock-Weathering Studies: Geology. **12**, 306-309.

LARROUMET, D., GREENFIELD, D., AKID, R., and YARWOOD, J., 2007, Raman spectroscopic studies of the corrosion of model iron electrodes in sodium chloride solution: Journal of Raman Spectroscopy. **38**, 1577-1585.

LASAGA, A. C., 1998, Kinetic theory in the Earth Science: Princeton, Princeton University Press.

LEE, M. R., BLUCK, B. J., and CHUNG, P. Y., 2006, Analysis of samples of Glasgow Building sandstone for composition and alteration due to urban surface deposition and weathering: Glasgow, University of Glasgow, p. 2-14.

LEFEVRE, R. A., and AUSSET, P., 2002, Atmospheric pollution and building materials: stone and glass: Geological Society, London, Special Publications. **205**, 329-345.

LENG, L., 2008, Material Characterization: Introduction to Microscopic and Spectroscopic Methods: Singapore, Wiley.

LIANG, C., DAS, K. C., and MCCLENDON, R. W., 2003, The influence of temperature and moisture contents regimes on the aerobic microbial activity of a biosolids composting blend: Bioresource Technology. **86**, 131-137.

LIN, S. Y., LI, M. J., and CHENG, W. T., 2007, FT-IR and Raman vibrational microspectroscopies used for spectral biodiagnosis of human tissues: Spectroscopy-an International Journal. **21**, 1-30.

LITCHMAN, E., STEINER, D., and BOSSARD, P., 2003, Photosynthetic and growth responses of three freshwater algae to phosphorus limitation and daylength: Freshwater Biology. **48**, 2141-2148.

LOWRY, O. H., ROSEBROUGH, N. J., FARR, A. L., and RANDALL, R. J., 1951, PROTEIN MEASUREMENT WITH THE FOLIN PHENOL REAGENT: Journal of Biological Chemistry. **193**, 265-275.

MACEDO, M. F., MILLER, A. Z., DIONISIO, A., and SAIZ-JIMENEZ, C., 2009, Biodiversity of cyanobacteria and green algae on monuments in the Mediterranean Basin: an overview: Microbiology. **155**, 3476-3490.

MACHILL, S., ALTHAUS, K., KRUMBEIN, W. E., and STEGER, W. E., 1997, Identification of organic compounds extracted from black weathered surfaces of Saxonean sandstones, correlation with atmospheric input and rock inhabiting microflora: Organic Geochemistry. **27**, 79-97.

MADSEN, F. T., and MULLER-VONMOOS, M., 1989, The Selling Behaviour of Clays: Applied Clay Science, 143-156.

MATSUOKA, N., 2001, Microgelivation versus macrogelivation: towards bridging the gap between laboratory and field frost weathering: Permafrost and Periglacial Processes. **12**, 299-313.

MAURICE, P. A., VIERKORN, M. A., HERSMAN, L. E., FULGHUM, J. E., and FERRYMAN, A., 2001, Enhancement of Kaolinite Dissolution by an Aerobic Pseudomonas mendocina Bacterium: Geomicrobiology Journal. **18**, 21 - 35.

MCALISTER, J. J., SMITH, B. J., and CURRAN, J. A., 2003, The use of sequential extraction to examine iron and trace metal mobilisation and the case-hardening of building sandstone: a preliminary investigation: Microchemical Journal. **74**, 5-18.

MCDONALD, C., and DUNCAN, H. J., 1979, Particle size distribution of metals in the atmosphere of Glasgow: Atmospheric Environment (1967). **13**, 977-980.

MCGREEVY, J. P., and SMITH, B. J., 1982, Salt Weathering in Hot Deserts: Observations on the Design of Simulation Experiments: Geografiska Annaler. Series A, Physical Geography. **64**, 161-170.

—, 1985, The spalling of quartz overgrowths during experimental salt weathering of a sandstone: Micron and Microscopica Acta. **16**, 277-279.

MCGREEVY, J. P., WARKE, P. A., and SMITH, B. J., 2000, Controls on Stone Temperatures and the Benefits of Interdisciplinary Exchange: Journal of the American Institute for Conservation. **39**, 259-274.

MCKINLEY, J. M., CURRAN, J. M., and TURKINGTON, A. V., 2001, Gypsum formation in non-calcareous building sandstone: a case study of Scrabo sandstone: Earth Surface Processes and Landforms. **26**, 869-875.

MCKINLEY, J. M., WARKE, P., LLOYD, C. D., RUFFELL, A. H., and SMITH, B. J., 2006, Geostatistical analysis in weathering studies: case study for Stanton Moor building sandstone: Earth Surface Processes and Landforms. **31**, 950-969.

MCNEILL, G. W., 1999, Variations in the Weathering Rate of Scottish Gravestones as an Environmental Signature of Atmospheric Pollution: Environmental Geochemistry and Health. **21**, 365-370.

MILLER, A., DIONÍSIO, A., and MACEDO, M. F., 2006, Primary bioreceptivity: A comparative study of different Portuguese lithotypes: International Biodeterioration & Biodegradation. **57**, 136-142.

MITCHELL, J. G., and TAKA, A. S., 1984, Potassium and argon loss patterns in weathered micas: Implications for detrital mineral studies, with particular reference to the triassic palaeogeography of the British Isles: Sedimentary Geology. **39**, 27-52.

MOROPOULOU, A., BISBIKOU, K., TORFS, K., VAN GRIEKEN, R., ZEZZA, F., and MACRI, F., 1998, Origin and growth of weathering crusts on ancient marbles in industrial atmosphere: Atmospheric Environment. **32**, 967-982.

MOROPOULOU, A., HARALAMPOPOULOS, G., TSIOURVA, T., AUGER, F., and BIRGINIE, J. M., 2003, Artificial weathering and non-destructive tests for the performance evaluation of consolidation materials applied on porous stones: Materials and Structures. **36**, 210-217.

MOTTERSHEAD, D., GORBUSHINA, A., LUCAS, G., and WRIGHT, J., 2003, The influence of marine salts, aspect and microbes in the weathering of sandstone in two historic structures: Building and Environment. **38**, 1193-1204.

NEFF, D., BELLOT-GURLET, L., DILLMANN, P., REGUER, S., and LEGRAND, L., 2006, Raman imaging of ancient rust scales on archaeological iron artefacts for long-term atmospheric corrosion mechanisms study: Journal of Raman Spectroscopy. **37**, 1228-1237.

NIENOW, J. A., MCKAY, C. P., and FRIEDMANN, E. I., 1988, THE CRYPTOENDOLITHIC MICROBIAL ENVIRONMENT IN THE ROSS DESERT OF ANTARCTICA - LIGHT IN THE PHOTOSYNTHETICALLY ACTIVE REGION: Microbial Ecology. **16**, 271-289.

O'CONNOR, J., RAY, A., FRANKLIN, B., and STUART, B., 2001, Changes in teh physical and chemical properties of weathered Maroubra Sandstone in Sydney: AICCM Bulletin. **26**.

OLLIER, C., 1991, Ancient Landforms, Belhaven Press.

OMELON, C. R., POLLARD, W. H., and FERRIS, F. G., 2006a, Chemical and ultrastructural characterization of high arctic cryptoendolithic habitats: Geomicrobiology Journal. **23**, 189-200.

—, 2006b, Environmental controls on microbial colonization of high Arctic cryptoendolithic habitats: Polar Biology. **30**, 19-29.

—, 2007, Inorganic species distribution and microbial diversity within high arctic cryptoendolithic habitats: Microbial Ecology. **54**, 740-752.

ORTEGA-CALVO, J. J., HERNANDEZ-MARINE, M., and SAIZ-JIMENEZ, C., 1991, Biodeterioration of building materials by cyanobacteria and algae: International Biodeterioration. **28**, 165-185.

PARNELL, J., TAYLOR, C. W., THACKREY, S., OSINSKI, G. R., and LEE, P., 2010, Permeability data for impact breccias imply focussed hydrothermal fluid flow: Journal of Geochemical Exploration. **In Press, Corrected Proof**.

PEEL, R. F., 1974, Insolation weathering: some measurements of diurnal temperature changes in exposed rocks in the Tibesti region, central Sahara: Zeitschrift für Geomorphologie.

PETERSON, G. L., 1977, A simplification of the protein assay method of Lowry et al. which is more generally applicable: Analytical Biochemistry. **83**, 346-356.

PHOENIX, V. R., BENNETT, P. C., ENGEL, A. S., TYLER, S. W., and FERRIS, F. G., 2006, Chilean high-altitude hot-spring sinters: a model system for UV screening mechanisms by early Precambrian cyanobacteria: Geobiology. **4**, 15-28.

PHOENIX, V. R., KONHAUSER, K. O., ADAMS, D. G., and BOTTRELL, S. H., 2001, Role of biomineralization as an ultraviolet shield: Implications for Archean life: Geology. **29**, 823-826.

PIFFY, A. F., 1979, Geography and Soil Properties London, Methuen.

PLAS, L. V. D., and TOBI, A. C., 1965, A chart for judging the reliability of point counting results: American Journal of Science. **263**, 87-90.

POTTS, M., and FRIEDMANN, E. I., 1981, Effects of water stress on cryptoendolithic cyanobacteria from hot desert rocks: Archives of Microbiology. **130**, 267-271.

PRICE, D. G., 1995, Weathering and weathering processes: Quarterly Journal of Engineering Geology and Hydrogeology. **28**, 243-252.

PRIETO, B., SILVA, B., CARBALLAL, R., and DE SILANES, M. E. L., 1994, Colonization by lichens of granite dolmens in Galicia (NW Spain): International Biodeterioration & Biodegradation. **34**, 47-60.

PRIKRYL, R., LOKAJÍCEK, T., SVOBODOVÁ, J., and WEISHAUPTOVÁ, Z., 2003, Experimental weathering of marlstone from Prední Kopanina (Czech Republic)--historical building stone of Prague: Building and Environment. **38**, 1163-1171.

PŘIKRYL, R., MELOUNOVÁ, L., VAŘILOVÁ, Z., and WEISHAUPTOVÁ, Z., 2007, Spatial relationships of salt distribution and related physical changes of underlying rocks on naturally weathered sandstone exposures (Bohemian Switzerland National Park, Czech Republic): Environmental Geology. **52**, 409-420.

REICHE, P., 1962, A survey of weathering processes and products, University of New Mexico Press.

RIPPKA, R., DERUELLES, J., WATERBURY, J. B., HERDMAN, M., and STANIER, R. Y., 1979, Generic Assignments, Strain Histories and Properties of Pure Cultures of Cyanobacteria: J Gen Microbiol. **111**, 1-61.

RODRIGUEZ-NAVARRO, C., and DOEHNE, E., 1999, Salt weathering: Influence of evaporation rate, supersaturation and crystallization pattern: Earth Surface Processes and Landforms. **24**, 191-209.

SABBIONI, C., and ZAPPIA, G., 1992, Decay of Sandstone in Urban Areas Correlated with Atmospheric Aerosol: Water Air and Soil Pollution. **63**, 305-316.

SAIZ-JIMENEZ, C., 1995, Deposition of anthropogenic compounds on monuments and their effect on airborne microorganisms: Aerobiologia. **11**, 161-175.

SASS, O., and VILES, H. A., 2006, How wet are these walls? Testing a novel technique for measuring moisture in ruined walls: Journal of Cultural Heritage. **7**, 257-263.

SCHLESINGER, W. H., PIPPEN, J. S., WALLENSTEIN, M. D., HOFMOCKEL, K. S., KLEPEIS, D. M., and MAHALL, B. E., 2003, COMMUNITY COMPOSITION AND PHOTOSYNTHESIS BY PHOTOAUTOTROPHS UNDER QUARTZ PEBBLES, SOUTHERN MOJAVE DESERT: Ecology. **84**, 3222-3231.

SEABURG, K. G., PARKED, B. C., WHARTON, R. A., and SIMMONS, G. M., 1981, TEMPERATURE-GROWTH RESPONSES OF ALGAL ISOLATES FROM ANTARCTIC OASES1: Journal of Phycology. **17**, 353-360.

SEAWARD, M. R. D., 1997, Major impacts made by lichens in biodeterioration processes: International Biodeterioration & Biodegradation. **40**, 269-273.

SEBASTIÁN, E., CULTRONE, G., BENAVENTE, D., LINARES FERNANDEZ, L., ELERT, K., and RODRIGUEZ-NAVARRO, C., 2008, Swelling damage in clay-rich sandstones used in the church of San Mateo in Tarifa (Spain): Journal of Cultural Heritage. **9**, 66-76.

SELBY, M. J., 1993, Hillslope materials and processes / M.J. Selby ; with a contribution by A.P.W. Hodder: Oxford, England :, Oxford University Press.

SÉRGIO DE MELO, M., and CÉSAR FONSECA GIANNINI, P., 2007, Sandstone dissolution landforms in the Furnas Formation, southern Brazil: Earth Surface Processes and Landforms. **32**, 2149-2164.

SMALL, R. J., 1972, The study of Landforms: Cambridge, Cambridge University Press.

SMITH, B. J., GOMEZ-HERAS, M., and MCCABE, S., 2008a, Understanding the decay of stone-built cultural heritage: Progress in Physical Geography. **32**, 439-461.

SMITH, B. J., and MCGREEVY, J. P., 1988, Contour scaling of a sandstone by salt weathering under simulated hot desert conditions: Earth Surface Processes and Landforms. **13**, 697-705.

SMITH, B. J., SRINIVASAN, S., GOMEZ-HERAS, M., BASHEER, P. A. M., and VILES, H. A., 2008b, Experimental studies of near-surface temperature cycling and surface wetting of stone and its implications for salt weathering: Salt weathering on buildings and stone sculptures conference procedings

SMITH, B. J., TURKINGTON, A. V., WARKE, P. A., BASHEER, P. A. M., MCALISTER, J. J., MENEELY, J., and CURRAN, J. M., 2002, Modelling the rapid retreat of building sandstones: a case study from a polluted maritime environment: Geological Society, London, Special Publications. **205**, 347-362.

SOUZA-EGIPSY, V., WIERZCHOS, J., SANCHO, C., BELMONTE, A., and ASCASO, C., 2004, Role of biological soil crust cover in bioweathering and protection of sandstones in a semi-arid landscape (Torrollones de Gabarda, Huesca, Spain): Earth Surface Processes and Landforms. **29**, 1651-1661.

SPERL, J., and TRCKOVA, J., 2008, Permeability and Porosity of Rocks and their Relationship Based on Laboratory Testing: ACTA Geodynamica Et Geomaterialia. **5**, 41-47.

SUIHKO, M.-L., ALAKOMI, H.-L., GORBUSHINA, A., FORTUNE, I., MARQUARDT, J., and SAARELA, M., 2007, Characterization of aerobic bacterial and fungal microbiota on surfaces of historic Scottish monuments: Systematic and Applied Microbiology. **30**, 494-508.

SVENSSON, C., and JAKOB, D., 2002, Diurnal and seasonal characteristics of precipitation at an upland site in Scotland: International Journal of Climatology. **22**, 587-598.

SVENSSON, C., JAKOB, D., and REED, D. W., 2002, Diurnal characteristics of heavy precipitation according to weather type at an upland site in Scotland: International Journal of Climatology. **22**, 569-585.

TERHEIDEN, K., 2008, Simultaneous measurement of vapor and liquid moisture transport in porous building materials: Building and Environment. **43**, 2188-2192.

THOMACHOT, C., and JEANNETTE, D., 2002, Evolution of the petrophysical properties of two types of Alsatian sandstone subjected to simulated freeze-thaw conditions: Geological Society, London, Special Publications. **205**, 19-32.

—, 2004, Effects of iron black varnish on petrophysical properties of building sandstone: Environmental Geology. **47**, 119-131.

TLILI, A., SMITH, D. C., BENY, J.-M., and BOYER, H., 1989, A Raman microprobe study of natural micas: Mineralogical Magazine. **53**, 165-79.

TÖRÖK, Á., 2003, Surface strength and mineralogy of weathering crusts on limestone buildings in Budapest: Building and Environment. **38**, 1185-1192.

TUCKER, M. C., 1981, Sedimentary Petrology: Oxford, Blackwell Science.

TURKINGTON, A. V., MARTIN, E., VILES, H. A., and SMITH, B. J., 2003, Surface change and decay of sandstone samples exposed to a polluted urban atmosphere over a six-year period: Belfast, Northern Ireland: Building and Environment. **38**, 1205-1216.

TURKINGTON, A. V., and PARADISE, T. R., 2005, Sandstone weathering: a century of research and innovation: Geomorphology. **67**, 229-253.

URQUHART, D. C. M., JONES, M. S., NICHOLSON, K. A., WAKEFIELD, R. D., and YOUNG, M. E., 1995, Biological growth, biocide treatment, soiling and decay of sandstone buildings and monuments: Edinburgh, Historic Scotland

VESTAL, J. R., 1988, Biomass of the cryptoendolithic microbiota from the Antarctic desert: Appl. Environ. Microbiol. **54**, 957-959.

VILES, H., 1995, Ecological perspectives on rock surface weathering: Towards a conceptual model: Geomorphology. **13**, 21-35.

VILES, H. A., 2002, Implications of future climate change for stone deterioration: Geological Society, London, Special Publications. **205**, 407-418.

VILES, H. A., and GOUDIE, A. S., 2004, Biofilms and case hardening on sandstones from Al-Quwayra, Jordan: Earth Surface Processes and Landforms. **29**, 1473-1485.

VINCENT, W. F., and HOWARD-WILLIAMS, C., 1989, Microbial communities in southern Victoria Land streams (Antarctica) II. The effects of low temperature: Hydrobiologia. **172**, 39-49.

WAKEFIELD, R., JONES, M., WILSON, M., YOUNG, M., NICHOLSON, K., and URQUHART, D., 1996, Investigations of decayed sandstone colonised by a species ofTrentepohlia: Aerobiologia. **12**, 19-25.

WANG, A., FREEMAN, J., and KUEBLER, K. E., 2002, Raman Spectroscopic Characterization of Phyllosilicates, 33rd Annual Lunar and Planetry Science Conference: Houston, Texas.

WANG, W. H., 1992, Origin of reddening and secondary porosity in Carboniferous sandstones, Northern Ireland: Geological Society, London, Special Publications. **62**, 243-254.

WARKE, P. A., MCKINLEY, J., and SMITH, B. J., 2006, Variable weathering response in sandstone: factors controlling decay sequences: Earth Surface Processes and Landforms. **31**, 715-735.

WARKE, P. A., and SMITH, B. J., 1998, Effects of direct and indirect heating on the validity of rock weathering simulation studies and durability tests: Geomorphology. **22**, 347-357.

WARKE, P. A., SMITH, B. J., and MAGEE, R. W., 1996, Thermal response characteristics of stone: Implications for weathering of soiled surfaces in urban environments: Earth Surface Processes and Landforms. **21**, 295-306.

WARSCHEID, T., and BRAAMS, J., 2000, Biodeterioration of stone: a review: International Biodeterioration & Biodegradation. **46**, 343-368.

WARSCHEID, T., OELTING, M., and KRUMBEIN, W. E., 1991, Physico-chemical aspects of biodeterioration processes on rocks with special regard to organic pollutants: International Biodeterioration. **28**, 37-48.

WEBER, J., and LEPPER, J., 2002, Depositional environment and diagenesis as controlling factors for petro-physical properties and weathering resistance of siliciclastic dimension stones: integrative case study on the 'Wesersandstein' (northern Germany, Middle Buntsandstein): Geological Society, London, Special Publications. **205**, 103-114.

WEBSTER, R. G. M., ANDREW, C. A., BAXTER, S., MACDONALD, J., ROCHA, M., THOMSON, B. W., TONGE, K. H., URQUHART, D. C. M., and YOUNG, M. E., 1992, Stonecleaning in Scotland: Aberdeen, Historic Scotland and Scottish Enterprise.

WELTON, R. G., CUTHBERT, S. J., MCLEAN, R., HURSTHOUSE, A., and HUGHES, J., 2003, A preliminary study of the phycological degradation of natural stone masonry: Environmental Geochemistry and Health. **25**, 139-145.

WHALLEY, W. B., and MCGREEVY, J. P., 1985, Weathering: Progress in Physical Geography. **9**, 559-581.

WIERZCHOS, J., and ASCASO, C., 1996, Morphological and chemical features of bioweathered granitic biotite induced by lichen activity: Clays and Clay Minerals. **44**, 652-657.

WIERZCHOS, J., ASCASO, C., SANCHO, L. G., and GREEN, A., 2003, Iron-Rich Diagenetic Minerals are Biomarkers of Microbial Activity in Antarctic Rocks: Geomicrobiology Journal. **20**, 15 - 24.

WILLIAMS, R. B. G., and ROBINSON, D. A., 1981, Weathering of sandstone by the combined action of frost and salt: Earth Surface Processes and Landforms. **6**, 1-9.

WILSON, M. A., HOFF, W. D., and HALL, C., 1995, Water movement in porous building materials--XIII. Absorption into a two-layer composite: Building and Environment. **30**, 209-219.

WILSON, M. J., BAIN, D. C., MCHARDY, W. J., and BERROW, M. L., 1972, Clay-Minerals studies on some caboniferous sediments in Scotland: Sedimentary Geology.

WINKLER, E. M., and SINGER, P. C., 1972, Crystallization Pressure of Salts in Stone and Concrete: Geological Society of America Bulletin. **83**, 3509-&.

WINKLER, E. M., and WILHELM, E. J., 1970, SALT BURST BY HYDRATION PRESSURES IN ARCHITECTURAL STONE IN URBAN ATMOSPHERE: Geological Society of America Bulletin. **81**, 567-&.

WOODCOCK, N., and STRACHAN, R., 2000, Geological History of britain and Ireland, Blackwell Science, p. 423.

WRIGHT, J. S., 2000, The spalling of overgrowths during experimental freeze-thaw of a quartz sandstone as a mechanism of quartz silt production: Micron. **31**, 631-638.

YOUNG, M. E., 1997, Biological growths and their relationship to the physical and chemical characteristics of sandstones before and after cleaning: Aberdeen, The Robert Gordon University.

YOUNG, M. E., URQUHART, D. C. M., and LAING, R. A., 2003, Maintenance and repair issues for stone cleaned sandstone and granite building façades: Building and Environment. **38**, 1125-1131.

ZOGHLAMI, K., and GÓMEZ-GRAS, D., 2004, Determination of the distribution of consolidants and interpretation of mercury porosimetry data in a sandstone porous network using LSCM: Microscopy Research and Technique. **65**, 270-275.